This is a reproduction of a library book that was digitized by Google as part of an ongoing effort to preserve the information in books and make it universally accessible.

Google™ books

https://books.google.com

D 105.9:
20-292
FED DOCS

~~C 26.7/2 2-985/35-3~~

~~L.C. SUBJECT HEADINGS WEEKLY LISTS~~

D 105.9 = 20-292

ORDP 20-292

ORDNANCE CORPS PAMPHLET

ORDNANCE ENGINEERING DESIGN HANDBOOK

SURFACE-TO-AIR MISSILE SERIES

PART TWO, WEAPON CONTROL

STANFORD UNIVERSITY
DEC 1962
GOV'T DOCUMENT DIVISION

ORDNANCE CORPS

JUNE 1962

OFFICE OF THE CHIEF OF ORDNANCE
Washington 25, D. C., 29 June 1962

ORDP 20-292, Part Two, Weapon Control, forming part of the Surface-to-Air Missile Series of the Ordnance Engineering Design Handbook, is published for the information and guidance of all concerned.

H. F. BIGELOW
Major General, USA
Chief of Ordnance

OFFICIAL:
ALFRED A. ROBINSON
Colonel, Ord Corps
Executive Officer

OFFICIAL
COPY

DISTRIBUTION: Special

ORDNANCE CORPS PAMPHLET **ORDP 20-292**

ORDNANCE ENGINEERING DESIGN HANDBOOK

SURFACE-TO-AIR MISSILE SERIES

PART TWO, WEAPON CONTROL

CONSISTING OF

CHAPTERS 6—7

FOREWORD

The Surface-To-Air Missile Series is part of a group of handbooks covering the engineering principles and fundamental data needed in the development of ordnance equipment, which (as a group) constitutes the Ordnance Engineering Design Handbook Series.

The Surface-To-Air Missile Series is initially comprised of seven numbered Parts, each of which is published as a separate volume and assigned an Ordnance Pamphlet (ORDP) number. These designations, together with arrangement into Chapters and Chapter titles, are as follows:

ORDP 20-291 PART ONE — System Integration
  Chapter 1 — Introduction
  Chapter 2 — Operations Research
  Chapter 3 — Systems Engineering
  Chapter 4 — Systems Test and Evaluation
  Chapter 5 — Logistics and Support

ORDP 20-292 PART TWO — Weapon Control
  Chapter 6 — Fire Direction and Coordination
  Chapter 7 — Guidance and Control

ORDP 20-293 PART THREE — Computers
  Chapter 8 — Computers

ORDP 20-294(S) PART FOUR — Missile Armament (U)
  Chapter 9 — Warheads
  Chapter 10 — Fuzes

ORDP 20-295(S) PART FIVE — Countermeasures (U)
  Chapter 11 — Electronic Countermeasures

ORDP 20-296 PART SIX — Structures and Power Sources
  Chapter 12 — Power Sources
  Chapter 13 — Launchers
  Chapter 14 — Airframes
  Chapter 15 — Propulsion

ORDP 20-297(S-RD) PART SEVEN — Sample Problem (U)
  Chapter 16 — Sample Problem

The seven parts comprising the Surface-To-Air Missile Series codify the interacting elements which must be considered in defining an air defense problem and proceeding to a preliminary SAM system design concept. **Because of the breadth involved and the phase of development covered, this series of handbooks does not contain the data required to design any component of the weapon system. Rather, the subjects are covered in a manner intended primarily to assist the systems engineer in recognizing and integrating the design parameters of a total SAM system.** Additionally, it is hoped that the handbooks will: aid Ordnance engineers in drafting missile system requirements and evaluating resultant proposals, assist an expert in one field desirous of knowing the relation of his work to other component fields in the total missile system concept, and acquaint the new engineer with missile system development and associated problems. Extensive reference lists augment the text for those who wish to investigate derivations, proofs and design detail.

Arrangement for publication of the handbooks comprising the Surface-To-Air Missile Series was made under the direction of the Ordnance Engineering Handbook Office, Duke University, under contract to the Ordnance Corps, U.S. Army. The copy was prepared by the General Electric Company,* Light Military Electronics Department, Utica, New York, under subcontract to the Ordnance Engineering Handbook Office.

Comments on, and requests for copies of this handbook should be addressed to: Ordnance Engineering Handbook Office, Ordnance Liaison Group, Box CM, Duke Station, Durham, N.C

---

*H. P. Frankenfield — Project Manager; H. Edward Niebuhr — Editor

PREFACE

Part Two of the Surface-To-Air Missile Series contains Chapters 6 and 7. The subjects covered deal with the detection and evaluation of an enemy threat and the provision of data required to assign and guide the SAM to the threat so that a *kill* can be effected.

Chapter 6, "Fire Direction And Coordination", is primarily concerned with the following SAM system functions: search and detection, identification and evaluation, weapon assignment, acquisition, tracking, and engagement. The material included is intended to facilitate parametric studies related to these functions and enable the systems engineer to select appropriate modes of operation for their implementation. To avoid duplication, radar is emphasized here and infrared is covered in Chapter 7.

Chapter 7, "Guidance And Control", deals with the *nervous system* of the missile, that is, those functions which insure that the missile is brought to the required proximity and attitude to fulfill its mission. Included are discussions of available schemes for obtaining guidance information and controlling missile motion.

TABLE OF CONTENTS

Paragraph *Page*

CHAPTER 6

FIRE DIRECTION AND COORDINATION

6-1 INTRODUCTION 6-1
6-1.1 PURPOSE OF CHAPTER 6-1
6-1.2 FUNDAMENTAL PROBLEM 6-1
6-1.3 SEARCH AND DETECTION 6-1
6-1.4 IDENTIFICATION AND EVALUATION 6-3
6-1.5 WEAPON ASSIGNMENT AND INTERCOMMUNICATIONS 6-3
6-1.6 ACQUISITION, TRACKING AND ENGAGEMENT 6-5
6-1.6.1 Command Guidance 6-5
6-1.6.2 Beam Rider 6-5
6-1.6.3 Active Homing 6-6
6-1.6.4 Semi-Active Homing 6-6
6-1.6.5 Passive Homing 6-6
6-2 RADAR RANGE EQUATION 6-6
6-2.1 GENERAL 6-6
6-2.2 RADAR RANGE COMPUTATIONS 6-7
6-2.3 EFFECTIVE TARGET AREA 6-12
6-3 RADAR COMPONENTS AND TECHNIQUES 6-12
6-3.1 ANTENNAS 6-12
6-3.1.1 General 6-12
6-3.1.2 General Antenna Engineering Data 6-12
6-3.1.3 Search Antennas 6-20
6-3.1.4 Track Antennas 6-22
6-3.2 TRANSMITTERS 6-24
6-3.2.1 General 6-24
6-3.2.2 Microwave Transmitting Tubes 6-24
6-3.2.3 Pulser and Power Supply Considerations 6-25

TABLE OF CONTENTS (cont)

Paragraph *Page*

CHAPTER 6 (cont)

6-3.3 RECEIVERS, GENERAL 6-28

6-3.3.1 Design Considerations for Countermeasures and ECM 6-29

6-3.3.2 Receiver Noise Figure 6-29

6-3.3.3 Typical Overall Receivers 6-29

6-3.3.4 Bandwidth 6-31

6-3.3.5 Selectivity 6-32

6-3.3.6 Stability 6-32

6-3.3.7 Video Amplifiers 6-33

6-3.3.8 I-F Amplifiers 6-34

6-3.3.9 R-F Amplifiers 6-35

6-3.3.10 Parametric Amplifier 6-37

6-3.3.11 Maser 6-40

6-3.3.12 Sources of Noise 6-40

6-3.3.13 Measurement Techniques 6-41

6-3.3.14 Tables and Graphs 6-43

6-3.4 DETECTION 6-45

6-3.4.1 General 6-45

6-3.4.2 Non-coherent Integration 6-45

6-3.4.3 Coherent Integration 6-52

6-3.4.4 MTI Detection 6-54

6-4 SEARCH RADAR EVALUATION 6-60

6-4.1 GENERAL 6-60

6-4.2 DISCERNIBILITY FACTOR 6-60

6-4.2.1 Dependence on Product of I-F Bandwidth and Pulse Length 6-61

6-4.2.2 Effects of Video Bandwidth and Sweep Speed 6-63

6-4.2.3 Dependence Upon Pulse Repetition Frequency 6-64

6-4.3 INFLUENCE OF SCANNING 6-65

6-4.4 ADDITIONAL NOISE SWEEPS 6-70

TABLE OF CONTENTS (cont)

Paragraph *Page*

CHAPTER 6 (cont)

6-4.5 SCANNING RADAR RANGE COMPUTATIONS 6-71
6-4.6 PROBABILITY OF DETECTION 6-77
6-5 TRACKING RADARS, ANALYSIS AND DESIGN 6-82
6-5.1 GENERAL 6-82
6-5.2 TRACKING RADAR TYPES 6-82
6-5.2.1 Conical Scan and Lobe Switching 6-82
6-5.2.2 Amplitude Monopulse 6-89
6-5.2.3 Phase Monopulse 6-96
6-5.2.4 Combination Monopulse 6-99
6-5.3 ERROR SOURCES 6-102
6-5.3.1 General 6-102
6-5.3.2 Thermal Noise 6-103
6-5.3.3 External Radio Noise 6-103
6-5.3.4 Rain and Ground Clutter 6-107
6-5.3.5 Servo Noise and Servo Dynamic Errors 6-109
6-5.3.6 Target Scintillation Effects 6-118
6-5.3.7 Propagation Errors 6-123
6-5.3.8 Combining Errors 6-143
6-5.4 SAMPLE CALCULATIONS AND CHARTS 6-145
6-5.4.1 Parameters of the Calculations 6-145
6-5.4.2 Thermal Noise — Echo Tracking 6-161
6-5.4.3 Beacon Operation 6-161
6-5.4.4 Examples 6-162
6-5.4.5 Other Error Sources 6-165
REFERENCES 6-166

CHAPTER 7

GUIDANCE AND CONTROL

7-1 INTRODUCTION 7-1
7-1.1 GENERAL 7-1

TABLE OF CONTENTS (cont)

Paragraph *Page*

CHAPTER 7 (cont)

7-1.2 RELATIONSHIP OF GUIDANCE AND CONTROL WITH THE WEAPON SYSTEM 7-1
7-1.3 GUIDANCE PHASES 7-1
7-2 GUIDANCE MODES 7-3
7-2.1 GENERAL 7-3
7-2.2 LINE-OF-SIGHT (BEAM RIDER) TRAJECTORY 7-4
7-2.3 PURSUIT COURSE 7-6
7-2.4 MODIFIED PURSUIT COURSE 7-6
7-2.5 CONSTANT BEARING COURSE 7-11
7-2.6 PROPORTIONAL NAVIGATION 7-11
7-2.7 PERTURBATION ANALYSIS 7-13
7-2.7.1 Nominal Trajectory 7-13
7-2.7.2 Perturbations 7-13
7-2.8 SENSOR REQUIREMENTS 7-14
7-3 GUIDANCE SERVO LOOPS 7-17
7-3.1 GENERAL 7-17
7-3.2 LINEAR FEEDBACK CONTROLS 7-19
7-3.3 PRIMARY GUIDANCE LOOP 7-20
7-4 FLIGHT CONTROL 7-21
7-4.1 GENERAL 7-21
7-4.2 SPECIAL FEATURES 7-21
7-4.3 AIRFRAME AS A LOOP ELEMENT 7-22
7-4.3.1 Coordinate Systems and Nomenclature 7-22
7-4.3.2 Equations of Motion 7-24
7-4.3.3 Launch Phase Models 7-25
7-4.3.4 Low Dynamic Pressure Models 7-25
7-4.3.5 Aerodynamic Forces 7-29
7-4.3.6 High Dynamic Pressure Models 7-30
7-4.4 CLOSED LOOP AIRFRAME CONTROL — AUTOPILOTS 7-33

TABLE OF CONTENTS (cont)

Paragraph *Page*

CHAPTER 7 (cont)

7-4.4.1 General ... 7-33
7-4.4.2 Attitude Control ... 7-33
7-4.4.3 Attitude Rate Control ... 7-35
7-4.4.4 Lateral Control ... 7-39
7-4.5 TYPICAL CONTROL SYSTEM ... 7-39
7-4.5.1 Proportional Systems Versus Off-On And/Or Digital Systems ... 7-40
7-4.6 COMPONENT CONSIDERATIONS ... 7-40
7-4.6.1 Signal Requirements ... 7-41
7-4.6.2 Amplifiers ... 7-41
7-4.6.3 References — Sensors ... 7-42
7-4.6.4 Actuators ... 7-43
7-4.6.5 Environmental Considerations ... 7-43
7-5 KINEMATICS ... 7-44
7-5.1 GENERAL ... 7-44
7-6 SENSORS ... 7-44
7-6.1 GENERAL ... 7-44
7-6.2 MIDCOURSE GUIDANCE SENSORS ... 7-44
7-6.2.1 Basic Measurements ... 7-44
7-6.2.2 Radar ... 7-45
7-6.2.3 Inertial ... 7-49
7-6.2.4 Celestial ... 7-58
7-6.3 TERMINAL GUIDANCE SENSORS ... 7-59
7-6.3.1 Radar ... 7-59
7-6.3.2 Infrared ... 7-61
7-6.3.3 Ultraviolet ... 7-63
7-6.3.4 Optical ... 7-63
7-6.3.5 Hybrid ... 7-65
7-7 TERMINAL GUIDANCE SEEKERS ... 7-65
7-7.1 GENERAL ... 7-65

TABLE OF CONTENTS (cont)

Paragraph *Page*

CHAPTER 7 (cont)

7-7.2 SEEKER FUNCTIONS 7-65
7-7.2.1 Target Acquisition 7-65
7-7.2.2 Target Tracking 7-72
7-7.3 RADAR SEEKERS 7-73
7-7.3.1 Conical Scan 7-73
7-7.3.2 Amplitude Monopulse 7-73
7-7.3.3 Phase Monopulse 7-73
7-7.3.4 Combination Monopulse 7-74
7-7.3.5 Additional Aspects of Radar Seekers 7-74
7-7.4 INFRARED SEEKERS 7-74
7-7.4.1 Radiation Laws 7-77
7-7.4.2 Detectors 7-80
7-7.4.3 Atmospheric Transmission 7-82
7-7.4.4 Spectral and Spatial Discrimination 7-88
7-7.4.5 Infrared Range Equations 7-89
7-7.4.6 Optical Materials 7-91
7-8 GUIDANCE STUDIES 7-91
7-8.1 GENERAL 7-91
7-8.2 SYNTHESIS 7-91
7-8.3 BANDWIDTH 7-91
7-8.4 PRIMARY LOOP SYNTHESIS 7-94
7-8.5 PERFORMANCE EVALUATION 7-94
7-8.5.1 Criteria 7-94
7-8.5.2 Simulation 7-94
REFERENCES 7-97

LIST OF ILLUSTRATIONS

Fig. No.	*Title*	*Page*
6-1	Intercept Geometry for Sample SAM Mission	6-2
6-2	Radar Coverage Charts	6-4
6-3	Transmitter Power Above 1.0 Watt	6-8
6-4	Wavelength Factor	6-9
6-5	Target Area Function	6-10
6-6	Receiver Gain Factor	6-11
6-7	Slant Range as a Function of Total System	6-11
6-8	Taper Versus Sidelobe Level — Parabolic Reflector	6-14
6-9	Aperture Beamwidth Constant Versus Sidelobe Level (No Phase Errors)	6-15
6-10	Antenna Gain Loss Due to Phase Errors	6-17
6-11	Average Effect of Random Phase Error on Sidelobe Level	6-18
6-12	Rectangular Waveguide Data, Nomograph	6-19
6-13	Hyperboloid-to-Paraboloid Diameter Ratio versus Magnification	6-21
6-14	Amplitude Monopulse Design Curves	6-23
6-15	Typical Radar Receivers, Block Diagram	6-30
6-16	Basic Video Amplifier, Block Diagram	6-33
6-17	Typical R-F and I-F Noise Figure Performance	6-37
6-18	Typical Parametric Up-converter	6-38
6-19	Typical Receiver Noise	6-39
6-20	Noise Voltage Versus Overall Bandwidth	6-42
6-21	Differential Phase Shift Versus Gain Bias	6-44
6-22	Examples of Basic Non-Coherent Systems, Block Diagram	6-46
6-23	Examples of Basic Coherent Systems, Block Diagram	6-47
6-24	Integration Gain	6-49
6-25	Single Scan Detection Probability Versus S/N Ratio	6-50
6-26	S/N Ratio Loss, Detection Time Greater than Integration Time	6-51

LIST OF ILLUSTRATIONS (cont)

Fig. No.	*Title*	*Page*
6-27	Integration Loss, Non-Coherent Versus Coherent (Probability of Detection)	6-53
6-28	Integration Loss, Non-Coherent Versus Coherent (False Alarm)	6-54
6-29	Clutter Frequency Spread Due to Internal Motion Noise, Nomograph	6-57
6-30	Clutter Frequency Spread Due to Scanning, Nomograph	6-58
6-31	Pulse-to-Pulse Cancellation and its Velocity Response	6-59
6-32	S/N Ratio for Minimum Discernibility as a Function of I-F Bandwidth and Pulse Length	6-61
6-33	S/N Ratio for Minimum Discernibility as a Function of Video Bandwidth and Pulse Length	6-62
6-34	S/N Ratio for Minimum Discernibility as a Function of Pulse Length Presented on Observer's Screen	6-63
6-35	Pulse Repetition Function	6-64
6-36	S/N Ratio for Minimum Discernibility as a Function of Pulse Repetition Frequency	6-65
6-37	S/N Ratio for Minimum Discernibility as a Function of Beam Angle and Signal Presentation Time	6-66
6-38	S/N Ratio for Minimum Discernibility as a Function of Beam Angle and Scanning Rate	6-67
6-39	S/N Ratio for Minimum Discernibility as a Function of PRF	6-68
6-40	Particular Example of the Scanning Function	6-69
6-41	Effects of Scanning	6-70
6-42	S/N Ratio for Minimum Discernibility as a Function of Sweep Recurrence Frequency	6-71
6-43	S/N Ratio for Minimum Discernibility as a Function of PRF for Constant Sweep Recurrence Frequency of 3200 PPS	6-72
6-44	Scanning Function	6-73
6-45	Scanning Function Versus Pulse Hits Per Target Traverse	6-74
6-46	Indicator Collapsing Function	6-75
6-47	Receiver Representation Factor	6-77
6-48	Single Scan Probability of Detection Versus Range	6-78

LIST OF ILLUSTRATIONS (cont)

Fig. No.	*Title*	*Page*
6-49	Target Displacement During One Scan Versus Target Velocity and Scan Rate	6-79
6-50	Fifty Percent Single Scan Detection Range Necessary for Ninety Percent Cumulative Detection Probability at Range R_{90}	6-80
6-51	Correlation of 90 Percent Cumulative Detection Probability Range With 50 Percent Single Scan Detection Range	6-81
6-52	Conical Scanning	6-82
6-53	Conical Scan Radar	6-83
6-54	Round Trip Antenna Patterns — One Beamwidth Squint	6-85
6-55	Round Trip Antenna Patterns — 0.4 Beamwidth Squint	6-86
6-56	One-Way Antenna Pattern — One Beamwidth Squint	6-87
6-57	$\Delta - \Sigma$ Comparison	6-90
6-58	Four-Horn Monopulse Radar	6-92
6-59	Amplitude Monopulse	6-93
6-60	Logarithmic Amplitude Comparison	6-94
6-61	Logarithmic Receiver Characteristic	6-94
6-62	Logarithmic Amplitude Comparison Antenna Pattern	6-95
6-63	Phase Monopulse	6-97
6-64	Interferometer Sensitivity	6-98
6-65	Combination Monopulse	6-100
6-66	Combination Monopulse Radar	6-101
6-67	External Noise Factor (Referenced to Ideal Receiver Noise)	6-105
6-68	Addition of Scalar Quantities Expressed in Decibels	6-106
6-69	Target Area Factor	6-108
6-70	Typical Servo Response Curves	6-111
6-71	Frictional Drags on a Servomechanism	6-112
6-72	Constant Velocity Servo Errors	6-113
6-73	Basic Type I Servo Open Loop Response	6-114
6-74	Pass Course Geometry	6-114
6-75	Dynamic Errors of a Type I Servo Azimuth Tracking a Target on a Horizontal Pass Course	6-116

LIST OF ILLUSTRATIONS (cont)

Fig. No.	*Title*	*Page*
6-76	Servo Systems Employing ECS Correction	6-117
6-77	Spectra of Fading (Amplitude Scintillation)	6-121
6-78	Showing How Wander Arises from the Distorted Wavefronts Reflected from a Complex Target	6-122
6-79	Regions of Propagation Phenomena	6-124
6-80	Effect of Reflection on the Radar Beam Assuming Flat Earth, No Diffraction or Refraction	6-125
6-81	Geometry of the Reflection Problem	6-126
6-82	Interference Errors in a Combination Monopulse	6-127
6-83	Maximum Elevation Errors of Phase Monopulse	6-128
6-84	Interference Errors in a Combination Monopulse Having Amplitude Comparison in Elevation	6-129
6-85	Attenuation Due to Diffraction	6-130
6-86	Minimum Elevation Without Diffraction Loss	6-132
6-87	Elevation Errors Due to Knife-Edge Diffraction	6-133
6-88	Atmospheric Attenuation at Sea Level (Assuming One Percent Water Vapor Content)	6-133
6-89	Attenuation by Rain and Fog (at 18°C)	6-134
6-90	Attenuation by the Ionosphere	6-135
6-91	Refraction by the Ionosphere	6-136
6-92	Calculation of Refraction Assuming Linear Index of Refraction	6-137
6-93	Common Variations of Refraction with Altitude for Low Altitudes	6-139
6-94	Refraction by a Piecewise Linear Refractive Index Profile	6-141
6-95	Aid to RMS Addition	6-144
6-96	Combining Errors — Example I	6-145
6-97	Combining Errors — Example II	6-146
6-98	Nominal Beamwidth Versus Aperture	6-149
6-99	Conversion of Aperture Width to Wavelengths	6-150
6-100	Interferometer Sensitivity	6-151
6-101	Servo Filter Factor	6-152

LIST OF ILLUSTRATIONS (cont)

Fig. No. *Title* *Page*

6-102 Transmitter Power in DB Above 1.0 Watt 6-153
6-103 Range Loss 6-154
6-104 Nominal Gain, DB, Based on Cosine Illumination 6-155
6-105 I-F Bandwidth Factor 6-156
6-106 Typical Receiver Noise Figures 6-157
6-107 Crystal Beacon Sensitivity 6-158
6-108 Beamwidth or Angular Noise 6-159
6-109 Wavelength Factor 6-160

7-1 Missile Guidance Phases 7-2
7-2 Frequency Spectra for Various Beam Rider Turning Rates 7-5
7-3 Line-of-Sight Geometry 7-6
7-4 Line-of-Sight Trajectories for Various Launch Angles 7-9
7-5 Beam Rider Turning Rate Geometry 7-10
7-6 Normalized Curves of Turning Rates For Various Initial Launch Angles and Speed Ratios 7-10
7-7 Pursuit Course Geometry 7-10
7-8 Modified Pursuit Course Geometry 7-10
7-9 Turning Rate Criterion for Modified Pursuit 7-11
7-10 Constant Bearing Geometry 7-11
7-11 Proportional Navigation Geometry 7-12
7-12 Proportional Navigation Course $\phi_o = 60°$, $p = 2$ 7-12
7-13 Coordinate System for Analysis of Proportional Navigation Trajectories 7-13
7-14 Missile Trajectories for Initial Aiming Error. (K_c = Effective Navigation Constant.) (a) Displacement; (b) Velocity; (c) Acceleration. $X_T = 0$ 7-15
7-15 Required Missile Acceleration for Constant Target Acceleration 7-16
7-16 Missile Acceleration Ratios Versus Navigation Constant 7-17
7-17 Simplified Servo Loop 7-19
7-18 Primary Guidance Loop 7-20

LIST OF ILLUSTRATIONS (cont)

Fig. No.	*Title*	*Page*
7-19	Flight Control System Pitch Channel, Block Diagram	7-21
7-20	Missile Stability and Body Axes	7-22
7-21	Missile Pitch Angle and Flight Path Angle	7-23
7-22	Missile Acceleration Outside the Atmosphere	7-26
7-23	Missile Angular Acceleration, $\dot{\omega}$	7-27
7-24	Airframe Pitch Response to Deflection of Control Surfaces — Low Dynamic Pressure	7-28
7-25	Attitude Controller — Low Dynamic Pressure	7-28
7-26	Effect of Aerodynamic Forces Upon Missile Axes Within the Atmosphere	7-29
7-27	Airframe Attitude Control Within the Atmosphere	7-33
7-28	Flight Control System Root Locus	7-34
7-29	Variation of Airframe Short Period Characteristics With Altitude	7-36
7-30	Locus of $1 + GH = 0$	7-37
7-31	Airframe Pitch Rate Controller Within the Atmosphere Root Locus Plot	7-37
7-32	Additional Root Locus for Attitude Rate Control	7-38
7-33	Pitch Channel Diagram	7-39
7-34	Sensor Operating Frequencies	7-45
7-35	Beacon Radar System, Block Diagram	7-46
7-36	Command Coding Scheme	7-47
7-37	Typical Doppler Frequency Spectrum	7-48
7-38	Typical Doppler Radar, Block Diagram	7-48
7-39	Gyro Vector Relationship	7-50
7-40	Free Gyro with Two Pickoffs	7-51
7-41	Spring Restrained Rate Gyro	7-52
7-42	Floated Rate Integrating Gyro	7-53
7-43	Typical Gyro Configuration with Requirements	7-54
7-44	Gyro Accelerometer	7-55
7-45	Seismic Accelerometer	7-56
7-46	Stabilized Platform	7-57

LIST OF ILLUSTRATIONS (cont)

Fig. No.	*Title*	*Page*
7-47	Typical Command Guidance Stable Platform, Block Diagram	7-58
7-48	Active Seeker, Block Diagram	7-59
7-49	Continuous Wave Semi-Active Seeker, Block Diagram	7-60
7-50	Electromagnetic Spectrum	7-61
7-51	Spectral Distribution of Black Body Radiation	7-63
7-52	Possible Scan Patterns	7-66
7-53	Scanning (Search Mode)	7-66
7-54	Conical Scan (Track Mode)	7-67
7-55	Intercept Geometry	7-67
7-56	Maximum Look Angle Required for Successful Intercept	7-68
7-57	Region of Possible Intercept	7-68
7-58	Radar Section of Typical Active Pulsed-Radar Seekers	7-70
7-59	Radar Section of Typical Semi-Active Coherent Pulsed-Radar Seeker	7-71
7-60	Integration and Detection Section of a Typical Coherent Pulsed-Radar Seeker	7-71
7-61	Typical Boresight Shift for a Combined Antenna-Radome	7-73
7-62	Typical Infrared Seeker	7-75
7-63	AM and FM Reticles	7-76
7-64	Amplitude Modulation Error Signal	7-77
7-65	Typical IR Seeker System, Block Diagram	7-77
7-66	Nomograph for Calculation of IR Radiation	7-79
7-67	Responsivity and Noise Energy Density for a Long and a Short Time Constant Detector	7-81
7-68	Detectivity for Two Detectors of Figure 7-67	7-82
7-69	NEP Versus Spectral Response for *PbS* Detector	7-83
7-70	NEP Versus Wavelength of Various Detectors	7-84
7-71	*Jones "S"* Versus Wavelength for *PbS* Detectors	7-84
7-72	Transmission Versus Wavelength for H_2O and CO_2	7-86
7-73	Wavelength Versus Altitude for H_2O and CO_2	7-87
7-74	Amplitude Modulation Reticle, Checkerboarded for Spatial Discrimination	7-89

LIST OF ILLUSTRATIONS (cont)

Fig. No. *Title* *Page*

7-75 Optical System for Tracking 7-90

7-76 Optical System for Search 7-90

7-77 Airframe Bending Mode Excitation 7-94

7-78 Kill Probability from Adjoint System 7-96

LIST OF TABLES

Table No. *Title* *Page*

6-1 EXTERNAL CHARACTERISTICS OF PULSE TRANSMITTING TUBES 6-26

6-2 TRANSMITTER TUBE PHASE CHARACTERISTICS 6-27

6-3 I-F AMPLIFIER DYNAMIC RANGE CAPABILITIES 6-43

6-4 TYPICAL TRACKING RADAR PARAMETERS 6-88

6-5 COMPARISON OF TRACKING RADAR TYPES 6-91

6-6 TYPICAL RAINFALL INTENSITIES 6-107

6-7 STANDARD DEVIATION OF CLUTTER PARTICLE VELOCITIES 6-110

6-8 VALUES OF WANDER FOR PROPELLER DRIVEN AIRCRAFT 6-123

6-9 PARAMETERS OF "STANDARD" ATMOSPHERES 6-138

6-10 SAMPLE CALCULATION OF REFRACTION ERROR 6-142

6-11 RANGE DEPENDENCE OF TRACKING ERRORS 6-147

7-1 NOMENCLATURE FOR PARAGRAPH 7-2 7-4

7-2 SUMMARY OF FLIGHT PATH CHARACTERISTICS .. 7-7/7-8

7-3 GUIDANCE MEASUREMENT REQUIREMENTS 7-17

7-4 GUIDANCE MODE MECHANIZATION REQUIREMENTS 7-18

7-5 COORDINATE SYSTEMS NOMENCLATURE 7-24

7-6 SUMMARY OF THREE-DEGREE-OF-FREEDOM TRANSIENT RESPONSE PROPERTIES 7-31

LIST OF TABLES (cont)

Table *Page*

7-7 THERMAL LIMITATION OF HYDRAULIC FLUIDS 7-43

7-8 GENERAL COMPARISON OF ACTIVE, SEMI-ACTIVE AND PASSIVE RADAR SYSTEMS 7-62

7-9 COMPARISON OF VARIOUS SEEKER SYSTEMS 7-64

7-10 DETECTOR TIME CONSTANTS 7-85

7-11 INFRARED TRANSMITTING MATERIALS 7-92

CHAPTER 6

FIRE DIRECTION AND COORDINATION

6-1 INTRODUCTION

6-1.1 PURPOSE OF CHAPTER

This chapter is intended to present the general design considerations encountered in the system design of the fire direction and coordination portion of a surface-to-air missile system. Obviously the specific treatment of any single system is beyond the scope and space limitation of this chapter, but the reader should bear in mind that documentation supporting such systems as the NIKE-AJAX, NIKE-HERCULES, HAWK and REDEYE include many fine references illustrating specific design approaches. These references are recommended to the reader for both their approach to the complete SAM problem and also their specific subsystem design solutions. It is the purpose of this chapter to furnish the tools for the initial system design and evaluation of future SAM systems.

Subsystem and component design approaches is far too large a subject for this chapter; however, the use of such publications as the MIT Radiation Lab Series (published by the McGraw-Hill Book Co., 1947) are strongly recommended and, as this chapter progresses, references are listed for each major topic to enable interested readers to investigate solutions with minimum literature searching.

It will be noted that the emphasis here is on radar whereas Chapter 7 covers infrared as related to the SAM system. This is only one example of how these two chapters augment each other, indicating that the reader should be familiar with the contents of both in order to obtain a more complete picture of the detection-tracking-guidance problem.

Computers, countermeasures, and fuzes as related to the fire direction and coordination problem are also discussed in other chapters of this handbook.

6-1.2 FUNDAMENTAL PROBLEM

The primary problem in any missile weapon system is the detection, location and identification of the target to be destroyed.

After locating the target to be destroyed, the next problem is an evaluation of the target to be engaged to determine when the target will be within the effective range of the SAM and, if possible, that the target does represent a threat to the area being defended.

In the case of multiple enemy targets and multiple SAM systems, the problem of target evaluation also leads to the problem of weapon assignment since it becomes tactically desirable to eliminate all of the hostile targets by efficiently utilizing the firepower of other adjacent SAM systems.

At this point, the problem becomes one of determining the threat's position with accuracy and guiding the SAM to the threat and detonating a warhead at the proper time to destroy the threat.

The last major problem to be encountered in Fire Direction and Coordination is the communications between adjacent ground systems to coordinate the engagement of targets and also to communicate with early warning nets on future target assignments and battle engagement progress.

The major problems are then: search and detection; identification and evaluation; weapon assignment; acquisition, tracking and engagement; and intercommunications. These problems will be analyzed and discussed individually and the general approach towards their solution will be developed.

6-1.3 SEARCH AND DETECTION

The type of device selected to perform the search and detection function required in the SAM system can be an application of optics, radar, infrared, or acoustics depending on the performance requirements required for the system.

Normally radar is selected when the weapon system is required to be capable of all weather operation, long range detection and day and night operation. For the purpose of this chapter, radar is selected as the means of detection but the use of infrared and optics in future system design should not be ignored because where their application will satisfy the system requirement, excellent performance with little system complexity will result.

An explicit example of an IR application is the modern REDEYE surface-to-air missile being developed to defend against low flying aircraft. The missile is small enough to fire from the shoulder and the entire means of detection and guidance is a small IR seeker located inside the missile. The weapon is pointed at a threat and when the seeker acquires, the missile is fired and guided by the IR seeker to impact. Thus, radar is not necessarily the answer to all detection problems since weapon size, weight, complexity and accuracy requirements may dictate other types of detection devices.

The first consideration in the design of a detection radar is, quite naturally, what type or types of targets are considered to be the threat. The threat must be defined before any considerations of a search radar can proceed. The target size, altitude, velocity and low altitude capability must be established to define the design requirements of the detection radar. As an illustration, a SAM system is to be designed to protect specific ground installations from enemy attack by high flying aircraft having the following characteristics:

target velocity	V_T ft/sec
flying altitude	H ft
bomb release line	R_L (slant range ahead of ground target)
target size	A_t yds^2

The target will be intercepted and destroyed at position (1) by the SAM. The *minimum* slant range at intercept must be equal to the slant range R_L to destroy the threat before the bombs are released. To do this, the aircraft must be detected at point 2 and the distance 1-2 is equal to $V_T(T_{FM} + T_R)$

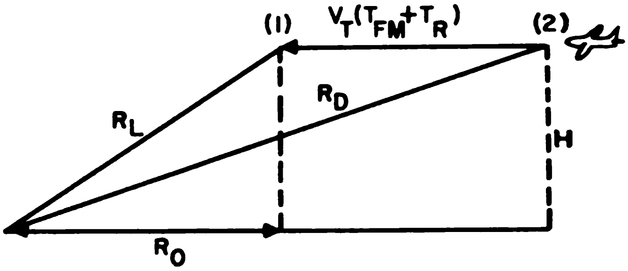

Figure 6-1. Intercept Geometry for Sample SAM Mission

Where $V_T =$ target velocity
$T_{FM} =$ time of flight of defensive missile
$T_R =$ reaction time (time from target detection to SAM launch)

Therefore the *minimum* radar detection range (R_D) of the proposed system is:

$$R_D = \left\{ \left[R_o + V_T(T_{FM} + T_R)\right]^2 + H^2 \right\}^{1/2} \qquad (6\text{-}1)$$

(for single interception only)

From the discussion above, the detection radar designer has been forced to be concerned with the definition of the threat and two system considerations, T_{FM} and T_R. In the initial system design, it is important to keep the distance V_T ($T_{FM} + T_R$) at a minimum in order to keep the radiating power requirements and therefore the physical size of the search radar reasonable.

From the example of the threat, a radar detection scheme could be designed with an antenna, transmitter, receiver and presentation system compatible for the job. If other threats are added to the detection system requiring detection of aircraft at lower altitudes a required detection curve resembling Figure 6-2 can be constructed. In the final analysis of the detection curves, the higher velocity targets at high altitudes dictate the maximum detection problems since, for the bombing aircraft, the bomb release line (R_L) increases with the aircraft flying altitude.

Additional design requirements that the detection designer must consider prior to the radar design is the problem of ground clutter on low flying targets and the effect of the earth's curvature on detecting low altitude targets as shown in Figure 6-2.

A set of requirements as furnished to the detection design should include:

(a) description of threat with velocity range and altitude range

(b) size and weight limitation

(c) the output data requirements such as azimuth and range or azimuth, elevation and range and the accuracy required

(d) total system reaction time

(e) time of flight versus range of target

(f) countermeasures to be expected

From this the designer must optimize to obtain the most volume coverage and detection range for the least amount of power and weight with the required accuracy.

6-1.4 IDENTIFICATION AND EVALUATION

A very real part of detection is the problem of determining what has been detected. To a ground radar, a reflector has been detected. By the use of MTI (Moving Target Indicator) schemes and Doppler techniques, it can be determined that the detected reflector is moving but still the fact that the detected target is friendly or hostile requires Identification, Friend or Foe (IFF) techniques. Several IFF techniques have been employed in operational fire control and SAM systems to date. Briefly some of these are:

(a) Air Corridor – designated flight lanes known to both friendly aircraft and detection radars.

(b) Electronic Interrogation and Reply Systems

(1) radio voice link

(2) microwave coded interrogation and coded reply presented on the radar visual indicators near the detected targets

(3) visual identification from airborne interceptors and ground installations

The IFF problem is necessarily of a magnitude larger than the design of any particular SAM weapon system since all ground defensive installations; commercial aircraft; Army, Navy and Air Force and NATO aircraft must be integrated and use common systems and techniques. In addition, the security of any one system must be beyond enemy comprehension or must be flexible and provide for continuous changes in order to maintain security.

The system engineer will usually have access to the existing IFF equipment design information which must be considered in the design of his fire control system. Applicable literature on current systems is available in the Air Force and Army libraries.

After identifying a detected target as a foe, the problem is to evaluate his position and flight path to determine when the target will be within the effective missile range of the system and if the hostile target represents a threat to the area being defended by the SAM system. In the case of multiple targets, the evaluation should include which target must be engaged first and how many others can be destroyed before they can accomplish their particular mission. It is important to remember at this point the reaction time (T_R) since the time consumed while performing target IFF and evaluation becomes a part of the total reaction time which will increase the required detection radar range and necessarily the size and weight of the radar.

6-1.5 WEAPON ASSIGNMENT AND INTERCOMMUNICATIONS

The general requirement for weapon assignment is usually generated as a means to maximize the kill capability of a group of SAM systems against a multiple target attack.

Since any one SAM system can be saturated with targets and it is very possible for two or

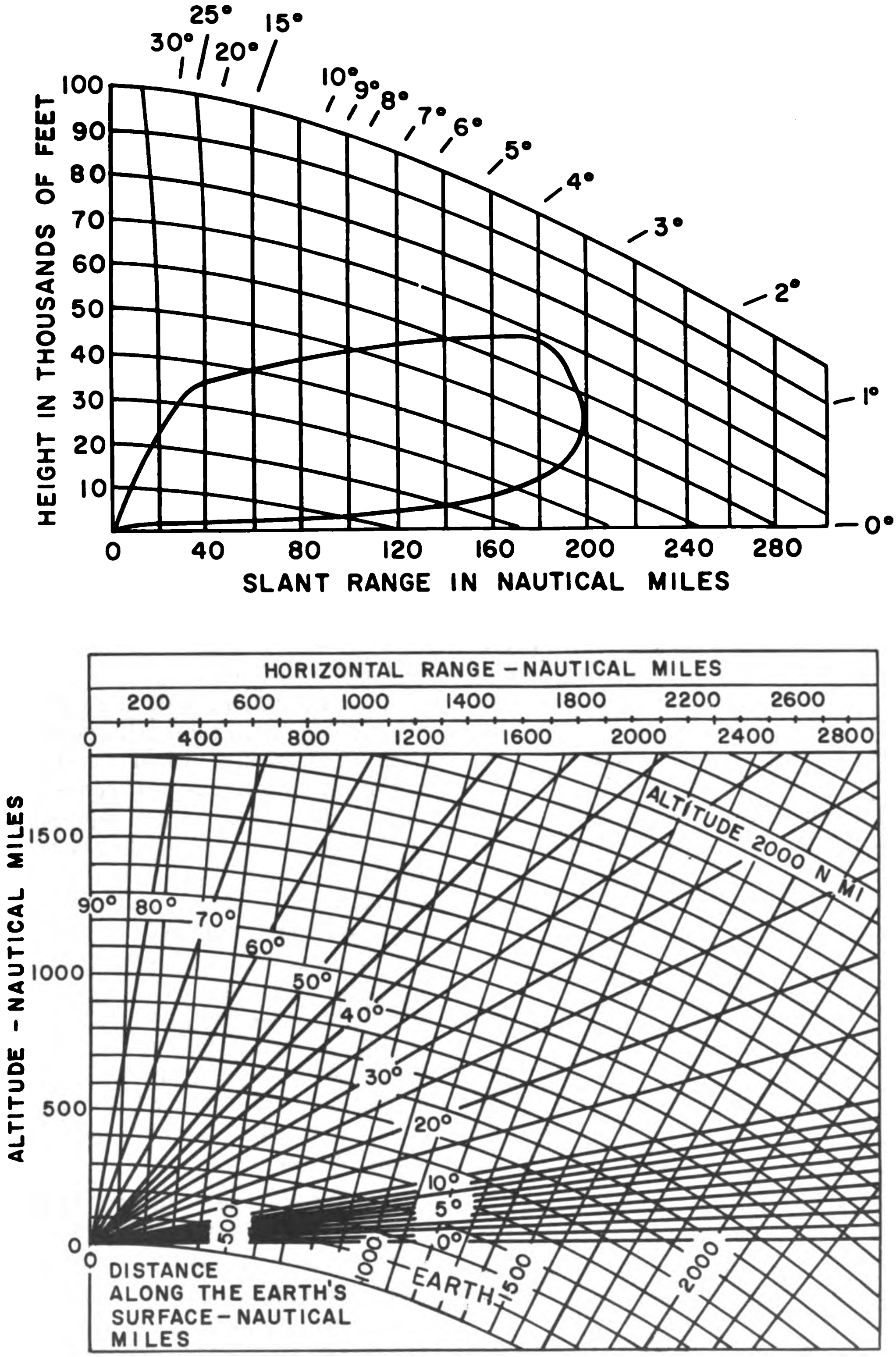

Figure 6-2. Radar Coverage Charts

more adjacent systems to engage the same target and permit a succeeding threat to go unchallenged, a fire coordination and weapon assignment system is most desirable. The advantages of a system with weapon assignment are:

(a) long range search and tracking information is provided to the SAM systems

(b) IFF information is available to local SAM systems including friendly aircraft activity

(c) target designation is provided from an overall area defense standpoint to each individual SAM system

(d) target engagement status is obtained from local SAM systems so that any hostile targets that slip through may be designated to another SAM system

The system engineering problem in weapon assignment becomes one of establishing a coordination philosophy. The equipment required to implement the problem requires no inventions but does require a vast quantity of complex computing, transmitting, receiving and display equipment.

Rather than try to illustrate the equipment design problems involved in this subject, the readers are urged to review the current AN/MSG-4 anti-aircraft defense system which was designed to coordinate the NIKE-HERCULES, NIKE-AJAX and HAWK SAM systems over a widely dispersed area into a uniform defensive force for engaging hostile aircraft. It has been designed to be a self-contained, mobile system capable of coordinating the anti-aircraft defenses of an air space of 100,000 square miles. The system is a typical implementation of a weapon assignment and intercommunications system concept.

6-1.6 ACQUISITION, TRACKING AND ENGAGEMENT

The last consideration in the design of a fire direction and coordination subsystem of a SAM system is the acquisition, tracking and engagement phases. These terms are defined as:

acquisition – the actual transfer of a detected target from the search radar to the tracking radar

tracking – the condition where a target is being watched by radar at a high data rate (continuous or sampled) for obtaining target position information which can be used to calculate launch orders for the SAM guidance

engagement – the period from SAM launch to target intercept (burst)

Several types of systems will be considered and the requirements on the ground system will be listed.

6-1.6.1 Command Guidance

The necessary minimum ground equipment required to implement a command guidance approach are:

(a) detection (acquisition) radar
(b) target tracking radar
(c) missile tracking radar
(d) computer
(e) launcher

The detection radar detects the threat and transfers the target to the target tracking radar. The target tracking radar determines the target position coordinates and transfers them to the computer. The missile tracking radar acquires the SAM on the launcher and tracks the missile through its flight path to the target and transmits necessary commands to the missile in order to intercept the target. In addition, it may transmit the burst command to the missile.

The computer, from the continuous position information received from the tracking radars, computes the intercept point, launch orders, and the necessary missile steering orders that the missile tracking radar must transmit to the missile in order to fly an intercept course.

6-1.6.2 Beam Rider

The essential elements of equipment in a beam rider SAM system are:

(a) detection radar
(b) tracking radar
(c) capture radar
(d) computer
(e) launcher

The detection radar transfers the target to the tracking radar and the SAM flies along the tracking radar beam to intercept the target. In order to initially get the launched SAM in the tracking radar beam, a capture radar (or Mode) is usually used to track the launched missile and guide it over to the tracking radar beam. The computer in this case is a much simpler device and is principally used to calculate the necessary launcher coordinates, and is also used when a capture radar is used to guide the capture beam to the target tracking radar beam.

6-1.6.3 Active Homing

In the active homing guidance type SAM system, the essential system elements are:

(a) detection radar
(b) tracking radar*
(c) homing airborne guidance
(d) computer
(e) launcher

The detection radar locates the target and from the target position data, the computer calculates the missile launch coordinates and initial steering orders. In this case, the airborne guidance in the missile is a small radar. After the missile is launched it must search, acquire and track the intended target and compute the necessary steering orders necessary to intercept the target. The missile path is initially determined by the pre-launch computer orders until it acquires the target.

6-1.6.4 Semi-Active Homing

In the semi-active guidance type SAM system the necessary ground equipment requirements are:

(a) detection radar
(b) tracking and illumination radar
(c) computer
(d) launcher

The ground tracking radar must provide two functions:

(a) obtain target position to calculate initial launch orders.
(b) track and illuminate the threat unt intercept.

After the SAM is launched, its guidanc system, which is primarily a receiver, searche for energy that is being transmitted by th tracking radar and reflected off the target. Th missile seeker acquires this reflected signal an computes the necessary course to fly to intercept the target.

6-1.6.5 Passive Homing

In a passive homing guidance type SAM system, the target becomes the source of energy used for guidance. The energy must be sound, light, heat or radio frequency waves. After detecting a target and launching a SAM, the SAM seeker homes on the target which is radiating energy. The essential system elements in this type of guidance scheme are:

(a) detection radar
(b) computer
(c) airborne seeker guidance
(d) launcher

Some of these types of systems require more ground equipment while other guidance schemes require more airborne equipment. The real purpose of this introduction into types of SAM systems is to illustrate some of the functions which are required of the ground equipment in each type system so that the material introduced in the radar range equation in paragraph 6-2, the search radar evaluation in paragraph 6-4, and the tracking radar evaluation in paragraph 6-5 can be modified to fit the type of system being considered.

6-2 RADAR RANGE EQUATION

6-2.1 GENERAL

The analysis of radar performance is generally statistical in nature. The transmitted and received signal is most always competing with jamming and/or noise power. In addition, the size of the target as seen by the radar often fluctuates over a large range of values in a random fashion.

The radar range equation is an attempt to calculate the expected signal strength that can be expected from a certain target under specific conditions. The designer should be aware that there will be variations in the various parameters and that the process of correlating the statistical effects of jamming, noise, and signal level are more applicable to the subject of detection. The intent of this section is to provide aid in calculating the signal level from the target.

---

*The detection radar may have to be supplemented by a target tracking radar depending on the data rate and accuracy of data from the detection radar.

P_t transmitted power

G_t transmitter antenna gain, relative to an isotropic radiator, at azimuth Θ, and elevation Φ

R range to target

A_e effective target area (typical values chosen are the peak, mean, median, minimum; except for simple shapes the values will all be different)

A_r effective receiving aperature at Θ and Φ

P_r received signal power

δ system losses including components and atmospheric effects

$$P_r = \frac{P_t \cdot G_t \cdot A_e \cdot A_r}{\delta\, (4\,\pi R^2)^2} \text{ round trip equation} \qquad (6\text{-}2)$$

$$P_r = \frac{P_t \cdot G_t\,(\Theta, \Phi)\, A_r}{\delta \cdot 4\,\pi R^2} \text{ beacon (one way)} \qquad (6\text{-}3)$$

If P_t is the peak power, the P_r is peak; if P_t is average power, then P_r is average power.

The total noise against which the signal P_r must compete is given by

$$N_p = K\, T_s\, B \qquad (6\text{-}4)$$

where

K = Boltzmann's constant. $4.01(10)^{-21}$ watts/cycle°K

T_s = System Noise Temperature, commonly given as $\overline{NF}T_o$, where $\overline{NF}$ is the receiver noise figure and T_o is 290°K. Recent advances in receiver techniques lead the designer to consider other noise sources such as the ground, sky, antenna and duplexer. The effect of all these must all be included in T_s.

B = the receiver bandwidth (for pulse systems $B \approx \frac{1}{\text{Pulse Length}}$)

The combination of equations 6-2 and 6-4, and 6-3 and 6-4 gives signal-to-noise ratios.

$$S/N = \frac{P_t\, G_t\, A_e\, A_r}{\delta\, (4\,\pi R^2)^2\, KT_s B} \quad \text{round trip} \qquad (6\text{-}5)$$

$$S/N = \frac{P_t\, G_t\, A_r}{\delta\, 4\,\pi R^2\, KT_s B} \quad \text{beacon} \qquad (6\text{-}6)$$

In equations 6-2 and 6-5, A_r is related to G_r by

$$A_r = \frac{G_r \lambda^2}{4\,\pi} \qquad (6\text{-}7)$$

For the case where a common antenna is used for transmit and receive and T_s is given by $\overline{NF}T_o$, then

$$S/N = \frac{P_t\, A_e\, G^2 \lambda^2}{(4\,\pi)^3\, \overline{NF}\, KT_o B\, \delta\, R^4} \quad \text{(round trip)} \qquad (6\text{-}8)$$

For unity signal-to-noise ratios

$$R = \left[\frac{P_t\, A_e\, G^2 \lambda^2}{(4\,\pi)^3\, \overline{NF}\, KT_o B\, \delta}\right]^{1/4} \qquad (6\text{-}9)$$

6-2.2 RADAR RANGE COMPUTATIONS

To provide a rapid and convenient means for computing the performance of a radar system, the radar equation can be rewritten in terms of db values above certain reference levels. The reference levels are chosen to be R_o (which is set equal to 1.0 meter) for the terms involving distance, length and area; and 1.0 watt for the power terms. Thus, radar equation 6-9 becomes:

$$\left[\frac{R}{R_o}\right]^4 = \left[G^2\right] \times \left[P_t\right] \times \left[\frac{\lambda}{4\,\pi R_o}\right]^2 \times \left[\frac{A_e}{4\,\pi R_o}\right] \times \left[\frac{1}{\overline{NF}}\right] \times \left[\frac{1}{\delta}\right] \times \left[\frac{1}{KT_o B}\right] \qquad (6\text{-}10)$$

Taking the logarithm of both sides and multiplying through by 10, equation 6-10 becomes:

$$10 \log R^4 = 20 \log G + 10 \log P_t + 20 \log \frac{\lambda}{4\,\pi} + 10 \log \frac{A_e}{4\,\pi} + 10 \log \frac{1}{\overline{NF}} + 10 \log \frac{1}{KT_o B} + 10 \log \left[\frac{1}{\delta}\right] \qquad (6\text{-}11)$$

For convenience and future reference, the terms of the right hand side of equation 6-11 have been individually plotted and designated as follows:

db_{ant} = generally given in terms of db; see antennas (paragraph 6-3.1)

$db_p = 10 \log P_t$ (Figure 6-3)

$db_\lambda = 20 \log \frac{\lambda}{4\pi}$ (Figure 6-4)

$db_a = 10 \log \frac{A_c}{4\pi}$ (Figure 6-5)

$db_{NF} = 10 \log \frac{1}{NF}$ (not plotted – obtain by measurement only)

$db_n = 10 \log \frac{1}{KT_oB}$ (Figure 6-6)

db_δ = round trip db losses

To accomplish the range computation, the algebraic sum of these individual db values nee only be determined and the corresponding rang obtained from Figure 6-7.

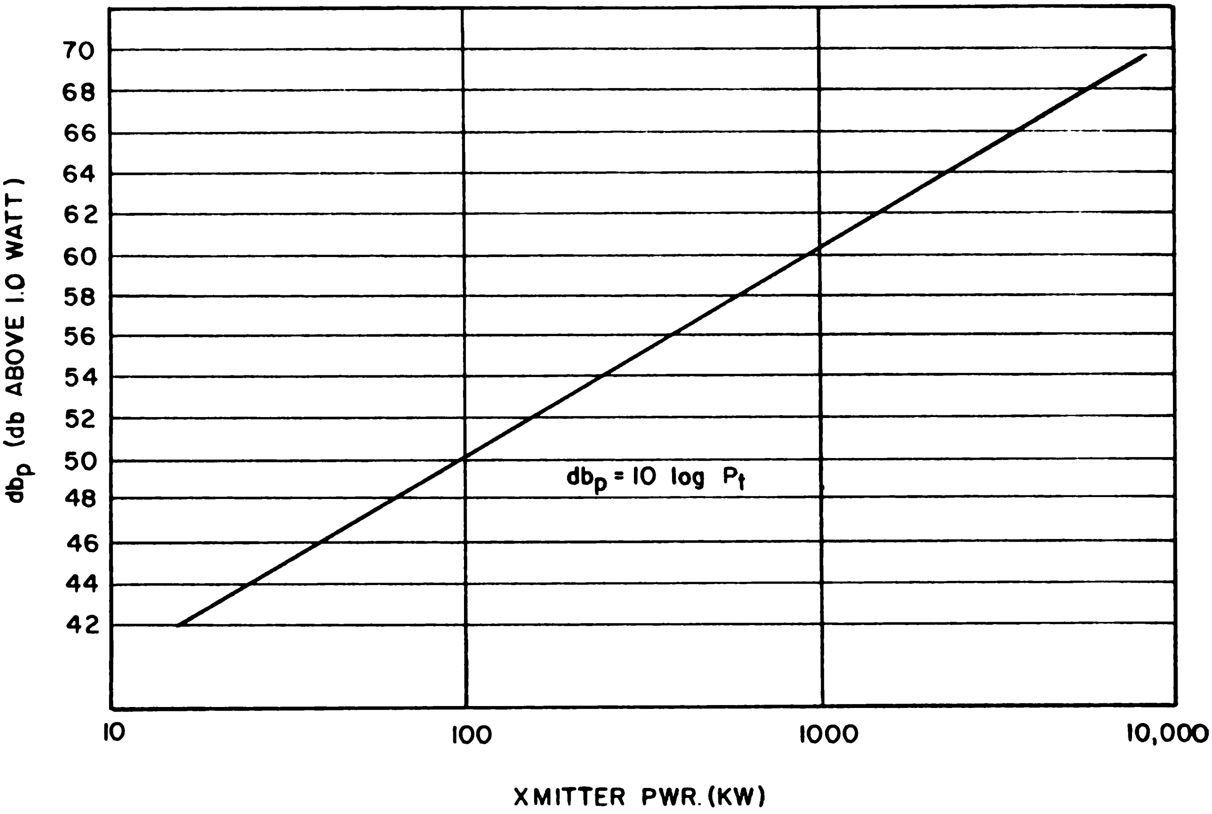

Figure 6-3. Transmitter Power Above 1.0 Watt

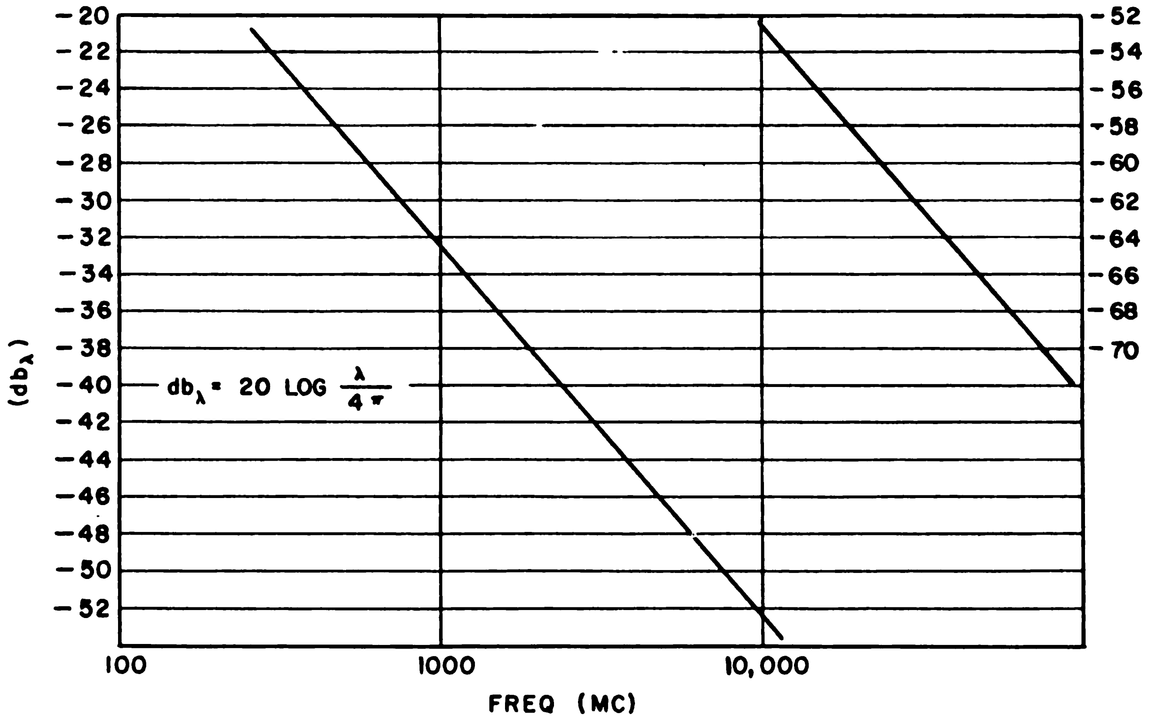

Figure 6-4. Wavelength Factor

For clarity, the method of computation and use of the curves that follow will be illustrated using a fictitious radar system XYZ whose system constants are given below:

antenna gain:	40.2 db one way
azimuth beam width:	0.9°; elevation beam width – 2.17°
frequency:	2800 mc
transmitter power:	800 kw peak
pulse length:	2.0 usec
receiver noise figure (including duplexer):	—12 db
receiver IF* bandwidth:	1.3 mc
losses: (round trip)	1.0 db

---

*Note that bandwidth must be wide enough to pass the pulse length.

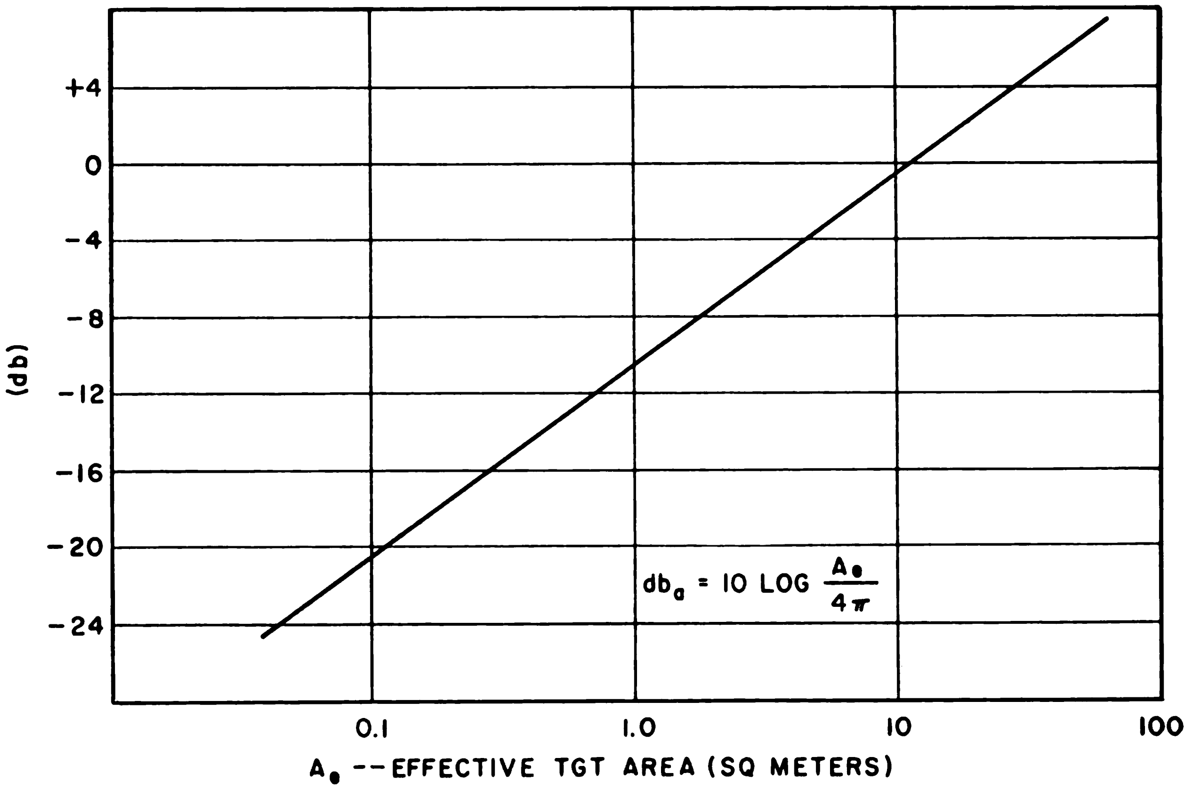

Figure 6-5. Target Area Function

Problem: To find the db S/N range on a typical aircraft whose mean area is 4.7 m^2 (The result will be *mean* range.)

antenna gain (two way): 2 × 40.2 db	db_{Ant}			+ 80.4
transmitter power: 800 kw	db_p	(#1) =		+ 59.0
frequency: 2800 mc	db	(#2) =	−41.4	
target size: 4.7 m^2	db_a	(#3) =	− 4.3	
receiver noise figure: −12 db	db_{NF}	=	−12.0	
receiver IF bandwidth: 1.3 mc	db_n	(#4) =		+142.9
(pulse length = 2.0 usec.)				
Losses: 1.0 db	db_L	=	− 1.0	
totals			−58.7 db	+282.3 db
net db_R	223.6			

slant range (Figure 6-7) = 238 statute miles

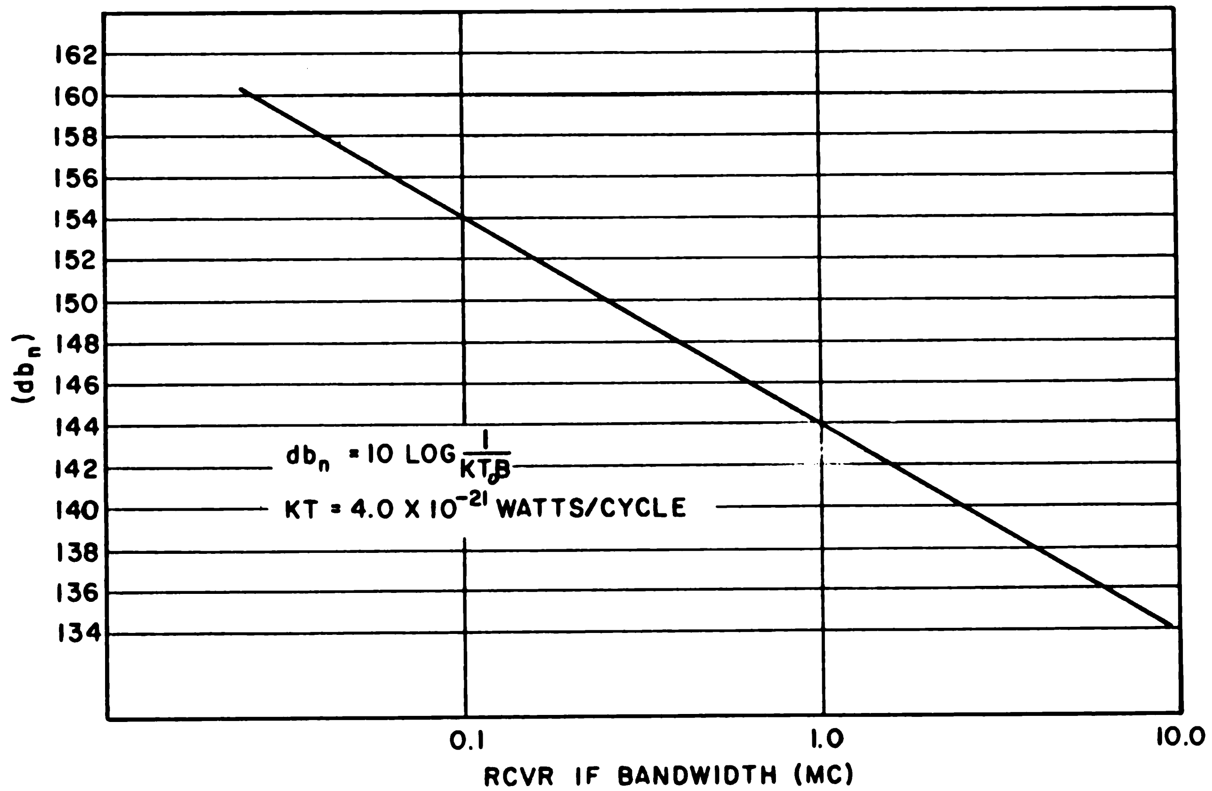

Figure 6-6. Receiver Gain Factor

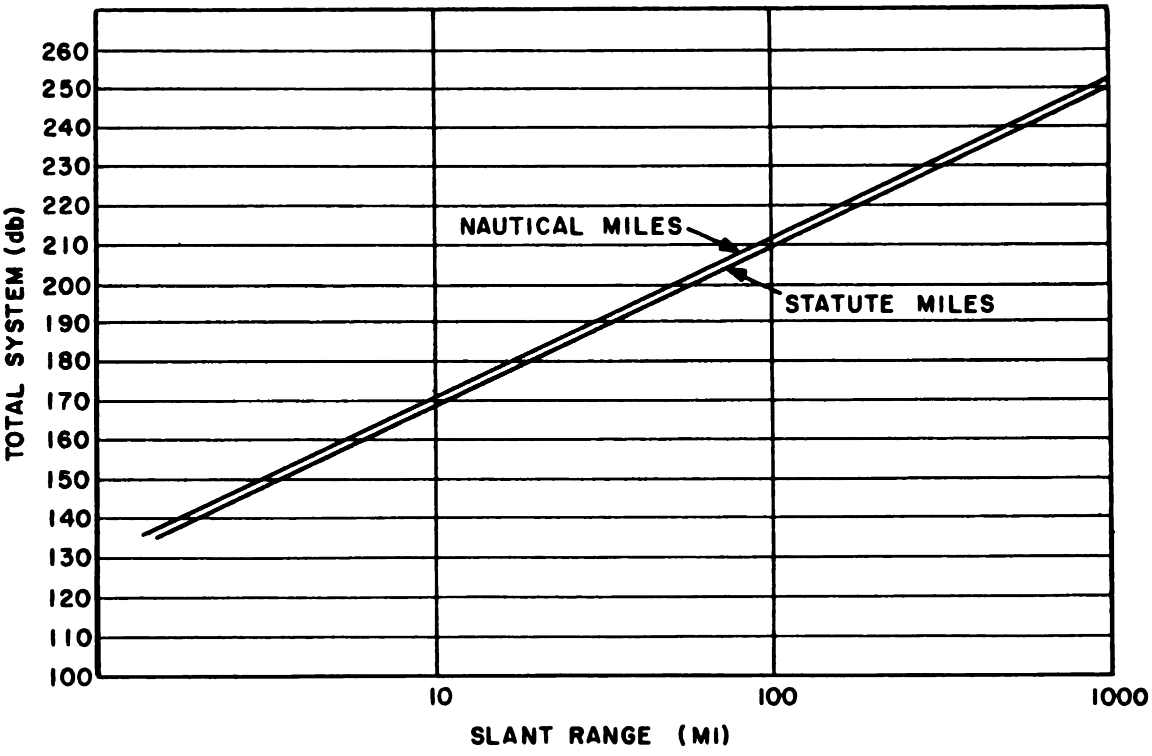

Figure 6-7. Slant Range as a Function of Total System

6-2.3 EFFECTIVE TARGET AREA

The effective target area factor (A_e) is probably the most difficult parameter of all to specify definitely and conclusively. Its evaluation for reflecting surfaces other than extremely elementary ones (such as spheres, flat plates, corner reflectors, etc.) is virtually impossible to compute, and this is especially true for the case of multicurved surfaces such as usually encountered in aircraft targets. Consequently, direct radar measurements obtained for radar systems whose parameters are known must be used; even so, such measurements often result in controversy and must be interpreted with caution.

Many radar designers have preferred to use flight test data obtained under scanning conditions in an attempt to arrive at mean values of effective target areas for various aircraft. To do this, the flight test range data is observed; the maximum reliable range of the system is judged; and the effective target area is computed from that range value. This *maximum reliable range* is by no means the maximum range observed on the system, nor is it a value which falls into the region of solid coverage. Rather, it is an in-between value selected in the vicinity of the range at which target "shows" on approximately 50 percent of the scans are received. This method has been applied to many systems to establish values of effective target areas for fighter and bomber aircraft. Typical values for World War II aircraft are 1.2 and 4.7 square meters for fighters and bombers respectively.

6-3 RADAR COMPONENTS AND TECHNIQUES

6-3.1 ANTENNAS

6-3.1.1 General

The basic purpose of a radar antenna is to concentrate the transmitted energy into a solid angle of some arbitrarily shaped cross-section and in some cases to provide a particular power distribution inside this angular region. Within the limitations imposed by the particular application and by the laws of nature, the antenna designer must strive to obtain the best compromise between the many conflicting requirements.

In the past, radar antennas were fundamentally designed as either search or track antennas. Recently there has been some degree of functional overlap. The track antenna may provide a limited search function and the search antenna may provide rough tracking in one or both planes during initial track acquisition, or one antenna system may provide first a search and later a track function. For the future, ferrites and other devices promise track-while-search capabilities with electronic beam steering permitting many targets to be tracked on a time-shared basis.

To date, solutions to the many antenna applications have been imaginative and varied. No attempt will be made here to describe these various configurations, since for the most part, they represent specific solutions to specific problems. References have been included which describe many of these antennas in some detail. A few systems not widely described due to their recent application are mentioned. If feasible, references are given and design information included. For the most part however, the information contained in this section is as practical and general as possible.

6-3.1.2 General Antenna Engineering Data

In view of the great number of possible microwave antenna configurations (involving parabolic, hyperbolic, spherical, plane and specially shaped reflectors as well as metallic lenses, dielectric lenses, arrays, dipoles, horns and dielectric radiators), determination of the complete performance of all except the simplest design requires a good deal of special calculation and experiment. References 1, 2, 3, and 4, discuss most of these various components in some detail and indicate the procedure for calculating the far-field diffraction pattern from an arbitrary aperture distribution. In the practical case, it is often difficult to obtain an accurate expression for the aperture field distribution which can be easily hand-integrated. In such cases, numerical integration by a digital computer is indicated. A comprehensive treatment of this procedure is given by reference 5.

Many of the antenna configurations required for radar applications produce a pencil beam from a plane-phased aperture distribution. Because of the relation which exists between the far-field patterns and the secondary aperture distribution, certain important parameters can be specified without regard to the specific configuration. Since horn-fed reflector systems are still the most popular type of radar antenna, design data are presented with this in mind. Correction factors for other configurations are indicated where applicable.

RELATION BETWEEN BEAMWIDTH AND SIDELOBES

In general, tapering the illumination of a uniformly phased aperture from a maximum in the center to a low value at the edges will broaden the beamwidth and reduce the sidelobe amplitude. The degree to which the sidelobes are reduced however, depends to a large extent on the shape of the amplitude distribution as well as the value of the edges. This is demonstrated by Figure 6-8, which shows the spread in first sidelobe values normally experienced with different types of feeds and parabolas of different focal length to diameter ratios. Phase errors and aperture blocking tend to raise the sidelobes above the values shown and these are taken into account in later figures.

The beamwidth for a given aperture is similarly dependent on the shape of the amplitude distribution. Without knowing the exact amplitude function, the value of edge taper is of limited aid in determining the beamwidth.

There is, however, a practical relationship between the beamwidth and sidelobe levels indicated by Figure 6-9. The curve labeled "NO BLOCKING" was derived by numerous calculations of practical aperture distributions. A large number of experimental check points have shown excellent agreement.

The effect of aperture blocking due to primary feeds, waveguide runs, support struts, etc., has been calculated in the usual manner, by considering an out-of-phase field at the center of the aperture. A shadow area of 2 percent and 4 percent of the total aperture is indicated by the dashed lines. While these curves have not had the experimental verification of the solid curve, they are, nonetheless, believed to be indicative of the degradation due to aperture blocking.

Besides giving a practical relation between beamwidth and sidelobe level for an arbitrary aperture size, Figure 6-9 provides a means for determining the penalty for lowering the sidelobe level without increasing the beamwidth. For example, determine the increase in aperture diameter necessary to permit obtaining a —25 db first sidelobe instead of a —20 db sidelobe. Assuming 2 percent aperture blocking in both cases, the required diameter becomes $D_2 = \frac{77}{66} D_1 = 1.17 D_1$, an increase of 17 percent. If phase errors are present, an even larger diameter is required, as explained in a later paragraph.

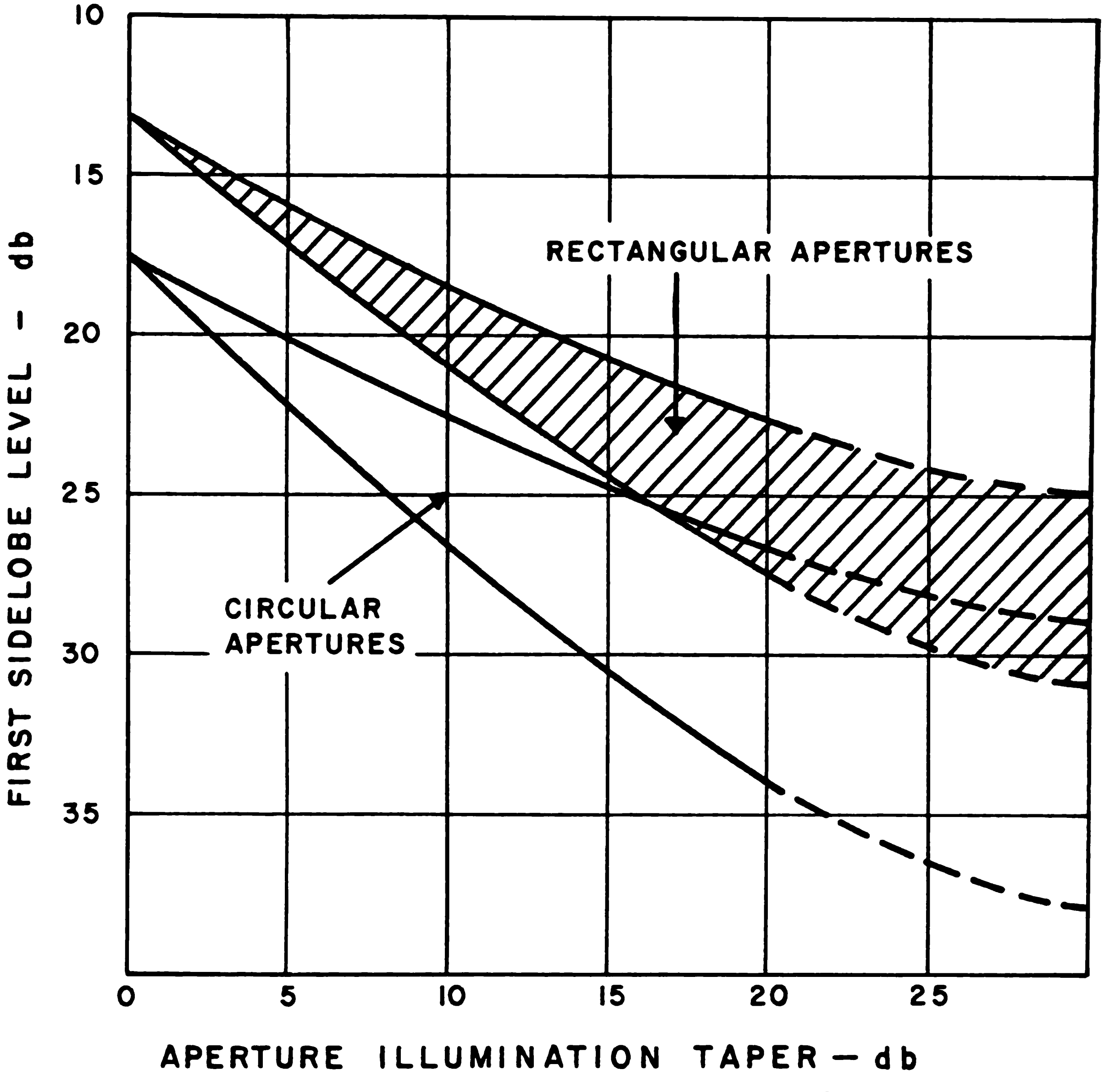

Figure 6-8. Taper Versus Sidelobe Level — Parabolic Reflector

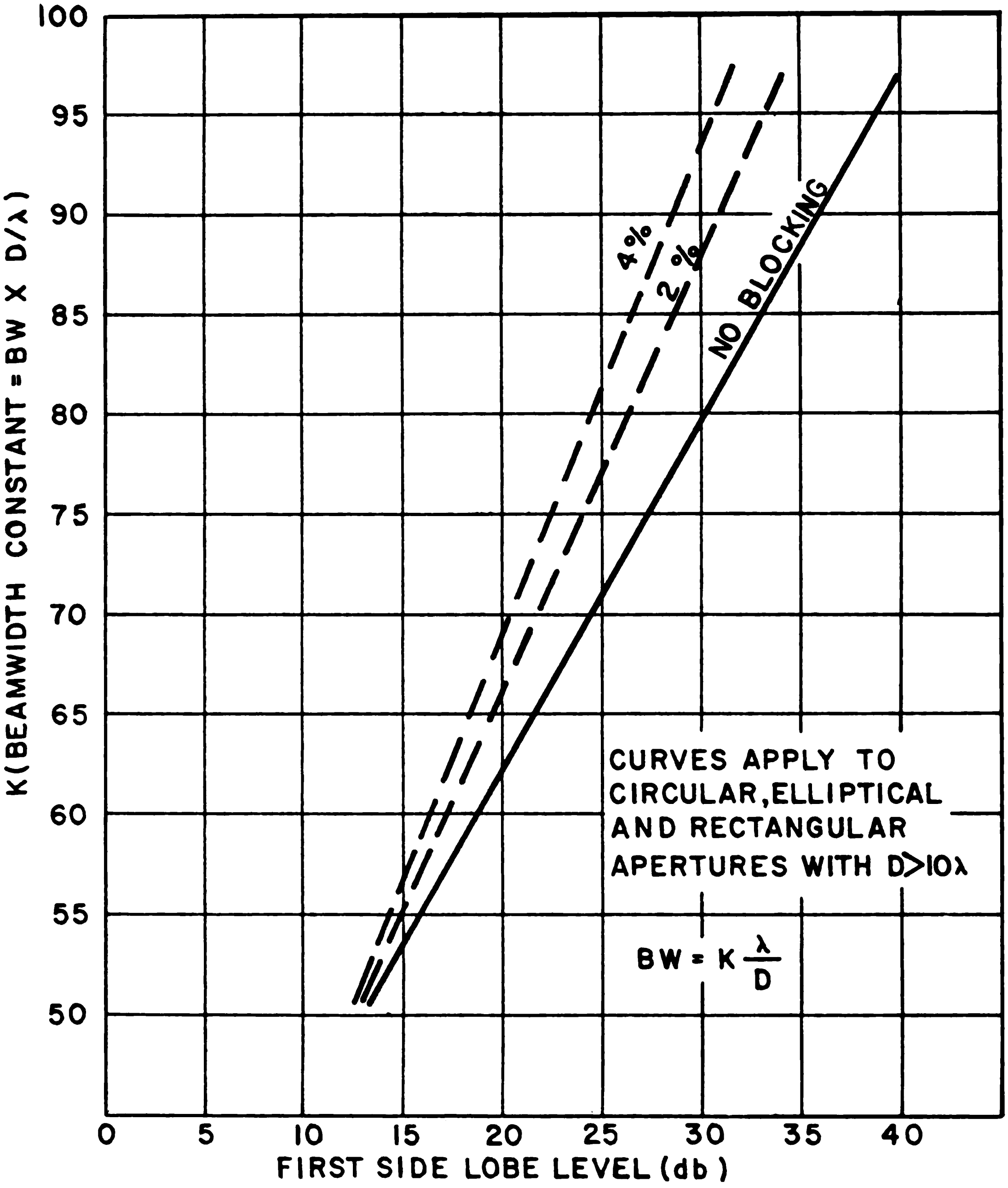

Figure 6-9. Aperture Beamwidth Constant Versus Sidelobe Level (No Phase Errors)

ANTENNA GAIN

The gain of a constant-phase aperture has a theoretical maximum when the field intensity over the aperture is uniform. This is given by

$$G = \frac{4\pi A}{\lambda^2} \qquad (6\text{-}12)$$

where A is the aperture area and λ, the wavelength. In practice however, the gain is generally 1.5 to 2 db below this value even if the antenna is designed for maximum gain. If the design emphasis is on low sidelobe levels, the result is an increase in beamwidth, spreading most of the energy over a larger solid angle. In such a case, the gain may be as much as 6 db below the theoretical maximum. This ratio of actual gain to maximum gain is sometimes referred to as antenna efficiency.

Several factors serve to determine antenna efficiency. Not all of the power radiated by the feed is intercepted by the reflector; that portion which escapes is commonly termed spillover. In a properly designed antenna, spillover loss usually amounts to about 1 db or less. A second factor is the shape of the aperture amplitude distribution. This determines its efficiency in concentrating the available energy into a narrow beam. Those distributions which result in lower sidelobes also tend to have lower efficiencies. In a design for maximum gain, aperture efficiency may be 90 percent corresponding to ½ db reduction in gain. A distribution which provides very low sidelobes may have an aperture efficiency of only 30 or 40 percent resulting in 4 or 5 db gain reduction. A third factor included in the definition and measurement of gain is the ohmic loss in the reflecting surfaces and the attenuation in the primary feed, including transmission line back to the point of gain measurement. One might also lump in the loss due to r-f leakage through a perforated or slatted reflecting surface. This combined loss is normally no more than a few tenths of a db. The last factor in a practical antenna, which reduces the gain, is deviations from a plane-phase front in the aperture. These phase errors also affect sidelobe level and are of sufficient importance to be treated separately in a following paragraph.

Without benefit of knowing the contributions from each of the above loss factors, a fairly reliable gain estimate can be made on the basi of the 3 db beamwidths in the two principa planes, vertical (Θ_V) and horizontal (Θ_H).

A reduction in gain caused by reduced aperture efficiency or smaller aperture size is reflected by an increase in beamwidth. Spillover power and ohmic losses, on the other hand, represent a fractional loss in gain which is independent of the other factors. For average pencil beams (less than 10° beamwidth) produced by circular apertures, the gain can be estimated by

$$\text{db gain} = 10 \log \frac{27000}{\Theta_V \Theta_H} \qquad (6\text{-}13)$$

For cosecant-squared antennas, the gain is about 1½ db less than the indicated value due to the gradual falloff of gain in the elevation plane. The gain of a two dimensional broadside array (excluding corporate structure losses) is about 1½ db greater than the value calculated from the above relation. This results from elimination of spillover loss and also from arraying elements of high end-fire directivity.

As a result of lower spillover loss and space attenuation, the gain of a parabolic cylinder fed by a line source is about ½ db higher than the indicated value. This figure, however, neglects loss in the line source feed and the net gain, including this loss, is usually comparable to the gain calculated for the circular aperture.

EFFECT OF PHASE ERRORS ON GAIN AND SIDELOBES

Figure 6-10 shows the loss of gain due to phase errors. Curves A, C, and D were plotted on the basis of information contained in references 6 and 7.

The correlation interval, c, refers to the distance, on the average, for which random type contour errors become essentially independent. In the case of a two-dimensional array of many elements with independent phase errors, the correlation interval equals the element spacing (approximately) and the abscissa scale is doubled since the reflector error affects the phase front both before and after reflection. There exists an upper limit to the maximum gain which can be realized by increasing the aperture dimensions. This limit is set by the rms deviation of the reflector contour. Due to the temperature expansion of metal, dimensional changes

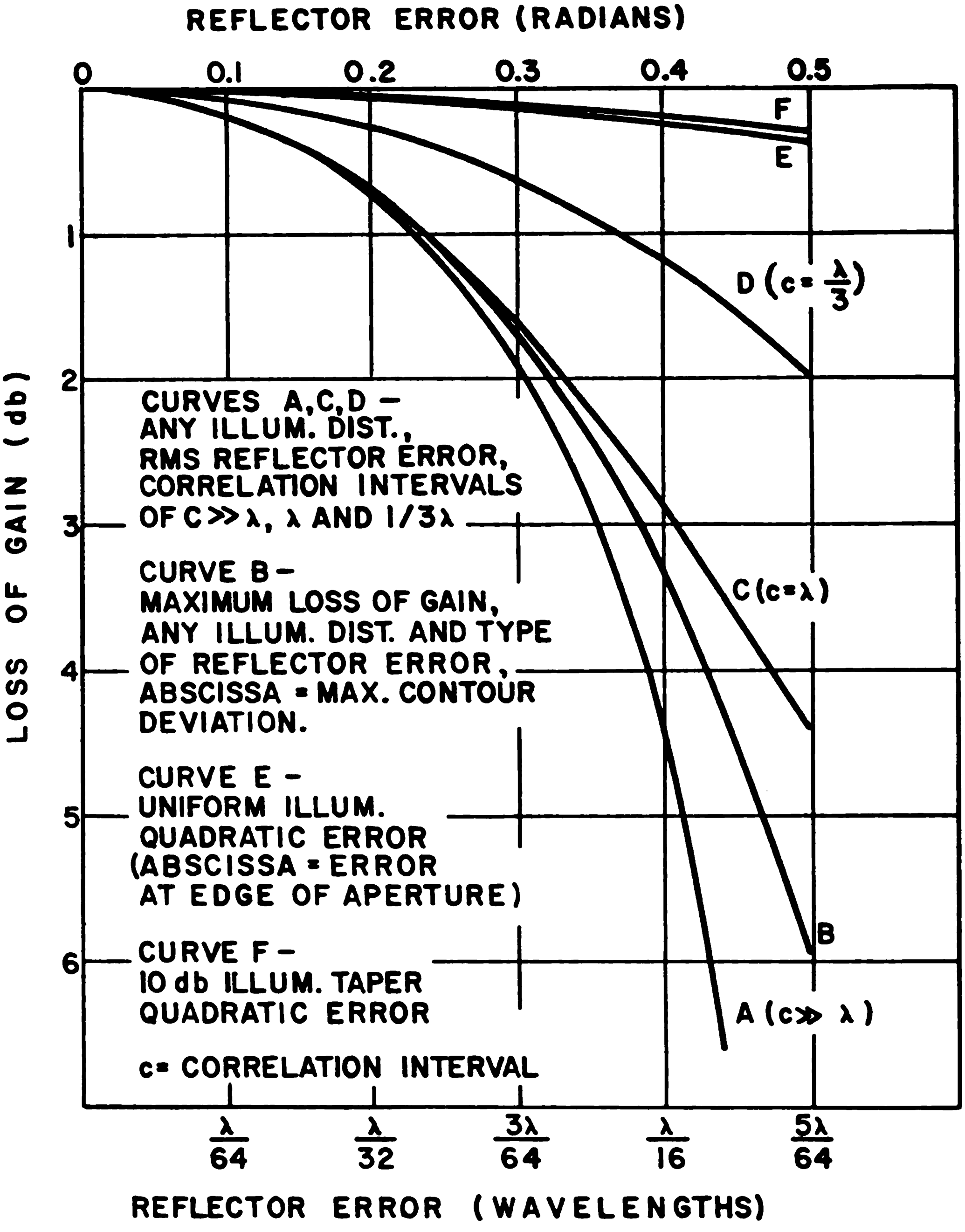

Figure 6-10. Antenna Gain Loss Due to Phase Errors

might be on the order of one part in ten thousand. This would limit the maximum gain of a paraboloid to about 70 db (references 1 and 6).

If the reflector errors are not random in nature but have some unusual distribution, the maximum possible loss in gain can be found from Figure 6-10 by curve B.

A warp in the reflector of the form ar^2, $(0 \leqq r \leqq 1)$ has the effect shown by curves E and F. An equivalent error also results from displacing the phase center of the feed axially from the focal point of the reflector or from taking antenna patterns with a spherical incident wavefront. The usual far-field condition of $2D^2/\lambda$ for example, corresponds to an aperture phase error of 1/16 λ at the edge or an equivalent quadratic reflector error of 1/32 λ. From curves E and F it can be seen that the gain will be reduced from the true (plane wavefront) value by less than 0.1 db. Although not shown, the first sidelobe is more sensitive an indicator of phase error than the gain and a —20 db first sidelobe would increase to nearly —19 db for this amount of phase error. Since the feed is adjusted for "best patterns" on the range, in the course of adjustment it would be defocused slightly to compensate for the finite range distance and yield a measured value of —20 db. The actual sidelobe level with an incident plane wave would then be closer to —19 db. For very low sidelobe antennas, the effect is even more pronounced and a range requirement of $3D^2/\lambda$ or $4D^2/\lambda$ is sometimes more desirable.

Figure 6-11 indicates the average sidelobe increase resulting from random reflector contour errors. If the beamwidth is different in the

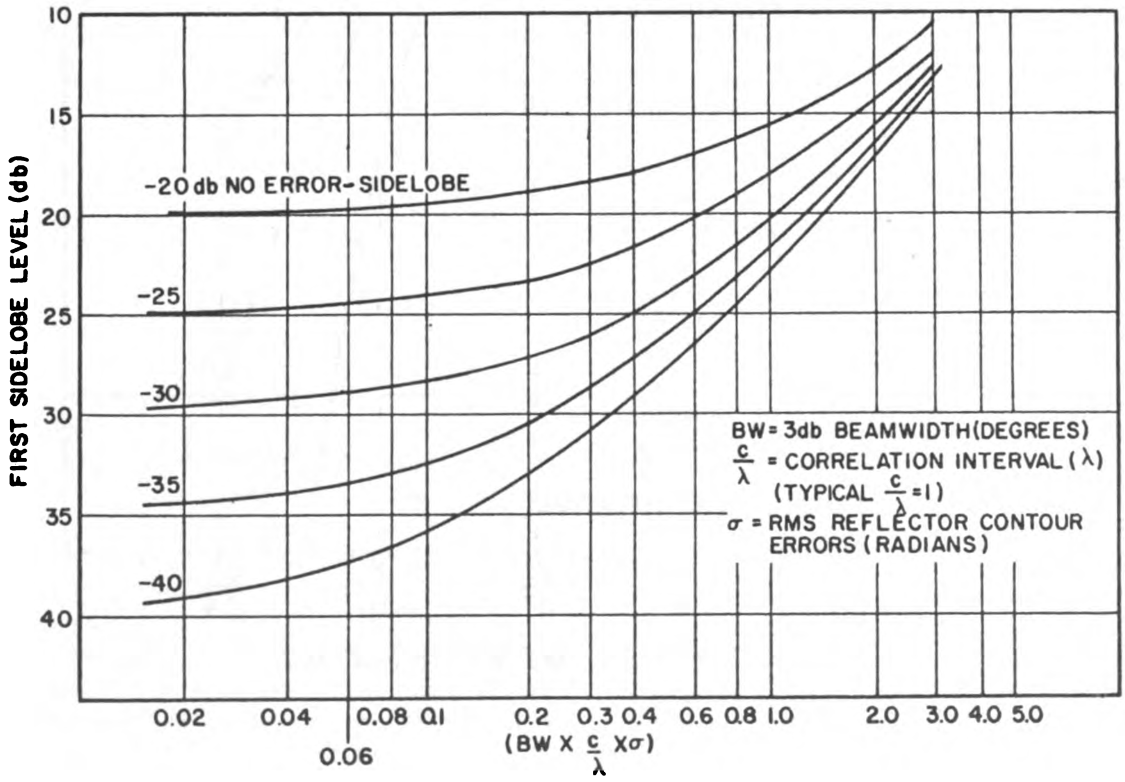

Figure 6-11. Average Effect of Random Phase Error on Sidelobe Level

o principal planes the average should be used the calculation. The difficulty in obtaining ry low sidelobes is obvious. The *no-error sidebe* refers to the value previously chosen in igure 6-9, and includes the effects of any aperre blocking which may be present.

ARTIALLY OPEN REFLECTORS

In general, the reflecting surfaces of large ntennas are made of perforated sheets, gratngs or mesh to reduce wind loading and weight. he feasibility of a partially open reflector is etermined by the required contour accuracy nd type of fabrication best suited for the paricular application.

Gratings (including flatwise strips, edgewise strips and round bars) provide a polarized reflecting surface. The element spacing is limited to $\lambda/1 + \sin \Theta$ (where Θ is the angle between the incident ray and the grating normal) if undesirable *grating lobes* are to be prevented.

Symmetrically perforated sheets, screens and mesh are used to provide a non-polarized reflecting surface. These materials are also better suited for some methods of antenna construction.

Data on r-f transmission and wind resistance for a variety of screens and gratings are available in references 8 and 9.

PRIMARY FEEDS AND PATTERNS

Usually, final antenna pattern calculations are based on experimental primary feed patterns. For purposes of initial calculation however, it is desirable to have approximate primary patterns available.

The nomograph labeled Figure 6-12 was taken from page 405 of reference 3. This nomograph provides data for constructing power patterns of rectangular waveguide apertures up to two wavelengths and thus covers almost all primary feed applications. Page 407 of the same reference provides a similar nomograph for circular feed apertures. Information on dielectric radiators is given by reference 10.

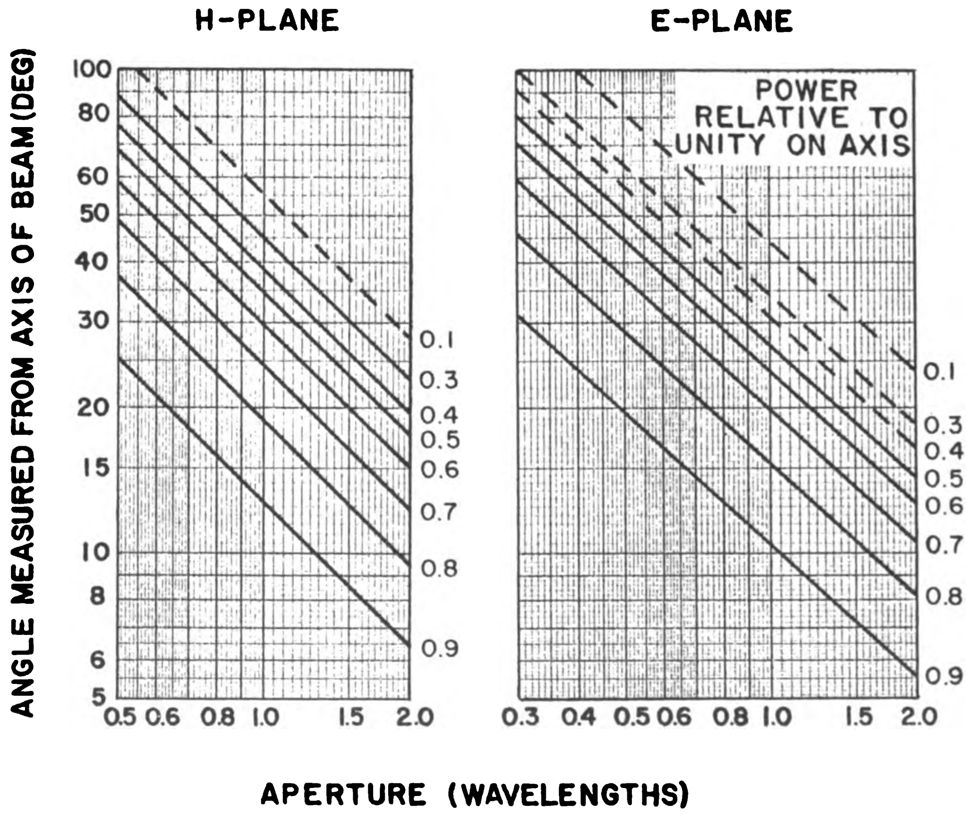

Figure 6-12. Rectangular Waveguide Data, Nomograph

WAVEGUIDE

The guide wavelength (λ_g) can be easily calculated knowing the free-space wavelength (λ) and the cut-off wavelength (λ_c).

$$\frac{1}{\lambda^2} = \frac{1}{\lambda^2} + \frac{1}{\lambda^2_c} \qquad (6\text{-}14)$$

For rectangular waveguide carrying the dominant TE_{10} mode, $\lambda_c = 2a$, where a is the internal broad-wall (H-plane) dimension.

Reference 11 lists values of the above wavelengths, for eleven standard rectangular waveguides which cover the frequency range from 1000 to 42,000 mc.

Reference 12 provides charts and graphs for determining power handling capacities of waveguide systems. Rectangular, coaxial and cylindrical waveguides are considered for both cw and pulsed-power applications.

6-3.1.3 Search Antennas

The many search antennas which have been devised can be lumped into several major categories; namely, rotating antennas, point source scanners, line source scanners and two-dimensional scanning arrays.

ROTATING ANTENNAS

Antennas of this type are usually designed to provide a cosecant-squared elevation pattern and a low sidelobe azimuth pattern. References 1 and 2 describe a number of techniques for obtaining this type of coverage. To maintain a smooth elevation pattern, reflector tolerances are usually required to be one thirty-second of a wavelength or better.

POINT SOURCE SCANNERS

Many different configurations have utilized a moving point source to scan through a small solid angle or over an angular sector. References 13, 14, and 15 give a number of specific examples.

For scan sectors on the order of ±5 to ±8 beamwidths, long focal length paraboloids are sometimes used. The off-axis characteristics of a paraboloid are treated in reference 16.

For applications where sidelobe requirements are not too severe, the axial depth can be considerably shortened by using a Cassegrain antenna system. This is a double reflector system employing a paraboloid for the main reflector and a hyperboloid for the sub-reflector. The hyperboloid is positioned between the vertex and focal point of the main reflector. Eccentricity of the hyperboloid is chosen such that one focus is coincident with the focal point of the paraboloid, while the conjugate focus is located near the paraboloid vertex. This permits the moving point source feed system to be conveniently fed from the rear of the main dish. The effective focal length of the Cassegrain antenna is MF, where M is the magnification factor and F is the paraboloid focal length. For a hyperboloid of eccentricity e, $M = \frac{e+1}{e-1}$. The space attenuation factor is also the same as for a paraboloid of focal length MF. The ratio of hyperboloid diameter to paraboloid diameter determines the aperture blocking and this ratio is plotted in Figure 6-13 as a function of the magnification M and the F/D of the main dish.

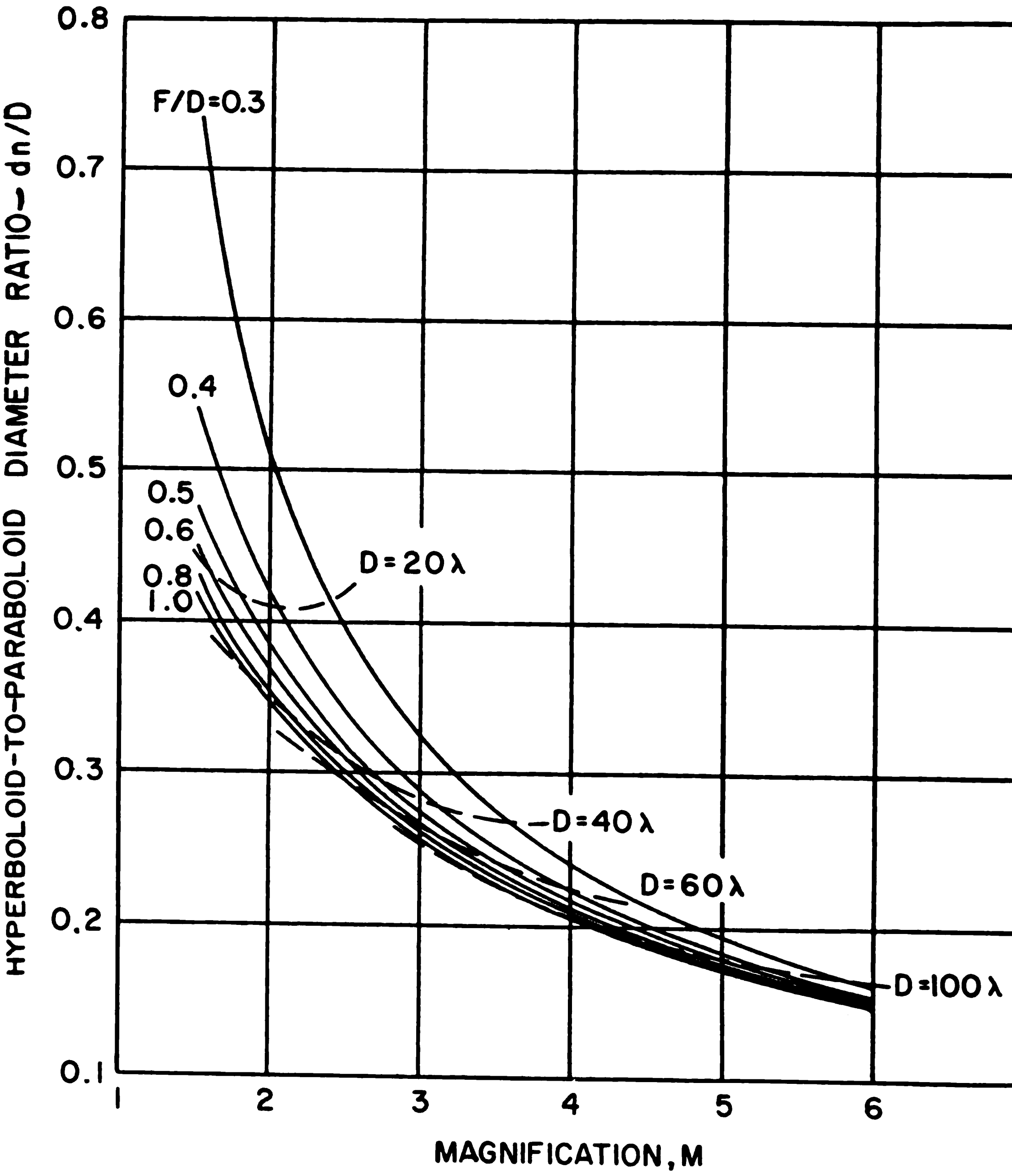

Figure 6-13. Hyperboloid-to-Paraboloid Diameter Ratio versus Magnification

The dashed lines indicate the limit on M if the hyperboloid is to be kept in the far-field, $(2d^2/\lambda)$ of the feed, assuming a 10 db illumination taper. These represent safe limits and in some cases, this distance has been reduced experimentally to d^2/λ while maintaining acceptable antenna patterns.

Another point source scanning antenna, recently popular, is the parabolic torus reflector fed by an organ pipe scanner or other moving source feed. This system has wide angle capabilities without beam deterioration, due to its symmetry. Sidelobe levels are good except for two *eye lobes* in the 45° planes below the main beam. By a proper choice of parameters, these can be kept below -17 db. Reference 17 gives a detailed description of the parabolic torus reflector.

The Luneberg Lens has received considerable attention in the past few years as a system ideally suited for scanning wide angles or volumes in space. The lens is a sphere of varying index of refraction and has the property of focusing a plane incoming electromagnetic wave into a point on the surface, diametrically opposite the point of entry. Chief drawback to the use of the dielectric lens as a transmitting antenna, has been the limited power handling capability. There are a great number of papers on this lens available in the literature. Reference 18 describes the standard Luneberg Lens and some possible variations.

LINE SOURCE SCANNERS

For sector scanning a beam with low sidelobes, a line source feeding a parabolic cylinder is often used. Some examples of applicable line sources include the Foster scanner[1], the Tin Hat lens fed by a moving point source[14 15], frequency scanned arrays[13 15] and lately, ferrite phase shifting arrays[19].

The first two examples have the advantage of a linear sawtooth scan and can be used to scan sectors up to 60 degrees or more. Frequency arrays have the undesirable feature of a non-linear scan and ferrite arrays are presently limited in application by temperature sensitivity and average power capability.

TWO-DIMENSIONAL SCANNING ARRAYS

Many new techniques have been developed for pointing a beam in space by electronically phasing a two-dimensional array of elements. These and other methods of *inertialess scanning* are presented in reference 19. Present day limitations in the use of ferrite materials to control the phase of array elements, is the result of their temperature and frequency sensitivity.

6-3.1.4 Track Antennas

The highest accuracy tracking antennas being made today use some form of monopulse to provide angular error signals. Reference 20 provides a thorough discussion of monopulse in all its forms and also makes a comparison between monopulse and sequential lobing systems. Also included is a discussion of most of the design problems without examples of specific solutions.

One of the most popular of the monopulse tracking systems uses amplitude-amplitude comparison. As an initial guide in the feed horn design, Figure 6-14 is included. This shows the size of the feed horn apertures required for 2.5 or 3 db secondary beam crossover as a function of the paraboloid F/D. Several experimental check points have shown close agreement with the calculated curves.

If conventional horn feeds are used with F/D ratios below 0.5, the H-plane dimension becomes very close to cut-off for the TE_{10} mode. This results in difficult impedance matching and necessitates very close machining tolerances. Sometimes dielectric loading of the feeds is employed to extend the point of dominant mode cut-off. This requires careful design in order to maintain a distinct feed horn phase center coincident in both planes. An indistinct phase center leads to a comparison of signals with a complex phase function and limits the tracking accuracy. The effect of feed assembly errors on angular accuracy is the subject of references 21, 22, and 23.

There are a number of possible monopulse feed configurations which depart from a simple cluster of contiguous horns. Combining networks can be used to provide effectively different horn combinations for transmit and for error sensing on receive. Each of these requires a special analysis.

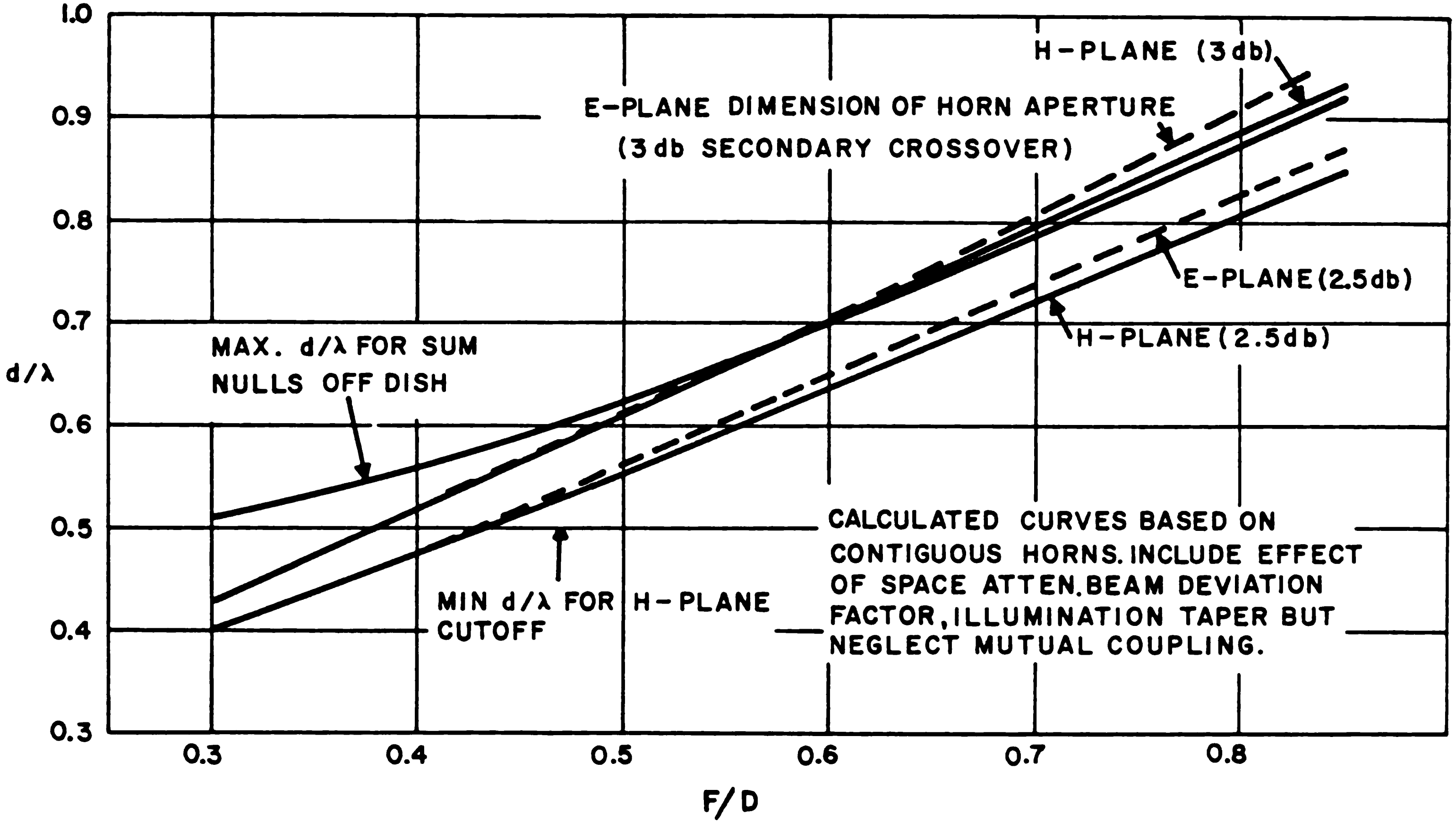

Figure 6-14. Amplitude Monopulse Design Curves

To reduce the physical depth of the antenna reflector system, a Cassegrain geometry is sometimes used. The effective focal length of *MF* (discussed in the preceding section) should be used in Figure 6-14 to determine the size of the feed horn apertures. This and other double-reflector systems are described in reference 24.

6-3.2 TRANSMITTERS

6-3.2.1 General

A transmitter is a device used to generate high frequency oscillations of energy level sufficient to properly illuminate or excite a radar target at some distant point. The fundamental objectives of the transmitter are essentially two fold, first, to generate the necessary energy level at the required operating frequency and second, to generate the energy with the required degree of frequency, time and amplitude stability.

Two basic approaches may be employed in transmitters. The first is the power oscillator transmitter where a single oscillator tube provides the necessary r-f energy. This approach has the advantage of minimum complexity, size and weight. The disadvantage is that since the oscillator must usually generate and deliver large amounts of power, heating of the oscillator tube structure, and variations in antenna loading, lead to relatively poor frequency stability. The second approach is the MOPA (master oscillator power amplifier) transmitter in which the frequency is generated in a highly stable low power oscillator circuit and amplified up to the required power level by means of succeeding power amplifier stages. A higher degree of complexity results, but this approach must be employed where excellent transmitter stability is a prime system consideration.

DESIGN CONSIDERATIONS

The following factors must be known and weighed before a transmitter design can be undertaken:

*(a) peak r-f power output required
(b) average r-f power output required
*(c) pulse length required
*(d) pulse repetition rate required
(e) carrier frequency or range of frequencies required
(f) phase, amplitude, and pulse time s bility required
(g) bandwidth required
(h) degree of complexity allowable
(i) overall efficiency desired
(j) size and weight allowable.

The factors listed above are determined p marily by the characteristics of the type transmitting tubes employed and the puls equipment, and/or the d-c power supplies us to operate the tubes. These characteristics w be discussed further in subsequent sections.

PULSED AND NON-PULSED CW TRANSMITTERS

The most common type of radar transmitt is the pulsed version. Much higher peak pow output for short intervals of time may be ol tained from transmitting tubes than from th same tube type operating in a non-pulsed mod In practice, many tubes are designed only fo pulsed operation and can not be operated un pulsed. Furthermore, most of these tube type are limited to very specific-maximum puls lengths, ten microseconds being a typical value The pulse shape is generally approximately rec tangular, although an appreciable reduction i the amount of r-f spectrum can be achieved by employing shaped (such as cosine, cosine squared, etc.) pulses. Since any practical pulsing system will result in a finite change in the d-c voltage applied to a transmitting tube during a pulse, and since all transmitting tubes have a phase delay versus voltage characteristic (*FM*), this problem must be analyzed to insure compatibility with overall system considerations. Non-pulsed transmitters, on the other hand, present a constant load on the sources of d-c operating voltage and hence the only essential phase shift variations will be due to the ripple content of the power supplies employed.

6-3.2.2 Microwave Transmitting Tubes

Most transmitting tubes can be classified into three broad categories:

(a) grid controlled tubes, exemplified by triodes, tetrodes, and pentodes – These tubes are generally limited to the lower frequencies (up to about 400 megacycles) when significant amounts of power are to be realized. They may be used as either oscillators or amplifiers and are available in either pulsed or non-pulsed versions.

---

*These factors apply to pulsed transmitters only.

(b) velocity modulated tubes, exemplified by klystrons, traveling wave tubes, and backward wave oscillators – These tubes generally are most practical at frequencies above 400 megacycles. The large klystron and traveling wave tubes are customarily employed as amplifiers. The reflex klystron and backward wave oscillator are employed as low powered frequency determining elements. All of these tube types may be available in either pulsed or non-pulsed versions.

(c) cross field tubes, exemplified by magnetrons and amplitrons operate over approximately the same frequency as the preceding group – Magnetrons are always used as oscillators and amplitrons are generally used as amplifiers. Both types may be available in the form of pulsed and non-pulsed versions.

GENERAL EXTERNAL CHARACTERISTICS

The previously described broad categories of transmitting tubes all have several important external characteristics as shown in very general form in Table 6-1. The first column is intended to show the operating frequency and power output characteristics that may be achieved without an extensive development program being undertaken. The variation of power output between the frequency extremes shown is not linear, but rather, falls off rapidly with frequency. The other factors of typical gain, operating voltage and efficiency will serve as a general guide in determining the relative complexity and size that a transmitter using the various tube types will entail. The r-f bandwidths shown are approximate maximums for high power tubes. Generally, the greater the bandwidth required, the lower the efficiency possible with a given tube type.

PHASE CHARACTERISTICS

Table 6-2 shows typical phase characteristics encountered in various amplifier tube types. With velocity modulated tubes the values of total phase length are typical for high power tubes, but they may be many times greater with low power tubes.

WEIGHTED VALUES OF TUBE CHARACTERISTICS

Reference 25 contains much useful information in selecting transmitting tubes. Included are a series of curves relating the relative desirability of various tube characteristics in terms of assigned weighing factors.

6-3.2.3 Pulser and Power Supply Considerations

Pulsers may be divided into roughly three categories: those using gas filled tubes as switches, those using vacuum tubes as switches, and those using saturating magnetic elements as switches. In general, all pulsers must have a high voltage d-c power supply which charges some form of energy storage element between pulses. The switching action, initiated to produce a constant amplitude pulse to the transmitter tube, may discharge either part or all of the energy in the storage element during one pulse time interval. It is in this respect that basic pulser circuits vary.

GAS TUBE PULSER CHARACTERISTICS

The gas tube pulser, usually called the line type pulser, consists of five basic elements having functions as follows:

(a) high voltage d-c power supply – This device steps up and rectifies a-c power line voltage. The rectified output is filtered to reduce the ripple to the degree prescribed by system considerations.

(b) resonant charging circuit – A charging reactor is selected to be resonant with the capacity of the energy storage element in the period equivalent to the interpulse time. The storage element is thereby charged to approximately twice the voltage of the d-c power supply.

(c) pulse forming network – This element is an artificial transmission line consisting of properly selected values of inductance and capacitance. During the resonant charging period the energy required for one pulse is stored in the line capacitance. The number of sections used in the line determines the rise time, fall time and flatness of the pulse generated upon discharge.

TABLE 6-1. EXTERNAL CHARACTERISTICS OF PULSE TRANSMITTING TUBES

	Typical Ranges		Amplification	Typical Power Gain	Typical DC Pulse Operating Voltage	Typical Efficiency	Typical Bandwidth	Remarks
	Frequency	Peak Power						
Triode & Tetrode	200 mc	500kw	Oscillator or Amplifier	10-20DB	5000kw 50kv	200mc 50%	1%	External RF Circuits Must be Designed
	3000mc	100w			100w 1kv	3000mc 10%		
Klystron	400mc	40,000kw	Amplifier	30-60DB	40,000kw 300kv	400mc 45%	5%	RF Circuits Built in External Focusing Required
	30,000mc	10kw			10kw 10kv	30,000mc 10%		
Reflex Klystron	1200-30,000mc	1w	Oscillator	-	< 1kv	50%	-	Voltage Tunable
Backward Wave Oscillator	3000-10,000mc	1w	Oscillator	-	< 2kv	10%	-	Voltage Tunable
Traveling Wave Tube	400mc	10,000kw	Amplifier	30DB	10,000kw 250kv	30%	10%	Similar to Klystron Amplifier 3-5 Years Behind
	10,000mc	1000kw			1000kw 100kv			
Magnetron	400mc	10,000kw	Oscillator	-	10,000kw 100kv	50%	-	Most Commonly Used Power Oscillator
	10,000mc	1000kw			10,000kw 50kv			
Amplitron	400mc	10,000kw	Amplifier	10DB	10,000kw 100kv	60%	10%	High Efficiency Gain
	10,000mc	1000kw			1000kw 50kv			

TABLE 6-2. TRANSMITTER TUBE PHASE CHARACTERISTICS

TUBE TYPE	TYPICAL PHASE SENSITIVITY
AMPLITRON	$\Delta\phi = 0.4°$ for 1% $\frac{\Delta I}{I}$
KLYSTRON	$\frac{\Delta\phi}{\phi} = \frac{1}{2}\ \frac{\Delta E}{E}$ $\phi \approx 5 \quad \phi = 9°$ for 1% $\frac{\Delta E}{E}$
TWT	$\frac{\Delta\phi}{\phi} = \frac{1}{3}\ \frac{\Delta E}{E}$ $\phi \approx 10 \quad \Delta\phi = 12°$ for 1% $\frac{\Delta E}{E}$
TRIODE	$\Delta\phi = 0.5°$ for 1% $\frac{\Delta I}{I}$
TETRODE	$\Delta\phi = 0$ to $0.5°$ for 1% $\frac{\Delta I}{I}$

(d) switch tube – This tube, usually a hydrogen thyratron, is triggered into conduction at the instant a pulse is required.

(e) pulse transformer – This device is the third element of a series circuit consisting of the pulse forming network, the switch tube, and the pulse transformer. The amplitude of the primary pulse, usually less than 30 kilovolts, is then stepped up to the necessary voltage level and applied to the transmitter tube being pulsed. At the end of one pulse essentially all of the energy is removed from the storage element and it is recharged for the next pulse during the interpulse period.

HARD TUBE PULSER CHARACTERISTICS

The hard tube pulser operates essentially the same as the line type pulser except that:

(a) resonant charging is not employed

(b) instead of a pulse forming network, a large storage capacitor is employed, which normally delivers only a small fraction of its energy on one pulse

(c) on many circuits a pulse transformer may not be required but this is done at the expense of operating pulser components at much higher voltage levels than in the line type pulser.

On velocity modulated tubes a variation of the conventional hard tube pulser is sometimes employed. Some klystrons and TWT's can be supplied with a modulating electrode which can be pulsed with respect to the cathode to turn on the beam in these tubes. The switch tubes therefore usually handle much less average power than in the conventional hard tube pulser, but the pulsing circuitry becomes somewhat more complex.

SATURATING REACTOR PULSERS CHARACTERISTICS

These pulsers bear a similarity to line type pulsers. Their principle of operation is based on resonantly charging a capacitor. When the capacitor reaches its peak charging voltage, a series reactor saturates and discharges the first capacitor into a second smaller capacitor which is then resonantly charged to a higher voltage in a shorter period of time. by going thru a number of successive stages of this type a short pulse can be formed. This pulse in turn is stepped up by a pulse transformer and applied to the transmitter tube as a line type pulser. It is sometimes possible to incorporate silicon controlled rectifiers in the low level, long charging period stages to simplify the construction of this pulser type.

RELATIVE MERITS OF PULSERS

(a) line type pulser

(1) The pulse is formed at relatively low voltage, generally resulting in smaller overall size and weight.

(2) Only the energy for one pulse is stored in each interpulse interval resulting in very limited fault current in an arcing transmitter tube.

(3) The pulse shape is a function of the characteristics of the pulse forming network and the pulse transformer.

(b) hard tube pulser

(1) The pulse is formed at relatively high voltage, generally resulting in large overall size and weight.

(2) Very high energy is present in storage capacitor at all times, resulting in extremely high fault current in an arcing transmitter tube unless protective circuits are employed.

(3) The pulse droop is a function of the storage capacitor size and the pulse transformer (if a transformer is used). The hard tube pulser produces the most rectangular pulse possible when properly applied.

(c) saturating reactor pulser

(1) The pulse is formed at relatively low voltage probably resulting in the smallest overall size and weight of any pulser.

(2) Time jitter and time drift may result from the variation in magnetic characteristics of the core steels.

(3) Energy per pulse characteristics are identical to the line type pulser.

(4) The pulse shape is a function of the characteristics of the last stage pulse forming network, the saturated reactance of the last stage and the pulse transformer characteristics.

6-3.3 RECEIVERS, GENERAL

In a typical radar system, the receiver is located both physically and electrically between the r-f plumbing and the data utilization and display equipment. It forms that element in the radar system which amplifies the returned signal so that it may be fully utilized by the remaining portion of the system. In some of the more modern sophisticated systems some form of pulse coding may be used which makes the signal more readily identifiable to the receiver. By making use of known signal characteristics, such as frequency, pulse length and prf, the designer is able to tailor his design so as to optimize receiver performance which will permit only the reception of a particular type of signal and make possible the rejection or at least the distinct reduction in sensitivity to other unwanted signals.

Unlike the home radio or the communications receiver, the radar receiver is required to have a very wide dynamic range capable of handling signals of various strengths almost simultaneously. This is true because operational conditions preclude the existence of an operator whose response time will be sufficiently rapid to instantaneously set the gain of the receiver to suit the needs of the rapidly changing signal strength.

The radar receiver may also be differentiated from the common radio receiver because the radar receiver seldom has its own independent and physically separate antenna. Instead it is necessary to share a signal receiving antenna with a powerful nearby transmitter making use of a very high speed transmit-receive switch to make possible this antenna sharing. Since no such switch is perfect, leakage through the r-f plumbing into the receiver channel is always a matter of concern for the radar receiver designer.

The communications receiver, as well as the home radio receiver, ordinarily operates with only very narrow overall bandwidths. A typical range of bandwidth for such receivers might be ten to thirty kc. On the other hand, the radar receiver may operate utilizing a very much wider bandwidth. For example, the receiver designer is confronted with a basic principle in many designs that the overall bandwidth of the receiver is inversely proportional to the pulse length. For instance, a one microsecond pulse length will require a bandwidth of approximately one megacycle. There do exist modern receivers, however, which must accept pulses of a millisecond or more in length, which means that the overall bandwidth will be comparable to that of a good radio receiver.

A final distinguishing characteristic of the radar receiver is the fact that it operates on extremely weak signals. This requires continuous seeking on the part of the designer for very high sensitivity and low noise front ends.

One characteristic which the radar receiver has in common with the radio receiver is the prevalent use of the super heterodyne technique. Single conversion is the most popular although double and even triple conversion are often necessary in order to obtain the very narrow bandwidth optimum for millisecond pulse radars. This means that i-f amplifiers will constitute the heart of the amplifying portion of the radar receiver. The various forms that this amplifier can take will be discussed with their applications in later sections.

6-3.3.1 Design Considerations for Countermeasures and ECM

The radar receiver will seldom operate in an environment free of any type of interfering signal. In reality and in practice there is always sufficient man-made and natural interference to constitute a constant threat to the effectiveness of any receiving system. To reduce and overcome this menace, various types of enhancement schemes which improve signal-to-jamming ratio in the presence of jamming are available. (See Chapter 11.) The designer therefore must consider that the primary function of the radar receiver may well be to receive signals satisfactorily in a highly adverse or jamming environment. Jammer powers and sophistication are continually being advanced and improved so that the receiver designer is always pushed to find new ways to minimize the effects of these interfering signals.

6-3.3.2 Receiver Noise Figure

One of the most important parameters the receiver designer must consider is receiver noise figure or receiver noise factor. These are two names for virtually the same thing. Very wide bandwidth receivers are usually rated in terms of noise figure instead of sensitivity in microvolts input signal for a given signal-to-noise ratio. This method of rating a receiver is less confusing where receivers vary widely in bandwidth. Though it can be shown that the calculation of noise factor is independent of bandwidth, this method of rating by noise factor must be related to bandwidth in order to fully evaluate a radar system.

The noise factor of a receiver, or of any network, is defined as the ratio of the available input to output signal-to-noise power ratio.

$$F = \frac{S_i/N_i}{S_o/N_o} \qquad (6\text{-}15)$$

where F = system noise figure

S_i = available signal input power

N_i = available noise input power

S_o = available signal output power

N_o = available noise output power

This equation indicates that the ideal receiver would be one where the noise factor F is equal to 1.0. When the noise factor F is expressed as a power ratio in db, it is termed *noise figure* of the receiver. This is its most common terminology and the one most commonly encountered in military specifications. This receiver noise figure is one of the major parameters in determining overall system noise figure. (See paragraph 6-2.)

6-3.3.3 Typical Overall Receivers

Three typical receiver block diagrams are given in Figure 6-15. They differ primarily in the head end. In each case the head end determines, to some degree, the selectivity of the receiver and primarily determines the overall noise factor obtainable.

The first receiver shown has an r-f amplifier as its head end. If the input circuit is properly designed, this first tube will determine the overall noise factor providing, of course, that the first tube has sufficient amplification to override any noise produced in either the second stage or the first converter. This is true because summation of non-coherent noise is always in an rms fashion so that the noise generated inside the tube, as compared with

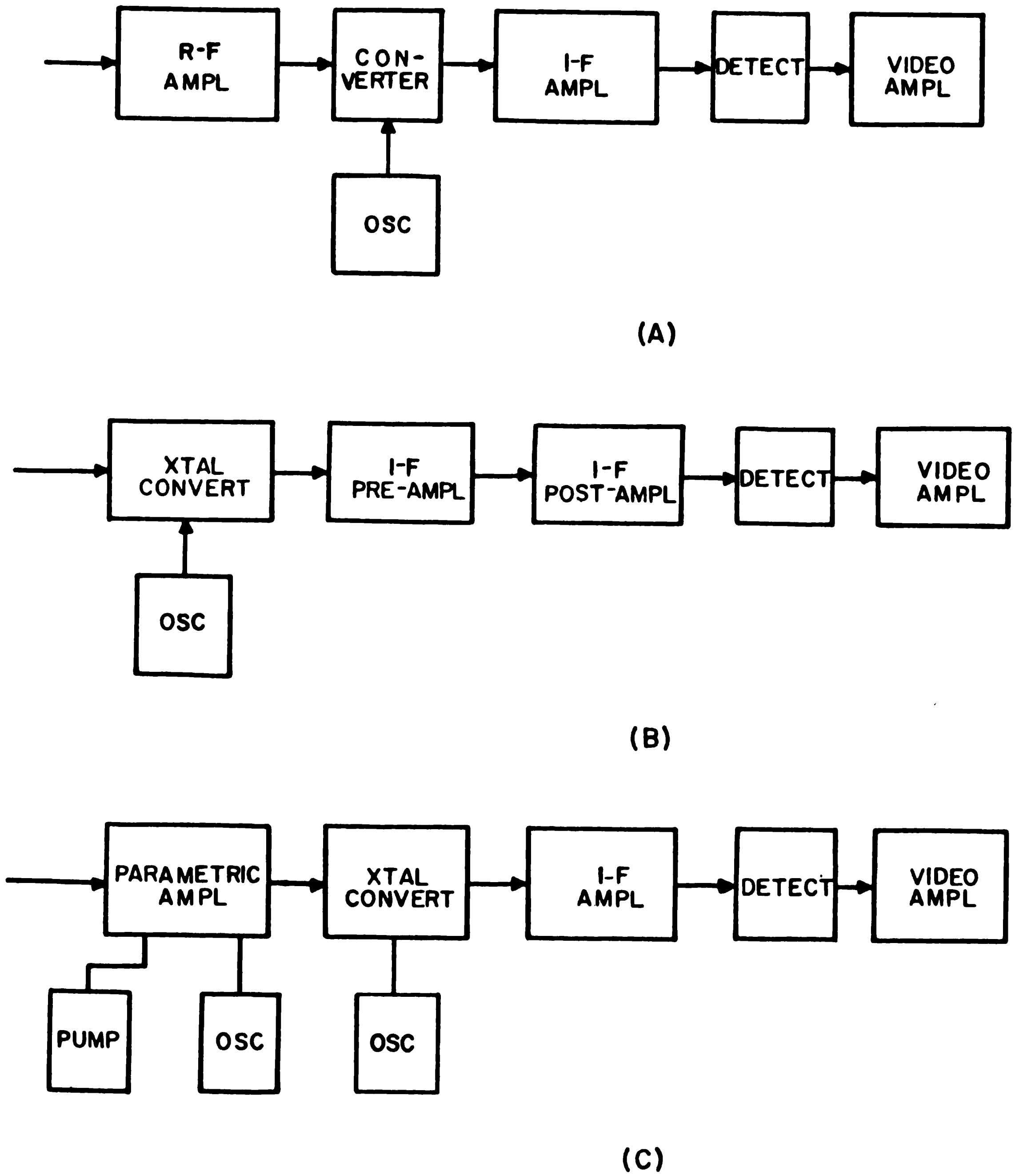

Figure 6-15. Typical Radar Receivers, Block Diagram

the input noise on the grid of the tube which enjoys a gain to the plate of the tube, will always appear as a much less important factor than the noise input from the preceding stages. Typical r-f amplifier tubes that could be preferably used over the lower frequency ranges are usually of the coplanar type. These may be of such types as the 2C39, the 7077, the 6299 and the 416B. The noise factor of these tubes in the range from 400 megacycles to a 1000 megacycles would vary between 5 and 10 db. A more detailed discussion of r-f amplifiers, their design and their characteristics is given in paragraph 6-3.3.3.

The second typical receiver uses a crystal converter as its first stage. Though a preselector would appear desirable with this arrangement, it is seldom used. The frequency range of operation can now be extended to K_u band and even beyond since the performance in regard to noise figure for crystals varies very little over this range. The noise figure of a crystal mixer is a function of conversion loss which is relatively independent of frequency. With the best crystals it is possible to obtain a receiver with a noise figure varying from 6 to about 12 db over this frequency range. A necessary part of such a successful head end presumes that it is carefully matched to a low noise cascade i-f stage using such low noise tubes as the GE 7077 or the Western Electric 417A.

From this discussion it is evident that the receiver design employing an r-f stage in the 60 to a 1000 megacycle range has only a slight advantage as far as noise figure is concerned. Since most radar receivers were originally located where spurious responses from other systems were not likely to be troublesome, the receiver using the crystal converter was simpler, hence more reliable. Therefore, the crystal converter for a first stage in a radar receiver has been used in the majority of head end applications.

In order to avoid the degradation which would be suffered if the local oscillator signal contained excess noise, a balanced crystal arrangement is often preferred. This popularly takes two forms, the so-called magic T balanced mixer and the hybrid coupler mixer. Both of these arrangements cause the oscillator injected noise to be cancelled out in the input circuits of the first i-f stage since its phase is reversed in the two crystals.

Insofar as sensitivity and noise figure are concerned, both the r-f and crystal converter receiver head ends have been improved recently by the addition of the parametric amplifier which is shown as the third receiver block diagram in Figure 6-15. With the best parametric amplifier available today it is possible to improve the noise factor of a receiver by a factor of three to one for frequencies up to C-band (5000 megacycles). The parametric amplifier uses a special diode. Due to the variable reactance obtained in this diode which responds to applied pump energy, low noise amplification at the signal frequency is accomplished. However, little is known about the performance of such amplifiers for frequencies above 5000 megacycles and it may be presumed that crystal converters will enjoy popularity in the region above 5000 megacycles for some time.

6-3.3.4 Bandwidth

The amount of selectivity which is incorporated in radar receivers is determined both by the type of pulse and by the local oscillator-transmitter stability. The i-f bandwidth generally must be wide enough to give a reasonably accurate pulse shape reproduction. If the i-f bandwidth is too narrow, the pulse will appear rounded on the corners instead of square, and all the possible energy of the pulse will not be satisfactorily passed through the chain of i-f amplifiers. Accurate pulse reproduction is particularly important in tracking radars. If the i-f bandwidth is too wide, excess noise is amplified into the output of the receiver and the signal-to-noise ratio will be correspondingly degraded. In general, the i-f bandwidth must be at least $\frac{1}{\text{pulse length}}$. For example, if the pulse length is 10 microseconds, the i-f amplifier pass band must be at least 100 kc. In many instances the receiver bandwidth is made appreciably wider because either special functions must be performed by the receiver or stability considerations dictate the wider i-f bandwidth. Only in the case of extremely stable oscillators, which are either cavity or crystal stabilized, will the minimum bandwidth suitable for faithful pulse reproduction be possible. An excellent discussion of optimum receiver bandwidth for various types of pulse shapes is given in Volume 24, MIT Radiation Lab Series, page 208.

6-3.3.5 Selectivity

Radar receivers usually are not required to furnish a given performance when operating very close to adjacent or alternate channels. In view of this, desensitization specification and selectivity figures at alternate frequencies usually are not made part of the specifications. Instead, as indicated above, the bandwidth of the receiver is determined by the type of pulse to which a receiver must respond. Neglecting for the moment such interference consideration as man-made or natural jamming, the selectivity associated with individual i-f stages is such that gain and bandwidth considerations are often more important than skirt selectivity. For a nominal bandwidth, a single tuned coil or coupling element is frequently used. For a wider bandwidth, double tuned i-f transformers may be called upon to perform the bandwidth controlling function. Where very wide bandwidths are required, multiple-tuned coupling elements with staggered tuning may be used.

In cases where it has been necessary to add adjacent channel selectivity to the radar receiver, a very practical solution has been the use of a pre-selector. Ideally this pre-selector would be one which would accept only the frequencies required to reproduce a desired pulse and reject all other frequencies. A voltage tunable version of this type is the forward wave amplifier. This, in many instances, particularly at X-band, requires such high Q elements as to preclude a successful design. Instead the designer is required to make use of passive devices, such as cavities or microwave line filters. For these, an additional consideration is insertion loss. Ordinarily the sharper the filter, the greater the insertion loss. Since this transmission loss subtracts from the sensitivity of the receiver, this is another design consideration which determines the practical bandwidth of the preselector. Though not many are presently used, primarily because of their insertion loss factors, it appears that there may be a distinct advantage in having a matching i-f filter between the first converter and the i-f amplifier.

6-3.3.6 Stability

The radar receiver is ordinarily required to raise a receive signal from the microvolt level up to approximately the one volt level. This amounts to about a 120 db voltage gain. Any unwanted feedback loop must be minimized as much as possible to avoid instability.

Stability problems are generally of two types – overall and individual stage. Overall stability problems are those where the undesired feedback loop is around the entire receiver. These problems may be aggravated by:

(a) increasing the overall gain requirements
(b) reducing the size of the amplifier
(c) poor filtering in the power supply mains
(d) inadequate shield enclosures

and in general, by increasing the operating or the intermediate frequency amplifier frequency. A logical solution to reduce the overall feedback is to divide the high gain amplifier into a pre-amp and a post-amplifier to reduce the total gain present in any one amplifier strip.

Another way of minimizing instability is to make use of the double or triple superheterodyne technique. The amount of gain contained in the receiver at any one frequency is reduced; for instance, 60 db of gain at the high i-f and 60 db of gain at the low i-f.

Another means of avoiding overall feedback is to keep the interconnecting leads which are fed to each amplifier well separated whether they are coaxial or straight wire. The individual amplifier stages should also have a reasonable physical separation in their mounting. They should be well grounded both through the coaxial cables and through direct contact to any mounting strip bracket.

Feedback or instability around an individual stage may be controlled by controlling

(a) the maximum gain of the stage
(b) the plate-to-grid capacity of the tube
(c) the impedance into which the tube works
(d) the by-passing of the output currents so they do not recirculate to the input of a particular tube or to another stage of the overall amplifier.

Pentodes used as amplifier tubes usually have a high gain. Potential instability may be controlled by grid-bias cathode degeneration or by lowering the plate voltage. A decided advantage of the pentode, however, is that the grid-capacity is several orders of magnitude lower than the typical triode so that this feedback path is reduced to a minimum.

The impedance into which the tube works can ordinarily be made either low enough to be ignored, or if high, have the phase of the impedance be such that it will cause no feedback problem. One of the most important considerations in individual stage feedback or instability is that of by-passing the proper area or element in the tube. Where a screen grid tube is used, it is very important to have a proper screen by-pass capacitor. It can be shown, in addition, that a certain amount of under by-passing of the screen may neutralize the effects of grid-plate capacity. This implies that the condenser must return to a true ground potential point (preferably on the chassis itself), and the condenser itself must have the lowest possible residual lead inductance.

The next most important by-pass is the plate return by-pass. This condenser is returned to d-c ground, and if so, then the cathode also must have a good low impedance by-pass to allow the a-c current from the chassis ground to flow back into the cathode from which they originated. The cathode by-pass also allows the other currents, such as those due to screen current, to flow back to the cathode of the individual tube. It is ordinarily good practice to make the cathode by-pass at least ten times smaller an impedance at the operating frequency than that of the self-biasing cathode resistor.

The remainder of this discussion of receiver design considerations will cover the individual building blocks of the receiver. Where necessary, typical block diagrams will be given. Typical performance characteristics as well as important design considerations will be included in the discussion and will be supplemented by graphs and other diagrams.

6-3.3.7 Video Amplifiers

This is a device used to amplify, shape (if necessary), limit and otherwise process the video signal so that it may be made useful for displays, computers, or for range and error tracking circuitry. In its most elementary form the video amplifier may take the form shown in Figure 6-16. External control signals such as gates and triggers may be introduced in addition to the basic video. Other types of circuits which are called upon to act on the signal in a video fashion are:

(a) automatic gain control (AGC)

(b) automatic frequency control (AFC)

(c) sensitivity time control (STC)

(d) fast time constant (FTC)

For a more complete discussion of each of the above see Volume 23 of MIT Radiation Lab. Series.

TYPICAL REQUIREMENTS

Unless otherwise specified it may be assumed that the video detector is an amplitude rather

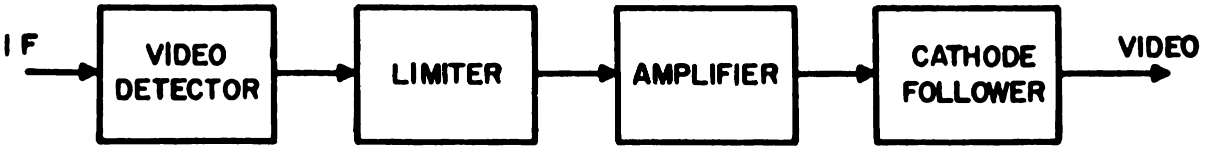

Figure 6-16. Basic Video Amplifier, Block Diagram

than a phase detector. Its time constant is usually made 10 to a 100 times greater than $\frac{1}{f}$ where f = the i-f amplifier frequency. However, this relationship generally is non-critical and wide variations are permissible. It is important in radar tracking systems to have good high frequency response without droop. A final consideration to the video amplifier designer is the avoidance of all undesired distortion in the video amplifiers such as pulse stretching or long recovery time after a large block of signals like ground clutter. Proper filtering of the power leads is important because the video amplifier lower cutoff frequency may be close to the power frequency being used. It is also important in the physical and electrical construction to take adaquate precautions to minimize hum pickup.

Transistors, triode tubes and pentodes can be successfully used as video amplifiers. Usually a video amplifier has a low output impedance when it takes on the role of a line driver.

LIMITERS

Where the output of the video circuitry is to be fed directly to a PPI or some similar form of display it becomes necessary to limit the video. This is because of the very limited dynamic range (10 to 15 db) of the PPI. Signals much above noise very often tend to cause undesirable blossoming on the PPI screen. Transistor, tube, and diode limiters are being used, though the tube type seems to be preferred.

BANDPASS CHARACTERISTICS

Once the limit level is set, not much further gain is required in the video amplifier. Ten to sixteen db is a typical range of post limiter gain values. The designer finds this low level of gain both desirable and convenient since it makes it easier to cope with hum pickup, transients, and unwanted gates, as well as spurious responses. Obviously amplitude limiting is not possible when such amplitude comparing circuits as error detectors or Doppler data are involved. The lower limit of the bandwidth of a video amplifier is ordinarily determined by the repetition rate. The upper limit is determined by the received pulse rise time desired. Because of the absence of filaments, a transistor video amplifier is inherently less troubled with hum pick-up than a tube video amplifier.

6-3.3.8 I-F Amplifiers

An i-f strip or intermediate frequency amplifier is the distinguishing characteristic portion of the superheterodyne system, since all the gain is obtained at one frequency and only the head end is tuned. This permits repeatable stage design and reasonable selectivity characteristics to be used.

INPUT-OUTPUT CHARACTERISTICS

Typical i-f amplifiers may be categorized in several fashions. The first of these is the relation by which the output voltage is made to vary as a function of the input voltage. The most elemental of the receivers is the linear receiver whereby the output voltage is a linear function of the input voltage. A representative range of linear characteristics would be about 40 db. Greater ranges of linear characteristics can be obtained by a careful design. A second type in this category is the log receiver, i.e. the output is a log function of the input voltage. A final type of amplifier scheme which is most often used in tracking or scanning beam systems is that by which the output voltage is related to the input voltage by means of an AGC servo loop. By means of a good AGC, the output voltage can be held to within a narrow range over perhaps an 80 db range of input signals. The linear receiver is often used in the more simple type of search radar. The log receiver is most popular in the more sophisticated search radars or preceding some type of MTI processing.

INTERSTAGES

A second way of categorizing i-f amplifiers is by means of the interstage coupling circuits. Basically those most commonly used fall into three types. These are: the single tuned amplifier, the transformer coupled amplifier and the stagger tuned amplifier. A single tuned amplifier has good transient response; however, the overall bandwidth reduces as stages are seried together. Both the staggered tuned and the transformer coupled amplifier have transient responses which are inferior to that of the synchronously tuned amplifier. However, where a wider bandwidth than can be furnished by the synchronously tuned amplifier is required, the transformer coupled amplifier is able to cover the bandwidths up to 15 megacycles. A fourth and somewhat unrelated type of amplifier, whose interstage may be a form of one of the above three, is the feedback pair. Because of its high gain bandwidth ratio when used with such new tube types as the E180F, this type of amplifier is being sought as a means of optimizing circuitry.

CHOICE OF INTERMEDIATE FREQUENCY

At first the designer is confronted with a seemingly infinite choice of i-f frequencies. As a matter of practicality this choice is actually somewhat limited. Considerations such as image rejection, stability requirements, availability of components and general know-how may govern the final choice. One of the most popular intermediate frequencies is 30 megacycles. It can be shown that this frequency lies about midway within a lower plateau where the overall noise figure of a crystal converter system can be optimized. In X-band systems where image rejection or AFC problems must be taken into consideration, 60 megacycles is often used.

CHOICE OF COMPONENTS

The miniature vacuum tube types which are in common use in i-f amplifier stages offer a somewhat limited selectivity. In addition to the E180F already mentioned, three other popular types of tubes are in common use. These are the 5654/6AK5W, the 6AU6 and the 6AH6. Of the latter three the 6AU6 has a considerably higher reliability rating. A tube type related to the 5654 is the 5725/6AS6W or the suppressor grid control tube. This tube has a reasonably good control characteristic because of a moderate gm available on the suppressor grid. It is often used where gating and gain is required because the signal can still be amplified from grid to plate while sufficient control, established by means of the suppressor grid, can be used to provide adequate gain reduction or gating. Among the subminiature tubes available, should system design considerations call for their use, are the 5702, 6843 and 6205. Transistors which may have useful applications are the 2N502 and 2N1141. A high alpha cut-off characteristic is very desirable in the latter.

HEAD END AND LOW NOISE DESIGN CONSIDERATION

Here, for reasons of low internal tube noise, a triode or simple transistor must be used in place of a tetrode or a pentode. These devices are generally operated with the grid grounded or with a low impedance in the plate of the tube because of the high grid-plate capacitance and the large feedback which can occur at the common i-f frequencies. A typical two stage combination is the Wallman cascade which consists of a cathode grounded stage followed by a grounded grid stage. This satisfies the needs for stability as well as low noise performance. Together these tubes are capable, with proper neutralization in the plate of the first stage, of realizing some of the lowest possible noise figures in the i-f head end. To date there is no comparable transistor circuitry capable of equivalent performance. A fuller discussion of this design technique is given in pages 127-137 of Volume 23 MIT Rad. Lab. Series.

6-3.3.9 R-F Amplifiers

The use of tubes as r-f pre-selectors or radar receiver systems offers some advantages in the region from L-Band downward. In the region up to about 600 megacycles a tube r-f amplifier offers the advantage of low noise sensitivity over a crystal mixer. There exists a gray area between 600 megacycles and L-Band where the decision between tube or crystal must be based on other system performance requirements than those of low noise sensitivity.

Radar systems in the field today and anticipated in the future will probably operate at no lower r-f carrier frequency than 200 megacycles. Therefore the designer's need for low noise r-f amplifiers will be considered for frequencies or systems operating above that frequency only.

TUBES

Because of their definite superiority as low noise amplifiers only triodes need be considered for this application. Among the suitable triodes which may be considered are Western Electric 5280/416B, General Electric 6299 and General Electric 7077. All are co-planer triodes which are demonstratively superior as low noise performers. Of the three available circuit considerations (grounded grid, grounded cathode and cathode followers), only the first offers any real possibility of success as an r-f amplifier configuration. The grounded grid configuration has the following advantages:

(a) wide band matching
(b) stability
(c) good low noise characteristics

The principle difficulty lies in the necessity of gain controlling the grounded grid amplifier. The most convenient method of gain controlling in this stage would be to furnish a d-c bias to the grid, having first adequately by-passed this grid to a-c ground. However, as the frequency of the r-f amplifier is made higher, adequate, reliable by-passes are difficult to achieve in practice so that some other means of gain control must be sought. This usually takes the form of introducing an additional current into the cathode circuit so that the cathode is driven more positive thus causing an additional bias to cut off the tube.

LOW NOISE PERFORMANCE

In the VHF region, lumped constant circuits for r-f amplifiers can be used successfully; in the UHF region (400 megacycles or higher) distributed constant, cavity type construction begin to show superiority. A typical set of noise figure results which can be expected for head ends using tubes over the frequency range is shown as Fig. 6-17. This data was obtained from performance measurements on various systems. It should be pointed out that the triode r-f amplifier, by virtue of its plate-tuned selectivity curve, provides some image rejection capability for the remaining portions of this type receiver. This naturally gives it a certain superiority over the untuned crystal mixers. However, since the r-f amplifier usually consists of only one stage, or at the most two, it must be followed by some form of a converter – a crystal or a tube mixer. The tube converter will ordinarily have a much worse noise figure than the crystal converter, thereby requiring a higher gain of the r-f amplifier itself to offset this disadvantage.

POWER HANDLING CAPABILITIES

Typical r-f amplifier tubes are capable of handling safely duplexer leakage powers at least an order of magnitude greater than that which a crystal can withstand. The crystal mixer following the r-f amplifier can therefore use a lower performance crystal such as the IN25 to an advantage. The r-f amplifier will ordinarily limit and prevent overloading an IN25.

NEWER FORMS OF TUBES

Another form of r-f amplifier tube which may be used in the receiver is called the traveling wave tube. The TWT makes use of the slow wave structure which is confined within a beam of electrons. The electron beam is initially formed by a series of electro-static grids and in its traverse through the tube structure is confined within a helical structure by a strong magnetic field. Energy at the carrier frequency is coupled to the helix through the electron beam. A low noise characteristic is possible with this type of tube. Basically this is a wide band device; bandwidths of 50 percent or more are common. This characteristic implies that some form of filtering must be used subsequent to this tube if undesirable effects of image noise are to be avoided.

A typical receiver using a traveling wave tube head end would probably require double conversion with the first intermediate frequency lying at least in the VHF field to enable a practical wideband filter either at S or X band to be used. This would, in turn, permit the reduction of image sideband noise to a permissible level. The gain of this type of front end is ordinarily in excess of 20 to 25 db, and the noise figure range increases from 7 to 9.5 db at X-band.

Another form of the traveling wave tube is called a forward wave amplifier and uses feedback in its amplifying action. This acts much like the regular traveling wave tube with the exception that it is no longer broadband. Bandwidths are usually less than 1 percent although the gain is comparable to that of the TWT. Noise figures are slightly lower than obtained with the TWT, while the bandwidth is tunable across the operating band of the tube itself by electronically controlling the voltage on the feedback loop. Using this device it is possible, therefore, to have a rapidly tunable front end which is narrow and the fixed tuned filter referred to in the TWT description above is no longer necessary.

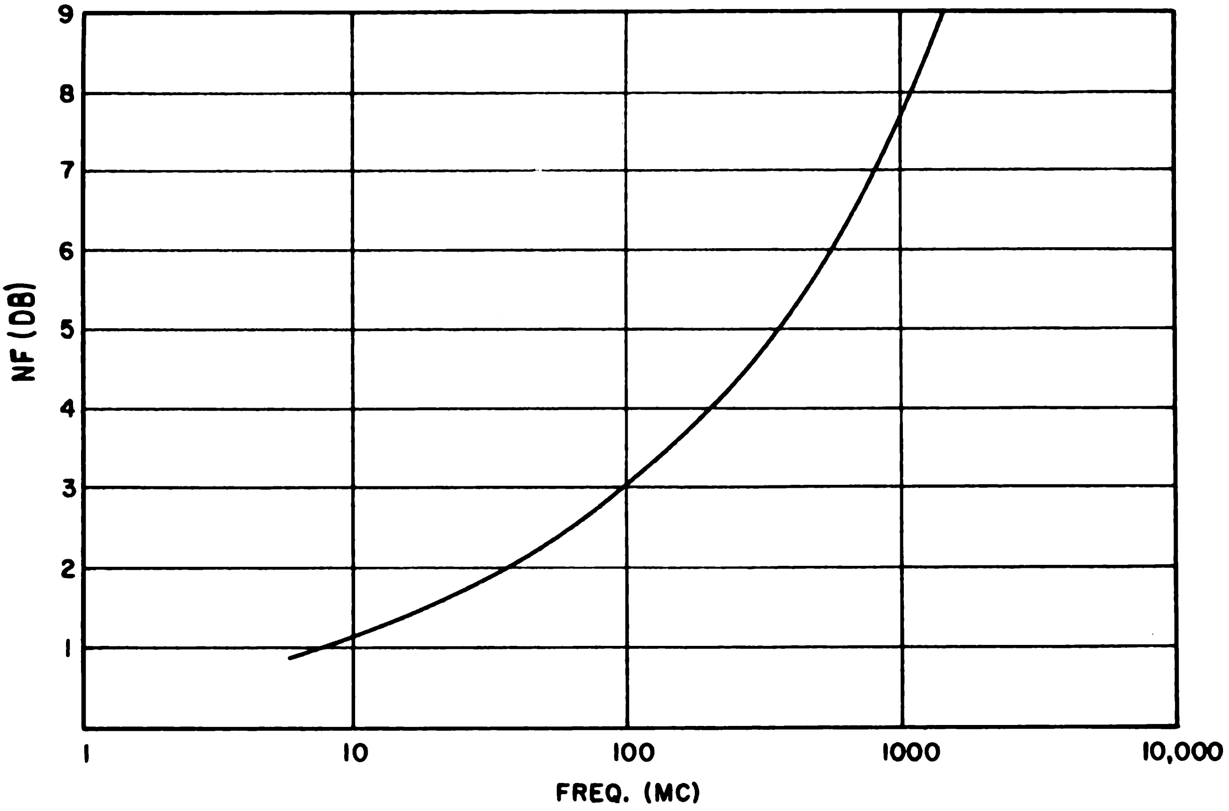

Figure 6-17. Typical R-F and I-F Noise Figure Performance

6-3.3.10 Parametric Amplifier

This type of amplifier is used as a low noise front end over a wide frequency range. It derives its action and benefits through the use of a variable reactance which is analagous to the variable resistance of ordinary diodes. By means of a high level local oscillator or "pump", this reactance (usually a capacitance) is caused to vary in synchronism with pump frequency. When a signal frequency is properly introduced into this circuit, energy from the pump is transferred to that of the signal frequency so that the output appears amplified.

Because this type of amplifier has a high d-c resistance, it does not have a crystal current monitoring possibility such as ordinary mixer diodes do. This means that some other tests for ascertaining the drive level must be in subsequent circuitry. The high impedance level of this amplifier offers a considerable low noise advantage since little noise current flows through the diode; thus, the shot noise is minimized.

TYPES

One of the earliest types of parametric amplifiers used was the so-called *up-converter*. This is the technique whereby a UHF frequency is up-converted to X-band by means of an X-band pump. The gain is directly proportional to the ratio of the sum of the pump frequency and the carrier frequency over the carrier frequency. In addition to the up-converter there are several other types of parametric amplifiers. Among them are the straight through amplifier whereby the input frequency is kept the same as the output frequency. This is a form of regenerative amplification and gains of 16 to 25 db have been realized over a very narrow band. This narrow band incidentally is one of the principal drawbacks of this method. The next type of parametric amplifier is the down-converter which is analagous in action to that of the common crystal converter. However, very little experimentation has taken place in this area and little knowledge concerning the overall characteristics of

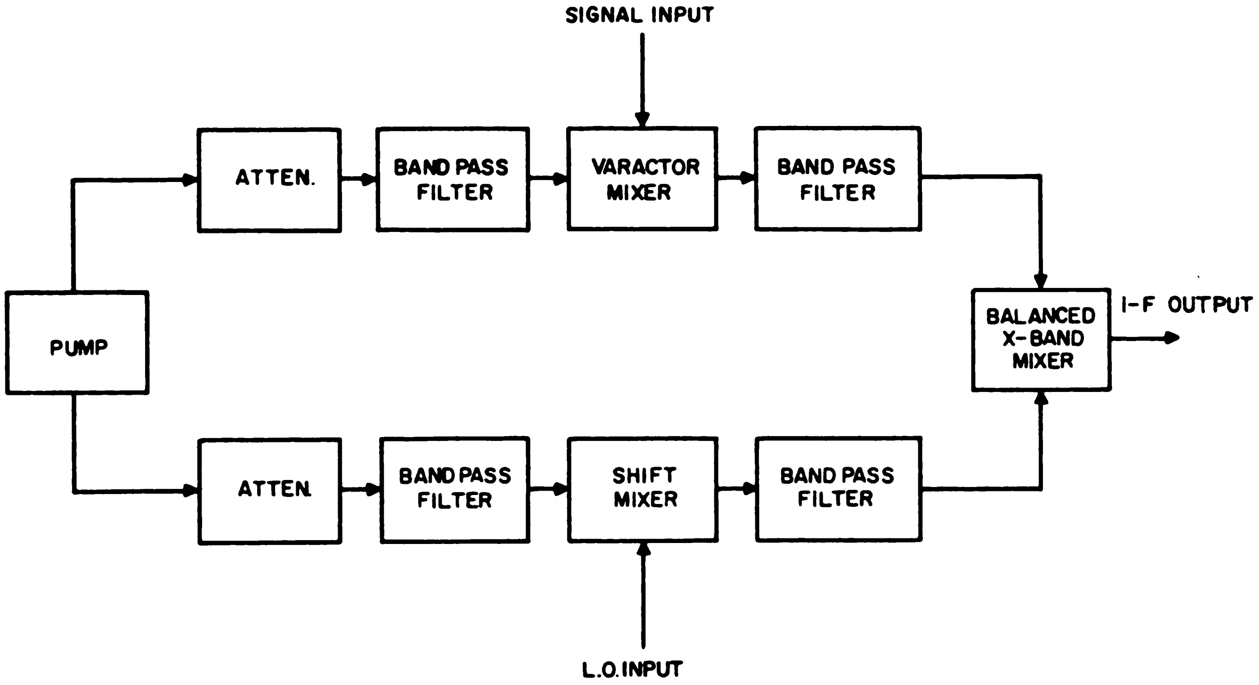

Figure 6-18. Typical Parametric Up-converter

this operation is available. A final type of parametric amplifier is the TWT parametric amplifier. This amplifier is reasonable broad band. (2 percent bandwidths are not unusual.) The amplifier itself is made up much like an ordinary TWT but its action depends on fast wave characteristics and their inter-action with a two times signal frequency pump source. Insufficient experimental data is available to describe the performance which can be expected of the TWT parametric amplifier.

By virtue of its versatility and inherent stability, the up-converter seems to be the most promising type of parametric amplifier. A block diagram of such a typical system is shown in Fig. 6-18. Fig. 6-19 shows the receiver noise figures with and without parametric amplifiers.

POWER HANDLING CAPABILITIES

A less publicized advantage of the parametric amplifier over other types of receiver head ends is their power handling capabilities. Experiments have indicated these devices should be capable of handling CW power levels up to 10 watts peak with a peak power level of almost 100 watts. This is several orders of magnitude

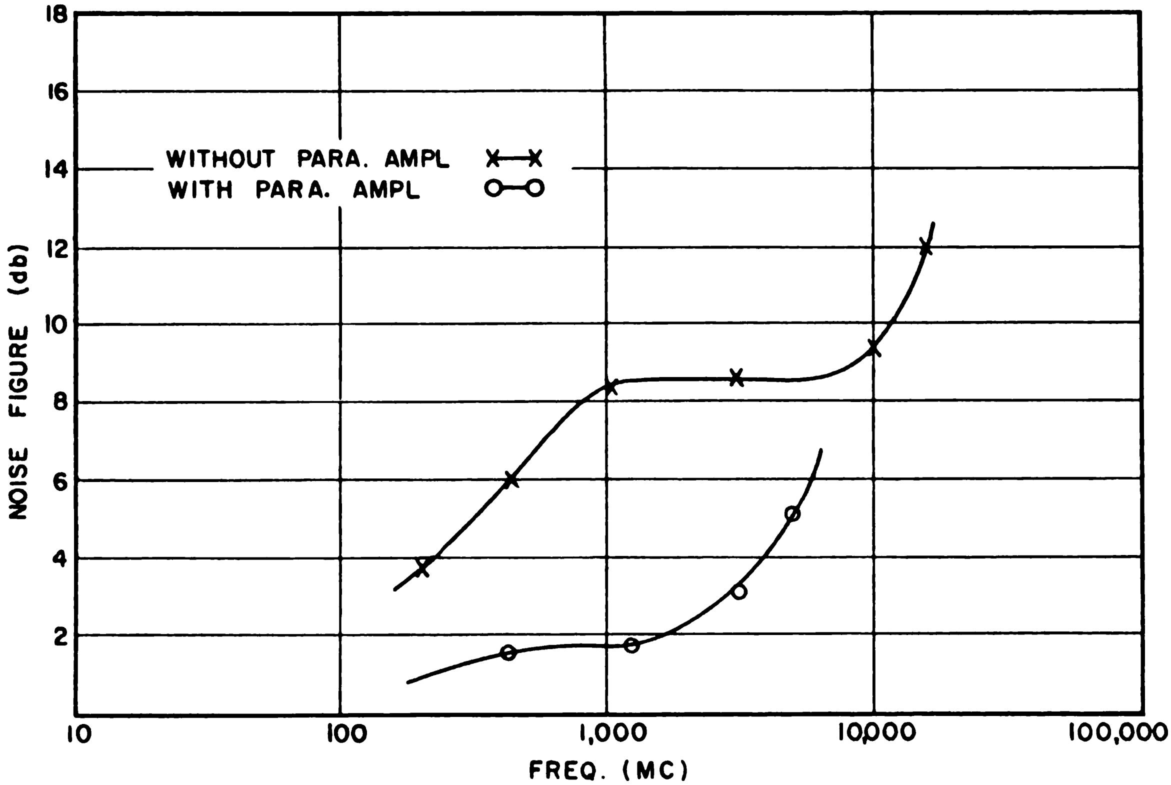

Figure 6-19. Typical Receiver Noise

better than any crystal or low noise tube and should make it possible for this device to become the eventual substitute for either tube or crystal front end.

ADDITIONAL DESIGN INFORMATION

Performance characteristics and other information concerning the parametric amplifier are available only in a few trade magazines such as IRE and internal company reports by those companies leading the investigation of the field such as General Electric, Bell Telephone, RCA and IBM.

6-3.3.11 Maser

The maser is another type of high sensitivity low noise front end which may have some special applications where weight and complexity are not design considerations. The maser amplifier differs from r-f amplifiers and other low noise front ends in two main ways. First, they make use of bound electrons rather than free electrons; second, they use r-f energy rather than d-c energy as a source of power for amplification. The magnetic moments of electrons in a stimulated emission state are the basis for the operations of the solid state maser.

The maser together with the parametric amplifier in its simplest form acts as a negative resistance. This means that it forms a regenerative amplifier and as such has a characteristic that the square root of power gain times bandwidth is a constant. The maser has one major defect: in order to have the full benefits of its operation, it must be operated in an atmosphere of either liquid helium or liquid nitrogen. In addition it requires a piece of material which has appropriate energy levels when placed in a d-c magnetic field. An assembly is also required that will not attenuate the strong r-f magnetic fields in the vicinity of the maser cavity. These three characteristics may limit employment of the maser in radar systems.

6-3.3.12 Sources of Noise

To the receiver designer one of the most important considerations is seeking a means to overcome all sources of noise. The sources of noise can be categorized as follows:

(a) tube noise itself
(b) crystal converter or mixer noise
(c) local oscillator noise
(d) man-made interferences
(e) natural noise

TUBE AND TRANSISTOR

In determining the initial noise figure of an i-f amplifier, tube and transistor noise is the major contributing factor. The noise may be of two kinds. The first of these is shot noise and exists because of irregularities in flow of the electron stream itself. The second is partition noise generated from separation of electrons from the flow which in turn induces voltages within grids or causes electrons to be emitted. Shot noise can exist in any kind of an electron stream, but because it has fewer external connections, a triode will ordinarily be much less noisy than a pentode or tetrode. Shot noise also occurs in microwave diodes but since there is no noise due to separation of the electron stream, partition noise can be largely ignored.

LOCAL OSCILLATOR

This is the noise which may be present in the local oscillators signal itself. In a good local oscillator at UHF band, the signal-to-noise ratio is ordinarily high enough so that this source of noise can be neglected. However, in the reflex klystron which ordinarily serves as a local oscillator for microwave signals, the signal-to-noise ratio is not high enough so that this source of noise can be ignored. Some means such as the balanced mixer, described earlier, or some other means must be used to cancel out local oscillator noise.

MAN-MADE

There are several man-made sources of noise interference which must be considered in the receiver design other than those which are generated by jammers. These include spark caps, distributors, and other similar types of arc-producing, hence noise producing circuitry. These man-made r-f interferences are ordinarily taken care of in the overall system design, so that by proper filtering on the a-c and d-c lines and utilization of shielded coaxial circuitry, they can be minimized.

NATURAL

Extremely quiet microwave amplifiers compels a closer examination of the noise sources which proceed the first low noise amplifier. These are the so-called natural noises. New designs involving characteristics which work to minimize this noise and maximize the incoming return signal must be given careful study. All the noises arising in the free space path from outer space to an antenna itself and the antenna's coupling to the first low noise amplifier must be considered.

An examination of the problem reveals that there are basically eight natural sources of noise:

(a) the sky
(b) re-radiation from absorbing medium
(c) leakage from a warm earth and a minor lobe pattern antenna
(d) poor radiation from a warm earth scattered by particles into the main lobe of the antenna
(e) finite conductivity of metallic antenna surfaces
(f) finite conductivity in transmission lines between the antenna and the low noise amplifier
(g) forward losses to any required duplexing components
(h) leakage from transmitter output stage to the converter

For many applications it is necessary to design a system where the sum of the external noise temperature is very much less than sky noise temperatures. A rule of thumb for this discussion should be to keep the individual excess noise temperatures at one order of magnitude less than the anticipated sky noise temperature.

The noise sources listed above can be described and catalogued as three types:

(a) transmission losses which form losses appearing in the antenna transmission lines and the duplexer
(b) the so-called warm earth noises which are those noises generated by the warm earth itself which reach the antenna
(c) radiation originating from beyond the ionosphere

This latter noise appears to be so fundamental that there seems to be no way of avoiding it. In the evaluation of sky noise, indications are that only 0.01 percent of the sky hemisphere has noise sources greater than 300°K, 2.5 percent are greater than 100°K and only 7 percent are greater than 25°K. Therefore, any object attempting to avoid detection by microwave equipment must avoid being observed against this predominately cold sky background. Obviously this condition is going to be difficult for most targets to accomplish. While sky noise is ordinarily considered as random and stretching uniformly throughout the frequency spectrum, it is actually somewhat frequency dependent. Cosmic noise or noise originating outside of the ionosphere has a negative slope with respect to frequencies so that when frequency is increased, less and less of this noise will cause troubles in a receiver. However, a more positive slope occurs when an examination is made of atmospheric noise characteristics generated by lightning or other similar natural sources.

6-3.3.13 Measurement Techniques

Another problem of the receiver designer is knowing whether the results for which he has designed have been achieved. It is possible for the designer of i-f circuitry to be deceived and misled as to the type of results he is obtaining. All equipment used in testing must be brought to a common low impedance ground. Failure to properly accomplish this basic and initial condition can make any later measurements and design efforts of little or no value.

In order to determine both the shape and the width of the receiver bandpass one of the most convenient means available to the designer is the swept oscillator. This in many instances feeds to the amplifier itself a constant or nearly constant signal output whose frequency is made to vary linearly. When this is fed into the receiver and the detected output together with the synchronous sweep is fed to a scope, the overall bandpass can be determined quite accurately. The reading of bandpass can be determined accurately by means of markers preferably generated external to the sweep generator itself and fed not to the amplifier but into the final detector itself and hence into the scope without passing through the amplifier. Interactions of any AGC loops and the swept oscillator must be minimized for the measurements to have any significance.

One of the best means of measuring gain of a receiver is by means of a modulated signal. Most signal generators have a capability of being modulated at either 400 or 1000 cycles. In the detection of this envelope and its variation as the input signal level is changed, the designer can use the insertion method of measuring receiver gain. This can be done by placing a step-attenuator whose steps are accurately known between the signal generator and the test receiver. An initial level is set using a traveling detector. Then the receiver itself is inserted beyond the attenuator and sufficient attenuation inserted so that the original signal level is re-set at the output of the traveling detector.

An oscilloscope examination of the overal swept bandpass of a receiver using the sweep generator described above should give a bandpass which, if the receiver is properly designed, will approach the desired bandpass very closely. Sharp peaks and valleys in the top sides of this bandpass are ordinarily indications of some type of undesirable regeneration. It should also be possible in a good receiver design to adjust the output of the amplifier by means of grid bias control through its entire range of adjustment so as to be certain that no unusual distortion of the overall swept bandpass occurs during such an adjustment.

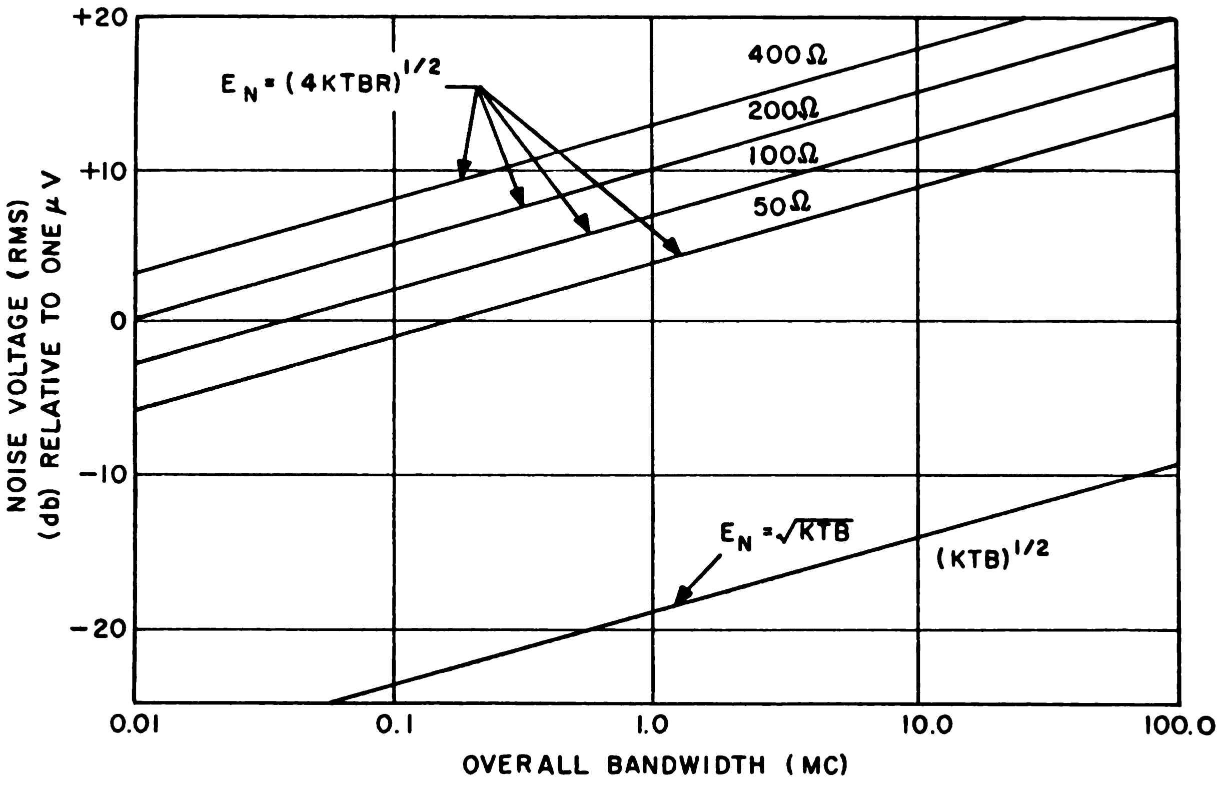

Figure 6-20. Noise Voltage Versus Overall Bandwidth

6-3.3.14 Tables and Graphs

A set of tables and graphs which cover some of the basic design elements is included as a final part of this section. The first of these, Fig. 6-19 shows the up-to-date performance of receivers with their noise figure optimized versus frequency. The upper line of the graph shows the receiver capability without using a parametric amplifier head end; the lower line shows the anticipated performance if a parametric amplifier is added to the receiver. Since it forms a part of the receiver designer's basic information several forms of curves showing the variation of Johnson noise with overall bandwidth are included in Fig. 6-20. Table 6-3 shows some dynamic range versus receiver type and the final graph showing phase shift versus AGC is shown as Fig. 6-21. This is often an important design consideration for monopulse receivers.

It is impossible in such a short discussion to give more than a broad brush to all facets of receiver design. For those wishing to delve into additional design considerations, references 44 through 54 give a broad enough coverage so that the receiver designer should be able to find most of the design principles he needs. Of invaluable use to the beginning receiver designer are Volumes 23, 18 and 16 of the MIT Radiation Laboratory Series.

TABLE 6-3. I-F AMPLIFIER DYNAMIC RANGE CAPABILITIES

I-F AMP TYPE	DESIGN WITH NO SPECIAL PRECAUTIONS	DESIGNED WITH SPECIAL PRECAUTIONS
LINEAR	40 db	65-70 db
LOG	80 db	100 db
AGC	60 db	80-100 db

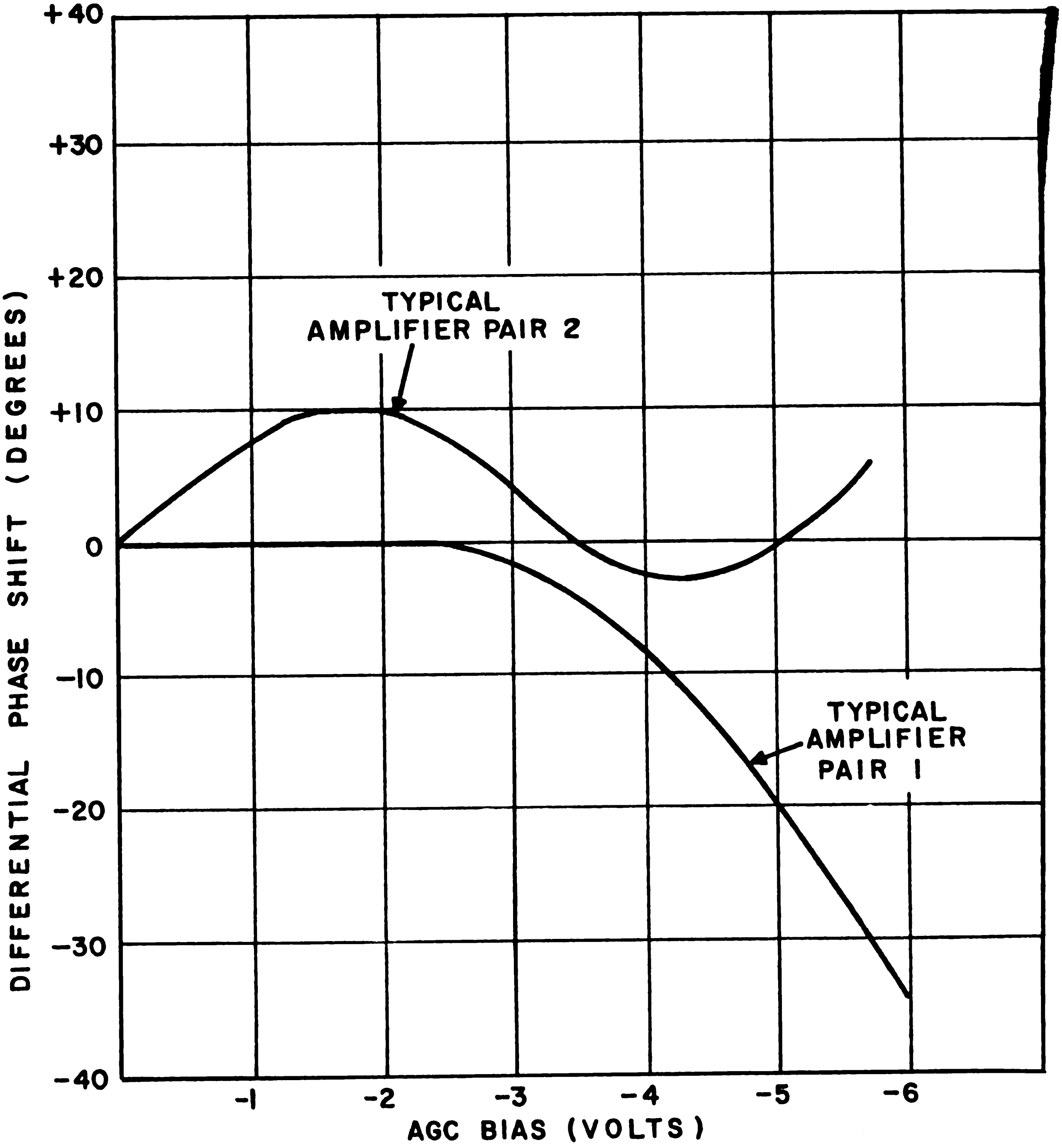

Figure 6-21. Differential Phase Shift Versus Gain Bias

6-3.4 DETECTION

6-3.4.1 General

The detection of a radar signal implies the discovery of echoes from a target. Detection may be accomplished either by an operator using visual indicators, or automatically by electronic detection circuitry. Several methods of detecting the signal are presented in this section along with design curves for calculation of the range at which a target can be detected to a specified degree of certainty cr probability.

For most radar systems an understanding of detection as defined above requires understanding of the signal processing from the i-f amplifiers to the visual indicator or threshold detection device. Several typical block diagrams of this are shown in Figures 6-22 and 6-23.

When a target return is not related or referenced to the transmitted signal in phase and frequency, then the system is said to be noncoherent and the detector detects the envelop of the return signal. If, however, the return signal is referenced to the transmitted signal in phase and frequency, the return signal is coherent and may be detected by referring to the phase of the transmitted signal.

The probability of detection of a target for a given range may be increased by integration (adding) of the target returns for a period of time (integration time). The signal can be integrated in the r-f stages, in the i-f stages, or in the video stages. Furthermore, there can be one or more linear or square law detectors present and the integration can be done in one or more steps and in at least two different ways. Fortunately, the various cases show little difference, with one marked exception. R-f and i-f integration are better than video integration for small signals (compared to noise). To take full advantage of i-f or r-f integration, the successive received pulses must be coherent.

Practical types of pulse integrators often take the form of narrow band audio filters having their center frequency at the pulse repetition frequency or some harmonic thereof. The action of such a filter can be understood by consideration of the frequency spectrum of a finite group of N pulses. The envelope of such a spectrum is simply the familiar $\frac{\sin x}{x}$ curve of a single pulse where the actual curve has appreciable values only in the neighborhood of the harmonics of the repetition frequency. The greater N, the more closely the spectrum cluster around these harmonics. Thus, the filter may be made narrower, excluding more and more noise, but retaining most of the signal energy.

6-3.4.2 Non-coherent Integration

Detection of a target may be accomplished either by an operator using a visual indicator such as an oscilloscope, or automatically with the aid of an electronic threshold detector. Radar performance with visual detection is discussed below in terms of a visibility factor, V, which is evaluated by experimental data using operators observing indicator displays. Automatic detection processes based on mathematical calculations of the radar detection range will then be described.

VISUAL DETECTION

The range equation may be written

$$R = \left[\frac{P_t G^2 \lambda^2 A_r}{(4\pi)^3 K T_0 B \overline{NF} V \delta} \right]^{1/4} \qquad (6\text{-}16)$$

where V is the visibility factor. All the factors described in the expression have been explained (see paragraph 6-2) except the term V. This factor can be viewed as a quantity which is chiefly concerned with the human reaction exhibited by a radar operator as various system parameters are varied. The parameters of V which contributes a major influence on the performance of the radar system are:

(a) product of i-f bandwidth and pulse length (BT_P)

(b) video bandwidth and sweep speed

(c) pulse repetition frequency (f_r)

The effects of V will be more fully explained in paragraph 6-4 and the relationship

$$V = \left[\frac{\frac{1}{2}(1+1)}{BT_P} \right]^2 \times \left[\frac{13}{f_r} \right]^{0.371} \qquad (6\text{-}17)$$

will be derived and a sample calculation on a radar system using visual detection will be illustrated.

Automatic detection of a signal is accomplished with the aid of a threshold device set to some predetermined bias level. The signal is detected when the output of the receiver exceeds

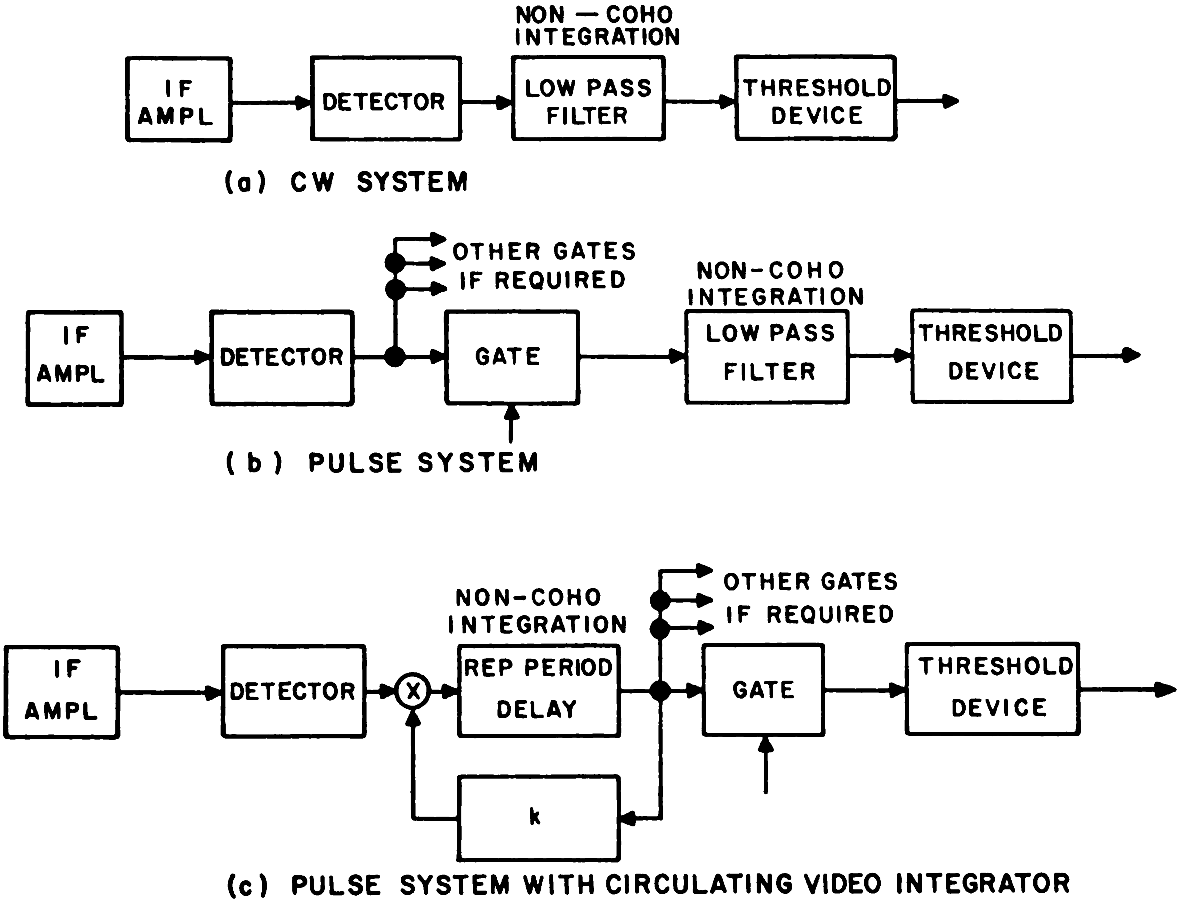

Figure 6-22. Examples of Basic Non-Coherent Systems, Block Diagram

this bias or threshold level. The bias level however, will be occasionally exceeded by noise alone and an erroneous detection or false alarm occurs. The average time between the intervals when noise alone exceeds the bias level is defined as the false alarm time.

The curves for finding the detection range for any specified probability of detection are based on calculations of the probability of the target (plus noise) exceeding the bias level, the bias level having been determined by the false alarm time.

Because of the complex echoing surface of many radar targets, the return echoes fluctuate in amplitude. The means of calculation of range as given here are based on the assumption that the returned signal energy per pulse is constant for the time on target during a single scan but fluctuates independently with a Rayleigh distribution from scan-to-scan.[55]

---

[55] Based on Swerling's Case I. This case gives the most pessimistic results for range. Swerling's Case II, in which the target fluctuates from pulse-to-pulse with a Rayleigh distribution would be applicable to a radar system employing pulse to pulse frequency agility.

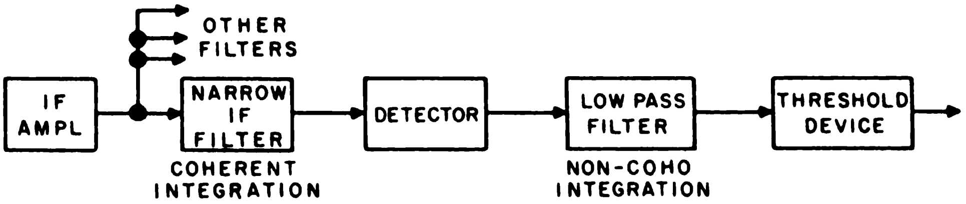

(a) CW SYSTEM

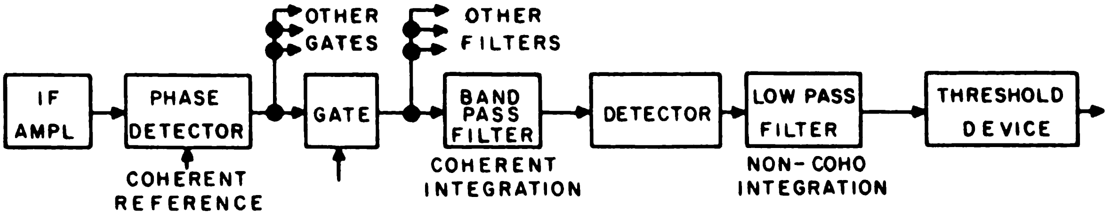

(b) PULSE SYSTEM (BLIND TO SIGN OF RANGE RATE)

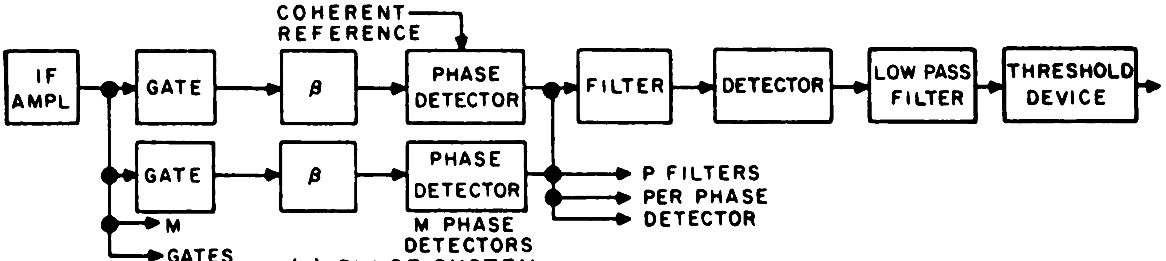

(c) PULSE SYSTEM

Figure 6-23. Examples of Basic Coherent Systems, Block Diagram

The probability of detecting a target at a given range has been shown to be essentially the same whether a square law or linear detector is used in the receiver.

To determine the range at which a target may be detected for a non-coherent pulsed radar system, the range equation may be written as:

$$R = \left[\frac{P_{av}\, G^2 \lambda^2 \quad A_e}{(4\pi)^3 K T_0 f_r \overline{NF}\, BT_p \delta} \quad \frac{1}{\overline{\overline{X}}}\right]^{1/4} \qquad (6\text{-}18)$$

For a pulsed signal, the signal-to-noise ratios given above are valid for $BT_r \geqq 1$. The optimum condition occurs at $BT_P \cong 1$, which will be assumed.

All the parameters of the radar system are known except $\overline{X}$. The value of $\overline{X}$ can be obtained as a function of the probability of detection and of two other parameters, n and N, which are the false alarm number and the number of pulses integrated respectively. n and N may be calculated using the following procedure:

(a) Determine the integration time (T_t). This will be a function of any system requirement which limits the time the target is in the beam – for example: scan rate, antenna beamwidth, and target velocity. It will be assumed that pulses are integrated over the full detection time.

For a scanning antenna, the integration time may be calculated as:

$$T_i = \frac{\phi}{w} \qquad (6\text{-}19)$$

where w is the antenna rotation velocity.

For a moving target, the pulses are changing in range and will not contribute at all to the integration when the range has changed by a pulse length. The integration time is calculated by assuming the pulses contribute their full amplitude when they are ½ the distance where they just fail to overlap, which results in:

$$T_i = \frac{T_p c}{4v} \qquad (6\text{-}20)$$

(b) The number of pulses integrated may now be calculated:

$$N = T_i f_r \qquad (6\text{-}21)$$

(c) The false alarm number, n, defined as the number of independent pulses of noise that occur during the false alarm time, may now be calculated. If the range sweep is continuous (no dead time within the repetition period), then

$$n = 0.693\,\frac{T_{fa}{}^{*}}{T_p} \qquad (6\text{-}22)$$

If the range sweep length or range under surveillance does not occupy the total time between repetition pulses, then:

$$n = 0.693\,T_{fa}\cdot f_r\cdot\eta \qquad (6\text{-}23)$$

$$\text{Where } \eta = \frac{2L}{cT_p} \qquad (6\text{-}24)$$

and L is the range sweep length.

To calculate the range, we may rewrite $\overline{X}$ as:

$$10\log\overline{X} = C(P_d) - I(n,N) \qquad (6\text{-}25)$$

C is the certainty loss, i.e., the penalty i range for increased certainty of detecting a tar get. I (integration gain) is the increase in sy stem performance resulting from the integra tion.

The range equation may be written simpl as:

$$10\log R = 10\log\left[\frac{P_{av}\,G^2\lambda^2 A_e}{(4\pi)^3 KT\,\overline{NF}\,f_r\,\delta}\right]^{1/4} + \frac{I-C}{4} \qquad (6\text{-}26$$

where values for I and C can be obtained from Figure 6-24 and Figure 6-25. These values of I and C are plotted based on the following assumptions:

(a) square antenna beamshape
(b) perfect integration
(c) integration time equals detection time
(d) $BT_p = 1$

A typical beamshape was taken from reference 56 and compared to the results found with a square beam. Calculations show a loss of approximately 2 db ($N \geq 10$) in signal-to-noise ratio for a shaped beam compared to an assumed square beam shape; therefore, this loss may be subtracted for calculations assuming a shaped beam.

Similar calculations show that an exponential integrator, one which discharges on an exponential curve, has a loss of approximately 1.8 db compared to the perfect integrator. This correction may be used for systems employing exponential integrators.

An optimum system results if pulses are integrated over all of the time available for detection. However, this is not always practicable. The amount of loss incurred if the detection time is greater than the integration time is indicated from Figure 6-26, where γ is the total number of pulses available during the detection time. The loss may be approximated from the curve. See reference 4 for a more exact calculation.

For a continuous wave system, the range equation may be written as:

$$10\log R = 10\log\left[\frac{P_{av}\,G^2\lambda^2 A_e}{(4\,\pi)^3 KT\,\overline{NF}\delta\,\Delta f_{cw}}\right]^{1/4} + \frac{I-C}{4} \qquad (6\text{-}27)$$

---

*0.693 is a constant resulting from the definition of false alarm time. The definition as given here, average time between false alarms, differs from Marcum's definition of being the time in which a false alarm has a 0.50 probable chance of occuring or $P_{fa} = (1-P)^n = \frac{1}{2}$.

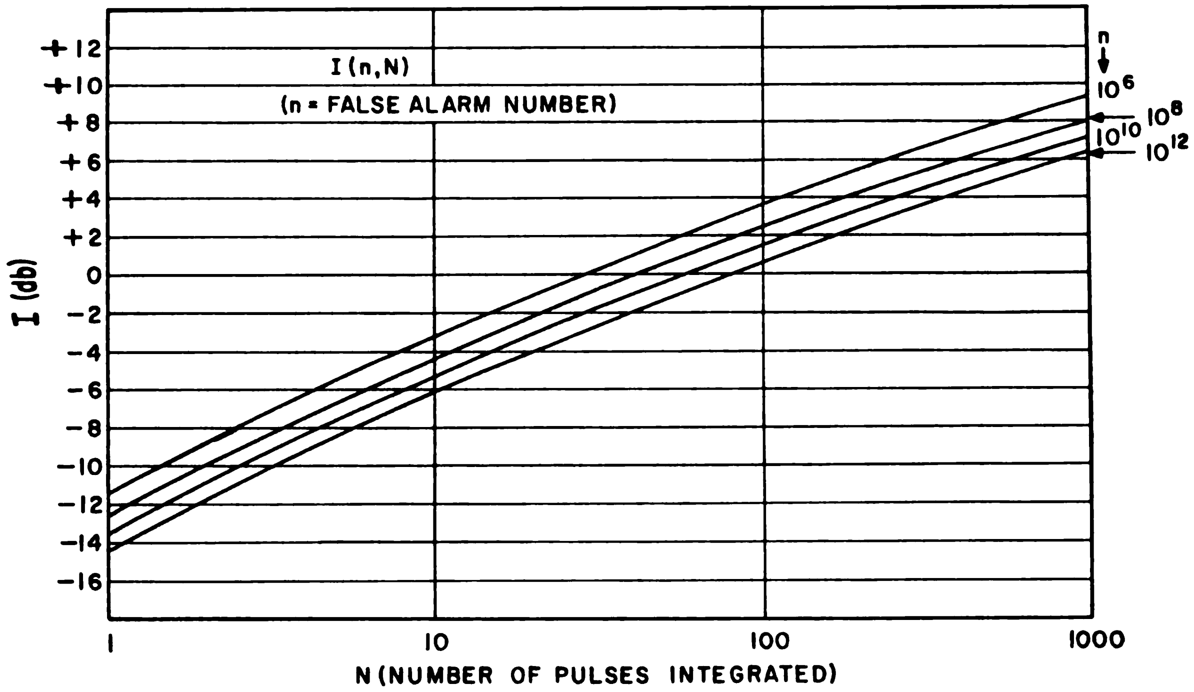

Figure 6-24. Integration Gain

where Δf_{cw} is combined r-f and i-f bandwidth of the receiver. An optimum CW system results if $T_i = \frac{1}{\Delta f_{cw}}$ where the integration time is assumed to equal the detection time. The number of chances for a false alarm in the false alarm time is:

$$n = 0.693\, T_{fa} \cdot \Delta f_{cw} \tag{6-28}$$

$N = 1$ as shown by:

$$N = T_i \Delta f_{cw} = 1 \tag{6-29}$$

$I\ (n,N)$ may now be found from Figure 6-24 and C from Figure 6-25.

The basic block diagrams of three non-coherent systems were given in Figure 6-22.

Figure 6-22a shows a continuous wave system which may be analyzed directly by the techniques described for a CW system.

Figure 6-22b shows the basic pulsed radar system. Different techniques may be used for instrumenting the range gate, such as a single gate, several gates, or a single moving gate scanning over a range. In terms of the type of gate used, η (see equation 6-24) may be more clearly written as:

$$\eta = \frac{2m}{c} \tag{6-30}$$

where m is the number of gates. This requires that the gate width is equal to the pulse width.

Figure 6-22c is a system employing a recirculating video integrator in which k is less than one to prevent regeneration. The advantage of this system is that integration before gating may be used thereby requiring only one integrator. This integrator is an exponential integrator. The integration time may be calculated as:

$$T_i = \frac{N}{f_r} = \log k \ \frac{1}{\varepsilon} \tag{6-31}$$

Equation 6-31 may also be applied for systems using a simple RC filter, that is:

$$T_i = RC = \frac{N}{f_r} \tag{6-32}$$

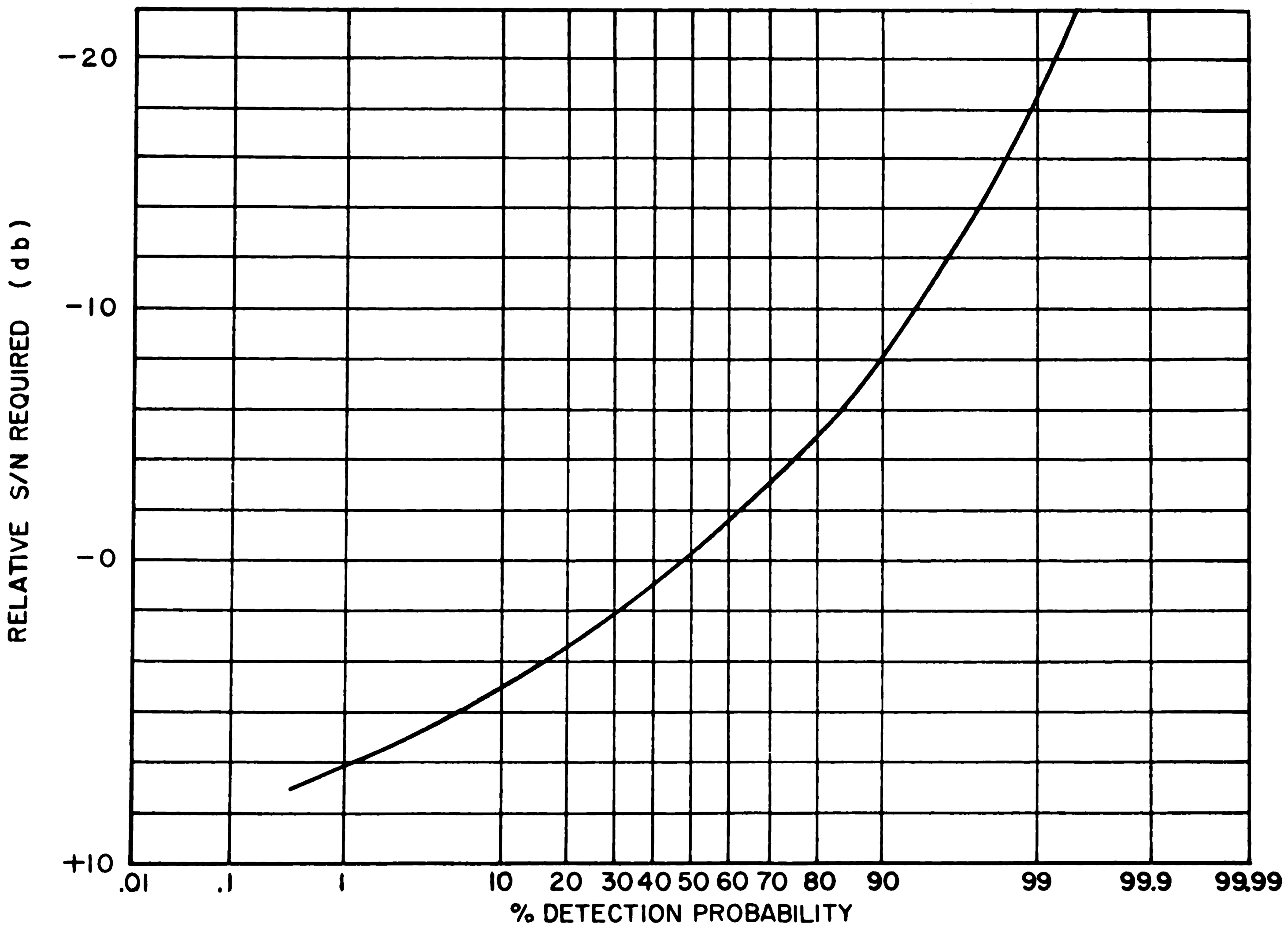

Figure 6-25. Single Scan Detection Probability Versus S/N Ratio

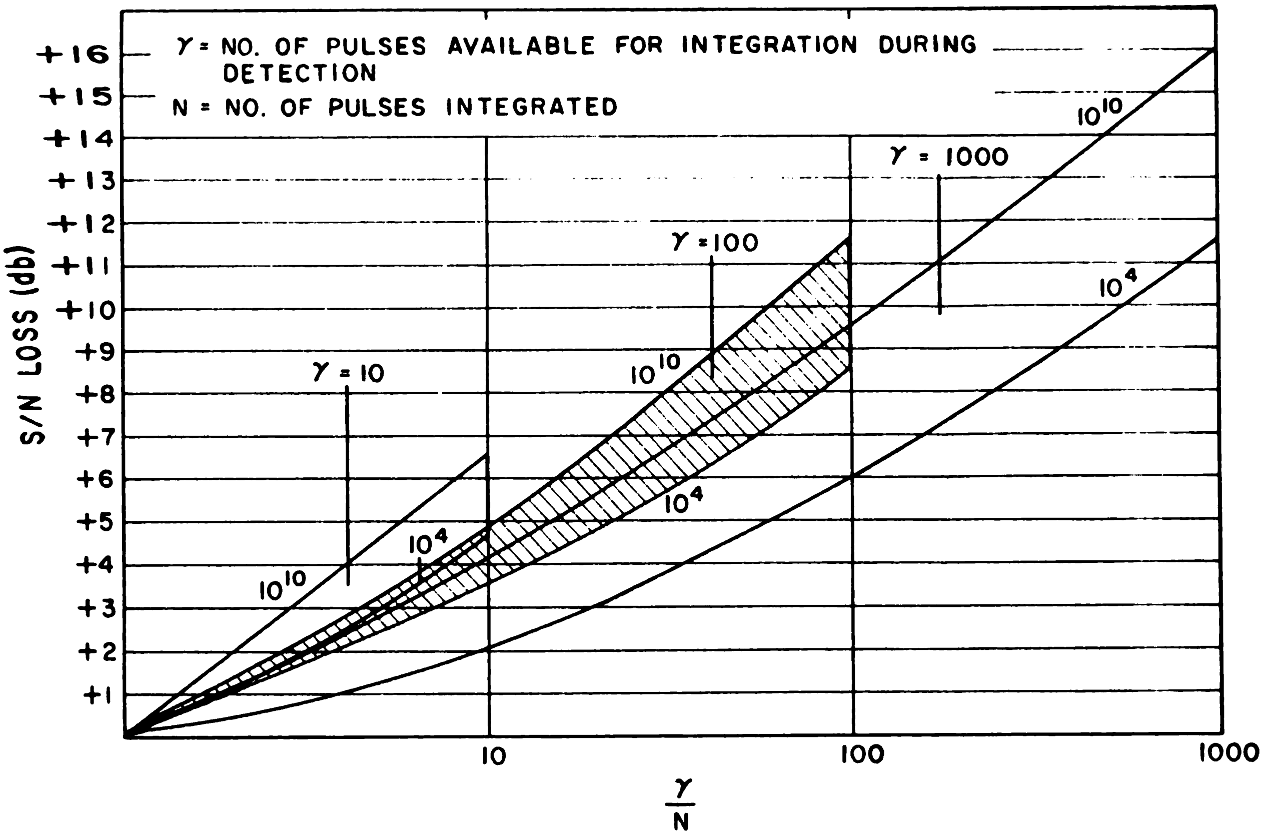

Figure 6-26. S/N Ratio Loss, Detection Time Greater than Integration Time

As a simple example for determining the detection range for a target, the following data will be assumed:

v = maximum target radial velocity = 350 mph
w = angular rate of antenna = 30°/sec
Φ = antenna beamwidth = 3°
f_r = pulse repetition rate = 500 pulses/sec
T_p = pulse length = 1 microsecond
T_{fa} = false alarm time = 10 min
T_d = required detection time = 25 sec
L = surveillance range = 20-80 miles

Assume an exponential integrator, a shaped antenna beam, and, for simplicity, assume the quantity inside the brackets of equation 6-26 is 40^4 miles, i.e.:

$$10 \log R = 10 \log (40^4)^{1/4} + \frac{I - C}{4} \qquad (6\text{-}33)$$

Find the range for a detection probability of 50 percent and 90 percent.

The integration time is determined as:

$$T_i = \frac{\Phi}{w} = \frac{3}{30} = 0.1 \text{ sec} \qquad (6\text{-}34)$$

however, from the target velocity*

$$T_i = \frac{T_p c}{4v} = \frac{10^{-6}(186{,}000)3600}{4(350)} = 0.05 \text{ sec} \qquad (6\text{-}35)$$

It is seen for a maximum velocity target, the pulses will not overlap for the entire time the target is in the beam, therefore, the integration time may be set as 0.05 second.

From equation 6-21:

$$N = T_i f_r = 0.05(500) = 25 \qquad (6\text{-}36)$$

During the detection time, the antenna will scan the target twice, therefore, γ, number of pulses available for integration during the detection time, is:

$$\gamma = 2(25) = 50 \qquad (6\text{-}37)$$

Since the range of interest is from 20 to 80 miles, n is calculated from equations 6-23 and 6-24.

$$n = \frac{0.693\, T_{fa} f_r\, 2L}{cT_p} = 0.693$$

$$\frac{(10)(500)(2)(80\text{-}20)(60)}{(186{,}000)(10^{-6})} = 1.3 \times 10^8 \qquad (6\text{-}38)$$

Now the detection range may be determined:

	$P_d = 50\%$	$P_d = 90\%$
Integration gain (Fig. 6-24) $n = 1.3 \times 10^8, N = 25$	−1.5	−1.5 db
Certainty loss (Fig. 6-25)	0	−8.0 db
Additional factors: $\gamma/N = 50/25 = 2$ (Fig. 6-26)	+1.5	+1.5 db
Loss of shaped beam compared to square beam	−2.0	−2.0 db
Loss of exponential integrator compared to perfect integrator	−1.8	−1.8 db
TOTAL	−3.8	−11.8 db

Then:

$$10 \log R_{50\%} = 10 \log \left[40^4\right]^{1/4} - \frac{3.8}{4} \qquad (6\text{-}39)$$

therefore

$R_{50\%} \cong 32$ miles

and by similar computations:

$R_{90\%} \cong 20$ miles

6-3.4.3 Coherent Integration

GENERAL

Several examples of coherent systems were given in Figure 6-23. In this section the method of calculating the detection range for non coherent systems will be extended for making similar computations for coherent systems. This is done by making direct use of the preceding figures and adding any necessary corrections.

For initial system design, having comparisons of alternatives in clear form is sometimes more valuable than a means of exactly calculating performance of a specific system. One such comparison is the relative performance of post-detection and predetection integration. Figures 6-27 and 6-28 are taken from reference 57 and illustrate this comparison quite clearly. The integration loss is defined as the ratio of signal required for a given probability of detection when post-detection integration is used to the corresponding signal required if predetection integration is used. N represents the amount of post-detection integration in the first case, and may be considered as either a number of pulses or as a bandwidth ratio. It is interesting to note that the integration loss varies little with either the false alarm time or the probability of detection.

RANGE CALCULATION

The CW system of Figure 6-23a is basically the same as the non-coherent CW system. However, several narrow velocity filters or Doppler

---

*It should be recognized that a maximum velocity target will move approximately 1.2 miles from scan-to-scan making this calculation pessimistic for incoming targets. For an analysis of the effect on the probability of detection of a target moving from scan-to-scan see paragraph 6-4.6.

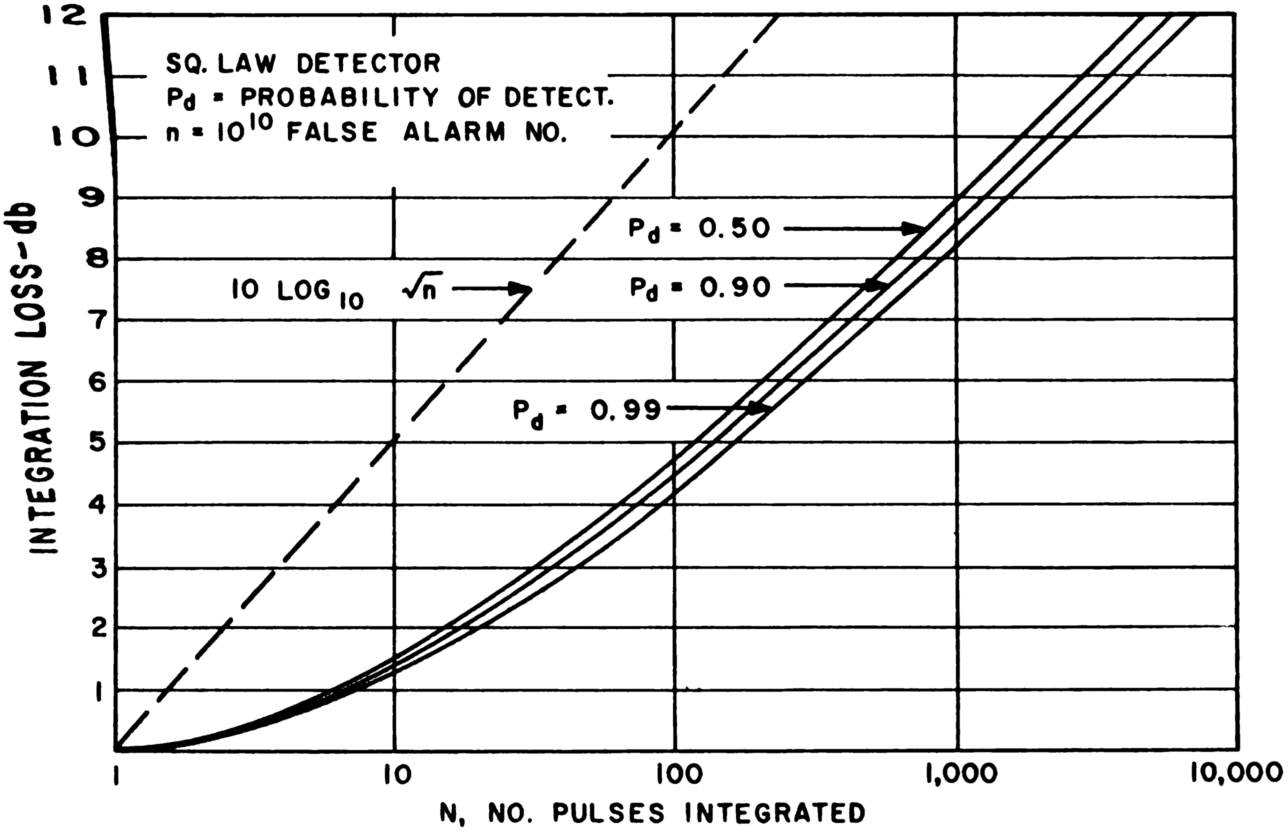

Figure 6-27. Integration Loss, Non-Coherent Versus Coherent (Probability of Detection)

filters have been added. The false alarm number then becomes

$$n = 0.693\ T_{fa}\, f_d\, N \qquad (6\text{-}40)$$

where N is the number of velocity filters and f_d is the bandpass of the filters. N may be calculated as before but by replacing $\Delta\, f_{ow}$ with f_d

$$N = T_i\, f_d \qquad (6\text{-}41)$$

Equation 6-27 may now be employed for determining the range.

The system of Figure 6-23b uses a phase detector to convert the signal to video. It is seen that this system does not retain the sign of the radial range rate; that is, outgoing targets are indistinguishable from incoming targets.

After gating, the noise power spectrum is approximately flat to $\frac{f_r}{2}$. The Doppler filter will increase the signal-to-noise ratio by a factor of $\frac{f_r}{2f_d}$. Equation 6-26 then becomes

$$10 \log R = 10 \log \left[\frac{P_{av}\, G^2 \lambda^2\, A_e}{(4\pi)^3\, KT\, 2\, f_d\, \overline{NF}\, \delta}\right]^{1/4} + \frac{I - C}{4} \qquad (6\text{-}42)$$

As before, $N = T_i f_d$ and the false alarm number is

$$n = 0.693mp\ T_{fa}\, f_d \qquad (6\text{-}43)$$

Where m is the number of gates and p is the number of Doppler filters.

The system of Figure 6-23c employs gating before the final mixer. Each range gate is

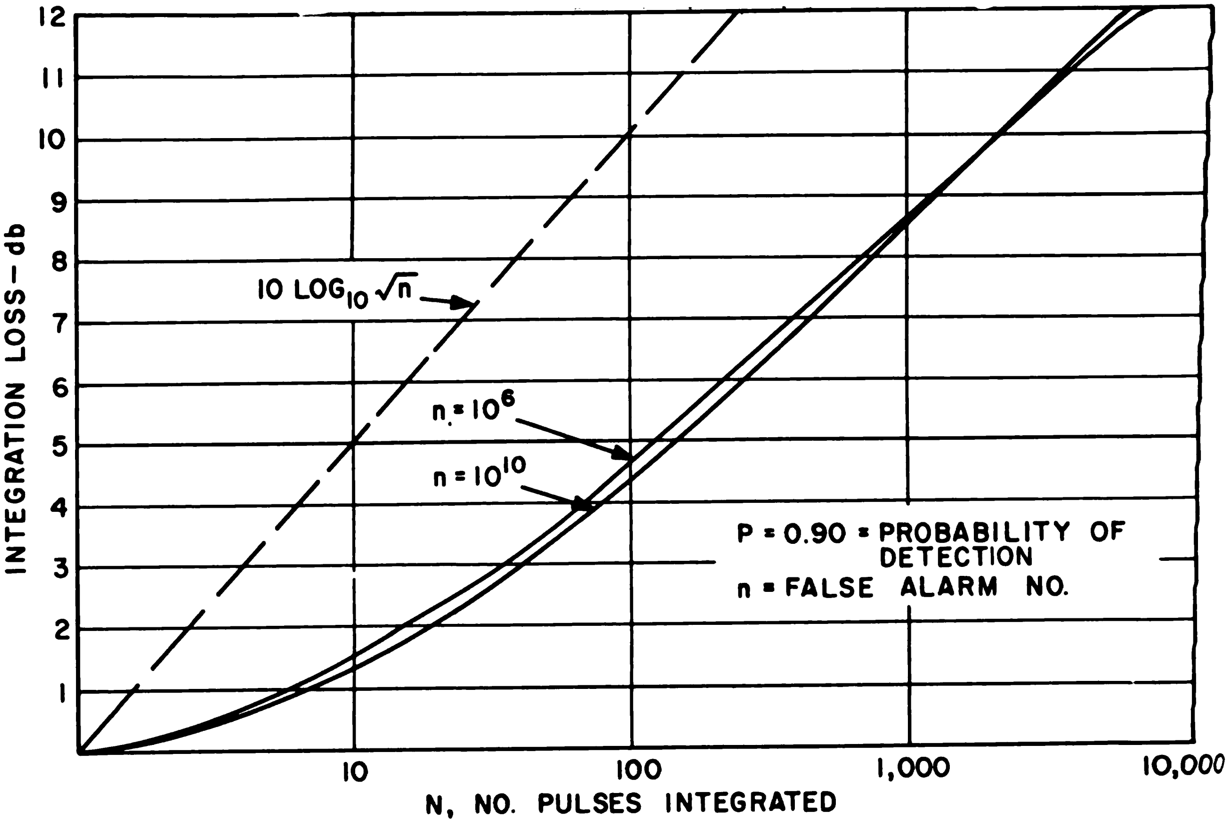

Figure 6-28. Integration Loss, Non-Coherent Versus Coherent (False Alarm)

followed by a filter β of bandwidth f_r centered at the first i-f frequency. It is seen that the sense of the target range velocity is preserved. The signal-to-noise ratio is improved by f_r/f_d in going from the first i-f to the detector which is twice the improvement of the preceding system. For a given velocity range under surveillance, this system, however, must monitor twice the Doppler frequency band as the preceding system (assuming both positive and negative range rate targets are of interest). Equation 6-42 may be employed directly by removing the 2 in the denominator. It is seen that this system gives a 3 db improvement in signal-to-noise ratio.

An extention of the foregoing analysis may be used to analyze the detection performance of other systems.

6-3.4.4 MTI Detection

GENERAL

The fundamental objectives in the design of an MTI radar are:

(a) maximum detection sensitivity to moving targets in clutter

(b) maximum cancellation of undesirable moving objects such as chaff.

The purpose of this section is to give a basic understanding of MTI techniques and the basic method for calculating the performance of an MTI system.

MTI is based on the principle that the return signal from a moving target is different from that of a stationary target. MTI receivers use this difference (the Doppler effect) in one form or another.[58]

In paragraph 6-3.4.1 it was noted that in a herent system, the signal may be detected ith a phase detector instead of an envelope etector. The amplitude of phase detected ideo varies as a function of the target velocity, ince the amplitude of the signal is proportional o the phase difference between the transmitted nd received signal.

Thus, if successive phase detected returns (MTI coherent video) are subtracted, a moving target will yield a finite residue since the successive video pulses vary in amplitude, but a stationary target will not yield a residue since the successive video pulses do not vary in amplitude. It would then seem that the ratio of the residue from a moving target is infinite compared to a cancelled stationary target. Unfortunately, this is not true for two reasons. It may be that at times the residue of a moving target is zero. Secondly, it is not possible to obtain complete cancellation of so-called stationary targets.

The residue of a moving target becomes zero because of the radar's velocity nulls or blind speeds. Velocity nulls occur when the moving target has a radial velocity such that the Doppler frequency is an integral multiple of the prf. The first null occurs at:

$$V = \frac{\lambda f_r}{2} \qquad (6\text{-}44)$$

Thus the target appears to be stationary when it travels a distance of $\lambda/2$ or a multiple of $\lambda/2$.

Range redundancy occurs when a system's range capability exceeds the range corresponding to the pulse repetition period. With a normal coherent system, the transmitted pulse is randomly phased but obtains coherence with the received signal by locking the coherent oscillator. Since the system locks the coherent oscillator with each transmitted pulse, then second time around (and higher order) targets are not coherent, but random in phase. Therefore they produce a residue from pulse-to-pulse.

Poor cancellation of stationary targets results from two basic reasons:

(a) instability of radar components

(b) returns from stationary targets appear as returns from moving targets due to internal motion of the targets, scanning, and radar platform motion

Instabilities of the radar components include variations in the prf, r-f frequency stability, cancellation equipment stability, etc. These cause pulse-to-pulse variation in the return signal.

The frequency spectrum of the internal motion of stationary targets, for example, are generated by trees and their leaves moving in the wind, waves in the ocean, and clouds slowly moving. Furthermore, when the antenna scans the target, the echoes from stationary targets vary due to the beam pattern and due to a finite number of hits on a given target.

Thus, the moving target in an MTI system is masked by radar instabilities (including velocity nulls and range redundancy), clutter due to environment, and scanning clutter.

CANCELLATION RATIO AND SUB-CLUTTER VISIBILITY

Two figures of merit for MTI performance are cancellation ratio and sub-clutter visibility.

The cancellation ratio (CR) is generally measured by presenting a pulse train to the cancellation equipment. The CR is then defined as the ratio of the output signal residue to the input signal (after accounting for latent loss or gain). It is seen that this is analogous to receiving returns from a truly stationary target by the cancellation equipment. This is a measure of the stability of the cancellation equipment and does not include the transmitter and receiver noise or stability. A more complete measurement would involve pointing the antenna at a fixed target, but such a target is hard to find and care must be exercised for the results to be meaningful.

Sub-clutter visibility (SCV) is defined as the ratio of input power from clutter to input power from a moving target for equal power outputs from the cancellation equipment. SCV gives a measure of how much clutter, both internal and external, can be present without completely obscuring a moving target. The clutter spectrum will vary with radar location and radar range at a particular location and care must be taken to specify the clutter spectrum when quoting SCV.

In some cases, the SCV is defined as the ratio of the input power from a fixed target and from an optimum speed target $\left(v = \frac{\lambda f_r}{4}\right)$ for equal power outputs from the cancellation unit. This is an optimistic figure for SCV since it compares the strongest moving target signal with a clutter that is proportional to only the radar instabilities.

In order to predict the operation of an MTI radar in its natural environment, a theoretical set of calculations for SCV can be made. In these calculations the CR is assumed infinite. If the CR is known, then the actual SCV can be found as:

$$SCV_{(actual)} = \frac{1}{\frac{1}{SCV_{(CR=\infty)}} + \frac{1}{CR}} \qquad (6\text{-}45)$$

CALCULATION OF CLUTTER ATTENUATION

The amount of clutter attenuation is found by multiplying the unit pulsed clutter spectrum by the unit power response of the MTI system and then comparing the power of the original clutter spectrum with the power of the residue clutter spectrum. Thus the clutter attenuation on a power basis is given as:

$$\frac{1}{\alpha} = \frac{\int_{-\infty}^{+\infty} W(f) \left|\left[H(f)\right]\right|^2 df}{\int_{-\infty}^{+\infty} W(f) \quad df} \qquad (6\text{-}46)$$

$W(f)$ = pulsed clutter spectrum (normalized)

$H(f)$ = velocity response characteristic (transfer function of cancellation unit, normalized)

$|H(f)|^2$ = power response of *MTI* cancellation unit

By assuming infinite CR, the only clutter present will be clutter external to the radar and scanning clutter. The clutter spectrum shape is usually assumed Gaussian, with a standard deviation proportional to the type of clutter present. Nomographs for internal motion clutter and for scanning clutter are shown in Figures 6-29 and 6-30.

SAMPLE CALCULATION FOR SINGLE PULSE TO PULSE CANCELLATION

The unit power response for a MTI syste is found by squaring the magnitude of t velocity response characteristic. The veloci response characteristic for a single delay li cancellation unit (see Figure 6-31a) is show in Figure 6-31b. This response may be obtaine simply by noting that the video pulses from th MTI receiver are amplitude modulated at Doppler frequency f_d. Thus the pulse amplitud at a time t is given by:

$$y_1 = \cos W_d t \qquad (6\text{-}47)$$

and for the next pulse:

$$y_2 = \cos W_d(t + T_r) \qquad (6\text{-}48)$$

T_r = pulse repetition period (6-49)

The cancelled video pulse is therefore:

$$y = 2 \sin \frac{W_d T_r}{2} \sin W_d \left(t + \frac{T_r}{2}\right) \qquad (6\text{-}50)$$

The magnitude of the cancelled pulses will be:

$$y = 2 \sin \frac{W_d T_r}{2} \qquad (6\text{-}51)$$

Thus, as f_d goes from $-\infty$ to $+\infty$, R will be a series of positive half sine waves.

As was mentioned previously, the unit power response curve may be found by squaring the velocity response curve. For single cancellation this would be in the form of 4 $\sin^2 W_d t$.

The clutter attenuation for a single cancellation unit is thus given by:

$$\alpha = \frac{\int_0^{\frac{f_r}{2}} W(f)\, df}{4 \int_0^{\frac{f_r}{2}} W(f) \sin^2 \frac{W_d T_r}{2}\, df} \qquad (6\text{-}52)$$

For an example of this calculation consider the following:

Let: $f_t = 3{,}000$ mc ($\lambda = 10$ cm) $f_r = 900$ cps
With heavily wooded hills and 20 mph wind the frequency spread of the clutter due to internal motion is $\sigma_{im} = 5$ cycles/sec. (found in Figure 6-29).

If the scan rate is 6 rpm and if the antenna diameter is 4 feet, then frequency spread of the clutter due to scanning is $\sigma_a = 2$ cycles/sec. (found in Figure 6-30).

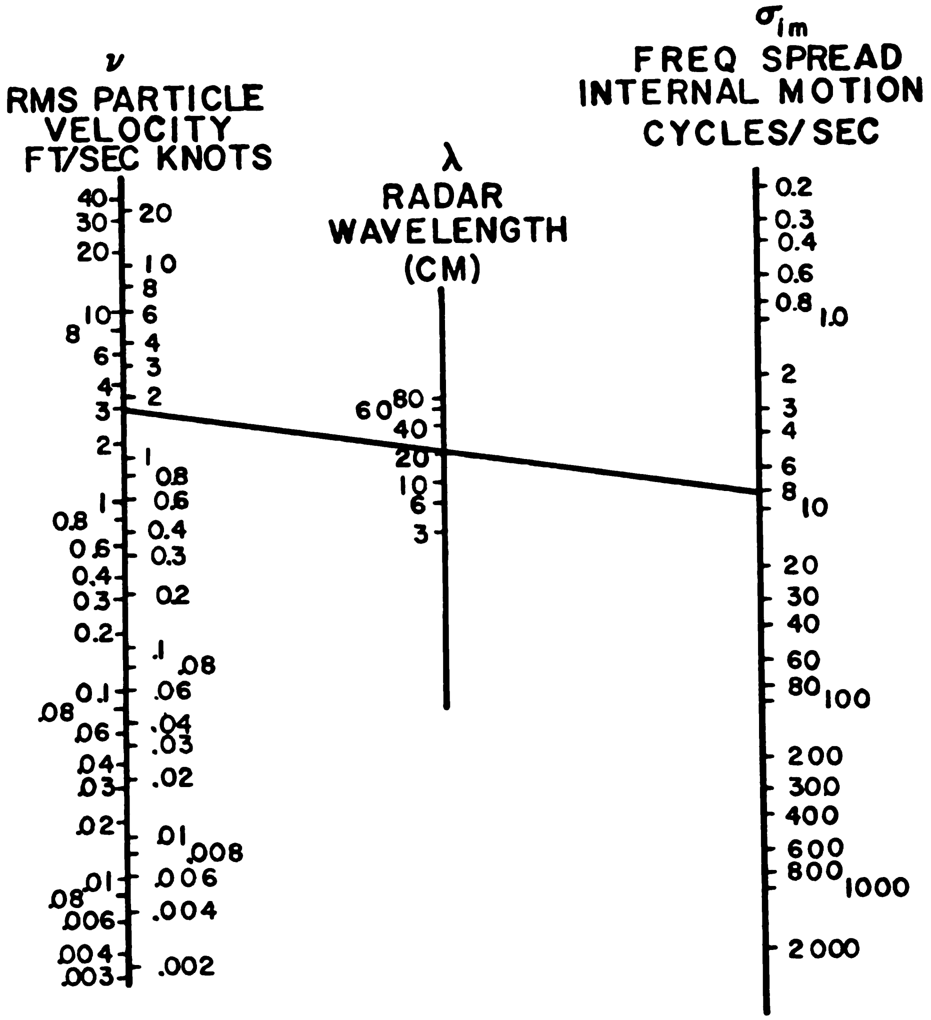

$1 \text{ knot} = \frac{6080 \text{ ft.}}{\text{hr}}$

v knots	
0.01	Sparsely wooded hills - calm
0.50	Heavily wooded hills - 20 mph
1.8	Sea echo windy
2.0	Window Jamming
3.9	Rain Clouds

Figure 6-29. Clutter Frequency Spread Due to Internal Motion Noise, Nomograph

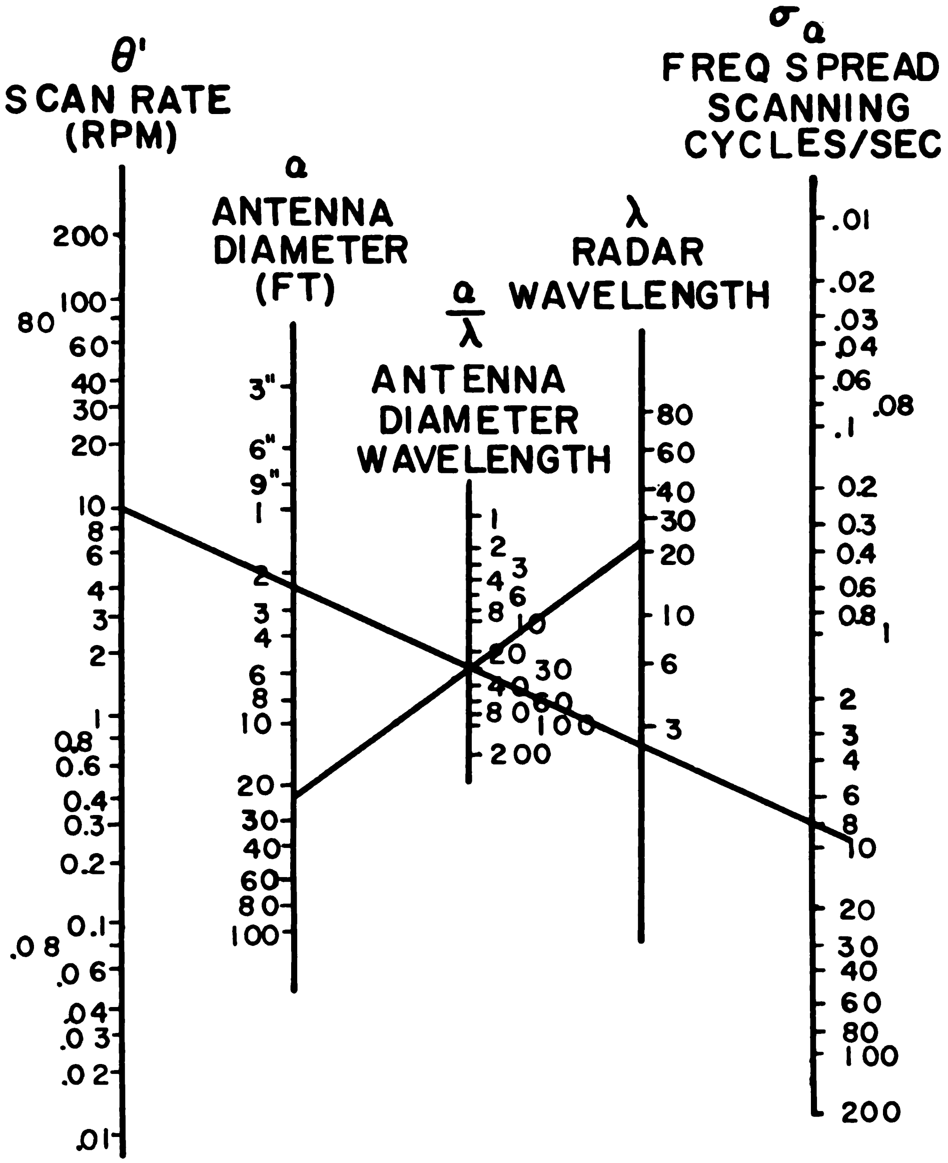

Figure 6-30. Clutter Frequency Spread Due to Scanning, Nomograph

The total clutter frequency spread is found from:

$$\sigma_c^2 = \sigma_{im}^2 + \sigma_a^2 \qquad (6\text{-}53)$$

$$\sigma_c^2 = 29 \qquad (6\text{-}54)$$

The normalized power spectrum of the clutter is:

$$W(f) = \frac{1}{\sqrt{2\pi\sigma_c^2}}\,\varepsilon^{-\frac{f^2}{2\sigma_c^2}} \qquad (6\text{-}55)$$

or in this case:

$$W(f) = \frac{1}{\sqrt{58\pi}}\,\varepsilon^{-\frac{f^2}{58}} \qquad (6\text{-}56)$$

The power response for the single delay cancellation unit is:

$$|H(f)|^2 = 4\sin^2\frac{W_d T}{2} = 4\sin^2\frac{f_d}{900} \qquad (6\text{-}57)$$

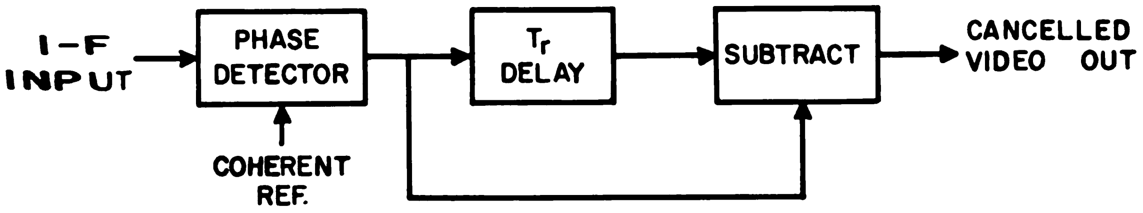

(a) ELEMENTARY PULSE-TO-PULSE CANCELLATION

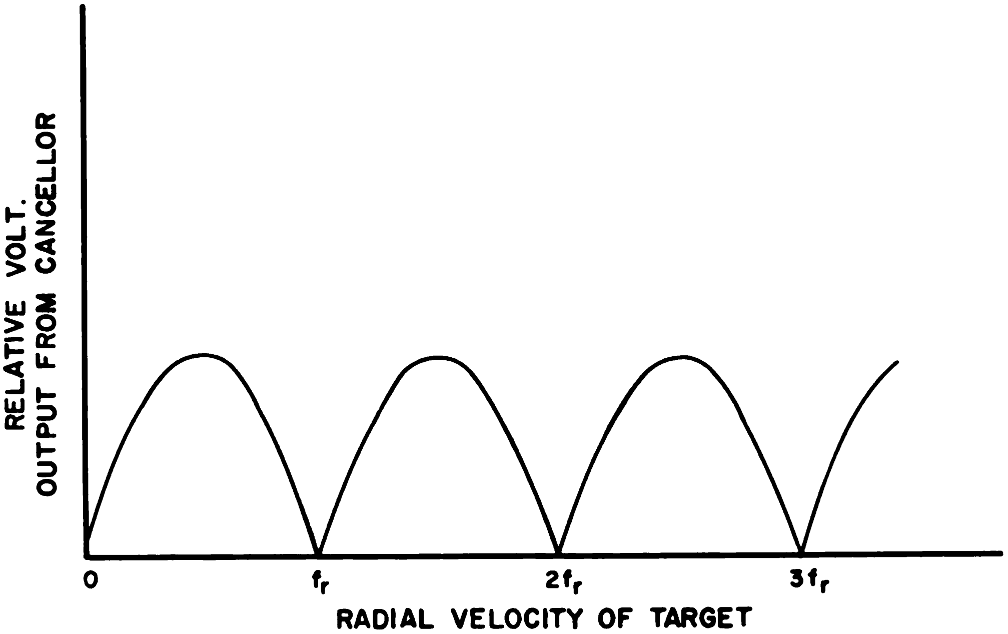

(b) VELOCITY RESPONSE OF A PULSE-TO-PULSE CANCELLOR

Figure 6-31. Pulse-to-Pulse Cancellation and its Velocity Response

The clutter attenuation is given by:

$$\frac{1}{\alpha} = \frac{4\int_0^\infty \frac{1}{\sqrt{58\pi}} \varepsilon^{-\frac{f^2}{58}} \sin^2 \frac{f_d}{900}\, df_d}{\int_0^\infty \frac{1}{\sqrt{58\pi}} \varepsilon^{-\frac{f^2}{58}}\, df_d} \qquad (6\text{-}58)$$

The CW clutter spectrum can be used in place of the pulsed clutter spectrum as long as the σ_c of the clutter is much less than the prf. Limits of 0 to ∞ may be used for the integrals under their stipulation also.

Thus

$$\alpha = \frac{1/2\sqrt{58\pi}}{4\left[\,1/4\sqrt{58\pi}\left(1 - e^{-\frac{58}{900^2}}\right)\right]} = 7000 = 38.5 \text{ db} \qquad (6\text{-}59)$$

SYMBOLS

b	video bandwidth
B	receiver i-f bandwidth
c	velocity of light
C	certainty loss
f	frequency
f_d	Doppler bandwidth
f_r	pulse repetition frequency
Δf_{cw}	combined r-f & i-f bandwidth
G	antenna power gain (one way)
$H(f)$	velocity response characteristic
I	integration gain
KT	Boltzmann's constant × absolute temperature
L	range sweep length or range under surveillance
m	number of range gates
n	false alarm number
N	number of pulses integrated
$\overline{NF}$	receiver noise figure
p	number of Doppler filters
P_t	peak transmitter power
P_d	probability of detection
P_{av}	average transmitter power
R	range
T_i	integration time
T_p	pulse length
T_{fa}	false alarm time (average time between false alarms)
v	radical target velocity
V	visibility factor
T_r	pulse repetition period
w	antenna rotation velocity
W_d	Doppler frequency (radians/sec)
$W(f)$	pulsed clutter spectrum
$\bar{x}$	signal-to-noise ratio
y	pulse amplitude
α	attenuation
β	filter bandwidth
γ	total number of pulses available during the detection time
δ	dimensionless loss factor which accounts for atmosphere absorption, r-f plumbing losses, etc.
η	number of independent noise samples in the range under surveillance
λ	wavelength
A_e	mean scattering cross section of target
σ_a	frequency spread of clutter from antenna scanning
σ_c	frequency spread of clutter
σ_{im}	frequency spread of clutter from clutter internal motion
ϕ	antenna beamwidth

6-4 SEARCH RADAR EVALUATION[59]

6-4.1 GENERAL

This section relates to manual acquisition search radars; automatic acquisition is considered in paragraph 6-3.4. For the manual acquisition radar, the radar range equation is modified to include a new factor called the discernibility factor, V.

The minimum discernible peak power required for the received pulses to be barely visible in the presence of noise is defined as:

$$P_{min} = NF \times V \times KTB \tag{6-60}$$

To determine radar detection range, P_r is set equal to P_{min};

$$R = \left[\frac{P_t\, A_e\, G_t\, G_r\, \lambda^2}{(4\pi)^3\, \overline{NF}\, V\, KT_oB\, L}\right]^{1/4} \tag{6-61}$$

All of these factors have been covered except V.

6-4.2 DISCERNIBILITY FACTOR

The discernibility factor (V) can be viewed as more or less of a "catchall" quantity which chiefly concerned with the human psycho- gical reaction exhibited by a radar operator s various system parameters are varied. A mprehensive list and discussion of all the arameters that should be included in *V* would e very lengthy; so, only those parameters hich contribute a major influence on the per- ormance of a radar system will be selected here.

First the parameters to be considered will be listed; the results will be described of controlled experiments which have been made in an attempt to evaluate their effects. The parameters and effects to be discussed are:

(a) dependence on the product of i-f bandwidth and pulse length

(b) effects of video bandwidth and sweep speed

(c) dependence upon pulse repetition frequency

6–4.2.1 Dependence on Product of I-F Bandwidth and Pulse Length

The noise power which is passed by an i-f amplifier is directly proportional to the i-f bandwidth, so that in order to achieve a low noise level system, it is desirable to reduce the i-f bandwidth to as low a value as possible. On the other hand, when one attempts to pass a series of repetitive rectangular pulses through an i-f amplifier and still retain a faithful reproduction of the pulse shapes in the output, the bandwidth of the amplifier must be relatively wide so as to pass the major share of the contributing harmonics. These two considerations contradict one another from the standpoint of simultaneously achieving the most signal and the least noise, but if we are interested in the signal-to-noise ratio (S/N), it should be expected that there must be an optimum bandwidth-pulse length product which will yield the best value of S/N. One of the best means of establishing this value is by direct observation of a system employing controlled parameters wherein a large number of independent observations are made by many operators. The results may then be analyzed on a statistical basis and plotted according to any desired probability of success. Figure 6-32 shows the results of such a procedure. The i-f bandwidth-pulse

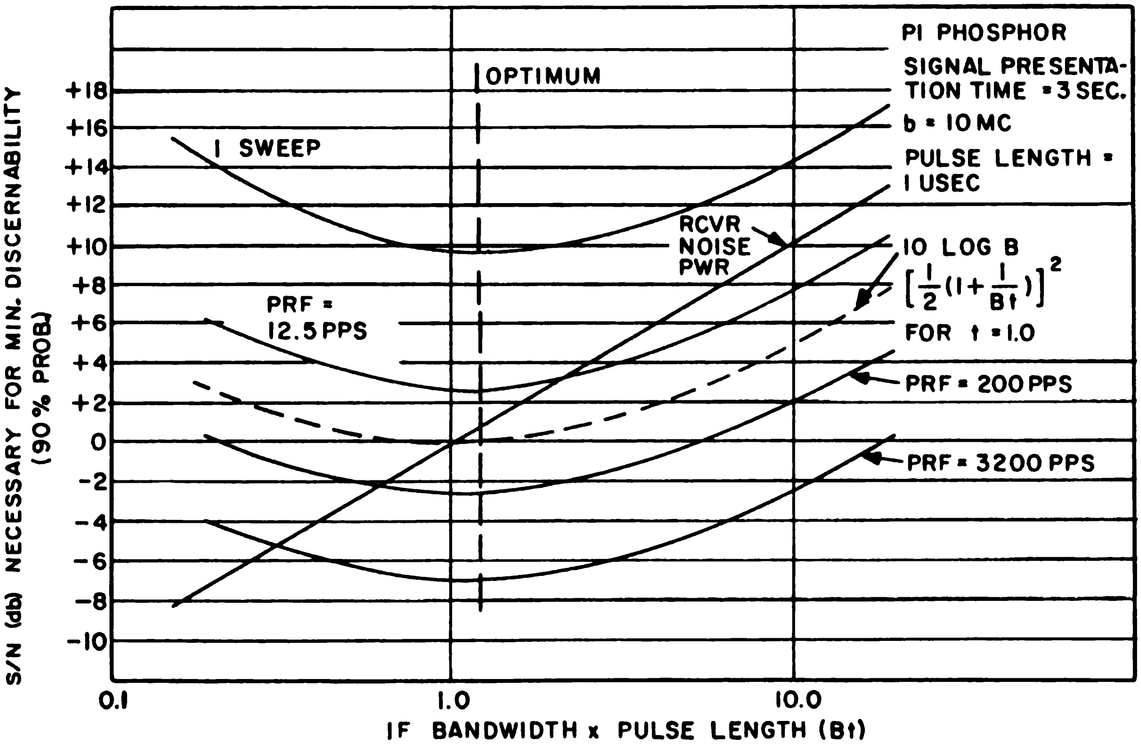

Figure 6-32. S/N Ratio for Minimum Discernibility as a Function of I-F Bandwidth and Pulse Length

length product is plotted against the S/N necessary for a minimum discernible display on the basis of 90 percent probability of success. The optimum product of i-f bandwidth and pulse length is rather broad but centers about the value of 1.2.

The general shape of all the curves is essentially the same, independent of the pulse repetition frequency so that it is possible to curve-fit the data on the basis of B and t alone. This has been accomplished according to the following expression. (This is done in terms of db in order to facilitate computations.)

$$\text{db} = 10 \log B \left[\frac{1}{2}\left(1 + \frac{1}{Bt}\right)\right]^2 \qquad (6\text{-}62)$$

To illustrate the excellence of curve fit, this function is plotted as the dashed curve in Figure 6-33.

Now, to write this function into the rad equation, it is clear that the entire function

$$B\left[\frac{1}{2}\left(1 + \frac{1}{Bt}\right)\right]^2 \qquad (6\text{-}63)$$

must appear in the denominator of equation 6-61. But, upon examination of equation 6-61, factor B already appears in its proper place in the denominator; hence, only an additional factor is needed of

$$\left[\frac{1}{2}\left(1 + \frac{1}{Bt}\right)\right]^2 \qquad (6\text{-}64)$$

Or, if this factor is included in V,

$$V\alpha\left[\frac{1}{2}\left(1 + \frac{1}{Bt}\right)\right]^2 \qquad (6\text{-}65)$$

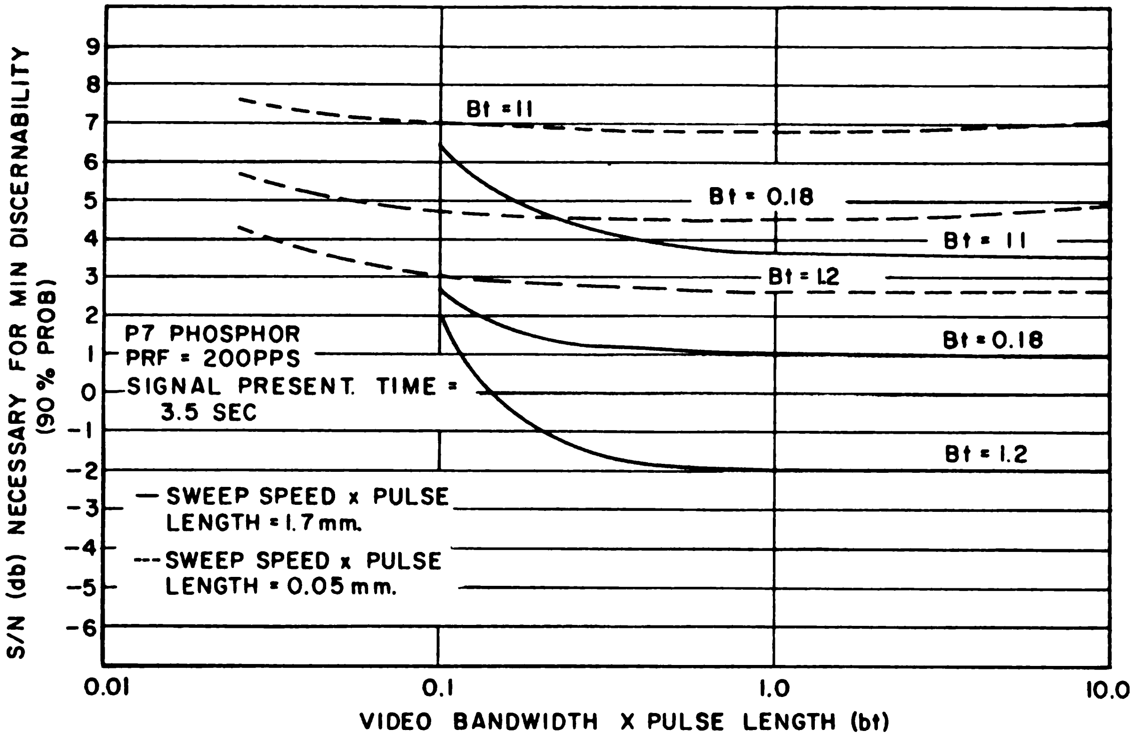

Figure 6-33. S/N Ratio for Minimum Discernibility as a Function of Video Bandwidth and Pulse Length

-4.2.2 Effects of Video Bandwidth and Sweep Speed

The effect of limiting the video bandwidth is different from the effect of limiting the i-f bandwidth, even in the case of a linear detector. This statement may seem somewhat surprising but the linear detector records only the absolute value of the i-f envelope so that cross-modulation products will develop. Thus, the video noise emanating from a linear detector will be of a different character (Rayleigh) from that of the i-f amplifier (Gaussian) and the effect of reducing the video bandwidth will be different from the effect of reducing the i-f bandwidth. This effect can be illustrated by again returning to the statistical results obtained from direct experiment under controlled conditions. Figure 6-33 shows the variation of minimum discernible S/N which results from varying the video bandwidth-pulse length product (*bt*). The two sets of curves illustrate the effect of fast and slow sweep speeds (*st*), that is, the physical length of the signal presented on the CR indicator. Each set is plotted for the optimum value of *Bt* (1.2) and two extremes (0.18 and 11.0). It is clearly shown that as long as the video bandwidth-pulse length product (*bt*) is greater than about 0.5, no effect can be placed on this parameter. As a result, the *bt* function is not entered in the discernibility factor (*V*) as long as the engineer realizes that the value of *bt* should be greater than 0.5.

Figure 6-33 also indicates that the sweep speed-pulse length product (*st*) is a factor requiring consideration, but only two values of *st* are shown (1.7 mm an 0.05 mm). In order to obtain a better view of this function, the experimental curves in Figure 6-34 are included

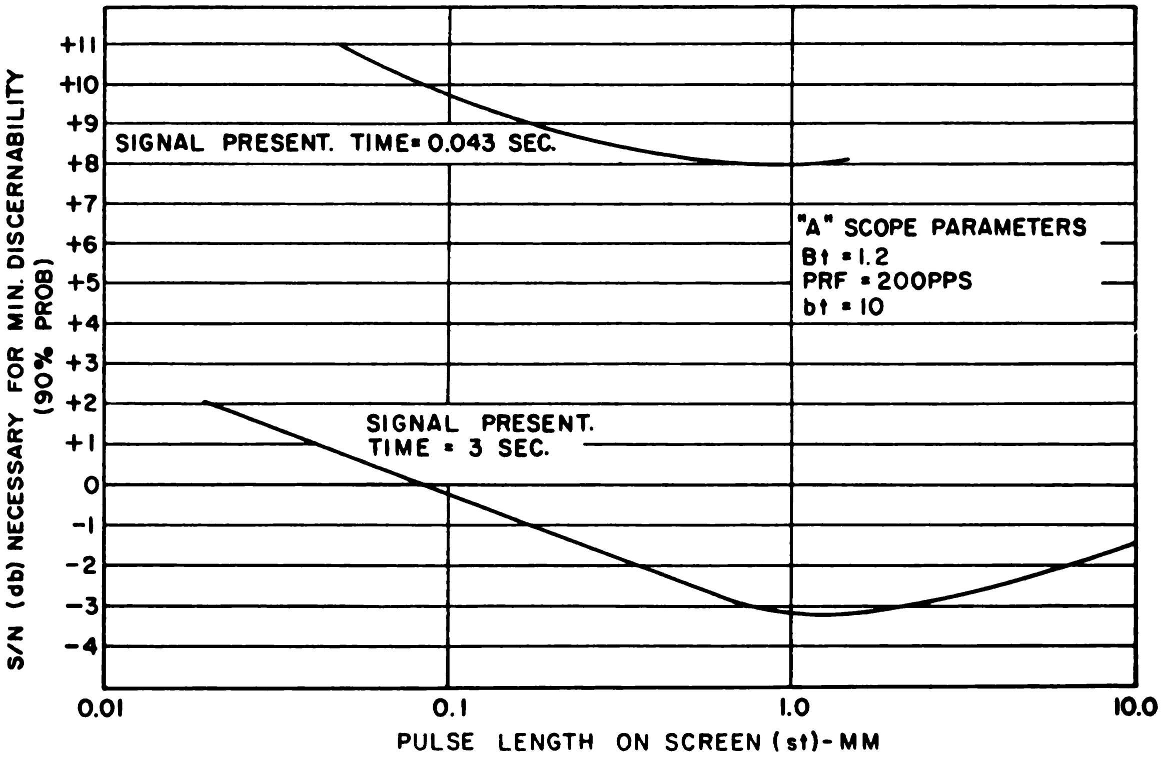

Figure 6-34. S/N Ratio for Minimum Discernibility as a Function of Pulse Length Presented on Observer's Screen

which show the effect of varying *st* over a wide range of values. The results here show the selective effect that the observer's eye and brain mechanism have on the observer's ability to distinguish a readable signal under conditions of various pulse (and noise) lengths presented on the screen. The curves clearly show that the observer responds best when the signal and its noise are made approximately one mm in length. That is, if the eye and brain preferentially select events having a spatial separation of one mm, then the eye and brain mechanism have somewhat the same effect as a low pass filter in that they have difficulty in resolving events which are closely spaced (or which contain high frequencies as far as the eye and brain are concerned).

In present day radar indicators, the presented spot size is generally in the vicinity of the optimum size of 1.0 mm so that generally this effect need not be considered in the radar design. For this reason, the spot size function is not included in the expression for V as such. The reader should be mindful of this effect, however, when and if special cases arise where it should be considered.

6-4.2.3 Dependence Upon Pulse Repetition Frequency

The radar pulse repetition frequency is functional in the performance of a radar system from the standpoint of both searchlight (where the radar antenna beam remains fixed on the target) and scanning conditions. For the moment, however, this function is considered from the standpoint of searchlight conditions only, leaving its dependence in the scanning case for later discussion. (See Figure 6-35 for searchlight conditions.)

In order to present this function for searchlight conditions, only the values of Figure 6-32 need to be cross-plotted at the optimum value of $Bt = 1.2$, thereby obtaining the top curve of Figure 6-36 (which describes the function for a P1 phosphor). Other experiments have shown that a gain of about 1.5 db is obtained when a P7 phosphor is substituted for the P1; thus the corresponding results are plotted for a P7

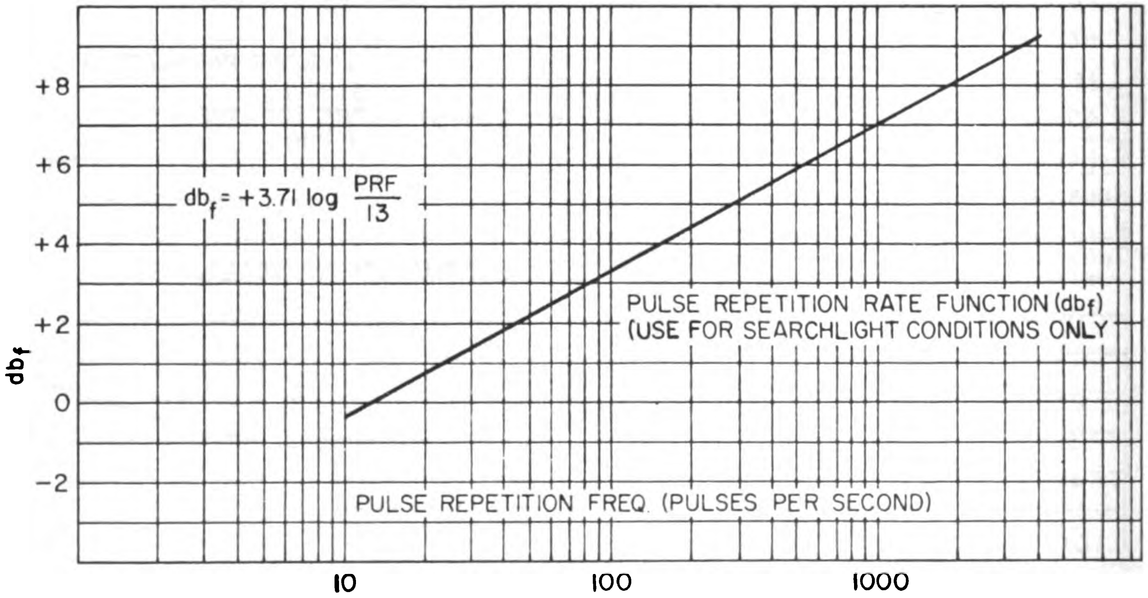

Figure 6-35. Pulse Repetition Function

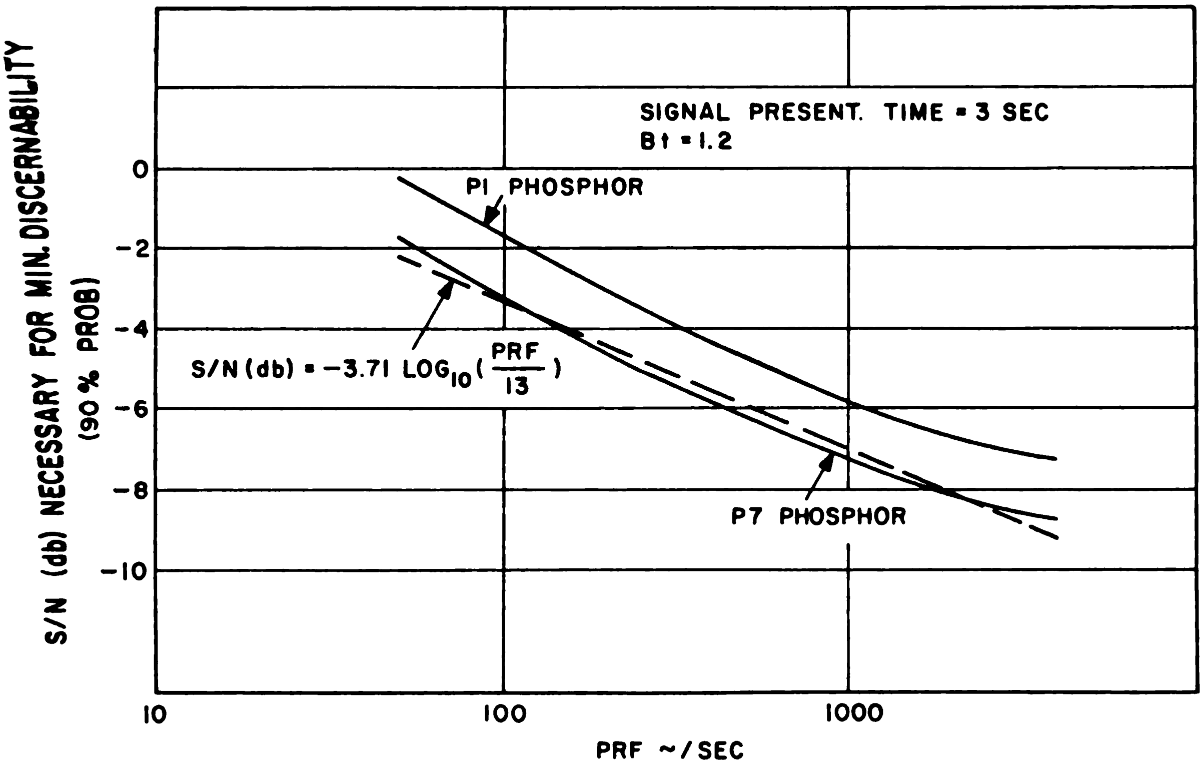

Figure 6-36. S/N Ratio for Minimum Discernibility as a Function of Pulse Repetition Frequency

phosphor on Figure 6-36 as shown. Since most concern is with the use of a P7 phosphor and it is desirable to include its function in the discernability factor (V), the prf function for a P7 phosphor has been approximated as shown by the dashed line in Figure 6-36. This line fits the P7 phosphor within approximately 0.5 db over the range of prf usually encountered (50 to 4000 pps), and its expression is

$$S/N\ (db) = -3.71 \log_{10} \frac{prf}{13} \qquad (6\text{-}66)$$

or, in order to include this as a factor of V, the expression is rewritten as

$$V \alpha \left[\frac{13}{prf}\right]^{0.371} \qquad (6\text{-}67)$$

At this point, the discernability factor (V) can be formulated for searchlight conditions by combining expressions 6-65 and 6-67 into a common quantity. Thus:

$$V = \left[\frac{1}{2}\left(1 + \frac{1}{B^t}\right)\right]^2 \times \left[\frac{13}{prf}\right]^{0.371} \qquad (6\text{-}68)$$

(For Searchlight Conditions ONLY)

As a result, the radar equation for searchlight conditions is written by combining equations 6-61 and 6-68 as follows:

$$R = \left[\frac{P_t A_e G_t G_r \lambda^2}{(4\pi)^3 \overline{NF} KTB \left[\frac{1}{2}\left(1 + \frac{1}{B_t}\right)\right]^2 \left[\frac{13}{prf}\right]^{0.371}}\right]^{1/4}$$

*(For Searchlight Conditions ONLY)** (6-69)

6-4.3 INFLUENCE OF SCANNING

When the radar antenna is made to scan through a target at a particular rate, the signal presentation time (and hence the number of signal pulses) will be vastly reduced from those values obtained under searchlight conditions. The chief parameters are:

(a) the scanning rate of the antenna
(b) the antenna beamwidth in the scanning plane
(c) the prf

---

*Searchlight condition refers to non-scanning radar.

The signal presentation time is, of course, functional with (a) and (b). In order to ascertain the magnitude of the effect of scanning, the results of three experiments are described and an attempt is made to generalize a solution to the problem.

In the first experiment, a PPI indicator was used with a constant rotational period of 8 seconds. The prf was held constant at 800 pps and the presentation time was varied between wide limits. The results appear in Figure 6-37. The minimum discernible signal varies as the square root of either the signal presentation time o the beam angle over most of the range considered, although small deviations exist at bot ends of the plot. For very large beam angle (greater than 45 degrees), it is understandabl that the signals are less easily distinguished. since the operator has difficulty in viewing the entire arc. Also, for very small beam widths (less than one degree) the geometrical size of the signal spot becomes smaller than one mm, so that one would expect a decrease in performance similar to the effect of decreasing the sweep

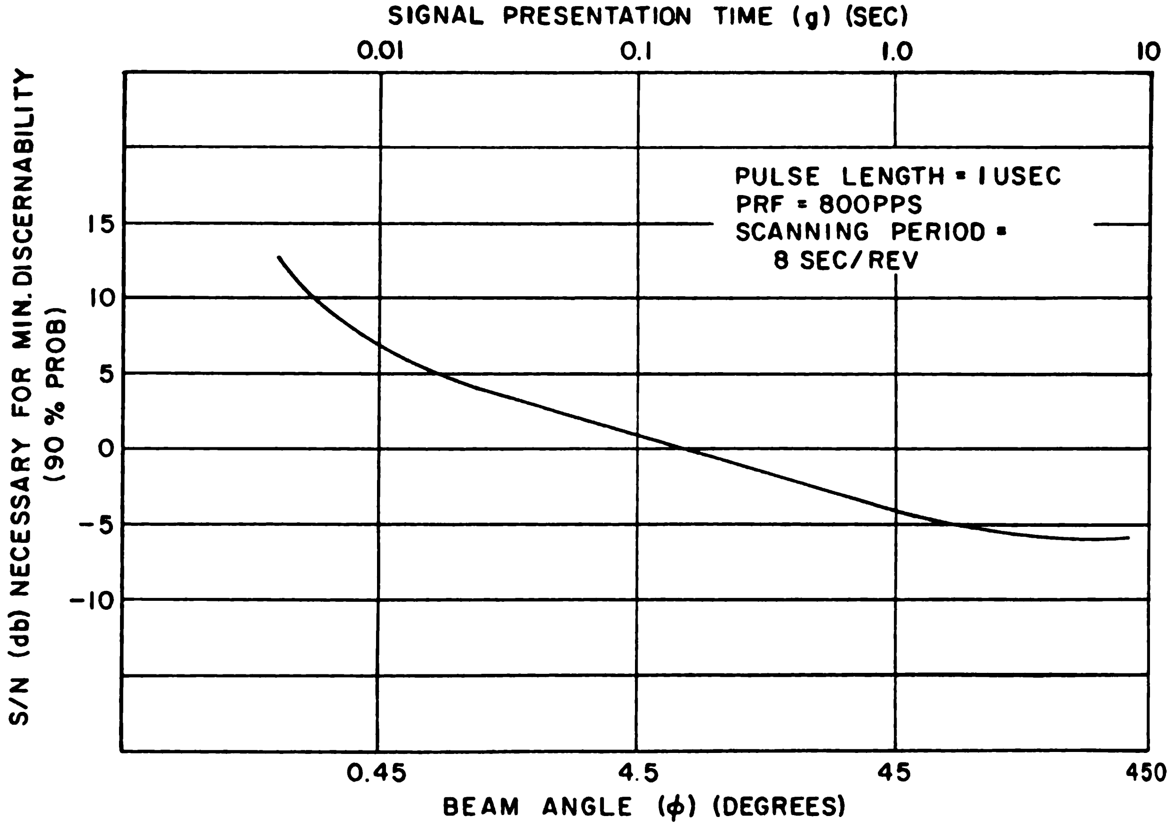

Figure 6-37. S/N Ratio for Minimum Discernibility as a Function of Beam Angle and Signal Presentation Time

speed. In other words, here again the eye and brain have a tendency to discriminate against geometrically small signals in favor of wider ones. The general shape of the curve of Figure 6-38 is important since it shows that, for a specific number of hits per target traverse, no essential change of minimum discernible signal is caused by the geometrical arc length of the presented signals. This conclusion contradicts the widespread opinion that a long arc length is more easily discernible in the presence of noise than is a shorter arc length. To substantiate this conclusion more firmly, another experiment has been performed wherein the signal presentation time and the prf were held constant and the beam angle was changed by varying the scanning frequency. The results are shown in Figure 6-38. From a presentation standpoint, it is evident that, for beam angles between one degree and 45 degrees, then antenna beam width itself has little to do with the minimum discernible signal. However, the prf and antenna scanning frequency are usually fixed in a radar system and therefore the number of presented signal pulses is proportional to the beam angle.

The results of a third experiment can now be reviewed wherein the antenna scanning rate was held constant at 5 rpm; the beam width was constant at 2 degrees (which results in a signal presentation time of 1/15 second) and the prf was varied over wide limits. The results are shown in Figure 6-39. Under these conditions, the minimum discernible signal varies approximately as the square root of the repetition rate; hence, it is functional with the square root of the number of pulse hits.

The data illustrated by the solid curve of Figure 6-39 was obtained under conditions which simulated an antenna scanning in PPI fashion insofar as the antenna beam width is concerned, but the presented pulse train contained pulses of equal magnitude. In the case of an actual antenna system where the presented pulses vary in magnitude according to the round trip antenna pattern shape, the original data should be modified thereto. Such modification indicates

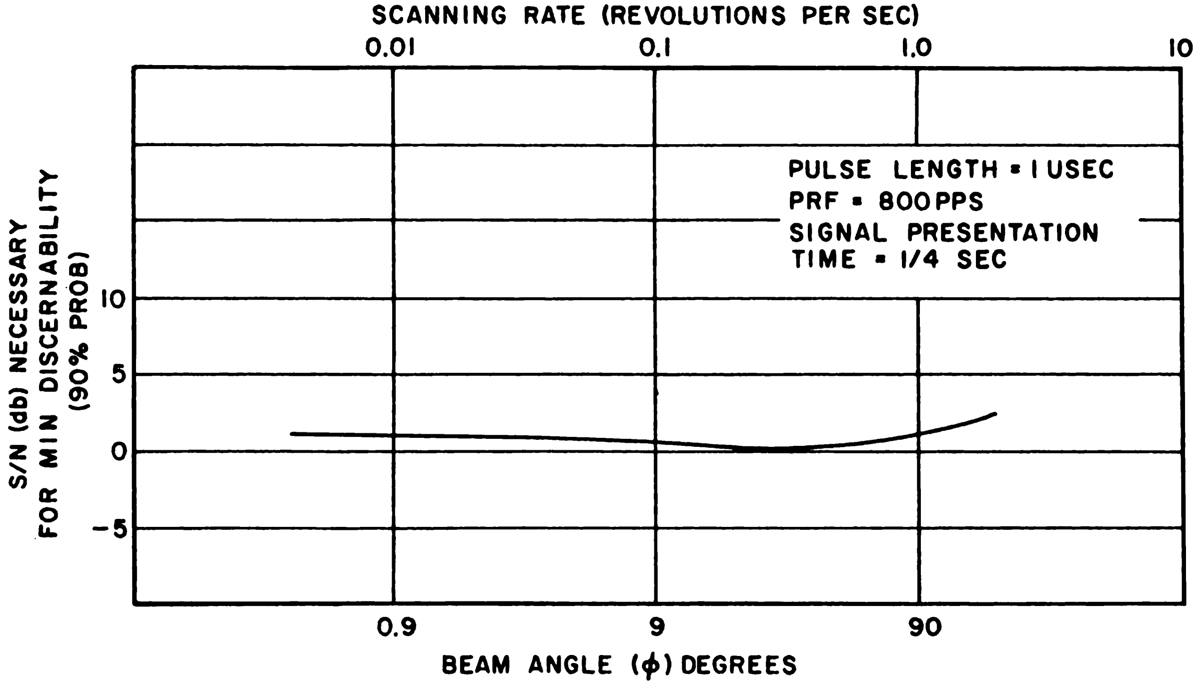

Figure 6-38. S/N Ratio for Minimum Discernibility as a Function of Beam Angle and Scanning Rate

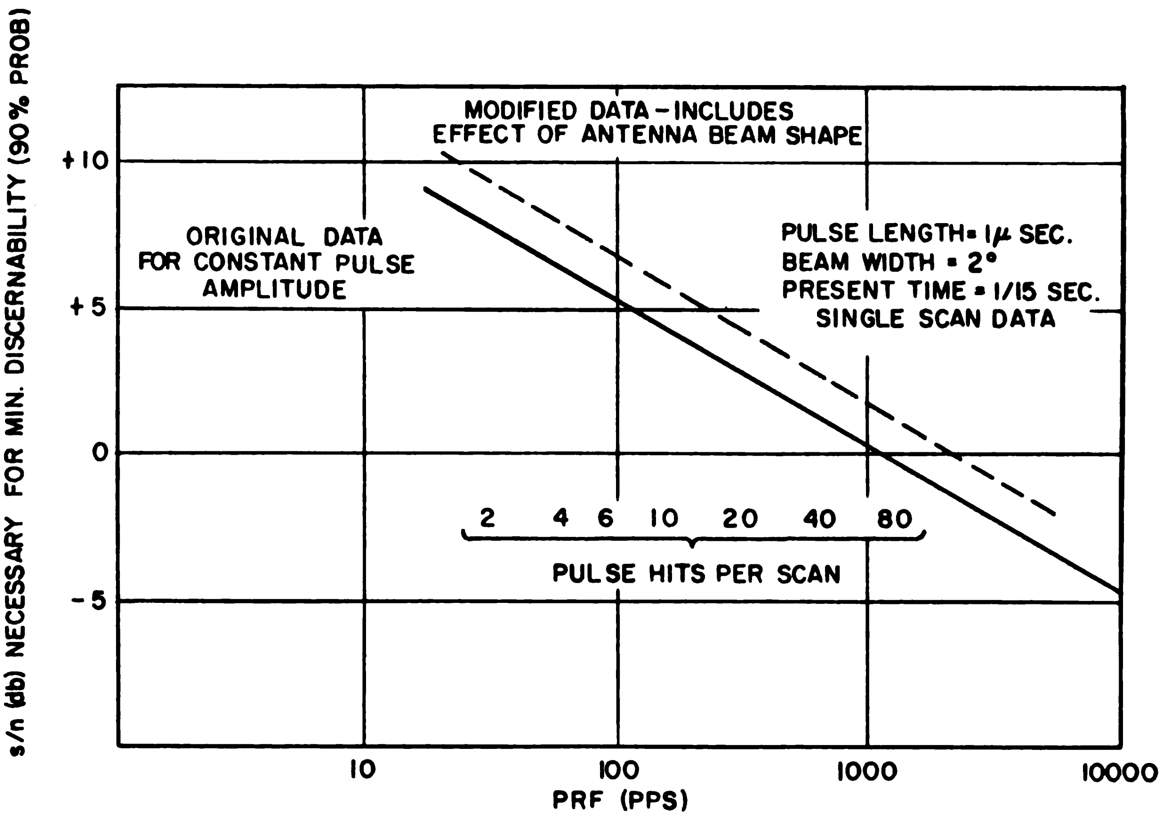

Figure 6-39. S/N Ratio for Minimum Discernibility as a Function of PRF

that 1.5 db must be added to the original data, giving the results shown by the dashed curve of Figure 6-39.

At this point, it is a simple matter to generalize the results of the last three experiments by stating that the S/N (in power) necessary for minimum discernibility is directly proportional to the square root of the product of the beam width and prf. This relationship is true only for single-scan operation provided the scanning frequency is adjusted between certain limits, and is not true at all for multiple-scan operation. The reasoning behind this statement stems from the consideration of a new parameter, i.e., the maximum time over which effective pulse-to-pulse integration can be effective (called the *integration time*). It would normally be expected that the integration time would be functional with the type phosphor employed and the remembering characteristics of the human eye, but experiments have shown that its value is substantially constant (at somewhere between 4 and 10 seconds) independent of the persistence characteristics of the phosphor. Thus, in a scanning radar system, a loss would be anticipated due to scanning until the antenna scanning rate has been increased to such a value that the antenna beam remains on the target for a period less than the integration time. However, if the antenna rotational speed is increased, the loss due to scanning is simply proportional to the square root of the ratio of the number of searchlighting pulses to the number of scanning pulses (this ratio is $360°/\phi$.).

Having thus established the behavior of the scanning loss function at the extremities of the scanning rates (very low and very high) and knowing that the scanning loss in the intermediate region is inversely proportional to the square root of the number of pulse hits per scan, a set of curves can be presented which describe the relationship between prf, antenna beam width (ϕ) and the antenna rpm. For example, suppose a particular condition exists where the prf is constant at 400 pps and the variation in the minimum discernible signal is determined as the antenna beam width and rotational rate are varied. Employing the arguments discussed above, a set of curves, similar to those shown in Figure 6-40 can be constructed, which shows clearly the behavior due to scanning. The integration time has been set at 5 seconds, and, with this value, close inspection will reveal that an excellent fit has been obtained for correlating the central portions of the curves with their extremities. For example, the 5 second integration time dictates that, with a 1 degree beam width, no appreciable loss will result until the antenna beam remains on the target for less than 5 seconds (or, until the antenna rotational rate exceeds 0.033 rpm). Thus, 0.033 rpm is the lower *breaking point* in the curve for a one degree beamwidth. On the other hand, the upper breaking point will occur at 12 rpm where scan-to-scan integration begins. Also, the central portion of the curve must satisfy the dashed curve of Figure 6-39 (which it does). Finally, the difference between the extremities of the $\phi = 1$ degree curve must satisfy the square root of $360^\circ/\phi$ relationship, which turns out to be 12.8 db (which also agrees with the curve). With the behavior of these curves in mind, the more general set of curves shown in Figure

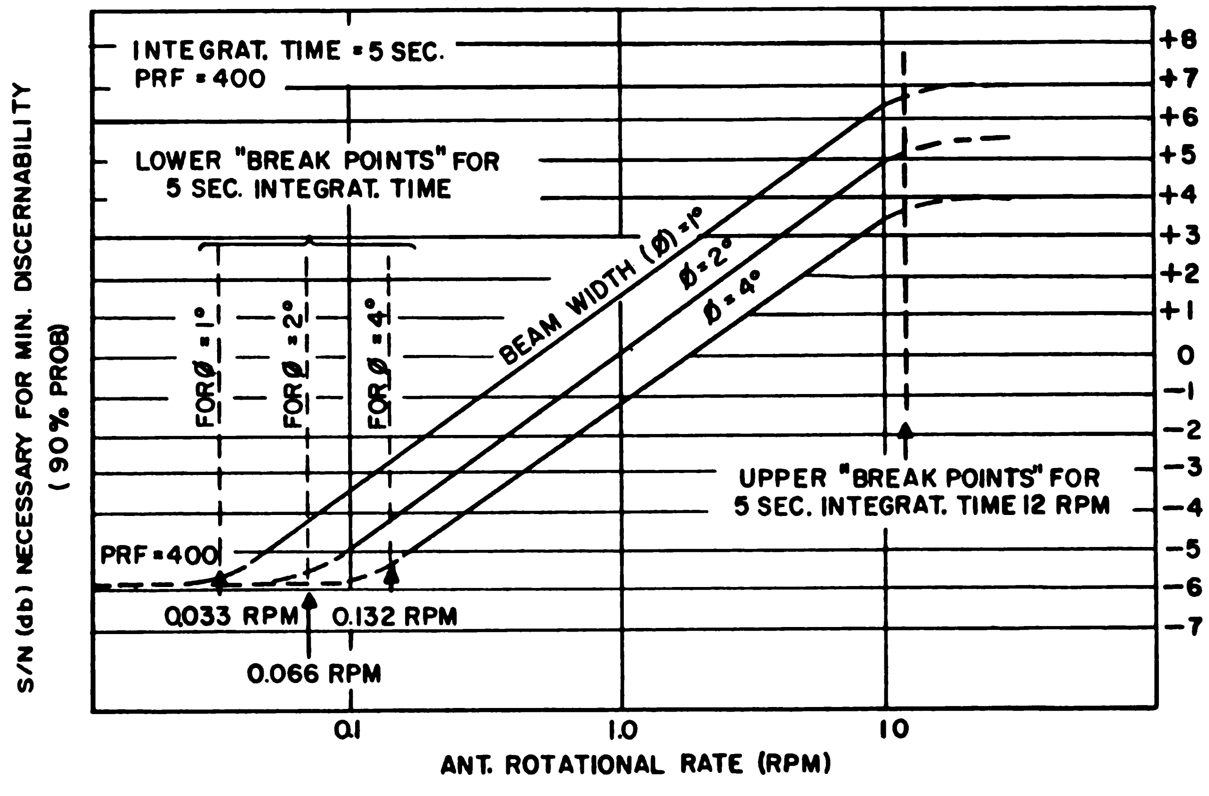

Figure 6-40. Particular Example of the Scanning Function

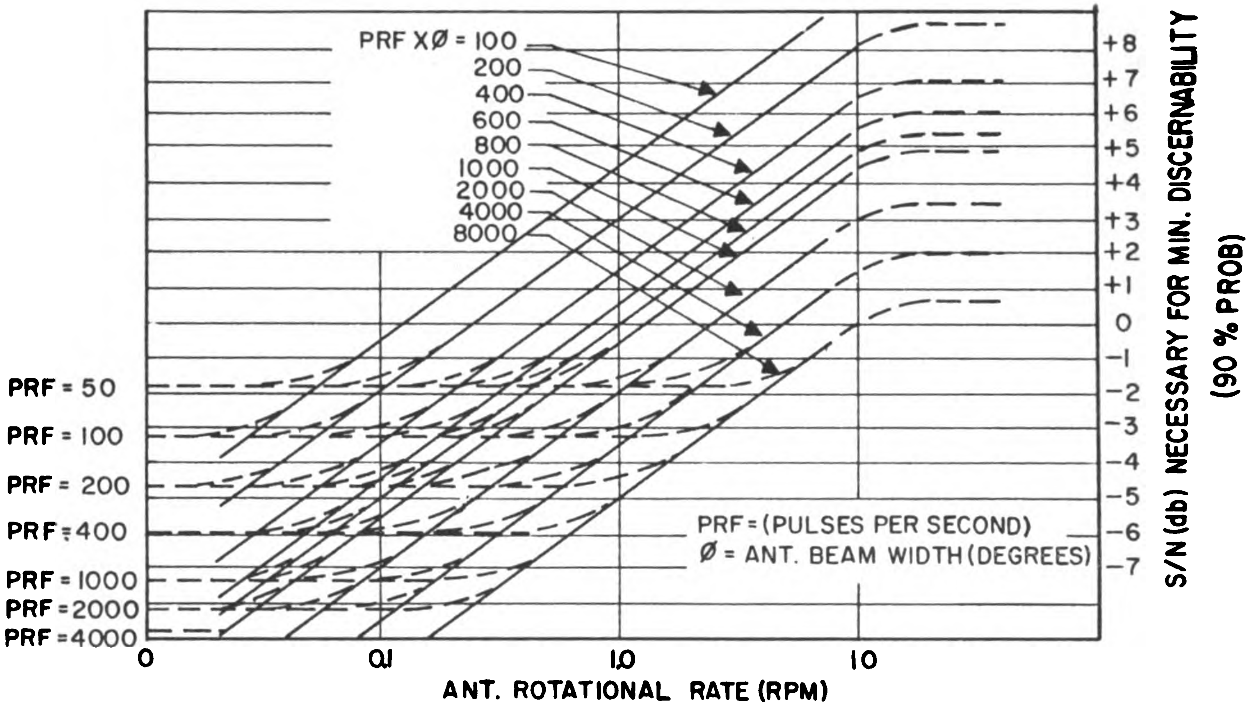

Figure 6-41. Effects of Scanning

6-41 can be plotted. Included are various values of prf and the central region is plotted in terms of the product of prf times the antenna beam width in degrees.

6-4.4 ADDITIONAL NOISE SWEEPS

In certain types of radar systems (especially three-dimensional scanning systems) the situation is likely to arise where the indicator presentation contains additional noise sweeps which lie superimposed on those sweeps which contain the usual signals and noise. A particular example of this is the PPI presentation of a system which contains an elevation scanning function as well as an azimuthal rotational rate.

To evaluate the detrimental effect of such additional noise sweeps on the minimum discernible signal, the results of two experiments will be considered. From the results of Figure 6-42 it can be seen that the signal threshold power is directly proportional to the square root of the sweep recurrence frequency, while the results shown in Figure 6-43 show that, over most of the scan, the signal threshold power is inversely proportional to the first power of the signal recurrence frequency.

Thus, if N_N equals the total number of sweeps presented and N_S of these contain signals while the rest contain noise, only then

$$P_{min} \text{ (threshold power) } \propto \frac{N_N}{N_S} \qquad (6\text{-}70)$$

When N_N equals N_S, this relation clearly leads to the familiar square root relationship between the threshold power and the total number of observations.

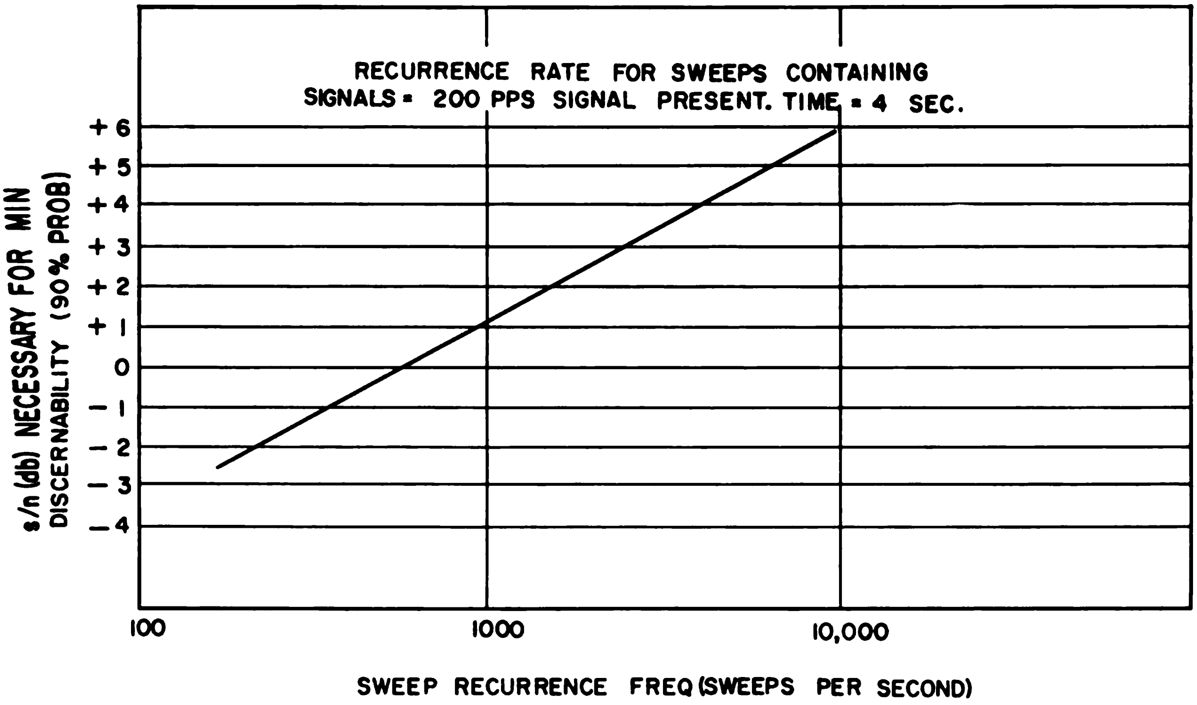

Figure 6-42. S/N Ratio for Minimum Discernibility as a Function of Sweep Recurrence Frequency

6-4.5 SCANNING RADAR RANGE COMPUTATIONS

The computations involved for the range determination of a scanning system are identical with those involved in the case of searchlight conditions with two major exceptions:

(a) The prf function (db_F) used under the conditions of searchlight must be replaced by the scanning function db_H described in Figure 6-44. This scanning function illustrates the interdependence of the repetition rate, antenna beam width in the scanning plane, and the antenna rotational rate.

Note: If the target velocity is high, such that the scan-to-scan traces are not superimposed on the indicator, the engineer may individually compute the pulse hits per target traverse and employ the db_H figure obtained from Figure 6-45 instead of referring to Figure 6-44.

(b) In addition to (a) above, the situation may arise (especially in the case of three-dimensional scanners) where additional noise sweeps are presented superimposed on those sweeps which contain the target signals. In this case, the engineer must apply an indicator collapsing loss db_c, which can be obtained from the curve of Figure 6-46. This loss should be included over and above those other system parameters listed above.

An example of the procedure used for determining the maximum reliable range of a scanning system appears as Example 1. Here, the same system constants are considered as were employed in the example used for radar range equation calculations on fictitious radar system XYZ with the additional stipulation that the antenna is made to rotate at 6.0 rpm in azimuth.

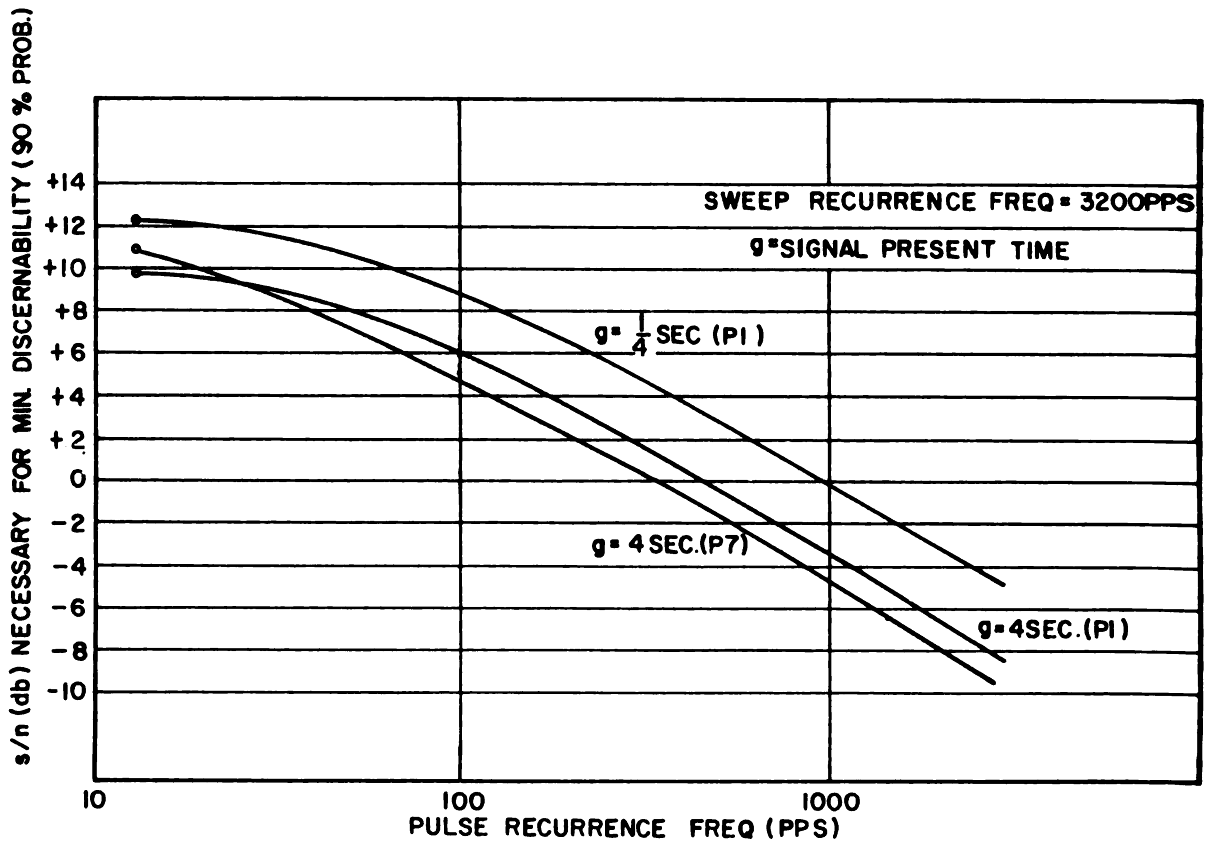

Figure 6-43. S/N Ratio for Minimum Discernibility as a Function of PRF for Constant Sweep Recurrence Frequency of 3200 PPS

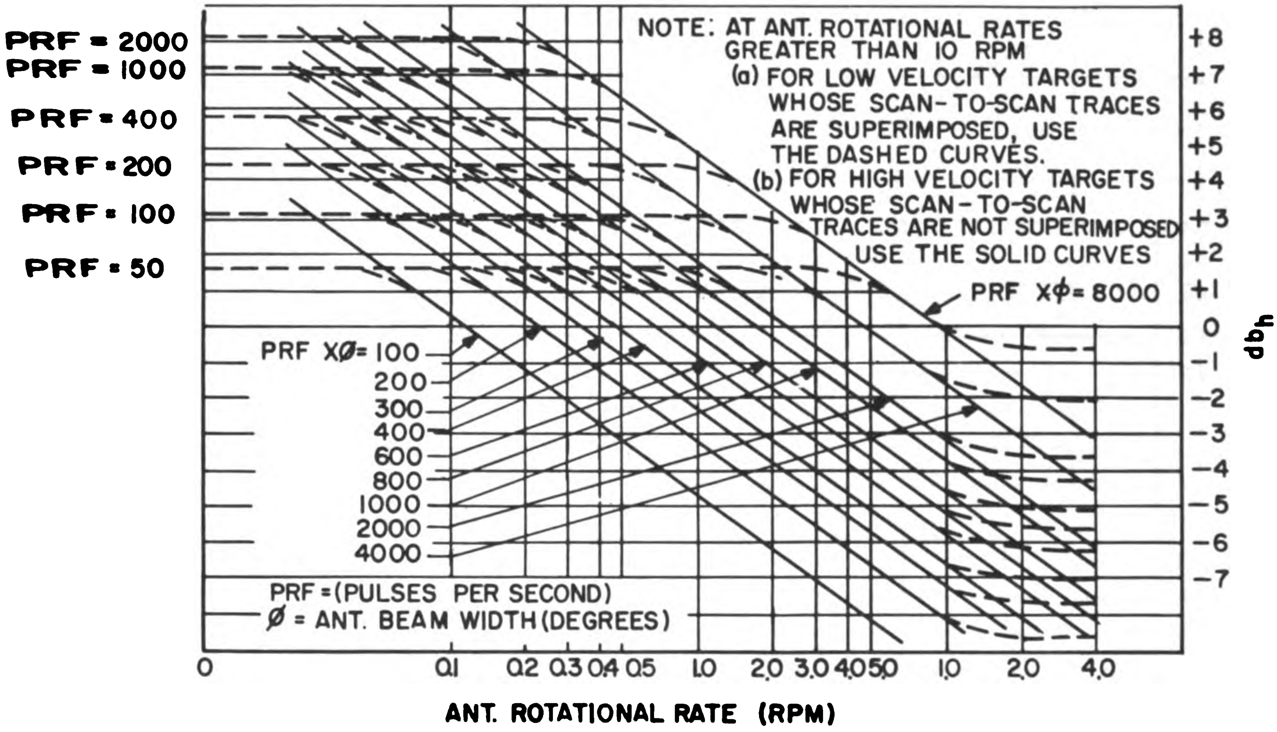

Figure 6-44. Scanning Function

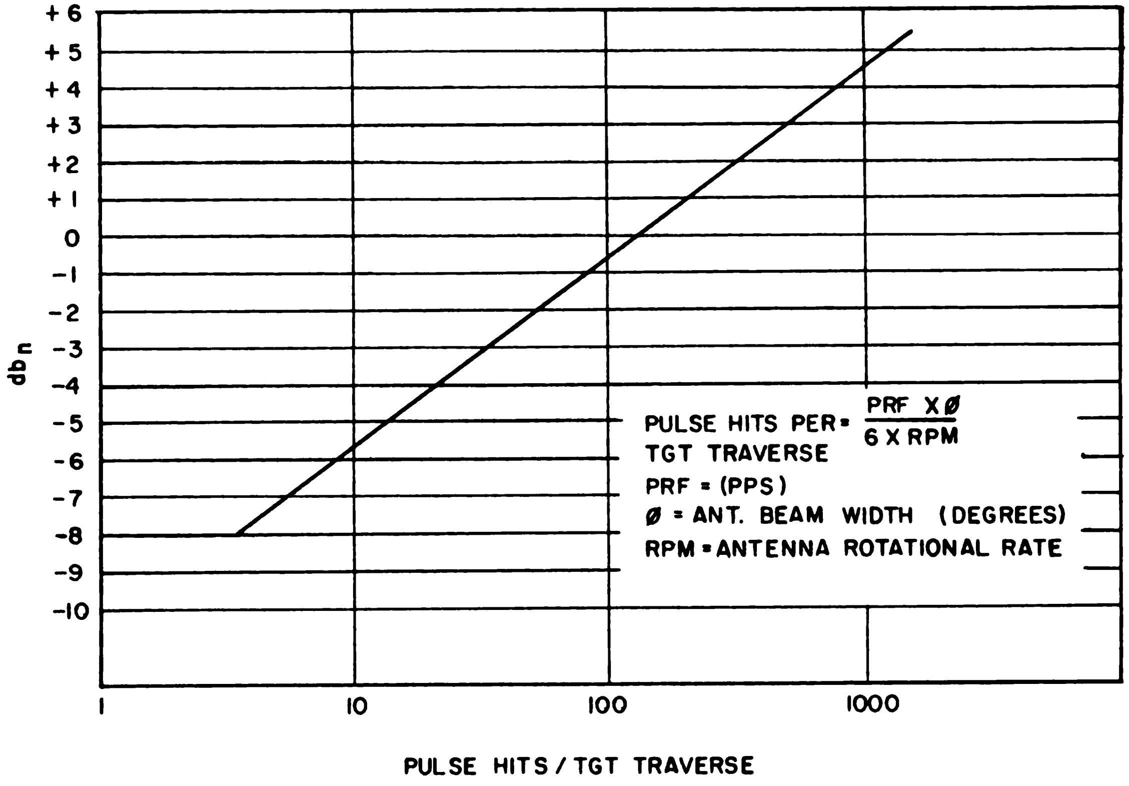

Figure 6-45. Scanning Function Versus Pulse Hits Per Target Traverse

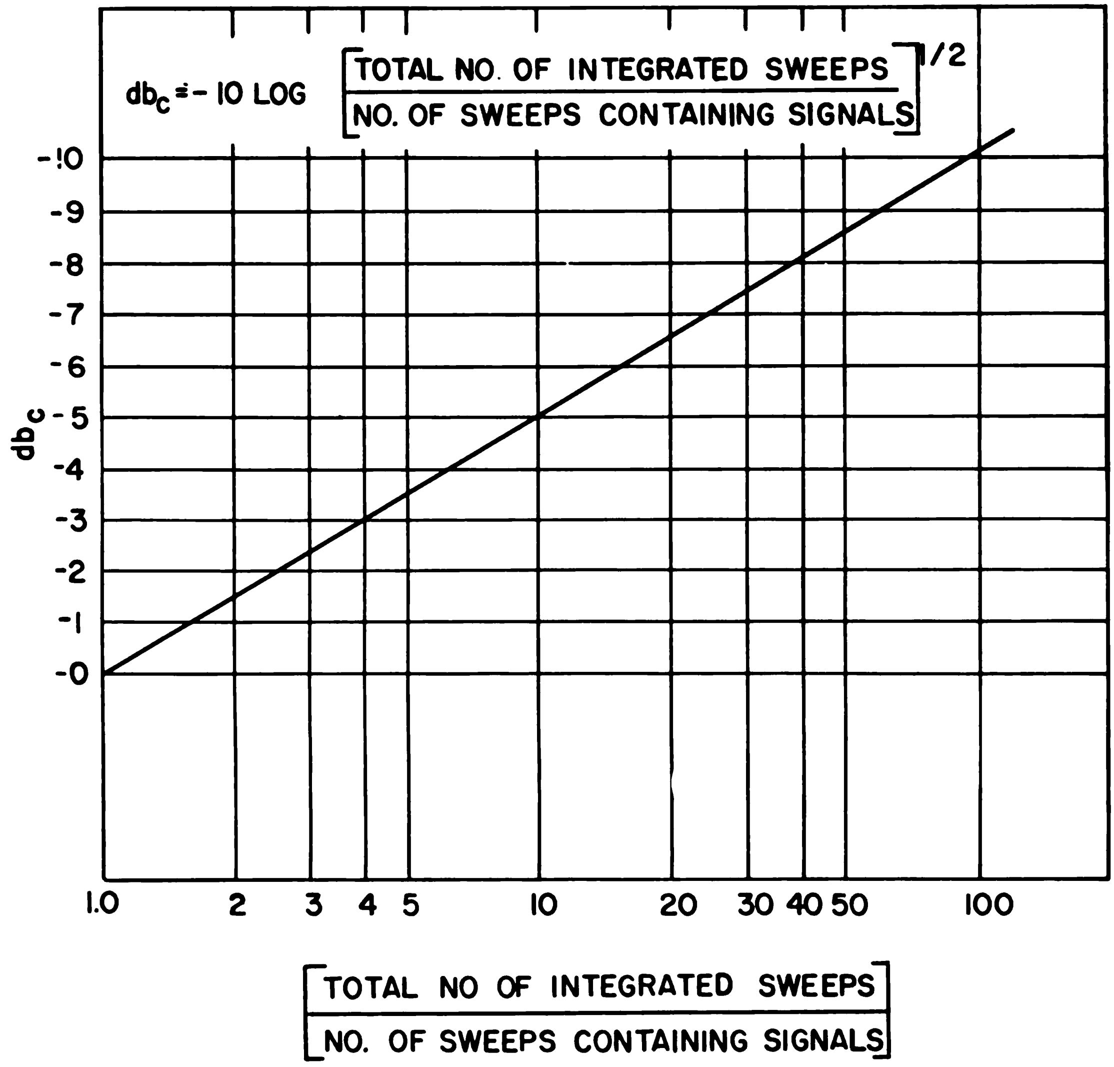

Figure 6-46. Indicator Collapsing Function

EXAMPLE 1
COMPUTATION OF MAXIMUM RELIABLE RANGE FOR RADAR SYSTEM *XYZ*
(UNDER SCANNING CONDITION OF 6.0 RPM)

Antenna Gain (two way) : 2 × 40.2 db	db_{Ant}		=		+80.4
Transmitter Power : 800 kw	db_P	Fig. 6-3	=		+59.0
Frequency : 2800 mc	db_λ	Fig. 6-4	=	−41.4 db	
Target Size : 4.7 M^2	db_A	Fig. 6-5	=	−4.3 db	
Receiver Noise Figure : −12 db	db_{NF}		=	−12.0 db	
Receiver i-f Bandwidth : 1.3 mc	db_n	Fig. 6-6	=		+142.9 c
Pulse Length : 2.0 usec					
Bt : (if bandwidth × pulse length) = 1.3 mc × 2 usec = 2.6	db_{tb}	Fig. 6-47	=		3.2 d
Losses : 1.0 db	db_L		=	−1.0 db	
Az. Beam Width (ϕ) = 0.9° $prf \times \phi$	db_H	Fig. 6-44	=	−6.4 db	
Rep. Rate (prf) = 300 pps = 270					
Az. Rotational Rate = 6.0 rpm					

Note: db_H may be obtained from Fig. 6-45 by computing the "pulse hits per target traverse." For example:

$$\text{Pulse hits} = \frac{prf \times \phi}{6 \times rpm} = \frac{300 \times 0.9}{6 \times 6} = 7.5$$

and, from Fig. 6-45 $db_H = -6.4$ db.

Total	−65.1 db	+285.5 db
		−65.1 db
Total System db =		+220.4 db

Slant Range Fig. 6-7 = 200 Statute Miles; this is the mean range. Note that this is different from the 238 miles calculated in paragraph 6-2.

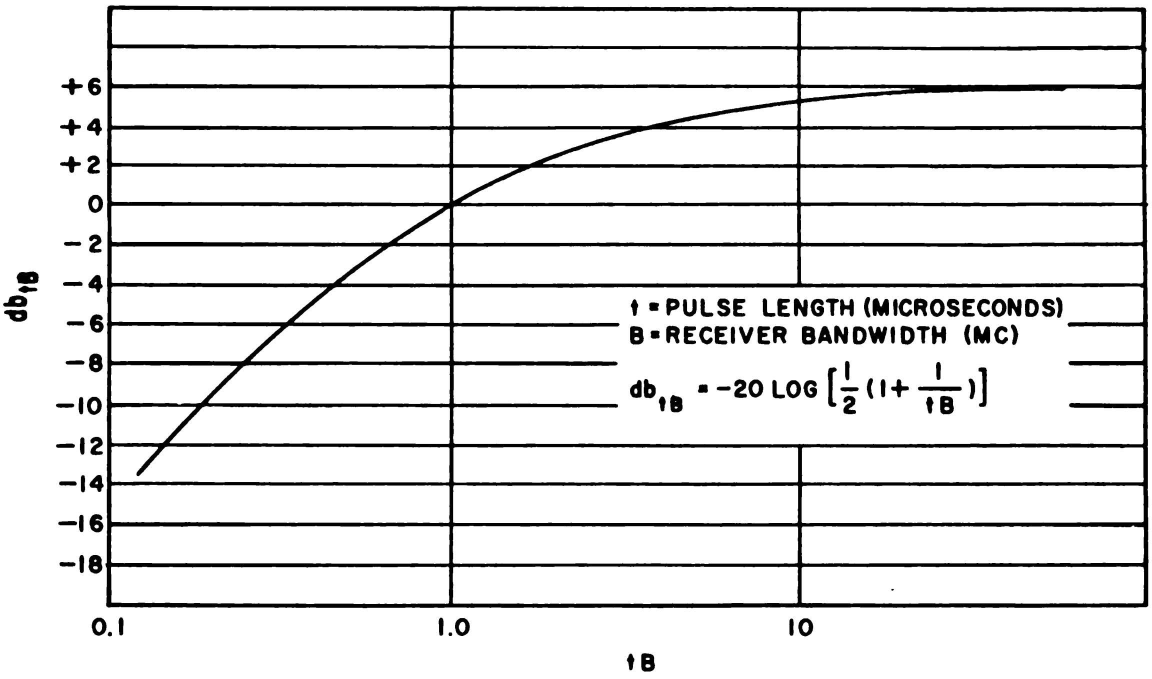

Figure 6-47. Receiver Representation Factor

6-4.6 PROBABILITY OF DETECTION[60]

Figure 6-48 shows the probability of detecting a target returning a signal with a Rayleigh distributed amplitude. Range is presented in normalized fashion, based on the range at which the single scan detection probability is 50 percent.

The cumulative detection probability for a given range is the probability of detecting an incoming target on at least one scan by the time it reaches that range. It depends on target speed and course and on the scan rate of the radar.

Figure 6-49 enables the easy calculation of the increment in target range between scans. This quantity is used in Figure 6-50 to normalize the range quantities so that they may be presented in a simple and useful form. To use the curve, δ is found from Figure 6-49 and is known in the problem at hand. The curve will then yield the normalized value of the other range parameter.

Figure 6-51 is included for convenience. The first quadrant of this curve is identical to Figure 6-50. The second and fourth quadrants can be used to convert the range parameter from miles to dimensionless forms.

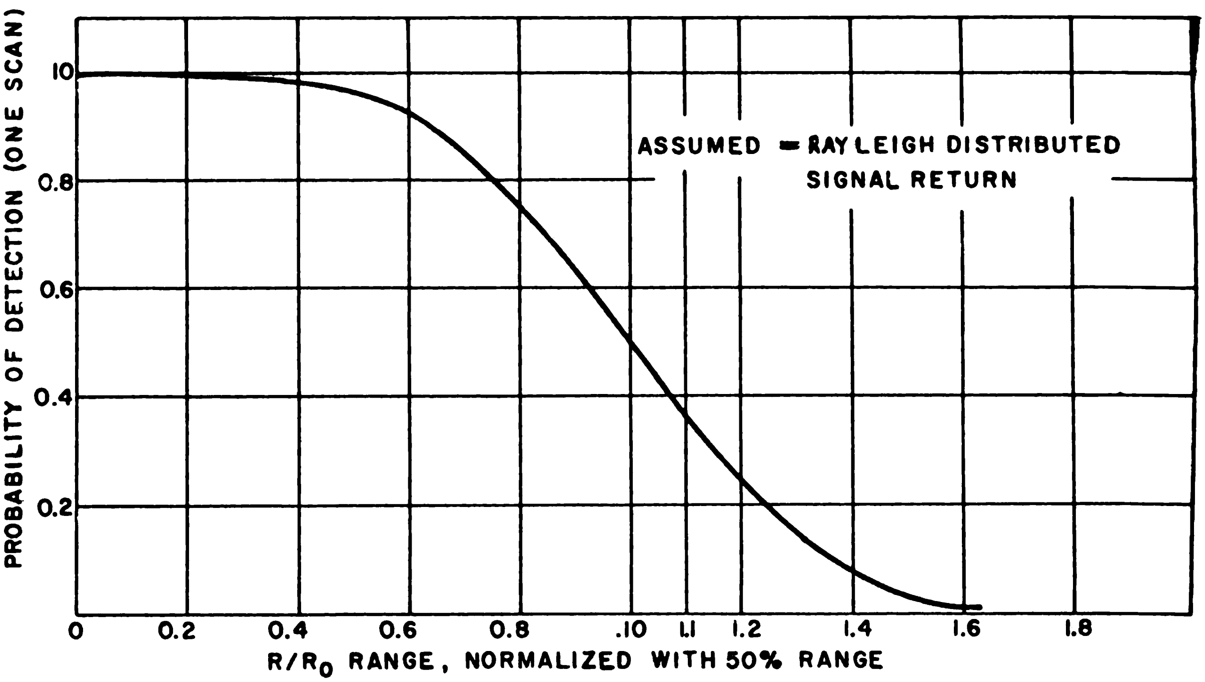

Figure 6-48. Single Scan Probability of Detection Versus Range

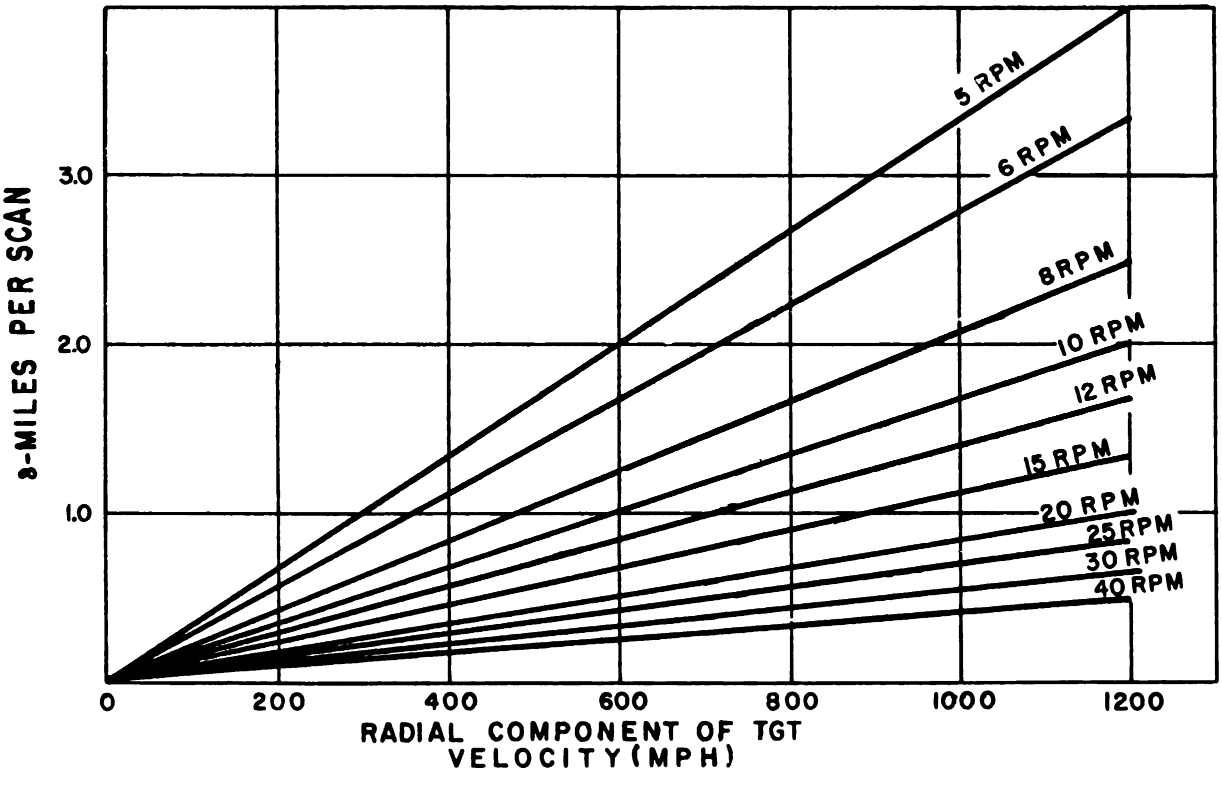

Figure 6-49. Target Displacement During One Scan Versus Target Velocity and Scan Rate

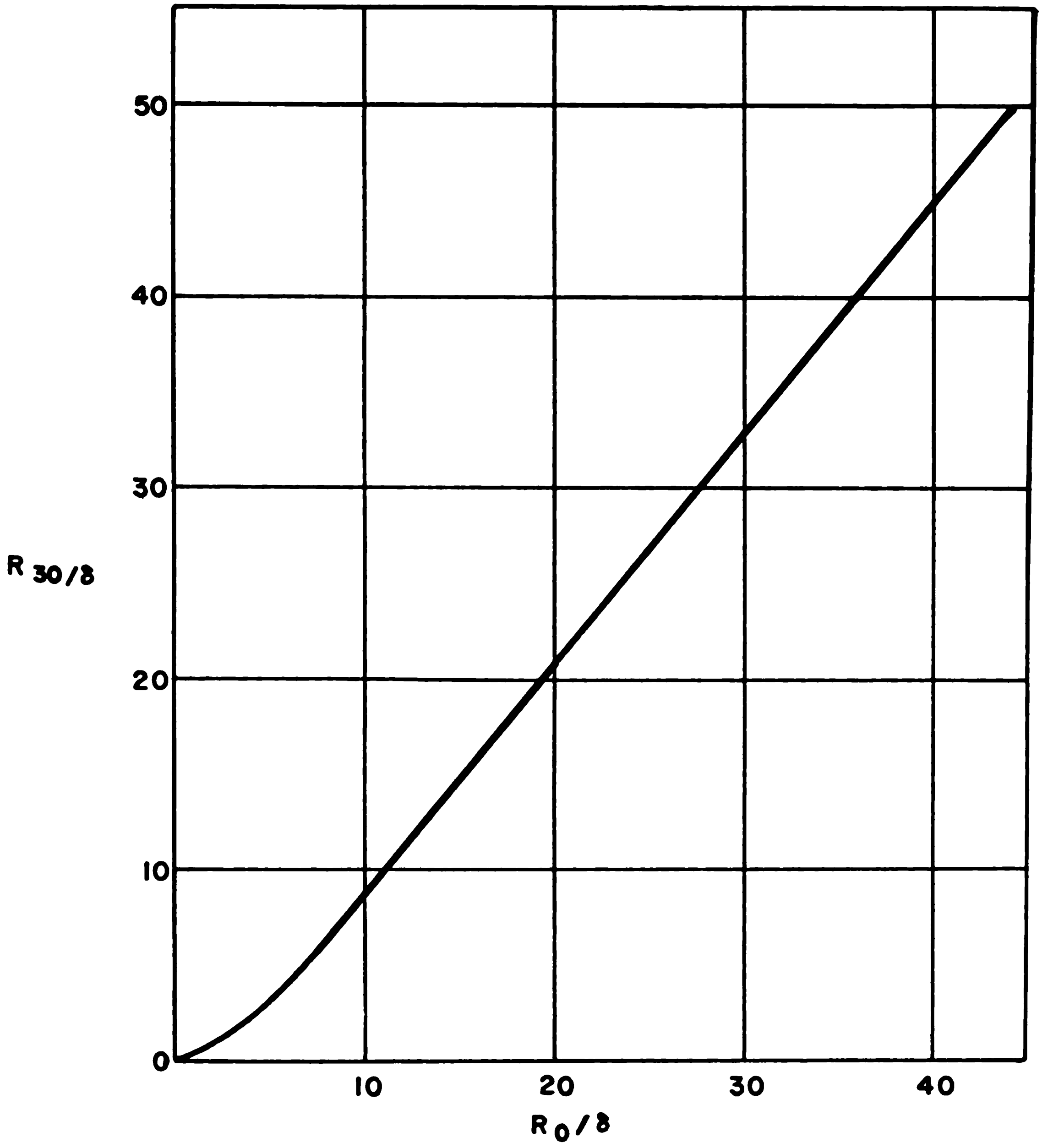

Figure 6-50. Fifty Percent Single Scan Detection Range Necessary for Ninety Percent Cumulative Detection Probability at Range R_{90}

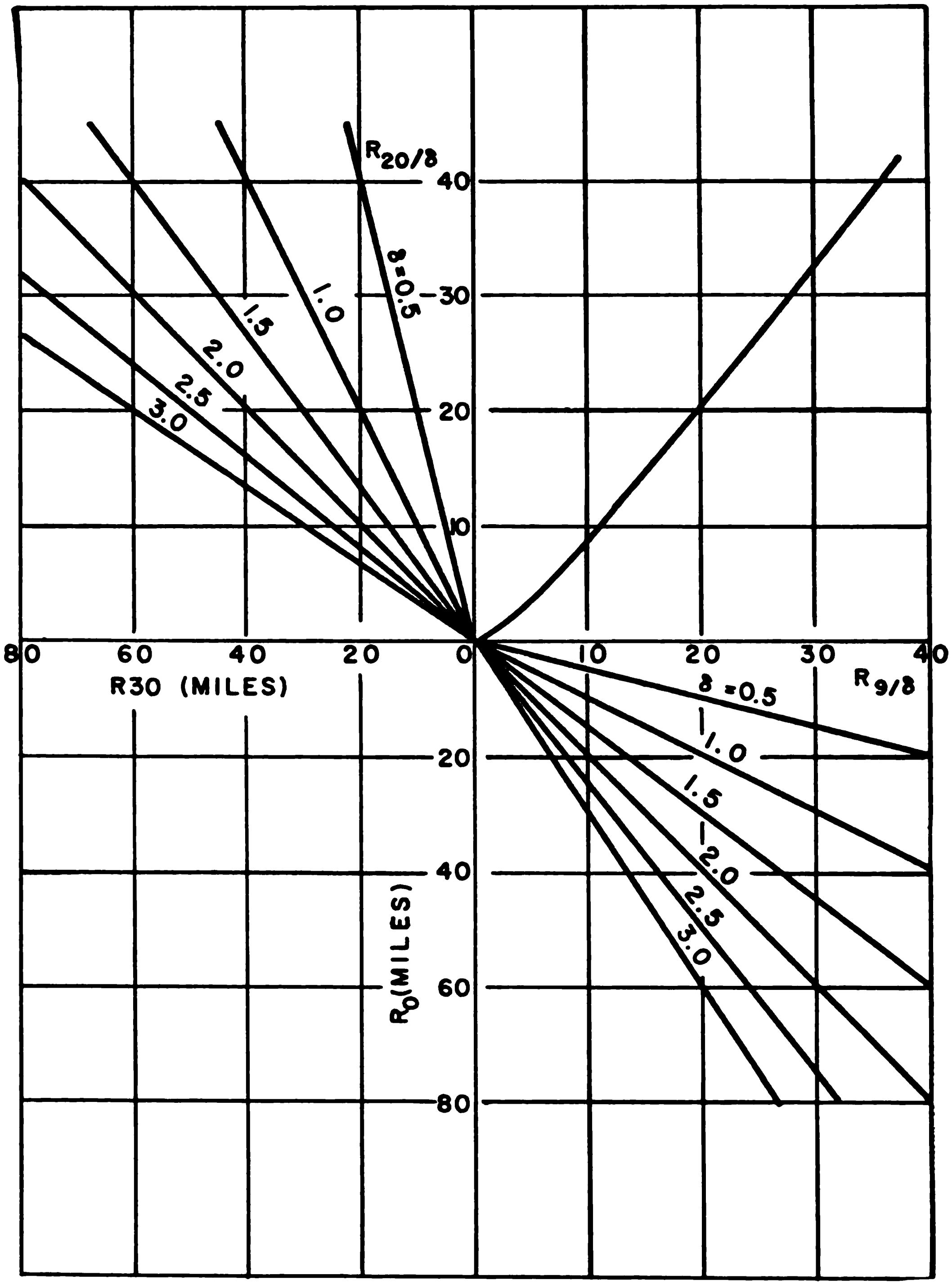

Figure 6-51. Correlation of 90 Percent Cumulative Detection Probability Range With 50 Percent Single Scan Detection Range

6-5 TRACKING RADARS, ANALYSIS AND DESIGN

6-5.1 GENERAL

The purpose of this section is to serve as an introduction and guide to the design techniques and problems of tracking radars. A description and analysis of the various tracking techniques and a system for analyzing common sources of tracking errors is presented with the necessary graphs and sample calculations to facilitate a rapid and convenient method for computing and analyzing the problems encountered in tracking radar design.

6-5.2 TRACKING RADAR TYPES

6-5.2.1 Conical Scan and Lobe Switching

The simplest method of radar tracking consists of manually maximizing the echo received by a pencil beam radar. The difficulty with such a simple approach is that a decrease in the signal level may be due to increasing range, target fluctuation or the target moving off the center of the beam. In the latter case, decrease of the signal gives no hint in which direction the beam must be moved in order to recenter the target.

A number of methods have evolved to overcome these difficulties. In the case cited above the operator would learn to jitter the beam back and forth to find the target. The simplest mechanical approach is to do the same thing. A single beam is either rotated in a small circle or switched rapidly back and forth a fraction of a beam width by switching between two r-f feeds. These methods are both sequential lobing. The former method, conical scanning, is p tured in Figure 6-52. In this manner the tar may be centered by keeping the received sig at a constant level. When the target moves center, the received signal will show a modul tion at the lobing (switching or conical sca ning) frequency. Furthermore, it is appare that if this modulation can be compared in pha with the position of the beam it will indica the direction of the target from the boresig or center of the lobing pattern.

In a conical scan radar, the beam is usuall caused to wobble either by rotating a paraboli dish about an axis tilted with respect to th focal line of the dish or, more commonly, b rotating or nutating the feed. Whichever method is used to scan, a two-phase reference generator is attached to the scanner. The received signal, after detection, is then compared with these reference voltages in order to detect an error in two orthogonal directions. The error so derived, when small, is proportional to the deviation off-boresight and may be used as an error signal for azimuth and elevation servos. Because of the orthogonality of the two reference voltages when they are properly phased, the error signals are completely separated; that is, the balanced detectors produce a signal only for errors in the plane of the proper servo control.

The magnitude of the error signals so derived would be a function of target size and range if an automatic gain control were not used, as shown in Figure 6-53. This circuit maintains a constant magnitude of the average signal output. The effect is to normalize the error

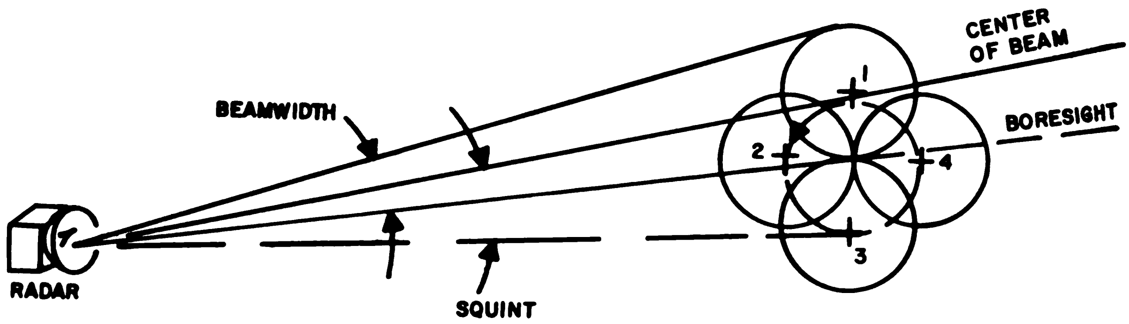

Figure 6-52. Conical Scanning

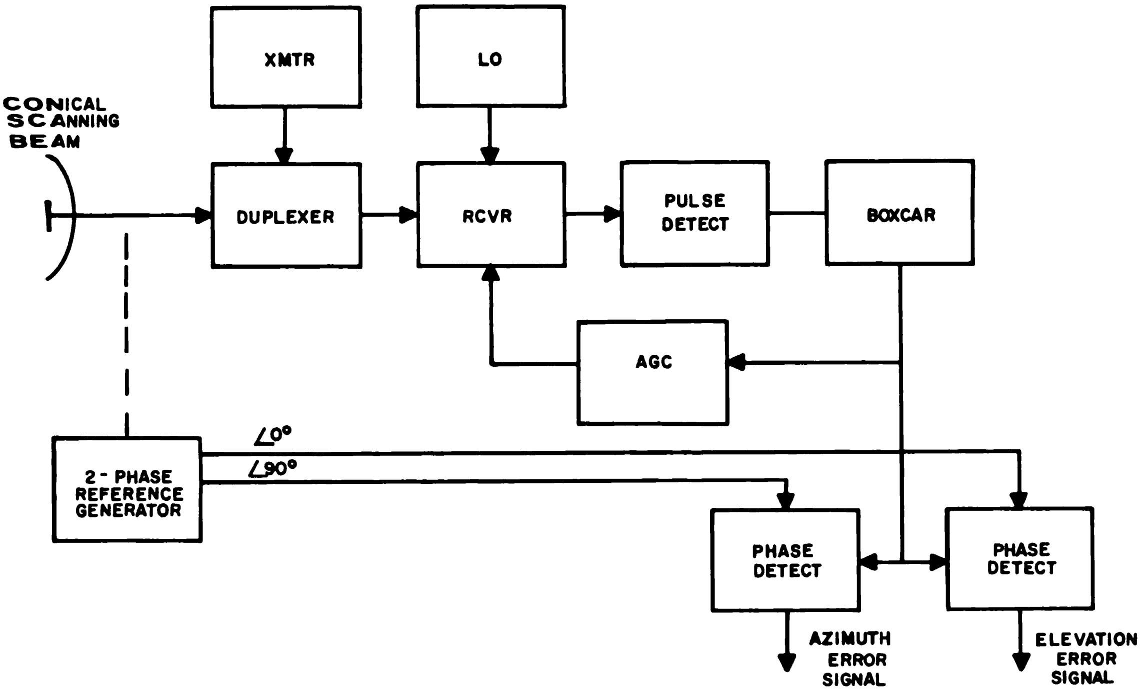

Figure 6-53. Conical Scan Radar

signals so that they are proportional only to the angular distance off-boresight.

A quantity of interest in all tracking systems is sensitivity — the ratio of angular error or deviation from the boresight to the electrical error signal. The automatic gain control is fundamental to this concept also. Obviously the sensitivity would be meaningless without some form of AGC, since additional amplifiers or transformers could raise it ad infinitum. The sensitivity, K_S is therefore usually expressed in a dimensionless form. It is often taken, also, on a per beamwidth basis and this will be done here. That is, if the beamwidth is Θ, the angular error ε, the error voltage Δ, and the received signal strength S, then:

$$\frac{\Delta}{S} = K_s \frac{\varepsilon}{\Theta} \tag{6-71}$$

Since the AGC has normalized the Δ signal by the signal S for the conical scan, this is only a measure of the signal modulation due to the angular error ε. This modulation is determined by the beam shape and squint angle, or angle of the scanning cone.

Note that equation 6-71 assumes that a linear relationship exists between the angle error and the Δ signal. Obviously this is untrue for large angles but it is a good approximation with proper squint angles near the boresight. The minimization of tracking errors is usually desirable. The sensitivity will be more strictly defined as the rate-of-change of normalized error signal with angle error per beamwidth, evaluated at zero error.

The antenna patterns may be chosen either for maximum sensitivity or for maximum linearity, but not both. Usually, maximum sensitivity is desirable for conical scanning since at all times the signal from the receiver will contain an rms amount of noise N. In this case the output of the radar will be:

$$\frac{\Delta + N}{S + N} \tag{6-72}$$

In cases of interest for accurate tracking, the signal-to-noise is high so that this is approximately:

$$\frac{\Delta}{S}+\frac{N}{S}=K_s\frac{\varepsilon}{\Theta}+\frac{N}{S} \qquad (6\text{-}73)$$

This is then used as an error signal by a servo system which generally has a filtering action and can be characterized by a filter factor K_f. This reduces the effective rms noise so that when the servo error is reduced to zero the target is still off the boresight, i.e., it has an rms error angle ε defined by:

$$K_s\frac{\varepsilon}{\Theta}+\frac{1}{K_f}\frac{N}{S}=0 \qquad (6\text{-}74)$$

or

$$\frac{\varepsilon}{\Theta}=\frac{1}{K_s K_f}\frac{N}{S} \qquad (6\text{-}75)$$

This sensitivity may be evaluated from the antenna pattern which quite often approximates the pattern produced by an aperture with illumination varying across the aperture in a cosine fashion.

Figure 6-54 shows the round trip voltage patterns *A* and *B* of a conical scan or sequential lobing radar with a squint angle equal to the beamwidth of the antenna. The average signal, ½ $(A + B)$, will be proportional to the average of the pattern in its two extreme positions which correspond to the positions *A* and *B* as seen in Figure 6-54. A target off the boresight will cause a modulation of the average signal with a peak-to-peak amplitude proportional to the difference between the two patterns $(A - B)$. This modulation is what is detected by the conical scan. The AGC circuits cause it to be measured only in terms of the percent modulation of the average signal.

If it is assumed that this peak-to-peak value can be taken also as the peak-to-peak of the component of scanning frequency in the modulation, the amplitude of the error signal is given by:

$$\Delta=\frac{1}{2}(A-B) \qquad (6\text{-}76)$$

In which case, since the average signal is:

$$S=\frac{1}{2}(A+B) \qquad (6\text{-}77)$$

then:

$$\frac{\Delta}{S}=\frac{A-B}{A+B} \qquad (6\text{-}78$$

This gives a means of evaluating the sensitivity. From Figure 6-54 near the boresight, it is seen that $(A+B)$ is just unity, while $(A-B)$ varies essentially linearly with the normalized angle. From the figure, slope of the Δ/S versus ε/Θ curve can be measured. Near the zero error point:

$$\frac{(A-B)}{(A+B)}=2.88\,(\varepsilon/\Theta) \qquad (6\text{-}79)$$

By comparison with equation 6-71, equation 6-78 then leads to the following value of sensitivity for an echo tracking conical scan radar with one beamwidth squint:

$$K_s=2.88 \qquad (6\text{-}80)$$

Other configurations of the antenna will have sensitivities which can be calculated similarly. For example, Figure 6-55 shows the patterns for a squint of 0.4 beamwidth which produces a wide region of linearity in the error signal characteristic and Figure 6-56 shows the one-way patterns for the same conditions as above. These patterns would be applicable for tracking a beacon. It is seen that the slope of the Δ/S patterns can be reduced, for symmetrical patterns, to the slope of the pattern at the cross-over divided by the value of the pattern at cross-over. From Figure 6-56 this yields, for beacon tracking conical scan with one beamwidth squint:

$$K_s=\frac{1.05}{0.707}=1.49 \qquad (6\text{-}81)$$

The squint angle may be adjusted to give maximum sensitivity or maximum linearity of the Δ signal with displacement from the boresight. It may be noted from the form of equations such as 6-81 that the linearity of pattern which is of importance is actually the linearity of the pattern of Δ/S versus angle. This pattern can be readily calculated from Δ and *S* patterns and plotted. In general, this pattern will exhibit linearity over a much larger angle than the difference pattern alone. Table 6-4 lists more values for sensitivities of conical scanners.

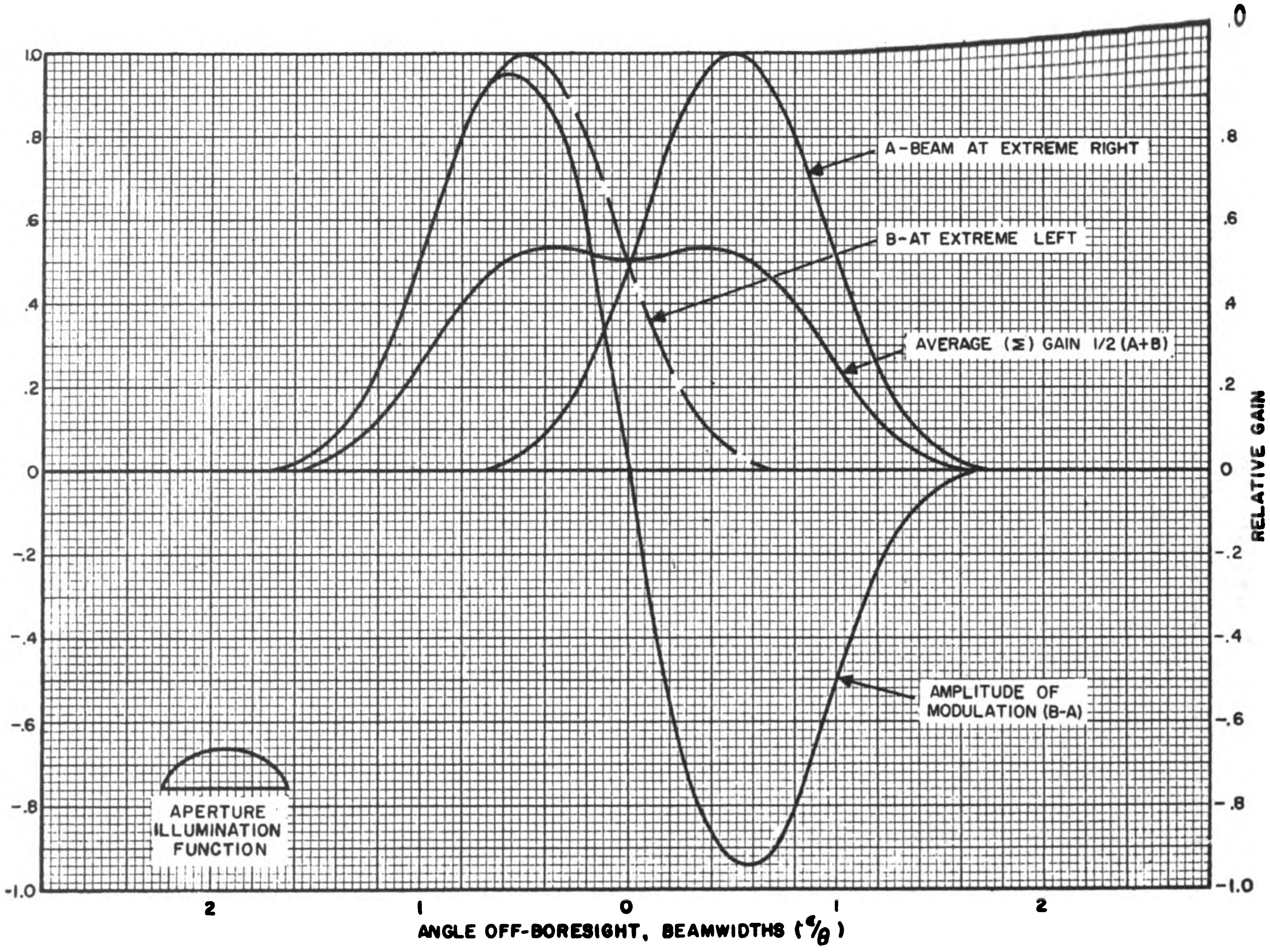

Figure 6-54. Round Trip Antenna Patterns — One Beamwidth Squint

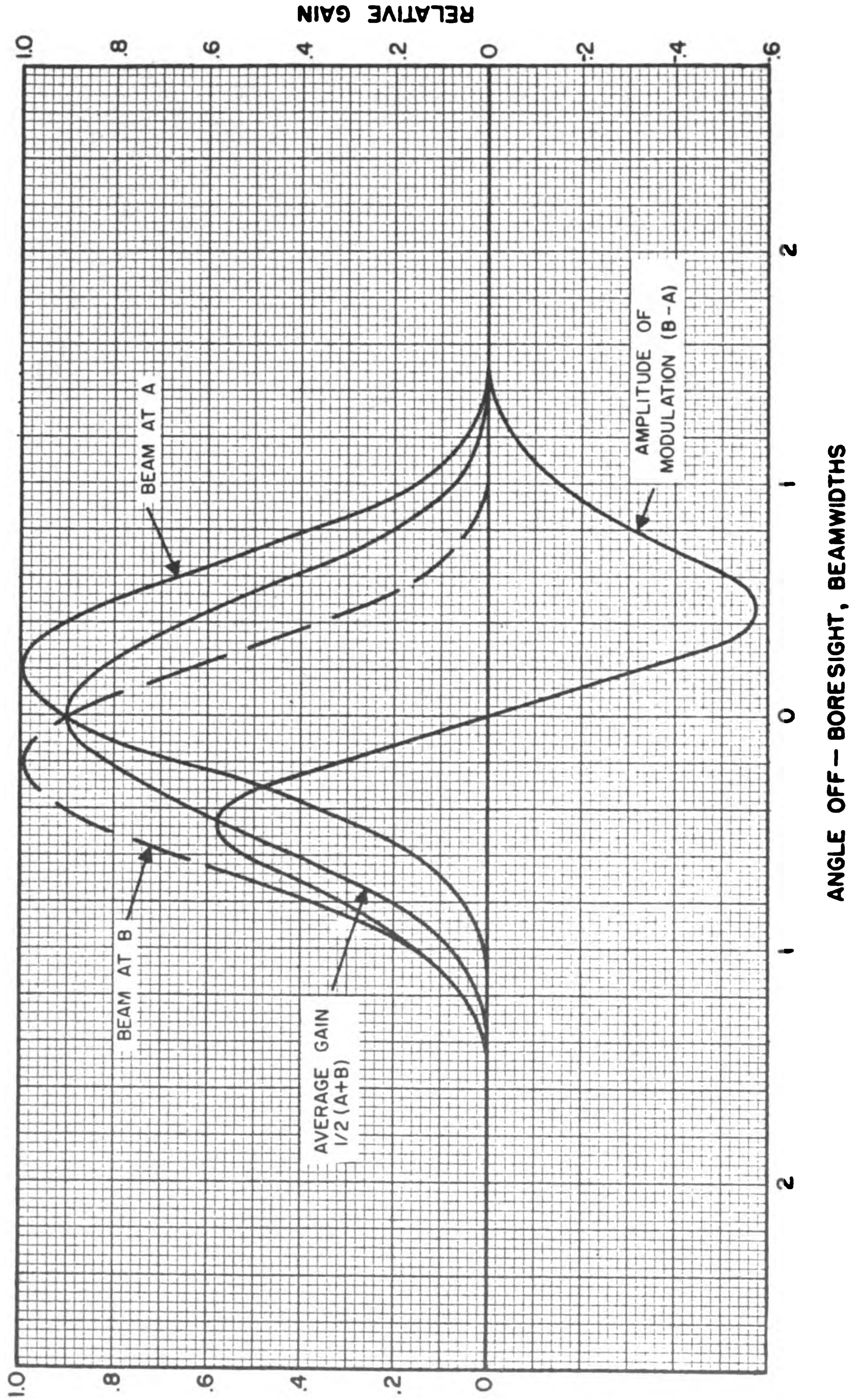

Figure 6-55. Round Trip Antenna Patterns — 0.4 Beamwidth Squint

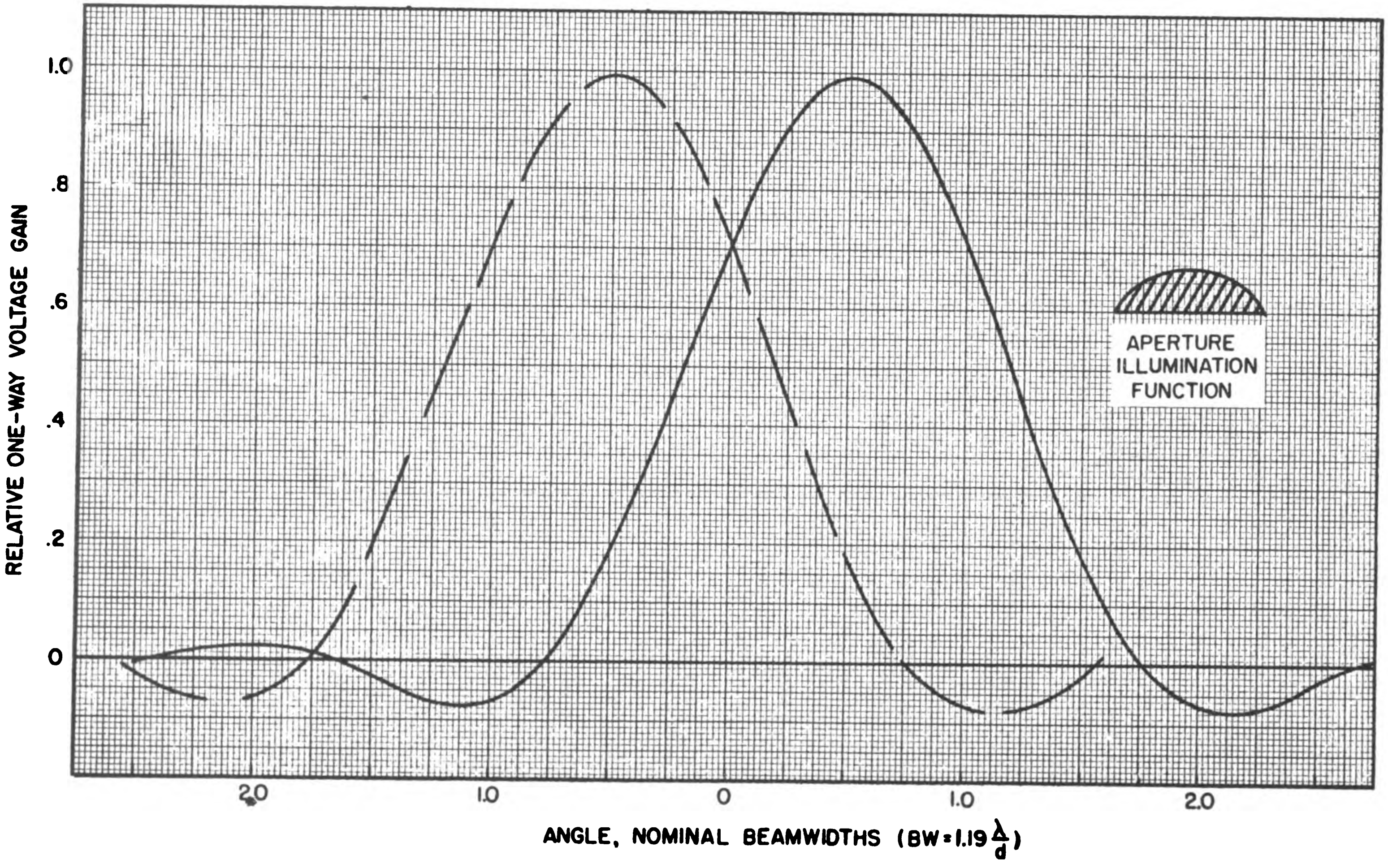

Figure 6-56. One-Way Antenna Pattern — One Beamwidth Squint

TABLE 6-4. TYPICAL TRACKING RADAR PARAMETERS

Radar Type		Squint, beam-widths,Δ -or- Phase center separation, aperture widths	Loss of gain, oneway, db*	Angular Sensitivity K_s	
				RatioΔΔ	DB
Conical Scan:					
Echo**	Maximum sensitivity	1.0	3.0	2.88	9.2
	Linear error	0.4	0.5	1.06	0.5
Beacon**	Maximum sensitivity	1.36	5.8	2.26	7.1
	Linear error	0.8	1.9	1.12	1.0
	3 db crossover	1.0	3.0	1.49	3.5
Amplitude Monopulse:					
4 feed**	Optimum gain-sensitivity product	0.9	2.0	1.30	2.3
	Linear error	0.8	1.4	1.12	1.0
2 feed	Log comparison with 3 db crossover	1.0	2.6	1.39	2.8
Phase Monopulse:					
4 feed**	Optimum gain-sensitivity product	0.45	-0.7***	1.69	4.6
	No overlap	0.5	0.0	1.88	5.5
	1/3 overlap (low sidelobe)	0.33	-0.2***	1.26	2.0
Combination Monopulse:					
No overlap, optimum Amplitude axis gain-sensitivity product**	Phase	0.0	2.5	1.88	5.5
	Amplitude	0.92		1.34	2.5
AN/TPQ-10(XN-1)ΔΔΔ	Phase	0.367		1.24	1.9
	Amplitude	1.09	3.0	2.03	6.1

*Compared to gain of total aperture, assuming cosine illumination.
**Based on cosine illuminations from all feeds.
***Increased gain, relative to cosine illumination.
ΔBased on the nominal beamwidth for the aperture with cosine illumination (1.19 λ/d).
ΔΔVolts/volt/beamwidth, based on the same nominal beamwidth of note 4.
ΔΔΔEmpirical data.

Note that the squint angle also causes a loss boresight antenna gain relative to that realed in the direction of maximum gain.

The concept of sensitivity has been developed rom a theoretical view. In practice, the patterns which might be measured would be the omposite S and Δ/S patterns. Because of their ature, these may be called sum and difference, r sum and delta patterns. The significance of this will be more apparent for monopulse radars.

Conical scan radars have some other significant characteristics including susceptibility to error due to amplitude modulation of the received signal and fading. Most radar targets exhibit fading at frequencies such that the conical scanner senses the modulation and erroneously treats it as an error signal. This leads to angular errors in tracking. Another characteristic follows from the fact that in conical scanning or sequential lobing the angular error information is carried on the scanning frequency. After detection and filtering, this signal will contain noise from two sidebands of the lobing frequency carrier. This leads to less noise improvement by filtering or servo action than is experienced by equivalent monopulse trackers.

6-5.2.2 Amplitude Monopulse

The difficulties experienced by sequentially lobing radars due to their scanning frequency are decreased when the scanning frequency is increased. Amplitude monopulse may be thought of as sequential lobing at infinite frequency. A single r-f pulse is simultaneously fed from separate horns into the same reflector, or fed to separate antennas. The two lobes produced are squinted. In the case of a single reflector, this is achieved by moving the feeds slightly off the focal point or line. The returned signal can be compared directly in the same manner as for conical scan except the difference between the signals in the two lobes is constant rather than modulated at a scanning or lobing frequency.

The most direct way to do this might be to have a separate receiver for each horn, the outputs of which are detected and compared. In practice, it is common to use an r-f hybrid to form sum and difference of the separate antenna lobes. This has a number of advantages. It enables use of an AGC circuit that performs the function of normalizing the output as was done in the sequential lober. It removes the need for maintaining very closely matched amplitude response in two receivers, since the actual receiver gain in the sum-difference ($\Sigma - \Delta$) system determines only the sensitivity of the signal and cannot cause a change of the zero position, or boresight shift. Figure 6-57 shows such a $\Sigma - \Delta$ system for one axis. The action of such a system is exactly analogous to the conical scan in free space. Antenna patterns would look just like those shown in Figure 6-56.

At least one more feed is required to use such a system for two-axis tracking. Normally two are added to give a four-horn system such as that of Figure 6-58. This system uses the horns in pairs to derive error signals for the two axes. By using hybrids as shown, the error signal in azimuth, or $\Sigma\Delta$ signal is given by:

$$\Sigma\Delta = A - B + C - D = (A + C) - (B + D) \tag{6-82}$$

Similarly, the elevation error is:

$$\Delta\Sigma = (A + B) - (C + D) \tag{6-83}$$

This system makes optimum use of the received signal. Other systems could be readily devised that would compare only A and B for azimuth error and A and C, say, for elevation error. This obviates the necessity for the fourth feed, but causes a nonsymmetrical pattern and less than optimum use of the received signal.

The sensitivity of an amplitude monopulse radar is found from the same procedure as that used for conical scan, with one important difference. Because the target is simultaneously illuminated by both lobes, the effect of the transmitting antenna pattern is the same on the signal returned in any receiving lobe. Because of this, one-way voltage patterns must be used for either echo or beacon-tracking in calculating sensitivity of monopulse radars.

Practically, in a monopulse radar the antenna patterns of interest are the sum and difference patterns, not the patterns from separate feeds. The sum pattern, determined by all the feeds, fixes the total signal strength incident on the

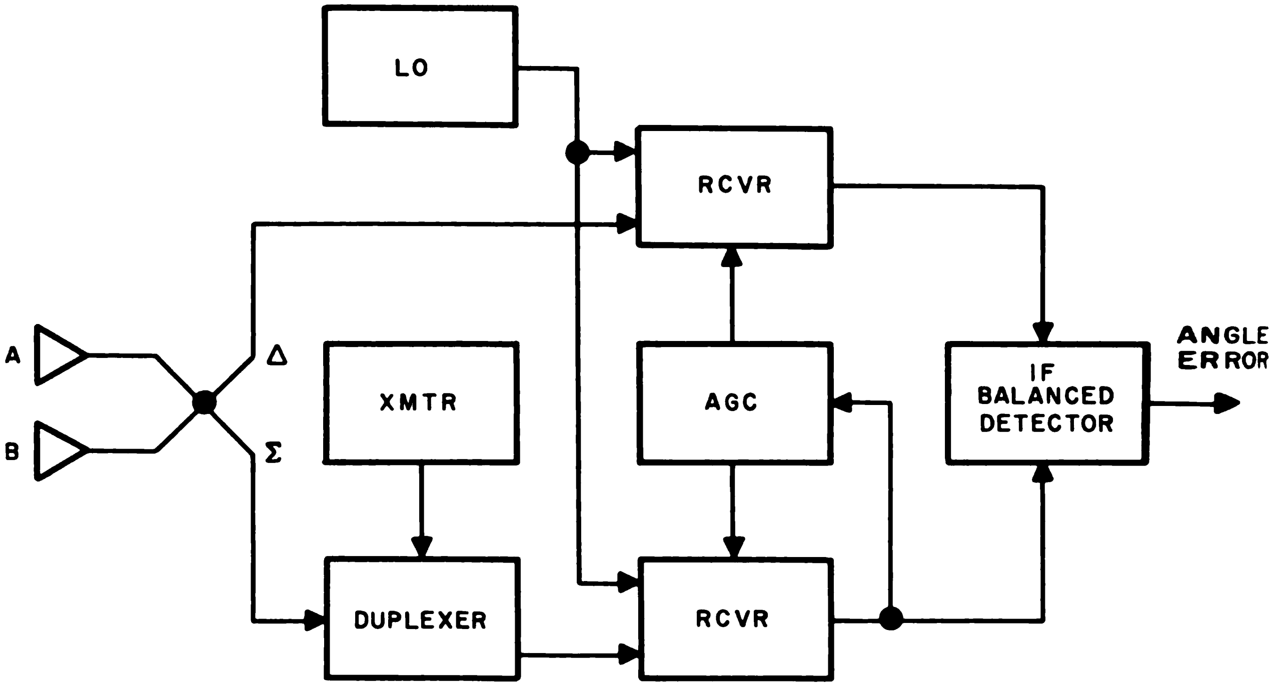

Figure 6-57. $\Delta - \Sigma$ *Comparison*

target as well as the receiving gain for ranging purposes and signal-to-noise calculations. These one-way sum and difference patterns have shapes like those shown in Figure 6-59. (Difference patterns in either axis are similar.) It is actually the Δ/Σ or normalized difference pattern that is of interest due to the use of AGC circuits. The sensitivity is found from the slope of this Δ/Σ pattern at its zero (on the boresight). There is, of course, nothing to prevent the design of equipment that has different patterns in its separate axes and therefore unequal sensitivities in the two directions. So, in general, two sensitivities must be specified for a four-horn system and errors must be determined separately for each axis.

The noise errors are found from the same reasoning as that used for conical scan. Assuming large signal-to-noise ratios, when the Δ signal is zero, the noise, decreased by the filter factor, determines the angle error, according to the formula:

$$\frac{\varepsilon}{\Theta} = \frac{1}{K_s K_f} \frac{N}{S} \tag{6-84}$$

Both the sensitivity K_s and signal S, (through its dependence on the sum-pattern gain) depends on squint angle. An optimum value of squint exists. If only the angular error due to noise is considered, the optimum is achieved when the product $K_s G$ is a maximum. The gain that is applicable is round-trip on one-way voltage gain for echo or beacon tracking respectively. (As pointed out above, in monopulse radars, K_s is equal for either type tracking.)

On the other hand, in some applications it may be desired to adjust the squint for the optimum linearity of error signal versus error angle. For four horn amplitude comparison, the significant characteristics of these two important configurations are given in Tables 6-4 and 6-5. Reference 61, especially the second quarterly report, covers the variations of sensitivity and gain in monopulse radars in more detail. It should be emphasized that the optimum performance in a tracking system is obtained when the gain-sensitivity product is maximum and not for maximum sensitivity alone.

TABLE 6-5. COMPARISON OF TRACKING RADAR TYPES[*]

Radar Type		Extent of Linear Error Signal, Beamwidths[**]	Figure of Merit, db[Δ]
Conical Scan:			
Echo	Maximum sensitivity	0.5	0.2
	Linear error	1.9	-3.5
Amplitude Monopulse:			
4 feed	Optimum gain-sensitivity product	1.7	-1.7
	Linear error	2.4	-1.8
2 feed	Log comparison with 3 db crossover	-wide- See Note 2	-2.4
Phase Monopulse:			
4 feed	Optimum gain-sensitivity product	0.45	6.0
	No overlap	0.4	5.5
	1/3 overlap (low sidelobes)	0.6	2.4
Combination Monopulse:			
No overlap, optimum Amplitude axis gain-sensitivity product	Phase	0.4	0.5
	Amplitude	1.7	-2.5

[*] Same systems as listed in Table VI-4.

[**] Five percent linearity: based on cosine illuminations. Use of Δ-Σ comparison. Thus the linearity is that of the pattern. The range of linear error signal may be increased by the use of nonlinear circuits.

Logarithmic comparison will be linear over as great an angle as the lobe patterns approximate a Gaussian curve, which may be several beamwidths.

[Δ] Angular sensitivity times loss of gain, two way, (less 3 db for conical scan due to decreased filter factor). Note that this comparison is only with respect to errors due to thermal noise. All types of tracker will have much higher noise errors for off-boresight tracking due to loss of gain and loss of sensitivity.

---

[*] Same systems as listed in Table 6-4.

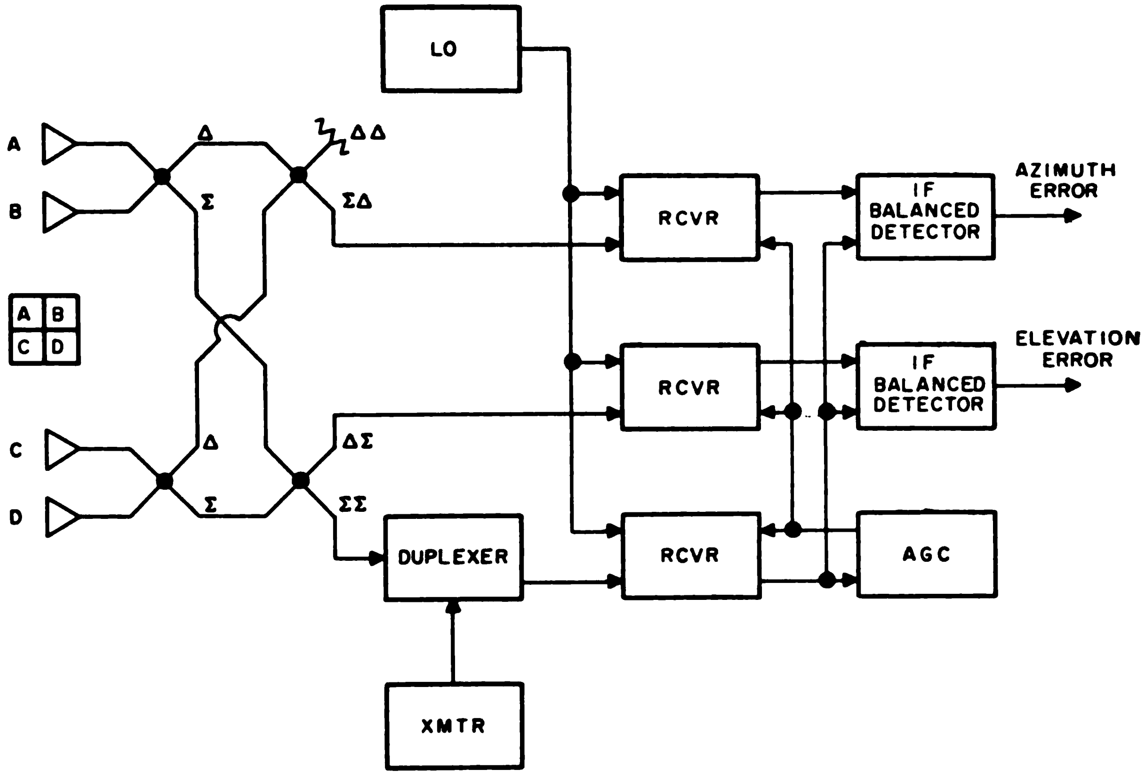

Figure 6-58. Four-Horn Monopulse Radar

A number of variations from the sum-difference type of amplitude monopulse are possible. In some cases it may be desirable to avoid the use of AGC. This can be done by placing a 90-degree phase shift in the Δ signal before detection and then recombining the sum and delta signals (see Figure 6-59d). The result is a pair of signals that differ in phase by an angle proportional to Δ/Σ. Assuming small error angles, if these two signals are processed through separate receivers and phase detected, this system also detects Δ/Σ and has the same sensitivity as the previous system. However, since the video detection is a phase detection the receivers may be limiting. This relaxes the requirements of gain matching at the expense of requiring phase matching between two channels. This method can be extended to a four-horn system easily. Also, although Figure 6-59d shows the conversion using two hybrids and a

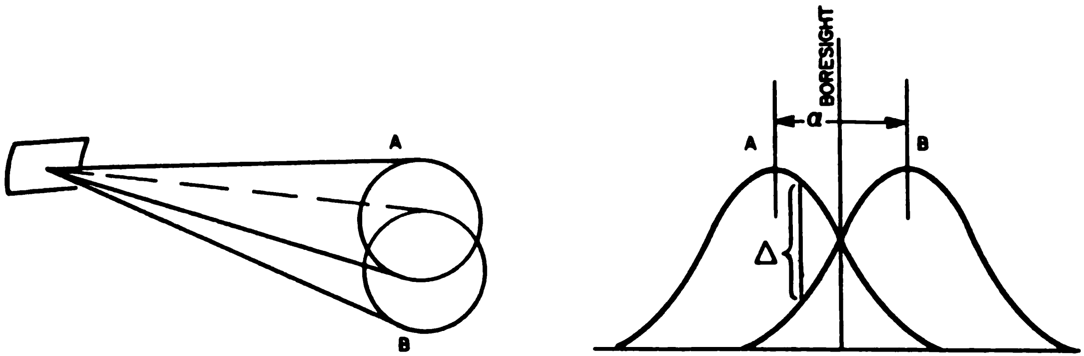

a. SQUINTED BEAMS

b. AMPLITUDE DIFFERENCE Δ DEPENDS ON SQUINT α, ANTENNA PATTERNS, AND ERROR ANGLE Σ.

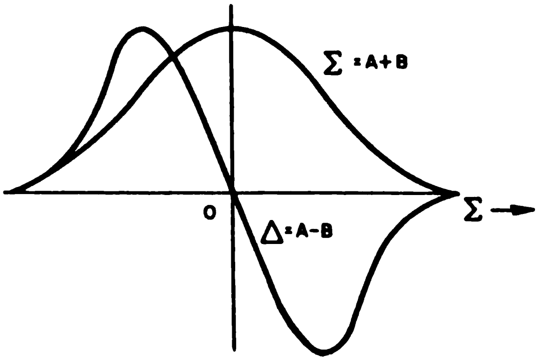

c. SUM & DIFFERENCE PATTERNS

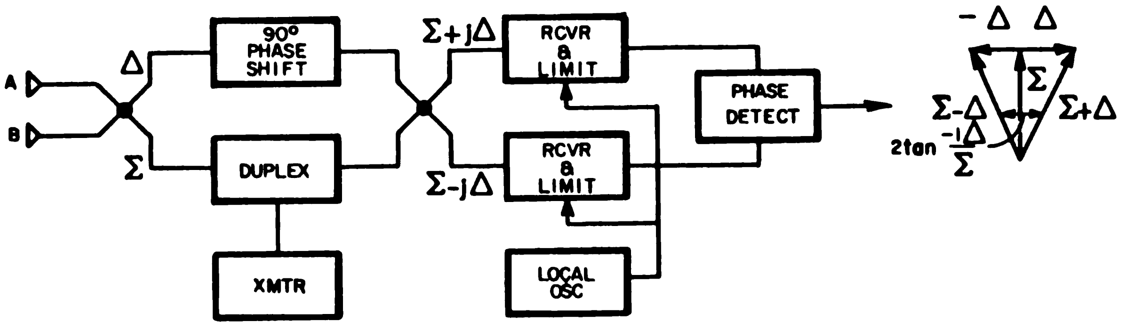

d. CONVERSION TO PHASE DETECTION

Figure 6-59. Amplitude Monopulse

phase shift, a single device (the short-slot hybrid) will perform the conversion directly. However, duplexing is then more complex.

A variation of the same technique recombines the sum and delta signals at intermediate frequency and phase detects. In this way boresight shifts due to long runs of waveguide are minimized.

Another type of amplitude comparison that is of importance is logarithmic comparison, as seen in Figure 6-60. This system uses completely separate receiving channels and receivers of logarithmic response as seen in Figure 6-61. It requires separate duplexing and close-gain matching of the two receivers. It has at least three significant advantages:

(a) it eliminates the requirement for AGC circuits

(b) because of the absence of the time delay associated with AGC circuits, it presents the error signal for a given target instantaneously

(c) the error signal due to a target off b sight can be made proportional to distance off boresight over a very w angle

The latter two attributes are particularly us ful for tracking within the beam by electron means, as opposed to boresight tracking b servoing the antenna. This system has bee used for height finding in cases where mul lobed patterns were used. For this reason, th angular sensitivity and angular error at angl off the boresight are of interest.

Assume that the shapes of both of the lobes shown in Figure 6-62 are Gaussian. In terms of the squint angle, α and beamwidth of one lobe. Θ, the signals in either channel, for a target off boresight and angle ϕ are proportional to:

$$A \sim e^{-1.39\frac{(\alpha/2+\phi)^2}{\Theta^2}}, B \sim e^{-1.39\frac{(\alpha/2+\phi)^2}{\Theta^2}} \tag{6-85}$$

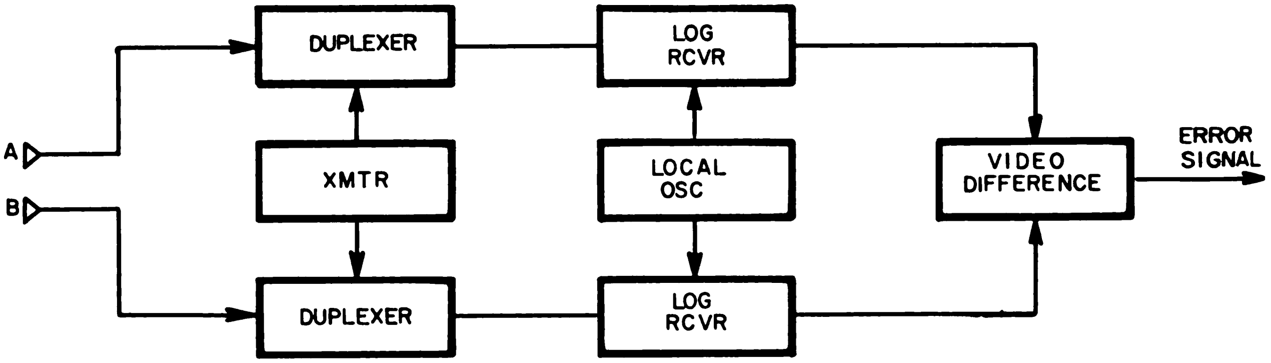

Figure 6-60. Logarithmic Amplitude Comparison

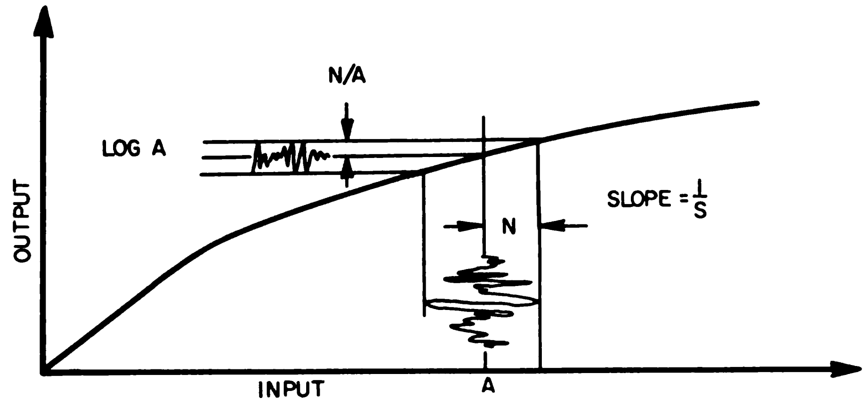

Figure 6-61. Logarithmic Receiver Characteristic

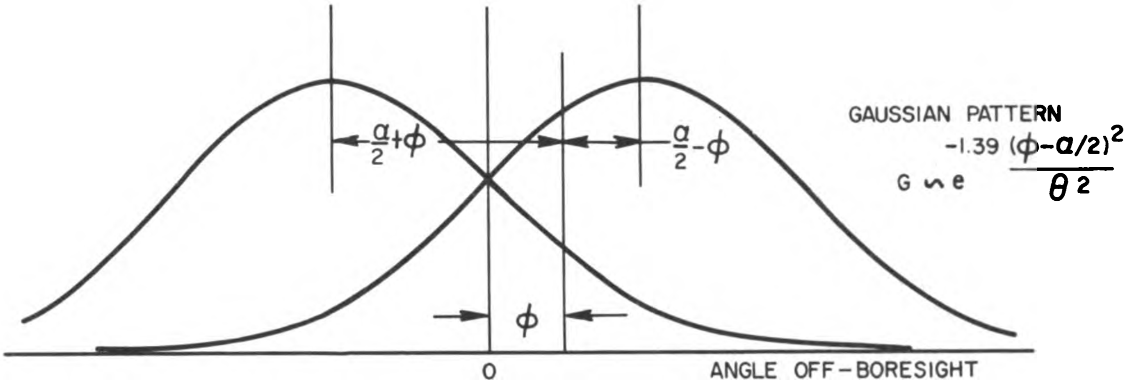

Figure 6-62. Logarithmic Amplitude Comparison Antenna Pattern

Taking the logarithm of these with the receiver response and then the difference, yields an output

$$\log B - \log A = \frac{2.78\,\alpha\,\phi}{\Theta^2} \qquad (6\text{-}86)$$

The output is linearly related to the position, therefore, over as wide an angle as the antenna pattern approximates a Gaussian curve.

The noise in the output of a nonlinear receiver can be related to the input by approximating the receiver characteristic as a straight line if the signal-to-noise level is high. The slope of the line is the derivative of the receiver characteristic as shown in Figure 6-61. Since the derivative of the logarithm is the reciprocal, an input noise, N, in one channel produces noise output, N/A where A is the signal input. The total noise in the output of video difference circuit is the rms total since the noise is random. We assume that noise input to each receiver is the same. Any subsequent filtering will reduce this noise by a filter factor K_f. Therefore the angular error due to the noise, ε, can be obtained by setting this noise equal to the expression of equation 6-86:

$$\frac{2.78\,\alpha\,\varepsilon}{\Theta^2} = \frac{1}{K_f}\sqrt{\left(\frac{N}{A}\right)^2 + \left(\frac{N}{B}\right)^2} \qquad (6\text{-}87)$$

or, equivalently, this relationship can be stated as:

$$\frac{\varepsilon}{\theta} = \frac{1}{2.78\,\alpha/\Theta\,K_f}\,\frac{N}{AB}\sqrt{A^2+B^2} \qquad (6\text{-}88)$$

Even though no sum signal is directly derived in this system, we can think in terms of one. This facilitates the off-boresight noise analysis. This sum signal is the signal calculated on the basis of the sum pattern gain and is:

$$S = \sqrt{A^2+B^2} \qquad (6\text{-}89)$$

In terms of this signal equation 6-88 can be put into the usual form:

$$\frac{\varepsilon}{\Theta} = \frac{1}{K_s K_f}\,\frac{N}{S} \qquad (6\text{-}90)$$

with:

$$K_s = \frac{2.78\,\alpha/\Theta}{\dfrac{A}{B} + \dfrac{B}{A}} \qquad (6\text{-}91)$$

However, from equation 6-85:

$$\frac{A}{B} = e^{-2.78\frac{\alpha}{\Theta}\frac{\phi}{\Theta}} \qquad (6\text{-}92)$$

From which:

$$K_s = \frac{1.39\,\alpha/\Theta}{\cosh 2.78\,\dfrac{\alpha}{\Theta}\,\dfrac{\phi}{\Theta}} \qquad (6\text{-}93)$$

One point to notice about this relation is that although the sensitivity on the boresight ($\phi = 0$) increases with increased squint, the sensitivity for other angles may be drastically reduced. For example, on the peak of one lobe the sensitivity is:

$$K_s = \frac{1.39\,\alpha/\Theta}{\cosh 2.78\,(\alpha/\Theta)^2} \qquad (6\text{-}94)$$

Also at this point there is a loss of signal due to the lower sum pattern gain. It might for this reason be desirable to optimize this sensitivity.

An optimum can be found by the usual method of differentiating equation 6-94. The resulting transcendental equation yields a value of squint:

$$\alpha/\Theta = 0.73 \qquad (6\text{-}95)$$

For this value of squint, the sensitivity on boresight is 1.02, and that on the peak of a lobe is 0.776. A squint of one beamwidth results in boresight sensitivity of 1.39 and sensitivity on the peak of a lobe of 0.65. This is a difference of 6.6 db. In addition there may be a loss of round-trip gain of about 3 db so that the angular noise error may be almost 10 db higher on the peaks of the pattern than that on the boresight or crossover of the pattern. The error will of course increase even more for targets further from the boresight. In cases where many lobes are used (rather than just two), the loss of gain is less in general, but the loss of sensitivity is still large and should be accounted for in the design.

6-5.2.3 Phase Monopulse

If in the systems shown in Figures 6-57 and 6-58 the feeds are placed in the radar in such a manner that there is no squint between the lobes produced, but each is parallel to the boresight axis, all received signals will have equal amplitude. If, however, the lobes are displaced from each other as shown in Figure 6-63 there will be phase differences between them when the target is not on the boresight. This is due to the difference between the electrical path lengths from separate feeds to the target. The systems of Figures 6-57 and 6-58 can be used to detect this phase difference. Since the hybrids produce vector sum and difference signals, these signals are usable just as they were for amplitude comparison. As shown by the vector diagrams of Figure 6-63, the difference signals are for this case in quadrature with the sum. By simply adding 90 degrees of phase shift to the sum signal before using it in the balanced detectors, these difference signals are detected.

The sensitivity of phase comparison monopulse is easily calculated in terms of the separation of the apparent sources of the beams. These points are called phase centers. They are determined by the illumination patterns produced on the radar reflector by the separate feeds. A special case arises when two or more completely separate dishes are used, each with one feed. This device is usually called an interferometer. For either an interferometer or a phase monopulse having a common reflector the sensitivity based on $\Delta - \Sigma$ comparison is

$$K_s = \frac{\Delta/\Sigma}{\varepsilon/\Theta} \qquad (6\text{-}96)$$

In terms of the signals in each feed:

$$K_s = \frac{\Theta}{\varepsilon}\,\frac{B-A}{B+A} \qquad (6\text{-}97)$$

But from Figure 6-63 it may be seen that the signals A and B differ only in phase, so the vector quantity $B - A/B + A$ is the tangent of half the phase angle between A and B. If we base the sensitivity on a nominal beamwidth for a cosine illuminated dish, $\Theta = 1.19\,\lambda/d$ and:

$$K_s = \frac{1.19\,\lambda/d}{\varepsilon}\tan\frac{\pi\,a\sin\varepsilon}{\lambda} \qquad (6\text{-}98)$$

For small angles, near boresight, this is closely approximated by:

$$K_s = 1.19\,\pi\,a/d \qquad (6\text{-}99)$$

This relation is plotted in Figure 6-64.

By definition it is apparent that interferometer spacings cannot be closer than a ratio of a/d equal to unity. Similarly, the phase monopulse with the single reflector cannot have a phase center spacing greater than the aperture. Actually, there are a number of other limitations on the phase center spacing and thus the sensitivity. For the single antenna these limitations may be either loss of gain or high sidelobes. Assuming that the illuminations produced by the feed horns are cosinusoidal, then phase center separations of more than half the aperture will necessitate either an unilluminated center section of the antenna or part of the feeds spilled over the edges of the reflector. Even when the feeds are exactly a half aperture apart the pattern is generally unsatisfactory due to the high sidelobe levels. To get around these troubles the feeds are generally overlapped so that the phase center spacing is smaller. When this is done there may be some improvement in gain compared to the gain of a cosine illuminated aperture because of a more favorable illumination function. Generally sidelobe levels are acceptable with one-third overlap, or one-third aperture phase-center spacings. The very high sensitivities corresponding to interferometer spacings are not achieved without difficulty.

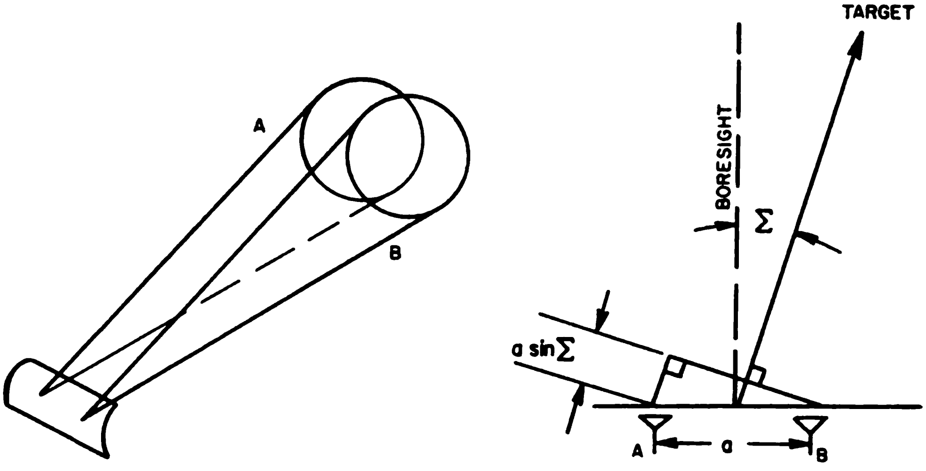

a. PARALLEL BEAMS

b. PHASE DIFFERENCE

$\phi = \frac{2\pi}{\lambda} a \sin\Sigma$

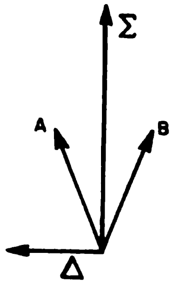

c VECTOR DIAGRAM – 2 HORNS

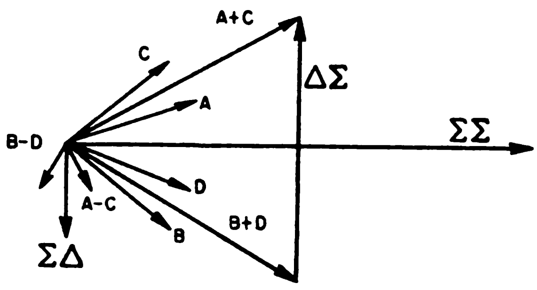

d. VECTOR DIAGRAM – 4 HORNS

Figure 6-63. Phase Monopulse

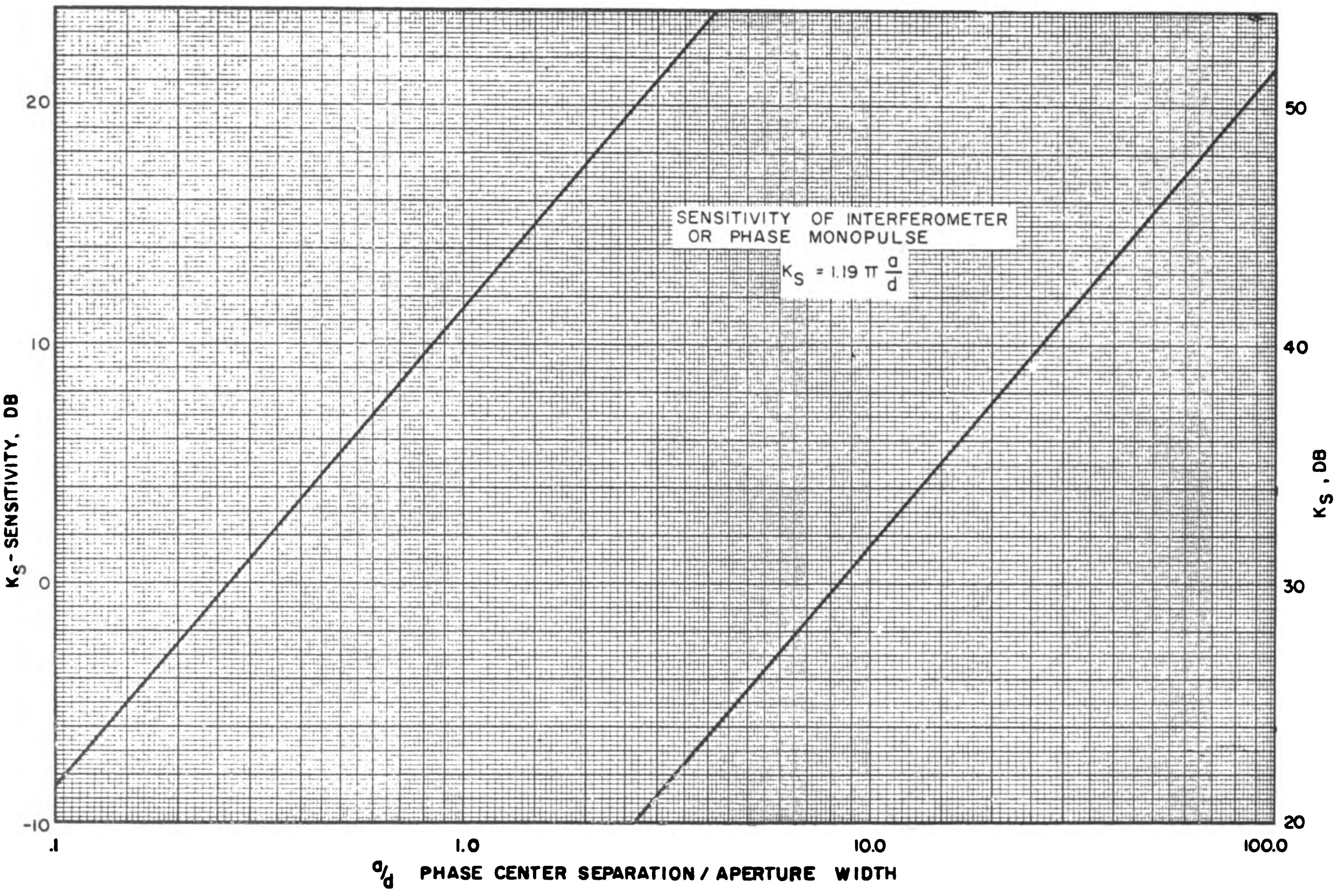

Figure 6-64. Interferometer Sensitivity

he source of trouble is redundancy. For any nterferometer there are numerous angles where he difference signal is zero, corresponding to ifferences in electrical path length from target o the two feeds of 0, λ, 2λ, 3λ, ... , etc. This orresponds to angles of 0, λ/*a*, 2λ/*a*, 3λ/*a*, . . . , tc. These multiple nulls may occur within he beamwidth of one of the interferometer dishes, in which case they may be mistaken for the center null. This redundancy must be resolved if the interferometer is to provide useful information. The resolution may be effected by use of a second interferometer with smaller spacing between dishes, by a separate monopulse system, or by any method available to give a coarse angular measurement.

Since the performance of the system depends on the sensitivity and the gain, an optimum phase center spacing exists for phase monopulse. It can be calculated on the basis of cosine illumination functions of each feed. In practice it will probably be adjusted empirically. The system engineer should bear in mind that it is the gain-sensitivity product that determines optimum performance. The gain that is applicable is the voltage gain, one-way or round trip depending on whether the application is echo or beacon-tracking. For the interferometer, of course, the gain does not depend explicitly on phase center spacing and the limitations on this spacing are imposed either by redundancy or mechanical considerations.

Again, Tables 6-4 and 6-5 list some typical characteristics of phase comparison systems and reference 6, Quarterly Report No. 2, goes into more detail on the calculation of sensitivities and gains. As a reminder, note that the beamwidths in that report as well as in the equations in this section refer to a nominal beamwidth of the total aperture involved and not to either the beamwidth of one lobe or to the beamwidth of the sum pattern. For interferometers the beamwidth is of course taken as the beamwidth of one dish, but the gain for the sum signal must include the gain of all dishes contributing.

6-5.2.4 Combination Monopulse

In the previous section it was noted that the same block diagram could be used for either phase or amplitude comparison, the differences between the two consisting of the difference in the antenna patterns and a 90-degree phase shift in the reference signal to the detector. Since this is so, it is possible to combine the two techniques in order to obtain two-axis (azimuth and elevation) tracking using only two antenna feeds. These are adjusted to give lobes which are squinted in one direction and have phase centers spaced in the other direction.

The boresight is then determined by the line along which the amplitude received in each feed is equal and the phase also is equal. For small displacements from this boresight in the plane in which the two lobes are squinted, the result is a difference of received amplitude between the feeds, but their phases remain equal. Similarly, for small displacements from boresight in the plane of the phase center separation, only phase difference results, as for phase monopulse. On Figure 6-65 are shown the vector diagrams for signals from a target displaced in both directions. The sum and difference are taken and the difference signal resolved into components in phase and in quadrature with the sum. The inphase difference is then a measure of the amplitude difference between the two lobes and the quadrature difference a measure of the phase difference. These signals may be used as error signals to drive tracking servos. A block diagram of a method used to generate these signals is shown in Figure 6-66. The resolution of the difference signal into inphase and quadrature components is achieved by the 90-degree phase shift in the sum reference signal for the balanced detectors.

The sensitivities of a combination system may be found in the same fashion as was done above for amplitude and phase comparison systems. The sensitivity in phase comparison will be exactly the same as that found for unsquinted case, i.e.:

$$K_s = 1.19\pi\, a/d \qquad (6\text{-}100)$$

where *a* is the phase center spacing and *d* the aperture width, the sensitivity being in volts per volt per nominal beamwidth.

In a practical application, equation 6-100 may be used to define the phase center spacing for future reference, rather than the sensitivity. Phase center separation cannot always be measured precisely and the sensitivity can. By defini-

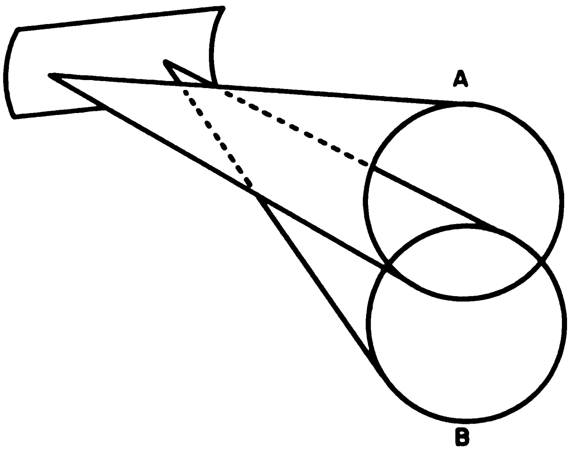

a. BEAMS SQUINTED IN ELEVATION PARALLEL IN AZIMUTH. (AN EXAMPLE–OTHER CHOICE OF AXES ARE POSSIBLE.)

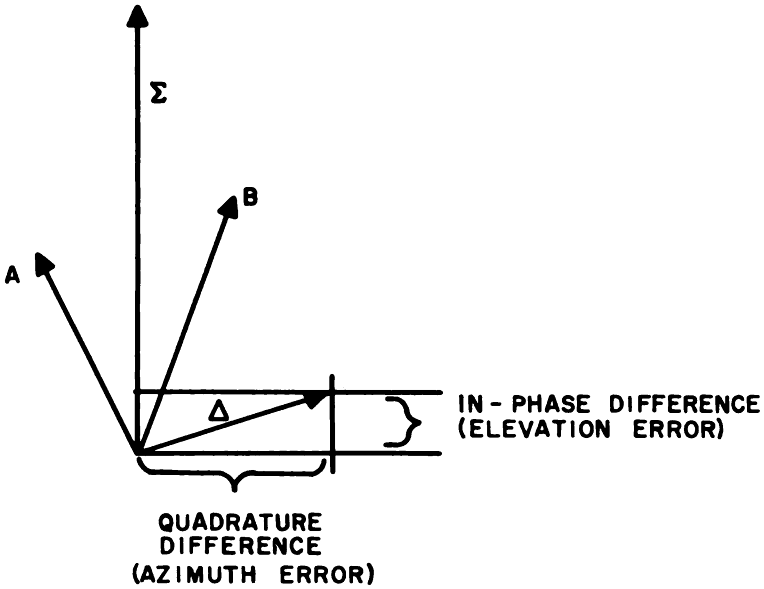

b. VECTOR DIAGRAM

Figure 6-65. Combination Monopulse

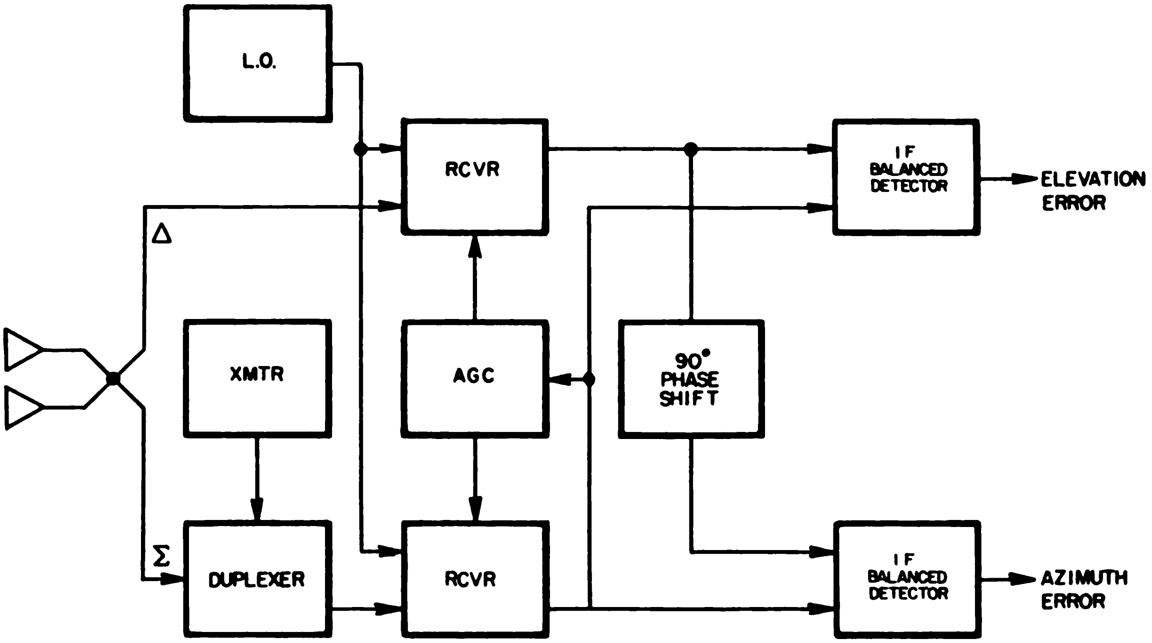

Figure 6-66. Combination Monopulse Radar

tion the sensitivity is the slope of the Δ/Σ pattern at its zero. For existing hardware, then, the sensitivity is often found empirically from pattern tests and may be adjusted to proper value in this fashion.

In the amplitude comparison plane, the sensitivity is also found from pattern tests when they are available. When they are not, sensitivity can be calculated in exactly the same manner as for pure amplitude systems. In fact, assuming the same illumination functions, the sensitivity is the same for equal values of squint.

The sum channel gain of a combination system, or the loss in gain compared to the same antenna with a single feed, is a difficult quantity to calculate. It involves, in general, vector summation of the patterns from the two horns and integration of this sum pattern over the solid angle of the pattern.

Table 6-4 gives some values of the loss of gain, including empirical values for the TPQ-10. Note that for the special case of no overlap of the feeds, or phase center spacing of one-half, the sum gain is easily computed, because the feeds are independent of each other. However, this configuration will seldom be practical, due to the high sidelobes that arise from such an illumination.

Even when the feeds do not overlap, the azimuth and elevation error signals of a combination monopulse are coupled together due to their formation from only two lobes. From the vector diagram of Figure 6-65 it may be seen that for finite phase angle, the inphase error signal will be a function of this angle even though it is primarily a function of amplitude difference. This characteristic causes combination monopulse to have somewhat higher errors due to certain causes, (wander and ground reflection) as discussed in the following sections.

6-5.3 ERROR SOURCES

6-5.3.1 General

A number of effects cause the angular information from a tracking radar to vary in a random or noise-like manner. In addition, there may be more consistent errors, such as refraction or the normal lag of a servo system.

The most common cause of angular noise in the radar output is the unavoidable thermal noise present in the radar. In some instances, other forms of radio noise (man-made, cosmic or atmospheric), may be of importance. Also, in skin-tracking radars, clutter return from rain or ground results in a greater dispersion in the angular information. The antenna servo has its own sources of noise, such as stiction or gear chatter. The nature of most targets encountered gives rise to noise in the angular output, caused by the scintillation of the target echo.

Fortunately the angular noise output of a tracking radar is considerably decreased due to the low-pass filter action of the antenna servos. The amount of improvement due to this filtering or integration can be calculated. If the servo (or filter of any kind) has a cutoff frequency of (f_c) and is assumed to approximate a single time constant filter, its power frequency response is given by:*

$$h(f) = \frac{1}{1 + (f/f_c)^2} \tag{6-101}$$

If the output of the radar is put through a boxcar circuit which is assumed ideal and the input to this circuit is Gaussian and white over a frequency range much greater than the prf,** the normalized power spectrum of boxcarred noise, either alone or in the presence of signal, is:

$$p(f) = \frac{2}{f_p}\left[\frac{\sin^2 \frac{\pi f}{f_p}}{\frac{\pi^2 f^2}{f_p}}\right] \tag{6-102}$$

where f_p is the pulse repetition frequency. The improvement in signal-to-noise power is then given by:

$$K_f^2 = \frac{\text{Noise Power in}}{\text{Noise Power out}} = \frac{1}{\int_0^\infty h(f)\, p(f)\, df} \tag{6-103}$$

If it is assumed that the cutoff frequency of the low-pass filter is much smaller than (f_p) the power spectrum can be considered constant over the passband of the filter.

$$K_f^2 = \frac{1}{\int_0^\infty \frac{1}{1 + (f/f_c)^2} \frac{2}{f_p}} = \frac{f_p}{\pi f_c} \tag{6-104}$$

For a conical scan or sequentially lobing radar, this expression requires some modification. The error signal on a conical scan is essentially modulating a carrier, the scanning frequency. Assuming this frequency is greater than the filter cutoff but much less than the pulse rate, the filter factor of the servo is less. For a bandwidth of f_c the reduction in noise amplitude is:

$$K_f = \sqrt{\frac{f_p}{2\pi f_o}} \tag{6-105}$$

This filter factor and the sensitivity of the tracking radar can be used to relate angular noise or error to the electrical noise in the output of the radar. The sensitivity factor (K_s), relates a displacement of the target from the boresight to the error signal output of the radar. In order that the error signal be independent of the exact size and range of target, all tracking systems have outputs normalized by the on boresight signal strength. Thus, if we normalize the target deviation or angular noise (ε) by the beamwidth (Θ):

$$\frac{\varepsilon}{\Theta} = \frac{1}{K_f K_s} \left(\frac{N}{S}\right) \tag{6-106}$$

The sensitivity factor has already been discussed for various types of tracking radar. Table 6-4 lists the sensitivities of common tracking radars.

---

*Because of the subsequent integration, this approximation introduces only small errors in calculation, regardless of the actual response curve.

**Corresponding to thermal or radio noise.

5.3.2 Thermal Noise

One of the largest sources of error in a track- g radar is usually the electrical noise in the tput of the radar. The effect of the noise on acking accuracy will depend on the signal-to- oise ratio. This can be computed in the usual ashion if the only noise source is considered be thermal noise.

For many applications thermal noise is the lominant error source to such an extent that ther sources may be neglected. If this is so, hen the voltage signal-to-noise ratio is given, or a skin-tracking radar, by:

$$\left(\frac{S}{N}\right)^2_{radar} = \frac{P_t G_t^2 \lambda^2 A_e L}{(4\pi)^3 R^4 N_f KTB} \qquad (6\text{-}107)$$

where:

P_t = radar peak power, watts

G_t = one-way antenna power radar gain, connected for the type tracking involved

λ = wavelength, meters

A_e = target echo area, square meters

R = target range, meters

N = noise figure of the radar receiver

KT = Boltzmann's constant × absolute temperature (watts per cycle)

B = radar bandwidth, cycles per second

L = losses in propagation and/or r-f circuitry

For a radar tracking an airborne beacon, the performance depends upon two separate transmissions. Accordingly, a full prediction of the performance depends on two calculations. We will first calculate the condition for triggering of the beacon by the radar and then calculate the performance of the tracking function.

In order to trigger the beacon, assuming it is a crystal receiver with a sensitivity (S) watts, the received signal at the beacon must be at least:

$$S \leq \frac{P_t G_t G_b \lambda^2 L}{(4\pi)^2 R^2} \qquad (6\text{-}108)$$

where:

G_b = beacon one-way antenna power gain

This expression does not depend explicitly on thermal noise, because the sensitivity of a crystal beacon is usually determined by the noise generated in the crystal. Unlike ideal thermal noise, this noise does not have a flat spectrum, but increases in power density with decreasing frequency. This is the basic reason why crystal receivers are far less sensitive than superheterodyne receivers and why the sensitivity is usually specified for a given crystal and receiver.

The more sensitive superheterodyne beacons depend for their triggering upon the signal-to-noise level in the same manner as the radar. If the beacon is adjusted to trigger at a given signal-to-noise level, (S/N), the condition for triggering is:

$$\left(\frac{S}{N}\right)^2_{beacon} \leq \frac{P_t G_t G_b \lambda^2 L}{(4\pi)^2 R^2 N_f KTB} \qquad (6\text{-}109)$$

where N_f and B are now respectively the noise figure and bandwidth of the beacon receiver.

Having successfully triggered a beacon, it is now necessary to calculate the signal-to-noise received at the radar in order to determine tracking accuracy. If the beacon transmits a peak power of (P_b) watts, the signal-to-noise at the radar will be given by:

$$\left(\frac{S}{N}\right)_{radar} = \frac{P_b G_b G_t \lambda^2 L}{(4\pi)^2 R^2 N_f KTB} \qquad (6\text{-}110)$$

N_f and KTB are in equation 6-110 which includes the radar receiver parameters.

Equations 6-107 through 6-110 are the basic radar equations for a tracking radar. They are more fully developed elsewhere, and need no proof here.

Anything that is done to improve or degrade the signal-to-noise at the radar will cause a corresponding effect on the tracking accuracy. Normally a tracking radar receives information at a high-data rate. If this information is smoothed by the action of a low-pass filter, a considerable improvement in performance can be attained.

6-5.3.3 External Radio Noise

The effect of thermal noise on the tracking radar accuracy has already been noted. Generally this thermal noise is the most important noise source in the microwave spectrum. For relatively low frequency radars, or in special radar environments, other noise sources external to the radar may become important. These may be of three types:

(a) *Atmospheric* noise originates in the earth's atmosphere from lightning, meteors, aurora, etc.

(b) *Cosmic* noise originates from discrete sources such as stars or from the extended area of the galactic plane.

(c) *Man-made* noise, from commutators, spark gaps, diathermy machines, etc., is most troublesome in heavily populated areas.

These external noise sources may be from relatively discrete sources such as the sun, or from extended sources such as the atmosphere. Their effect on the radar is then determined in part by the gain and orientation of the radar antenna. Figure 6-67* shows values for these noise sources compared to ideal receiver noise for an isotropic receiving antenna.

For convenience, these values are given in terms of a noise factor similar to the noise figure used to evaluate thermal receiver noise.

Cosmic noise sources are often specified in terms of brightness b, or temperature T_X and solid angle Ω, or flux density S. These are related by:

$$b = \frac{2\,K\,T_X}{\lambda^2} \tag{6-111}$$

$$S = b\Omega \tag{6-112}$$

where:

K is Boltzmann's constant
λ is wavelength

The power received by the radar is then, for random polarized noise:

$$P = \frac{1}{2} SAB \tag{6-113}$$

where:

A is receiving area
B is receiver bandwidth

This can be written as:

$$P = \left(\frac{\Omega}{4\pi}\,\frac{T_X}{T}\right)\left(\frac{4\pi A}{\lambda^2}\right)\left(KTB\right) \tag{6-113a}$$

where T is the standard temperature used in the radar equation, 290°K. In this form we recognized the receiving gain G and define the external noise factor:

$$N_X = \frac{\Omega}{4\pi}\,\frac{T_X}{T} \tag{6-113b}$$

This analysis is valid for small angles Ω, but when Ω is comparable to the beamwidth of the radar, the expression should be an integral and in general, the full gain of the antenna is not realized. For the case of Ω much greater than the beamwidth, this reduces to:

$$N_X\,G = \frac{T_X}{T} \tag{6-113c}$$

In any application, a correction should be made for the applicable gain of the antenna. On discrete sources the noise may be enhanced by the full gain of the antenna. On the galactic plane and probably on extended man-made noise sources, the realizable gain will be limited to 10 to 15 decibels. Conversely, when directed away from these sources, noise factor from the figure (reduced by the applicable antenna gain) is compared to receiver noise figure (Figure 6-107). The combined effect of both thermal and some external noise can be found readily since noise adds in power. Figure 6-68 facilitates addition of powers expressed in decibels. Since receiver noise figure and this noise factor are both measures of noise power, they can be added with the aid of this figure.

To illustrate the procedure outlined in the above paragraph suppose we have a radar operating at 500 megacycles tracking a target against a background of the galactic plane. Assume an antenna gain of 35 db and that the target is well above the horizon. Then, any man-made noise is attenuated by at least the full gain of the antenna but the galactic plane noise will be enhanced by 10 or 15 decibels. This yields a value of zero to five decibels for galactic noise. The man-made noise factor will be about −10 db and may be neglected. A reasonable receiver noise figure at this frequency is 6 db. The cosmic noise is then appreciable. The total noise factor, taking the pessimistic estimate of cosmic noise factor, is about 5 plus 3 or 8 db. This may be used in radar calculations in the same manner as receiver noise figure.

---

*Adapted from the curves presented on page 763 of reference 62.

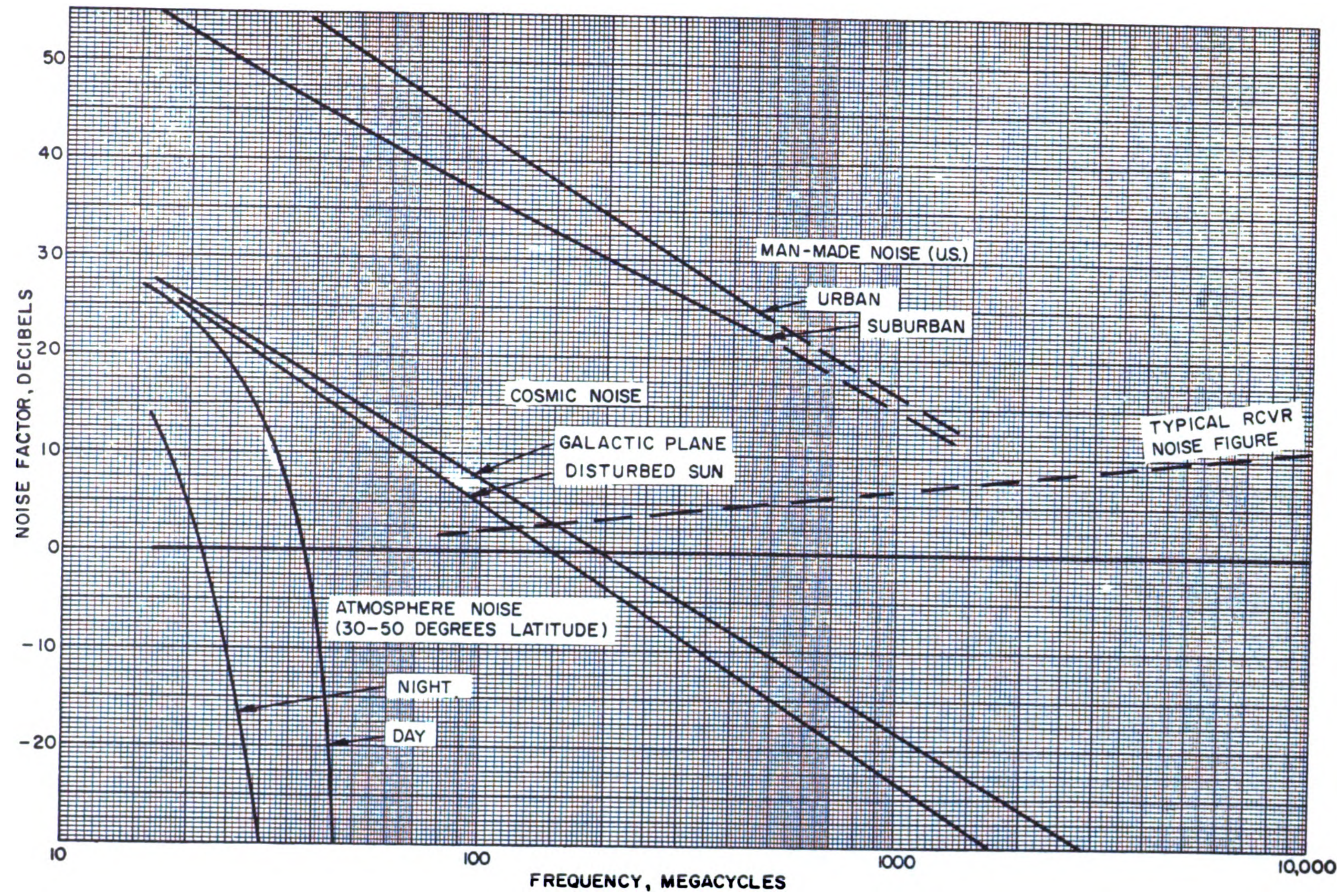

Figure 6-67. External Noise Factor (Referenced to Ideal Receiver Noise)

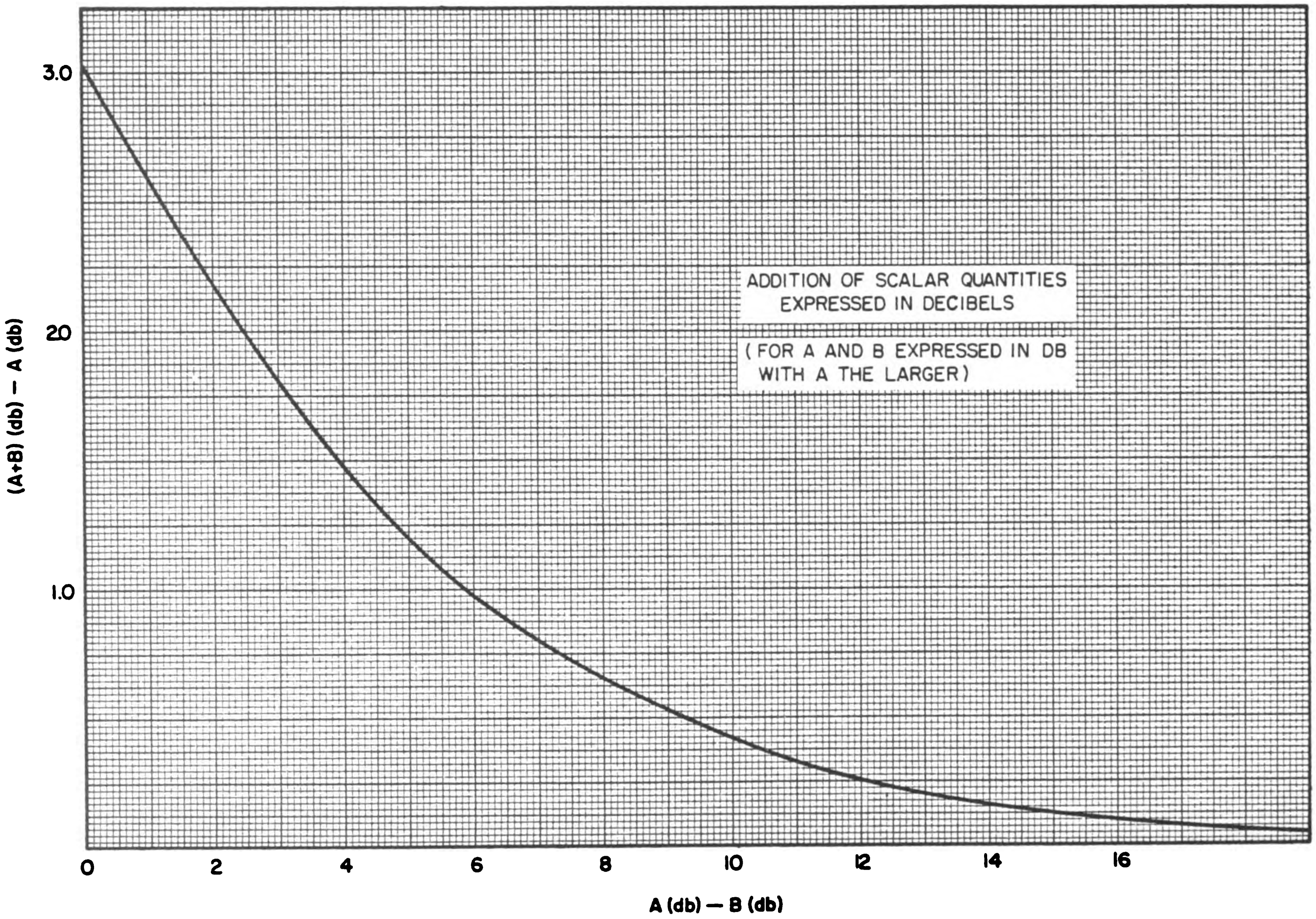

Figure 6-68. Addition of Scalar Quantities Expressed in Decibels

5.3.4 Rain and Ground Clutter

Clutter is an uncorrelated return from rain, liage, waves, etc. In general it has somewhat e same characteristics as noise and will have similar degenerative effect on tracking accuacy.

Because it is a reflection, the clutter spectrum s centered on the radar frequency and of limted width. This leads to its removal by moving arget indication (MTI) techniques. In addition, rain clutter, because of the spherical shape of the rain droplets, can be filtered in large measure by polarization techniques.

Rain cancellations with a circular polarizer have been measured up to 30 db. Ground clutter cancellation with the most refined techniques may be as high as 70 db, but with a single stage of cancellation 30 db can be expected.

The effect of clutter on the tracking radar without cancellation can be computed from the echo area of the clutter. For rain, the echo area is given by:

$$\sigma_r = \frac{\pi \Theta_a \Theta_e R^2}{4} \times \frac{cT}{2} \times \frac{300 (\bar{d})^6 N}{\lambda^4} \tag{6-114}$$

where:

σ_r = rain clutter echo area, square meters
Θ_a = azimuth beamwidth in radians
Θ_e = elevation beamwidth in radians
R = range, meters
c = velocity of light, meters/second
T = pulse duration, seconds
$\bar{d}$ = average rain drop diameter
N = rain density drops per cubic meter
λ = radar wavelength, meters

Typical rainfall intensities and their corresponding parameters are taken from Kerr[63] and tabulated in Table 6-6.

For ground clutter, assuming grazing incidence, the echo area is:

$$\sigma_g = \Theta_a R \times \frac{cT}{2} \times A_g \tag{6-115}$$

where:

A_g = specific echo area, meters/meter

For heavily wooded countryside, the specific echo area is about —4.5 db. For open plains it is about —13 db.

Having found the clutter echo area the clutter-to-signal level before cancellation will be given by the ratio of this echo area to the target echo area (see Figure 6-69). If the radar has MTI circuits or circular polarizers, the clutter-to-signal level will be less by the amount of cancellation.

In a search radar the combined effect of clutter and thermal noise can be computed by adding them in a power sense. In tracking however, it is desirable to calculate the errors induced by the two causes separately. They have different range dependence and different spectra.

The clutter-to-signal ratio can be used to calculate angular errors due to clutter using the same formula that is used for thermal or other noise. However, since the two fluctuations have different spectra, a filter factor for the clutter must be calculated as discussed below.

TABLE 6-6. TYPICAL RAINFALL INTENSITIES

Description of Rain	Intensity mm/hr	$\bar{d}$ (Meters)	N/Meter^3
Drizzle	0.25	1.0×10^{-3}	27
Moderate	2.5	1.3×10^{-3}	178
Heavy	12.5	1.9×10^{-3}	253

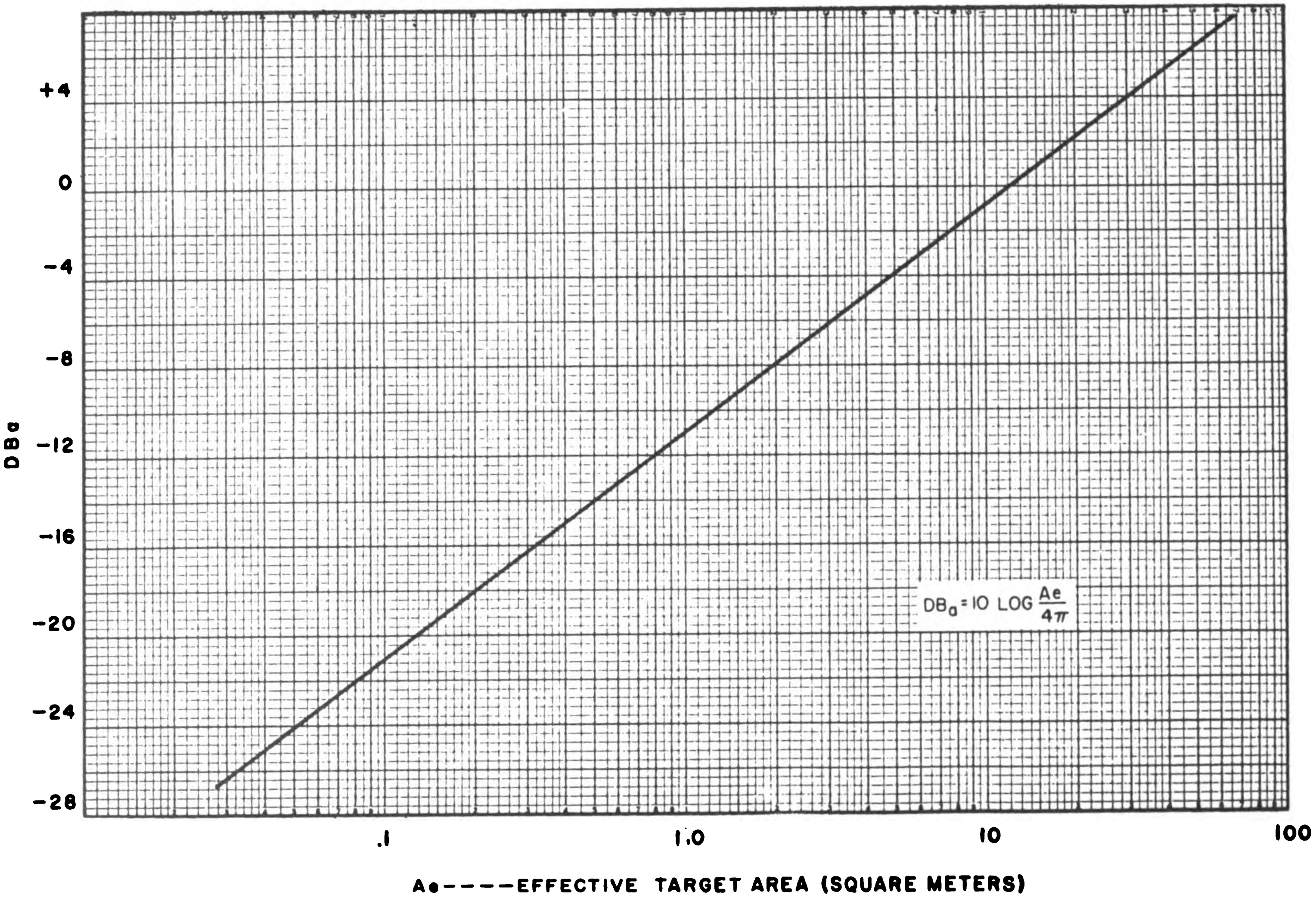

Figure 6-69. Target Area Factor

To calculate the effect of the servo filtering n clutter noise it is necessary to know the pectrum of the clutter. Because the width of his spectrum is much narrower than the prf, he filter factor derived for wide-band noise (such as thermal, atmospheric, etc.) does not pply. Actually this spectrum is often of comparable width to the servo bandpass. When this is so the filter factor for clutter must be calculated by actually multiplying the normalized power clutter spectrum $p(f)$ by the filter response $h(f)$ and integrating:

$$K_f^2 = \frac{1}{\int_0^\infty h(f)\, p(f)\, df} \qquad (6\text{-}116)$$

If the clutter spectrum is much narrower than the filter bandpass there will be no improvement due to filtering and the filter factor is unity. If the clutter spectrum is several times as wide as the filter bandpass then the filter factor may be approximated by formulas similar to those found for wideband noise. Clutter spectrums for ground clutter, rain clutter or window are usually approximated as Gaussian. This is borne out by empirical results.

Then the normalized spectrum is given by:

$$p(f) = \frac{2}{\sqrt{2\pi f_n^2}}\, e^{-\frac{f^2}{2 f_n^2}} \qquad (6\text{-}117)$$

where f_n^2 is the variance of the spectrum. The power out of the filter is given as before by the integral of the filter power response times the normalized power spectrum. However, if f_n is much larger than f_c, the amplitude of the power spectrum may be considered constant over the passband:

$$K_f^2 = \frac{1}{\int_0^\infty \frac{1}{1 + (f/f_c)^2} \frac{2}{\sqrt{2\pi f_n^2}}\, df} = \sqrt{\frac{2}{\pi}}\, \frac{f_n}{f_c} \qquad (6\text{-}118)$$

We can, therefore, calculate the effect of the filter on the clutter if the spectral width of the clutter is known. To find this, note that clutter is caused by Doppler return from a random group of scatterers or clutter particles. The clutter is then characterized by a variance and a standard deviation of clutter particle velocities and this deviation is related to the standard deviation of the clutter spectrum by the Doppler formula:

$$f_n = \frac{2 V_c}{\lambda} \qquad (6\text{-}119)$$

where λ is the radar wavelength in meters and V_c the standard deviation of clutter velocities in meters per second. Typical values of this standard deviation are given in Table 6-7.

There are two possible complications to this picture of the clutter spectrum which may infrequently arise. If the radar is on a moving platform and is a coherent radar, the entire clutter spectrum is translated in frequency by the Doppler shift due to platform motion. Another effect arises in a conical scanning radar. The motion of the beam gives rise to scanning clutter which broadens the clutter spectrum. Clutter may cause large errors in a conical scan system since the clutter may be present on one side of the scanning pattern but not the other.

No discussion has been made of sea clutter. A word of caution is called for. The spectrum of sea clutter is not the random affair that was seen for ground clutter. Due to the wave action, sea clutter sometimes exhibits strong peaks at discrete frequencies.

Another point to be borne in mind is that ground clutter will be attenuated beyond the radar horizon. For this reason ground clutter is probably a limitation on tracking accuracy in only rare applications where surface targets are being tracked or where the radar is elevated and tracking low-flying targets. Beacon operation is normally not affected by clutter returns, but if necessary the procedure above can be followed similarly for beacon operation.

Clutter errors can be combined with other errors by methods discussed in paragraph 6-5.3.8.

6-5.3.5 Servo Noise and Servo Dynamic Errors

Most tracking radars function by driving a large dish or array in such a manner as to keep its boresight aligned with the moving target. The servomechanisms required to drive these antennas have faults and limitations which may cause appreciable angular error. Also, even trackers that might use a stationary array

TABLE 6-7. STANDARD DEVIATION OF CLUTTER PARTICLE VELOCITIES

Clutter Type	Standard Deviation
Heavily wooded hills, 50 mph wind*	0.34 meters/second
Heavily wooded hills, 20 mph wind**	0.21
Sparsely wooded hills, calm**	0.017
Rain clouds**	1.93
Window**	1.06

*Calculated from curves given in Reference 63.
**Calculated from data given in Reference 64.

would probably utilize servos in driving phase shifters or attenuators.

One of the more important attributes of the servo from an accuracy viewpoint has been discussed previously. Normally the servo has a very narrow bandwidth. This can be an aid to accuracy by filtering much of the noise from various sources, or it may be a limitation to accuracy because of the associated longer response time for the servo. Concerning servo bandwidth it should be noted that the literature of servos defines noise bandwidth as the frequency where the open-loop servo response becomes less than unity. This should be distinguished from closed-loop half power point, although generally they will be almost equal values. This distinction is illustrated on the typical response curves of Figure 6-70.

In addition to the dynamic errors due to the finite response time of the servo and the noise admitted by the servo bandwidth, the servo itself will usually generate certain errors. A number of these are of a random or noise type. They may be due to gearing backlash, motor slot-locking, component nonlinearities, amplifier drifts, distortions due to loading, hum pickup, etc. Obviously such errors are a function of the mechanical system and are subject to the skill of the designer. These errors are usually small. An estimate of their value for a specific system is made in reference 65.

One of the common causes of tracking roughness is the nonlinearity of the friction forces in the servo mount. In many cases the linear analysis of servomechanisms assumes that all friction is viscous, i.e., proportional to velocity. Actually the friction force may vary with velocity in the fashion shown in Figure 6-71. There are a number of components to this characteristic. The sharp spikes near zero velocity represent stiction. Due to the higher coefficient of friction in the static case, a larger force is needed to start the motion than to continue it. This can cause considerable roughness at slow tracking rates. Some of the friction forces are coulomb friction. These depend only on the direction of mo-

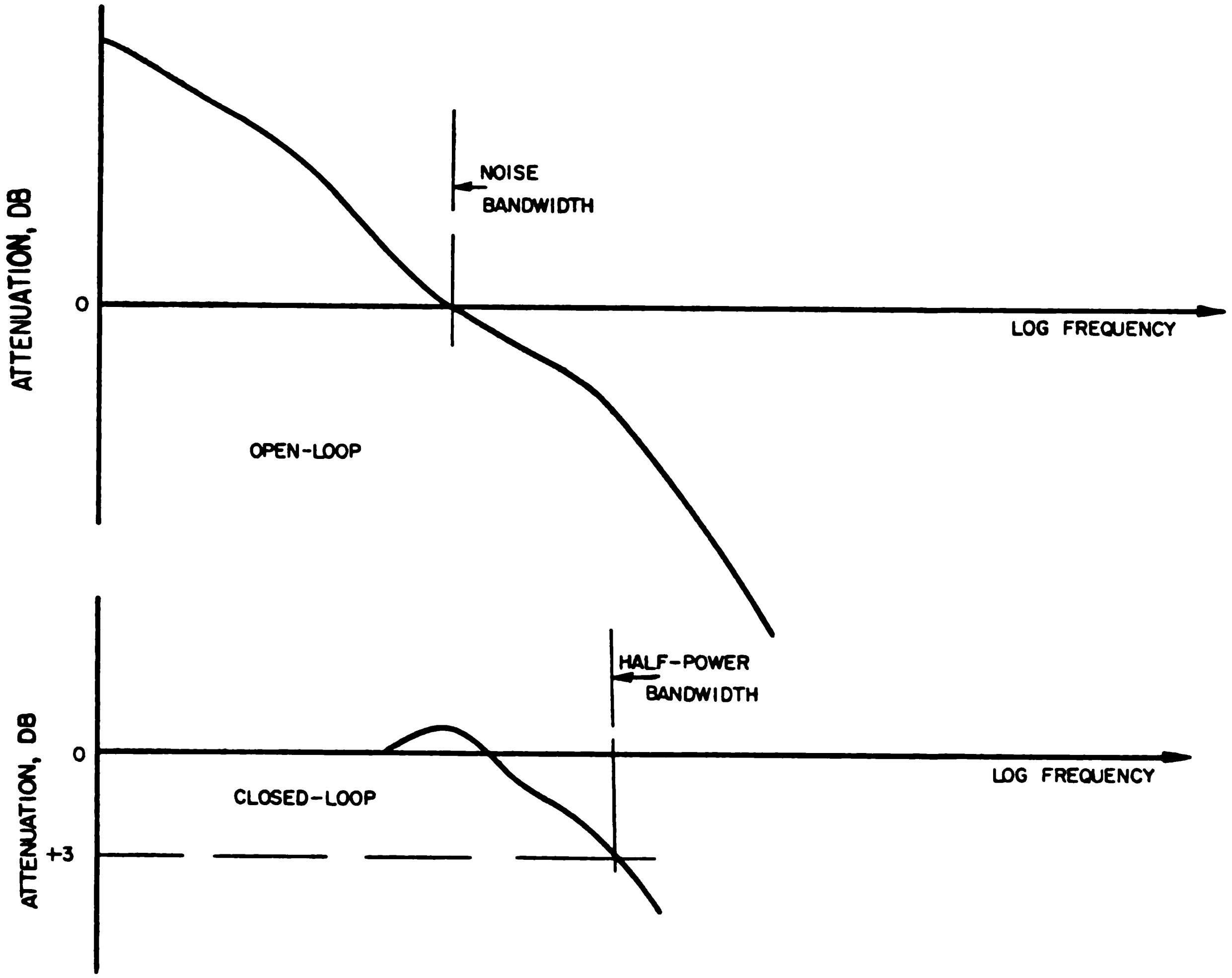

Figure 6-70. Typical Servo Response Curves

tion and are constant for all speeds. The remainder are viscous friction or drags (due to windage, etc.) that are proportional to higher powers of velocity. The stiction problem is alleviated by proper lubrication and is sometimes treated by the use of *dither*. This consists of adding a small alternating signal to the servo error signal to keep the servo in motion oscillating slightly about the target. Even when stiction is eliminated the coulomb friction requires a certain minimum force before motion can occur. This necessitates a minimum error. The net effect is to produce a *dead-band* about the target bearing. The servo can track at best only at the edge of this dead-band. In addition to this lag the velocity and acceleration of the target require more error signal to actuate the servo. To illustrate this, Figure 6-72 compares empirical data of servo error for constant velocity targets with an error of the form:

$$\varepsilon = \varepsilon_o + \frac{\overset{\prime}{\Theta}}{K\omega_1} \tag{6-120}$$

For the values taken the agreement is good. It might be noted that the value chosen for $K\omega_1$ is a reasonable one.

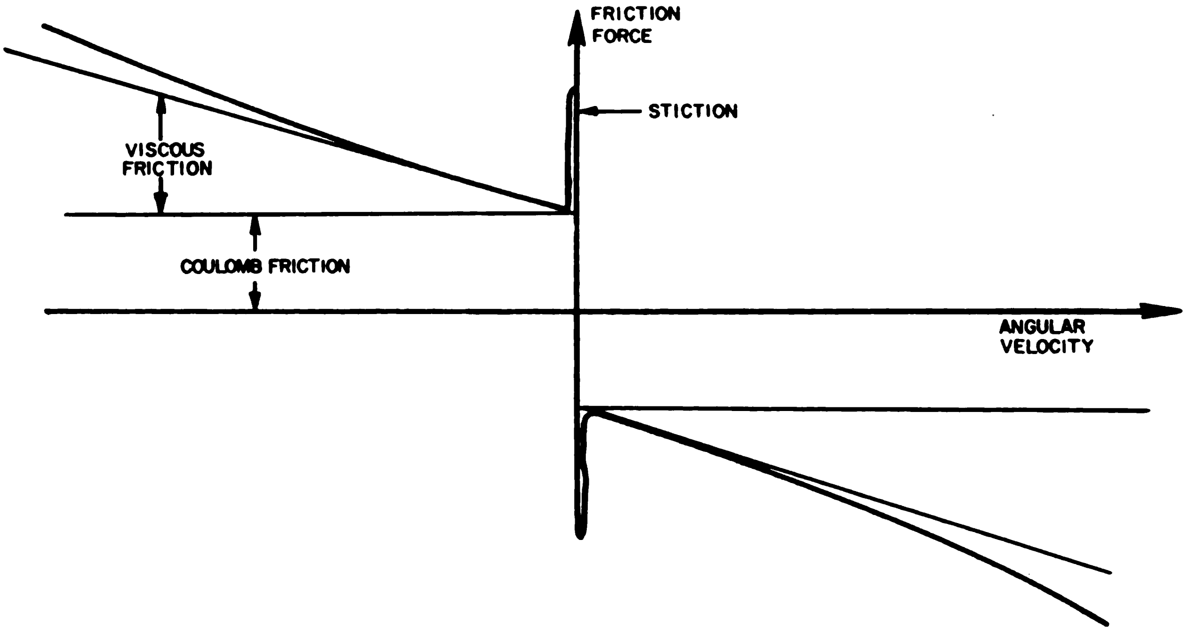

Figure 6-71. Frictional Drags on a Servomechanism

Disregarding for the present the *dead-band lag,* the dynamic errors of antenna servos may be analyzed in a straightforward fashion. Generally these servos are of Type I. They have one integrating element in their loop, such as a d-c motor. A basic Type I servo has an open-loop frequency response like that shown in Figure 6-73. In practice, although the servo loop will have a more complicated transfer function, it may be approximated for many purposes by this simpler characteristic. The transfer function pictured is of the form (where S is the complex frequency):

$$\frac{\Theta_o}{\varepsilon} = G(s) = \frac{\omega_o}{S\left(1+\frac{S}{\omega_1}\right)} = \frac{K}{\frac{S}{\omega_1}\left(1+\frac{S}{\omega_1}\right)} \tag{6-121}$$

If the error is assumed small, then Θ_o, the heading of the antenna, will be approximately equal to the azimuth of the target, Θ.* Then the error is given by:

$$\varepsilon(s) = \frac{S\,(1+S/\omega_1)}{\omega_o}\,\Theta(s) \tag{6-122}$$

In the time domain, this is:

$$\varepsilon\,(t) = \frac{\overset{\prime}{\Theta}}{\omega_o} + \frac{\overset{\prime\prime}{\Theta}}{\omega_o\,\omega_1} = \frac{\overset{\prime}{\Theta}}{K\,\omega_1} + \frac{\overset{\prime\prime}{\Theta}}{K\,\omega_1^{2}} \tag{6-123}$$

This error is a lag due to the rapid motion of the target. A common case of interest is the error associated with the pass course of a target. For target paths close to the radar the angular rates required of the servo may be very high. Figure 6-74 shows the geometry of the pass course problem assuming a target flying a straight, level line at altitude H and constant speed V. If the slant range to the target at its closest approach (crossover) is R_o and the elevation angle at the same time is ϕ_o, then the azimuth angle of the target at any time t is:

$$\Theta = tan^{-1}\frac{Vt}{R_o\cos\phi_o} \tag{6-124}$$

---

*More exact analysis as well as treatment of elevation and range aspects of the pass course problem are given in references 66 and 67.

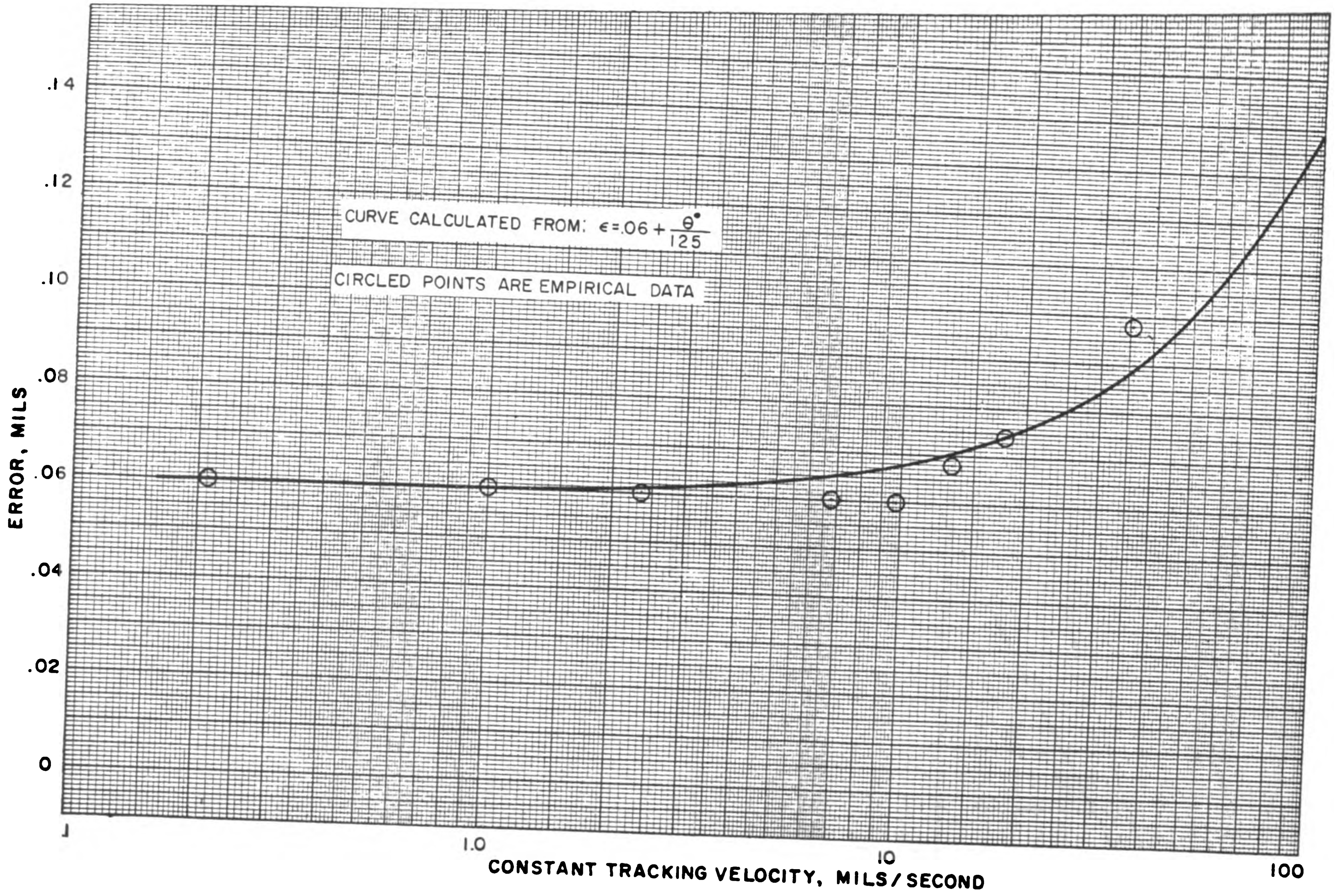

Figure 6—72. Constant Velocity Servo Errors

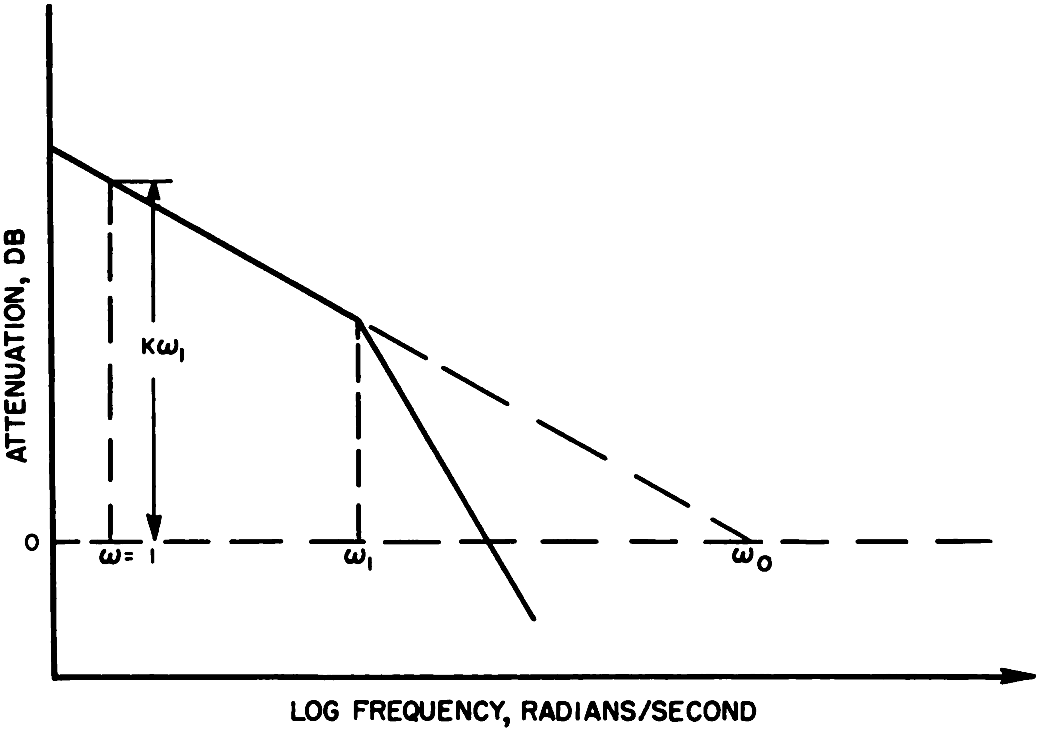

Figure 6-73. Basic Type I Servo Open Loop Response

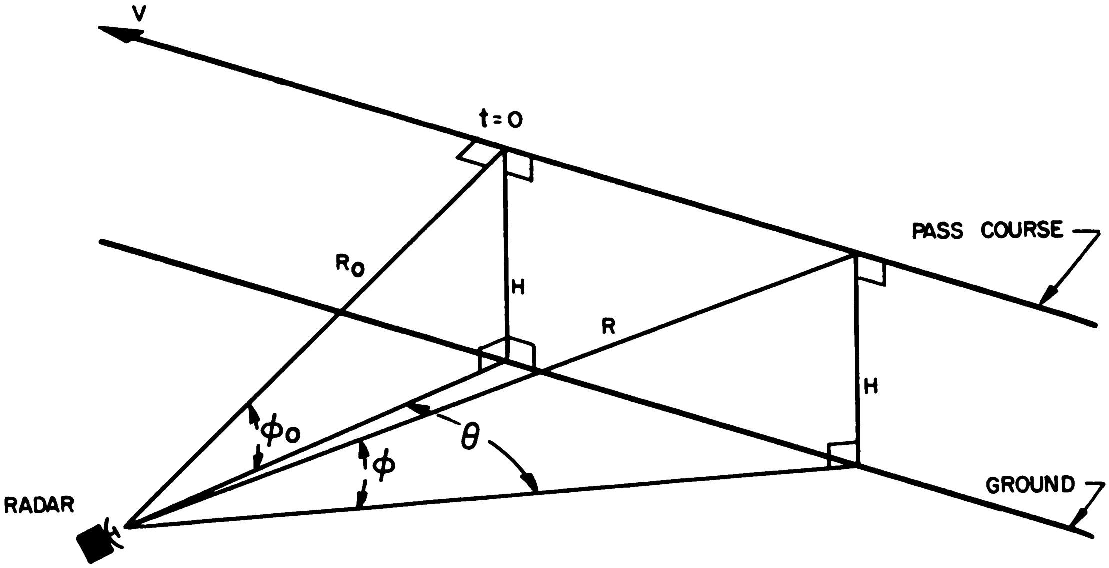

Figure 6-74. Pass Course Geometry

Successive differentiations yield:

$$\overset{\prime}{\Theta} = \frac{V}{R_o \cos \phi_o} \cos^2 \Theta \qquad (6\text{-}125)$$

$$\overset{\prime\prime}{\Theta} = 2\left(\frac{V}{R_o \cos \phi_o}\right)^2 \cos^3 \Theta \text{ sine } \Theta \qquad (6\text{-}126)$$

$$\overset{\prime\prime\prime}{\Theta} = 2\left(\frac{V}{R_o \cos \phi_o}\right)^3 \cos^4 \Theta \, (4 \text{ sine}^2 \Theta - 1) \qquad (6\text{-}127)$$

nese expressions can be used to find the error ; any angle Θ. However, we are generally ıterested in the maximum error, ε_{max}, which is efined from equation 6-124 by:

$$\frac{d\varepsilon}{dt} = 0 = \frac{\overset{\prime\prime}{\Theta}_m}{K\,\omega_1} + \frac{\overset{\prime\prime\prime}{\Theta}_m}{K\,\omega_1^2} \qquad (6\text{-}128)$$

Substituting for the derivatives; and solving for

$$\frac{V}{\omega_1 R_o \cos \phi_o}$$

which we denote by a:

$$\frac{V}{\omega_1 R_o \cos \phi_o} = a = \frac{\tan \Theta_m}{1 - 4 \sin^2 \Theta_m} \qquad (6\text{-}129)$$

Figure 6-76 shows this relationship which defines the angle Θ_m at which the maximum error occurs. The maximum error is found with this value of Θ_m. It will be convenient to rearrange equation 6-124 to put it in the form:

$$\varepsilon_m K = \left[\frac{\overset{\prime}{\Theta}}{\omega_1} + \frac{\overset{\prime\prime}{\Theta}}{\omega_1^2}\right]_{\Theta = \Theta_m} \qquad (6\text{-}130)$$

$$= a \cos^2 \Theta_m + 2\,a^2 \cos^3 \Theta_m \sin \Theta_m$$

It may be seen that the quantity a determines the maximum error. This is as expected since a is the ratio of the maximum angular rate of the target to the bandpass of the servo. Equation 6-130 is also plotted on Figure 6-75.

Note that for small values of $\frac{V}{\omega_1 R_o \cos \phi_o}$ (less than 0.2) that $\varepsilon_{max} K$ is equal to it. That is:

$$\frac{V}{R_o \cos \phi_o} < 0.2\,\omega_1 ; \; \varepsilon_{max} = \frac{\frac{V}{R_o \cos \phi_o}}{K\,\omega_1} \qquad (6\text{-}131)$$

Also note that any dead-band lags add directly to these dynamic errors unless corrected. In a given application the values of the servo constants K and ω_1 will be limited by stability and the mechanical resonant frequency of the antenna structure respectively. This resonance should be at least one to two octaves higher than the servo-passband, not only to prevent resonant response, but also to limit the errors in the servo due to nonlinearities such as wind-up in the gear train. To give an idea of the magnitudes involved; the TPQ-5 (XE-1) antenna showed resonance in azimuth at 10 to 12 cycles and the servo drive had a half-power bandwidth of three to four cycles.[68] In elevation the bandwidth, which corresponds to ω_1 of two to three cycles, was the same, but the resonant frequency was about seven cycles. This was close enough to cause difficulty. What values of K and ω_1 are feasible for a given application will depend on a highly detailed estimate of the antenna characteristics in a given application. In fact the angular error due to the pass course target may in many instances serve to determine the required gain and bandwidth. This in turn may affect mechanical design and electrical characteristics of the entire system.

The subject of servo errors would be incomplete without some discussion of the techniques utilizing the servo error correction signal (ECS) to improve the tracking performance. Two possible methods of doing this are shown in Figure 6-76. The advantage is evident.

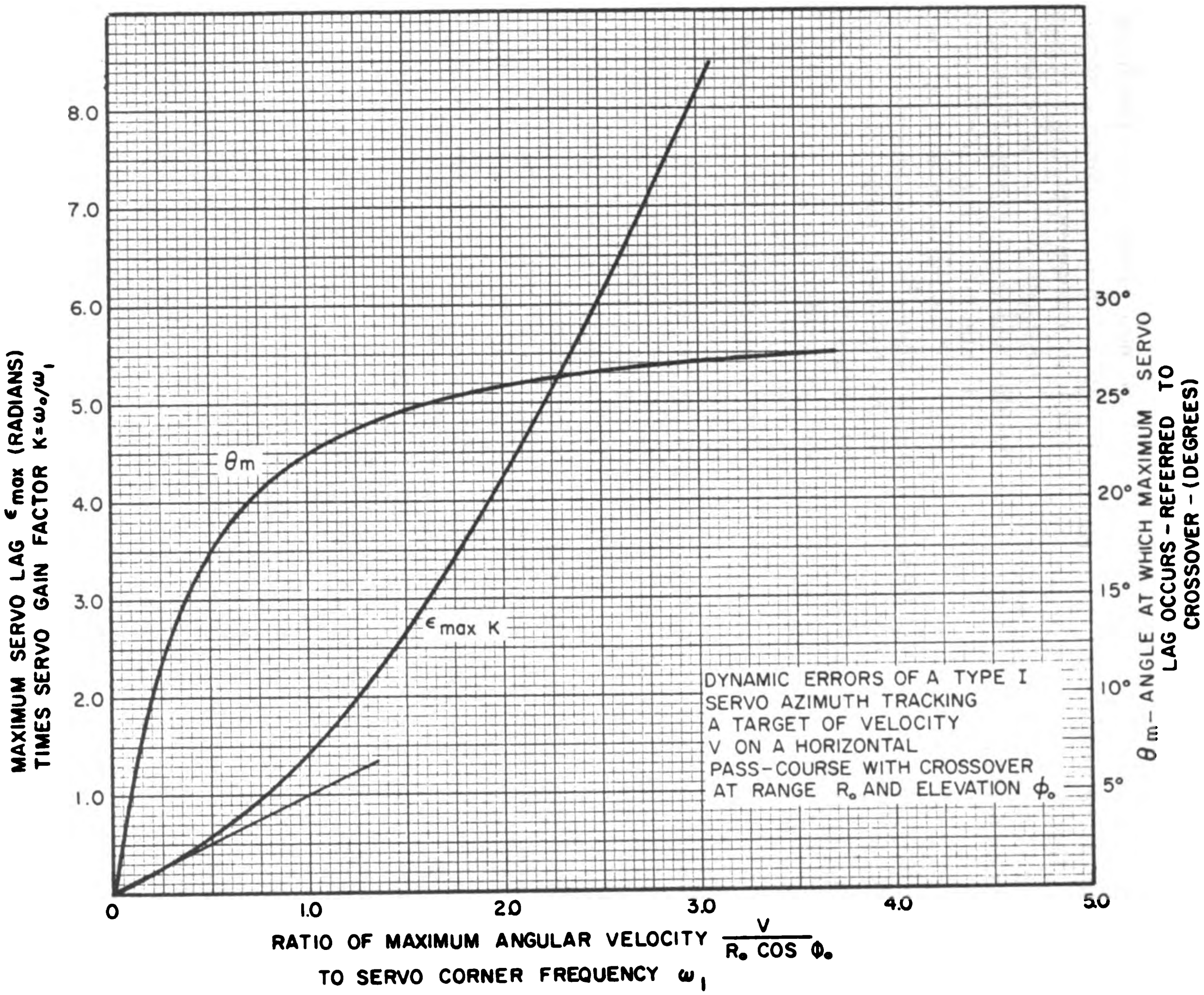

Figure 6-75. Dynamic Errors of a Type I Servo Azimuth Tracking a Target on a Horizontal Pass Course

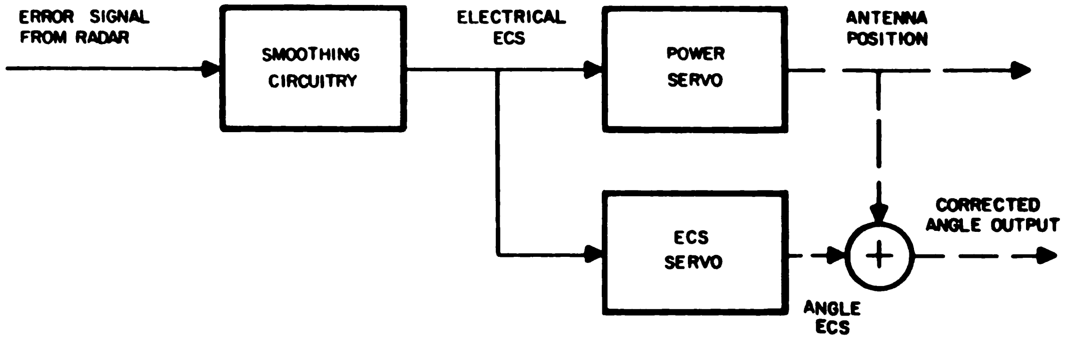

a. ADDITION OF ERROR CORRECTION SIGNAL TO ANTENNA POSITION TO PRODUCE ACCURATE ANGULAR POSITION INFORMATION

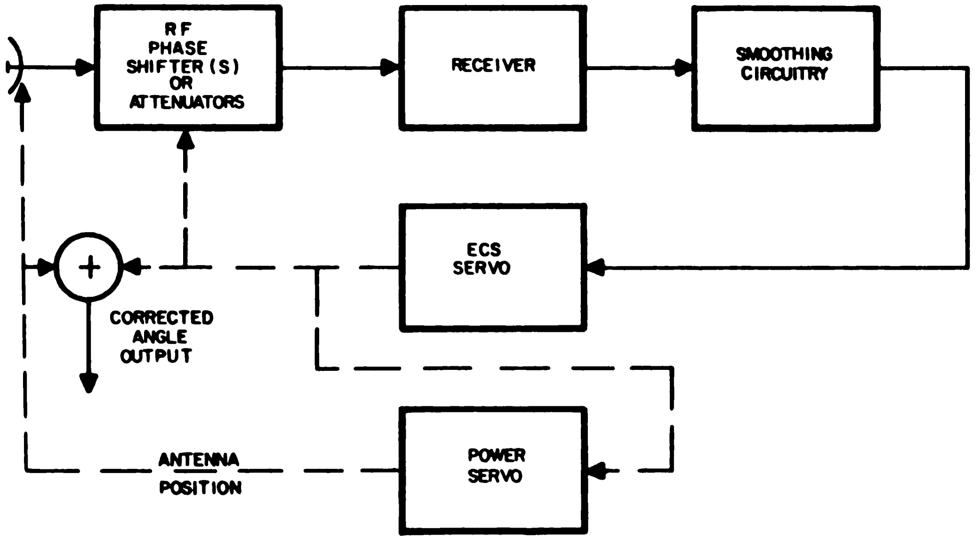

b USE OF RF ECS SYSTEM TO MAINTAIN SMALL SIGNAL IN RECEIVER AND CORRECT ANGULAR OUTPUT

Figure 6-76. Servo Systems Employing ECS Correction

In either case the ECS servo is an instrument servo which may be built with much more accurate components and higher frequency response. At the same time the narrow bandwidth of the smoothing circuitry serves to filter the noise from the radar. The noise, roughness and dead band of the power servo are compensated by the fast and accurate response of the ECS servo. Furthermore, the mechanical resonance of the antenna drive does not limit the ECS bandwidth as it does for the power servo.

This may often lead to a simpler and more economical power servo. Reference 69 treats r-f ECS systems in some detail.

6-5.3.6 Target Scintillation Effects

Most radar targets and especially aircraft, present complex surfaces of reflection to the incident radiation. Because of this, slight changes in target aspect may cause very great changes in the radar echo signal. Also, the apparent center of the target shifts. The terms glint, wander, scintillation and fading have all been used in various ways to describe these effects. In this section fading refers to the fluctuation in echo amplitude and wander refers to the angular variations of the apparent center of reflection. (These same two effects have sometimes been called amplitude modulation and glint; or amplitude noise and angle noise.) It is apparent that these effects are nonexistent (or at least minimized) for beacon operation so this section refers only to echo-tracking radars. Both fading and wander cause angular errors in certain types of tracking radars, but the errors are of different types. These are two distinct effects and their differences should be clearly understood.

FADING

Fading is a time variation of the total signal strength. Its cause is probably a combination of effects. The reflection from a complex target such as an aircraft exhibits a multilobed pattern. The lobes are narrow and close together, so very small changes in aircraft aspect may cause large changes in signal strength. Another possible cause of fading is so-called *differential Doppler reflection*. Because of the finite extent of the target the radial velocity is not constant for the entire target, even though the target is a rigid body. Also, for nonrigid targets, relative motion between parts of the targe gives rise to amplitude modulation. For example, propeller modulation is very marked i echoes from the head-on aspect of conventiona aircraft. The combination of these effects give rise to a noise-like amplitude modulation of the reflected signal strength.

The effect of fading on the radar depends on the type tracking involved. Because it is a fluctuation with time, monopulse or simultaneous comparison radars are affected only indirectly (the loss of signal strength enhancing the errors due to other effects). This is accounted for in the value of target echo area used, which is that echo area exceeded 50 percent of the time. Sequential lobers and conical scanning radars are affected more directly by fading. Variations of the echo in the period between lobe comparison results in a difference signal that is due to the fading, in addition to any difference signal that may be present because of the displacement of the target from boresight. This results in a component of fading noise in the difference or error signal. The amplitude of this noise depends on the fading characteristics of the target (which will in general depend on radar frequency) and the lobing frequency of the radar. However, since the error signal is standardized by dividing by the average signal (either by AGC or phase-detection techniques) the amplitude of the error due to this noise is, within limits, independent of range. It can therefore be computed if the spectrum and percent modulation of the fading are known for a given target.

Spectra or determined errors exist for special cases, but little data of general usefulness is available. However, if the target is complex, it is often assumed that the scan-to-scan returns are composed of random signals from numerous point targets. This leads to a Gaussian probability distribution for any component of the echo, or a Rayleigh distribution for the amplitude of the echo. If the target return is considered to consist of these random signals plus a steady component, the amplitude distribution should approach a Gaussian. Empirical measurements* verify this.

---

*Reference 70. Measurements on an SNB type aircraft. This reference states that measurements were also made on an F94 jet, but does not give distribution functions for this A/C.

Assume the Rayleigh distribution and evalu- e the effect of fading. The probability of a gnal amplitude (x) is:

$$p(x) = \frac{x}{\sigma^2} e^{-\frac{x^2}{2\sigma^2}} \qquad (6\text{-}132)$$

To evaluate the deviation, use the usual efinition of target area as that area exceeded 0 percent of the time. If the signal calculated n the basis of this area is S, then:

$$p(x > s) = \tfrac{1}{2} = \int_s^\infty \frac{x}{\sigma^2} e^{-\frac{x^2}{2\sigma^2}} dx \qquad (6\text{-}133)$$

Performing the integration:

$$\tfrac{1}{2} = - e^{-\frac{x^2}{2^2}} \Big|_s^\infty \qquad (6\text{-}134)$$

Thus: $ln\, 2 = \frac{s^2}{2\sigma^2}$ (6-135)

And: $\sigma^2 = \frac{s^2}{2\, ln^2} = 0.721\, s^2$ (6-136)

Now the part of the return that produces fading noise is only the difference from the average echo. To evaluate this noise calculate the rms value of this difference from the average. Call this N_f and the average signal return x_{av}. The rms and average values are calculated by multiplying a variable by the time that it exists in an interval and dividing by the length of the interval. However, the probability distribution only expresses the relative portion of the time that these quantities have a given value. Therefore:

$$x_{av} = \int_0^\infty x\, p(x)\, dx \qquad (6\text{-}137)$$

$$N_f = \sqrt{\int_0^\infty (x - x_{av})^2\, p(x)\, dx} \qquad (6\text{-}138)$$

The average value can be computed directly:

$$x_{av} = \int_0^\infty \frac{x^2}{0.721\, s^2} e^{\frac{x^2}{1.442\, s^2}} dx \qquad (6\text{-}139)$$

$$= \sqrt{\frac{\pi\,(1.442\, s^2)}{4}} = 1.06\, s$$

This simply states that the average value of a Rayleigh distributed signal is equal to 1.06 of the median value. The integral of equation 6-138 may be expanded to:

$$N_f = \sqrt{\int_0^\infty x^2\, p(x)\, dx - 2\, x_{av} \int_0^\infty x\, p\,(x)\, dx - x_{av}{}^2 \int_0^\infty p(x)\, dx} \qquad (6\text{-}140)$$

But the last two integrals are respectively x_{av} and unity. The first integral defines the rms value of the total signal:

$$x_{rms} = \sqrt{\int_0^\infty x^2\, p(x)\, dx}$$

$$= \sqrt{\int_0^\infty \frac{x^3}{0.721\, s^2} e^{-\frac{x^2}{1.442\, s^2}} dx}$$

$$= 1.20\, s \qquad (6\text{-}140a)$$

Equation 6-140 is then:

$$N_f = \sqrt{x^2_{rms} - x_{av}{}^2} = \sqrt{(1.45 - 1.13)\, s^2}$$

$$= 0.55\, s \qquad (6\text{-}141)$$

This indicates a basic noise-to-signal ratio for fading noise of a Rayleigh character, of about 55 percent. As with other forms of noise, this will be improved by filtering. To determine the amount of filtering improvement, remember that this discussion of fading applies only to sequential lobers, so that the signal is carried in the side bands of the lobing frequency. Also, fading spectra are narrow-banded compared to pulse rates. The filter factor derived for wideband noise therefore does not apply to fading noise. It can be calculated from the filter power response, $h(f)$, and fading power spectrum, $p(f)$, by integration:

$$K_f{}^2 = \frac{1}{\int_{-\infty}^{\infty} h(f)\, p(f)\, df} \qquad (6\text{-}142)$$

Note that the limits of integration must extend from minus infinity because the noise is on the lobing frequency carrier. If the servo band is very narrow compared to the fading spectrum, the spectrum may be considered constant over the integration as was done in previous calculation. If A_{f_l} is the amplitude of the normalized power spectrum at the lobing frequency f_l:

$$K_f{}^2 = \frac{1}{\int_{-\infty}^{\infty} \frac{1}{1 + (f/f_c)^2} A_{f_l}\, df} = \frac{1}{\pi\, f_o\, A_{f_l}} \qquad (6\text{-}143)$$

Typical spectra for an R4D (C-47) type aircraft are shown in Figure 6-77[71]. The effects of propeller modulation are quite noticeable. To calculate fading noise for other targets, spectrum information should be found if possible. In the absence of empirical information, it is possible to calculate a spectrum by the differential Doppler theory. The target is considered composed of point targets corresponding to the major parts of the airframe in geometry and with echo strengths weighted according to the silhouette of the part.[72,73] Such calculations are too lengthy and tedious. However, some information concerning the spectrum can be calculated rapidly. If the sweeping assumption is made that the target in the broadside position is represented by a uniformly illuminated slot of length equal to the length of the target, a beat frequency can be calculated by considering the lobes of the reflection pattern. These will be spaced apart by an angle:

$$\Theta = \frac{\lambda}{2l} \qquad (6\text{-}144)$$

where l is the length of the target and λ the radar wavelength. These lobes give a large component of amplitude modulation at a frequency given by:

$$f = \frac{V}{R\,\Theta} = \frac{2Vl}{R\,\lambda} \qquad (6\text{-}145)$$

where V is the target velocity and R the range. Calculations of this sort made in reference 74 show good correlation with strong frequencies observed in empirical measurements. The calculations should be better for targets similar to long cylinders such as missiles.

WANDER

Although a great deal has been said of fading, it is probably a less important scintillation than that fluctuation of the center of reflection called wander. This is true only because of the increasing use of monopulse type radars (which are not susceptible to fading errors) over the sequential lobers. Both types of tracker are susceptible to wander errors.

The physical cause of this wander is the same as the cause of fading. The complex target shape reflects a wave front which has ripples and kinks in it unlike the idealized spherical wave front reflected from a point target. Since an tracking system is basically measuring th angle of approach of the wave front, these ripple can cause an error in the angle sensed by th device (see Figure 6-78). Small fluctuations o target aspect and/or vibrations cause this angle error to vary in a noise-like manner about some mean position. It is important to note that the mean position is not necessarily the geometrical center of the target. Generally, however, because of the randomness of the fluctuations, the mean error will be small compared to the instantaneous excursions.

Like fading, wander may be analyzed by considering a group of point targets with appropriate weight and geometry to approximate the actual target. Based on an analysis of this sort,[73] the various types of tracking radars have equal performance with regard to wander with the exception of combination monopulse. Because of the two-beam nature of combination monopulse systems, interaction between beams occurs in the presence of wander. This can lead to very large errors in one axis compared to those for other tracking methods. For short range applications, if wander is the dominant source of error, the ratio of elevation sensitivity to azimuth sensitivity of the combination monopulse has an optimum value which depends upon the shape of the target. If equal errors in the two axes can be tolerated, for typical aircraft targets the elevation sensitivity should be about twice the azimuth sensitivity. Under this condition, the error in either axis will be about 3 db larger than for other systems. The optimum ratio of sensitivities arises from the shape of the aircraft silhouette. For targets extending equally in azimuth and elevation, or whose orientation is random, the two sensitivities should be equal. For targets such as rising missiles which extend further in elevation than azimuth, azimuth sensitivity should be larger than elevation sensitivity.

Calculation of the errors due to wander is hampered by a lack of empirical data. Available information shows rms values of the wander measured in feet at the target of from 0.05 to 0.30 times the span of the aircraft for a front or rear aspect and about twice as much for the side aspect. A combination of theoretical and

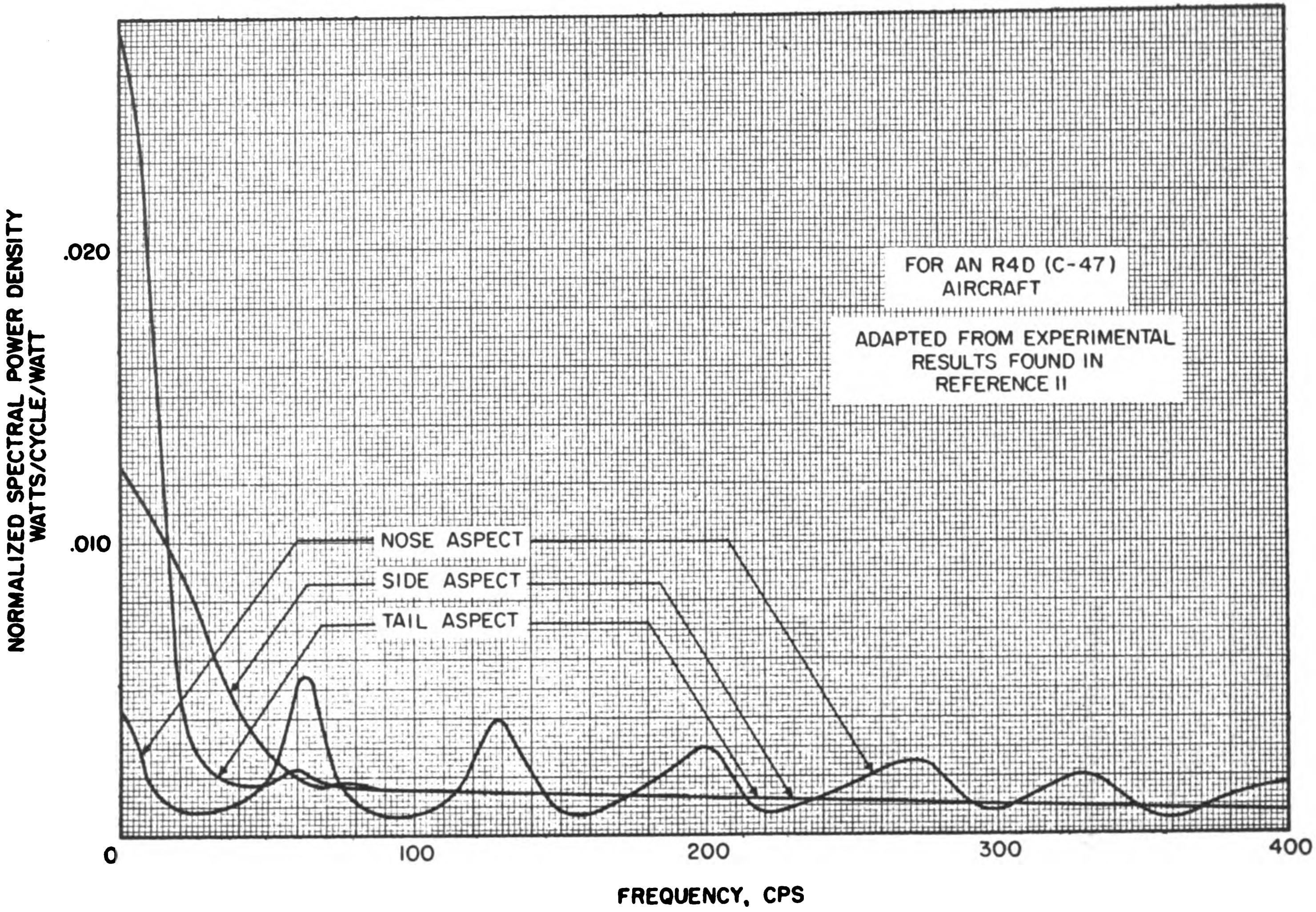

Figure 6-77. Spectra of Fading (Amplitude Scintillation)

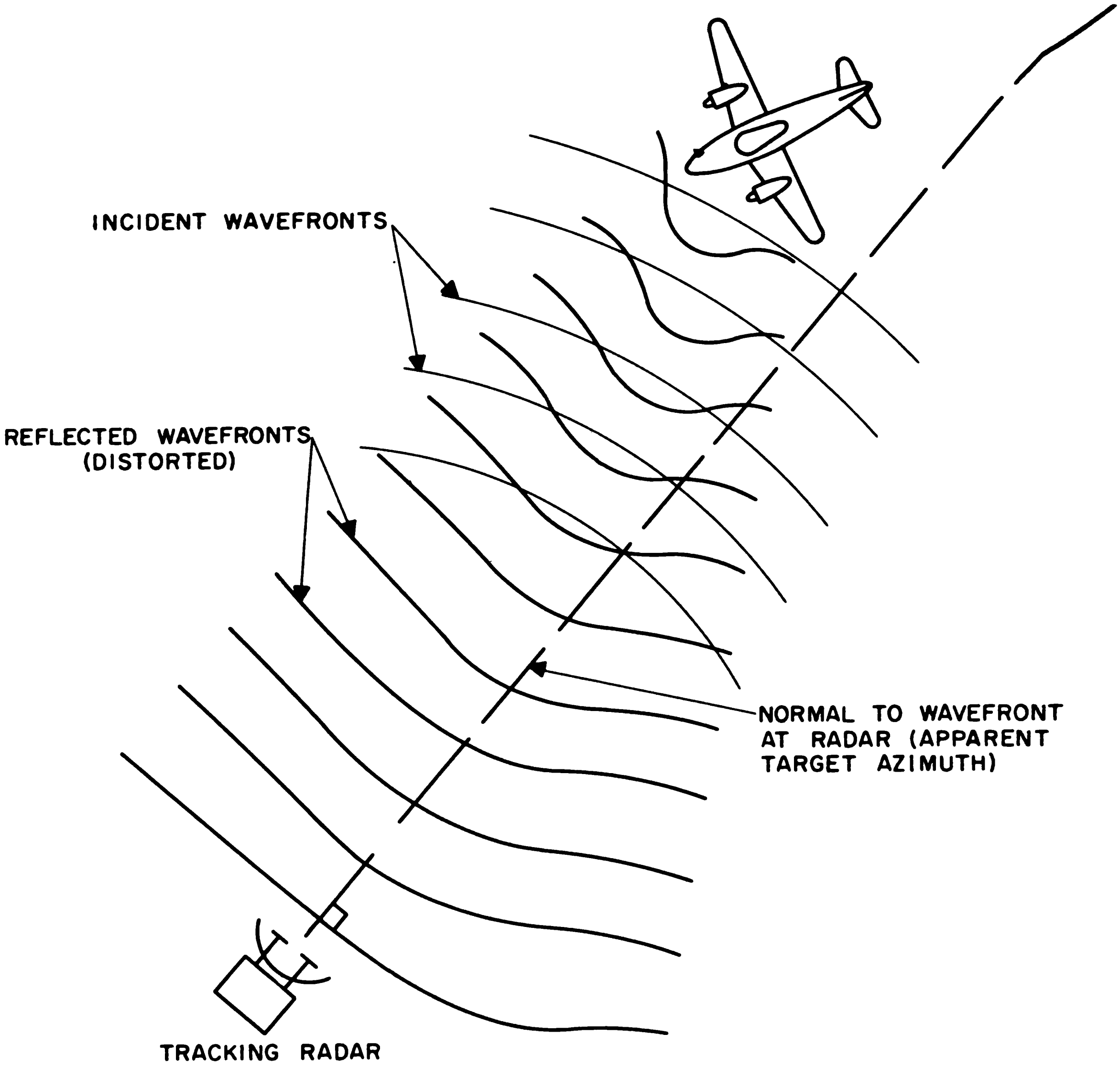
INCIDENT WAVEFRONTS
REFLECTED WAVEFRONTS (DISTORTED)
NORMAL TO WAVEFRONT AT RADAR (APPARENT TARGET AZIMUTH)
TRACKING RADAR

Figure 6-78. Showing How Wander Arises from the Distorted Wavefronts Reflected from a Complex Target

empirical work at Hughes has led them to propose the values of wander[74] (in feet at the target) given in Table 6-8.

As mentioned above, the spread of observed values differs widely from these values.

The spectrum of wander noise is very narrow. For the R4D (C-47) aircraft empirical spectra given in reference 73 are six to ten cycles wide. Whether this is representative is not known. In a given application, if the spectrum of the wander or angle noise is known, the filter factor can be calculated as before:

$$K_f^2 = \frac{1}{\int_0^\infty h(f)\, p(f)\, df} \tag{6-146}$$

TABLE 6-8. VALUES OF WANDER FOR PROPELLER DRIVEN AIRCRAFT

For single-engine aircraft:	0.162 x span of aircraft
For twin-engine aircraft:	0.138 x span of aircraft
For four-engine aircraft:	0.115 x span of aircraft

If only the cutoff frequency (f_n) of the wander spectrum is known the filter factor may be approximated by:

$$K_f \approx \sqrt{\frac{f_n}{f_c}} \qquad (6\text{-}147)$$

where as before, f_c is the servo bandwidth.

CONCLUSION

The calculation of errors due to scintillation effects, which may be very important, depends upon empirical information. Much more information is needed in order to predict these errors with confidence and design for minimizing them. Care should be used in tabulating empirical results. Much of the data available is of limited usefulness because of a lack of information about the conditions under which it was gathered. For example, as indicated by equation 6-145, the fading spectrum is affected by target velocity, dimensions and range, as well as frequency of the radar. Yet the target information is not supplied in the reference from which the curves of Figure 6-77 are taken. In other papers, the data is difficult to evaluate because it is not clearly specified whether the noise has been filtered by the servo. Future empirical work should avoid these difficulties.

In concluding, it should be mentioned that frequency agility techniques have a striking and salutary effect on errors due to scintillation. Since scintillation effects are very frequency sensitive, rapid random frequency shifts cause the scintillation noise to be raised to a frequency range well above the servo passband. The theory of this effect is stated in reference 75 and empirical measurements are presented in reference 76.

6-5.3.7 Propagation Errors

All of the usual phenomena of classical optics occur to significant degree in microwave propagation. These propagation effects may be limiting sources of error in many applications. At elevation angles of less than a beamwidth, *reflection* of the radar energy from the surrounding terrain will cause interference with the signal propagated directly. The errors so caused may be very severe. *Diffraction* of microwaves is usually so small that it is neglected, yet at grazing angles in certain situations it may be more important than interference. Because the earth's atmosphere varies greatly in refractive index, any propagation through this medium suffers *refraction*, or bending. The effect may cause large errors even at fairly high elevation angles. Finally, *attenuation* by the atmosphere may so weaken the radar signal that other sources of noise become more serious in producing angular errors.

Figure 6-79 illustrates the regions in which various propagation phenomenon usually predominate.

REFLECTION

For most short range systems, interference due to reflection is probably the worst propagation problem. This causes effects similar to fading and wander, but which may be much more pronounced.

The interference is due to multipath propagation. Figure 6-80 illustrates how the beam is affected. The ground reflection may be thought

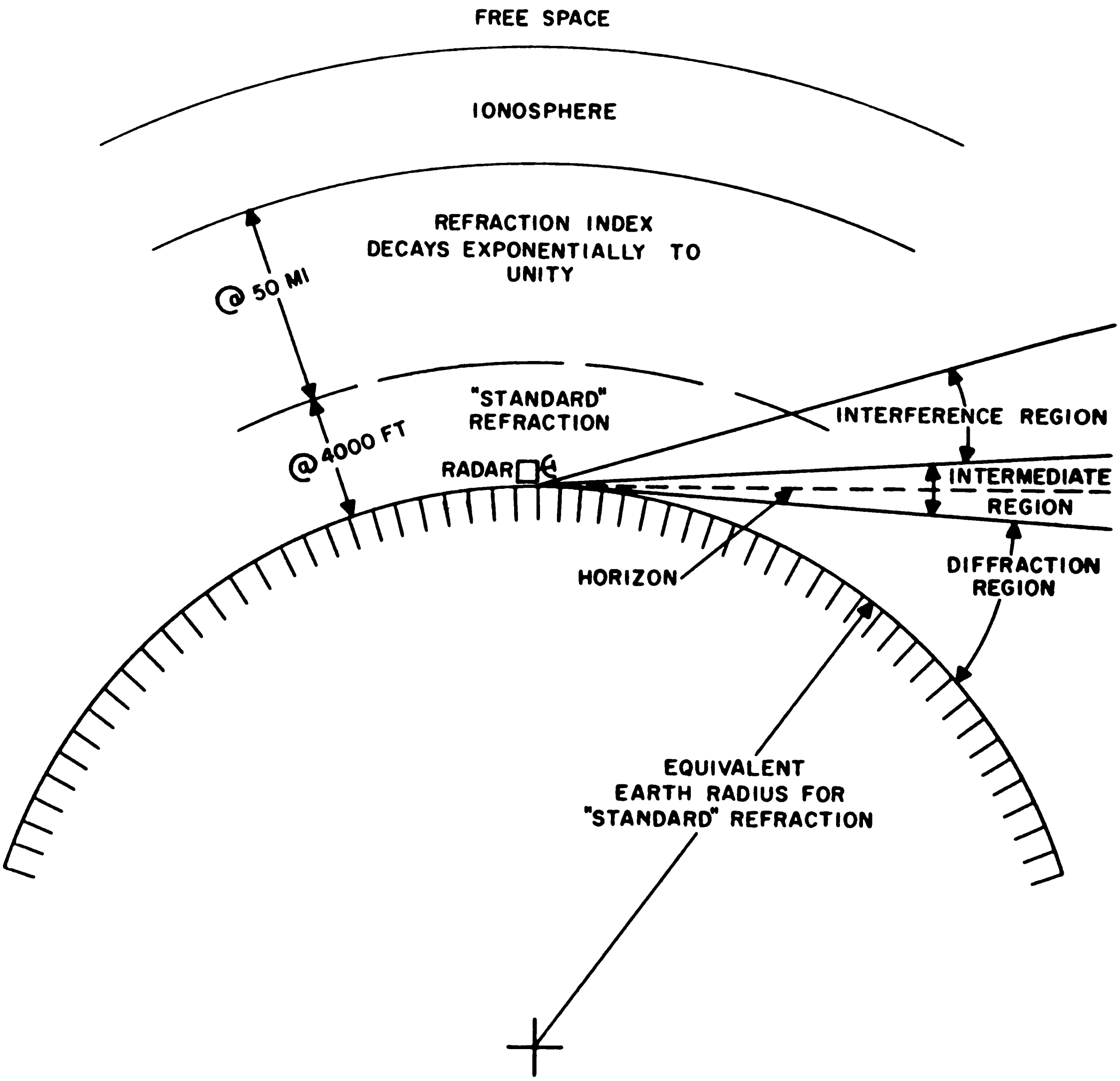

Figure 6-79. Regions of Propagation Phenomena

of as an image beam. The intensity and relative phase of this beam will depend on terrain and frequency, as well as radar height and beam shape. However, where the two beams overlap they cause alternately constructive and destructive interference.

The usual reflecting surface is the ground or sea, so that the largest errors are in elevation. However, large nearby objects such as steep mountains may give rise to appreciable reflection in the horizontal plane. Obviously the effect is worse for targets at low elevation angles. Highly attenuated sidelobes and narrow radar beams help to decrease the minimum angles at which the interference is tolerable.

The size of the errors due to interference will depend upon frequency, beam shape, and terrain, but an estimate of the frequency of this interference fading and wander can be made in a straightforward fashion. From Figure 6-81 the

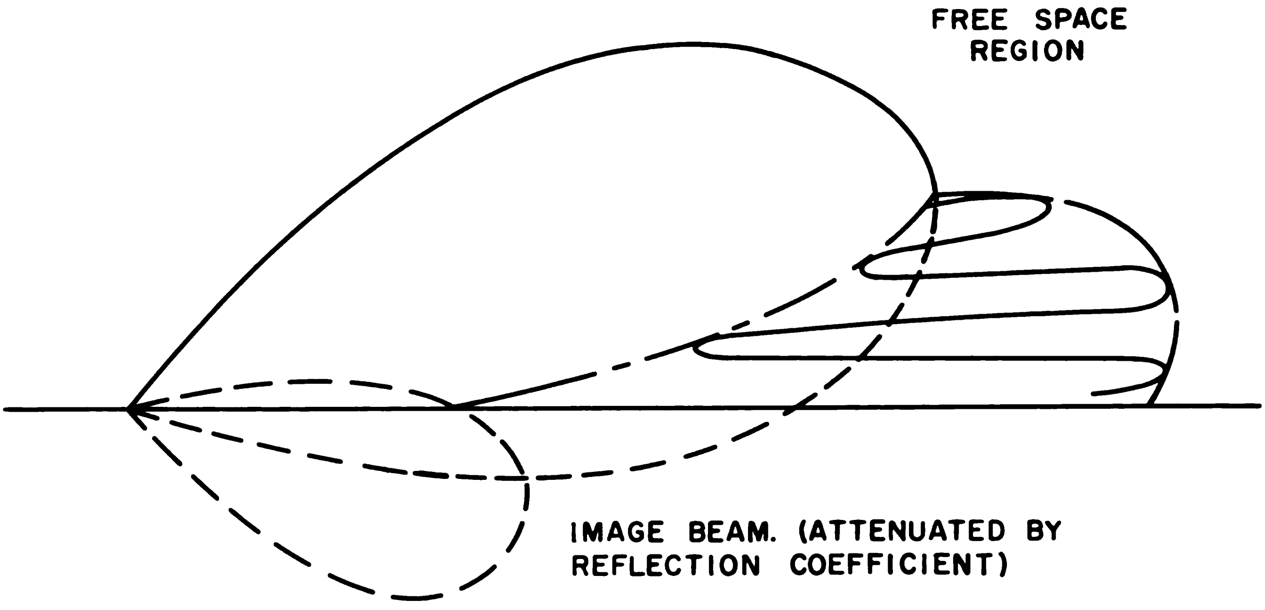

Figure 6-80. Effect of Reflection on the Radar Beam Assuming Flat Earth, No Diffraction or Refraction

phase difference between direct and reflected return, neglecting the phase change due to reflection and assuming a plane earth is:

$$\begin{aligned}\phi &= \frac{2\pi}{\lambda}\left[\sqrt{(h_1+h_2)^2+d^2}-R\right] \\ &= \frac{2\pi R}{\lambda}\left[\sqrt{1+\frac{4\,h_1\,h_2}{R^2}}\;-1\right]\end{aligned} \qquad (6\text{-}148)$$

Now, in order to have the beam so low as to include reflection, normally $h_2 << R$. (This may not be a valid assumption for an airborne tracker). Under this condition the binomial approximation to the radical leads to:

$$\Theta = \frac{4\pi\,h_1\,h_2}{\lambda R} \qquad (\Theta \text{ in radians}) \qquad (6\text{-}149)$$

This phase difference is changing, causing a modulation of the return at a frequency given by (assuming constant altitudes):

$$f = \frac{1}{2\pi}\,\frac{d\Theta}{dt} = \frac{2\,h_1\,h_2}{\lambda R^2}\,\frac{dR}{dt} \qquad (6\text{-}150)$$

It might be convenient for comparison, to write this in the form:

$$f = \frac{h_1}{h_2}\left(\frac{h_2}{R}\right)^2 f_d \qquad (6\text{-}151)$$

where f_d is the Doppler frequency of the return. For an aircraft target velocity of 500 meters per second (at 1100 mph), elevation angle of one degree and an x-band radar height of ten feet, this frequency is about 1/10 cycle per second. Thus, the effect of this fading on a sequentially lobing radar should be slight and is insignificant on monopulse systems. The wander due to the modulation, however, will be troublesome and will probably be unimproved by filtering.

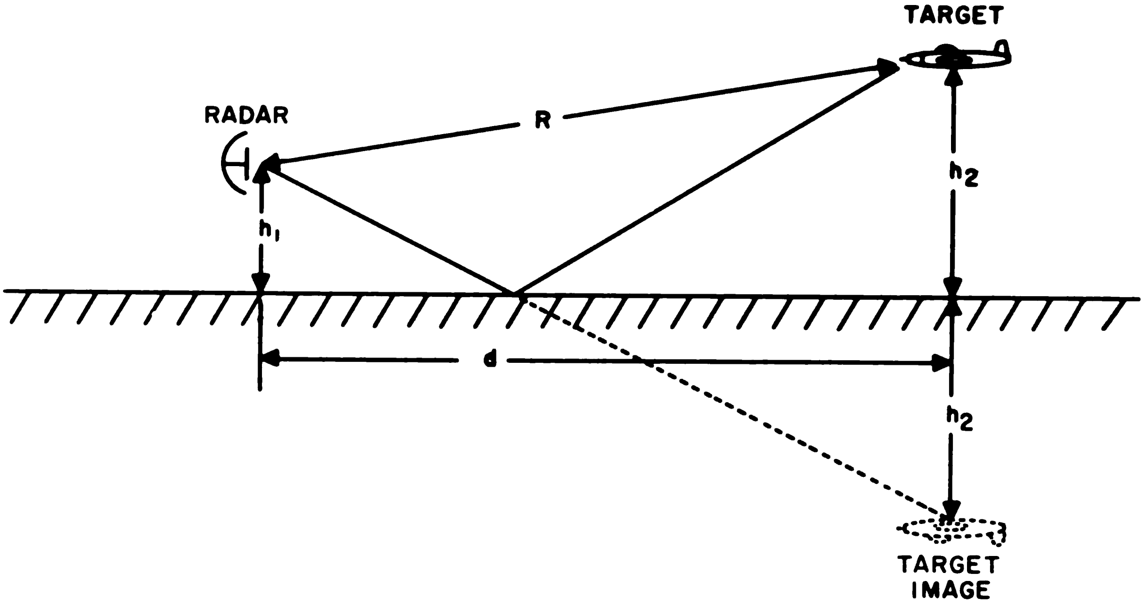

Figure 6-81. Geometry of the Reflection Problem

The magnitude of the error depends upon the ratio of the reflected signal amplitude to the direct signal amplitude and therefore the effective reflection coefficient of the terrain. Some experimental values for this coefficient are given in reference 63. However, the values vary widely with terrain, frequency and angle of incidence. The reflected signal will probably be of the same order of magnitude as the direct signal until attenuated by the beam shape. The advantage of low sidelobes is apparent. However, these and the narrow beam only make it possible to go lower without having this effect become significant. It is necessary to avoid the region where the effect occurs, especially if elevation tracking is required, but also for azimuth tracking unless the terrain is very flat.

Figure 6-82 and 6-83 are the maximum possible errors for monopulse radars due to reflection from the ground surface.[77] These curves are based on an assumption of total reflection with random phase. The advantage of the lower sidelobes in the tapered (cosine) illumination is apparent. Empirical results indicate that these are pessimistic estimates, probably due to the roughness and therefore reduced reflection coefficient of actual sea surface or terrain.

The errors that are derived from this effect have been measured in some cases to be of the order of degrees and elevation may appear to be negative. The effect will occur for all type of radars, but will be somewhat more marked for combination monopulse. It was noted above that this type system will have larger errors than any other due to scintillation wander. The same is true for wander due to interference. Note also that wander in elevation will cause an apparent wander in azimuth in the combination system. For example see Figure 6-84. Very great caution should be exercised in applying combination monopulse for low-angle tracking.

A very good reference giving interference region field strengths for isotopic antennas is reference 78.

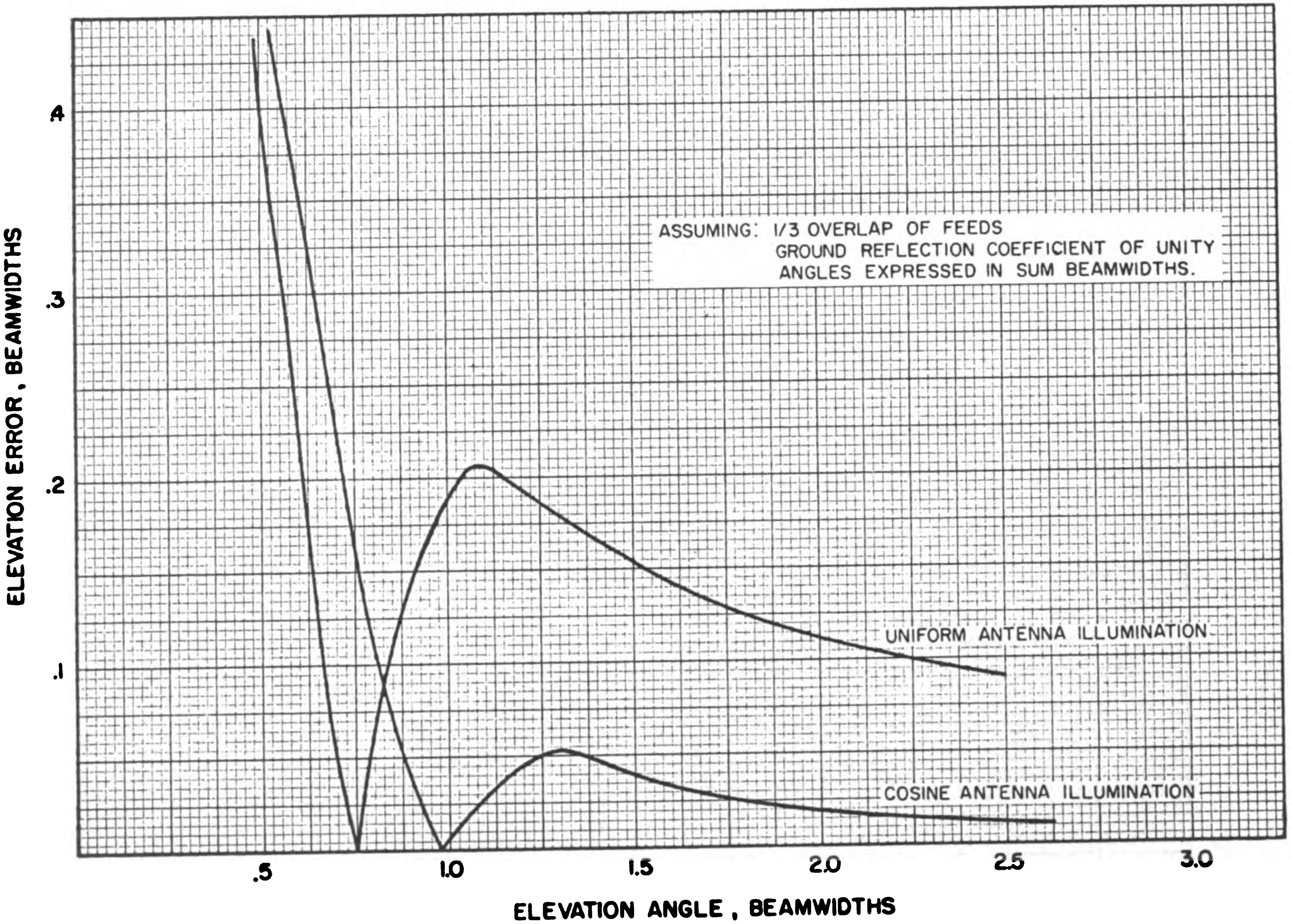

Figure 6-82. Interference Errors in a Combination Monopulse

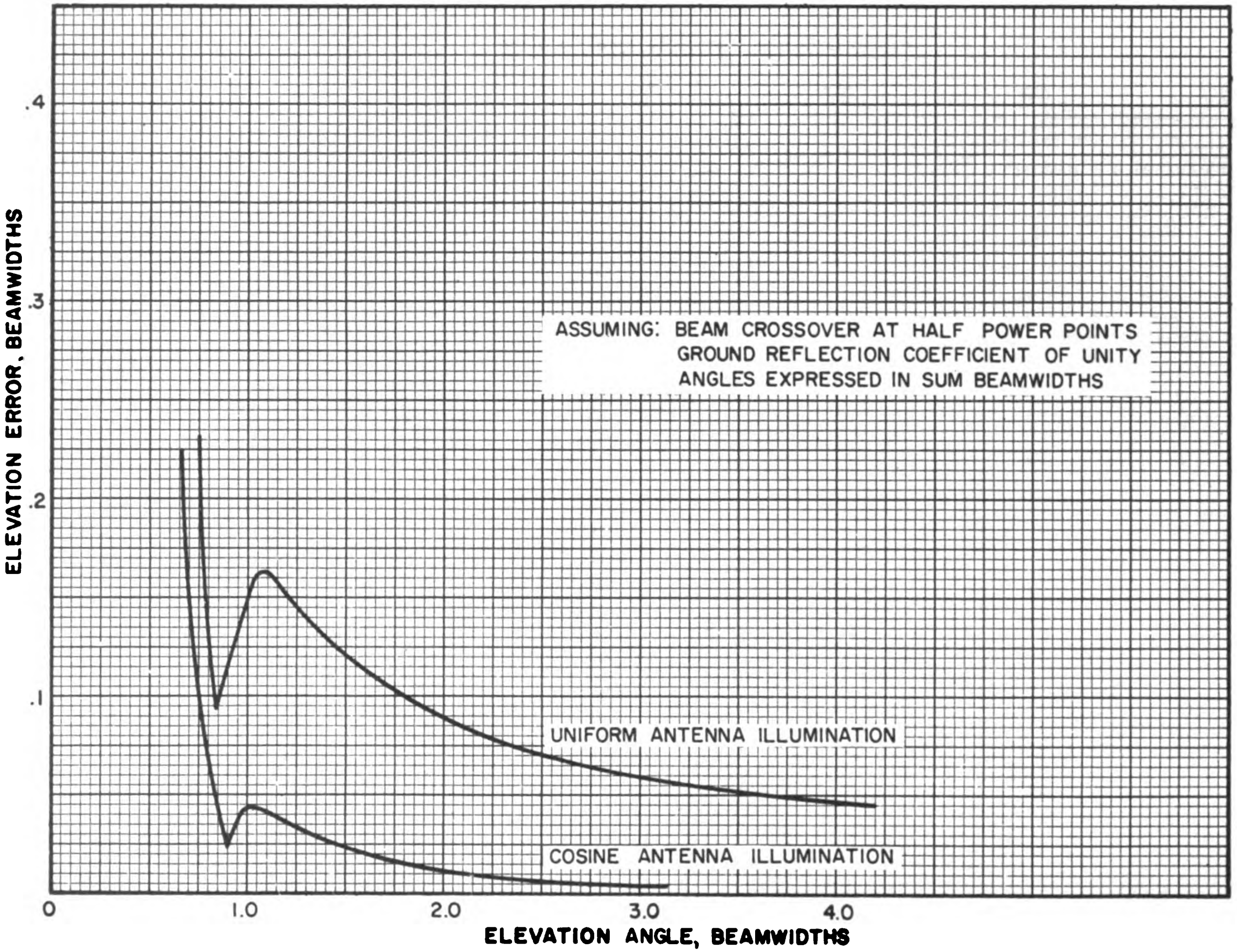

Figure 6-83. Maximum Elevation Errors of Phase Monopulse

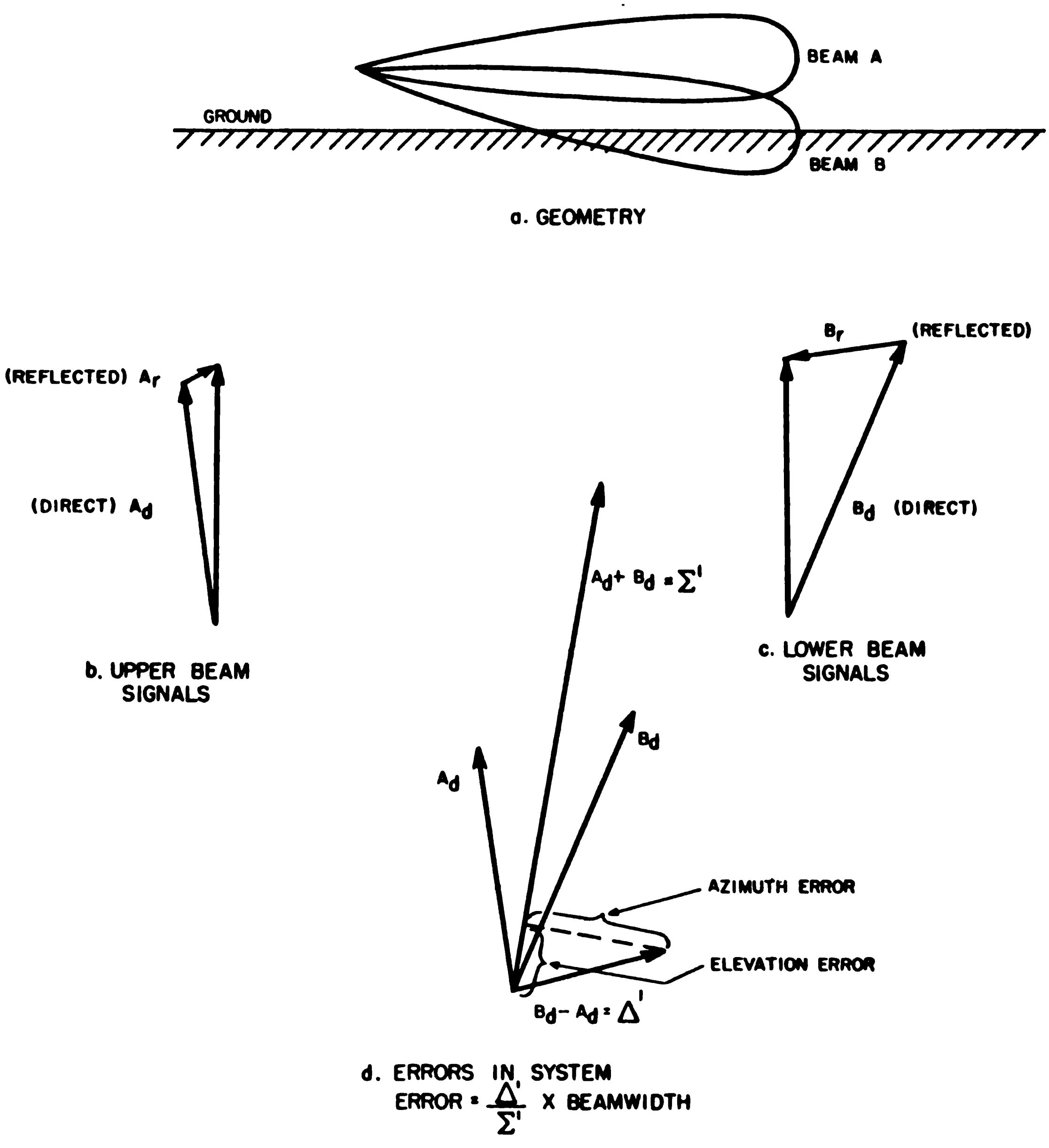

a. GEOMETRY

b. UPPER BEAM SIGNALS

c. LOWER BEAM SIGNALS

d. ERRORS IN SYSTEM

ERROR $= \frac{\Delta'}{\Sigma'}$ X BEAMWIDTH

Figure 6-84. Interference Errors in a Combination Monopulse Having Amplitude Comparison in Elevation

DIFFRACTION AND ATTENUATION

Two effects cause a loss in radar signal strength relative to the free space propagation usually assumed in the radar equation. In a tracking radar, loss of signal causes larger errors due to thermal or other types of noise. A discussion of these two sources of signal loss, diffraction and atmospheric attenuation is given below. Both are subjects of complexity. It is the intent to give an indication of the regions where the effects are significant and their order of magnitude with references for more complete evaluation of the effect.

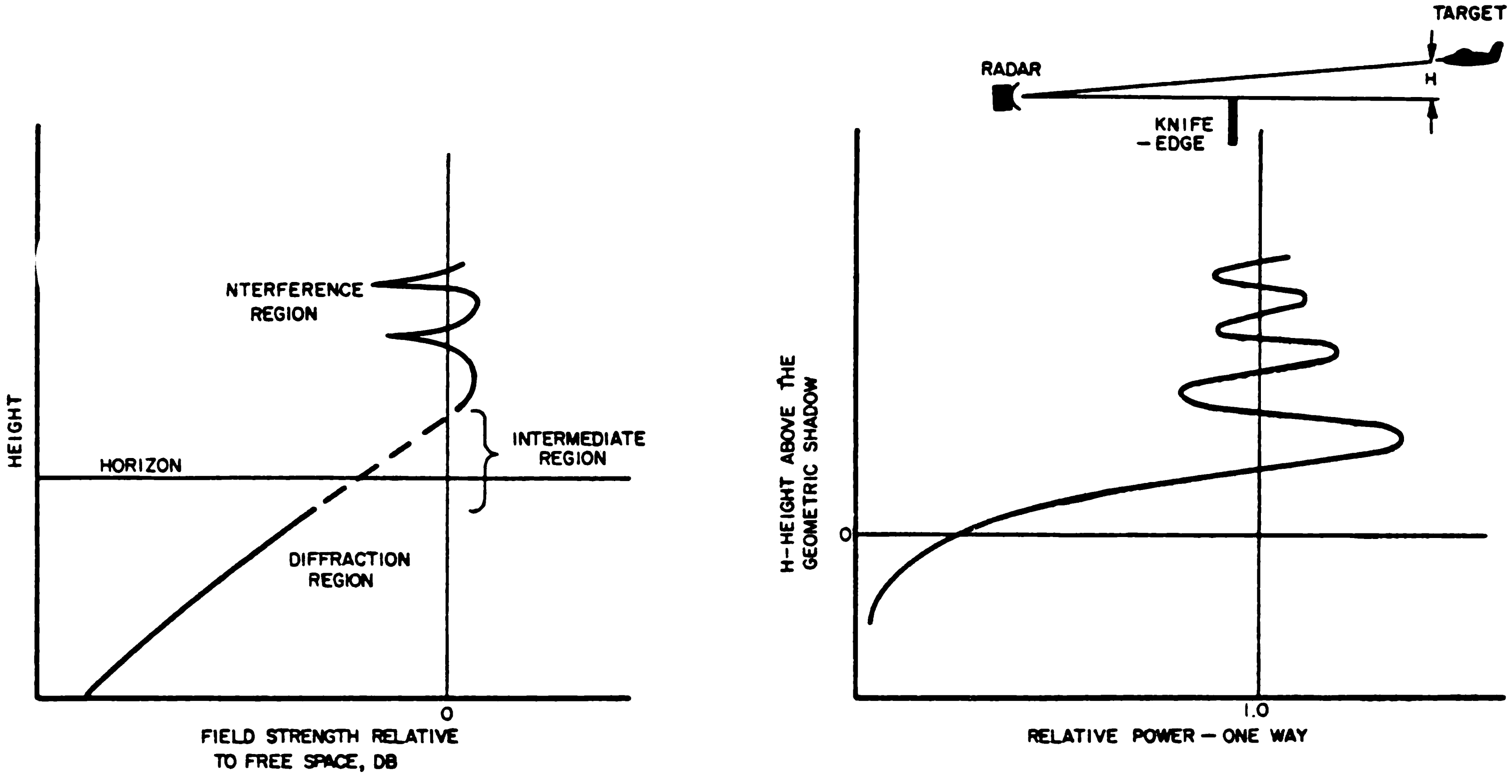

a. DIFFRACTION BY THE SMOOTH EARTH

b. KNIFE-EDGE DIFFRACTION

Figure 6-85. Attenuation Due to Diffraction

Two types of diffraction are of interest to the radar engineer — so called *straight-edge* diffraction and diffraction around the spherical earth. Both effects are demonstrated by the field strength profiles of Figure 6-85. Physically, diffraction can most easily be understood in terms of Huygen's principle of wave propagation which states that each point on a wave front is the source for a wavelet radiating isotropically. The effect of all points on the wave therefore determines successive wave fronts and field strengths.

Because of the interaction of diffraction and reflection effects over a smooth earth, the calculation of field strength very near the horizon becomes impractical. Thus the fields in this region, called the intermediate region, are commonly interpolated from calculated values for the regions where one cause or the other predominates.

The only result of diffraction by the smooth earth that is significant is the loss of signal relative to free-space propagation. At the higher radar frequencies this effect extends only a few mils above the horizon. At lower frequencies, however, signal loss due to diffraction occurs at higher elevation angles (up to about a degree at 500 megacycles). This is illustrated by Figure 6-86. Unfortunately, propagation curves from which Figure 6-86 was adopted do not cover the centimeter wavelengths, so the dotted portion is extrapolation. Actual calculation of the field strength in the regions of diffraction is complex. The method is presented in reference 63.

The spherical diffraction, because it occurs only over a very small region of space and causes only loss of signal strength, is of less concern to the tracking radar engineer than straight-edge diffraction. This is usually calculated on a mathematical model consisting of a spherical wave passing a semi-infinite plane. The "shadow" of the edge of this plane has no sharp boundary, but a diffraction pattern as shown in Figures 6-85 and 6-87. As abstract as this knife-edge model may seem, diffraction fringes closely related to those predicted by this simple theory are observed in practice. Reference 79 shows empirical signal versus height curves for L-and S-band systems that exhibit very clear diffraction patterns, although there is no sharp ridge in the adjacent terrain.

Figure 6-87 shows the angular errors that may arise from straight-edge diffraction. This error is the actual deviation of the normal to the wave front from a direction radial to the target. In addition, the motion of the target through the diffraction fringes will cause fading and wander effects.

The curves shown are arbitrary examples. For other cases the effects may be more pronounced. Therefore, some thought should be given to diffraction in very low elevation angle applications. The siting of the radar will have a large bearing on the severity of the effect. A protecting ridge may have the advantage of reducing interference due to reflection and reducing the maximum range at which ground clutter is observed, but it may offset this by producing very great loss of signal and some angular deviation of the wave front. The calculations of knife-edge diffraction, which are straightforward, are outlined in reference 80 or in most optics textbooks.

Probably a more serious source of signal loss than diffraction is the attenuation of microwave energy in passing through the earth's atmosphere. This loss of signal stems from two physical causes. In another section we discussed rain clutter. Obviously the energy in this clutter return was taken from the transmitted power. This is one cause of atmospheric attenuation — scattering. This is most important with the shorter wavelength propagating through clouds or precipitation. The other cause of attenuation is absorption, or conversion of the microwave energy to heat by the molecules of oxygen and water vapor in the atmosphere. Figure 6-88 shows the attenuation versus frequency due to these causes. The atmospheric conditions assumed in this picture are, according to the source,[81] relatively dry. However, reference 63, speaking of the same water vapor concentration, states that it is typical for temperate zones.

In the presence of rain or fog the tropospheric attenuation is greatly increased. The calculation of these attenuations is made in reference 63. Figure 6-89 is taken from this source. Note that these curves are calculated for a temperature of 18°C (65°F). For temperature as low as 0°C

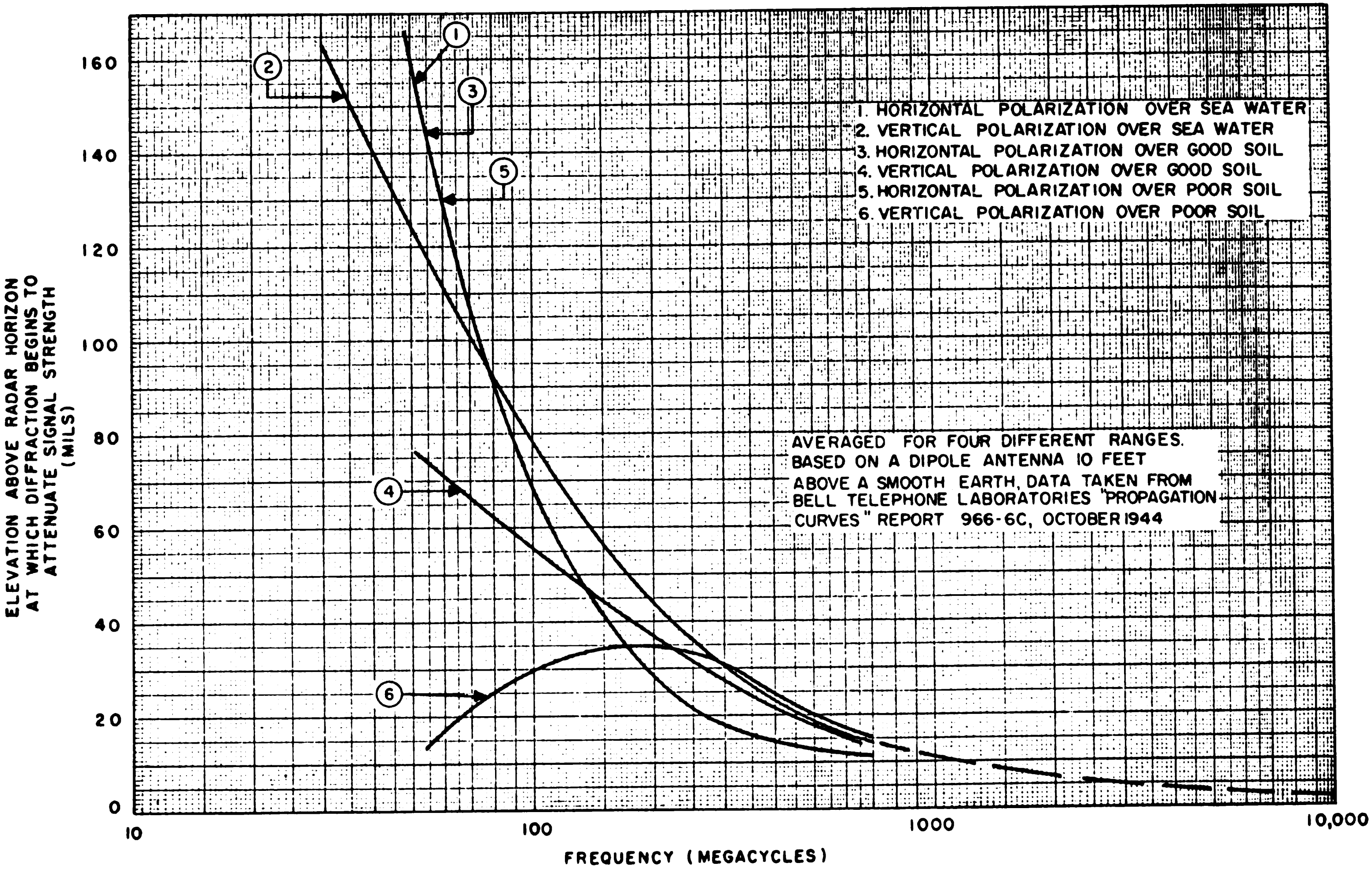

Figure 6-86. Minimum Elevation Without Diffraction Loss

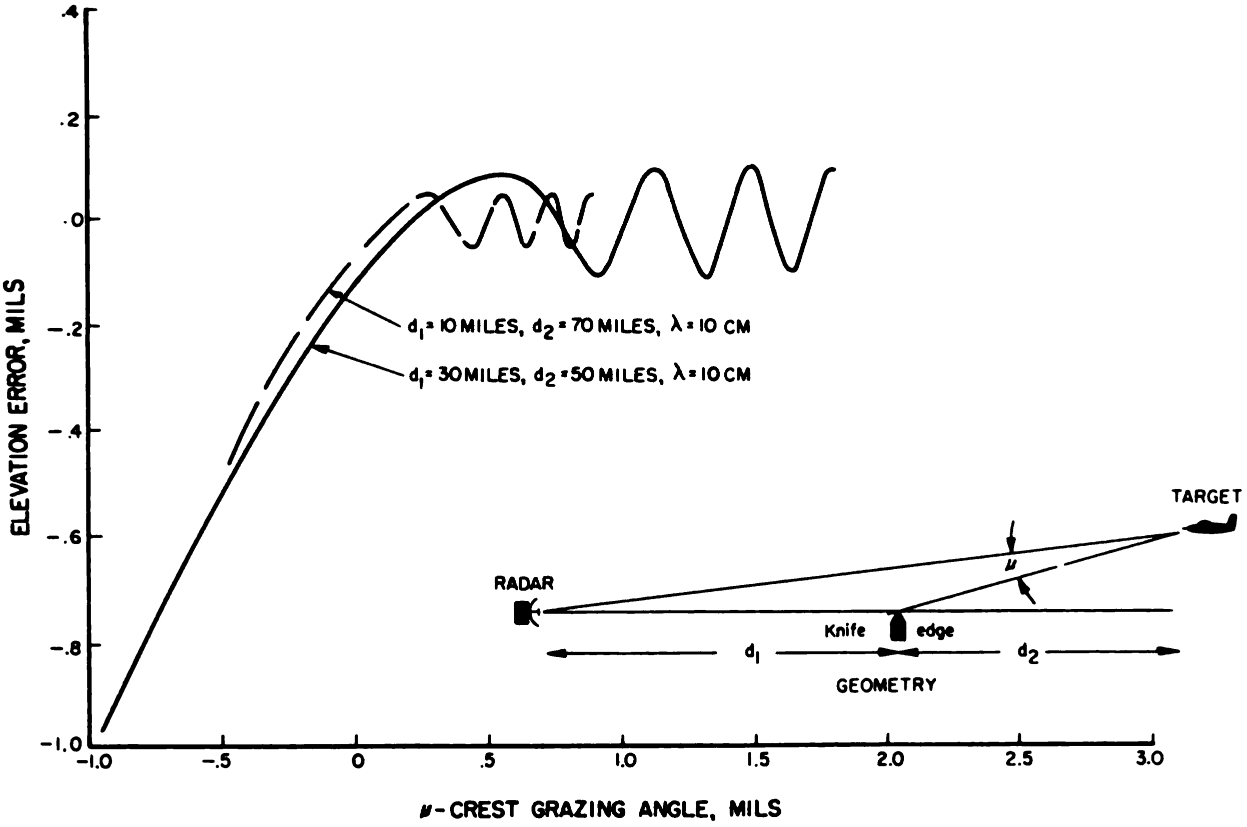

Figure 6-87. Elevation Errors Due to Knife-Edge Diffraction (From Reference 16)

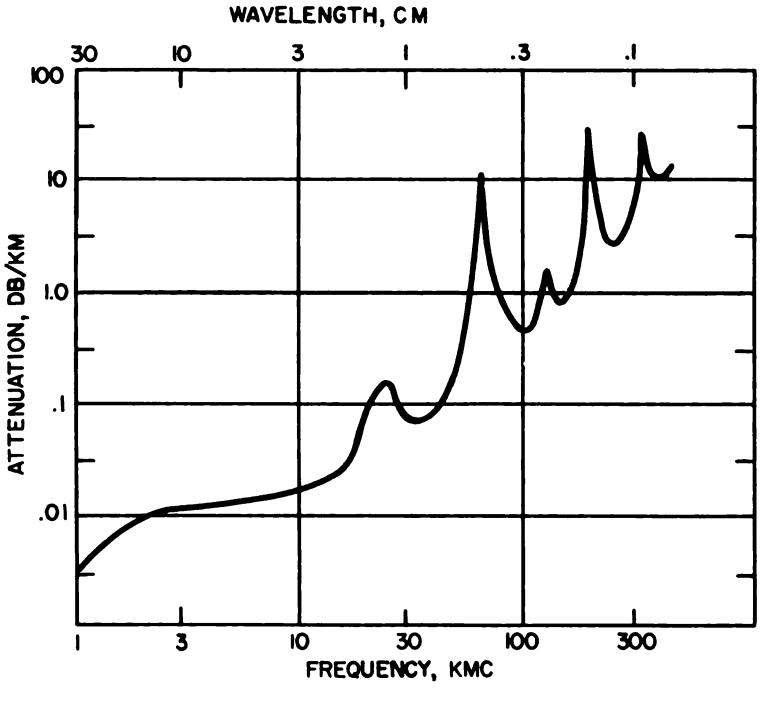

Figure 6-88. Atmospheric Attenuation at Sea Level (Assuming One Percent Water Vapor Content)

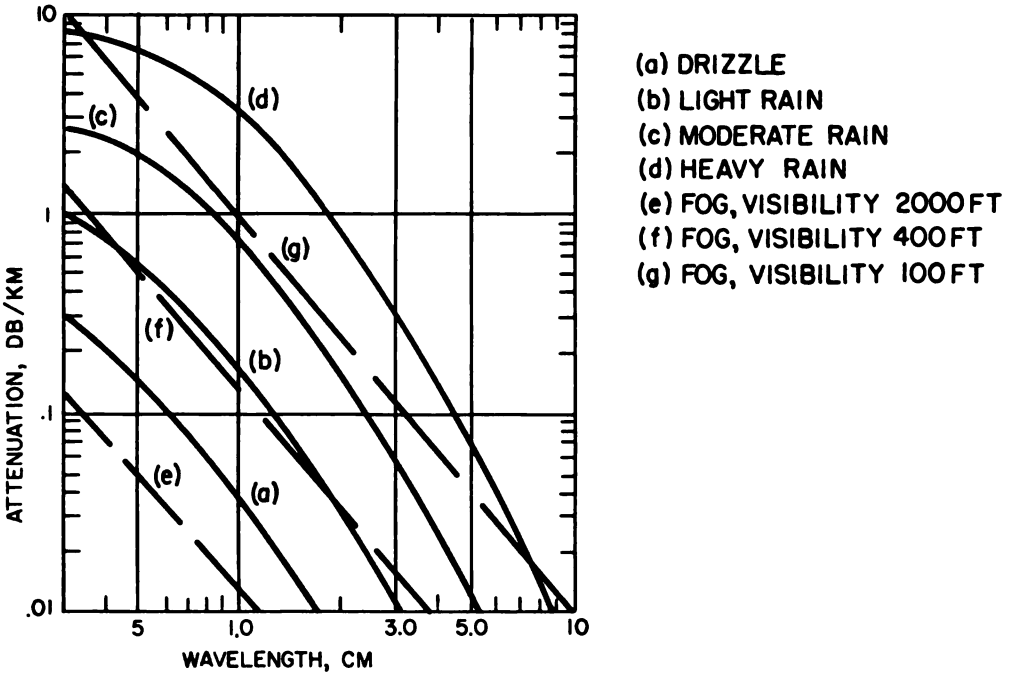

Figure 6-89. Attenuation by Rain and Fog (at 18°C)

and as high as 40°C the attenuation may vary by a factor of two, being higher at lower temperatures and lower at the higher temperatures.

Still another source of attenuation in a tracking radar may be the ionosphere. Because this region occurs at altitudes of 50 or more miles, it will be applicable only to missile or satellite trackers. The attenuation is also very slight. Figure 6-90 shows typical one-way attenuations of radio energy in passing through the daytime ionosphere. Night time attenuations are only about a tenth of those shown.

REFRACTION

In recent years, the bending of the radar beam by the atmosphere has become a principal source of error in tracking radars. This is primarily due to the advancing state-of-the-art which is reducing errors from other causes. The requirement for more refined long range trackers has made this problem the subject of considerable study and fairly good methods exist for calculating and correcting refraction errors if sufficient meteorological data are available.

Refraction occurs in both the lower atmosphere, or troposphere and the ionosphere. However, the causes of the two refractions are quite different.

The causes of *tropospheric refraction* are to be found in the composition of the atmosphere. The index of refraction of air, n, can be expressed in terms of temperature, T, (°K), pressure p (millibars) and partial water vapor pressure, e (millibars) as:

$$(n-1)\,10^{-6} = \frac{79}{T}\left(p + \frac{4800\,e}{T}\right) \qquad (6\text{-}152)$$

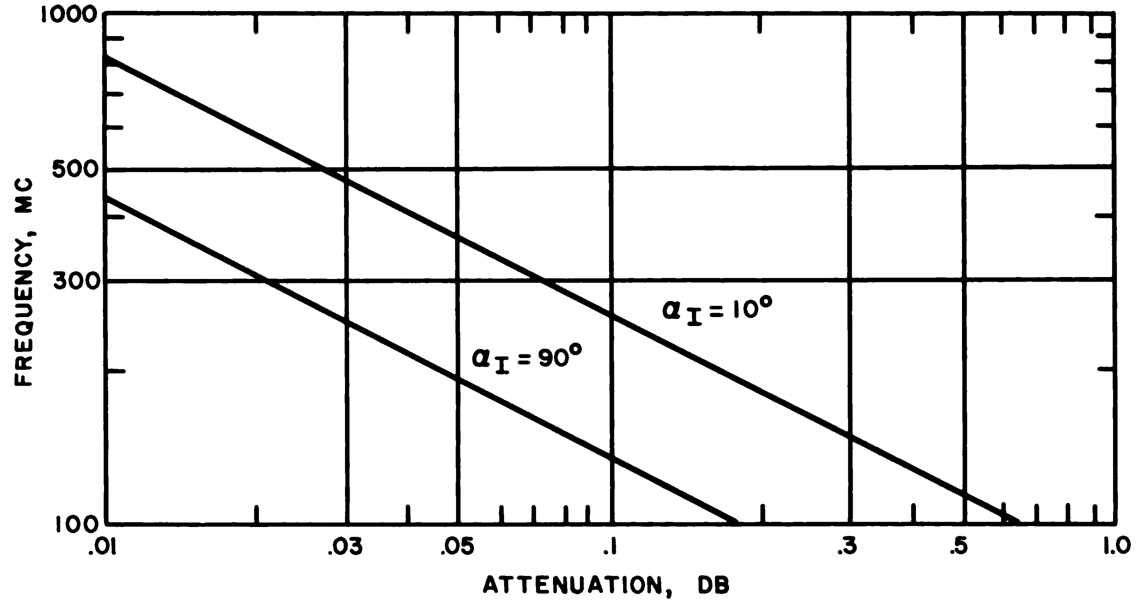

Figure 6-90. Attenuation by the Ionosphere

The refractivity is essentially independent of frequency in the frequency range from 100 to 30,000 megacycles. The difficulty in predicting refraction stems from the extreme variability of these quantities in the lower atmosphere. Quite often the atmosphere is stratified with cold layers and hot layers causing so-called inversions.

Ionospheric refraction is of growing interest for missile and satellite tracking. Index of refraction of dielectrics is usually greater than one. This is the case with the troposphere. The index gradually reduces with altitude to the free-space value of unity. However, at higher altitudes the ionized plasma of the ionosphere causes an index of refraction less than unity. Radio waves are therefore refracted. This refraction, unlike that of the troposphere, is very frequency sensitive. It is, in fact, total refraction by the ionosphere, sometimes called reflection, that makes possible sky-wave radio communications. At radar frequencies the refraction is small, but may be appreciable. It should be noted that to a large extent this refraction compensates itself. That is, the rays are bent in passing through, but come out of the ionosphere almost parallel to their path upon entering it. This is similar to the familiar passage of light through a window pane. In fact the only reason the beam is not exactly parallel to itself leaving the ionosphere is the curvature of the ionosphere. At low angles, the side-ways displacement of the beam may cause appreciable angular error (parallax) at the radar if not accounted for, especially if the target is at moderate height. This may be a larger source of error than the angular deviation. These effects are shown in Figure 6-91. Reference 82 calculates ionospheric refraction for a number of cases. At 400 megacycles the maximum error is of the order of a half mil. It decreases rapidly with frequency and increased elevation angle.

In most applications, the tropospheric refraction is most significant. A number of models have been developed to represent the index of refraction variation with altitude. At higher altitudes theoretical deductions, backed by experiment, suggest an index which decays exponentially from its surface value to its free space value of one with a height constant of 25,000 feet. Algebraically this is:

$$(n-1)\,10^{-6} = N = N_o\, e^{-\frac{z}{25,000}} \qquad (6\text{-}153)$$

This model seems generally valid from altitudes of about 30,000 feet up[82] and a good average atmosphere at lower altitudes.

In particular, note that for low altitudes this model is well approximated by a linear variation of index with a slope given by:

$$\frac{dN}{dZ} = \frac{dn}{dz}\,10^{-6} = -\frac{N_o}{25,000} \qquad (6\text{-}154)$$

From which:

$$\frac{dn}{dZ} = -\frac{N_o}{250} \times 10^{-8} \qquad (6\text{-}155)$$

If the index of refraction is known by any means, it is possible to calculate the path of a ray from optics. Snell's law of refraction for a sperically stratified medium is written as:

$$n_o\, a \cos \alpha_o = n(a+Z)\cos \alpha \qquad (6\text{-}156)$$

where α is the angle the rays make with the horizontal and a the actual earth radius (see Figure 6-92). This can be put in the form:

$$\frac{n_o}{n} = \left(1 + \frac{Z}{a}\right)\frac{\cos \alpha}{\cos \alpha_o} \approx \frac{\cos \alpha}{\cos \alpha_o} + \frac{Z}{a} \qquad (6\text{-}157)$$

If we now note, since n is very close to unity, that:

$$\frac{n_o}{n} \approx 1 + n_o - n \qquad (6\text{-}158)$$

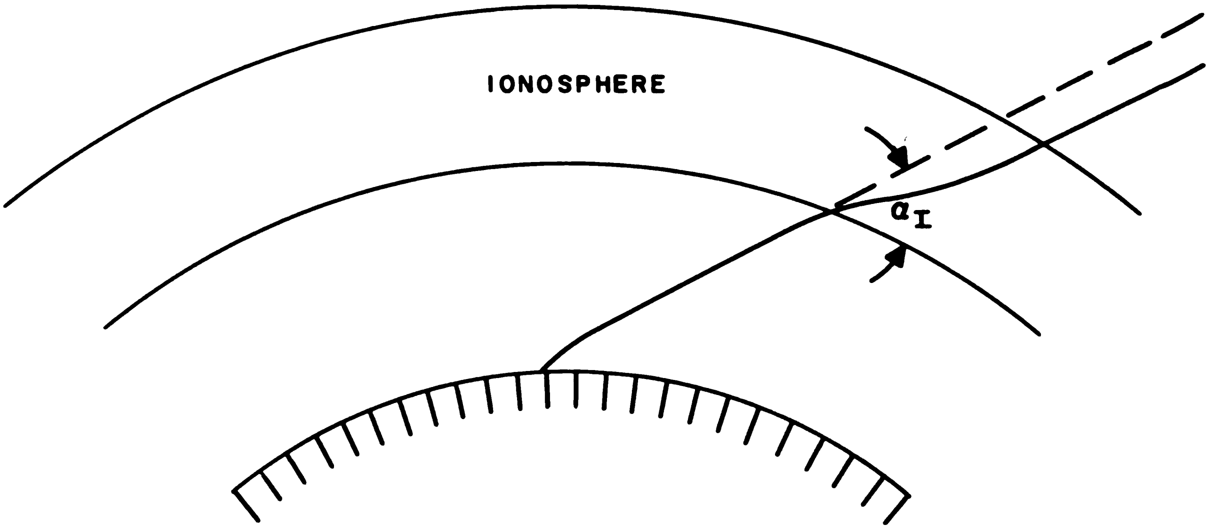

Figure 6-91. Refraction by the Ionosphere

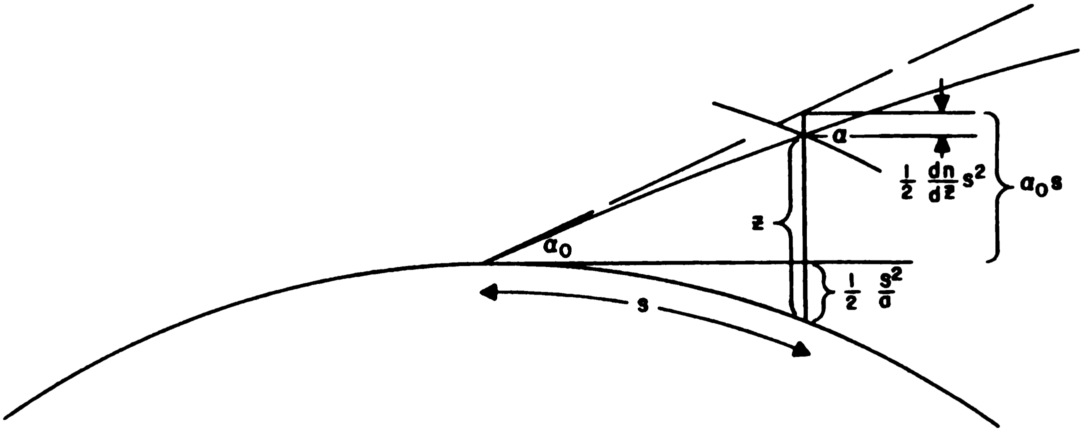

Figure 6-92. Calculation of Refraction Assuming Linear Index of Refraction

and that cos α can be approximated as (since $(\alpha - \alpha_o)$ is very small):

$$\cos\left[\alpha_o + (\alpha - \alpha_o)\right] = \cos\alpha_o - (\alpha - \alpha_o)\sin\alpha_o \tag{6-159}$$

Then equation 6-157 can be written as:

$$1 + n_o - n = 1 - (\alpha - \alpha_o)\tan\alpha_o + \frac{Z}{a} \tag{6-160}$$

which can be put in the form:

$$\frac{Z}{\tan\alpha_o}\left(\frac{n - n_o}{Z} + \frac{1}{a}\right) = \alpha - \alpha_o \tag{6-161}$$

The angle α_o is now assumed to be small, so then $\tan\alpha_o \approx \alpha_o$ and the range is small compared to a, so that the ground range (S) is given by:

$$S = \frac{Z}{\tan\alpha_o} \tag{6-162}$$

Then equation 6-161 becomes:

$$\alpha = \frac{dZ}{dS} = \alpha_o + S\left(\frac{n - n_o}{Z} + \frac{1}{a}\right) \tag{6-163}$$

If a linear variation in index is assumed, then the term involving the index is constant and the equation may be integrated directly, with the result:

$$Z = \alpha_o S + \frac{1}{2}\left(\frac{dn}{dZ} + \frac{1}{a}\right)S^2 \tag{6-164}$$

This equation is the basis for the equivalent earth radius, a', which is given by:

$$\frac{1}{a'} = \frac{dn}{dZ} + \frac{1}{a} \tag{6-165}$$

When using approximations involved in the derivation, the tangent of the angle is taken equal to the angle and ranges are assumed much less than earth's radius. Neither of these is really a limitation on the result, however. The most basic assumption, a linear variation of index with altitude, is valid at best only to a few thousand feet.

The concept of an equivalent earth radius to account for refraction effects, although convenient, is limited in usefulness. Nothing has been said of the value of the equivalent earth radius. However, this is a very important point. Table 6-9 lists the parameters of several so-called standard atmospheres. Note that the 4/3 figure commonly used is only a special case. Also note that equations 6-152, 6-155 and 6-165 enable the calculation of an equivalent earth radius for any known surface meteorological conditions.

The well-behaved index of refraction (i.e., one that is linear or exponential with altitude) is unfortunately of rare occurrence. In the absence of complete meteorological data it is the best model we can postulate. However, the index may vary in a number of ways, corresponding to various meteorological phenomena. From equation 6-164 or Figure 6-93 the curvature of the ray in a linear index environment is given by dn/dZ.

A logical extension of the analysis given for linear index profile is to approximate the atmosphere by successive layers, each having a linear index, but of different gradient. The general trend of any atmosphere will be for the index to decrease, but due to temperature

TABLE 6-9. PARAMETERS OF "STANDARD" ATMOSPHERES[83]

Type Atmosphere	Rate of Change of Index of Refraction with Altitude $(\frac{dn}{dz})$	Equivalent Earth Radius Ratio $\frac{a'}{a} = 1/1 + a\frac{dn}{dz}$	Where Applicable:
Optical	-0.8×10^{-8} ft.	6/5	Only for visible light.
Standard	-1.2×10^{-8}	4/3	Radio refraction in temperature zones under ideal conditions.*
Tropical	-1.8×10^{-8}	8/5	Radio refraction in tropic zones under ideal conditions.*
Tropical Dry	-2.4×10^{-8}	2	Radio refraction in desert or semiarid tropic area under ideal condition.*

*Ducting may be common for all models. Accuracy of all models decreases above altitudes of 4000 feet.

inversions or high evaporation over large bodies of water the index may decrease nonuniformly over certain altitude regions. This then reverses the sign of the curvature of the ray giving rise in extreme uses to trapping or ducting effects.

Atmospheric conditions that give rise to ducting are shown in Figure 6-93. Note that the refractive modulus is shown:

$$M = \left(n - 1 + \frac{Z}{a}\right)10^6 \tag{6-166}$$

Note also that:

$$\frac{dM}{dZ} = \left(\frac{dn}{dZ} + \frac{1}{a}\right)10^6 = \frac{10^6}{a'} \tag{6-167}$$

Where a' is the equivalent earth radius as previously defined. That is, dM/dZ is the curvature of the ray with respect to the ground surface. When dM/dZ is negative, the rays are bent back toward the ground with curvature more than that of the earth, so that refraction may be total for certain ray paths. Therefore these regions of negative dM/dZ are ducts. These ducts are normally fairly narrow, so only energy incident at very small angles is actually trapped. However, errors in elevation angle at higher incidence angles may be appreciable.

As hinted above, the path of a ray can be calculated by approximating the index profile as a sequence of straight lines and evaluating each region separately. From Figure 6-92 note that the error in a region h high will be given by:

$$\Delta x_1 = \frac{1}{2}\left(\frac{dn}{dZ}\right)_1 S_1^2 \tag{6-168}$$

but $\alpha_1 S_1 \approx h_1$ therefore:

$$\Delta x_1 = \frac{h_1^2}{2\alpha_1^2}\left(\frac{dn}{dZ}\right)_1 \tag{6-169}$$

There is also an angular deviation in the direction of the ray at the end of the first region. Since the region has a linear index, the ray path is a circular arc of radius:

$$\rho_1 = \frac{1}{\left(\frac{dn}{dZ}\right)_1} \tag{6-170}$$

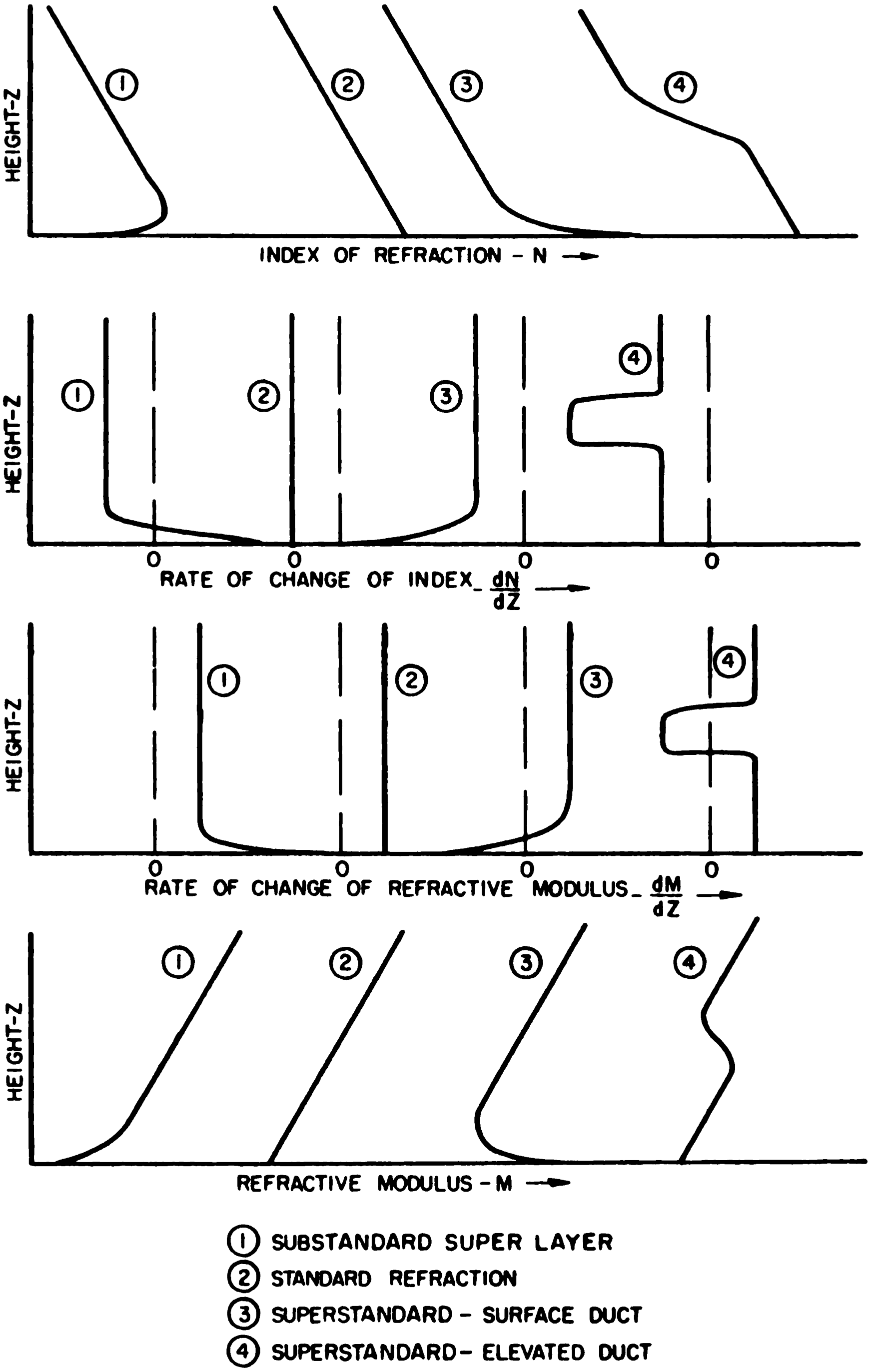
HEIGHT-Z
①
②
③
④
INDEX OF REFRACTION - N →
HEIGHT-Z
①
②
③
④
0
0
0
0
RATE OF CHANGE OF INDEX_ dN/dZ →
HEIGHT-Z
①
②
③
④
0
0
0
0
RATE OF CHANGE OF REFRACTIVE MODULUS_ dM/dZ →
HEIGHT-Z
①
②
③
④
REFRACTIVE MODULUS - M →
① SUBSTANDARD SUPER LAYER
② STANDARD REFRACTION
③ SUPERSTANDARD - SURFACE DUCT
④ SUPERSTANDARD - ELEVATED DUCT

Figure 6-93. Common Variations of Refraction with Altitude for Low Altitudes

The angular deviation is therefore:

$$\Delta\alpha_1 = \frac{S_1}{\rho_1} = S_1 \frac{dn}{dZ}_1 \qquad (6\text{-}171)$$

This angular deviation will contribute to the total error a linear distance:

$$\Delta\alpha_1 \sum_{i=2}^{N} S_i = S_1 \left(\frac{dn}{dZ}\right)_1 \sum_{i=2}^{N} S_i \qquad (6\text{-}172)$$

The contribution of successive regions is similarly evaluated. The total error can be put in the form:

$$x = \sum_{j=1}^{N} \frac{1}{2} \left(\frac{dn}{dZ}\right)_j \left(\frac{h_j}{\alpha_j}\right)^2 + S_j \left(\frac{dn}{dZ}\right)_j \sum_{i=j+1}^{N} S_i \qquad (6\text{-}173)$$

The angular error at the radar is then x/R. Again replacing S_i, this can be written as:

$$\text{E} = \frac{x}{R} = \frac{1}{R} \sum_{j=1}^{N} \frac{h_j}{\alpha_j} \left(\frac{dn}{dZ}\right)_j \left[\frac{1}{2}\frac{h_j}{\alpha_j} + \sum_{i=j+1}^{N} \frac{h_i}{\alpha_i}\right] \qquad (6\text{-}174)$$

Noting that approximately $R = \sum_{1}^{N} \frac{h_j}{\alpha_j}$; equation 6-174 can be written in the equivalent form:

$$\text{E} = \frac{1}{R} \sum_{1}^{N} \frac{h_j}{\alpha_j} \left(\frac{dn}{dZ}\right)_j \left[R - \frac{1}{2}\frac{h_j}{\alpha_j} - \sum_{i=1}^{j-1} \frac{h_i}{\alpha_i}\right] \qquad (6\text{-}175)$$

The α_i in this equation are the angles that the ray makes with the i^{th} layer and may vary appreciably. However, since the curvature with respect to the earth is given by the equivalent earth radius and the stratification is assumed to be spherical, then:

$$\alpha_{i+1} = \alpha_i - \Delta\alpha_i + \frac{S_i}{a + \sum_{1}^{i} h_k} \qquad (6\text{-}176)$$

$$= \alpha_i - \frac{h_i}{\alpha_i} \left[\left(\frac{dn}{dZ}\right)_i + \frac{1}{a + \sum_{k=1}^{i} h_k} \right]$$

This recurrence formula can be used to calculate the incidence angles a_i since the starting angle a_1 will be known.

The application of equations 6-174, 6-175 and 6-176 is best illustrated by a simple exampl Suppose the problem is to find the error i elevation angle if the measured elevation ang is five degrees and the index profile is as show in Figure 6-94. The approximate target heigh H_t is first found from the law of Cosines. I the range is measured to be 125,000 feet the (the earth's radius is 2.08 x 10^7 feet):

$$H_t = \sqrt{a^2 + R^2 + 2\,a\,R \sin\alpha_o} - a = 11{,}620 \text{ fee}$$

This is used to find the height of the last altitude increment. Calculation of the elevation angle error is performed in Table 6-10.

This method of calculating refraction errors is a straightforward extension of the concept of an equivalent earth radius. One advantage of the method is that it calculates the error directly, lending itself to calculations with slide rule or desk calculator. A more rigorous method of calculating refraction with a piecewise linear approximation is given in reference 84. However, this method arrives at the error only by subtraction of large calculated quantities which necessitates machine calculation. It is also a great deal more tedious. Still another method, used in reference 82, to calculate this refraction, is a step-wise approximation to the index profile. This method will generally require very short increments of height to produce accurate information.

The present method, like the others, has limitations in its application. The height increment must be taken small enough to justify the approximation of linear variation of index and small enough that the path length of the rays in any incremental shell are small compared to the radius of that shell. Since the derivation assumed small angles ($\tan \alpha \approx \alpha$) the accuracy of the method will decrease with elevation angle. However, at elevation angles below 30 degrees this probably will be negligible in comparison with the uncertainty of meteorological data. At higher angles, because of less refraction, the method will decrease in absolute accuracy (mils of error) slowly.

This method may also be used with an atmospheric model consisting of concentric spherical shells which are inclined to the local horizontal by calculating angles with respect to this tilted frame of reference.

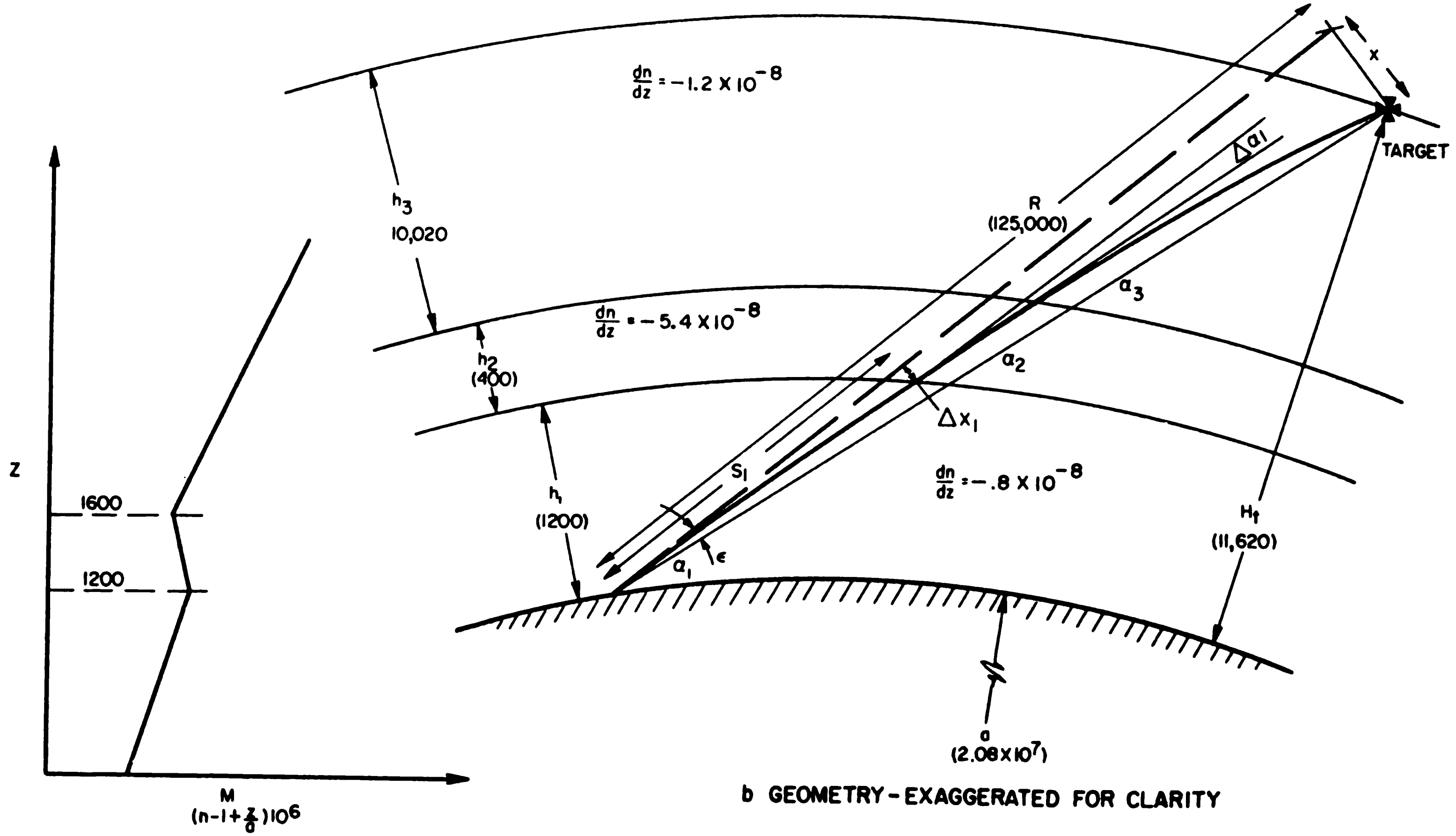

a INDEX PROFILE

b GEOMETRY - EXAGGERATED FOR CLARITY

Figure 6-94. Refraction by a Piecewise Linear Refractive Index Profile

TABLE 6-10. SAMPLE CALCULATION OF REFRACTION ERROR

Zone No. j	Zone Height h_j (ft.)	Index Gradient $(\frac{dn}{dz})_j$ (1/ft.)	$(\frac{dn}{dz})_j + \frac{1}{a}$	Elevation Angle α_j (radians)	$\frac{h_j}{\alpha_j}$	$\sum_{j+1}^{N} \frac{h_i}{\alpha_i}$	$1/2 \frac{h_j}{\alpha_j} + \sum_{j+1}^{N} \frac{h_i}{\alpha_i}$	$(\frac{dn}{dz}) \frac{h_j}{\alpha_j} \left[1/2 \frac{h_j}{\alpha_j} + \sum_{j+1}^{N} \frac{h_i}{\alpha_i}\right]$
1	1,200	-0.8×10^{-8}	4.0×10^{-8}	0.0868	13,830	120,940	127,855	14.1
2	400	-5.4×10^{-8}	-0.6×10^{-8}	0.0862	4,640	116,300	118,620	29.7
3	10,020	-1.2×10^{-8}	3.6×10^{-8}	0.0862	116,300	---	58,150	81.3

$$\sum_{I}^{N} (\frac{dn}{dz})_j \frac{h_j}{\alpha_j} \left[1/2 \frac{h_j}{\alpha_j} + \sum_{j+1}^{N} \frac{h_i}{\alpha_i}\right] = 125.1 \text{ feet}$$

$$\text{therefore,} \quad E = \frac{125.1}{125,000} = 0.001001 \text{ radian}$$

$$\approx 1.0 \text{ mils}$$

5.3.8 Combining Errors

A number of error sources have been dis- issed. They stem from a variety of effects. owever, the principal interest in them in a iven application is a utilitarian one. The com- ined effect on the radar performance is the nd result in which we are interested.

Fortunately, the errors do not accumulate n an arithmetic sense. Most of the errors are andom errors defined in terms of their rms alue, or standard deviation. This is true of all the errors of a noise-like nature. This includes thermal noise, ground and rain clutter, servo noise or tracking roughness, aircraft scintillation, (both fading and wander) and external noise sources whether cosmic, man-made or what-ever. All of these random errors add in an rms fashion. For example, if the error due to servo noise is ε_s, the error due to wander is ε_ω, and the error due to thermal noise is ε_N, all are computed for the same values of system parameters and they are the only appreciable error sources, the total error is:

$$\varepsilon_T = \sqrt{\varepsilon_s^2 + \varepsilon_\omega^2 + \varepsilon_N^2} \qquad (6\text{-}177)$$

This type addition may be facilitated by Figure 6-95.

A number of other errors in the mechanical parts of the radar may also have a random nature, but may not be time variant like noise so that in given radar they constitute a bias error. Usually this bias will be calibrated out, but in field use it may well creep back. In addition there are certain errors that are biasing by nature. The lag, or dynamic errors of the servo are notable examples. Propagation errors may well produce biasing errors unless corrected. This is particularly true of refraction errors. Correction on the basis of an equivalent earth radius will help to remove some of the bias so that the error is not only decreased but is made more random. Other propagation errors, due to interference or diffraction, will be more nearly random because they depend on target position which is itself a random variable.

In the usual practice, all errors are added in an rms sense, even when they are not random. This enables the total error expected to be presented in simple fashion and gives a good estimate of the expected error. Often, such estimates are not warranted. For example, a radar being used with a beam rider missile depends only on relative accuracy and the biasing errors are of little consequence.

The errors that have been discussed vary with many parameters, the most common of which is range. For a number of purposes the variation of radar error with range, a sort of accuracy profile, is desired.

For many cases this characteristic can be very quickly derived graphically. The basis for this is the range dependence of the various errors. They are, for most errors, proportional to an integral power of range. If such a relationship is drawn on paper having logarithmic scales in both variables, it plots as a straight line with slope equal to the applicable power of range. For example, wander errors are inversely proportional to range. Therefore a plot, on logarithmic paper, of the wander error alone is a line with a slope of minus one. This is shown on Figure 6-96 along with other errors. If the wander error is calculated for a single range it can be immediately plotted by drawing the line through the calculated point.

Similarly the error due to thermal and external noise sources will increase as the square of the range (for a skin tracking radar) due to the attenuation of the signal (assuming free-space propagation). This is also shown on the plot of Figure 6-96, as are servo noise and mount errors which are independent of range and the fading error that might occur in a conical scan radar, which is also independent of range. In combining these errors a useful property of this type presentation becomes apparent. The errors are asymptotic to these straight lines. Due to the rms addition the error is determined principally by one error, except where these straight lines cross. At these points the errors due to two effects are equal, so the total error is $\sqrt{2}$ times the error due to either. From this fact, or by actually adding components in an rms fashion, the total error is found as shown.

One situation that will require a little different treatment arises when two error sources have the same range dependence. However, this is easily treated by summing these two effects in an rms fashion for any given range. Their sums must of course still have the same range dependence. This is shown on Figure 6-97.

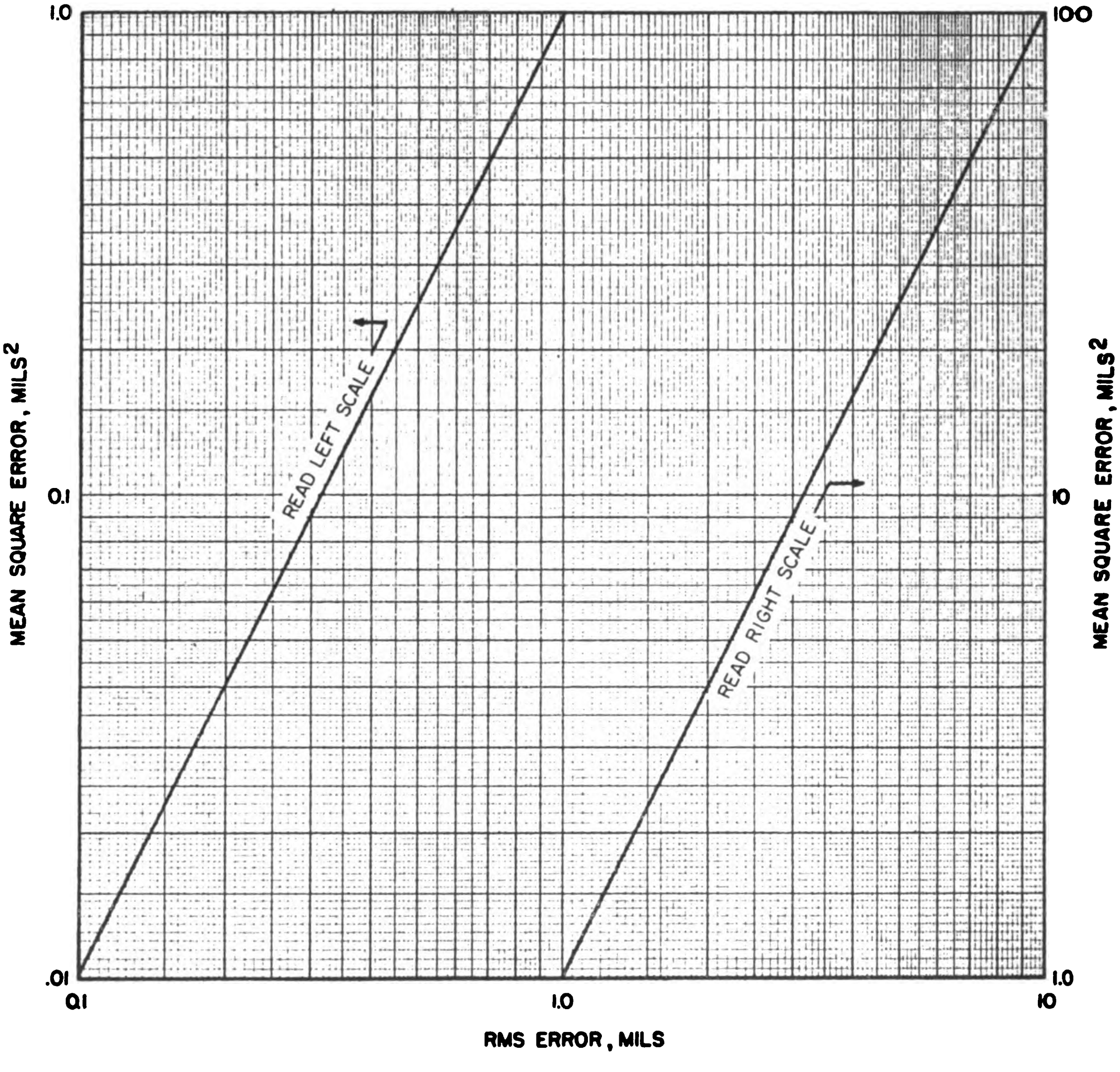

Figure 6-95. Aid to RMS Addition

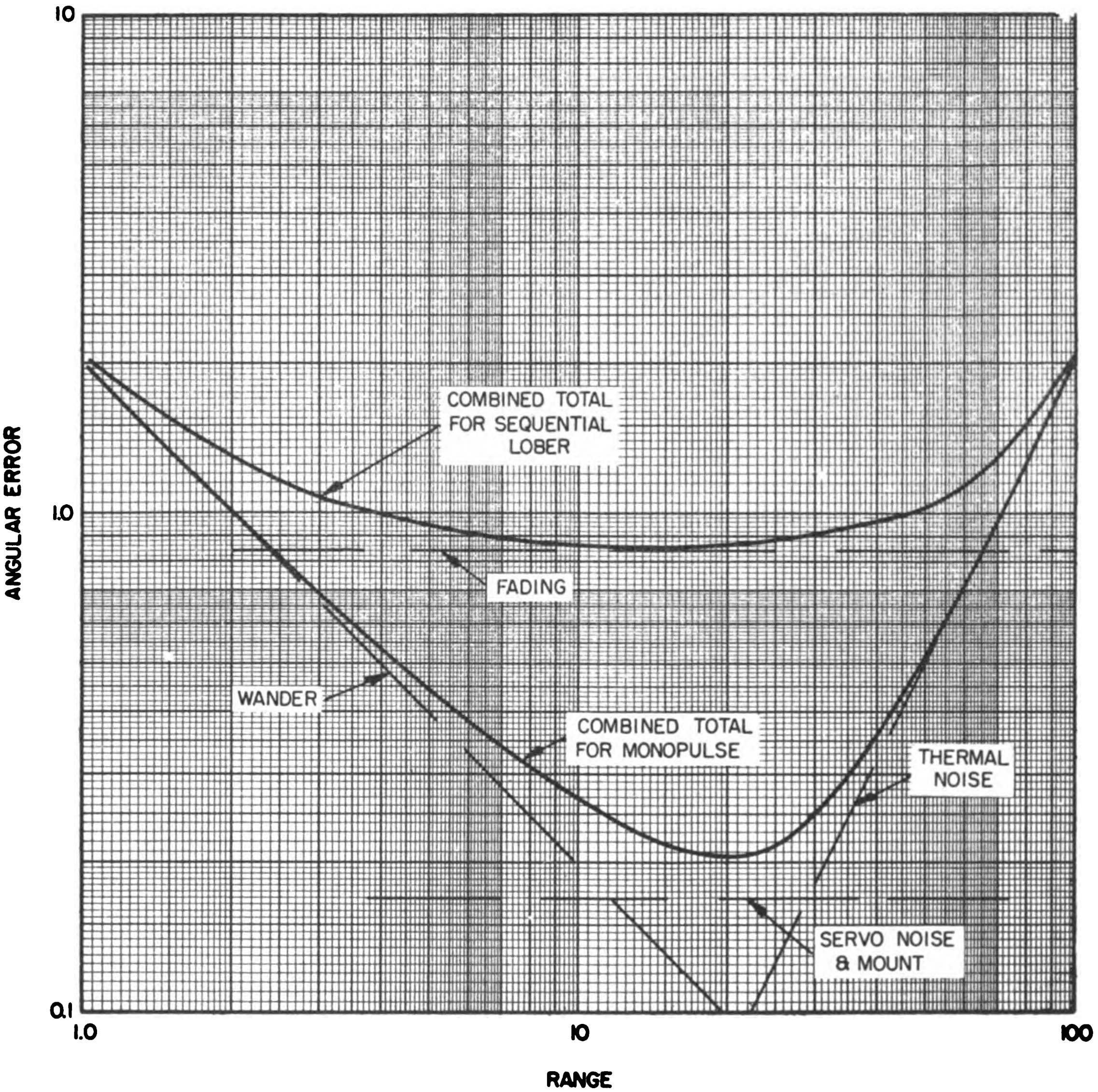

Figure 6-96. Combining Errors — Example I

Servo lag, assuming a certain target velocity and low elevation angles, will have the same range dependence as wander. Summing the two in an rms fashion yields the straight line marked combination in Figure 6-97. This is then combined with the other errors as before.

Table 6-11 shows the range dependence of the more common errors. An effect which is not taken into account is loss of signal due to attenuation by air or rain. This will cause the noise error characteristics to be other than the straight lines seen above. When these effects are appreciable the noise error will have to be calculated as a function of range or a correction that is a function of range must be made. The logarithmic calculation using the charts of paragraph 6-54 greatly facilitate this.

6-5.4 SAMPLE CALCULATIONS AND CHARTS

6-5.4.1 Parameters of the Calculations

In the calculation of radar performance in the presence of noise the following quantities are significant.

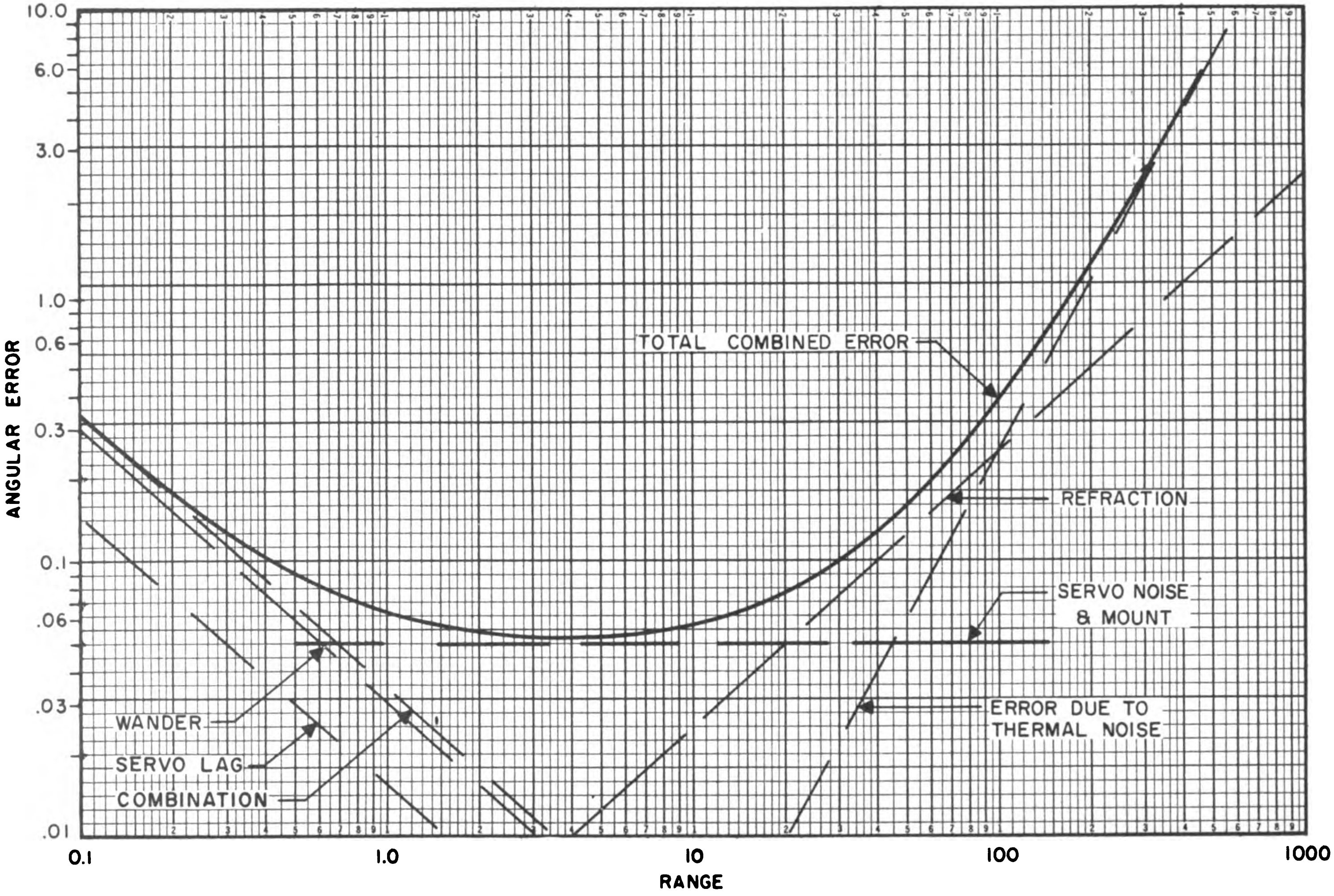

Figure 6-97. Combining Errors — Example II

TABLE 6-11. RANGE DEPENDENCE OF TRACKING ERRORS

Type Error	Proportional to:	Slope of Log Error versus Log Range Curve	Comments
Thermal or other noise sources Skin Tracking	R^2	+2	Neglecting attenuation by air or rain
Thermal or other noise sources Beacon Tracking	R	+1	Because of one-way transmission. Neglecting attenuation.
Rain clutter	R^2	+2	Because the clutter cell increases in volume as the square of the range. Only applicable for range at which rain is present.
Ground clutter	R	+1	Only applicable at ranges within the horizon where clutter is present.
Fading	1	0	Dependent only on target characteristics and only occurs for sequential lobing radars.
Wander	$\frac{1}{R}$	-1	At very short ranges the spectrum may be affected causing some deviation from this dependence.
Servo noise, mount errors, data take-off misalignment, etc.	1	0	Essentially fixed errors, although tracking roughness may be increased at longer ranges due to slow angular rates.
Servo dynamic errors	$\frac{1}{R}$	-1	Assuming fixed target speed and aspect.
Refraction	R	+1	Only good to first approximation. Generally, a more complex relationship.
Ground reflection and diffraction	--	--	Very dependent on specific geometry of radar and target positions, not specifically on range.

The half-power beamwidth, Θ, of a tracking radar is a more nebulous thing than that of a search radar. A quantity often used in calculation is a nominal beamwidth, based on the use of the given aperture with a single feed and a cosine illumination. This is shown in Figure 6-98 in terms of wavelengths of aperture (found from Figure 6-99). The advantage of this half-power beamwidth is only that the radar sensitivity often can be calculated easily in terms of it. In practice the quantity measured is the half-power beamwidth of a sum pattern. This is true of both monopulse and sequential lobers. Either beamwidth can be used for error calculations.

The angular sensitivity, K_S, of the radar depends on the beamshape of the radar and the type of lobe comparison used to obtain tracking information. It is often expressed in volts per volt per beamwidth. Care should be exercised in noting whether this denotes sum beamwidth or the nominal beamwidth discussed above. Sometimes sensitivity may be expressed in volts or millivolts per degree or radian. In this case what is expressed is K_S/Θ, and must be treated so in the calculations. Figure 6-100 gives sensitivity of an interferometer-type tracker. Table 6-4 lists sensitivities of some of the more common tracking configurations.

Filter factor, K_f, of a tracking radar reduces the errors due to noise by smoothing the radar output. It is less for conical scan radars than for comparable monopulse trackers. Figure 6-101 gives this factor.

The transmitted power of the radar, P_t, or of a beacon, P_b, determines the signal available at the receiver to be discerned above the noise. Figure 6-102 gives this power in decibels. If radiated isotropically through free space the power density decreases as the square of the distance R. For echo-tracking radars, due to the round trip, the received power varies inversely as the fourth power of R. These factors are shown in decibels in Figure 6-103.

The gain of the antenna, G_t, for the radar or, G_b, for a beacon, directs the transmitted power. Like the beamwidth it is less well-defined in the case of a tracking radar. The gain measured in practice is the sum gain. An often used yardstick of performance is a nominal gain based on the use of the give aperture with a single feed and cosine illumina tion. This is shown in Figure 6-104. This mus be corrected by an amount depending on th type tracker used. Typical corrections are liste in Table 6-4.

The wavelength of a radar, λ, determines with the gain of the device, the receiving are of the antenna, given by:

$$A = \frac{G_t \lambda^2}{4\pi} \qquad (6\text{-}178)$$

The echo area of a target A_e is usually known empirically. It is extremely complex to calculate for any but the simplest targets. It is usually given only as a statistical quantity (that area which is exceeded 50 percent of the time). This is necessary because the signal return from usual targets varies rapidly and randomly. Figure 6-69 shows this area for a number of typical targets.

In propagating through the atmosphere and in traversing some of its r-f waveguide and associated devices, notably duplexers, the microwave signal suffers an attenuation or loss, L. This is determined from knowledge of the atmospheric attenuation which may be very high in the presence of rain or fog (see Figures 6-88 and 6-89) and knowledge or an estimate of the circuitry losses.

In any receiver, thermal noise exists which cannot be eliminated without cooling the receiver. Because this noise is white, i.e., evenly distributed over all frequencies of interest, the amount of noise power in the receiver is proportional to, for the commonly used superheterodyne receivers, the intermediate frequency bandwidth, B. For a nominal value of temperature this theoretical thermal noise is given by Figure 6-105.

Since no receiver is ideal, the quality of the receiver is expressed in terms of noise figure, N_f, the ratio of actual receiver noise to the ideal thermal noise. This parameter is subject to change as the state-of-the-art progresses. Some typical values are shown in Figure 6-106 for the common types of microwave receivers. New techniques may cause marked improvements. Note that in the case of crystal mixers brackets are shown to indicate that the noise

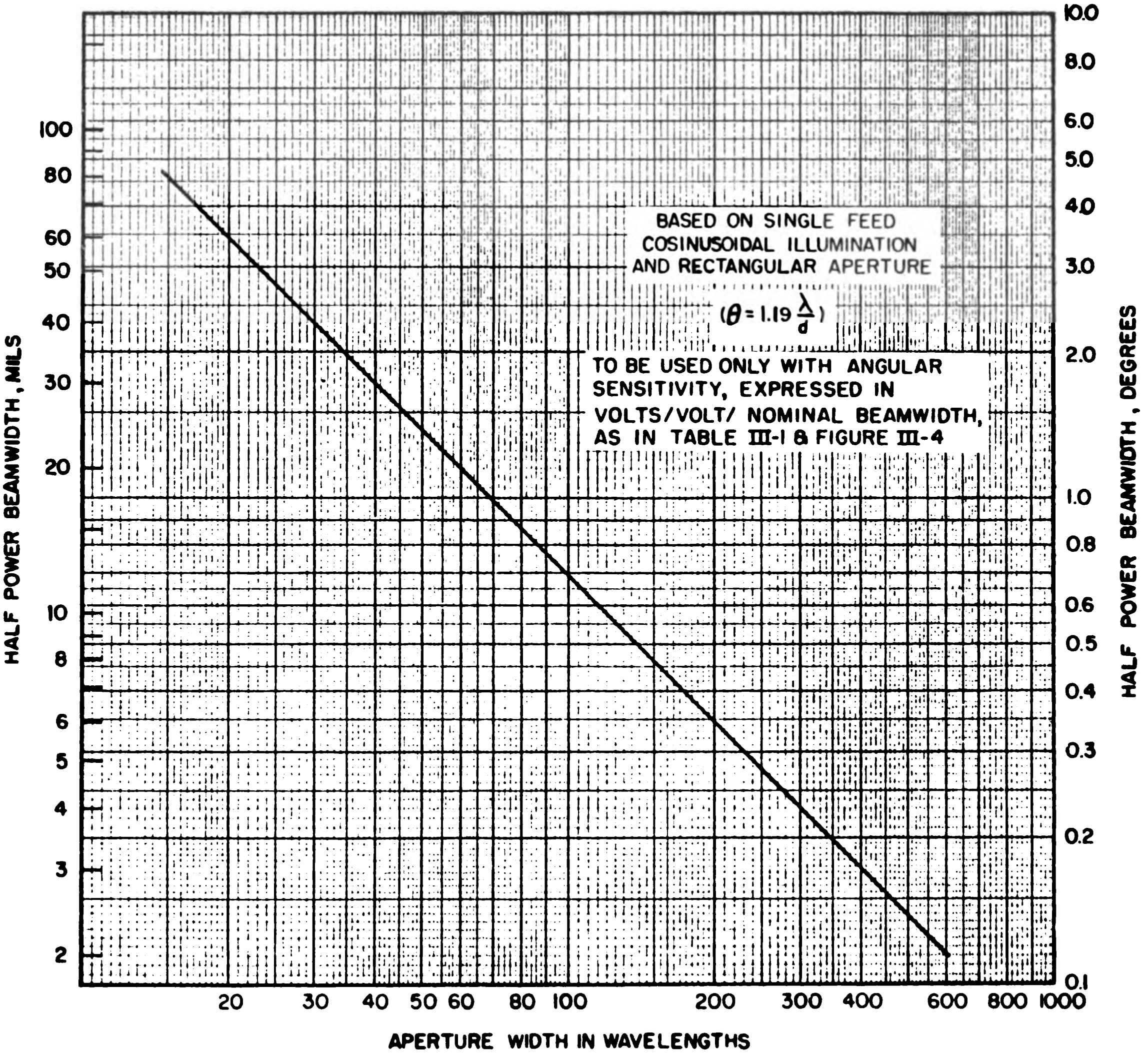

Figure 6-98. Nominal Beamwidth Versus Aperture

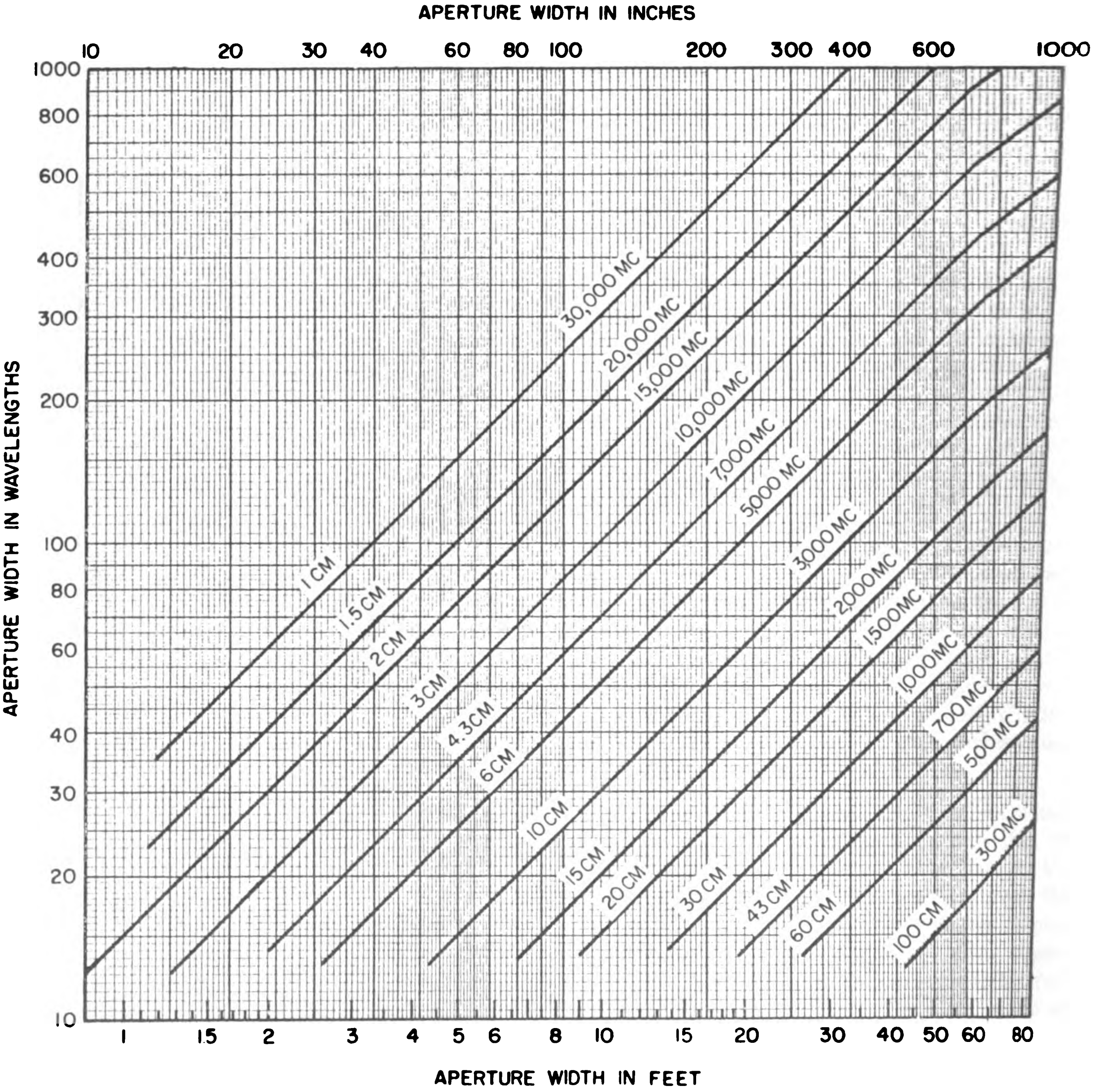

Figure 6-99. Conversion of Aperture Width to Wavelengths

figure may vary considerably with the skill of the circuit designer and between individual crystal diodes. A spread of values achieved with triode r-f amplifiers will also be found in practice. The figure shows the best noise figure that can be achieved.

In tracking beacons that use a crystal receiver converting directly from r-f to video, the performance of the receiver is usually specified in terms of a sensitivity, *S*. This is a measure of the smallest signal discernible from noise. This quantity is analogous to the product

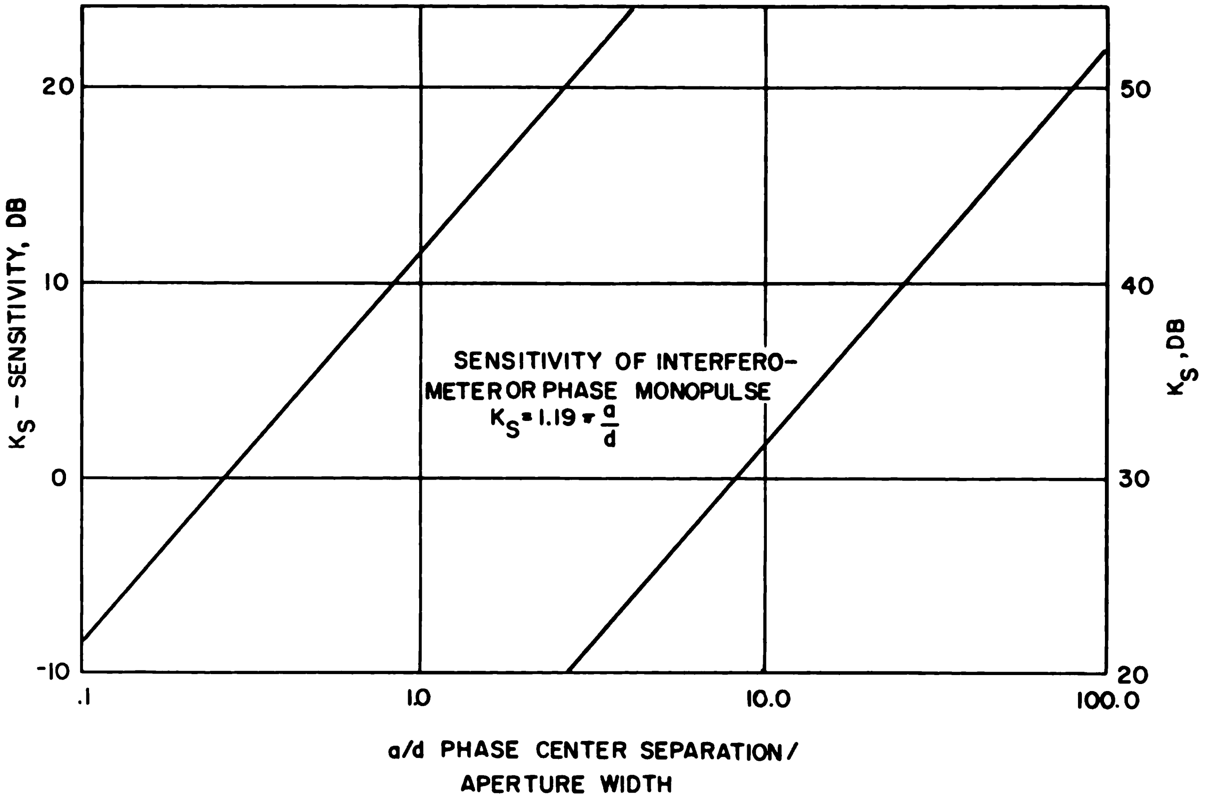

Figure 6-100. Interferometer Sensitivity

of noise figure and i-f bandwidth factor used to gauge the performance of the superheterodyne receiver. Figure 6-107 shows typical sensitivities for specific crystals. As in the chart for noise figures, a range of values is shown that is indicative of the range of values obtained in practice. The sensitivity shown is tangential sensitivity defined by that signal which raises the noise envelope, as seen on an oscilloscope, by a value equal to its peak-to-peak amplitude. This corresponds to a signal-to-noise ratio (rms) of approximately 4 db. The sensitivities are given in db above a milliwatt.

Finally the angular error, ε, is usually computed for separate axes, such as azimuth and elevation separately and is usually expressed in rms mils. Figure 6-108 shows the conversion from mils to decibels.

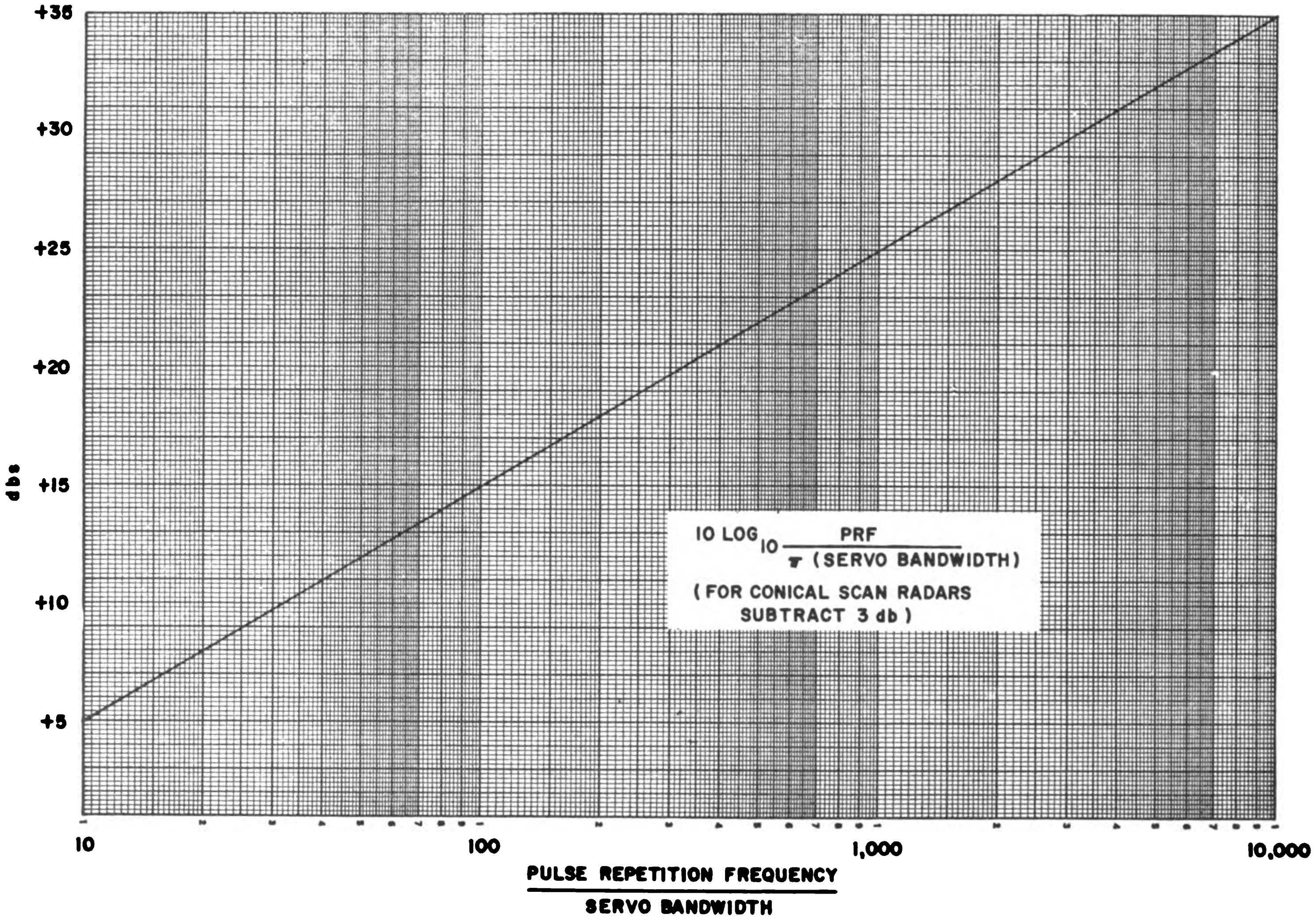

Figure 6-101. Servo Filter Factor

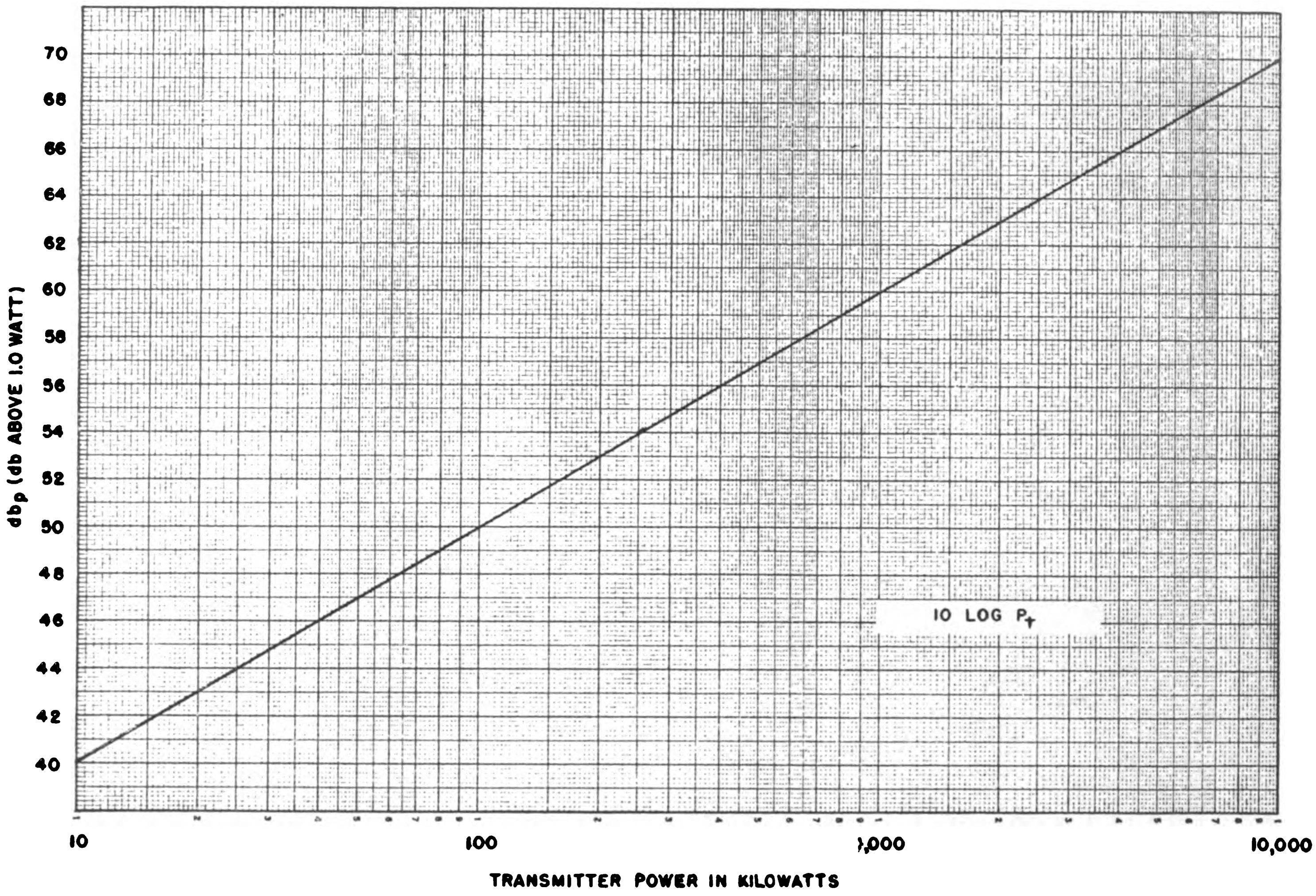

Figure 6-102. Transmitter Power in DB Above 1.0 Watt

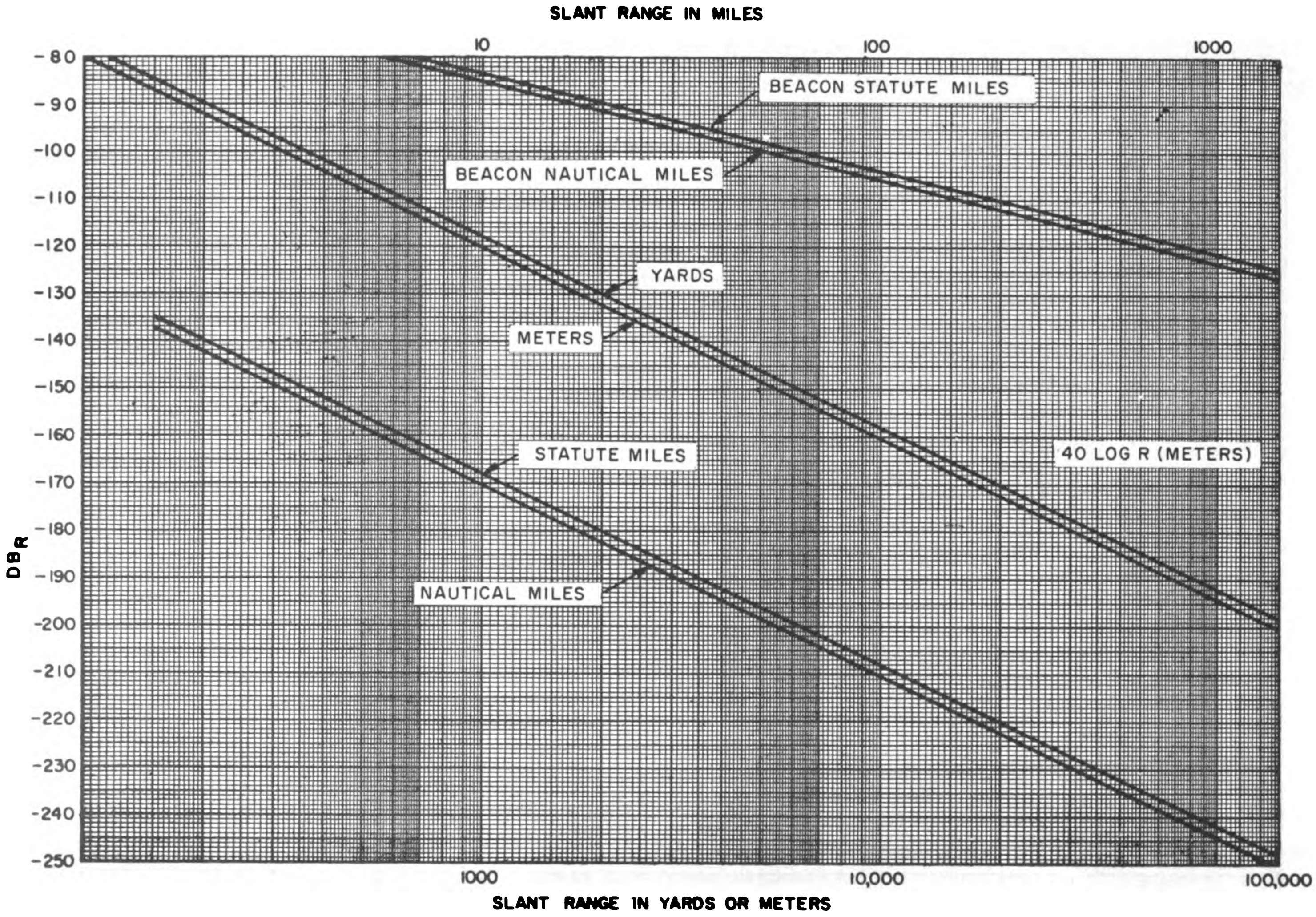

Figure 6-103. Range Loss

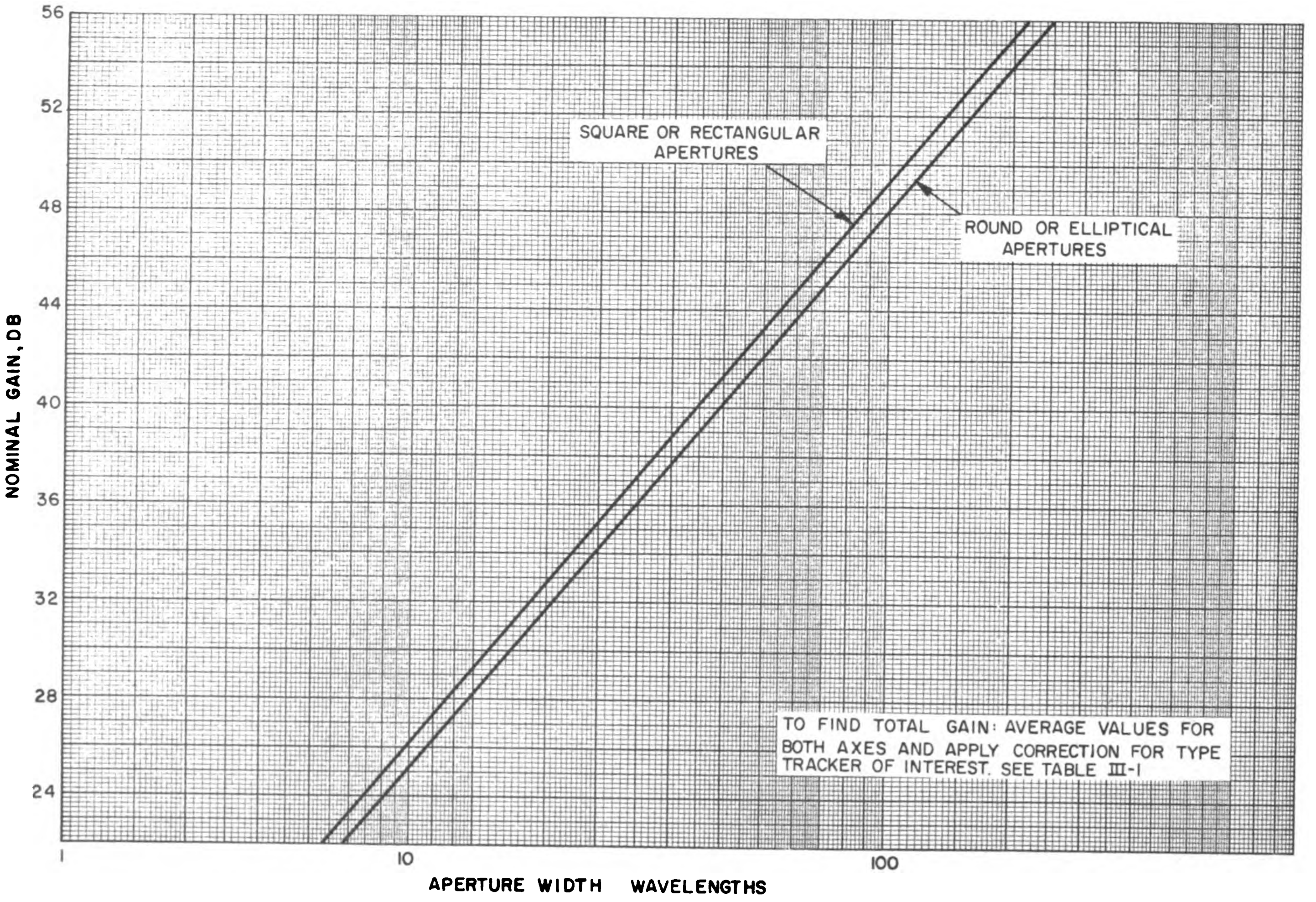

TO FIND TOTAL GAIN: AVERAGE VALUES FOR BOTH AXES AND APPLY CORRECTION FOR TYPE TRACKER OF INTEREST. SEE TABLE III-1

Figure 6-104. Nominal Gain, DB, Based on Cosine Illumination

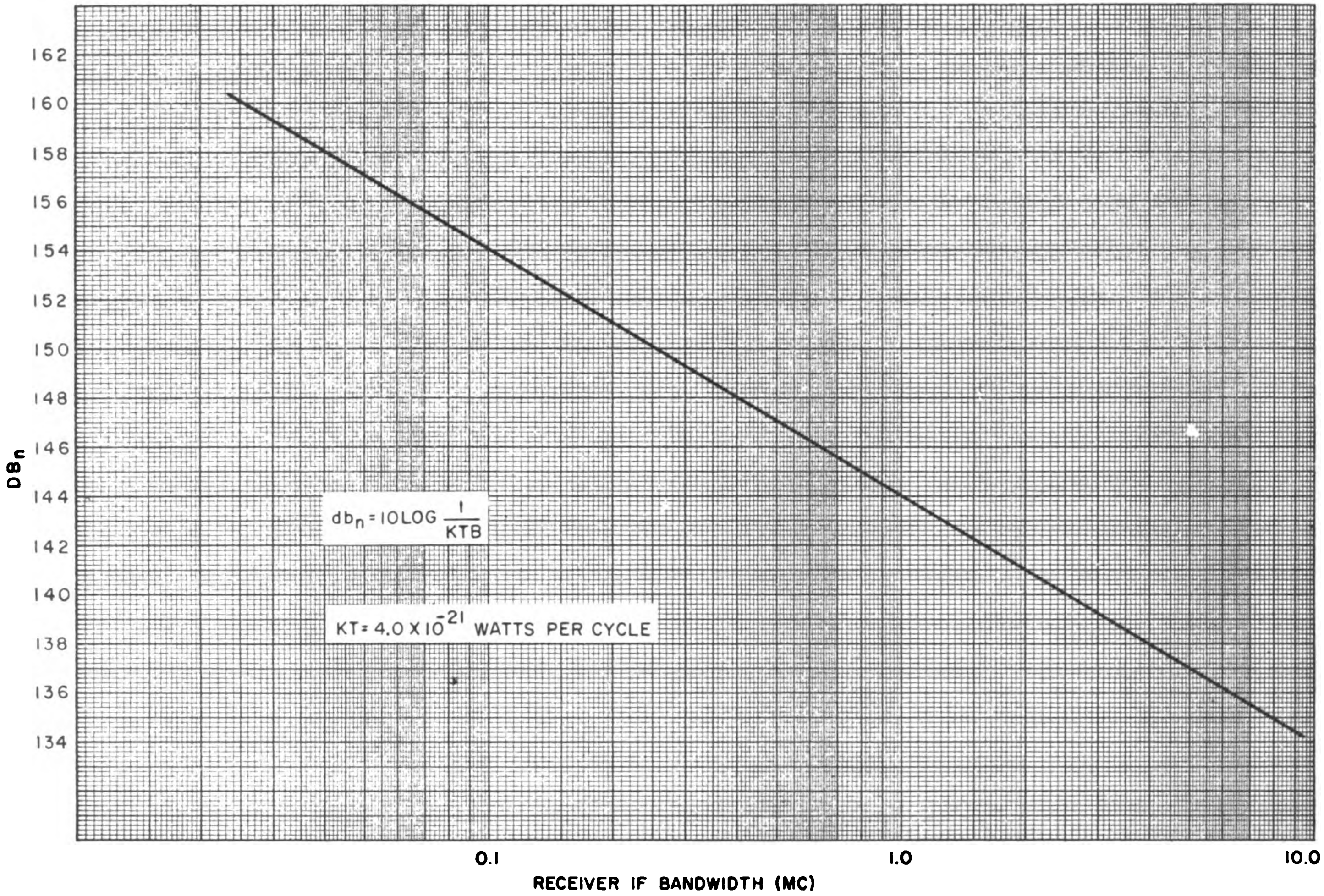

Figure 6-105. I-F Bandwidth Factor

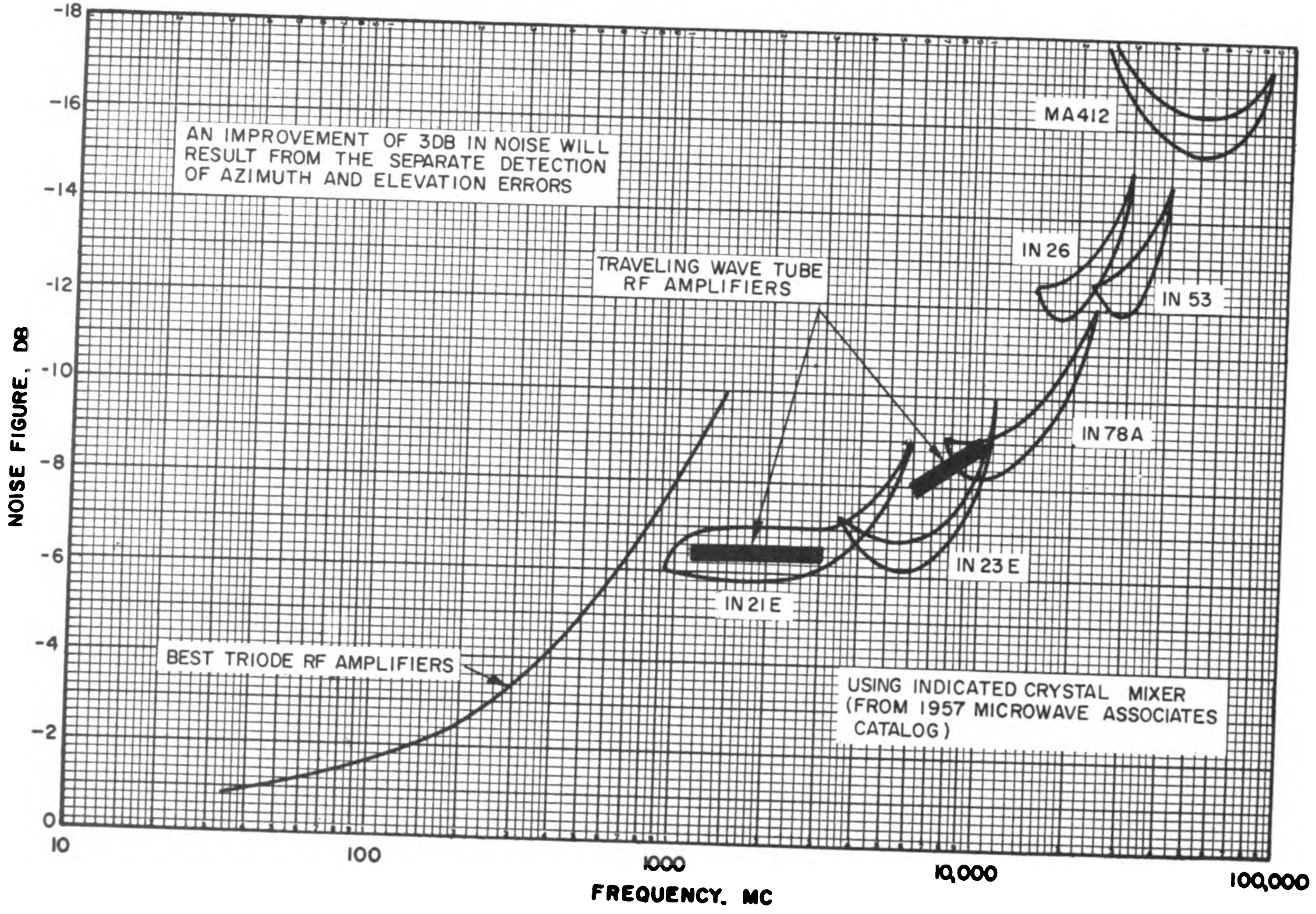

Figure 6-106. Typical Receiver Noise Figures

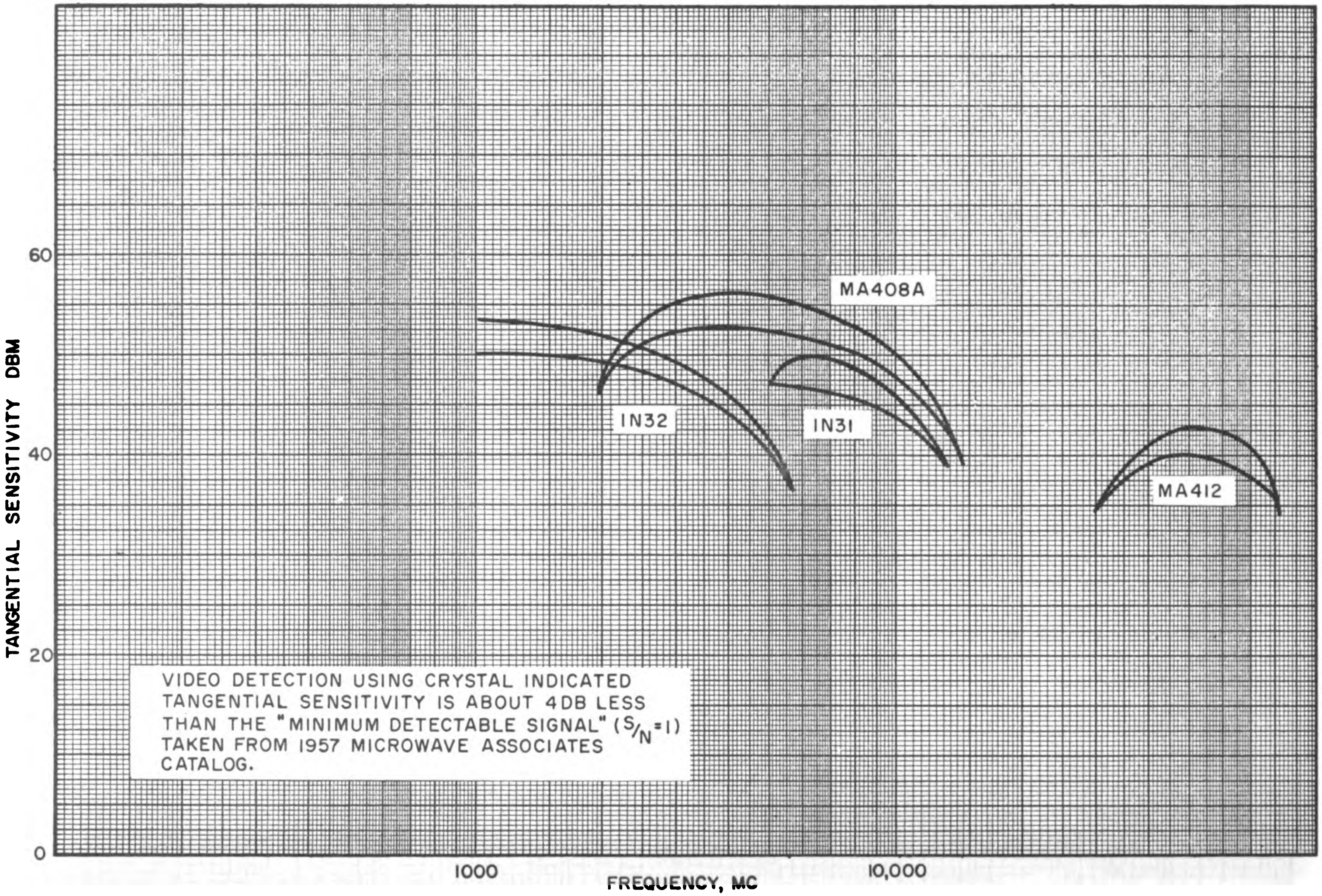

VIDEO DETECTION USING CRYSTAL INDICATED TANGENTIAL SENSITIVITY IS ABOUT 4DB LESS THAN THE "MINIMUM DETECTABLE SIGNAL" ($S/_N = 1$) TAKEN FROM 1957 MICROWAVE ASSOCIATES CATALOG.

Figure 6-107. Crystal Beacon Sensitivity

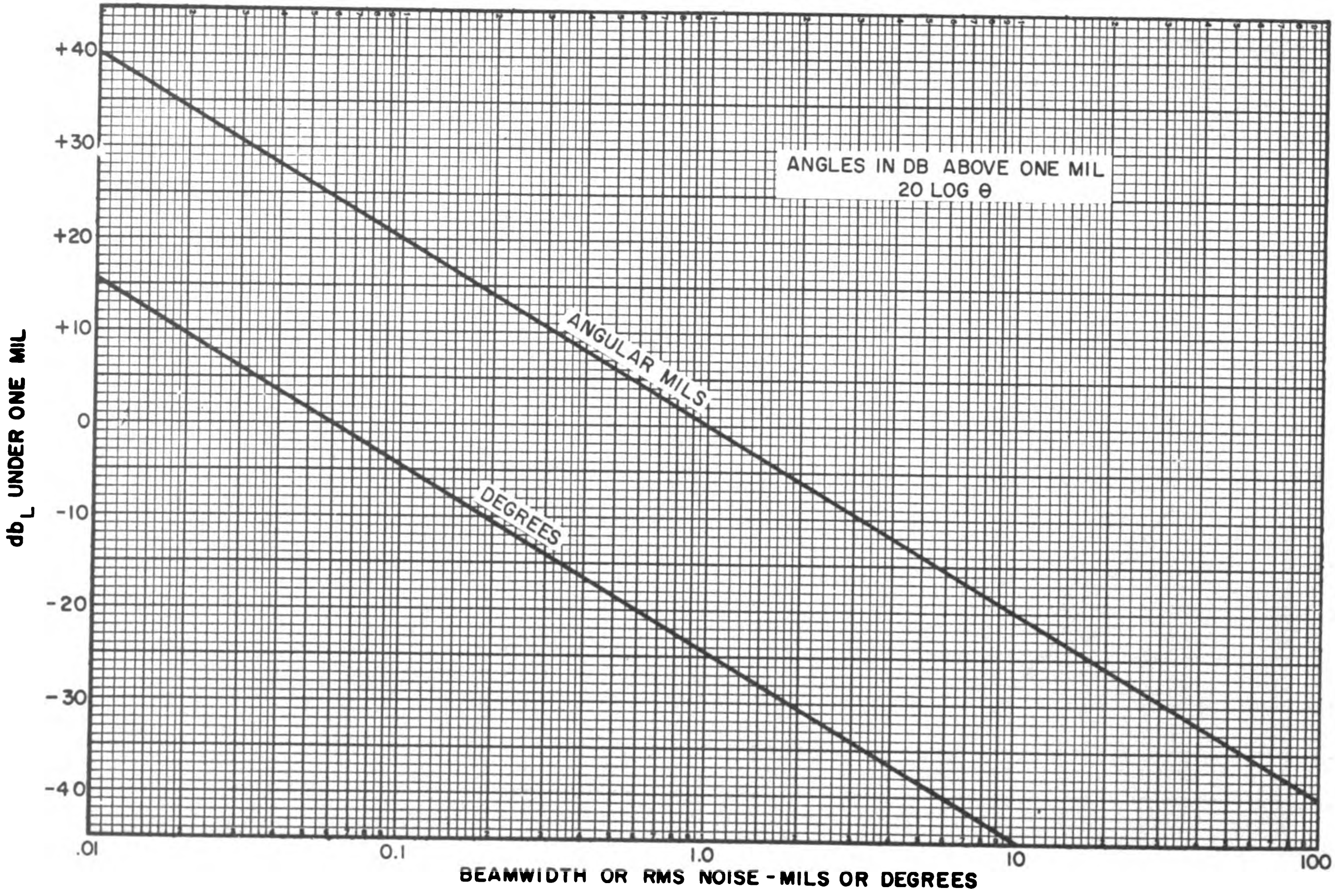

Figure 6-108. Beamwidth or Angular Noise

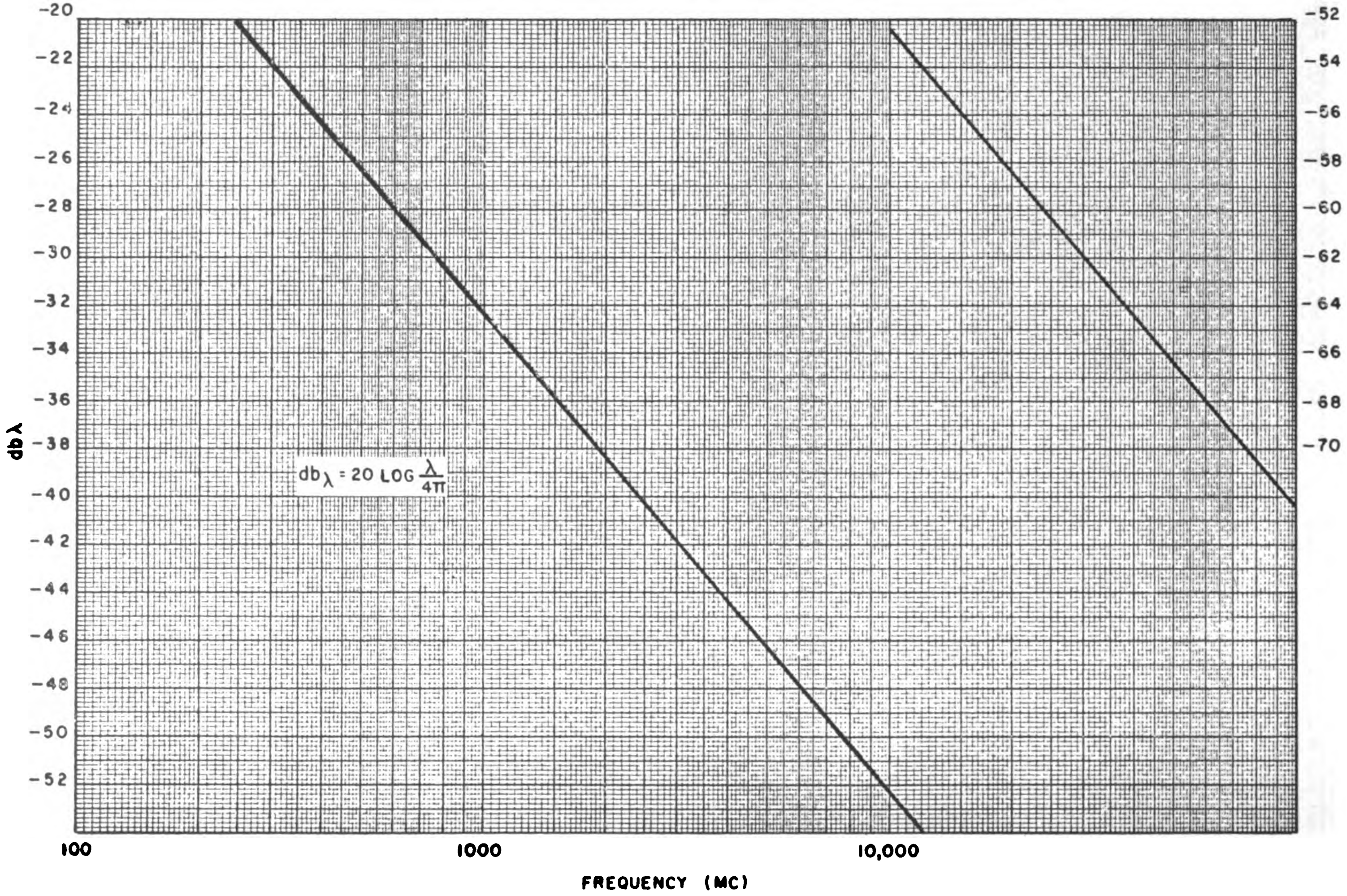

Figure 6-109. Wavelength Factor

-5.4.2 Thermal Noise — Echo Tracking

In accordance with the usual radar equation, for skin tracking, the voltage signal-to-noise in the front end of the radar is given by:

$$\left(\frac{S}{N}\right)^2 = \frac{P_t G_t^2 \lambda^2 A_e L}{(4\pi)^3 R^4 N_f KTB} \qquad (6\text{-}179)$$

In a tracking radar the servo driving the antenna acts as a low pass filter, decreasing the noise by a factor:*

$$K_f = \sqrt{\frac{f_p}{\pi f_c}} \qquad (6\text{-}180)$$

This thermal noise level manifests itself as an angular noise. The two quantities are related by an equation of the form:

$$\frac{S}{N} = \frac{\Theta}{\varepsilon K_f K_s} \qquad (6\text{-}181)$$

where

Θ = antenna beamwidth

ε = angular thermal noise error

K_f = servo filter factor

K_s = angular sensitivity

Combining equations 6-179 and 6-181 we can write for the tracking error due to noise:

$$\varepsilon = \frac{\Theta}{K_f K_s} \sqrt{\frac{(4\pi)^3 R^4 N_f KTB}{P_t G_t^2 \lambda^2 A_e L}} \qquad (6\text{-}182)$$

Each of the significant quantities in this equation can be stated logarithmically in terms of its ratio to some arbitrary unit. This is the basis for the charts given in this section. In most cases, the quantities are expressed directly in decibels when they are taken in MKS units. The constant $(4\pi)^3$ is contained in the decibel expressions for wavelength factor (Figure 6-109) and target echo area, respectively.

Note that the logarithmic quantities contain the proper power of the variable, so that they are summed directly with the exception of antenna gain. This is given in terms of one-way gain which is used in the beacon calculations described below.

Also note that Table 6-4 lists corrections to be made to the nominal gain of Figure 6-104 if this figure is used. A correction to the filter factor is indicated for conical scan and a detection factor is indicated on the chart of typical noise figures.

6-5.4.3 Beacon Operation

Beacon operation is equivalent to two one-way transmissions. Separate calculations must be made for each. For a crystal beacon receiver performance is usually specified in a sensitivity figure S. In order to trigger the beacon the signal must equal or exceed this sensitivity:

$$S \leq \frac{P_t G_t G_B \lambda^2 L}{(4\pi)^2 R^2} \qquad (6\text{-}183)$$

For superheterodyne beacons, performance depends on the noise figure of the beacon similar to the radar receiver:

$$\left(\frac{S}{N}\right)^2 = \frac{P_t G_t G_B \lambda^2 L}{(4\pi)^2 R^2 N_f (KTB)} \qquad (6\text{-}184)$$

The angular accuracy of the system depends upon the return link. The signal-to-noise in the front end of the radar will be:

$$\left(\frac{S}{N}\right)^2 = \frac{P_b G_b G_t \lambda^2 L}{(4\pi)^2 R^2 N_f KTB} \qquad (6\text{-}185)$$

The other considerations (filter factor, sensitivity) are the same as for skin tracking radar. The expression for angular error is in this case:

$$\varepsilon = \frac{\Theta}{K_f K_S} \sqrt{\frac{(4\pi)^2 R^2 N_f KTB}{P_b G_b G_t \lambda^2 L}} \qquad (6\text{-}186)$$

All of the above expressions can be readily calculated by addition using the logarithmic charts given in Figures 6-69, 6-98 – 6-109. The radar sensitivity, K_S, if not known in a given application, may be estimated from Table 6-4.

The logarithmic charts give values corresponding to the proper power of the variable. These values may be added directly. Examples are given below.

---

*For a conical scan radar this factor is $\sqrt{f_p/2\pi f_c}$, because the angular information is on a carrier, the scanning frequency.

6-5.4.4 Examples

EXAMPLE I

Find the azimuth thermal noise error in a phase monopulse radar having the following characteristics and skin tracking an aircraft of the F-80 type at a range of 30 miles.

Radar frequency	10,000 mc
I-f bandwidth	200 kc
Peak power	25 kw
Azimuth servo bandwidth	3.0 cps
Pulse repetition rate	800 cps
Antenna gain	40 db
Azimuth sensitivity	1:57 v/v/bw (Sum beamwidth)
Azimuth sum pattern beamwidth	1.5 degrees

The calculation is listed below, the data having been taken from the charts with minor exceptions. Since the sensitivity is known, it is converted directly to db. R-f losses are computed on the basis of a clear atmospheric attenuation of 0.0125 db per kilometer (found from Figure 6-89) and an assumed loss in r-f plumbing of one db. Since azimuth and elevation errors are detected separately, each contains only one component of noise so that a detection factor of 3 db is subtracted from the noise figure which is choosing an optimistic value (about 9 db) from Figure 6-106.

EXAMPLE I. CALCULATION OF ERROR — MONOPULSE-ECHO TRACKING

Beamwidth		— 28.0 db
Sensitivity	+ 3.9 db	
Filter factor	+ 19.3	
Power	+ 44.0	
Gain	+ 80.0	
Wavelength factor		— 52.4
Target echo area		— 18.0
R-f losses (0.6 db atmospheric + 1.0 db waveguide loss)		— 1.6
Range		—187.0
Noise factor (9 db less 3 db detection factor)		— 6.0
I-f bandwidth	+151.0	
	+298.2 db	—293.0 db
	= +5.2 db	

Therefore angular error in azimuth = 0.54 mil

EXAMPLE II

Find thermal noise error for the following conical scan radar when skin tracking aircraft of the F-86 type at a range of 15 miles.

Radar frequency	3000 mc
I-f bandwidth	500 kc
Peak power	100 kw
Antenna – circular parabolic dish in diameter	64 inches
Feed squinted one beamwidth	
Servo bandwidth	2.5 cps
Pulse repetition rate	1000 cps

This calculation is performed in much the same manner as the previous one, with the exception that the antenna characteristics are found from Table 6-4 for an echo tracking conical scan radar of maximum sensitivity. Also, the filter factor is less by three db due to the conical scanning.

The atmospheric loss is again calculated by recourse to Figure 6-88. (0.01 db per kilometer times (15 × 1.609) kilometers ≈ 0.2 db).

A low value of noise figure is chosen from Figure 6-106 and corrected for 3 db improvements by detection. From the final result it can be seen that for systems symmetrical in azimuth and elevation, this correction can be neglected if the end result desired is the total rms angular noise.

EXAMPLE II. CALCULATION OF ERROR – CONICAL SCAN-ECHO TRACKING

Beamwidth (nominal, for 64″ dish = 4.3°)		– 37.2 db
Sensitivity (per nominal beamwidth)	+ 9.2 db	
Filter factor (21.0 db, less 3 db due to conical scan)	+ 18.0	
Power	+ 50.0	
Gain (32.2 db less 3 db)	+ 58.4	
Wavelength factor		– 42.0
Target echo area		– 15.0
R-f losses (0.2 atmospheric + 1.0 plumbing)		– 1.2
Range		–175.0
Noise factor (at –6 +3)		– 3.0
I-f bandwidth	+147.0	
	+282.6 db	–273.4 db
	= +9.2 db	

Therefore angular error in azimuth = 0.33 mil

The total rms angular error, since the elevation channel of a conical scan radar is identical to the azimuth, is 3 db higher, or 0.47 degree.

EXAMPLE III

Find the range to which a crystal beacon of 45 dbm sensitivity will be triggered by the radar of Example I. Find the angular error at 30 miles due to thermal noise if the beacon has a transmitted power of 40 watts and due to shielding by the airframe, has an antenna gain of –6 db.

EXAMPLE III. CALCULATION OF ERROR — MONOPULSE-BEACON TRACKING

A. For the Beacon Performance:

Power	+ 44.0 db	
Radar gain (one-way)	+ 40.0	
Beacon gain		— 6.0 c
Wavelength factor		— 52.4
Loss (0.7 atmospheric +1.0 waveguide on same basis as in Example I)*		— 1.7
Beacon sensitivity (dbw = dbm + 30)	+ 75.0	
	+159.0 db	— 60.1 d
	= +98.9 db	

From the beacon curve of Figure 6-103, range = 55 miles

B. At 30 miles:

Beamwidth		— 28.0 dl
Sensitivity	+ 3.9 db	
Filter factor	+ 19.3	
Beacon power	+ 16.0	
Beacon gain		— 6.0
Radar gain	+ 40.0	
Wavelength factor		— 52.4
Loss (same as before)		— 1.6
Range (for beacon)		— 93.5
Noise factor (as before)		— 6.0
Bandwidth	+151.0	
	+230.2 db	—187.5 db
	= +42.7 db	

---

*Note that the calculation of atmospheric attenuation requires knowledge of the range, so that the actual solutio above is carried out by a process of iteration. This is very abbreviated due to the relative unimportance of th attenuation.

Therefore the thermal noise error is seen from Figure 6-108 to be less than 0.01 mil rms. Not that the value, although not given on the figure, can be extrapolated by noting that for 22.7 dl it would be 0.074 mil; therefore, for this case the answer is 0.0074 mil which is too small to b significant.

6-5.4.5 Other Error Sources

Since the aims of this section are broad, it has been necessary to narrow the focus on the problems of more general occurence, leaving a number of important aspects of the tracking problem relatively untouched. Most of the omissions contribute only small errors to the usual tracker, although in specific instances they may be of prime importance. They are for the most part of a practical nature, depending upon specific mechanical configurations and the skill of the designer. Some of the more important of these omissions are:

(a) Radome errors – propagation of the radar beam through a radome may cause boresight shifts. This can be calibrated out when the radome moves with the antenna. With a stationary radome, errors (calculated for common radome materials in reference 85) are less than a quarter mil.

(b) Alignment, leveling and boresighting errors – a number of errors and machining tolerances in the antenna mount combine to produce these errors. References 65 and 86 discuss these errors in detail.

(c) Sun and wind loading distortions – thermal and physical loads on the antenna structure may cause boresight shifts of appreciable magnitude. Reference 65 estimates the possible effects of sun loading on one particular system. These errors can be minimized by proper design and use of the equipment.

(d) R-f coupling errors – unwanted coupling between the separate feeds of most monopulse systems is unavoidable. Normally this source of angular error is small in comparison to others.

REFERENCES

1 *Aerials for Centimetre Wavelengths,* Cambridge University Press, 1950.

2 *Radiation Laboratory Series,* Vol. 12, McGraw-Hill Book Co., N.Y., 1949.

3 *Principles and Applications of Waveguide Transmission,* D. Van Nostrand Co., Princeton, 1950.

4 J. Kraus, *Antennas,* McGraw-Hill Book Co., N.Y., 1950.

5 *Study of Numerical Integration Methods for Antenna Pattern Calculations,* ASTIA #AD 160 855, 1958.

6 J. Ruze, "The Effect of Aperture Errors on Antenna Radiation Patterns", *Proc. of Symp. on Communication Theory and Antenna Design,* ASTIA #AD 117 067.

7 J. Robieux, *Influence of the Manufacturing Precision of an Antenna on its Performance,* ASTIA #AD 83 556, 1955.

8 W. Hayes, *Gratings and Screens as Microwave Reflectors,* Rad. Lab. Rept. No. 54-20, April 1, 1943.

9 H. Worthington Jr., *The Microwave Transmitting Properties of Metal Screens,* ASTIA #AD 36 136.

10 D. Kiely, "Dielectric Aerials", *Methuen's Monographs on Physical Subjects.*

11 "Tables of Constants for Rectangular Waveguide", *IRE Trans. on Microwave Theory and Techniques,* July, 1956.

12 L. Gould, *Handbook on Breakdown of Air in Waveguide Systems,* Microwave Associates, Inc., Reprinted December, 1957.

13 *Radiation Laboratory Series,* Vol. 26, McGraw-Hill Book Co., N.Y., 1949.

14 *Fourth Symposium on Scanning Antennas,* NRL, ASTIA #AD 205 443, April 1952.

15 *Georgia Tech – Scel Symposium on Scanning Antennas,* December, 1956.

16 K. Kelleher and H. Coleman, *Off-Axis Characteristics of the Paraboloidal Reflector,* NRL Rept. No. 4088, December, 1952.

17 K. Kelleher and H. Hibbs, *A New Microwave Reflector,* NRL Rept. No. 4141, May, 1953.

18 J. Huynen, "Theory and Design of a Class of Luneberg Lenses", *Wescon Convention Record,* Part I, 1958.

19 D. Kuhn et al., *Development of Ferrite Phase Shifters for Antenna Scanning,* GE Report No. R59ELS96, Syracuse, 1959.

20 D. Rhodes, *Introduction to Monopulse,* McGraw-Hill Book Co., N.Y., 1959.

21 *The Antenna Phase Characteristic and its Effect on the Performance of an Amplitude-Amplitude Simultaneous Lobing System,* Sperry Rept. No. 5251-2101, November, 1947.

22 I. Olin and R. Tompkins, *Performance of a Compact Monopulse Feed Assembly,* NRL Report No. 4428, September, 1954.

23 *A Mathematical Analysis of a Four-Lobe Monopulse System,* NAVORD Rept. No. 3162, December, 1955.

24 P. Hannan, *Principle of the Double Reflector Antenna,* Wheeler Labs. Rept. No. 658, 1955.

25 *Supplement A to Microwave Tube Study for Project 140,* July-September, 1958, contract DA-36-039SC-78178, GE.

26 G. Gray, "Inexpensive Square-wave Generator", *Electronics,* February, 1952.

27 B. Mills, "Transient Response of Cathode Followers in Video Circuits", *Proc. IRE,* Vol. 37, June, 1949, pp. 631-3.

28 J. Blewett and J. Rubell, "Video Delay Lines", *Proc. IRE,* Vol. 35, December 1947, pp. 1580-4.

29 L. G'Acoletto and H. Hohnson, "UHF Triode Design in Terms of Operating Parameters and Electrode Spacings", *Proc. IRE*, Vol. **41**, January, 1953, pp. 51-8.

30 G. Ford and E. Walsh, "The Development of Electron Tubes for a New Coaxial Transmission System", *BTSJ*, Vol. 30, October, 1951, pp. 1103-28.

31 R. Lowell, *A Low Noise Wide Band 200 MC Insertion Amplifier*, NRL Rept. No. 3979, May, 1952.

32 M. Dishal, "Theoretical Gain and Signal to Noise Ratio Obtained from the Grounded Grid Amplifier at UHF", *Proc. IRE*, Vol. 32, 1944, p. 276.

33 M. Strutt, "The Causes for the Increase of Admittances of Moderately High Frequency Amplifier Tubes on Shortwaves", *Proc. IRE*, Vol. 26, August, 1938, pp. 1011-33.

34 W. Ferris, "Input Resistance of Vacuum Tubes as Ultra High Frequency Amplifiers", *Proc. IRE*, January, 1936.

35 D. North, "Analysis of the Effects of Space Charge on Grid Impedance", *Proc. IRE*, January, 1936.

36 C. Starner, "The Grounded Grid Amplifier", *Broadcast News*, January, 1946.

37 A. Haeff, "Effect of Electron Transit Time on Efficiency of a Power Amplifier", *RCA Review*, July, 1939.

38 E. Spitzer, "Grounded Grid Power Ampiifiers", *Broadcast News*, October, 1946.

39 M. Jones, "Grounded Grid R. F. Voltage Amplifiers", *Proc. IRE*, July, 1944.

40 J. Rankin, "Receiver Input Connections for VHF Measurements", *RCA Review*, April, 1942.

41 H. Jamieson and J. Whipner, "Power Amplifiers with Disk-seal Tube", *Proc. IRE*, Vol. 34, 1946, p. 483.

42 C. Fay, "1.5 KW 500MC Grounded Grid Triode", *Proc. IRE*, July, 1951.

43 R. Peters, "UHF RF Amplifier Design", *TV Eng.*, July, 1951.

44 *An Experimental Investigation of the Properties of a Tuned-input Microwave Receiver*, ASTIA #AD 117 492.

45 *Development of Radar Receiver Incorporating Clutter-operated Anti-clutter Circuits*, ASTIA #AD 29 155, February, 1952.

46 E. Anderson, *Television Receiver Signal Circuit and AGC Considerations for Impulse Noise Immunity*, RCA Rept. No. LB836.

47 W. Whalley, "Design Considerations for Combination UHF and VHF Receivers", *Tele-Tech*, November, 1952, pp. 36-8.

48 J. Croney, "A Simple Log Receiver", *Proc. IRE*, Vol. 34, July, 1951.

49 Alred-Reiss, "An Anti-clutter Radar Receiver", *JIEE*, Vol. 95, part 3, November, 1948.

50 L. Morrison, "The Radar Receiver", *Proc IRE*, Vol. 26, October, 1947, p. 693.

51 R. Richardson, *Some Pulse-Doppler Radar Design Considerations*, Lincoln Lab TR-154, August, 1957.

52 L. Hoffman, *A Low Noise 215-225 MC Converter*, NRL Rept. No. 4765, June, 1956.

53 R. Peter, *Direct-Reading Noise-Factor Considerations and Measurement Techniques of UHF*, RCA Rept. No. LB866, June, 1952.

54 M. Lery, "Signal to Noise Ratio in Radar", *Wireless Eng.*, Vol. 24, December, 1947, pp. 349-52.

55 P. Swerling, *Probability of Detection for Fluctuating Targets*, Project RAND Research Memo 1217, March, 1954.

56 M. Johnson, *Expected Performance of a Video Integrator*, GE Rept. No. 54E113-23, Syracuse, 1954.

57 J. Marcum, *A Statistical Theory of Target Detection by Pulsed Radar*, ASTIA #AD 101 882, April, 1952.

58 J. Marcum, *A Statistical Theory of Target Detection by Pulsed Radar – Mathematical Appendix*, ASTIA #AD 101 882, July, 1948.

59 B. Brown, *The Factors Affecting Search Radar System Performance,* GE Rept. No. 51E111, Syracuse, 1951.

60 T. Connolly, *Cumulative Probability of Detection,* GE Rept. No. R57EMH38, 1957.

61 O. Linderman and G. Kirkpatrick, *Angular Accuracy Improvement,* (Five quarterly, one final report), GE Rept. No. 51E204, 1951.

62 *Reference Data for Radio Engineers,* 4th edition, ITT Corp., N.Y., 1956.

63 *Radiation Laboratory Series,* Vol. 13, McGraw-Hill Book Co., N.Y., 1951.

64 Kirkpatrick et al., *Anti-Clutter Techniques,* GE Rept. No. 51E236-6, Syracuse, 1951.

65 *HMEED, Error Analysis of Interim Tracker for WS107A-1,* GE, Syracuse, 1956.

66 Locke et al., *Principles of Guided Missile Design Series – Guidance,* D. Van Nostrand Co., Princeton, 1955.

67 Chestnut and Mayer, *Servo Mechanisms and Regulating Systems Design,* Vol. 2, John Wiley And Sons, N.Y., 1955.

68 T. Johnson, *16th Quarterly Technical Report on Radar Set AN/TPQ-5(XE-1),* GE Rept. No. R51GL64-17, Schenectady, 1951.

69 D. Kuhn and W. Nester, *Feasibility Study of RF ECS Systems,* GE Rept. No. R56ELS129, Syracuse, 1956.

70 A. Hastings et al., *Noise in Tracking Radars,* NRL Rept. No. 3929 (ATI 126243), January, 1952.

71 J. Meade et al., *Noise in Tracking Radars,* NRL Rept. No. 3759 (ATI 90876), November, 1950.

72 G. Millman, *An Analysis of the Angular Scintillation of Tracking Radar Systems,* GE Rept. No. R56ELS98, Syracuse, 1956.

73 K. Kuhn, *Radar Angular Tracking Error for a Complex Target Covering Variable Aspects,* GE Rept. No. R56ELS98, Syracuse, 1956.

74 R. Hogg, *A Critical Survey of Recent Work Covering Amplitude Modulation and Glint in the U.K. and U.S.A.,* Royal Aircraft Establishment Tech. Note GW323, Farnborough Hants, England, June, 1954.

75 C. Miller and F. Perry, *Effect of Frequency Diversity on Tracking Accuracy,* GE Rept. No. R56ELC30, Ithaca, 1956.

76 S. North and J. Patterson, *The Reduction of Scintillation by AJAX Techniques,* GE Rept. No. R58EMH4, Syracuse, 1958.

77 R. McFall, *First Quarterly Technical Report on Radar Set AN/TPQ-5(XE-1),* GE Rept. No. R51GL64, Schenectady, 1951.

78 Dodson et al., *Field Intensity Contours in Generalized Coordinates,* Radiation Lab Rept. No. 702, MIT, 1945.

79 *Symposium on Tropospheric Radio Wave Propagation Within the Horizon,* USN Electronics Lab. Rept. No. 409, San Diego, 1953.

80 H. Venema, *Accuracy Limitations in Low Angle Radar Tracking,* GE Rept. No. 52E245, Syracuse, 1952.

81 C. Wilcox, *Effects of Atmospheric Attenuation on Reconnaissance Antenna Design,* Scientific Rept. No. 1, AF 19(604)-1708, Hughes Aircraft, Culver City, 1957.

82 G. Millman, *Analysis of Tropospheric, Ionospheric and Extra Terrestrial Effects on VHF and UHF Propagation,* GE Rept. No. R56EMH31, Syracuse, 1956.

83 J. Boyd, *Effects of Atmospheric Conditions on Precision Tracking Radar,* LRA 19/6, Georgia Inst. of Tech., 1949.

84 J. Biggs, *Atmospheric Refraction in Radio Measurement,* GE Rept. No. R54A0505, Philadelphia, 1954.

85 Untitled Radome Study for General Electric Naval Ordnance Dept., Pittsfield, Mass., P.O. AOP80477, McMillan Laboratory, Inc., Ipswich, Mass., August, 1955.

86 T. Johnson, *Eighth Quarterly Technical Report on Radar Set AN/TPQ-5(XE-1),* GE Rept. No. R51GL64-9, Schenectady, 1953.

CHAPTER 7

GUIDANCE AND CONTROL

7-1 INTRODUCTION

7-1.1 GENERAL

The guidance and control subsystem is essentially the *nervous system* of the surface-to-air missile. Its function is to insure that the missile is brought to the required proximity (usually 10 to 100 feet) and attitude with respect to its target to fulfill the missile's mission.

It is the purpose of this chapter to provide concepts pertinent to the guidance and control design process. This includes a discussion of the standard schemes available for guiding the missile and controlling its motion as well as methods of evaluation.

7-1.2 RELATIONSHIP OF GUIDANCE AND CONTROL WITH THE WEAPON SYSTEM

As stated in Chapter 3, the interdependencies which exist among subsystems, coupled with the lack of information, makes the design and development task a formidable one. Servomechanism theory was mentioned as one aid available to the systems engineer for obtaining proper perspective in the development problem. *Regardless of how complex and how many fields of technology may be involved, the guidance and control system is basically a position servomechanism.* That is, the target supplies a reference input and the guidance and control system provides means for determining the error and reducing it. When viewed in this light, the general principles of servo design may be used as guides for developing the system.

Three primary questions should be answered:

(a) What are the "input characteristics"?

(b) What are the "control characteristics of the fixed elements"?

(c) What are the "desired response characteristics"?

A partial answer to (a) is generally provided when a threat or class of threats and associated operational characteristics are defined. The answers to (b) and (c) are difficult to obtain because of the lack of design information mentioned above. To execute the philosophy of simple parameterized studies and obtain answers to (b) and (c), the guidance and control engineer must be aware of basic results from several fields of technology. Then intelligent assumptions that permit reasonable appreciation of the relationship between the various subsystems can be made.

7-1.3 GUIDANCE PHASES

There may be as many as three distinct phases to the guidance problem – launch, midcourse, and terminal. The control problem in each phase is discussed in paragraph 7-4.

During the launch phase, the guidance function serves to reduce launch transients and to direct the missile to a point where midcourse guidance begins. Midcourse guidance serves to guide the missile during the mid-portion of the flight. It begins after the launch phase and guides the missile to the target area at which time the terminal phase begins. Terminal guidance is that portion of flight when all final corrections are made to direct the missile to the target. The terminal phase usually employs some type of target seeker to guide the missile.

Figure 7-1a illustrates how the three phases may be broken down utilizing three distinct guidance schemes. In the launch phase the missile is stabilized and gyros may be pre-set in conjunction with an altimeter to guide the missile to a point in space. At this point the missile levels out and is guided to the target area by radio command.

When the missile is within range of seeker lock-on, the seeker searches for the target. At seeker lock-on, the midcourse guidance is discontinued and the terminal phase begins. Dur-

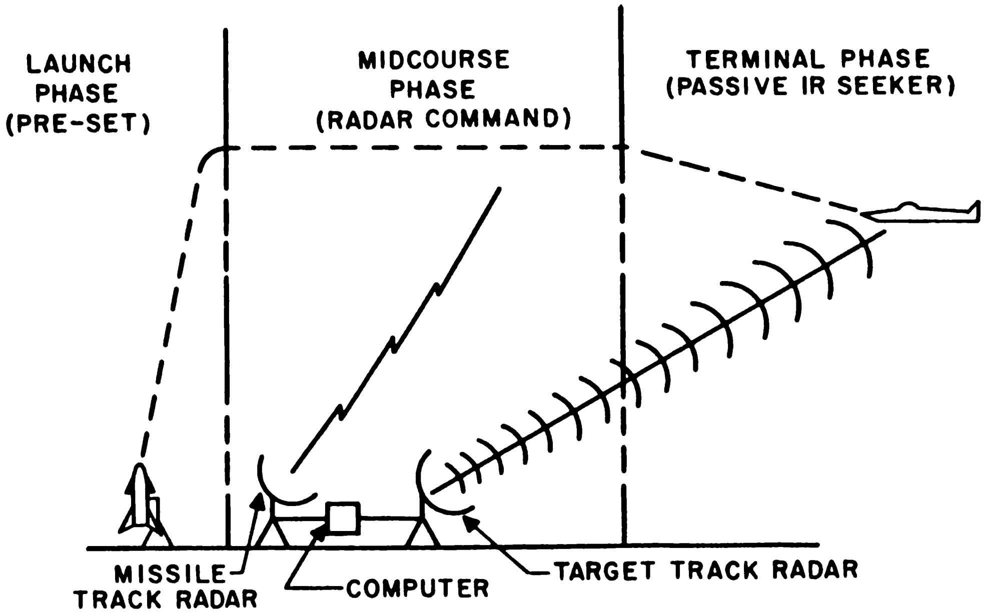

(a) THREE-PHASE GUIDANCE

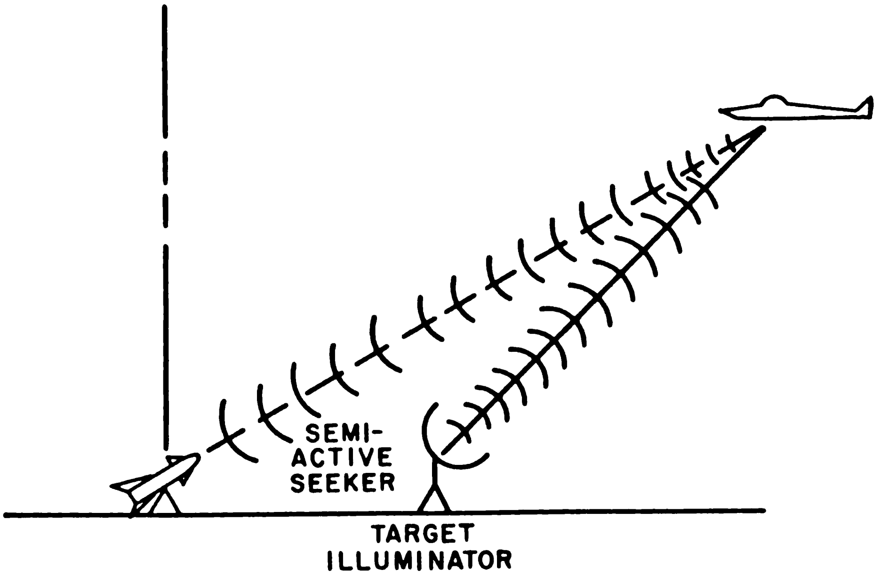

(b) TERMINAL PHASE
(SEMI-ACTIVE HOMING ALL THE WAY)

Figure 7-1. Missile Guidance Phases

ing this phase, the seeker directs the missile to a collision with the target.

It was previously stated that there may be as many as three guidance phases. It is possible however to have only one phase. This is illustrated in Figure 7-1b in which only the terminal phase is employed. Here the seeker locks on to the target while the missile is still on the launcher. After the seeker locks on, the missile is launched and the seeker directs the missile on a collision course with the target.

The two examples given in Figure 7-1 illustrate that the terminology of guidance phases must be qualified by specifying the guidance scheme or schemes employed.

7-2 GUIDANCE MODES[1]

7-2.1 GENERAL

The guidance subsystem of a SAM system is often classified according to the resulting trajectory.

This classification scheme is used because certain characteristics of the trajectory influence the design of the guidance system.

These characteristics are also helpful in evaluating various guidance systems for use in a given tactical situation.

The following discussion is restricted to the geometry and time relations for various trajectories. It should be noted that command guidance can be utilized with any of the guidance modes discussed here. However, because of the mechanization requirements (Table 7-4), command guidance is more compatible with the line-of-sight, or beam rider, mode than with the other guidance modes.

When implementing homing type missiles, additional effects to be studied include target maneuvers, tracking errors, and control system-missile time lags as well as limited missile acceleration capabilities and other nonlinearities. Although the aggregate of these effects presents a formidable analysis problem, simplified mathematical models which include one or two parameters have been investigated.[2-15] Results of such analyses, though simplified, should not be disregarded as they often present, in non-dimensionalized form, results that are useful for initial feasibility studies or trade-off estimates.

The applicable parameters include the trajectory, maximum turning rate, maximum lateral acceleration, flight time, and turning rate frequency spectrum. In general, the considerations are restricted to two dimensions with the following assumptions:

(a) The target travels a non-maneuvering, straight-line course.

(b) Both the missile speed and target speed are constant.

For beam rider guidance these are modified to:

(c) The control point is a stationary reference.

(d) The missile is launched from the control point.

In all cases except beam rider guidance, a two dimensional coordinate system is established in the plane defined by the missile and target velocity vectors. In beam rider guidance, a two-dimensional coordinate system is established in the plane determined by the target velocity vector and the line joining the point of control with that vector.

If V_M is the missile velocity and $\dot{\phi}_M = \left(\frac{d\phi_M}{dt}\right)$ its turning rate, then its lateral acceleration is obtained from

$$A_M = \left| V_M \dot{\phi}_M \right| \qquad (7\text{-}1)$$

(See Table 7-1 for definition of terms.) The turning rate frequency spectrum is defined as the Fourier Transform of the turning rate, namely

$$F(\omega) = \int_{-\infty}^{\infty} \dot{\phi}_M(t)\, e^{-j\omega t}\, dt; \; (j = \sqrt{-1}\,) \qquad (7\text{-}2)$$

Usually $F(\omega)$ cannot be obtained directly from $\dot{\phi}_M(t)$, and in these cases an approximation can be obtained by:

(a) fitting a polynomial

$$\dot{\phi}_M(t) = a + bt + ct^2 + --- \qquad (7\text{-}3)$$

to a plot of the missile turning rate or by:

(b) making an assumption concerning $\dot{\phi}_M(t)$ for $t > t_f$ where t_f is the missile flight time, i.e., t_f is the total time elapsed from launching $(t = o)$ until missile-target impact.

TABLE 7-1. NOMENCLATURE FOR PARAGRAPH 7-2

Subscript T refers to target

Subscript zero means initial value

Subscript M refers to the missile

V	-	speed
ϕ	-	missile turning rate
ϕ	-	angle between target velocity vector and the line-of-sight
A	-	lateral acceleration
ω	-	angular frequency
t	-	time
t_f	-	time of flight
r	-	instantaneous range
θ	-	elevation angle from control point to missile
k	-	constant in beam rider equations = pR
p	-	ratio of missile speed to target speed = $\frac{V_M}{V_T}$
R	-	target altitude
m	-	initial slope of beam rider trajectory
r_f	-	final range
ϕ_M	-	angle between missile velocity vector and a horizontal reference
δ	-	$\phi - \phi_M$ = deviation angle
γ	-	angle between heading and line of sight

In Figure 7-2 it was assumed that

$$\dot{\phi}_M(t) = 0 \text{ for } t < 0 \text{ and } t > t_f \tag{7-4}$$

so that

$$F(\omega) = \int_0^{t_f} \dot{\phi}_M(t)\, e^{-j\omega t}\, dt \tag{7-5}$$

7-2.2 LINE-OF-SIGHT (BEAM RIDER) TRAJECTORY

The line-of-sight course is one which a beam rider missile follows and is defined as *a course on which the missile is guided in order to remain on the line joining the target and point of control.*

Although it is assumed that the missile is launched from the control point, it is important to note that in practice a *capture* problem is always encountered. That is, the missile cannot be launched directly along the line-of-sight; also a transient period exists between launching and the time when the missile has been captured by the guidance beam and is directed along it.

The geometry for a missile launched from the control point is shown in Figure 7-3. The resulting trajectory differential equation, Table 7-2, is non-linear and unsolvable in closed form by ordinary methods. However, if the missile range, r, is expanded in a Taylor Series,

$$r = r_o + r_o'(\Theta - \Theta_o) + \frac{r_o''(\Theta - \Theta_o)^2}{2!} + \frac{r_o'''(\Theta - \Theta_o)^3}{3!} + \cdots \tag{7-6}$$

where

$$r_o' = \frac{dr}{d\Theta}\bigg|\, \Theta = \Theta_o;\ r_o'' = \frac{d^2r}{d\Theta^2}\bigg|\, \Theta = \Theta_o; \text{ etc.,} \tag{7-7}$$

The coefficients r_o, r_o', r_o'' can be evaluated from the initial boundary conditions

$$r_o = 0 \tag{7-8}$$

$\Theta_o = \arctan m$; $m =$ initial slope of trajectory

and the differential trajectory equation (and derivatives of it) yield the solution shown in Table 7-2. Figure 7-4 shows several line-of-sight trajectories for various initial launch angles and speed ratios.

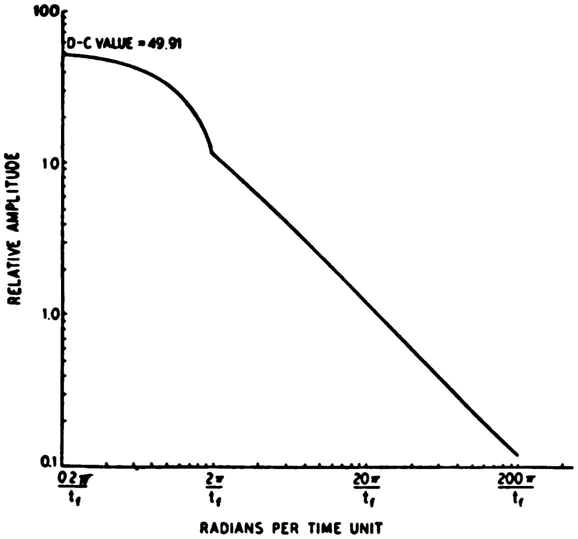

Frequency Spectrum of Beam-rider Turning Rate; $\theta_0 = 15°$, $p = 1.5$

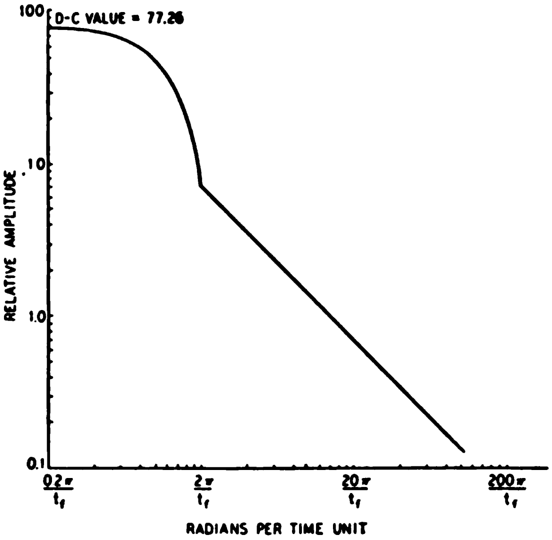

Frequency Spectrum of Beam-rider Turning Rate; $\theta_0 = 15°$, $p = 5$

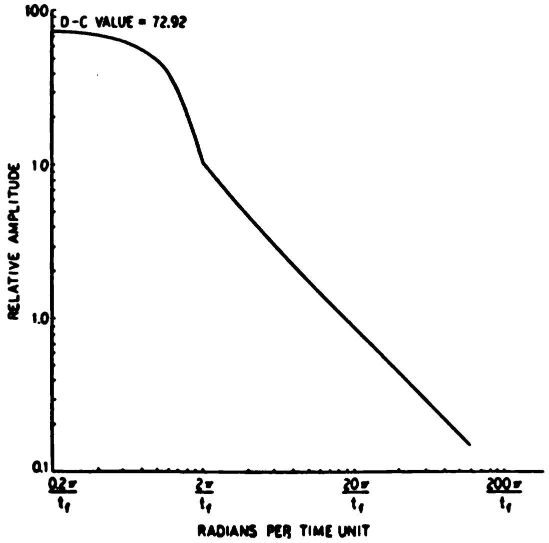

Frequency Spectrum of Beam-rider Turning Rate; $\theta_0 = 45°$, $p = 1.5$.

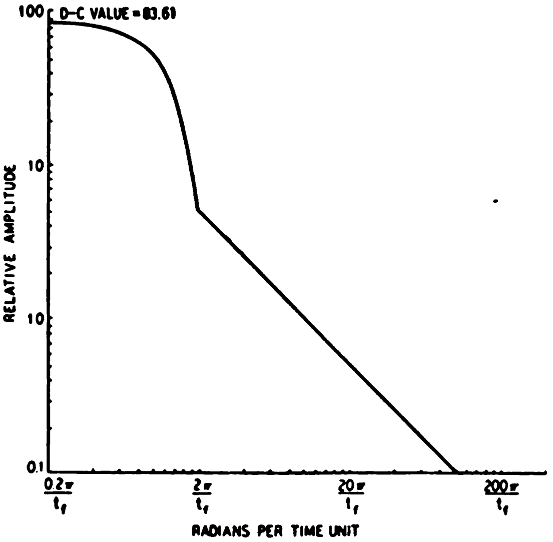

Frequency Spectrum of Beam-rider Turning Rate; $\theta_0 = 45°$, $p = 5$.

Figure 7-2. Frequency Spectra for Various Beam Rider Turning Rates

From: Arthur S. Locke, GUIDANCE, Copyright 1955, D. Van Nostrand Company, Inc., Princeton, N.J.

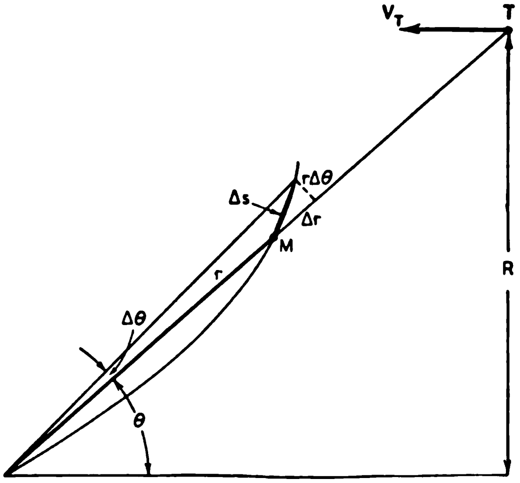

Figure 7-3. Line-of-Sight Geometry

From: Arthur S. Locke, GUIDANCE, Copyright 1955, D. Van Nostrand Company, Inc., Princeton, N.J.

The geometry for determining the beam rider missile turning rate is shown in Figure 7-5 which provides the result shown in Table 7-2.

Figure 7-6 shows several normalized plots of $\dot\phi$ for various initial launch angles and speed ratios.

The amplitude frequency spectrums of Figure 7-2 were obtained by fitting a cubic polynominal to the turning rate curves of Figure 7-6 and obtaining the absolute value of $F(\omega)$, $|F(\omega)|$, in accordance with equation 7-5. The ordinates represent relative amplitude and the abscissas represent radian frequency for the normalized time variable $\tau = t/t_f$.

7-2.3 PURSUIT COURSE

A pursuit course is defined as a course in which the missile velocity vector is always directed towards the instantaneous target position.

The geometry for a pursuit course is shown in Figure 7-7 for a receding target; i.e., a target with a velocity vector having a component along r (the missile-to-target range) that tends to increase r. The equations of motion are obtained from velocity components along and normal to r as

$$\begin{aligned} \dot r &= V_T \cos\phi - V_M && \text{(a)} \\ r\dot\phi &= -\,V_T \sin\phi && \text{(b)} \end{aligned} \qquad \textbf{(7-9)}$$

which have the solution shown in Table 7-2.

For an approaching target, both velocities cause a decrease in r so that equation 7-9 becomes

$$\begin{aligned} \dot r &= V_T \cos\phi - V_M && \text{(a)} \\ r\dot\phi &= V_T \sin\phi && \text{(b)} \end{aligned} \qquad \textbf{(7-10)}$$

whose solutions are also shown in Table 7-2. An explicit expression for elapsed time, which permits one to plot the trajectory for any particular case, can be obtained from equation 7-9 for a receding target and from equation 7-10 for an approaching target. The total flight time, t_f, is then obtained by setting $r = 0$ in the expressions for elapsed time. Turning rate and, hence, lateral acceleration are easily obtained from the equation for normal velocity components, i.e., equations 7-9b or 7-10b.

The value of $\dot\phi$ at impact is shown in Table 7-2 along with the maximum absolute value.

7-2.4 MODIFIED PURSUIT COURSE

When a non-zero, constant angle exists between the missile velocity vector and the line-of-sight from the missile to the target, a constant navigation or modified pursuit course results. The modified pursuit geometry is shown in Figure 7-8 where

$$\begin{aligned} \phi_M &= \text{missile heading from horizontal} \\ \delta &= \phi - \phi_M \end{aligned} \qquad \text{(7-11)}$$

The equations of motion are

$$\begin{aligned} \dot r &= V_T \cos\phi - V_M \cos\delta && \text{(a)} \\ r\dot\phi &= V_T \sin\phi + V_M \sin\delta && \text{(b)} \end{aligned} \qquad \text{(7-12)}$$

and can be integrated directly to provide the solution given in Table 7-2.

OF FLIGHT PATH CHARACTERISTICS

FLIGHT PATH	RATE, $\dot{\phi}$	REMARKS
LINE OF SIGHT COURSE	$\left(\frac{dr}{d\theta}\right)^2 \sqrt{\frac{r \cot \theta}{k^2 \csc^4 \theta - r^2}}\Big)$ ③	① Equation of motion is nonlinear. Solution is obtained by series expansion. ② Flight time expressed in term of final slant range; can be obtained also from $t\|_{\theta = \theta_f}$, θ_f = final elevation angle ③ $\dot{\theta}$ finite for $p > 1$
PURSUIT COURSE, OUTGOING TARGET	$\dot{r} = \frac{\cos \phi)^p}{\phi^{p-2}}$ $r\dot{\phi}$	④ $\lim_{r \to 0} \phi = 0$ ⑤ $t_f \leq \infty,\ p > 1$ ⑥ $\lim_{\phi \to 0} \dot{\phi} = 0,\ 1 < p < 2$ $= -4 V_T/K,\ p = 2$ $= -\infty,\ p > 2$ ⑦ $\|\dot{\phi}\|_{max}$ occurs at $r = 0$ if $p \geq 2$ $\|\dot{\phi}\|_{max} = \frac{V_T}{K}(1+p/2)^p \left[1-(p/2)^2\right]^{1-p/2}$ $1 < p < 2$ at $\phi = \cos^{-1} p/2$
PURSUIT COURSE, INCOMING TARGET	$\dot{r} = \frac{)^{p+2}}{\cos \phi)^p}$ $r\dot{\phi}$	⑧ $\lim_{r \to 0} \phi = \pi$ ⑨ $t_f \leq \infty,\ p > 1$ ⑩ $\lim_{r \to 0} \dot{\phi} = 0,\ 1 < p < 2$ $= 4 V_T/K_1,\ p = 2$ $= \infty,\ p > 2$ ⑪ $\|\dot{\phi}\|_{max}$ occurs at $r = 0$ if $p \geq 2$ $\|\dot{\phi}\|_{max} = \frac{V_T}{K_1} \frac{\left[1-(p/2)^2\right]^{1+p/2}}{(1-p/2)^p}$, $1 < p < 2$ at $\phi = \cos^{-1}(-p/2)$
MODIFIED PURSUIT	$\frac{\sin\phi + \eta \cos\phi]^{\frac{p \cos\delta}{\eta}}}{\sin\delta]^{\frac{p \cos\delta}{\eta} - 2}}$ $\dot{r} = V_T \Big(\frac{\cos\delta}{\eta}\Big).$ $r\dot{\phi} =$ $\frac{\cos\delta}{\eta} - 1$ $\overline{\ \eta \cos\phi_0\ }\Big]\Big\}$ ⑭	⑫ Trajectory spirals around target an infinite number of times and misses. ⑬ $t_f \leq \infty$ for $p > 1,\ \delta < \pi/2$ ⑭ $\Delta = \sin^{-1}(p \sin\delta)$, $\dot{\phi}(\Delta) = 0,\ \frac{p \cos\delta}{\eta} < 2$ $= \infty,\ \frac{p \cos\delta}{\eta} > 2$ $= F(\phi_0)\, p^4 \cos^4\delta,\ \frac{p \cos\delta}{\eta} = 2$
CONSTANT BEARING	$r = V_0$ $0 = V$	No practical implementation known - Important for kinematics linearization
PROPORTIONAL NAVIGATION	$\dot{r} = V_T) \left[\frac{r}{r_0}\right]^{K_4 e^{K_5}}$ $r\dot{\phi} =$ $\phi_m = a$	⑮ a = Navigation Constant $a = 1,\ \phi_0 = 0$ Pursuit Course $a = 1,\ \phi_0$ Fixed Modified Pursuit Course $\dot{\phi} = 0 \rightarrow$ Constant Bearing ⑯ Solution holds only for $a = 2$. For $a \neq 2$ use Numerical integration with $\alpha_0 = \gamma_0 + \phi_0$ ⑰ Closed form expression relating r & γ cannot be obtained. Use numerical integration ⑱ $\lim_{r \to 0} \phi = 0$ $p \cos\alpha_0 > -1$ $= \infty$ $p \cos\alpha_0 < -1$ $< \infty$ $p \cos\alpha_0 = -1$

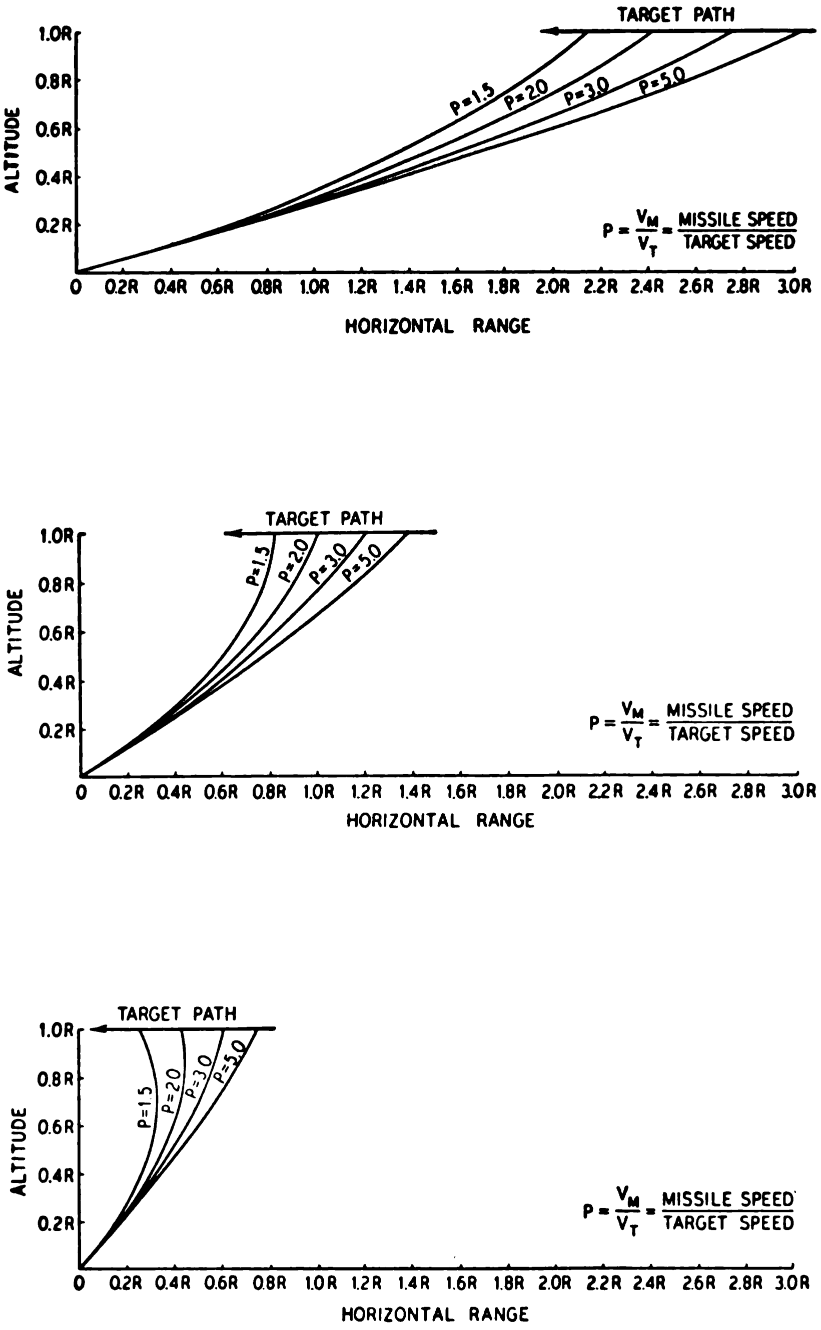

Figure 7-4. Line-of-Sight Trajectories for Various Launch Angles

From: Arthur S. Locke, GUIDANCE, Copyright 1955, D. Van Nostrand Company, Inc., Princeton, N.J.

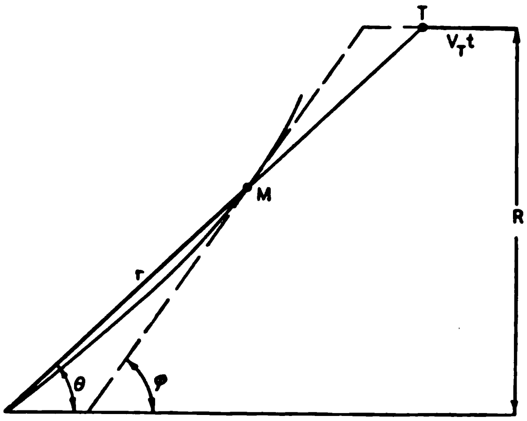

Figure 7-5. Beam Rider Turning Rate Geometry

From: Arthur S. Locke, GUIDANCE, Copyright 1955, D. Van Nostrand Company, Inc., Princeton, N.J.

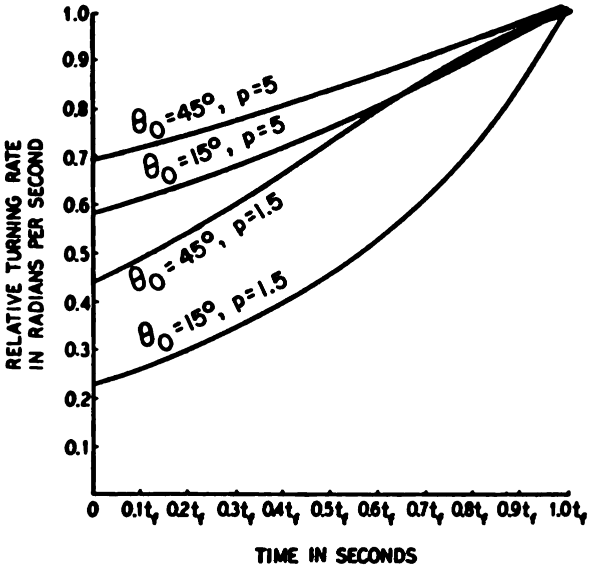

Figure 7-6. Normalized Curves of Turning Rates for Various Initial Launch Angles and Speed Ratios

From: Arthur S. Locke, GUIDANCE, Copyright 1955, D. Van Nostrand Company, Inc., Princeton, N.J.

Note that the solution takes different forms for $p^2 \sin^2 \delta < 1$ and $p^2 \sin^2 \delta = 1$. For $p^2 \sin^2 \delta > 1$, the trajectory is a spiral which does not provide an interception. An explicit expression for time can be obtained from equation 7-12 and from this, the value of total flight time can be obtained, as shown in Table 7-2. The turning rate is obtained from equation 7-11 as

$$\dot{\phi}_M = \dot{\phi} \qquad (7\text{-}13)$$

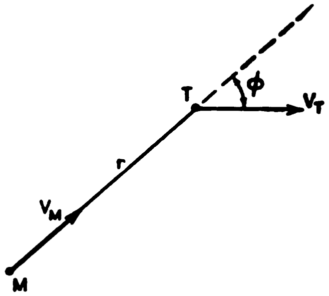

Figure 7-7. Pursuit Course Geometry

From: Arthur S. Locke, GUIDANCE, Copyright 1955, D. Van Nostrand Company, Inc., Princeton, N.J.

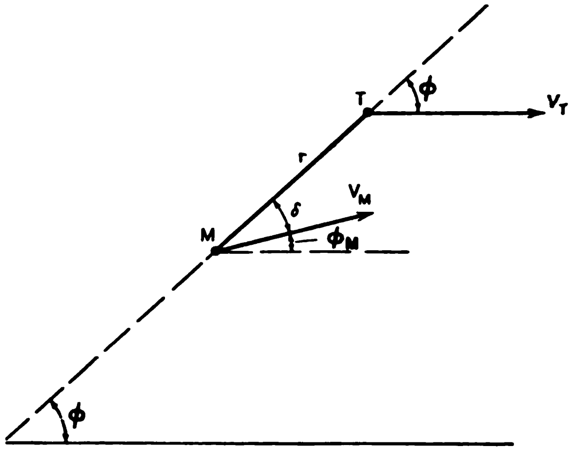

Figure 7-8. Modified Pursuit Course Geometry

From: Arthur S. Locke, GUIDANCE, Copyright 1955, D. Van Nostrand Company, Inc., Princeton, N.J.

Since δ is a constant and since a solution for r is available, equation 7-12b provides

$$\dot{\phi}_M = V_T \frac{p \sin \delta - \sin \phi}{r} \qquad (7\text{-}14)$$

Substituting the expression for r from Table 7-2 provides

$$\dot{\phi}_M = F(\phi_o) \cdot f\,(p, \delta, \phi) \qquad (7\text{-}15)$$

which is infinite when $\sin \phi = p \sin \delta$ or, when $\phi = \Delta$; where

$$\Delta = \arc \sin (p \sin \delta) \tag{7-16}$$

Under these conditions one can show that

$$\begin{aligned} \dot{\phi}(\Delta) &= 0, \frac{p \cos \delta}{\sqrt{1 - p^2 \sin^2 \delta}} < 2 \\ &= F(\phi_o) p^4 \cos^4 \delta, \frac{p \cos \delta}{\sqrt{1 - p^2 \sin^2 \delta}} = 2 \quad (7\text{-}17) \\ &= \infty, \frac{p \cos \delta}{\sqrt{1 - p^2 \sin^2 \delta}} > 2 \end{aligned}$$

Figure 7-9 shows the necessary relationship between p and $\sin \delta$ in order that ϕ remains finite. Values of $p \sin \delta$ in Region I result in infinite turning rates. In practice, the maximum turning rate is limited so that the missile will execute its maximum turn (for $p \sin \delta$ in Region I) until it cuts across the line of the target path and then either re-enters the proper course or is lost.

Since $A_M = |V_M \dot{\phi}|$ the acceleration will be finite only as long as $\dot{\phi}$ is finite, or in other words, when p and δ are such that one is in Region II of Figure 7-9.

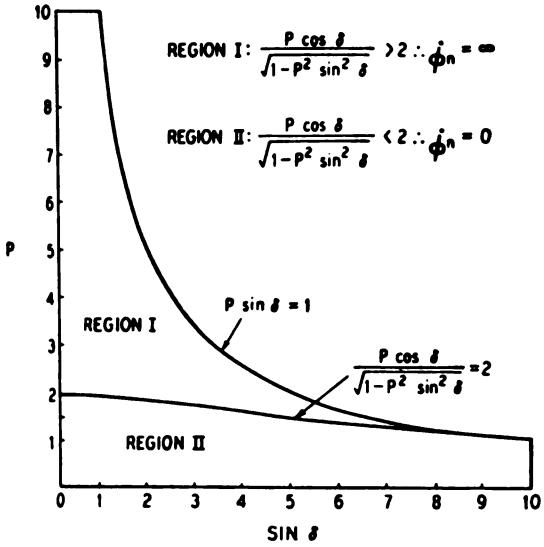

Figure 7-9. Turning Rate Criterion for Modified Pursuit

From: Arthur S. Locke, GUIDANCE, Copyright 1955, D. Van Nostrand Company, Inc., Princeton, N.J.

7-2.5 CONSTANT BEARING COURSE

A constant bearing course is one in which the line-of-sight from the missile to the target maintains a constant direction in space. That is, in Figure 7-10 which illustrates the constant bearing geometry, ϕ is a constant and hence $\dot{\phi} = 0$. The equations of motion are:

$$\begin{aligned} \dot{r} &= V_T \cos \gamma_T - V_M \cos \gamma_M \\ 0 &= V_T \sin \gamma_T - V_M \sin \gamma_M \end{aligned} \tag{7-18}$$

which provide the solution,

$$r = r_o + (V_T \cos \gamma_T - V_M \cos \gamma_M)\, t \tag{7-19}$$

Total flight time is obtained from equation 7-19 when $r = 0$. For a straight line target course, both the missile turning rate and, hence, lateral acceleration are zero, while for a constant speed maneuvering target and missile the missile acceleration cannot exceed that of the target.

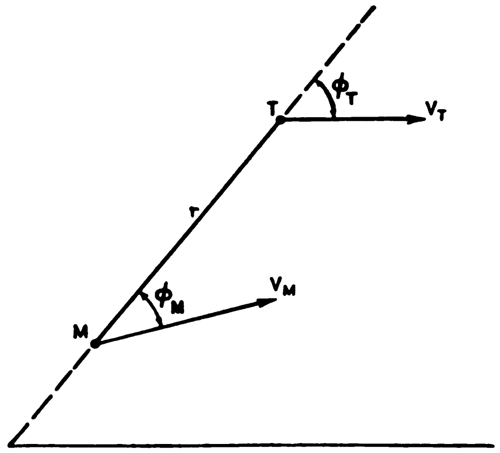

Figure 7-10. Constant Bearing Geometry

From: Arthur S. Locke, GUIDANCE, Copyright 1955, D. Van Nostrand Company, Inc., Princeton, N.J.

7-2.6 PROPORTIONAL NAVIGATION

A proportional navigation course is one in which the rate-of-change of missile heading is made directly proportional to the rate-of-rotation of the line-of-sight from the missile to the target. (See references 6 and 16 for a three dimensional definition.)

The geometry is shown in Figure 7-11 where the angle ϕ_M is the missile heading. The equations of motion are:

$$\dot{r} = V_T \cos\phi - V_M \cos(\phi - \phi_M) \quad \text{(a)}$$
$$r\dot{\phi} = -V_T \sin\phi + V_M \sin(\phi - \phi_M) \quad \text{(b)}$$
$$\dot{\phi}_M = a\dot{\phi} \quad \text{(c)}$$
$$\text{(7-20)}$$

or

$$\dot{r} = V_T \cos(\gamma + \phi_M) - V_M \cos\gamma \quad \text{(a)}$$
$$r\dot{\phi} = -V_T \sin(\gamma + \phi_M) + V_M \sin\gamma \quad \text{(b)}$$
$$\dot{\phi}_M = a\dot{\phi} = \left(\frac{a}{1-a}\right)\dot{\gamma} \quad \text{(c)}$$
$$\text{(7-21)}$$

Although the equations can be solved in closed form only when $a = 2$, numerical techniques can be used to obtain solutions in other cases. For $a = 2$, equation 7-21c reduces to

$$\dot{\phi}_M = 2\dot{\phi} = -2\dot{\gamma} \quad \text{(7-22)}$$

or

$$\phi - \phi_o = \gamma_o - \gamma \quad \text{(7-23)}$$

From Figure 7-11, $\phi = \gamma + \phi_M$ so that equation 7-23 may be written as

$$\gamma + \phi_M = \phi_o + \gamma_o - \gamma = \alpha_o - \gamma \quad \text{(7-24)}$$

where

$$\alpha_o = \phi_o + \gamma_o \quad \text{(7-25)}$$

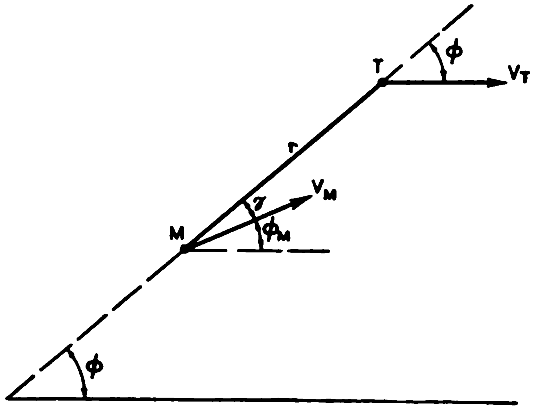

Figure 7-11. Proportional Navigation Geometry

From: Arthur S. Locke, GUIDANCE, Copyright 1955, D. Van Nostrand Company, Inc., Princeton, N.J.

while equations 7-21 a and b become

$$\dot{r} = V_T \cos(\alpha_o - \gamma) - V_M \cos\gamma \quad \text{(a)}$$
$$r\dot{\phi} = -V_T \sin(\alpha_o - \gamma) + V_M \sin\gamma \quad \text{(b)}$$
$$\text{(7-26)}$$

and provide the solution shown in Table 7-2. Explicit expressions for elapsed time and flight time cannot be obtained in closed form. Figure 7-12 illustrates the nature of the resulting trajectory for $a = 2$ and $\phi_o = 60°$. *Curve C* corresponds to having the *missile initially on a constant bearing course.* The turning rate can be obtained from the solution for r and equation 7-26b. The lateral acceleration then is

$$A_M = |V_M \dot{\phi}_M| = |aV_M\dot{\phi}| \quad \text{(7-27)}$$

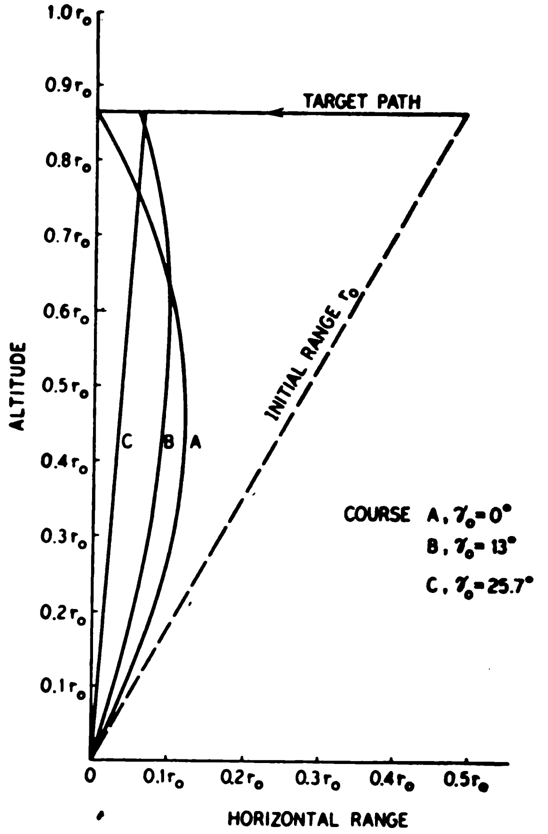

Figure 7-12. Proportional Navigation Course
$\phi_o = 60°, p = 2$

From: Arthur S. Locke, GUIDANCE, Copyright 1955, D. Van Nostrand Company, Inc., Princeton, N.J.

.7 PERTURBATION ANALYSIS

able 7-2 indicates that even for highly alized models the resulting solutions for jectory characteristics may be quite complex. e analysis problem is more difficult when get maneuvers, control lags, and limited celeration capability are considered.

To gain additional insight and simplified odels, considerable effort has been devoted to udying the perturbed motion of missiles in rious guidance modes. (See references 5, 6, , 10 and 12 through 20.)

Adler[6,19,20] has shown excellent agreement etween the perturbation approach outlined elow and the exact solutions. Results for pro-ortional navigation may be applied to the ursuit course by specializing to $a = 1$, $\phi_o = 0$. The modified pursuit course results from $\phi_o \neq 0$, $a = 1$.

7-2.7.1 Nominal Trajectory

In Figure 7-12 a particularly simple trajectory resulted when the missile was given the proper initial heading. For the perturbation analysis this trajectory, the constant bearing trajectory, is taken as a reference and deviations from it are studied. Nominal results may be obtained from Table 7-2 and are normally expressed as follows:

Closing speed

$$V_c = -(V_T \cos \gamma_T - V_M \cos \gamma_M) \tag{7-28}$$

Range

$$r = r_o - V_c t \tag{7-29}$$

Flight Time

$$t_f = \frac{r_o}{V_c} = T_o \tag{7-30}$$

Time-to-go to Collision

$$T = t_f - t = \frac{r}{V_c} \tag{7-31}$$

7-2.7.2 Perturbations

Since the line-of-sight orientation remains fixed in the constant bearing case, all angles can be measured from it. The reference path and perturbations are shown in Figure 7-13. Notice that missile and target position perturbations

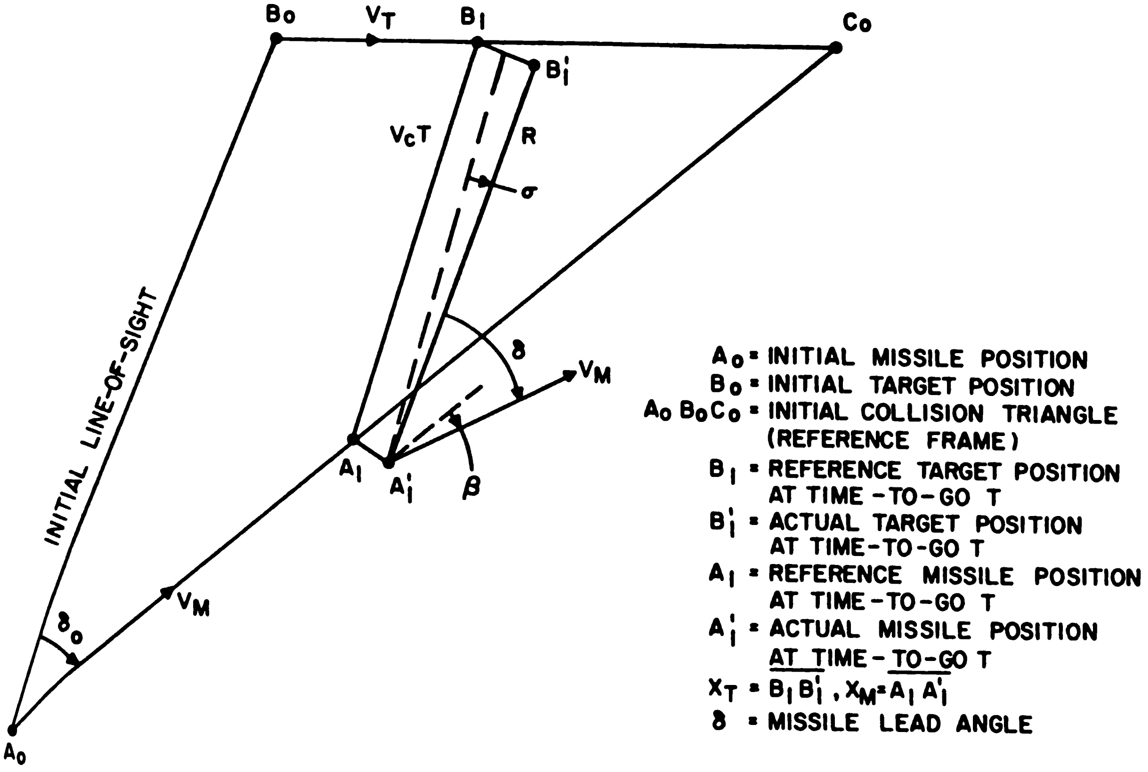

Bo
VT
B1
Co
B'1
VcT
R
σ
INITIAL LINE-OF-SIGHT
δ
VM
A1
A'1
β
VM
δo
Ao
Ao = INITIAL MISSILE POSITION
Bo = INITIAL TARGET POSITION
Ao BoCo = INITIAL COLLISION TRIANGLE (REFERENCE FRAME)
B1 = REFERENCE TARGET POSITION AT TIME-TO-GO T
B'1 = ACTUAL TARGET POSITION AT TIME-TO-GO T
A1 = REFERENCE MISSILE POSITION AT TIME-TO-GO T
A'1 = ACTUAL MISSILE POSITION AT TIME-TO-GO T
XT = B1B'1, XM=A1A'1
δ = MISSILE LEAD ANGLE

Figure 7-13. Coordinate System for Analysis of Proportional Navigation Trajectories

(Adapted from reference 20.)

may be resolved into components along and perpendicular to the reference direction, and that x_M, x_T are the perpendicular components. The line-of-sight perturbation angle is represented by σ and β is the missile velocity vector perturbation angle.

If the reference direction in Figure 7-11 is made to coincide with the initial line-of-sight, the following correspondence between Figure 7-11 and Figure 7-13 results:

$$\phi = \phi_o + \sigma = \sigma \; (\phi_o = 0) \qquad \text{(a)}$$

$$\text{(7-32)}$$

$$\phi_M = \phi_{Mo} + \beta = \delta_o + \beta \; (\phi_{Mo} = \delta_o) \qquad \text{(b)}$$

while equation 7-20c becomes

$$(\dot{\delta_o + \beta}) = a\,(\dot{\phi_o + \sigma})$$

or

$$\dot{\beta} = a\dot{\sigma} \qquad \text{(7-33)}$$

Expressions for x_M and σ are obtained from Figure 7-13 and small angle approximations.

$$\sigma = arc\ tan\left(\frac{X_T - X_M}{V_c T}\right) \qquad \text{(a)}$$

$$\dot{X}_M = V_M \sin(\delta + \beta) - V_M \sin \delta_o \qquad \text{(b)}$$

or $\qquad$ (7-34)

$$\sigma \simeq \left(\frac{X_T - X_M}{V_C\, T}\right) \qquad \text{(a)}$$

$$x_M \simeq (V_M \cos \delta_o)\,\beta \qquad \text{(b)}$$

$$\text{(7-35)}$$

Using equation 7-35 in equation 7-33 results in

$$\frac{d}{dt}\left(\frac{\dot{x}_M}{V_M \cos \delta_o}\right) = a\,\frac{d}{dt}\left(\frac{x_T - x_M}{V_c\, T}\right) \qquad \text{(7-36)}$$

or

$$T\dot{x}_M + \left(\frac{a\,V_M \cos \delta_o}{V_c}\right) x_M = \left(\frac{a\,V_M \cos \delta_o}{V_c}\right) x_T + T\dot{x}_{M_o} \qquad \text{(7-37)}$$

In equation 7-37, $\dot{x}_{M_o}$ is the initial perturbation velocity. It may be expressed also as an initial pointing error, $\beta_o = \dot{x}_{M_o}/V_M \cos \delta_o$. Fo trajectories A and B of Figure 7-12, β_o i —25.7° and —12.7° respectively.

For a reasonably accurate control system an small speed changes, the quantity $a\,V_M \cos \delta/V$ may be considered to remain constant. It is commonly referred to as the *effective navigation constant.*

$$K_e = \frac{a\,V_M \cos \delta_o}{V_c} \qquad \text{(7-38)}$$

In terms of K_e, equation 7-37 becomes

$$T\dot{x}_M + K_e\, x_M = K_e\, x_T + T\dot{x}_{M_o} \qquad \text{(7-39)}$$

Figure 7-14 shows the effect of initial aiming errors $(x_T) = 0$ while Figure 7-15 shows the missile acceleration that results from a step in target acceleration $(\dot{x}_{M_o} = 0)$,

$$x_T = \frac{1}{2}\,a_T t^2 = \frac{1}{2}\,a_T (T_o - T)^2 \qquad \text{(7-40)}$$

The final value of $\ddot{x}_M/a_t$ is shown in Figure 7-16 as a function of K_e.

Figure 7-16 indicates that a large value for K_e should be employed to reduce the acceleration required to counter a target manuever. In analyses that consider the effects of control system time lags and noise disturbances it is pointed out that the rms miss distance increases with K_e so that practically only values of K_e in the range of three to seven are of interest. (See references 6, 19 and 20.)

7-2.8 SENSOR REQUIREMENTS

The choice of guidance mode or trajectory affects the subsystems configuration in the sense of requiring the measurement of certain quantities. Basic measurements required for each of the five modes just considered are listed in Table 7-3 and common implementation requirements are shown in Table 7-4.

Additional measurement requirements are related to fuzing and autopilot requirements.

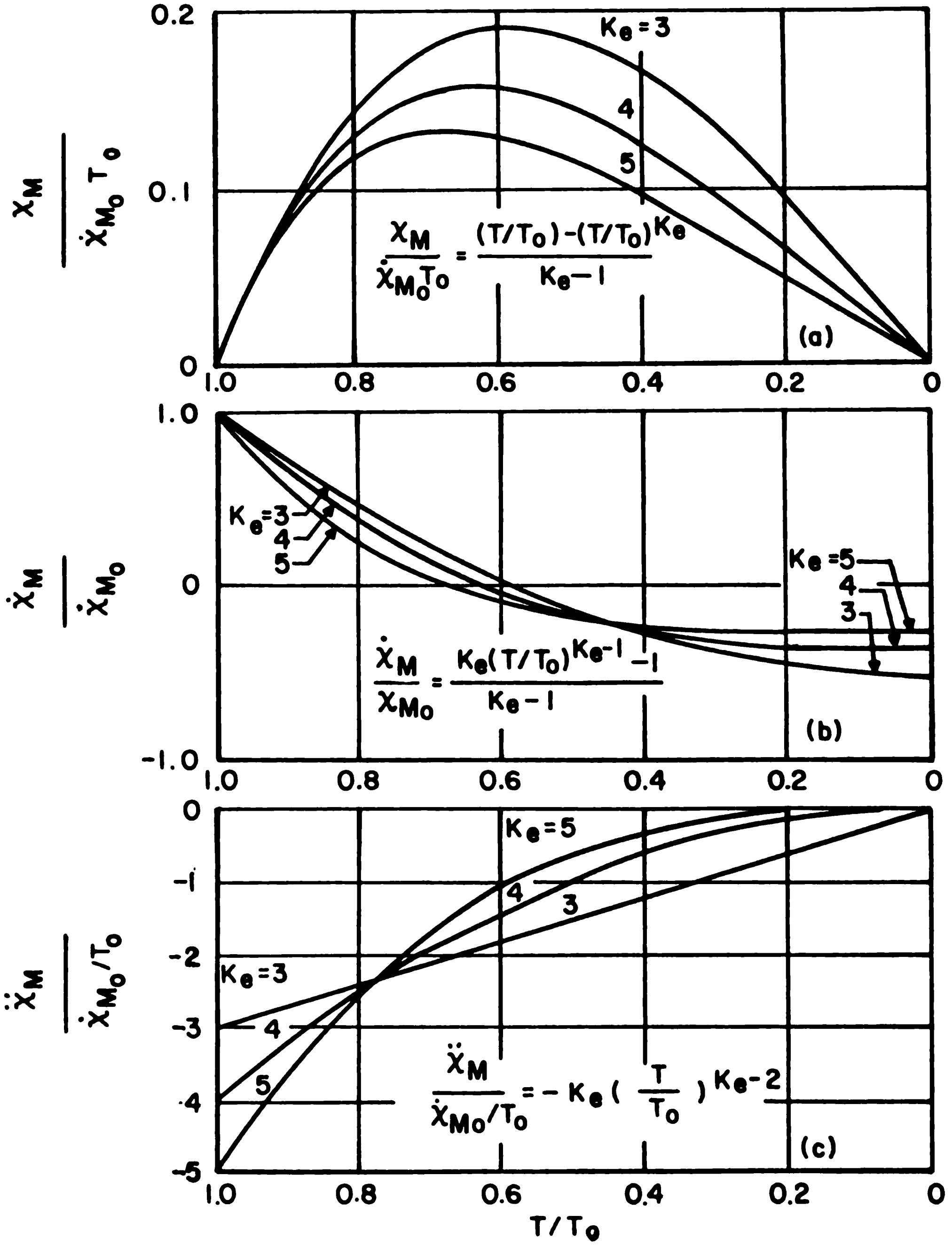

Figure 7-14. Missile Trajectories for Initial Aiming Error. (K_e = Effective Navigation Constant.) (a) Displacement; (b) Velocity; (c) Acceleration. $X_T = 0$

(Adapted from reference 20.)

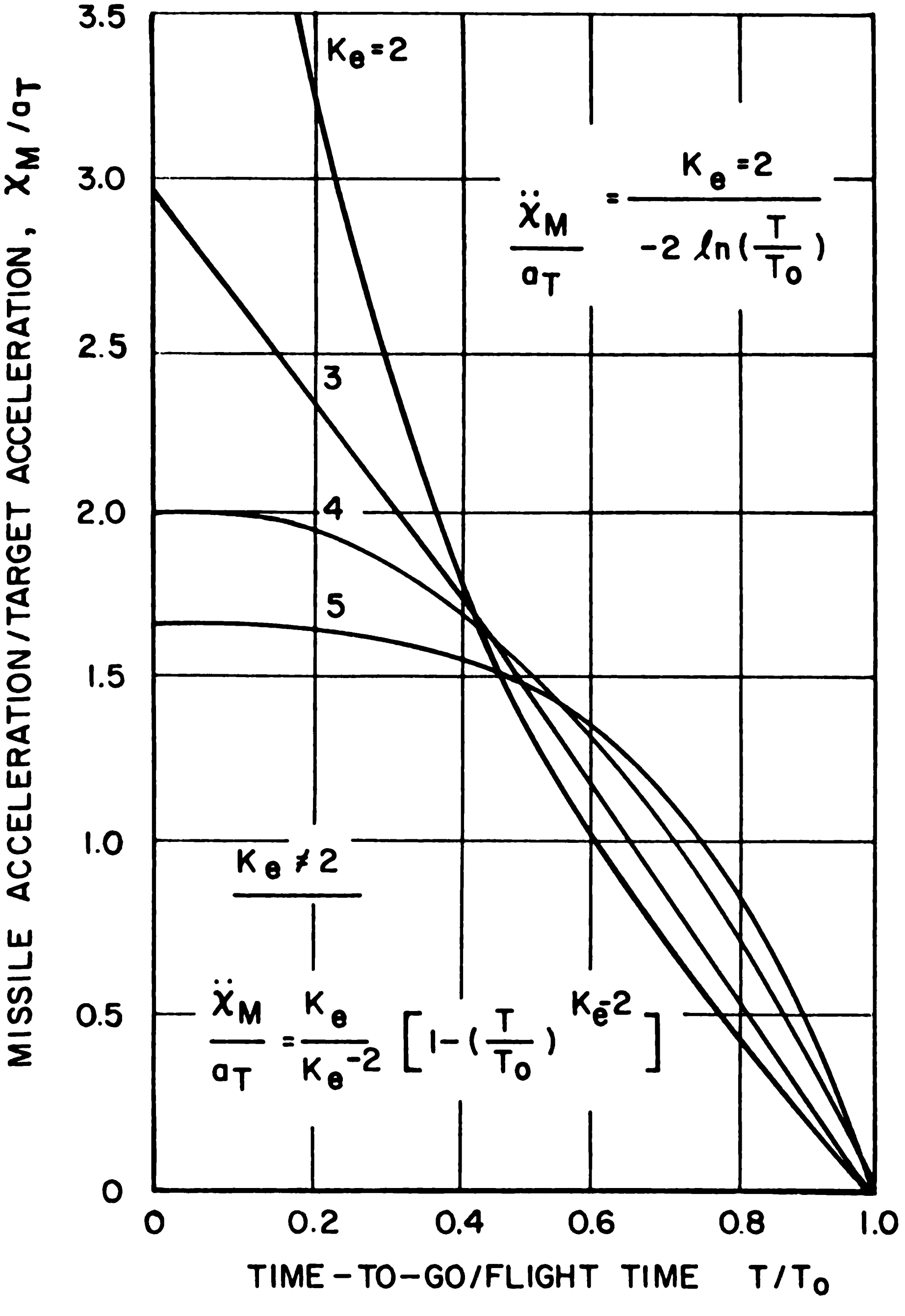

Figure 7-15. Required Missile Acceleration for Constant Target Acceleration

(Adapted from reference 20.)

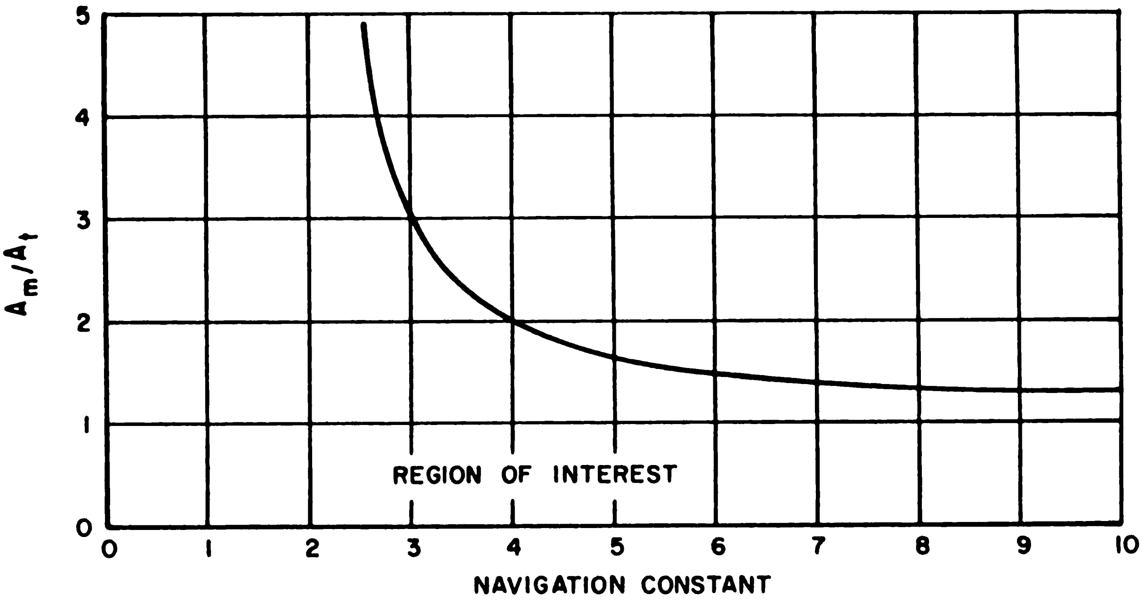

Figure 7-16. Missile Acceleration Ratios Versus Navigation Constant

TABLE 7-3. GUIDANCE MEASUREMENT REQUIREMENTS

Guidance Mode	Measured Quantities
Line-of-sight (beam rider)	Interceptor displacement from line-of-sight from ground reference point to target.
Pursuit	Angular displacement of interceptor velocity vector from line-of-sight from interceptor to target.
Modified pursuit	Angular displacement of interceptor velocity vector from pre-determined, fixed angle with respect to the line-of-sight from interceptor to target.
Constant bearing (collision)	Correct angle between line-of-sight between interceptor and target and interceptor velocity vector.
Proportional navigation	Angular rate of line-of-sight between interceptor and target.

Paragraph 6-1.6 of Chapter 6 considers this problem from the viewpoint of the fire direction and coordination problem.

7-3 GUIDANCE SERVO LOOPS

7-3.1 GENERAL

In the preceding section, parameters dictating required missile performance such as lateral acceleration and speed of response (frequency spectrum of turning rate) were obtained for several different flight paths. The physical system requires sensing the proper flight path parameter and operating on it in such a manner that the missile follows the prescribed trajectory, as outlined in paragraph 7-2.8.

Sensor characteristics are considered in later

TABLE 7-4. GUIDANCE MODE MECHANIZATION REQUIREMENTS

Guidance Mode	Command Guidance	Passive Homing	Active Homing	Semi-active Homing
Line-of-Sight	Ground Based Angle Tracker Data Link Roll Reference or Stabilizer	Not Applicable	Not Applicable	Ground Based Angle Tracker and Illuminator Missile Receiver Roll Reference or Stabilizer
Pursuit	Ground Based Radar Ground Based Computer Data Link Roll Reference or Stabilizer	Missile Seeker	Missile Radar Seeker	Ground Based Tracker and Illuminator Missile Semi-active Seeker
Modified Pursuit	Ground Based Radar Ground Based Computer Data Link Roll Reference or Stabilizer	Ground Based Radar Ground Based Computer Missile Seeker	Ground Based Radar Ground Based Computer Missile Radar Seeker	Ground Based Tracker and Illuminator Ground Based Computer Missile Semi-active Seeker
Constant Bearing	Ground Based Radar Ground Based Computer Data Link Roll Reference or Stabilizer	Missile Seeker Airborne Computer	Missile Radar Seeker, Computer Inertial Sensors (elec or electro-mech)	Ground Tracker and Illuminator Missile Semi-active Seeker and Ground Computer or A/B Computer
Proportional Navigation	Ground Based Radar Ground Based Computer Data Link Roll Reference or Stabilizer	Missile Seeker	Missile Seeker	Ground Tracker and Illuminator Missile Semi-active Seeker

tions. Here, the problem of *operating on the* oper *parameter* is discussed after illustrating e general closed loop nature of the guidance stem.

3.2 LINEAR FEEDBACK CONTROLS

It is not the purpose of this handbook to de- ive results from servo theory but rather to use hem to convey concepts useful for guidance and ontrol design. However, the remainder of this ection will summarize servo theory and outline he results obtainable with its use. References 21, 22, and 23 are recommended sources for the reader who requires more coverage than is given here.

The forces* acting upon the various components of any system and the resultant motions* of the components can be expressed as differential equations which describe the dynamic characteristics of the components. In general, the analysis problem constitutes one of determining the motion of components by solving the differential equations. Since the differential equations are usually nonlinear or have variable coefficients, much of the literature is concerned with approaches for obtaining approximate solutions by linearizing the equations or examining solutions in a period of time that is short when compared with that required for a significant change in the coefficients. The design problem, however, concerns, among other things, the specification of components that affect the differential equations in such a way that the resulting solutions have desirable properties. In either case, most problems are initially reduced to considering linear, constant coefficient, ordinary differential equations. (Exceptions may already be noted in paragraph 7-2. Another important class of exceptions is that of adaptive controllers.) When reduced to this form, a host of techniques from control system theory are available to accomplish the required modifications.

The simplest general servo is shown in Figure 7-17 where

$$C(s) = E(s)\,G(s) \qquad (7\text{-}41)$$

which is a notation indicating that the *Laplace Transform* of C is the product of the transforms of E and G.

$E(s) = R(s) - F(s)$ and:

R is the reference or command function. It is a measure of the condition desired.

C is the controlled variable. It is the actual condition which results from the command.

F is a function which is a measure of the actual condition (C), which is compared with the command (R).

E is the error resulting from this comparison. The presence of an error at (E) is an indication that the controlled variable (C) is not in correspondence with the desired command (R).

G is the forward gain function and represents the characteristics of the mechanism or process being controlled. It also includes the characteristics of that portion of the control system which

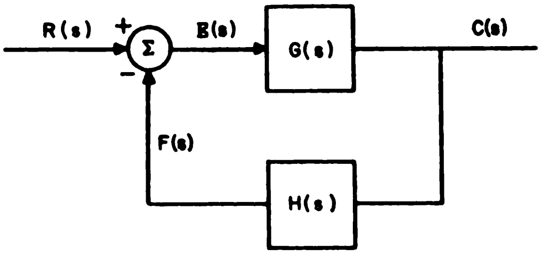

Figure 7-17. Simplified Servo Loop

---

*These are to be reviewed in a general sense. The forces include mechanical and electrical forces. Similarly, the motion may be a physical displacement or electrical quantity.

interprets the error signal and forces the controlled variable to closer correspondence with the command.

H is the feedback function and represents the characteristics of that part of the control system which measures the actual output (C), and transmits some function (F) of that output for the comparison with the command (R).

The importance of the feedback function (H) is demonstrated by manipulating equation 7-41 to obtain the output (C) as a function of the command (R).

$$C(s) = \frac{R(s)\,G(s)}{1 + G(s)\,H(s)} \qquad (7\text{-}42)$$

The closed loop transfer function is

$$\frac{C(s)}{R(s)} = \frac{G(s)}{1+G(s)\,H(s)} \qquad (7\text{-}43)$$

If the numerical gain of the open loop function is large compared to unity,

$$\left|\frac{F(s)}{E(s)}\right| = \left|G(s)\,H(s)\right| >> 1$$

then equation 7-43 becomes approximately G/GH or $1/H$. (The argument "s" is often omitted for compactness.) On the other hand, if

$$\left|\frac{F}{E}\right| << 1$$

equation 7-43 reduces to G. More detail is required if

$$\left|\frac{F}{E}\right| \cong 1$$

More particularly, considerable effort is usually devoted to finding those values of s for which $F/E = GH = -1$. Plots of such values are called root loci (the locus of roots of $1+G(s)\,H(s) = 0$) and are important in determining response and stability characteristics of closed loop systems.

7-3.3 PRIMARY GUIDANCE LOOP

The main loop of a guidance and control system is illustrated symbolically in Figures 7-17 and 7-18. The elements of Figure 7-18 are meant only to point out the major constituents of the loop. The sensing devices for instance may be carried completely within the missile or may be split between ground and airborne installations. The feedback function, $H(s)$ in Figure 7-17 and "kinematics" in Figure 7-18, is somewhat unique in that no physical equipment is involved. Rather, the kinematics is that set of relations from paragraph 7-2 that describes the flight path parameter of interest *in* terms of airframe attitude, position, etc. It is sometimes referred to as *geometry feedback* as discussed in paragraph 7-5.

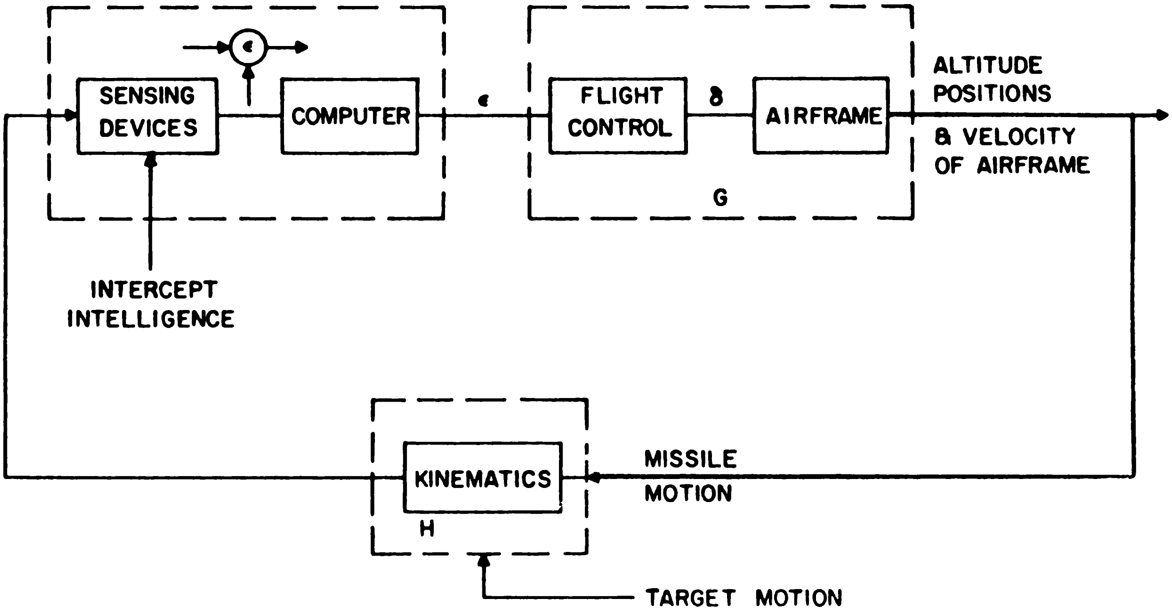

Figure 7-18. Primary Guidance Loop

An additional feature is that the computer ay not stand out as a separate element. The oming seeker usually employed with proortional navigation combines the properties of nsing and computing.

-4 FLIGHT CONTROL

-4.1 GENERAL

From the flight control standpoint, the guidance loop is considered only as a source of the ommand signal. This is labeled ε in Figure 7-18. Figure 7-19 shows a typical pitch control channel from a simple flight control system which could be a portion of the two blocks labeled *G* in Figure 7-18. Figure 7-19 is a closed loop system also.

7-4.2 SPECIAL FEATURES

In addition to controlling the airframe according to guidance loop commands, the *stability* of the responses must also be maintained. Sources of instability are divided into three classes:

(a) *static or attitude instability* – the tendency of the airframe to drift slowly from a desired attitude

(b) *dynamic or short period instability* –the tendency of the airframe to oscillate rapidly about a desired attitude

(c) *structural resonance* — the tendency of the airframe to vibrate at a frequency determined by the mass of the missile and the elastic properties of the body structure.

Thus, SAM flight control reduces to three separate, but interrelated problems:

(a) the overall guidance problem of commanding and holding an attitude or a scheduled program of attitude which will result in intercepting the target.

(b) damping out any short period oscillatory tendencies of the missile – these oscillatory tendencies may result from the aerodynamic characteristics of the flight environment or from resonances inherent in the attitude control loop.

(c) minimizing the excitation of the body bending modes of the airframe – these vibratory frequencies may be excited by aerodynamic forces at sonic and supersonic flight speeds or by the control system itself as a result of a combination of high frequency response of the control system and the improper placement of a sensor.

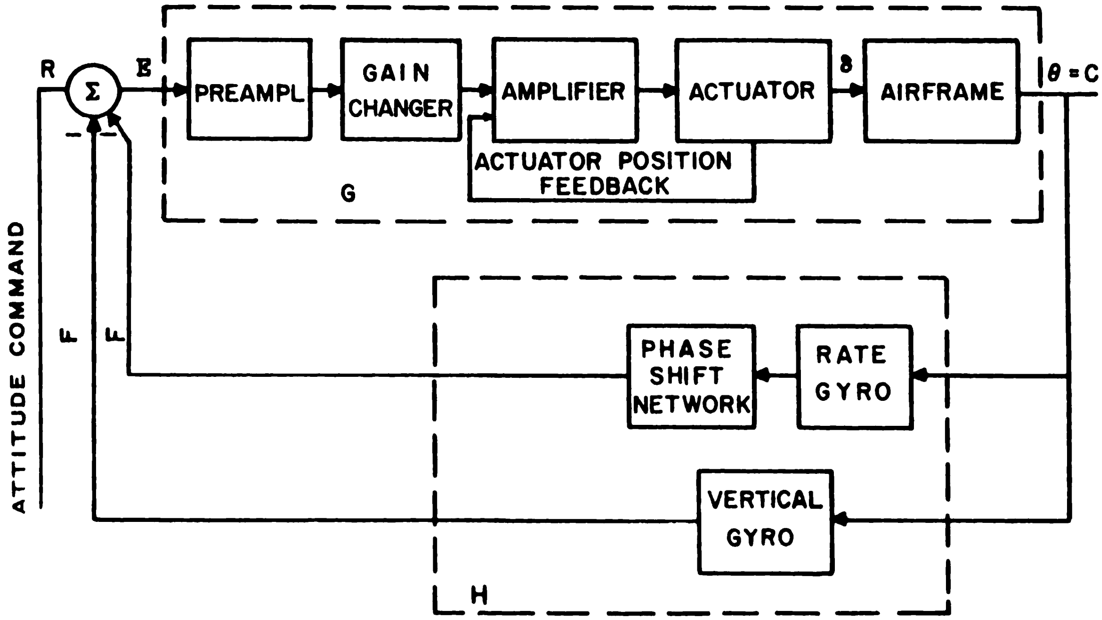

Figure 7-19. Flight Control System Pitch Channel, Block Diagram

7-4.3 AIRFRAME AS A LOOP ELEMENT[24-26]

The airframe is an excellent example of the simplification process discussed in paragraph 7-3.1. It is a complicated servo component with the result that its control characteristics change considerably during the launch, midcourse, and terminal phases of interception.[27] That is, the airframe transfer functions are generally different in each of the three flight regimes.

The differences are emphasized if the terminal phase occurs outside the significant atmosphere where aerodynamic effects are either nonexistent or negligible.

To provide effective control in these circumstances, the flight control subsystem must be capable of recognizing the changed airframe control characteristics and appropriately modifying the actuation signals supplied to it. The level of refinement for accomplishing this varies considerably and covers the range from not controlling the airframe to adaptive autopilots.*

Whether the controller continously or discretely adapts, the nature of the airframe transfer functions describe the element that must be controlled. The basis for obtaining these is outlined in following sections with some typical results. It should be noted that the coefficients (*K's* and *T's*) depend on various airframe properties as discussed in paragraphs 7-4.3.4 and 7-4.3.5.

7-4.3.1 Coordinate Systems and Nomenclature

Several coordinate systems are useful in the analysis of aircraft automatic control systems. (See references 24-26 and 32.) One is the *body axis system* shown in Figure 7-20.

---

*Although important, adaptive controllers are not considered in detail here, the essential point of any such discussion is simply that adaptive controllers extend the usefulness of simple models. Discussion and examples of adaptive controllers are contained in references 27-31.

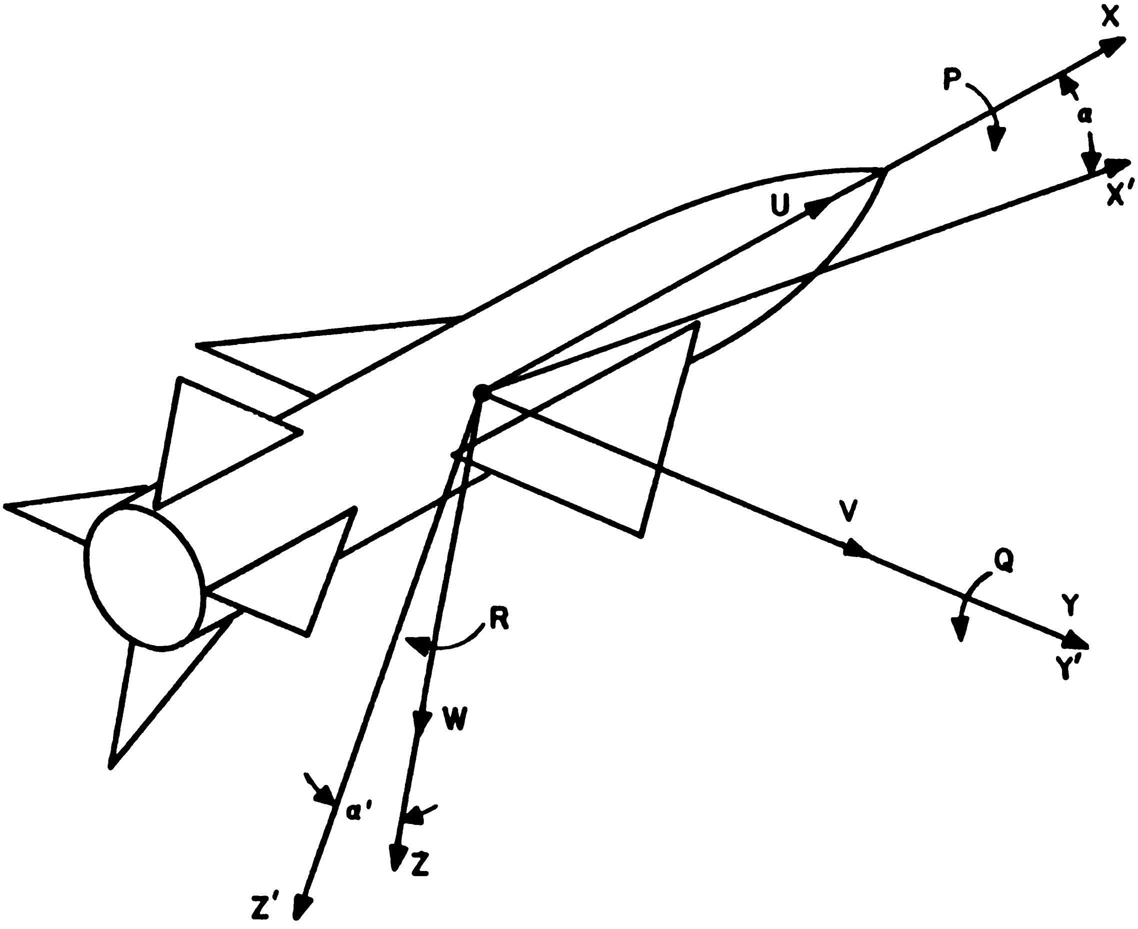

Figure 7-20. Missile Stability and Body Axes

These axes have their origin at the center of gravity of the missile and are oriented such that the X axis lies along the principal axis of the airframe, the Y axis is parallel to a line connecting wing tips, and the Z axis is perpendicular to the XY plane. In the case of a cruciform vehicle the Y and Z axis orientation is arbitrary. However, the Z axis is taken to be vertical and the Y axis horizontal when the missile is in level flight.

Another system utilizes the *stability axes.* They are usually the axes used for determining the stability characteristics of the aircraft. The set of axes to be used is a matter of preference or convenience depending on the problem involved. The stability axes differ from the body axes as shown in Figure 7-20. The X' axis is oriented along the velocity vector of the center of gravity. The Y' axis is identical with the Y axis. The angle between $X - X'$ and $Z - Z'$ is the angle of attack, α.

Since the direction of axis X' is into the relative wind, the stability axes are usually used for reference of all aerodynamic forces. Drag is considered along the negative X' axis and lift is considered along the negative Z' axis.

For the purpose of including the effects of gravity, two other angles are taken into consideration. As shown in Figure 7-21 these are the pitch angle, Θ, between the X axis and the horizontal, and the flight path angle, γ, between the X' axis and the horizontal.

Using either of these sets of axes, the motion of the airframe may be expressed in six degrees of freedom.

The nomenclature is shown in Table 7-5.

In the relatively small sample of nomenclature illustrated here there are ambiguities. Moments about the Z axis are given as N, while N is also sometimes used to represent acceleration along the Z axis or normal to the principal X axis of the aircraft. Also, Θ is used to indicate total pitch angle from the horizontal as well as pitch angle from any orientation that the X axis might have at the beginning of any specific transient.

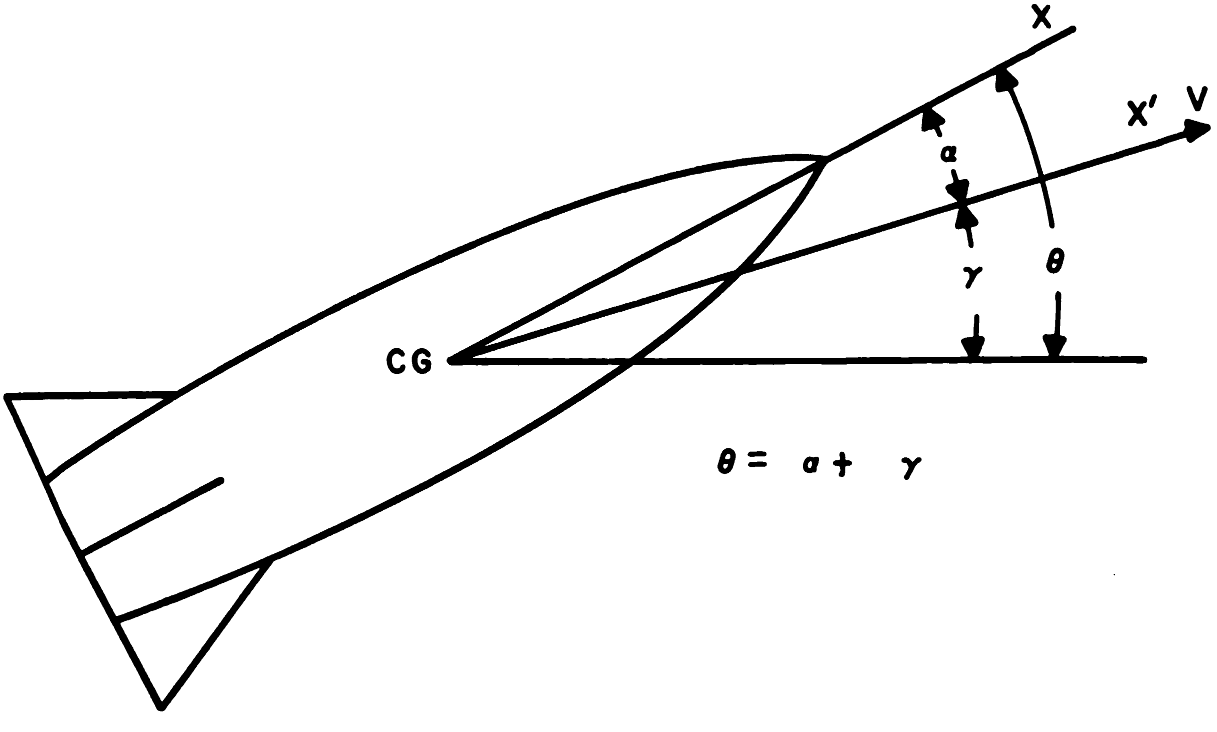

Figure 7-21. Missile Pitch Angle and Flight Path Angle

TABLE 7-5. COORDINATE SYSTEMS NOMENCLATURE

Condition	Symbol		
Linear Motion			
Axes	x	y	z
Velocity	x	y	z
	U	V	W
Acceleration	x	y	z
	U	V	W
	A		N
	Roll	Pitch	Yaw
Angular Motion About Axes			
Angle	ϕ	θ	ψ
Velocity	ϕ	θ	ψ
	P	Q	R
Acceleration	ϕ	θ	ψ
	P	Q	R
Forces	F_x	F_y	F_z
Torques or Moments About Axes	L	M	N
Moments of Inertia	I_{xx}	I_{yy}	I_{zz}
Moments of Momentum About Axes	h_x	h_y	h_z

7-4.3.2 Equations of Motion

Although a set of inertial axes may be used to express the equations of motion, the result is unduly complicated. Usually either body or stability axes are employed.

Although these references move with the missile, for flight control purposes it can be assumed that they remain stationary for an instant of time (Δ_t), during which the missile moves with respect to the stationary axes. The axes then reorient themselves with reference to the missile and another time period (Δ_t) is considered.

If these successive time periods approach zero in length, the equations which express motion with reference to inertial axes can be used instantaneously as representative of the airframe dynamics.[24]

The equations which describe the six degrees of freedom of the missile are

$$\overline{F} = \frac{d(m\overline{V})}{dt} \qquad (a)$$

$$\overline{M} = \frac{d\overline{H}}{dt} \qquad (b)$$

$$(7\text{-}44)$$

where $\overline{F}$ is the vector force acting on the airframe, $\overline{V}$ is the vector velocity, $\overline{M}$ is the moment and $\overline{H}$ the amount of momentum.

For any orthogonal set originating at the center of gravity and fixed relative to the airframe, the components of equation 7-44 become

$$
\begin{aligned}
F_x &= m(\dot{U} + QW - RV) \\
F_y &= m(\dot{V} + RU - PW) \\
F_z &= m(\dot{W} + PV - QU) \\
\mathbf{L} &= \dot{P}I_{xx} - \dot{Q}I_{xy} - \dot{R}I_{xz} + QR\ (I_{zz} - I_{yy}) \\
&\quad - PQI_{xz} - Q^2I_{zy} + R^2I_{yz} + PRI_{xy} \\
M &= \dot{Q}I_{yy} - \dot{R}I_{yz} - \dot{P}I_{xz} + PR\ (I_{xx} - I_{zz}) - \\
&\quad QRI_{xy} - R^2I_{xz} + P^2I_{xz} + PQI_{xz} \\
\mathbf{N} &= \dot{R}I_{zz} - \dot{P}I_{zy} + PQ\ (I_{yy} - I_{xx}) - PRI_{yz} \\
&\quad - P^2I_{xy} + Q^2I_{xy} + QRI_{xz}
\end{aligned}
\tag{7-45}
$$

where I_{xy}, I_{xz}, etc. are products of inertia. (Constant mass and position of c.g. have been assumed.)

The problem of obtaining transfer functions for the airframe centers about studying special cases of the set in equation 7-45 with $\overline{F}$ and $\overline{M}$ expressed in terms of thrust, gravity, and aerodynamic forces.

In winged vehicles, the *XZ* plane is one of symmetry; therefore, the terms containing the products of inertia I_{xy} and I_{xz} become zero. For cruciform missiles (symmetrical about the *X* axis) all products of inertia revert to zero when body axes are used. For most winged vehicles, the product of inertia term I_{xz} is small enough to be neglected when body axes are used. When stability axes are used and small angles of attack are considered, all products of inertia can be neglected. When large angles of attack are considered, the term I_{xz} cannot be neglected for winged vehicles whose slip angles are small. (The slip angle is the angle between the *X* axis and the projection of *V* on the yaw plane.) If the slip angle is large, I_{xy} and I_{yz} must also be considered for accurate analysis.

The differences just referred to between winged and cruciform airframes result from the method of making horizontal turns. The method of making such a turn by a winged vehicle is to roll and pitch. If a properly coordinated turn is made (no slip or skid) there is no rotation about the *Z* axis. The turning results from rotation in the pitch plane, around the *Y* axis, which assumes an angle ϕ with the horizontal because of roll. The only angle of attack is in the *XZ* plane.

Although a cruciform missile could make a horizontal turn maneuver in the same manner, it is usually more efficient to rotate the missile about the *Z* axis. This maneuver results in a lateral attack angle, ψ, which is the yaw angle when referenced to the flight path vector X'. If both the attack angle α and the yaw angle (lateral attack angle) become large, all products of inertia should be considered. Inertial coupling between rotational motion around each axis becomes significant to the stabilization of the missile.

Fortunately for most applications, attack angles are small and for an initial approximation all inertial coupling is ignored. For further simplification, the principal of superposition is assumed and each axis is treated separately for initial approximate calculations or simulations.

Whatever degree of complexity one uses in expressing the motion of the airframe, when the summation equations of forces and moments are written, the external forces acting upon the aircraft are thrust, gravity and the aerodynamic forces.

7-4.3.3 Launch Phase Models

The launch or boost phase presents the most challenging control problem since the mass, speed, dynamic pressure, and other airframe characteristics related to control change most drastically.

Linearized models of the airframe have been developed for this phase from several viewpoints. If no control is exerted during the boost phase, dispersion estimates can be obtained under the assumption of constant mass and average aerodynamic characteristics as discussed in references 26 and 33. The effects of pointing errors, initial yaw, gravity, initial angular velocity, thrust misalignment, wind, fin misalignment, and slow spin are included in a treatment of the motion during burning.

The problem of exerting control during this phase has recently been approached from the point of view of adaptive controllers.[27,34]

7-4.3.4 Low Dynamic Pressure Models

If the airframe parameters are relatively constant, the analysis problem is greatly simplified when aerodynamic forces are negligible. This is generally the case for extra-atmospheric flight. The same approach also yields approximate results for some period immediately after launch. In the absence of aerodynamic forces, however, control forces and moments must be obtained by thrust control.

The linear acceleration of the airframe is: $\bar{a} = \frac{\bar{T}}{m} + \bar{g}$ where $\bar{T}$ is the thrust vector and m is the mass. Although $\bar{T}$ is shown in Figure 7-22 as passing through the center of gravity along the X axis, a significant perturbation may result from thrust misalignment. This occurs when $\bar{T}$ is either non-collinear with X or, does not pass through the center of gravity, or both.

Figure 7-22 shows the accelerations of a missile outside the atmosphere. Assuming that the XZ plane is kept vertical, and thrust is perfectly aligned, the equations are as follows:

$$a_h = \frac{T}{m} \cos \Theta \qquad \text{(a)}$$

$$a_v = \frac{T}{m} \sin \Theta - g \qquad \text{(b)}$$

(7-46)

where a_h and a_v are the horizontal and vertical components of missile acceleration with reference to earth coordinates.

When control forces are considered, thrust misalignment must be accounted for. The angular acceleration of the airframe is best defined in terms of its components as indicated in Figure 7-23.

Control about the X (roll) axis is usually accomplished by varying thrust devices differentially and obtaining a couple about the X axis.

The area of extra-atmospheric control reduces to applying forces to a free body, observing the body's motion and varying the direction and/or magnitude of the forces until the desired missile attitude is obtained.

For linearized models the control moment is expressed as a linear function of a control deflection, δ_e:

$$M = K_M \delta_e \qquad (7\text{-}47)$$

For the pitch axis

$$M = I_{yy} \dot{Q} = K_{M_\Theta} \delta_e \qquad (7\text{-}48)$$

Defining M_{δ_e} by

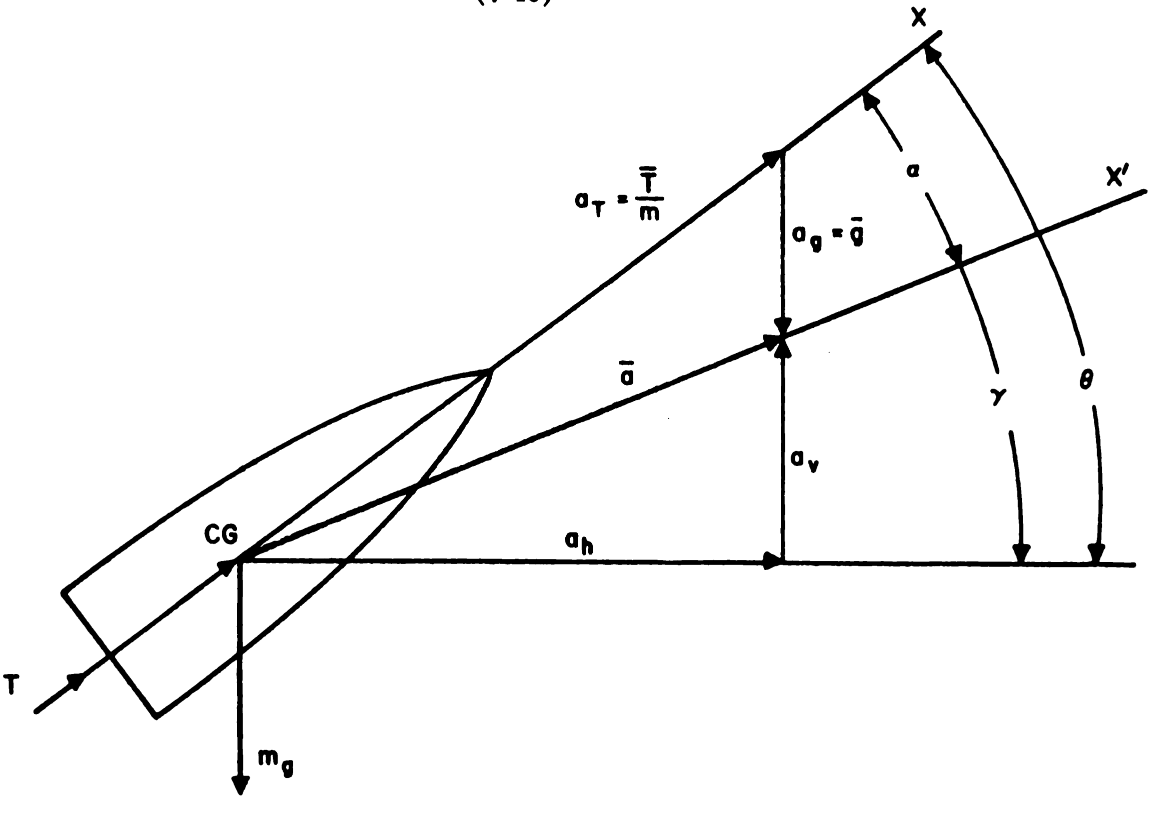

Figure 7-22. Missile Acceleration Outside the Atmosphere

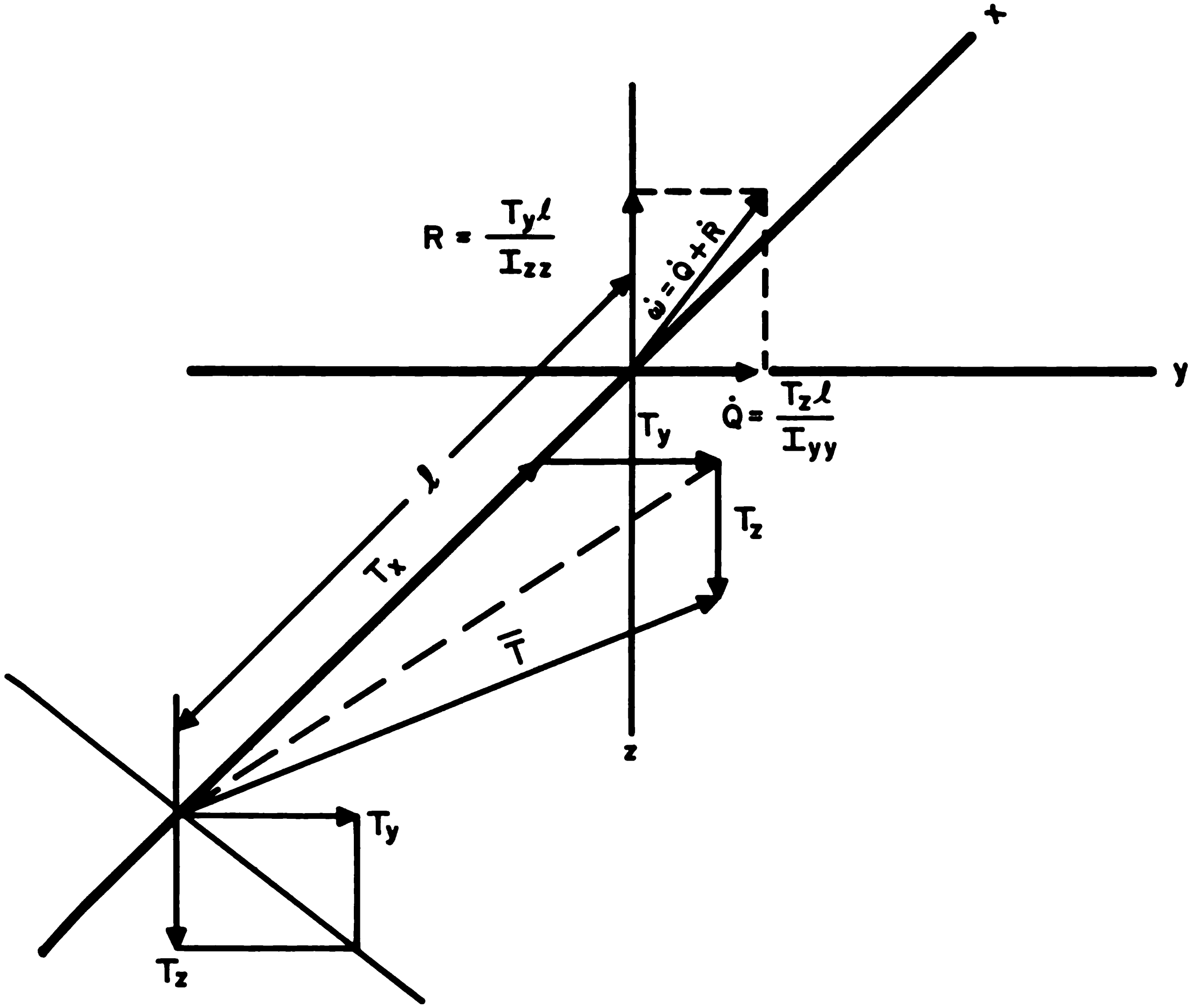
+
$R = \frac{T_y l}{I_{zz}}$
$\dot{\omega} = \dot{Q} + \dot{R}$
y
T_y
$\dot{Q} = \frac{T_z l}{I_{yy}}$
T_z
l
T_x
$\bar{T}$
z
T_y
T_z

Figure 7-23. Missile Angular Acceleration, $\dot{\omega}$

$$M_{\delta_e} = \frac{K_{M_\theta}}{I_{yy}} \tag{7-49}$$

provides

$$\dot{Q} = M_{\delta_e} \delta_e \tag{7-50}$$

K_{M_θ} is a torque coefficient containing the magnitude of the control force and related geometry. It is usually written as M_{δ_e} and is defined as the moment per unit deflection. In some cases M_{δ_e} is considered to contain the moment of inertia I_{yy} and, although equation 7-50 is actually an acceleration equation, it is still referred to as the moment equation. That is,

$$\dot{Q} = \ddot{\Theta}, \text{ and } \ddot{\Theta} = M_{\delta_e} \delta_e \tag{7-51}$$

This can be written as a transfer function in terms of the Laplace Transform parameter as

$$\frac{\Theta(S)}{\delta_e(S)} = \frac{M_{\delta_e}}{S^2} \tag{7-52}$$

and can be represented as shown in Figure 7-24. Figure 7-24 shows the block representing the airframe pitch response to a control deflection.

If a control loop using two sensors, one measuring pitch attitude, Θ, and the other pitch velocity $\dot{\Theta}$, is closed around the block, Figure 7-25 results.

Assuming that the flight control amplifier and actuator can be represented by the numerical gain, *K*, the forward function becomes

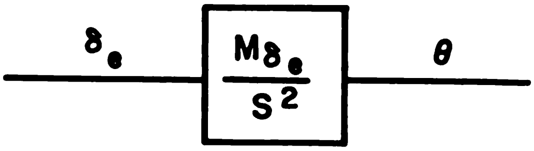

Figure 7-24. Airframe Pitch Response to Deflection of Control Surfaces — Low Dynamic Pressure

$$GH = \left(\frac{KM_{\delta_e}}{S^2}\right) H = \left(\frac{KM_{\delta_e}}{S^2}\right)(K_1 + K_2S) \qquad (7\text{-}53)$$

The closed loop transfer function is

$$\frac{\Theta(s)}{R(s)} = \frac{G(s)}{1 + C(s)\,H(s)}$$

$$= \frac{(1/K_1)\,(K\,M_{\delta_e}K_1)}{S^2 + K\,M_{\delta_e}K_2\,S + KM_{\delta_e}K_1} \qquad (7\text{-}54)$$

Equation 7-54 is well-known in servo theory as a *quadratic transfer function.* It is usually exhibited in standard form as

$$\frac{\Theta(s)}{R(s)} = \frac{G_o\omega_n^2}{S^2 + 2\xi\omega_n S + \omega_n^2} \qquad (7\text{-}55)$$

where ξ is the damping factor and ω_n the *natural* frequency. For equation 7-54, $\omega_n^2 = K\,M_{\delta_e}K_1$ and $2\xi\omega_n = K\,K_2\,M_{\delta_e}$. Since three parameters, *K*, K_1, K_2 can be adjusted in Figure 7-25, the three characteristics G_o, ξ, ω_n of equation 7-55 can be made to have desirable properties.

A simplified three dimensional model is obtained by writing similar equations for the remaining two axes. The equations of motion about the *X* and *Z* axes are similar, except for the magnitude of moments. With the absence of aerodynamic forces, control difficulties are

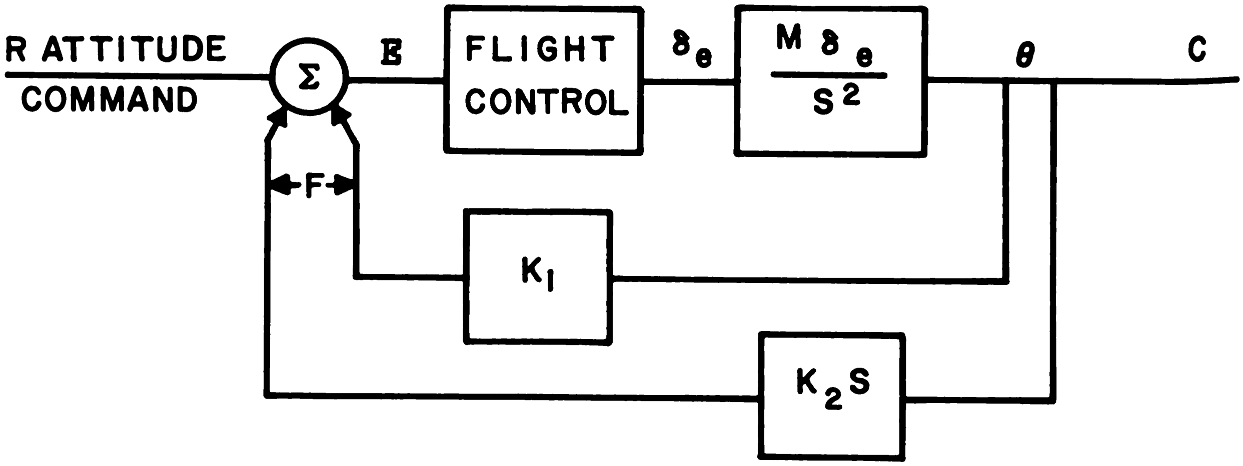

Figure 7-25. Attitude Controller — Low Dynamic Pressure

educed to those of mechanization and enironment.

7-4.3.5 Aerodynamic Forces

The flight control equations for flight outside the atmosphere have been given for the pitch axis in equations 7-46 and 7-54. When flight within the atmosphere is considered, these equations are complicated by aerodynamic forces (see Figure 7-26). The linear motion equation becomes

$$a_h = \frac{T}{m}\cos\Theta - \frac{L}{m}\sin\gamma - \frac{D}{m}\cos\gamma \qquad \text{(a)}$$

$$a_v = \frac{T}{m}\sin\Theta + \frac{L}{m}\cos\gamma - \frac{D}{m}\sin\gamma - g \qquad \text{(b)}$$

$$\text{(7-56)}$$

Without the aerodynamic forces, the accelerations, both horizontal and vertical, remain constant for any given thrust, weight, and attitude angle. As long as thrust is greater than weight, the speed increases continuously regardless of attitude. With aerodynamic forces, for any given thrust and weight, each attitude angle has a terminal speed associated with it due to drag forces which increase with speed. The flight path angle also changes with each change of attitude.

In the aerodynamic case, the total applied (external) forces and moments are usually approximated by a linear combination of effects of several variables. The pitch moment, for instance, from equation 7-45 becomes

$$M = \dot{Q}I_{yy} - \dot{R}I_{yz} - \text{- - -} + PQI_{xz} = M_{\delta_e}\delta_e + M_{\dot{\delta}_e}\dot{\delta}_e + M_a\alpha + M_{\dot{a}}\alpha + M_{\dot{\theta}}\dot{\Theta}, \text{ etc.} \qquad \text{(7-57)}$$

Each separate term M contains the characteristics of that function of the aircraft to which it applies. For instance

$$M_a = (C_{M_a})\,(qSC) \qquad \text{(7-58)}$$

where

q is the dynamic pressure, $q = \frac{1}{2}\rho U^2$

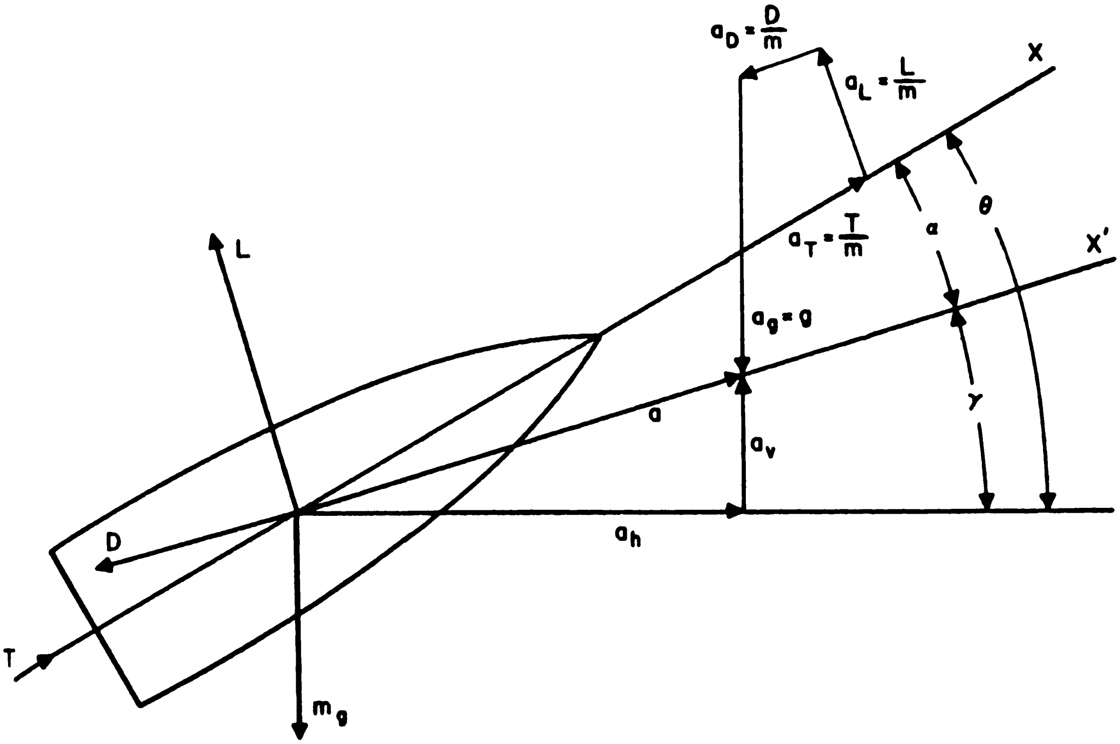

Figure 7-26. Effect of Aerodynamic Forces Upon Missile Axes Within the Atmosphere

U = relative wind speed

ρ = air density

s is the reference area (usually wing)

c is the reference distance (usually the mean aerodynamic chord of the wing)

C_{M_α} is an aerodynamic moment coefficient which may be derived analytically or empirically in a wind tunnel. M_α and C_{M_α} vary with α and are considered linear for small angles of attack.

At subsonic speeds the stability derivatives are a function of q and are approximately proportional to U^2.

At transonic and supersonic speeds, the aerodynamic forces which act on the airframe are more a function of airframe configuration than of velocity. The rate of change of any of the aerodynamic constants may vary widely and sometimes erratically as a function of velocity, depending on airframe configuration.

Similar expressions are obtained for the remaining equations in 7-45. The above expressions are linear in the various deflections and velocities. However, this is only an approximation which may be viewed as the result of retaining only the linear terms of a Taylor series expansion for the forces and moments. (See references 24-26 and 35.)

7-4.3.6 High Dynamic Pressure Models

When the midcourse and terminal phases occur within the significant atmosphere, the control problem is usually characterized by reasonably constant airframe parameters and dynamic pressure. With appropriate assumptions concerning the airframe and the motion involved, equation 7-45 can be reduced to separate sets of equations. The various special cases are usually referred to as the longitudinal and lateral modes.[24-26]

LONGITUDINAL MODE TRANSFER FUNCTIONS

The most often used results for the longitudinal mode result from reducing equation 7-45 to

$$F_z = m\,(\dot{W} - QU) \qquad \text{(a)}$$

$$M = \dot{Q}\, I_{yy} \qquad \text{(b)}$$

$$\text{(7-59)}$$

and introducing the aerodynamic forces. While this may seem to be a drastic reduction, useful engineering results have been obtained by this approach. The two-degree-of-freedom approximations presented above may be appreciated better if results of less drastic assumptions are examined first. The three-degree-of-freedom description uses equation 7-59 but in addition admits to changes in the forward speed, U. That is, the set

$$F_x = m\dot{U} \qquad \text{(a)}$$

$$F_z = m(\dot{W} - QU) \qquad \text{(b)} \qquad \text{(7-60)}$$

$$M = \dot{Q}(I_{yy}) \qquad \text{(c)}$$

is considered and perturbations from a nominal condition are studied. In terms of Figure 7-26, the transfer functions obtained from equation 7-60 are

$$\frac{u(s)}{\delta_c(s)} = \frac{K_u\,(T_1 S + 1)\,(T_2 S + 1)}{\Delta(s)} \qquad \text{(a)}$$

$$\frac{\alpha(s)}{\delta_c(s)} = \frac{K_\alpha\,(T_3 S + 1)\left(\frac{S^2}{\omega_4^2} + \frac{2\xi_4}{\omega_4} S + 1\right)}{\Delta(s)} \qquad \text{(b)}$$

$$\frac{\Theta(s)}{\delta_e(s)} = \frac{K_\Theta\,(T_5 S + 1)\,(T_6 S + 1)}{\Delta(s)} \qquad \text{(c)}$$

$$\Delta(s) = \left(\frac{S^2}{\omega_p^2} + \frac{2\xi_p}{\omega_p} S + 1\right)\left(\frac{S^2}{\omega_{sp}^2} + \frac{2\xi_{sp}}{\omega_{sp}} S + 1\right) \qquad \text{(d)}$$

$$\text{(7-61)}$$

Gravity effects are not included; u, α, Θ are the changes from nominal. The gains, time constants, damping factors and natural frequencies in these expressions are complicated functions of speed, air density, and airframe control parameters as indicated in the discussion of equation 7-58. The quantities needed to compute them for any given airframe may be estimated from Chapter 14 (Airframes) and references 25 and 26.

A transfer function for γ can be obtained from equation 7-61 by noting that $\Theta = \alpha + \gamma$.

In equation 7-61, ω_p is the natural frequency of the phugoid oscillation and ω_{sp} is that of the short period oscillation. The phugoid oscillation is a slow oscillation between altitude and forward speed. Representative values from the literature are

$\omega_{sp} \sim 10$ rad/sec
$\xi_{sp} \sim 0.25$ 1/sec
$\omega_p \sim 0.05$ rad/sec
$\xi_p \sim 0.05$ 1/sec

(Large deviations from these figures may occur. The damping factor may be negative or greater than unity in some cases.)

The significance of these results in terms of the two-degree-of-freedom approximation becomes clear if the time characteristics of the three-degree-of-freedom transient response are examined. The general nature of terms in the transient response is that of decaying oscillations.

The time required for the amplitude to decrease to half its initial value is

$$T_{1/2} = \frac{0.693}{\xi\,\omega_n}\ \text{sec} \qquad (7\text{-}62)$$

while the time for one oscillation is

$$P = \frac{2\pi}{\omega_n\sqrt{1-\xi^2}}\ \text{sec} \qquad (7\text{-}63)$$

The short period and phugoid characteristics for the representative data given above are summarized in Table 7-6.

TABLE 7-6. SUMMARY OF THREE-DEGREE-OF-FREEDOM TRANSIENT RESPONSE PROPERTIES

Mode	ω_n rad/sec	ξ	$T_{1/2}$ sec	P sec
Phugoid	0.05	0.05	280	126
Short Period	10	0.25	0.28	0.65

Thus, the short period transient is essentially completed before the phugoid terms have started to be significant. Actually, the transfer functions presented in this section are valid (in many SAM applications) for a period of time much less than those associated with typical phugoid modes.

The two-degree-of-freedom analysis provides simpler expressions which, for preliminary design purposes, can usually be approximated by

$$\frac{\alpha}{\delta} = \frac{K_{\alpha_1}}{\dfrac{S^2}{\omega_{sp}^2} + \dfrac{2\xi_{sp}}{\omega_{sp}}S + 1} \qquad \text{(a)}$$

$$\frac{\Theta}{\delta} = \frac{K_{\Theta_1}(T_6 S + 1)}{S\left(\dfrac{S^2}{\omega_{sp}^2} + \dfrac{2\xi_{sp}}{\omega_{sp}}S + 1\right)} \qquad \text{(b)}$$

$$\frac{\gamma}{\delta} = \frac{K_{\Theta_1}}{S\left(\dfrac{S^2}{\omega_{sp}^2} + \dfrac{2\xi_{sp}}{\omega_{sp}}S + 1\right)} \qquad \text{(c)}$$

(7-64)

where the relationship $\Theta = \alpha + \gamma$ has been used to obtain equation 7-46c. Representative values for T_6 are in the range of 1 to 10 seconds.

LATERAL DYNAMICS

The transfer functions of the lateral mode require the use of all six equations of motion. These, when simplified will yield two sets of transfer functions. One set gives side slip angle β, roll angle ϕ, and yaw angle ψ in terms of rudder deflection δ_R. The other set gives the same three angles in terms of aileron deflection δ_a.

$$\frac{\beta}{\delta_R} = \frac{K_{\beta R}(T_1 S - 1)(T_2 S + 1)(T_3 S + 1)}{(T_4 S + 1)(T_5 S + 1)\left(\dfrac{S^2}{\omega_D^2} + \dfrac{2\xi_D}{\omega_D}S + 1\right)}$$

(7-65)

(a)

$$\frac{\phi}{\delta_R} = \frac{K_{\phi R}(T_6 S - 1)(T_7 S + 1)}{(T_4 S - 1)(T_5 S + 1)\left(\dfrac{S^2}{\omega_D^2} + \dfrac{2\xi_D}{\omega_D}S + 1\right)}$$

(b)

$$\frac{\psi}{\delta_R} = \frac{K_{\psi R}\,(T_8 S + 1)\left(\frac{S^2}{\omega_1^2} + \frac{2\xi_1}{\omega_1} S + 1\right)}{S\,(T_4 S - 1)\,(T_5 S + 1)\left(\frac{S^2}{\omega_D^2} + \frac{2\xi_D}{\omega_D} S + 1\right)} \qquad \text{(c)}$$

$$\frac{\beta}{\delta_a} = \frac{K_{\beta a}\,(T_9 S - 1)\,(T_{10} S + 1)}{(T_4 S - 1)\,(T_5 S + 1)\left(\frac{S^2}{\omega_D^2} + \frac{2\xi_D}{\omega_D} S + 1\right)} \qquad \text{(7-66) (a)}$$

$$\frac{\phi}{\delta_a} = \frac{K_{\phi a}\left(\frac{S^2}{\omega_2^2} + \frac{2\xi_2}{\omega_2} S + 1\right)}{(T_4 S - 1)\,(T_5 S + 1)\left(\frac{S^2}{\omega_D^2} + \frac{2\xi_D}{\omega_D} S + 1\right)} \qquad \text{(b)}$$

$$\frac{\psi}{\delta_a} = \frac{K_{\psi a}\,(T_{11} S + 1)\left(\frac{S^2}{\omega_1^2} + \frac{2\xi_1}{\omega_1} S + 1\right)}{S\,(T_4 S - 1)\,(T_5 S + 1)\left(\frac{S^2}{\omega_D^2} + \frac{2\xi_D}{\omega_D} S + 1\right)} \qquad \text{(c)}$$

(The time constants T_1, T_2, T_3 . . . T_6 in these equations are not the same as those so numbered in the pitch equations.)

The denominators of all six of these transfer functions have three factors in common: ω_D the dutch roll frequency, T_5 the roll time constant, and T_4 the spiral divergence time constant.

Generally, all three transfer functions in a set must be taken into consideration when either yaw or pitch deflections are considered.

The factor containing T_4 indicates a positive real root which yields instability. This term represents the missile's tendency to spin if uncontrolled, thus the name, *spiral divergence.*

The time constant T_4 is very large in comparison to the time constant in the other factors. As a result, a control loop that will control the dutch roll mode will include control of spiral divergence. This factor can therefore be ignored to simpify the transfer function.

The *dutch roll mode* is a wobulating oscillation, that is: the excursions in roll and yaw are 90° apart in time so that the wing tip traces an approximate ellipse about the *y* axis. If for either set of equations, the oscillations in one plane can be damped out, the oscillations in the other plane are automatically damped proportionally. For control stabilization, each set can be represented by one equation.

$$\frac{\psi}{\delta_R} = \frac{K_{\psi R}\,(T_8 S + 1)\left(\frac{S^2}{\omega_1^2} + \frac{2\xi_1}{\omega_1} S + 1\right)}{S\,(T_4 S - 1)\,(T_5 S + 1)\left(\frac{S^2}{\omega_D^2} + \frac{2\xi_D}{\omega_D} S + 1\right)} \qquad \text{(7-67) (a)}$$

$$\frac{\phi}{\delta_a} = \frac{K_{\phi a}\left(\frac{S^2}{\omega_2^2} + \frac{2\xi_2}{\omega_2} S + 1\right)}{(T_4 S - 1)\,(T_5 S + 1)\left(\frac{S^2}{\omega_D^2} + \frac{2\xi_D}{\omega_D} S + 1\right)} \qquad \text{(b)}$$

To simplify these equations, the same method as was used in the pitch case can be used here. Only those acceleration equations which apply in the plane being considered will be used in the derivation.

For the yaw plane, the equations for yaw accelerations and sideslip acceleration will be used, and for roll, roll acceleration will be used. The resulting transfer functions are:

$$\frac{\psi}{\delta_R} = \frac{K_{\psi R1}}{S\left(\frac{S^2}{\omega_D^2} + \frac{2\xi_D}{\omega_D} S + 1\right)} \qquad \text{(a)} \quad \text{(7-68)}$$

$$\frac{\phi}{\delta_a} = \frac{K_{\phi a1}}{S\,(T_\phi S + 1)} \qquad \text{(b)}$$

These simplified transfer functions are sufficient in most cases for control analysis and ulation work. However, the aerodynamicist st in all cases assess the entire situation and ertain whether the approximations can be d.

n *the case of cruciform airframe configura- n, the aerodynamic situation in yaw is the me as in pitch.* The control transfer functions out the three axes are as follows:

$$\frac{\Theta}{\delta_e} = \frac{K_{\Theta e}\,(T_\Theta S+1)}{S\left(\frac{S^2}{\omega_{sp}^2}+\frac{2\xi_{sp}}{\omega_{sp}}S+1\right)} \qquad \text{(a)}$$

$$\frac{\psi}{\delta_R} = \frac{K_{\phi R}\,(T_\psi S+1)}{S\left(\frac{S^2}{\omega_{sp}^2}+\frac{2\xi_{sp}}{\omega_{sp}}S+1\right)} \qquad \text{(b)}$$

$$\frac{\phi}{\delta_a} = \frac{K_{\phi a}}{S\,(T_\phi S+1)} \qquad \text{(c)} \qquad \text{(7-69)}$$

Although, $\frac{\Theta}{\delta_e}$ and $\frac{\psi}{\delta_R}$ are identical in form, the constants are different since gravity must be considered when obtaining $\frac{\Theta}{\delta_c}$.

Flight control intelligence can be less complicated for the cruciform configuration since it does not have to roll to turn. A turn command may be fed to the flight control system as a yaw command.

7-4.4 CLOSED LOOP AIRFRAME CONTROL — AUTOPILOTS

7-4.4.1 General

The general problems of flight control were discussed in paragraph 7-4.1 before models of the airframe were available and again, briefly, in paragraph 7-4.3.4, where aerodynamic forces were considered negligible. The same approach can be used when aerodynamic forces are significant but the transfer functions of the airframe are different.

7-4.4.2 Attitude Control

Using the short period longitudinal transfer functions given in equation 7-64, the simple control loop used in the extra atmospheric case, Figure 7-25, becomes Figure 7-27. While not

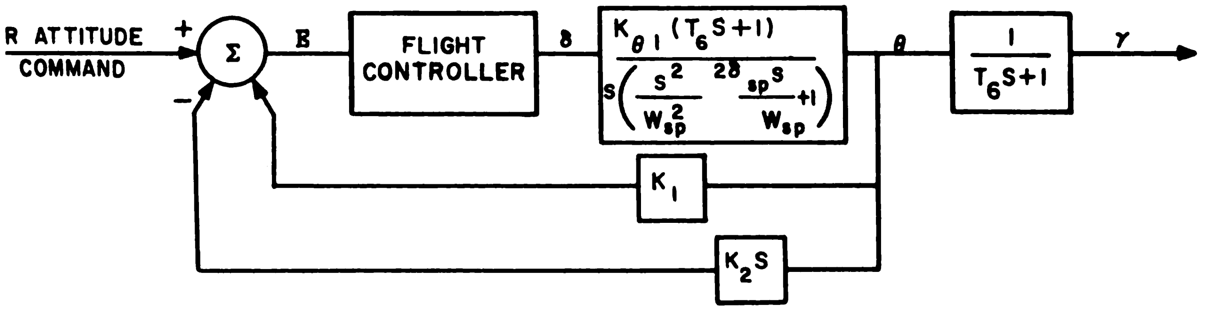
R ATTITUDE COMMAND
+
−
Σ
E
FLIGHT CONTROLLER
δ
$\frac{K_{\theta 1}(T_6S+1)}{S\left(\frac{S^2}{W_{sp}^2}\ \frac{2\delta_{sp}S}{W_{sp}}+1\right)}$
θ
$\frac{1}{T_6S+1}$
γ
K_1
K_2S

$$G = \frac{K K_{\theta 1}\,(T_6 s+1)}{s\left(\frac{s^2}{W_{sp}^2}+\frac{2\delta_{sp}s}{W_{sp}}+1\right)}$$

$$H = K_1\left(\frac{K_2}{K_1}S+1\right)$$

Figure 7-27. Airframe Attitude Control Within the Atmosphere

shown explicitly in Figure 7-24, control of α is implied by Θ control. The required relation, $\frac{\alpha}{\Theta}$, is easily obtained from equation 7-64a and b.

The transfer function between Θ and the commanded attitude R is

$$\frac{\Theta}{R} = \frac{G}{1 + GH} = \frac{K K_{\Theta 1} \; (T_6 S + 1)}{S \left(\frac{S^2}{\omega_{sp}{}^2} + \frac{2\xi_{sp}}{\omega_{sp}} S + 1 \right) + K K_{\Theta 1} \; K_1 \; (T_6 S + 1) \left(\frac{K_2}{K_1} \; S + 1 \right)} \qquad (7\text{-}70)$$

If the loop gain, $K K_{\Theta 1} K_1$ is large compared to unity, and if the product $\left(\frac{K_2}{K_1}\right) T_6$ is at least equal to $1/\omega_{sp}{}^2$, the transfer function can be approximated by

$$\frac{\Theta}{R} \simeq \frac{1}{H} = \frac{1/K_1}{\left(\frac{K_2}{K_1} S + 1 \right)} = \frac{1/K_1}{T_F S + 1} \qquad (7\text{-}71)$$

This is evident if the system root locus is plotted as shown in Figure 7-28.* As the gain is increased, the three open loop poles move as indicated by the arrows and the dominant pole (the one farthest in the positive real direction) approaches $\frac{-1}{T_F}$. The two complex roots become real. One has a large negative real value which provides a rapid decay transient while the other approximately cancels the numerator factor $(T_6 \delta + 1)$.

The desirability of operating with high loop gain deserves some consideration. During the

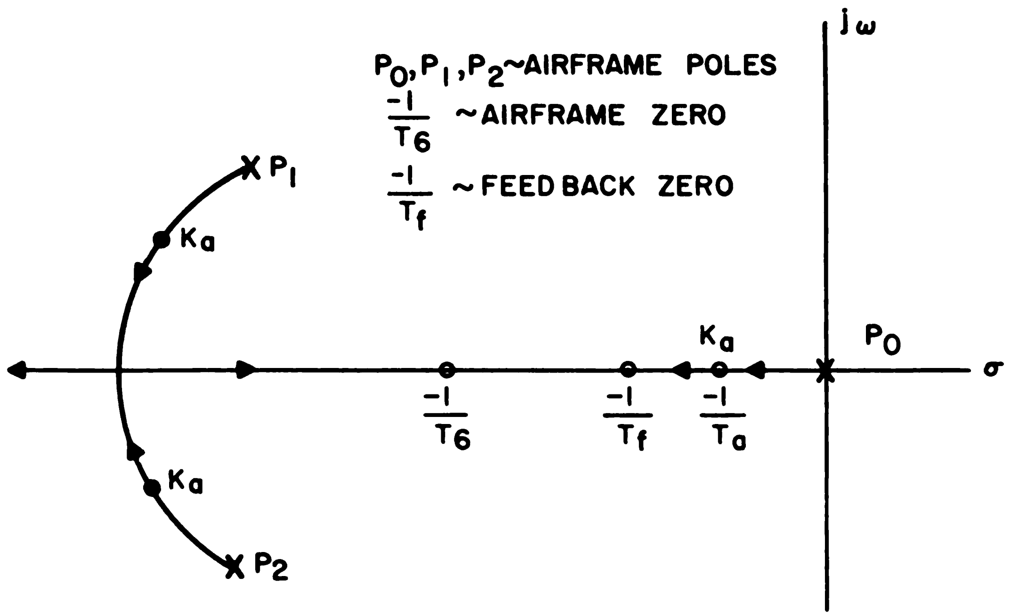

jω
P_0, P_1, P_2 ~AIRFRAME POLES
$\frac{-1}{T6}$ ~AIRFRAME ZERO
$\frac{-1}{T_f}$ ~FEED BACK ZERO
P_1
K_a
K_a
P_0
σ
$\frac{-1}{T6}$
$\frac{-1}{T_f}$
$\frac{-1}{T_a}$
K_a
P_2

Figure 7-28. Flight Control System Root Locus

midcourse phase when usually relatively small maneuvers are required, it is reasonable to assume quite small values for α. Under these conditions, $\Theta \simeq \gamma$ and attitude control provides sufficient path angle control with the result that the approximation given by equation 7-71 is reasonable. For terminal guidance, however, where significant attack angles are needed to provide maneuvers, and time lags are important, the gain approximation leads to

---

*All root locus plots in this chapter have no particular scale.

$$\frac{\gamma}{R} = \left(\frac{\Theta}{R}\right)\left(\frac{\gamma}{\Theta}\right) \cong \frac{1/K_1}{(T_F S + 1)} \cdot \frac{1}{(T_\theta S + 1)} \qquad (7\text{-}72)$$

As shown in Figure 7-28, $T_F > T_\theta$ so that equation 7-72 indicates quite sluggish path angle response. Even if the loop gain is operated at a value, K_a, to yield closed loop poles as indicated in Figure 7-28, the path angle response will involve a large time constant, T_a. With the open loop gain set at K_a, the approximation corresponding to equation 7-72 becomes

$$\frac{\gamma}{R} = \left(\frac{\Theta}{R}\right)\left(\frac{\gamma}{\Theta}\right) \cong \frac{K}{(T_a S + 1)} \qquad (7\text{-}73)$$

because under these conditions the factor $(T_\theta S + 1)$ is not cancelled by a closed loop pole but by (γ/Θ). Not much speed of response is obtained in this way however since $T_a > T_F$.

It should be noted that theoretically it is possible to obtain quite good closed loop response characteristics, regardless of the airframe transfer functions, by inserting proper compensation elements to cancel airframe poles and zeros. For various practical reasons this is not always accomplished[22] and some limitations on the approximate closed loop transfer functions are necessary. These are generally governed by the airframe characteristics. That is, the airframe of Figure 7-28 had sufficiently large ω_{sp} and ξ_{sp} that the approximations of equations 7-71, 7-72, and 7-73 were reasonable.

This will not be the case in Figure 7-32 where the airframe quadratic plays a significant role in determining the closed loop response. The operating condition is also significant as illustrated in Figure 7-29 which shows a representative variation of ω_{sp} and ξ_{sp} as a function of altitude for constant Mach number. Figure 7-29 is based on an *exponential atmosphere* which, while not accurate for some purposes, is sufficient to illustrate the nature of the changes in ω_{sp} and ξ_{sp}.

7-4.4.3 Attitude Rate Control

If the command signal in Figure 7-27 were a commanded pitch rate rather than pitch attitude, only rate feedback would be employed. That is, the feedback functions would be $K_2 S$ rather than $K_1 + K_2 S$ and the open loop transfer functions would be

$$GH = \left[\frac{K K_{\Theta_1} (T_\theta S + 1)}{S\left(\dfrac{S^2}{\omega_{sp}^2} + \dfrac{2\xi_{sp}}{\omega_{sp}} S + 1\right)}\right] (K_2 S) \qquad (7\text{-}74)$$

For equation 7-74, the closed loop transfer function is

$$\frac{\Theta}{R} = \frac{K K_{\Theta_1} (T_\theta S + 1)}{S\left[\dfrac{S^2}{\omega_{sp}^2} + \dfrac{2\xi_{sp}}{\omega_{sp}} S + 1 + K K_{\Theta_1} K_2 (T_\theta S + 1)\right]} \qquad (7\text{-}75)$$

Thus, the closed loop response with only attitude rate feedback has a pole at the origin and therefore, the steady state response to a constant input command is a constant pitch rate rather than a constant pitch angle. The locus of roots of the bracketed term in equation 7-75 is shown in Figure 7-30. Note that the airframe pole at the origin is cancelled by the pure rate feedback zero.

If the amplifier and actuator dynamic response is considered, the ideal K is modified to

$$\frac{\delta_e}{\varepsilon} = \frac{K}{(T_a S + 1)\left(\dfrac{S^2}{\omega_a^2} + \dfrac{2\xi_a}{\omega_a} S + 1\right)} \qquad (7\text{-}76)$$

The resulting open loop function, GH, is

$$GH = \frac{K K_{\Theta_1} K_2 (T_\theta S + 1)}{S\left(\dfrac{S^2}{\omega_{sp}^2} + \dfrac{2\xi_{sp}}{\omega_{sp}} S + 1\right)(T_a S + 1)\left(\dfrac{S^2}{\omega_a^2} + \dfrac{2\xi_a}{\omega_a} S + 1\right)} \qquad (7\text{-}77)$$

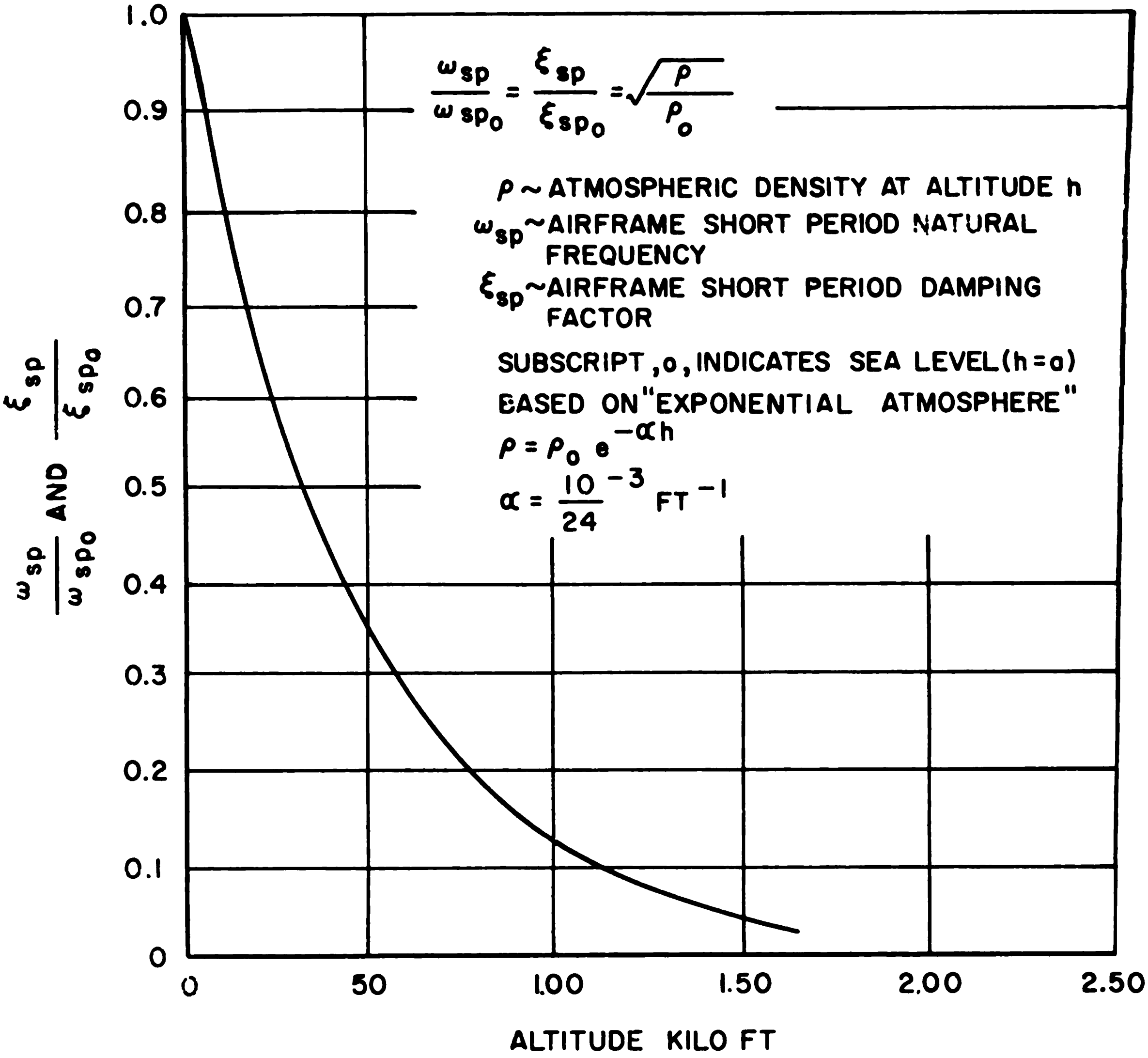

Figure 7-29. Variation of Airframe Short Period Characteristics With Altitude

The root locus plot may be more complicated as shown in Figure 7-31.

As the gain is increased, the short period oscillatory poles due to the airframe become over damped, but if the gain is increased further, another resonant pair of roots appears. If the open loop gain, $K K_{\theta 1} K_2$, lies between K_a and K_b, reasonably good path angle response can be obtained from a system of this type.

SMALL AIRFRAME DAMPING

The root locus in Figure 7-31 corresponds to a highly damped airframe. In case the airframe transfer function is not heavily damped, the nature of the root locus will change to that shown in Figure 7-32.

If the open loop gain is set to correspond to K_a in Figure 7-32, the closed loop response may be approximated by

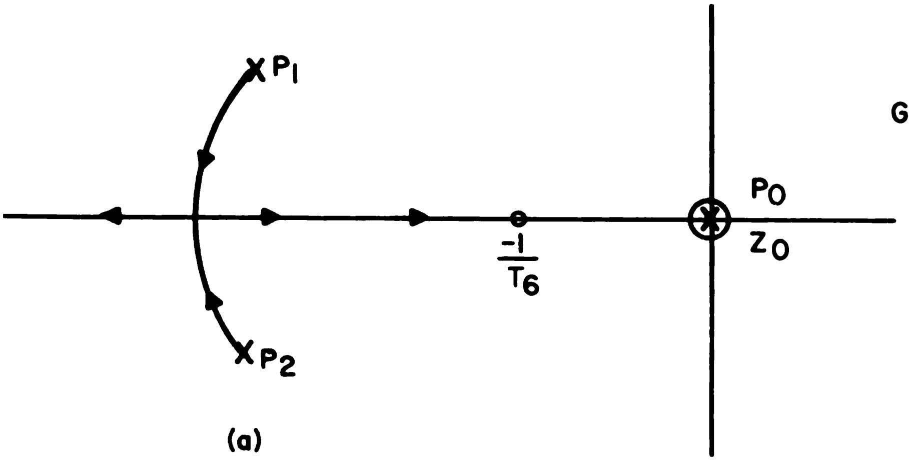

$$GH = \frac{K_2 K K_{\theta 1}(T_6 S + 1)}{\left(\frac{S^2}{\omega_{sp}^2} + \frac{2\xi_{sp}}{\omega_{sp}} S + 1\right)}$$

Figure 7-30. Locus of $1 + GH = 0$

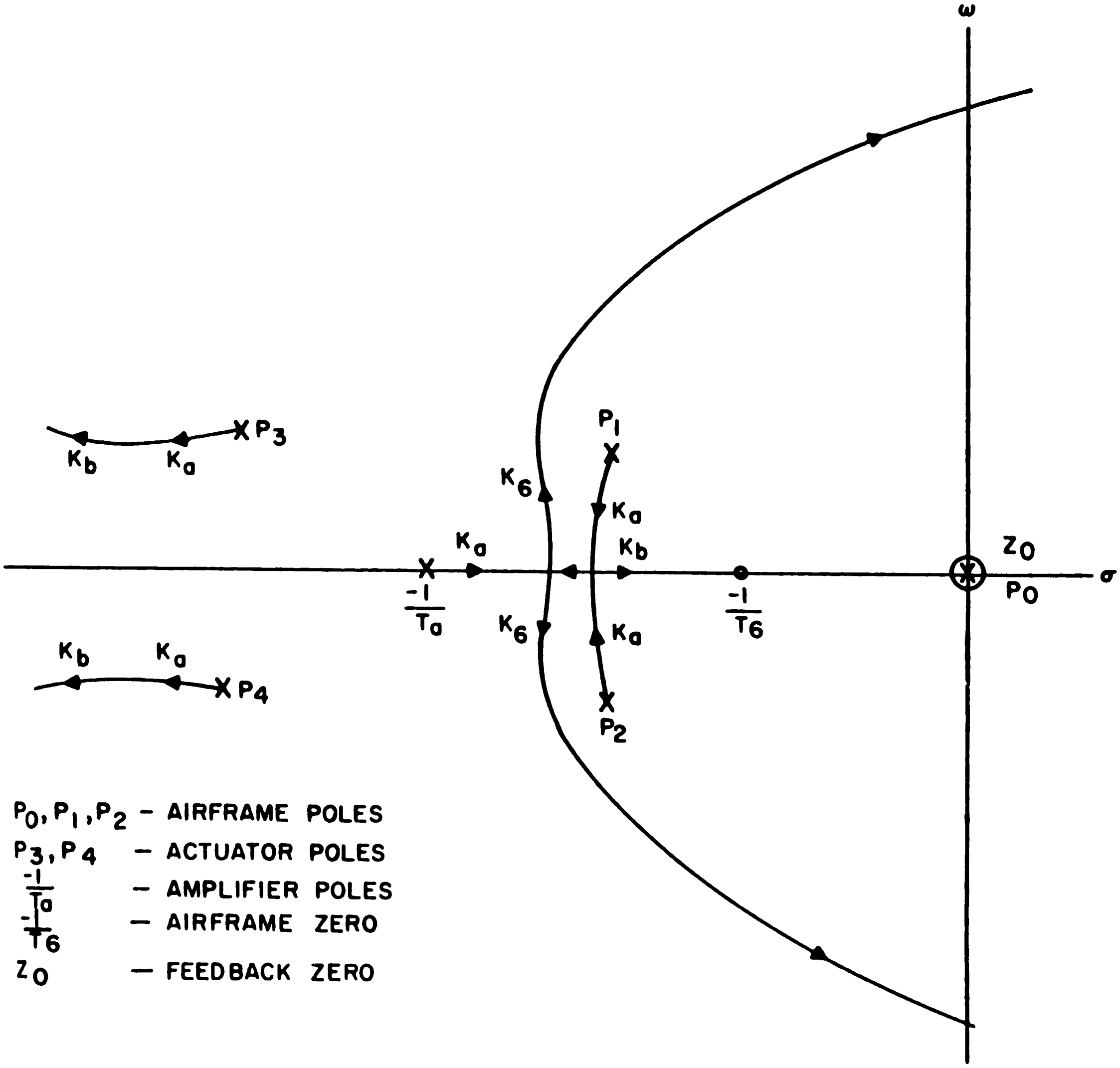

Figure 7-31. Airframe Pitch Rate Controller Within the Atmosphere Root Locus Plot

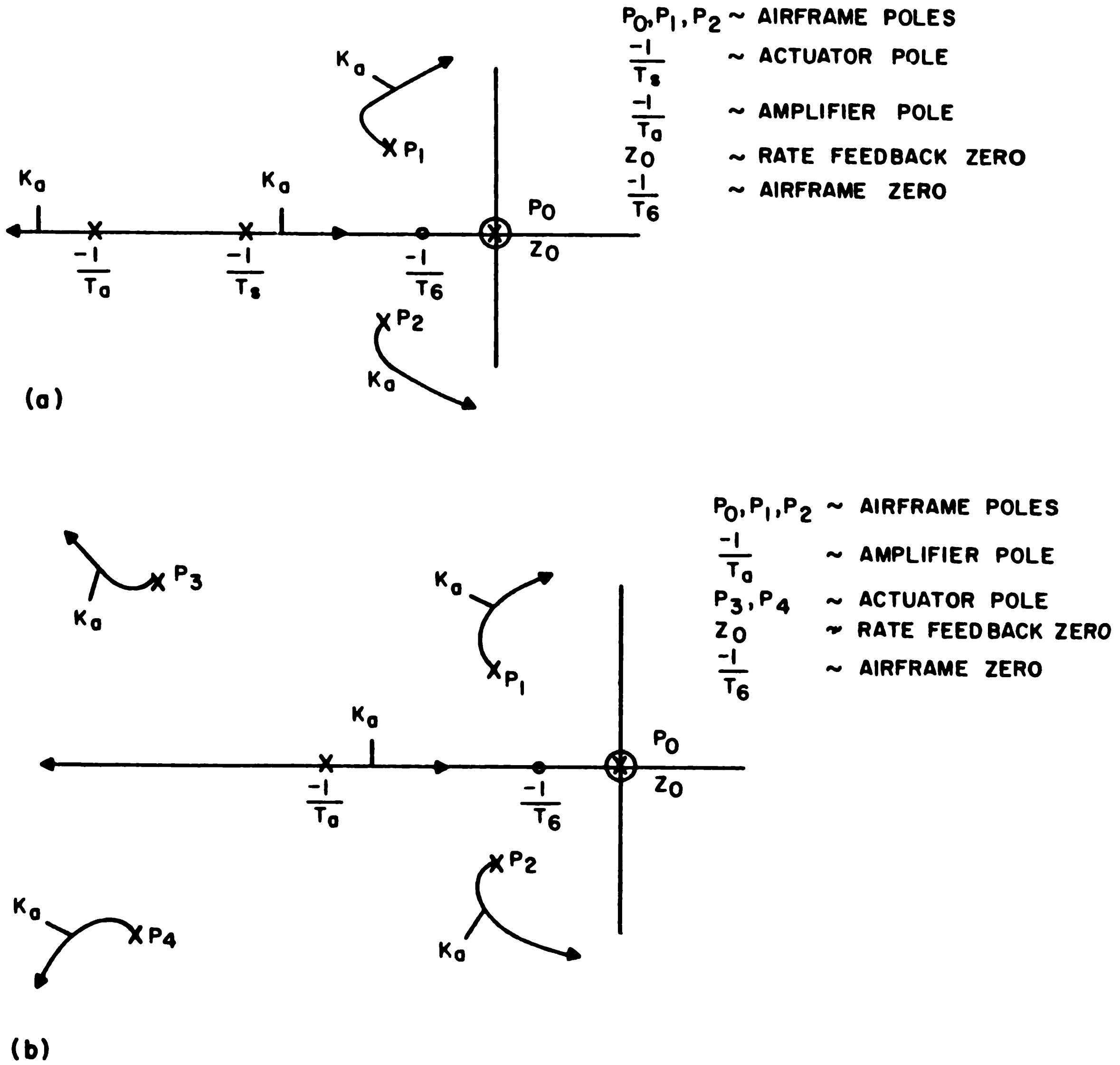
P_0, P_1, P_2 ~ AIRFRAME POLES
$\frac{-1}{T_s}$ ~ ACTUATOR POLE
$\frac{-1}{T_a}$ ~ AMPLIFIER POLE
Z_0 ~ RATE FEEDBACK ZERO
$\frac{-1}{T_6}$ ~ AIRFRAME ZERO
K_a
P_1
K_a
K_a
P_0
$\frac{-1}{T_a}$
$\frac{-1}{T_s}$
$\frac{-1}{T_6}$
Z_0
P_2
K_a
(a)
P_0, P_1, P_2 ~ AIRFRAME POLES
$\frac{-1}{T_a}$ ~ AMPLIFIER POLE
P_3, P_4 ~ ACTUATOR POLE
Z_0 ~ RATE FEEDBACK ZERO
$\frac{-1}{T_6}$ ~ AIRFRAME ZERO
P_3
K_a
K_a
P_1
K_a
P_0
$\frac{-1}{T_a}$
$\frac{-1}{T_6}$
Z_0
P_2
K_a
P_4
K_a
(b)

Figure 7-32. Additional Root Locus for Attitude Rate Control

$$\frac{\Theta(s)}{R(s)} = \frac{K'\,(T_6 S + 1)}{S\left(\dfrac{S^2}{\omega_o^{\,2}} + \dfrac{2\xi_o}{\omega_o} S + 1\right)} \qquad \text{(a)}$$

$$\frac{\dot{\gamma}(s)}{R(s)} = \left(\frac{\Theta(s)}{R(s)}\right)\left(\frac{\gamma(s)}{\Theta(s)}\right) = \qquad \text{(7-78)}$$

$$\frac{K'}{S\left(\dfrac{S^2}{\omega_o^{\,2}} + \dfrac{2\xi_o}{\omega_o} S + 1\right)} \qquad \text{(b)}$$

where ξ_o and ω_o are the damping factor and natural frequency of those roots on the airframe branches of the locus at K_a.

The pair of equations 7-78 is often presented in terms of the transform of $\dot{\Theta}$ and $\dot{\delta}$

$$\frac{\dot{\Theta}(s)}{R(s)} = \frac{K'\,(T_6 S + 1)}{\left(\dfrac{S^2}{\omega_o^{\,2}} + \dfrac{2\xi_o}{\omega_o} S + 1\right)} \qquad \text{(a)}$$

$$\text{(7-79)}$$

$$\frac{\dot{\gamma}(s)}{R(s)} = \frac{K'}{\left(\dfrac{S^2}{\omega_o^{\,2}} + \dfrac{2\xi_o}{\omega_o} S + 1\right)} \qquad \text{(b)}$$

4 Lateral Control

ng the simplified lateral transfer func- given in equation 7-69 and similar control , roll and yaw channels may be generated characteristics similar to those discussed iously. For the cruciform configuration δ_a differential deflection of control surfaces.

5 TYPICAL CONTROL SYSTEM

n previous sections, several elementary :k diagrams showed representative control tem configurations. The pitch channel dia- am shown in Figure 7-33 is only a slight riation from those previously shown. If we nsider the system of Figure 7-33 to be for a uciform missile, the block diagrams for the aw and roll channels will be identical to that own for pitch. The only essential difference ill be a different loop gain for roll. Also the roll channel will not include the linear accelerometer loop. The rate gyro is included in the system for short period damping and to make the pitch rate proportional to command. The accelerometer and the two filter networks are for the damping of body bending modes. (More detailed considerations of this aspect may be found in references 30, and 36-38.)

The essential difference of this system from those previously shown is the use of the integrating rate gyro.

By feeding both the command signal and the integrating rate gyro signal into the torquer, the gyro is made to operate in three functions. As a rate gyro, it is in parallel with the regular rate gyro in the short period damping function. Where a command signal is applied, the gyro is torqued and gyro reference is moved such that the gyro adds an additional rate command in

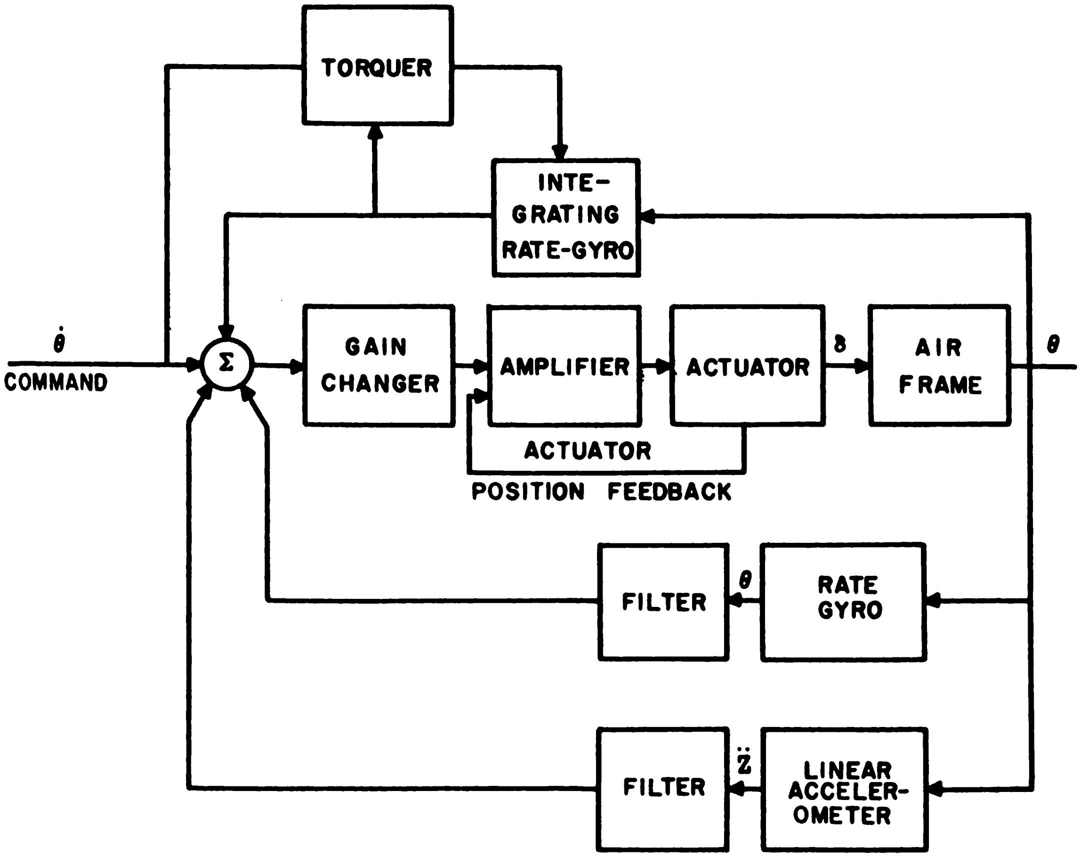

Figure 7-33. Pitch Channel Diagram

parallel with the direct command signal. When no command is applied, the gyro acts as an attitude reference and causes the missile to hold the attitude last called for until another pitch rate command is given.

Consider the transfer function of the airframe:

$$\frac{\Theta}{\delta_e} = \frac{K_{\Theta\delta_e}(TS+1)}{S\left(\frac{S^2}{\omega_{\kappa p}{}^2} + \frac{2\xi_{\kappa p}}{\omega_{\kappa p}}S + 1\right)} \qquad (7\text{-}80)$$

The constant, $K_{\Theta\delta_e}$, is far from constant but is a function of altitude, aircraft velocity and airframe configuration. As previously stated, all aerodynamic coefficients are approximately proportional to U^2 at subsonic speed. They are also proportional to ρ (the air density).

At transonic and supersonic speeds, the forces are still a function of speed and air density, but the functional relationships are determined by the airframe configuration.

Whatever these functional relationships are, they can be obtained for any flight condition by calculation, wind tunnel or actual flight tests.

This information can be stored in the gain changer of the control system. If, as flight conditions and $K_{\Theta\delta_e}$ change, the gain changer can be made to change the flight control system gain in an inverse manner, the loop gain of the system can be kept constant at a desired value. If this constant gain is possible, the missile's response to a given command will be the same for all flight control conditions.

Because of the importance of gain changing as speed ranges increase, there have been efforts to develop a self-adaptive gain changer which would be applicable to any or at least to many airframe configurations.[28-30,36,38] The general philosophy of these systems is that instead of measuring altitude and velocity, they measure the response of the aircraft itself, compare the actual response to what the response should be and change the gain in the desired direction.

7-4.5.1 Proportional Systems Versus Off-On And/Or Digital Systems

Only proportional flight control systems have been considered in this discussion. This is because relatively little has been done in flight control with off-on or bang-bang servos. (Several problems in optimal control theory lead to a bang-bang system. See section 4-15 of reference 28.) Also, little has been done in digital systems for SAM's.

Control requirements are becoming more complex and both range of travel and flight times are increasing. Greater speeds and the resulting higher temperatures make hot gas servos seem desirable. Hot gas servos will be much less complicated and offer less mechanical trouble in the servo itself, if they are simple bang-bang servos. The electronic systems controlling such servos may be less complicated if digital techniques are used. Also, the problem of the self-adaptive gain changer previously discussed seems to be more easily solved if the digital approach is used. Digital computer solution of flight control problems has been retarded due to the greater number of electronic components required. The lower reliability resulting from this greater number of components has been the main reason for this limitation of use. Greater component reliability linked with a more complex flight control problem will cause an increase in the use of digital equipment.

7-4.6 COMPONENT CONSIDERATIONS[23,39]

Basic flight control system requirements and methods for meeting them have been outlined without significant regard for practical constraints. Generally it is desirable that the requirements be met with a minimum of weight, volume, and cost, and high reliability.

To accomplish these objectives in any particular case requires considerable effort and more complete definition of the problem than is provided here. However, general guides can be offered towards meeting these goals.

Basic sensor characteristics are discussed in paragraph 7-6, but detailed data such as weight, power requirements, etc. are not included. The systems engineer would be wise to leave such considerations entirely to component or subsystem designers or utilize their more current knowledge. In such dealings, knowledge of the basic characteristics from paragraph 7-6 and the broad bounds discussed below will be helpful.

-4.6.1 Signal Requirements

NPUT

The input to the control system is in the form f a signal from the guidance system. Its purpose is to affect a change in the flight of he missile. A-c and d-c signals are used and both have their relative advantages. In proportional systems a-c signals require less circuitry than d-c signals.

LIMITING

The input command signal must be limited to a given magnitude. If the command signal is a rate command, it must not command a turning rate faster than the change of flight path capabilities of the airframe.

If the command is an attitude command, the magnitude of the signal that can be instantaneously applied must be limited to that allowed by the stability characteristics of the airframe.

In both cases, the limiting can best be done in the guidance system.

Limiting the rate of maneuver by limiting the command signal assumes a feedback signal that is reasonably proportional to missile motion. Limiting can also be accomplished by means of non-linear feedback.

SIGNAL TYPES

When accuracy and minimum zero drift are required, a-c amplifiers are usually used, and both input and feedback signals are a-c voltages. Direct current signals can be used in these cases if a modulator feeds the amplifier input. For more relaxed accuracy and drift specifications, an all d-c system may be used.

OUTPUT

The output of a flight control system is in terms of *L*, *M* and *N* (moments or torques about the roll, pitch and yaw axes). These moments can result from changes in aerodynamic forces resulting from the deflection of control surfaces. They can also result from thrust deflection, obtained either by deflection of the main thrust jets, by deflection of auxiliary jets or by turning fixed auxiliary jets on and off.

These means of obtaining control moments were listed in the descending order of power required for the actuator of the control device. The operation of a valve control on a stationary reaction rocket may take less than one watt. It may take several watts to rotate an auxiliary jet around its center of gravity, but it may also take one or more horsepower to operate aerodynamic control surfaces at supersonic speeds.

7-4.6.2 Amplifiers

TUBE AMPLIFIERS

Tube amplifiers, using regular miniature or subminiature tubes, are heavier and larger than other amplifiers. The weight per volume is low but weight is still greater than other types. There are other disadvantages in tube amplifiers. Due to the necessary high heat dissipation, the ambient temperature limit is usually 71°C with blower circulated cooling air. The other environmental difficulties are shock and vibration. Shock mounts and vibration isolators are necessitated by the internal construction of tubes. Cost is the only criterion in which the tube amplifier is competitive, but the high missile launching accelerations obviate their use in surface-to-air missiles.

TRANSISTOR AMPLIFIERS

The smallest, lightest, least expensive and most efficient flight control amplifiers available can be made with germanium transistors. Temperature has obstructed their use in military aircraft, especially missiles. Their upper limit of operation is 55°C and, above the aforementioned 71°C, they are useless.

Silicon transistors have all the advantages of germanium transistors except low cost. The high cost of silicon transistors may decrease considerably with improved manufacturing methods, and silicon purification. The problem of temperature is improved with silicon transistors since they are useable to 150°C.

CERAMIC TUBE AMPLIFIERS

In recent years extremely rugged ceramic vacuum tubes have been developed. They are several times bigger than transistors but smaller and much more suitable under shock and vibration conditions than previous tubes. The big advantage of ceramic tubes is their high ambient temperature limit. Their long time operating temperature range extends to 400°C. Their ability to operate properly at high temperatures exceeds most of the other circuit components.

EXPERIMENTAL AMPLIFIERS

The present types of amplifiers first discussed are by no means the ultimate in flight control amplifiers. Although the experimental types presently under consideration (masers and parametric amplifiers) are not directly applicable to flight control, their existance illustrates that means of obtaining amplification of an electrical signal have not been exhausted.

MAGNETIC AMPLIFIERS

Amplifiers which are all magnetic are not generally used in flight control systems because of their weight. However, when high electrical power is needed to drive the actuators, the magnetic output stage often becomes the best solution. One of the advantages of the magnetic amplifier stage is that it is possible to have either an a-c or d-c output. This can be obtained with either a-c or d-c input or both.

The present magnetic amplifier temperature limitation is predicated by the temperature limit of the silicon diodes used. This diode temperature limit is 25°C to 50°C above the silicon transistor working limit; that is 175°C to 200°C. Above 400°C there is irreparable damage to the magnetic properties of the core materials.

Core stress is another temperature difficulty with magnetic amplifiers. This results from temperature changes and different coefficients of expansion of core materials and potting or mounting materials. Mechanical stresses in the core materials result in changes of magnetic properties of the core. Another problem at 400°C with any type amplifier is insulation. As carrier frequencies are increased, the necessary size of magnetic amplifier components decreases. The types of insulation usable at high temperatures, especially with small wire used for core winding, are extremely limited.

PACKAGING TECHNIQUES

Current packaging techniques produce electronic equipment that varies from thirty to seventy-five pounds per cubic foot. Other components, actuator and sensors, average from 1½ to 2 times as heavy. The miniaturization of amplifiers which began with subminiature tubes, printed wire boards and transistors, is being carried to the extent of depositing point transistors, resistors and other components on glass or ceramics. This is termed *microminiaturization.* One hundred to three hundred components to the cubic inch is obtainable. This type of amplifier is still limited by the temperature limitations of the transistors used. A combination of the depositing technique with the use of ceramic tubes and high temperature magnetic amplifiers is possible.

The assembly technique that is most advantageous from the standpoint of temperature, size, weight, vibration, shock and long shelf life, is that of welding the components together instead of soldering them. In this procedure no support is used except that of the interconnecting wire, but, after being assembled in small throw-away modules, each module is potted in high temperature plastic. This is a much more difficult process to do either by hand or automation than printed wire dip soldering but it can be automated.

7-4.6.3 References — Sensors

The sensors that are normally included in a surface-to-air missile flight control system have already been named. They are vertical or free gyros, rate gyros, angular and linear accelerometers and in rare cases, stable platforms.

Choice of sensors for a given missile considering sensor range, accuracy, signal thresholds, saturation, etc., will depend upon missile characteristics, type of guidance, mission, and the type and characteristics of the target.

A drift of one degree in the attitude reference during the powered flight of a 5000-mile ICBM would result in a target error approaching 100 miles. The same one-degree drift during the flight of a surface-to-air missile would cause negligible error in its miss distance. This difference in accuracy is due to the SAM being controlled by a closed loop guidance system during the entire flight. Any slow drifts in attitude reference can be compensated for in the guidance system. In command guidance the missile components should be as light and inexpensive as is possible to control the missile dynamically while inherent errors can be corrected by the guidance system. Increases in weight, complexity, and cost of the guidance system are of lesser importance since the major portion is on the ground. In homing guidance systems, this is not the case, since the guidance system is also n the missile.

7-4.6.4 Actuators

The choice of actuators will depend on many things: the size, design and speed of the missile which will determine the hinge moments; the guidance philosophy which will determine the necessary response; and the type of available power supplies (including the weight and volume) that can be allotted.

For low horsepower actuation (small fraction of a horsepower) either two phase electric servo motors or small d-c motors are the simpler types of actuators for proportional systems. Also, single speed motors with two-way gear trains and differential clutches have been used. As power requirements increase with missile size, speed and maneuverability requirements, hydraulic systems are more feasible.

The most serious aspect of control actuators is that of supplying the power for them. In the case of electromechanical actuators, the primary power source will be either a battery or generator run by an auxiliary power unit (APU). (See Chapter 12, "Power Sources," for more detail.) Since one of these power sources is needed for the amplifier, there is no addition except in size. However, as more power is required, both power sources and motors become too heavy for practical use in the missile. In the case of a hydraulic system there are several means of supplying power.

(a) When a relatively short flight is considered, the use of a hydraulic reservoir pressurized by gas stored at several thousand psi is the cheapest and most practical way. The hydraulic fluid is dumped overboard as it is used.

(b) Another fluid jettisoning system receives its pressurization from tapping the combustion chamber of the missile or from a small separate combustion chamber (APU).

(c) As length of flight increases, or if actuator power and duty cycle increases, or both, it is more expensive, but better from the weight aspect, to reduce the stored fluid, increase the size of the APU driving the electrical generator, and drive a hydraulic pump as well. The hydraulic system becomes a closed system with the fluid recirculating rather than being jettisoned.

The problems connected with hydraulic systems are breakage of hydraulic lines, excessive leakage and temperature. The solution of the excessive leakage problem necessitates close machining tolerances which mean greater expense. The breakage of hydraulic lines results from vibration or from excessive hydraulic pressure. The temperature problem results from high ambient temperatures, the location of actuators close to the heat of the propulsion nozzles, and the heat generated in the hydraulic pump.

The temperature problem may be broken down into three problems: decomposition of hydraulic fluid, reduction of lubrication properties of the fluid, and damage to insulation of the electrical circuitry of the control solenoid.

The temperature limits for long time use of hydraulic fluids are shown in Table 7-7.

TABLE 7-7. THERMAL LIMITATION OF HYDRAULIC FLUIDS

Fluid	Temperature Point (°C)
Petroleum Base	125-150
Silicates	200
Silicone Oils	300

7-4.6.5 Environmental Considerations

TEMPERATURE

For surface-to-air missiles the temperature problem is not as great as for other missiles with greater range at supersonic speeds or for modern air launched missiles which must be launched from supersonic carriers.

The components which are deemed most susceptible to damage from temperature are the gyros.

If time of flight is such that a significant temperature problem exists, gyros and other components with low temperature limitations must be insulated or refrigerated or both.

HUMIDITY

The real criterion for design of humidity proof surface-to-air missiles is the storage requirement. Shelf storage for as much as five years necessitates hermetical seals or potting or both.

RELIABILITY

Because the missile is not recoverable, low cost has been and should be stressed when considering flight control or any other part of the missile. Reliability of systems and individual components should be stressed even more. It is better that a flight control system cost $20,000 and operate successfully 95 percent of the time than cost $5000 and operate successfully 60 percent of the time. When choosing components it is well to remember that the failure of a 25-cent resistor can result in the loss of thousands of dollars.

7-5 KINEMATICS

7-5.1 GENERAL

The basic kinematical relationships for each of several guidance modes were presented in paragraph 7-2. The extension of those definitions to three dimensions is important for both design and evaluation purposes, but guidance and control preliminary design usually is accomplished with two dimensional models.

There are several reasons for this apparently unscientific, incomplete, approach:

(a) Three dimensional equations are too complicated to yield to preliminary synthesis and design tools.

(b) Many of the equipment parameters that are needed to reasonably characterize three dimensional performance (and subsequently design decoupling and compensation filters) are unknown during preliminary design.

(c) To a first approximation, separate two dimensional models will adequately represent the three dimensional situation.

Although the above may appear to be begging the question, the two dimensional approach is in keeping with the desire to develop simple flexible models which are useful in the larger, more complex, weapon system problem. With the development of more powerful synthesis techniques may come the capability to characterize the general three dimensional situation in such a way that the results can be intelligently employed in preliminary design. For these purposes, as well as for evaluation, references 6, 7, 16, 19, 32, 40 and 41 may prove useful.

Regardless of the level of complexity at which one attempts to describe the guidance kinematics, it should be recognized that geometry feedback is the essence of guidance problems for it determines the basic sensor requirements given in paragraph 7-2.7.

7-6 SENSORS

7-6.1 GENERAL

The sensors needed in a guidance and control system may be generally divided into two functional classes — primary and secondary.

Primary sensors are used here according to Figure 7-18; that is, a primary sensor performs the function of detecting pertinent target information for the primary guidance loop. Secondary sensors are those associated with subsidiary control loops within the primary guidance loop. These include the attitude and rate gyros employed in the autopilot as well as accelerometers, etc.

Most primary sensors are based on devices that utilize high frequency radiation to detect target behavior and provide guidance error signals while secondary sensors operate at much lower frequencies. This is illustrated in Figure 7-34, which shows the potential source of all sensors.

In the following sections, means for achieving sensing are discussed in the context of guidance phases. The information needed for control (if any) during the launch phase is generally available from those devices considered under midcourse guidance in the next paragraph. The same applies to secondary sensors.

7-6.2 MIDCOURSE GUIDANCE SENSORS

7-6.2.1 Basic Measurements

It is necessary to know both target and missile locations. The measurements needed to determine target position are range, azimuth, and elevation. The same information plus attitude angle is needed for the missile. Radar can pro-

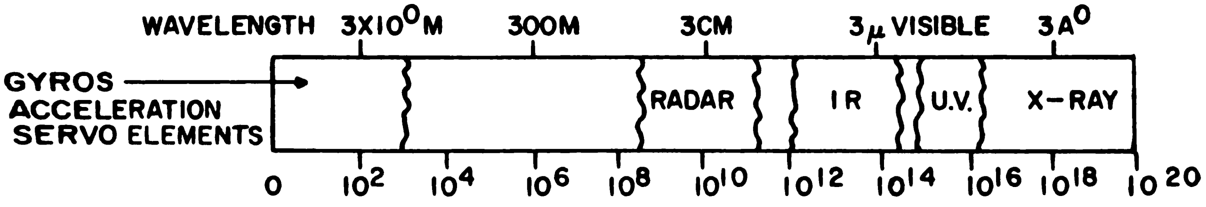

FREQUENCY CPS

Figure 7-34. Sensor Operating Frequencies

vide position measurements. (See Chapter 6, "Fire Direction and Coordination.") Attitude measurements are made by on-board inertial devices.

7-6.2.2 Radar[42]

The radar guidance problem was stated briefly in paragraph 6-1.6 of Chapter 6 from the point of view of Fire Direction and Coordination. Subsequent sections in Chapter 6 are useful in the design of airborne radar also. Thus, most of the following may be considered as an expansion, or restatement, of pertinent sections from Chapter 6 to include the guidance viewpoint.

BEACONS

Tracking the missile and sending commands to it increases the complexity of the radar. The ground radar must contain coding circuits to provide guidance commands during the midcourse phase. This is accomplished by means of a beacon in the missile; that is, a device that will transmit a signal when triggered on command from the ground radar. The radar interrogates or triggers, and the beacon replies by sending out a signal that is received by the radar. A block diagram of such a system is shown in Figure 7-35.

It was shown in the radar range equation in Chapter 6 that the required radar power varies inversely as the fourth power of free-space range. The beacon power varies only as the inverse square of range since one-way transmissions are involved. The power received by the beacon is given as

$$P_{R\,\max} = \frac{P_T\,(G_T)_{\max}\,(G_R)_{\max}\,\lambda_T^2}{16\pi^2 R_T^2} \qquad (7\text{-}81)$$

where

$P_{R\,\max}$ = maximum value of available peak power received by the beacon

P_T = peak value of power transmitted by the radar

G_T = maximum value of the gain of the transmitting antenna (radar)

G_R = maximum value of gain of receiving antenna (beacon)

λ_T = transmitted wavelength

R_T = range between radar and beacon

Letting P_{R-F} represent the peak value of available received power necessary to fire the beacon, and R_{TF} the corresponding range, and rearranging equation 7-81 gives

$$R_{TF} = \frac{\lambda_T}{4\pi}\left[\frac{P_T}{P_{R-F}}\,(G_T)_{\max}\,(G_R)_{\max}\right]^{1/2} \qquad (7\text{-}82)$$

If the beacon is at a range greater than that given by equation 7-82 it will not be triggered. For the beacon transmitter, the range of reply is given by

$$R_B = \frac{\lambda_B}{4\pi}\left[\frac{P_{TB}}{P_{RB}}\,(G_T)_{\max}\,(G_R)_{\max}\right]^{1/2} \qquad (7\text{-}83)$$

where

subscript B denotes beacon to radar

P_{RB} = Peak available received power required to give beacon signal on indicator of radar.

In designing a beacon radar system, it is desirable to have $R_{BF} = R_{TF}$; however, R_{BF} should be slightly larger than R_{TF} so that the radar operator may recognize the beacon return.

In Figure 7-35 a decoder is shown after the beacon receiver. (See paragraph 6-5.4.3 in Chap-

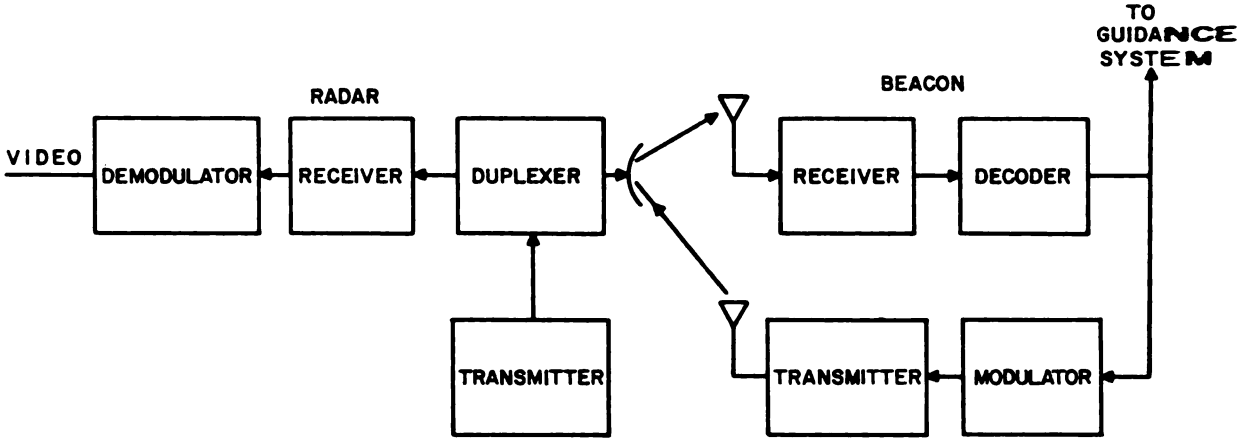

Figure 7-35. Beacon Radar System, Block Diagram

ter 6 for an example.) This decoder is used to insure recognition of the beacon and to maintain a secure communication link.

In command systems where the radar not only tracks the beacon but also sends commands, the beacon decoder can also feed the commands to the guidance system. The commands may be coded by frequency modulation of the pulse repetition frequency (prf) or by position modulation of the pulses.

The schemes for coding of commands are many; however, only one method will be described. In this system, a group of five pulses constitutes a command group. Two pulses are identifying pulses while the other three pulses contain roll, pitch, and yaw information. Figure 7-36(a) shows the five pulses. With no commands being transmitted, the pulses are spaced at 60 μsec intervals.

The first two pulses unlock the receiver. The receiver is designed such that a particular unlocking code can be set in prior to firing. The next three pulses transmit roll, pitch and yaw information in that order. By varying the pulse position in time, a command proportional to the pulse time position is obtained.

To illustrate the foregoing, consider Figure 7-36(b). Here the receiver is set to unlock with a 50 μsec spacing between the first two pulses. No roll command is sent; therefore, the position of the roll pulse is unchanged. Pitch and yaw commands are being sent; therefore, the pulses are displaced.

In order to reduce the effects of countermeasures, coding becomes quite intricate adding complexity to the radar. The disadvantages of using a system that requires coding during midcourse guidance must be weighed against the flexibility gained by the use of such a system.

DOPPLER DEVICES

Doppler radar systems make use of the frequency shift of a returned signal due to the relative motion between the target and the radar. Devices of this type have an important application in surface-to-air missiles, since they possess the capability of discriminating between a moving target and ground returns on a frequency basis.

The Doppler frequency is given by:

$$f_d = \frac{2\,(V_M + V_T)}{\lambda_o} = 2\,\frac{V_r}{\lambda_o} \qquad (7\text{-}84)$$

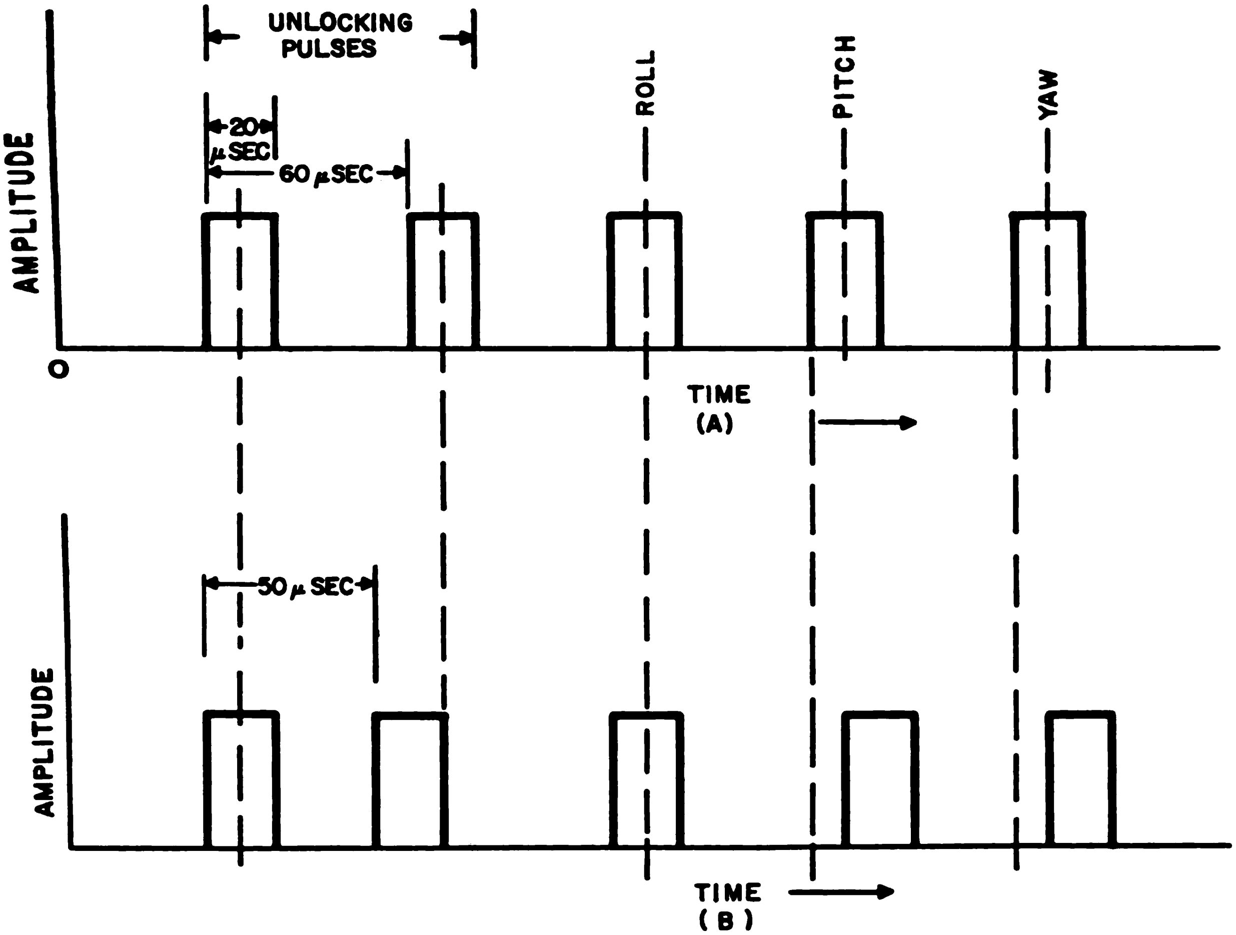

Figure 7-36. Command Coding Scheme

where

V_r = relative target velocity

V_M = the missile velocity component in the direction of the target

V_T = the target velocity component in the direction of the missile

λ_o = the transmitted wavelength.

In addition to a target return, ground clutter is received from all angles due to the sidelobes of the antenna. A typical frequency spectrum of the received energy is shown in Figure 7-37.

For a pulse Doppler system, side lobes will exist at multiples of the pulse repetition rate. Therefore, the pulse repetition frequency (f_R) must be selected such that,

$$f_R \geq \frac{2\,(V_{M\,\max} + V_{R\,\max})}{\lambda_o} \qquad (7\text{-}85)$$

to prevent the target Doppler from appearing in the upper side lobe clutter.

A typical Doppler radar block diagram is shown in Figure 7-38. The received signal is mixed in a coherent detector and passed on to the receiver, range gate, and the velocity filter. The velocity filter selects the Doppler spectral line of interest for control purposes. The amplitude modulation (at the scan frequency) is extracted in the scan filter, compared with the antenna scan frequency and quadrature error voltages are derived. These error voltages are used in the control system to produce corrections in the missile flight path.

Doppler radar for midcourse guidance may be one of several forms:

(a) active – CW Doppler
(b) active – pulse Doppler
(c) semi-active – CW Doppler
(d) semi-active – pulse Doppler

The operation of each type is fundamentally the same. The difference is in the way the equipment is employed. In the active system, all the radar equipment necessary for guidance is located in the missile. In the semi-active system, the tar-

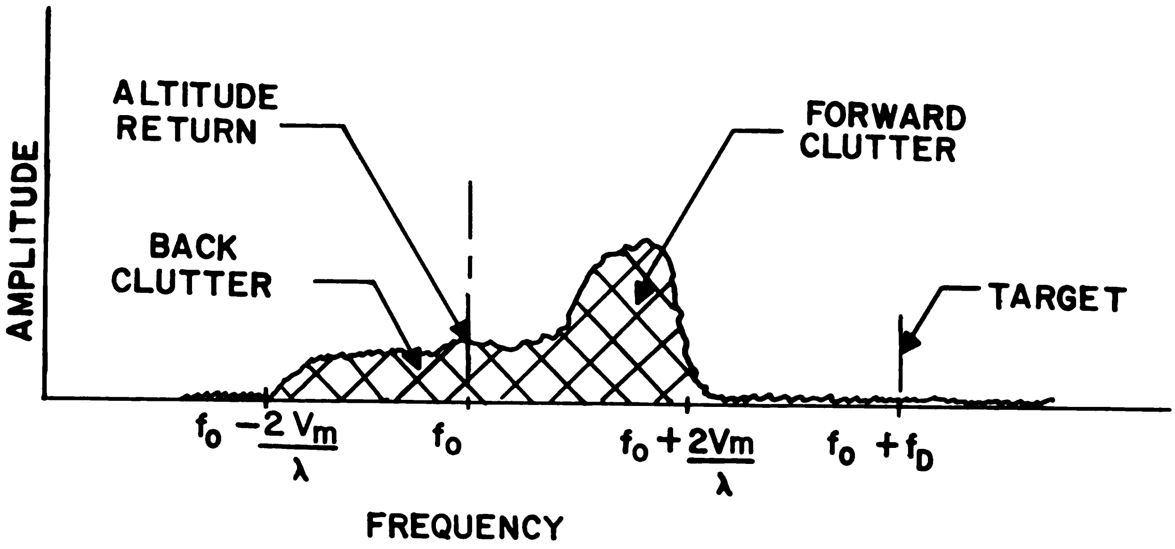

Figure 7-37. Typical Doppler Frequency Spectrum

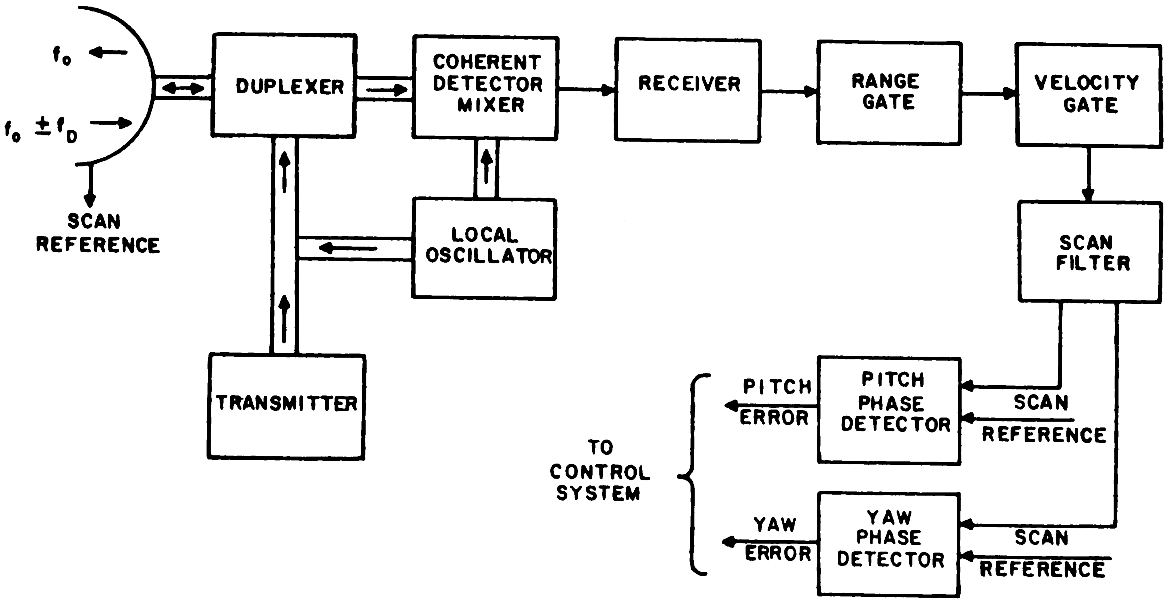

Figure 7-38. Typical Doppler Radar, Block Diagram

et is illuminated from a ground based trans-itter. The missile-borne receiver, in all forms, erives guidance commands by processing the arget reflections. For range capability analysis ee the cross references in paragraph 7-7 and eferences 42-45. For semi-active applications, ange product (the product of illuminator-to-target distance and target-to-receiver distance) must be used.

BEAM RIDER AND COMMAND[46]

For each of these modes the primary sensors are ground based. The major airborne equipment is a beacon (Figure 7-35) to accept and process transmitted error signals.

7-6.2.3 Inertial

The inertial devices in a missile can range from a simple gyro to a complete inertial platform to maintain a fixed reference in space. They are used for measuring:

(a) motion of the missile with respect to its own center of gravity

(b) motion of the missile center of gravity along the flight path

The first category defines the attitude of the missile. The second category defines missile location with respect to the launch point.

Roll, pitch and yaw positions and rate information are necessary to stabilize the missile. The position measurement provides an error from the desired attitude. The rate measurement can be utilized to damp out unwanted oscillations or can provide damping to prevent overshoot during attitude correction.

It is not necessary that both free and rate gyros be used together to obtain the required information. The guidance scheme is the determining factor. It may be possible that rate gyros combined with accelerometer signals can provide sufficient stabilization. In another guidance scheme, free gyros and a differentiating circuit to obtain rate information may be required.

Missile trajectory or path movement measurements can be more complex than attitude measurements. For trajectory measurement, there may not be a convenient reference or the reference may not be accurate enough to provide required overall system accuracy.

One way to sense movement along a path is to take advantage of the basic laws of motion, or simply that distance x, can be expressed as $\bar{x} = \int \bar{v}dt$ where $\bar{v}$ is instantaneous velocity. Since $\bar{v} = \int \bar{a}dt$, $\bar{a}$ being acceleration, distance can be calculated by measuring acceleration.

In missiles with a short time of flight (1-3 minutes) it is possible to attain attitude stabilization by using gyros and orienting three accelerometers to measure longitudinal, lateral, and transverse accelerations.

For missiles with longer flight times, gyro stabilization in itself does not provide the necessary accuracy and therefore more refined means for a stable reference are required. A gyro stabilized platform, which holds its orientation in space, provides a stable reference for the mounting of accelerometers. With the three orthogonal components of acceleration measured, the complete movement of the missile can be computed.

Measurement of the trajectory may also be accomplished by automating the celestial navigation that has been used for many years by ships. This type of guidance requires a stable platform, or similar *fixed reference*, and a star tracking telescope to determine the angular position of a star with respect to the platform. This information is then used to correct the drift in the platform.

GYROSCOPES[47]

The gyroscope is a spinning rotor supported in a gimbal system such that the spin axis has one or two degrees of freedom. Various sensing and control elements are attached to the framework to utilize the gyro for missile application.

Gyros serve as useful generators of intelligence because their behavior is referred to inertial space. The basic parts of a gyro are:

(a) a rotor and a device to drive it

(b) a gimbal system

(c) a pickoff

Other components are added depending upon the purpose and complexity of the gyro's intended use.

The vector equation describing the behavior of the gyro is:

$$\overline{M} = \overline{\Omega} \times \overline{H} \qquad (7\text{-}86)$$

where

$\overline{M}$ = applied torque

$\overline{\Omega}$ = absolute precessional angular velocity of the spin axis

$\overline{H}$ = rotor angular momentum

Figure 7-39 shows the relationship of the vectors.

This equation states that an applied torque $\overline{M}$ which tends to change the direction of the angular momentum vector $\overline{H}$ will cause the angular momentum vector to precess around an axis at right angles to the torque vector and the momentum vector. The precession is always in such a direction as to align the rotor rotation direction with the rotation of the applied torque. This means that a torque input will result in an angular velocity output and vice versa.

For all types of gyros, the environmental requirements are of utmost importance. Unless the environment is specified, the other parameters may be misleading. It is relatively simple for gyros to achieve very low drift rates under controlled laboratory conditions. In a more severe environment, the results may be somewhat different.

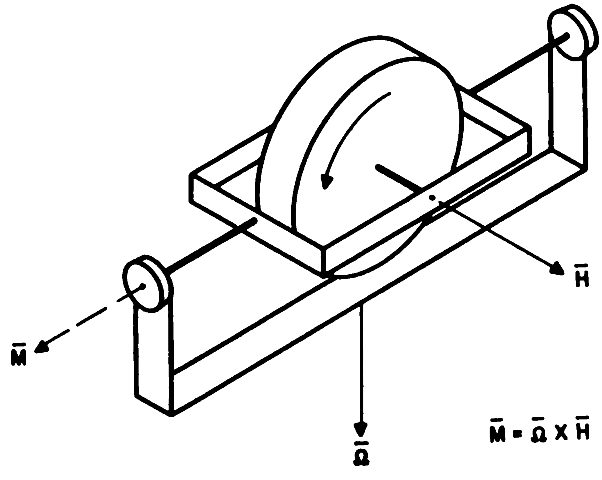

Figure 7-39. Gyro Vector Relationship

Temperature, shock, acceleration, and vibration are the important environmental characteristics. Most military equipment must perform adequately between −65°F and 170°F. The shock, acceleration, and vibration requirements depend upon the application. Some applications require withstanding shock up to 100 g's while others require only two or three g's.

A discussion of the basic gyro types and their individual parameters follows.

FREE GYRO (FIGURE 7-40)

A gyro with two degrees of freedom is termed a free gyro. The outer gimbal has 360° of freedom while the inner gimbal is usually limited to ±85° of freedom. This is to prevent gimbal lock which occurs at 90° inner axis displacement.

Free gyros are mechanically caged with the gyro case being used as a reference. Caging and uncaging is accomplished by remote control with indicator switches provided to indicate the caged or uncaged condition.

The signal from a free gyro is a voltage proportional to displacement with respect to the reference. By feeding the signal to an autopilot, corrections can be applied to the control surfaces of a missile to keep it stabilized in the correct attitude.

Some of the more important free gyro parameters are:

(a) *Drift* – This is defined as the undesired shift of the spin axis due to gimbal bearing friction and should be as low as possible. Total drift rates for free gyros are presently about 0.5° per minute with the state-of-the-art reducing this toward 0.2° per minute.

(b) *Output Non-Linearity* – This is the maximum deviation of the input-output curve from a straight line and can presently be kept to ± one percent full scale.

(c) *Run-up Time* – This is a function of the wheel size and type of power available. The time should be low in order to provide fast missile reaction time.

(d) *Caging Mechanism* – The device to orient the gimbals should cage them quickly and contribute little to uncaging de-

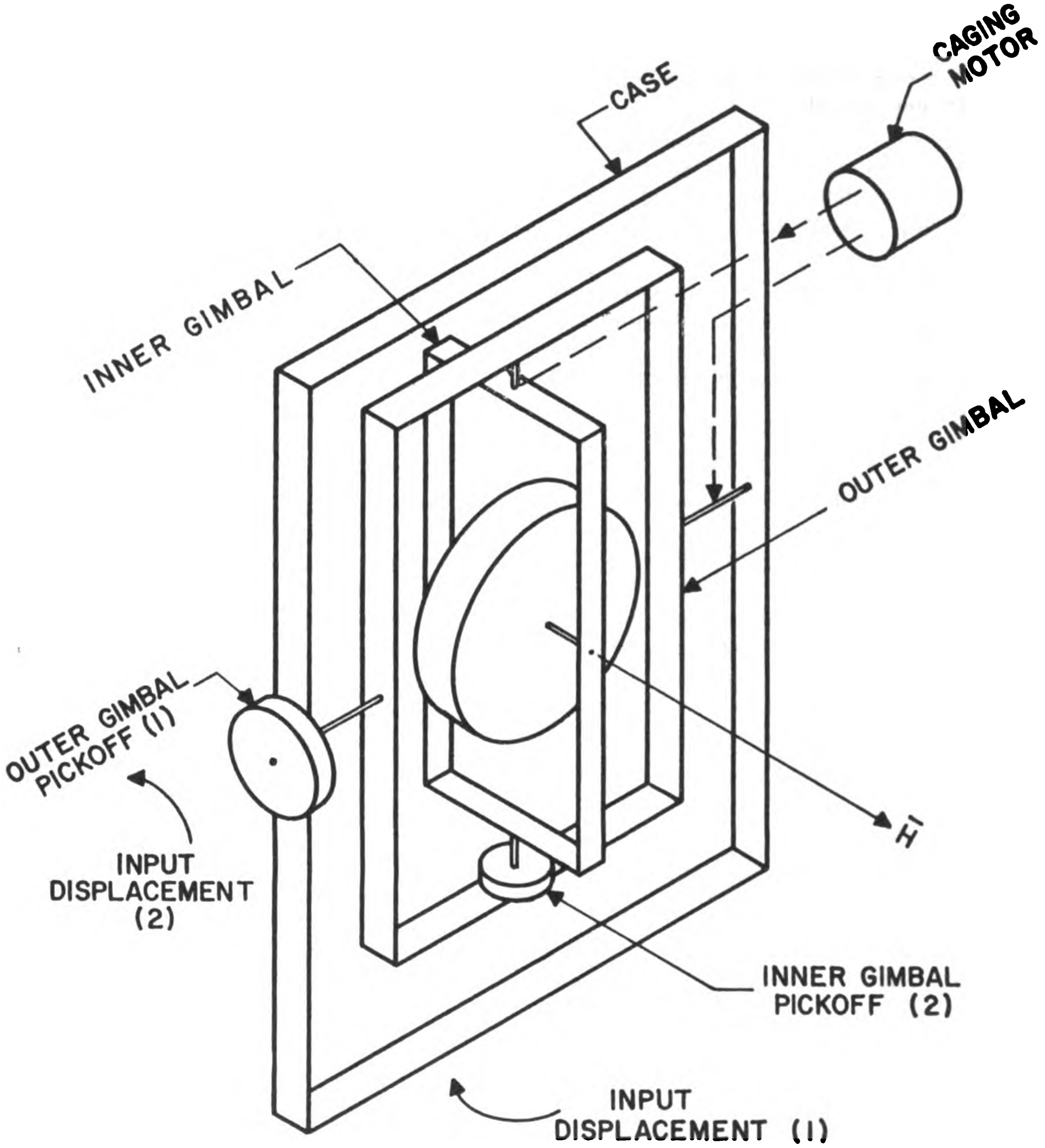

Figure 7-40. Free Gyro with Two Pickoffs

flection. This deflection upon uncaging should be kept as low as 0.05°.

RATE GYRO

Gyros with one degree of freedom are called rate gyros and serve to dampen the turning of a missile. Rate signals are compared with accelerometer signals and corrections are continuously applied to the control surfaces in order to prevent the missile from overshooting during a turn.

Parameters which must be considered for all rate gyros are:

(a) *Resolution* – This is the smallest change of input angular velocity discernible as a meaningful change of gyro output signal. Rate gyros with a maximum input of 10°

per second can attain 0.004° per second resolution while gyros with up to 400° per second usually attain a resolution of 0.02° per second.

(b) *Noise Level* – The noise level can be kept to as low as ± ½ percent full scale with a-c pickoffs. This value is harder to hold with d-c pickoffs during environmental tests.

(c) *Damping Factor* – The ratio of the actual damping to the critical damping at any given temperature defines the damping factor and should be from 0.5 to 0.8 critical.

(d) *Natural Frequency* – This is the dominant resonant mode of the gyro. It should be much higher than the rotational frequencies experienced by the missile in order to prevent resonance of the gyro.

(e) *Null* – Theoretically, the output signal for zero rate input should be zero. Due to inaccuracies in the pickoff, a null signal will occur. It depends upon the type of pickoff but should be kept very low.

For SAM application, two types of rate gyros are discussed.

(a) Spring Restrained Gyro (Figure 7-41) Springs are attached to the gimbal to cause the gimbal displacement to be proportional to the input rate rather than the input torque.

(b) Floated Rate Integrating Gyro (Figure 7-42)

In this single degree of freedom gyro, viscous restraint on the gimbal converts the input turning rate into a torque which is time integrated into a gimbal displacement. Therefore, the output gimbal displacement is proportional to the integral of the input rate. The fluid for restraint also serves to float the gyro gimbal which reduces bearing loading. Reduced loading means lower bearing friction which reduces the drift rate.

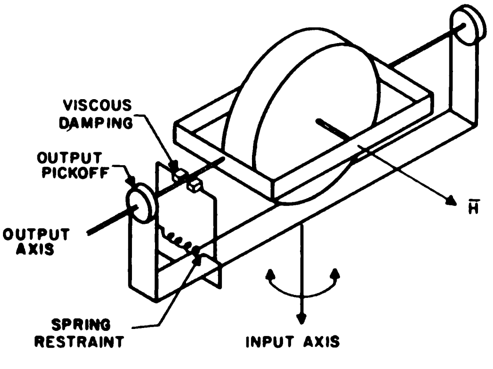

Figure 7-41. Spring Restrained Rate Gyro

Some of the prime considerations in rate integrating gyro applications are:

(a) *Drift* – Due to the low bearing friction resulting from gimbal floatation, the drift of rate integrating gyros is an order of magnitude lower than that of free gyros. A total drift as low as 1° per hour is attainable.

(b) *Warm-up Time* – This is the time required to bring the gyro up to operating temperature. It can vary depending upon whether heaters are used. Although the gyro will function, its operation will be sluggish if the fluid has not reached the proper temperature.

(c) *Torquer Linearity* – This is similar to the signal generator linearity. Since the torquer applies a restoring torque to the gyro, the signal should be proportional to the torque required.

(d) *Output Linearity* – Same as for a free gyro.

(e) *Characteristic Time Constant* – Since these gyros are used as part of a closed loop servo, the time constant should be specified. Response times of two to five milliseconds are considered adequate and most manufacturers have no trouble achieving this.

The parameters given for the various gyros are the most important ones. Figure 7-43 gives an example of specifying requirements for a rate gyro. The characteristics shown are typical but do not represent state-of-the-art limitations. (Figure 7-43 also shows a cut-away of the gyro.)

ACCELEROMETERS

Accelerometers may be of the gyro type or seismic type. The gyro can be used as an accelerometer by attaching a mass to the inner gimbal as shown in Figure 7-44. Under an acceleration, $\bar{a}$, the mass will exert a force $\bar{F} = m\bar{a}$ will

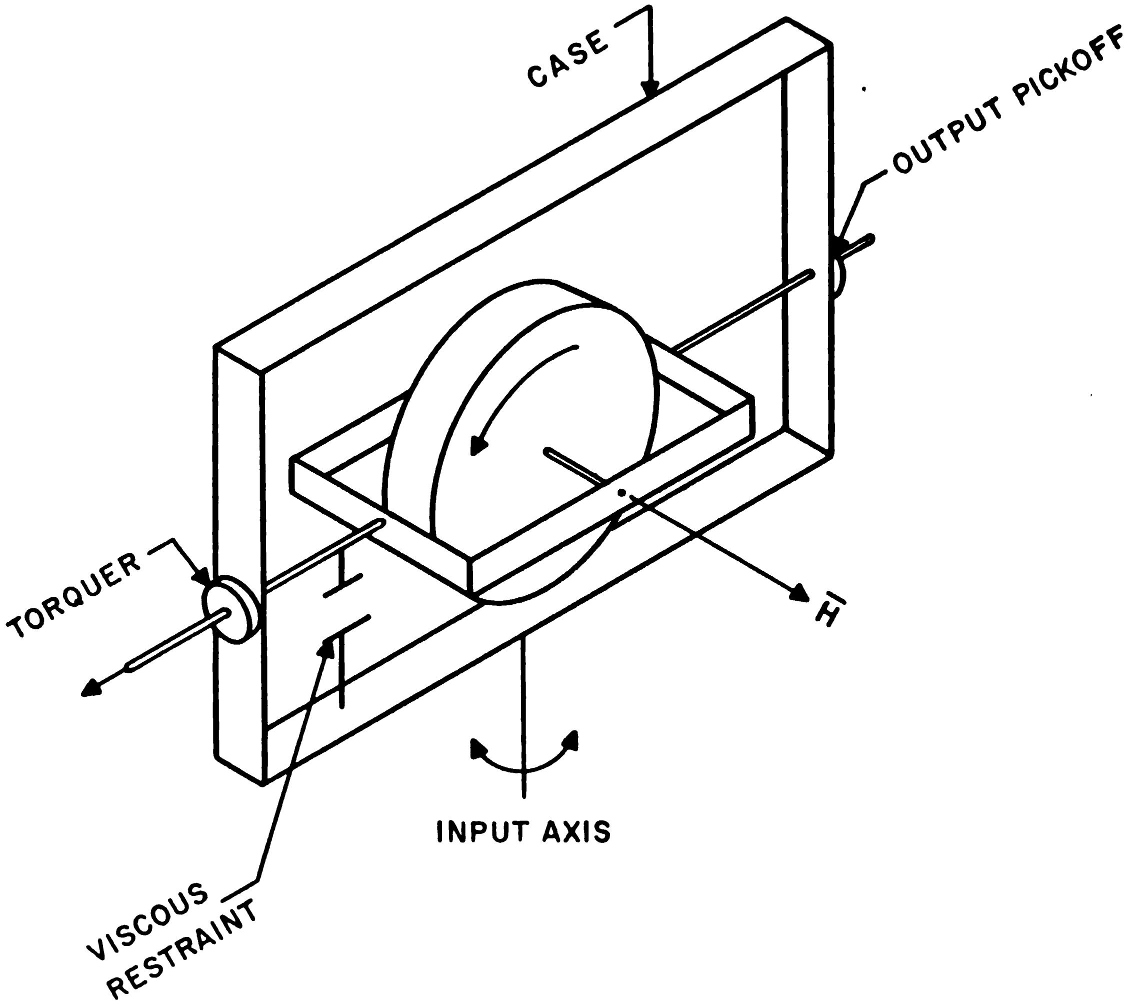

Figure 7-42. Floated Rate Integrating Gyro

be exerted on the weight. This results in a moment about the inner gimbal axis which tends to change the momentum vector, $\overline{H}$. Since the momentum vector resists a change in direction, the gyro precesses about the outer gimbal axis. The rate of precession is proportional to the acceleration input, and the angle of precession is proportional to the integral of the acceleration or velocity. Used in this manner, electrical pickoffs can give either acceleration or velocity data to the control system.

The seismic accelerometer, as shown in Figure 7-45, consists of a mass, spring, a means of damping, a movement reference and a supporting case. Under an external acceleration the summation of forces yields

$$m\ddot{x} + c\dot{x} + kx = -ma \qquad (7\text{-}87)$$

Redstone Arsenal Standard Rate Gyro*

Weight -- 2-1/2 lbs. max.

Size -- 3" x 3" x 6-1/2" max. rectangular space allotted

Gimbal Freedom -- ±3° max.

Gyro Motor
- 400 cps, 3 phase, 115V power
- 10.5 watts max., starting power
- 5.5 watts max., running power
- 1 minute max., run up time

Signal Generator
- Output -- 10V ± 10% for max. rate
- Signal proportional to angular rate within:
  - (1) ±5% of max. output, up to 15% of max. rate
  - (2) ± 10% of max. output, over 15% of max. rate
- Resolution 0.5% of max. rate
- Zero rate voltage -- 0.075V

Range
- Type 45 -- 0° to 45° per sec.
- Type 770 -- 0° to 770° per sec.

Natural Frequency
- Type 45 -- not below 10 cps
- Type 770 -- between 30 and 60 cps

Damping
- 0.5 to 0.8 critical

Life
- 100 hrs. accumulated running time (duty cycle - 15 min. on and 30 min. off)

Environmental Requirements
- Acceleration -- 40g each axis
- Shock -- 60g, 11 millisec. each axis
- Vibration -- 5-19 cps at 1.0" double amplitude
  - 20-2000 cps at 12g
  - 16g for 1 minute at resonant frequency

*This gyro was conceived by Redstone Arsenal as one which could fit a number of U.S. Army missiles with little or no no modification. Its purpose was not to provide a standard design to replace all gyros.

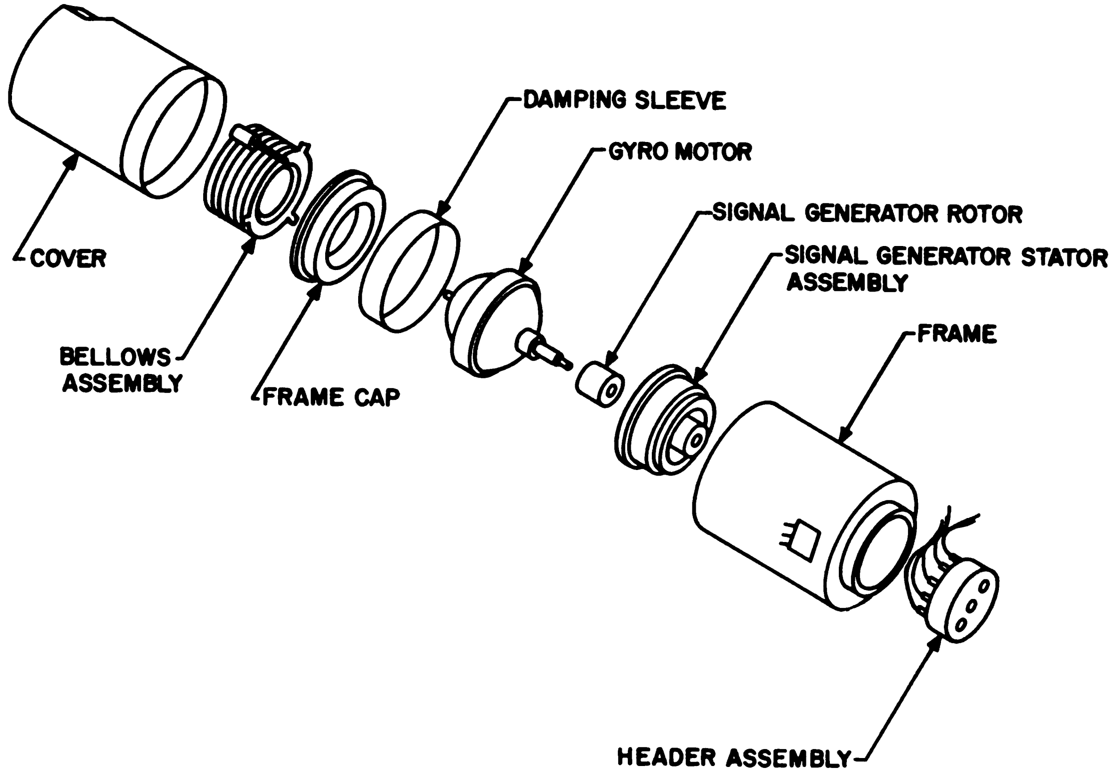

Figure 7-43. Typical Gyro Configuration with Requirements

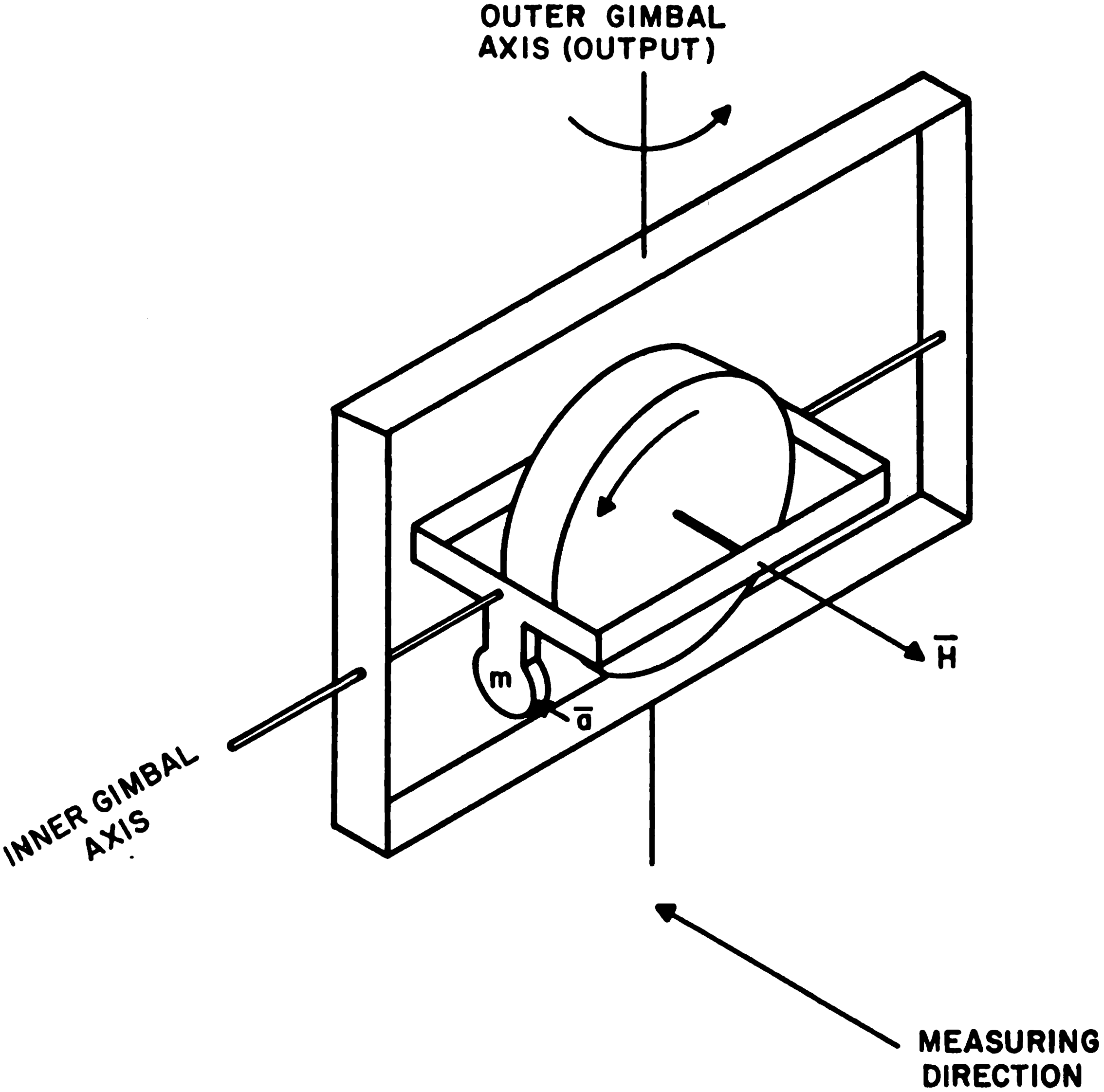

Figure 7-44. Gyro Accelerometer

where

a = external acceleration

x = deflection of mass measured from zero acceleration reference

m = mass

c = damping coefficient

k = spring constant

The minus sign denotes that the deflection of the mass is opposite in direction to the acceleration.

$$\text{Letting } \delta = \frac{C}{2\sqrt{km}} = \text{damping ratio}$$

$$= \frac{\text{damping coefficient}}{\text{critical damping coefficient}}$$

$$\omega_n = \sqrt{\frac{k}{m}} = \text{natural frequency}$$

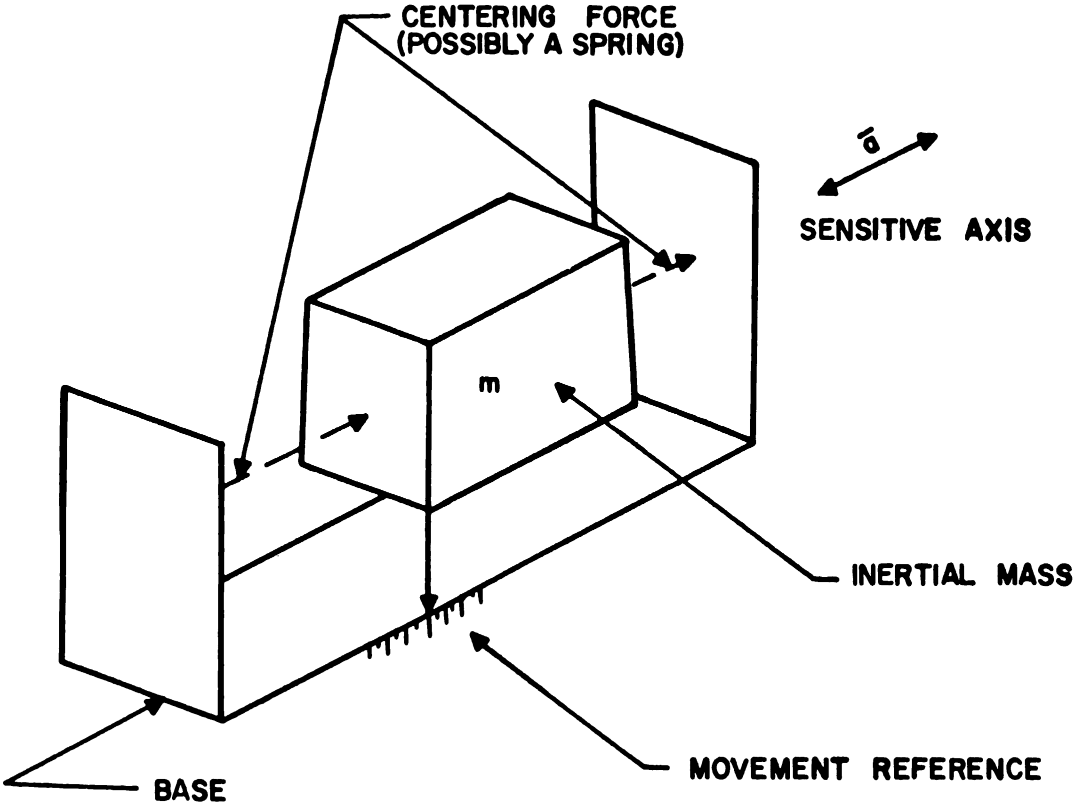

Figure 7-45. Seismic Accelerometer

Then it can be shown that in steady state, the response to a constant acceleration, *a*, is

$$x = \frac{-a}{\omega_n^2} \qquad (7\text{-}88)$$

Hence the deflection of the mass is inversely proportional to the square of natural frequency. This requires low natural frequencies (large masses or soft springs) in order to obtain large deflections.

In the design of this type of device the following factors are important:

(a) The friction, opposing movement of the mass, cannot be exactly zero. The friction therefore must be made as consistent as possible so that its effect upon the displacement can be accounted for in calibration.

(b) The centering force which is generally provided by a spring must also be precise and its characteristics well-known. It is often desirable to have the relationship between the force and the displacement of the spring as linear as possible. This requirement may call for using the spring over a small range of its possible travel accomplished by the use of limit stops to restrict movement to this small increment).

(c) The electrical pick-off of the accelerometer, especially if small accelerations are to be measured, must add very little friction to the device. Just as in the case of the gyro, the electrical devices must not destroy the mechanical precision of the instrument.

(d) Damping of the accelerometer movement is also a problem. Since the seismic accelerometer has all the requirements for mechanical resonance, it is entirely possible that vibration environment of the missile could make the device worthless. For this reason, damping is used to eliminate vibration disturbances. Since the viscosity of the fluid must be controlled to maintain uniform damping, this adds a constant temperature requirement to the use of the accelerometer.

y picking suitable values for the mass, ng constant, viscosity of damping, and fric- forces, this type of accelerometer can be le very sensitive to small accelerations. Un- tunately, as the sensitivity to minute acceler- ons goes up, so does the sensitivity to vibra- n disturbances. This vibration sensitivity and ssible resulting resonance tends to limit the e of this type accelerometer.

ABILIZED PLATFORMS

The stabilized platform is a platform sup- orted so as to retain its orientation with re- pect to space. In general, stabilization of the latform requires three gyroscopes mounted on it so that roll, pitch and yaw movements will be detected by a respective gyro. The electrical outputs of the gyros, which will signal any change in attitude, are used (through amplifiers) to drive the table back to its original position.

Thus, a table or platform, as shown in Figure 7-46, can be maintained at a constant spatial attitude by means of the torque motors driving about the gimbal pivots.

One advantage of this arrangement is that the sensing gyros move slightly about their gimbals before the table is driven in a manner to return the gyro to its original position. This restricts the movement of the gyro gimbals to a small angular motion. Thus, the gyro designer is faced with making a near perfect bearing for movement over a small angle instead of an entire 360° rotation.

Another advantage of the stabilized platform is the rigid surface it offers for the mounting of other guidance devices. Thus, with a stable table it is a simple matter to establish an inertial or spatial coordinate system for the accelerometers. If a missile trajectory requires unlimited angular movement of the missile, the stabilized

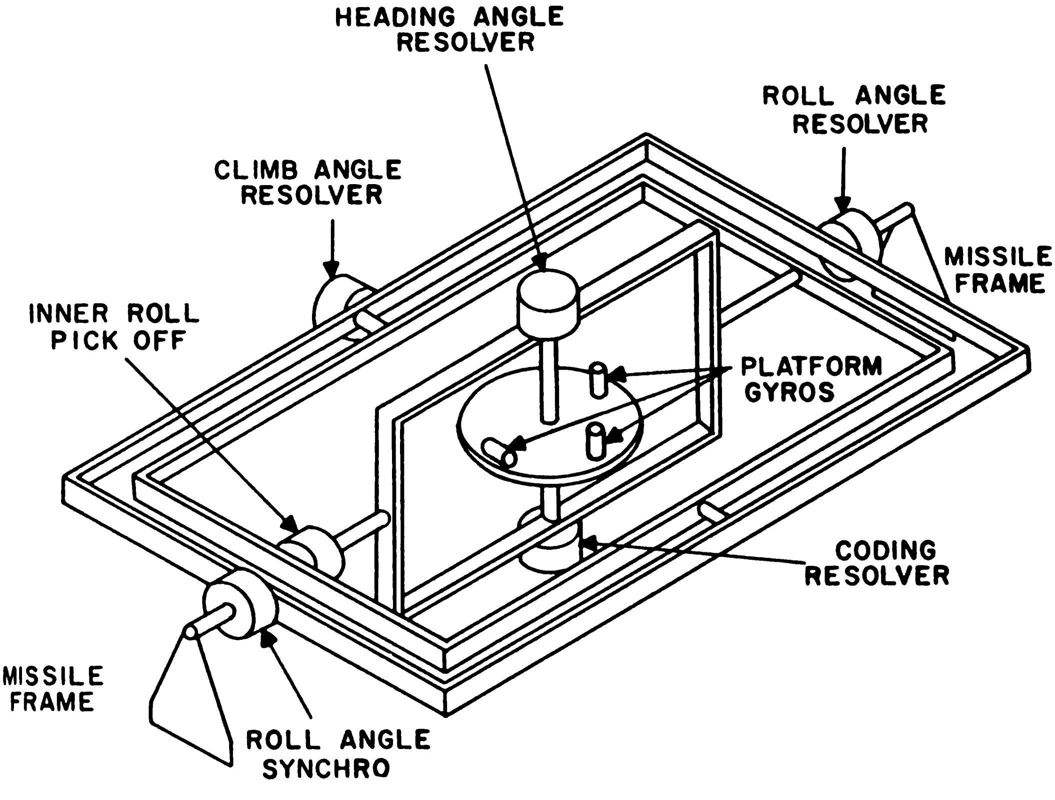

Figure 7-46. Stabilized Platform

platform must be mounted with a system of four gimbals and receive its electrical power through slip rings. If this is not the case, however, and the trajectory can be restricted, then three gimbals and flexible cables can be used.

The major disadvantages of stabilized platforms are their size, weight and power requirements. In addition to amplifiers, torque motors, sensing gyros and a gimbal system, they must have enough area to mount motion measuring devices, thus tending to be much larger and heavier than an airframe mounted measuring system.

A typical application for the stable platform in SAM systems is as a coordinate converter and inertial reference. In this scheme the platform can be used in conjunction with a command guidance system for midcourse guidance and a seeker for terminal homing. The purpose of the platform would be to:

(a) resolve commands from ground coordinate system to missile coordinate system
(b) resolve commands to position seeker head
(c) provide stable reference for mounting of sensors

Figure 7-47 shows a block diagram of platform utilization.

7-6.2.4 Celestial

Star trackers have an automatic telescope which can optically track a given star or planet. This telescope must be able to differentiate between the correct star and all others in or near its field of vision and track the star with a high degree of precision in angular position. Also the missile must contain an accurate time clock for the missile computer. An accurate spatial reference, which can be referrred to the earth must exist. The celestial system must be able to search and re-acquire a star should the tracking temporarily fail.

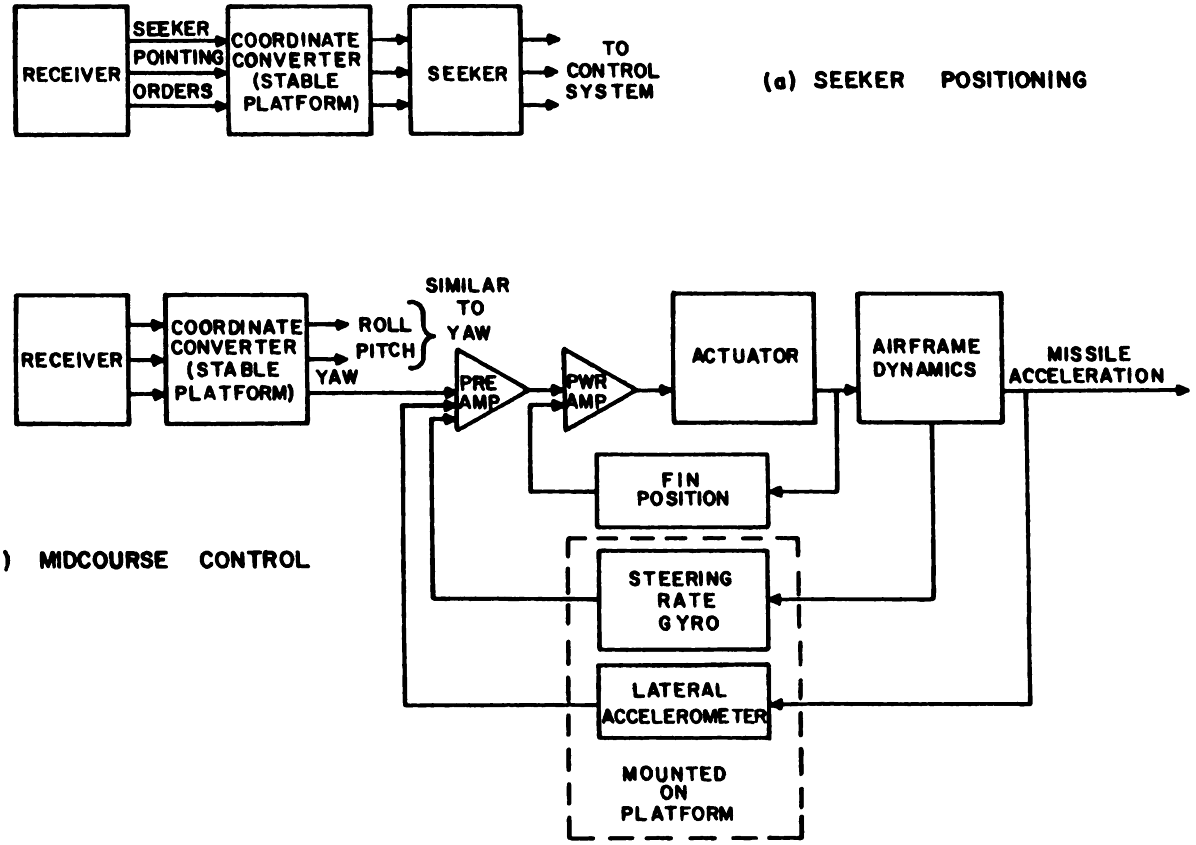

(a) SEEKER POSITIONING

(b) MIDCOURSE CONTROL

Figure 7-47. Typical Command Guidance Stable Platform, Block Diagram

If the above factors exist, it is possible, by conventional calculations, to determine the position of the missile relative to the earth from star positions.

With these requirements a device similar to the stabilized platform is necessary as a mounting device for the telescopes in order to preserve an attitude reference which can be referenced to the earth.

7-6.3 TERMINAL GUIDANCE SENSORS

In addition to the sensors needed for flight control, target sensing must also be provided. This can be obtained by radar, radio transmission, infrared, ultraviolet, or visible light. Sound is a distinguishing target characteristic; however, its propagation is slow when dealing with supersonic targets.

Regardless of the frequency utilized, the guidance mode dictates that the sensor must be fixed to the airframe or that it must be free to move independently. In the latter case both tracking and stabilization loops must be employed. The stabilization problem usually receives attention from the sensor designer so that in initial guidance studies only the tracking characteristics need be considered.

Also, much of the material presented in paragraph 7-7 for radar seekers and infrared seekers is applicable to any sensor. This is particularly true of the material on acquisition and tracking.

7-6.3.1 Radar

When employing radar in the terminal guidance phase, the tactical situation, number of targets, target characteristics, noise, missile attitude, and equipment complexity determine the system selection.

ACTIVE RADAR

In an active radar system, the transmitter and receiver are contained within the missile. A generalized block diagram of an active system is shown in Figure 7-48. The transmitter generates the signal and feeds it through the duplexer to the antenna. The echo is received by the antenna and passed through the duplexer microwave receiver, i-f amplifier and detector to the speed and range gate. From the speed gate, angle signals are derived to drive the antenna servos to follow the target. The range signal is fed back to the i-f amplifier to keep the echo centered in the range gate.

SEMI-ACTIVE RADAR

The semi-active radar system consists of a receiver in the missile and a transmitter located on the ground. The transmitter, referred to as the illuminator, sends out electromagnetic

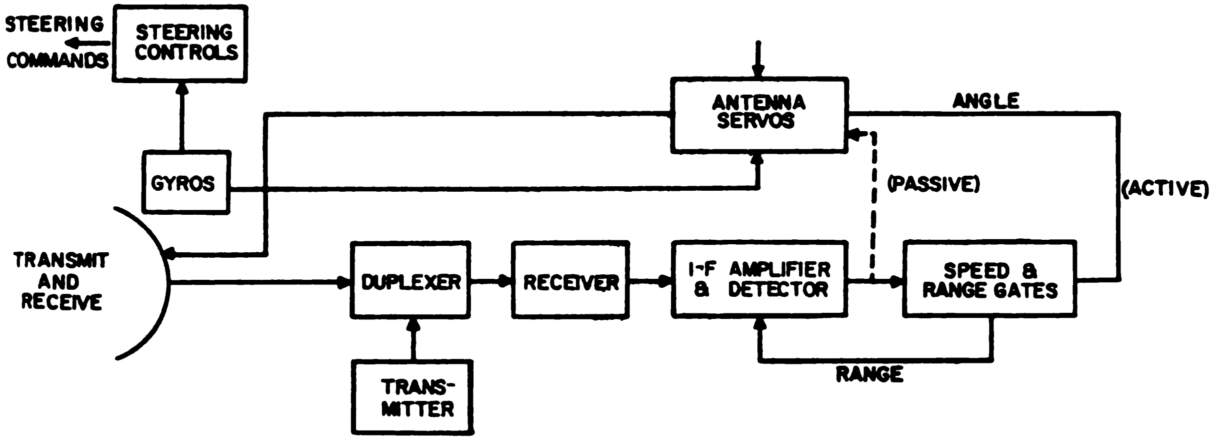

Figure 7-48. Active Seeker, Block Diagram

energy. This energy, reflected from the target, is picked up by the missile receiver. The receiver then locks on to this energy and causes the missile to home in on the target. The illuminator also transmits a synchronizing signal to a rearward-looking antenna. The purpose of this signal is to synchronize the missile guidance system with the illuminator. This makes it possible for the missile to measure range, range rate, or Doppler.

A generalized block diagram of a continuous wave semi-active seeker is shown in Figure 7-49. It operates in the following manner. Reflections from the target are received in the missile through the forward-looking antenna while the reference signal from the illuminator is received through the rearward-looking antenna. The rear signal is heterodyned with the local oscillator, amplified in the rear i-f amplifier and serves as a reference for coherent Doppler detection.

The forward-looking antenna receives the energy reflected from the target in the form of a Doppler shift signal. (The local oscillator is tuned to the illuminator frequency.) The target signal is heterodyned in the mixer to a lower frequency by the local oscillator. The signal is then amplified and heterodyned with the reference signal from the rear antenna. The Doppler amplifier further amplifies the signal. The speed gate then *locks on* to coherent signals within the Doppler spectrum. The signal is then resolved into pitch and yaw components by phase comparison with the scan reference signal. Voltages are then generated to steer the missile.

The semi-active seeker has the advantage over the active seeker of greater range. The missile also has less on-board equipment when the semi-active seeker is used since the transmitter is ground based.

PASSIVE RADAR

Passive radar seekers utilize electromagnetic energy from the target to provide homing signals. This electromagnetic energy may come from:

(a) radar transmitters

(b) radio transmitters

(c) electronic countermeasures equipment

The passive seeker is thought of as a device which homes on electromagnetic energy rather than strictly radar signals.

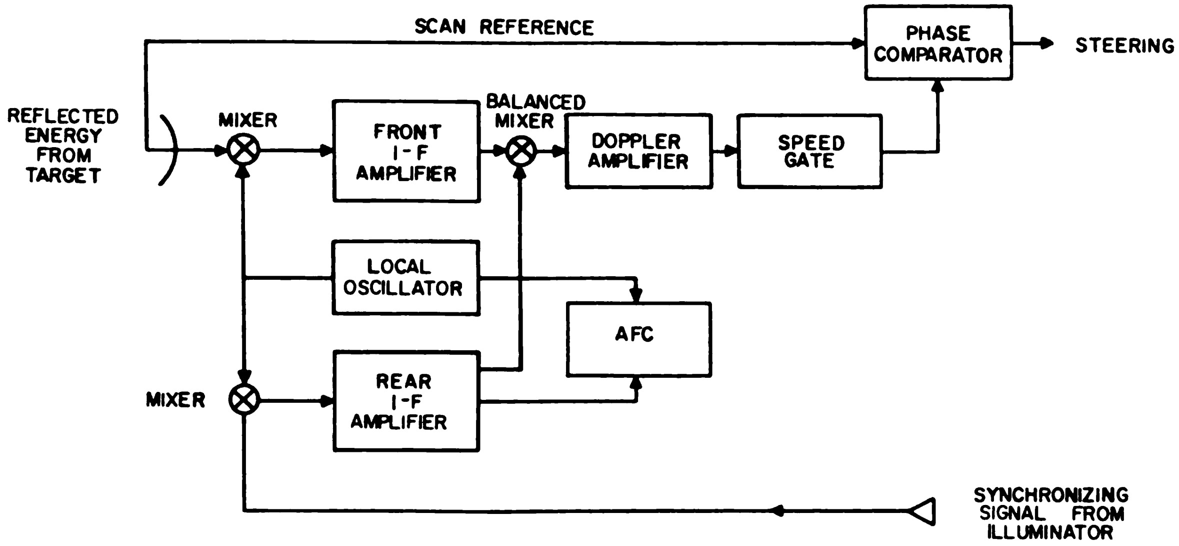

Figure 7-49. Continuous Wave Semi-Active Seeker, Block Diagram

Since the target will not intentionally provide n electromagnetic signal on which a missile ould home, it might appear that in the SAM ole there would be no requirement for a passive eeker missile. Such is not the case since the greatest application of this type of guidance is in conjunction with another system (command, active seeker, etc.). In this mode the passive seeker is used to home on jamming signals; thus when the primary guidance mode is jammed, the passive system can take over to continue guiding the missile.

The dotted line in Figure 7-48 illustrates a passive circuit used in conjunction with an active seeker. In the event of jamming, an angle tracking signal is obtained from the jammer noise signal in the i-f amplifier prior to the gates. This signal is fed to the antenna servo in place of the usual angle tracking signal. Rate signals from the gyros which measure the antenna tracking rate are fed to the steering controls.

GENERAL COMPARISON

The overall characteristics of radar systems are summarized in Table 7-8.

7-6.3.2 Infrared[48,49]

Infrared is an electromagnetic radiation whose frequency ranges from approximately one million to 100 million megacycles and falls between the visible and microwave regions as shown in the spectrum chart of Figure 7-50. Optical systems used to collect visible light are used to collect infrared radiation, although the optical elements themselves may be opaque to visible light. *Infrared radiation should not be confused with heat waves which are due to thermal convection or conduction through a medium.* Any object above absolute zero (−273°C) will radiate energy at all wavelengths due to molecular thermal action within the body. The term radiation refers to the continual emission of energy from the surface of a body and is in the form of electromagnetic waves identical to radio and light waves but differing in wavelength. These waves are propagated at the speed of light through a vacuum as well as air.

When radiant energy falls upon another body, some of the energy will be absorbed and converted to heat. The radiant energy emitted

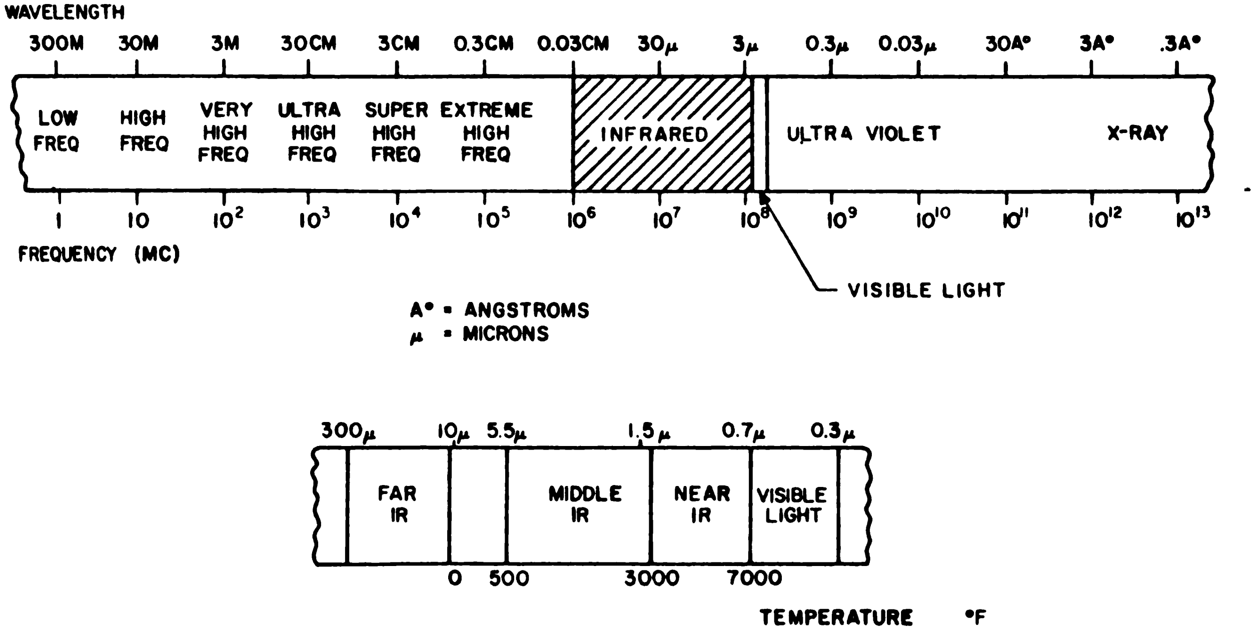

EXPANDED INFRARED SPECTRUM

Figure 7-50. Electromagnetic Spectrum

TABLE 7-8. GENERAL COMPARISON OF ACTIVE, SEMI-ACTIVE AND PASSIVE RADAR SYSTEMS

		Active	Semi-Active	Passive
Basic Equipment	Ground Based	Detection and Tracking Radar Computer	Detection Radar Tracking and Illumination Radar Computer	Detection Radar Computer
	Airborne	Seeker	Seeker	See Seeker "Application Note"
Over-all Range Capability		Greatest when used only for terminal guidance; system range determined by ground radar; accurate homing at long range provided by active seeker.	Generally inferior to active seeker system, because of homing uncertainties at long ranges	Uncertain
Guidance Information that Can Be Derived From Seeker		Range to Target Target Speed and/or Closing Rate Target Bearing	Range to target subject to errors from intercept geometry Target speed and/or closing rate when reference signals are transmitted from ground	Target bearing
Seeker Weight		Greatest	Low	Least
Problem Areas		In pulse systems, recovery time determines minimum effective seeker range	Target resolution; ground radar may illuminate several targets simultaneously -- Illumination radar must have high power and narrow beamwidth	
Application Notes		Weight generally limits application	Very effective when used "all the way" for relatively short-range intercepts.	Passive seekers are most often used in combination with active and semi-active seekers to give capabilities in jamming environment

by a surface depends upon the nature of the surface and its temperature. At low temperatures, the rate is small and of chiefly long wavelength. At higher temperatures, the radiation rate increases rapidly and the relative amount of energy at short wavelengths increases as shown in Figure 7-51. The peak radiant energy emitted from the surfaces shifts to shorter wavelengths as temperature increases.

A basic concept in infrared is that of a *black-body*. *A black-body absorbs all and reflects none of the energy falling on it.* Peak radiation from the black-body at 600°C occurs at 3.3 microns wavelength (1 micron = 10^{-4} cm). If the black-body temperature is raised to 1000°C, the peak shifts to 2.25 microns and the total radiation increases as the fourth power of absolute temperature.

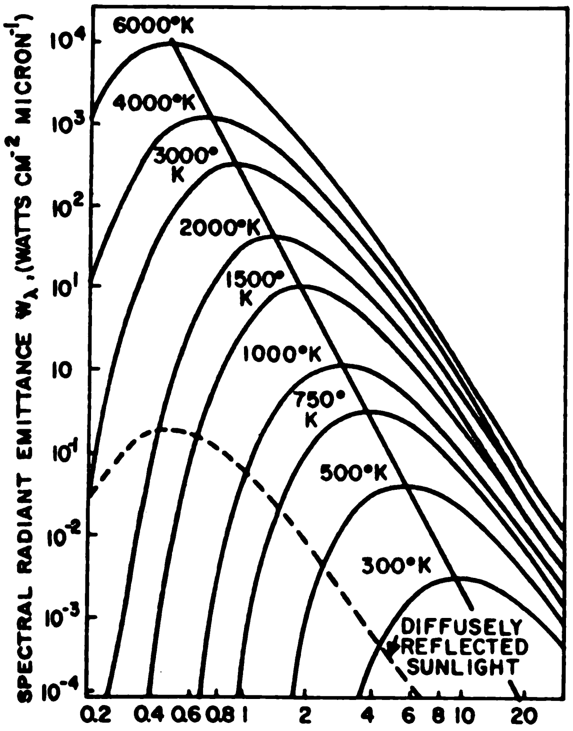

Figure 7-51. Spectral Distribution of Black Body Radiation

7-6.3.3 Ultraviolet

The ultraviolet spectrum falls between the visible and the soft x-ray spectra, the longest wavelength being about 0.3 micron and the shortest about 30 angstroms. Only limited data is now available on the emission of ultraviolet energy by military targets and the usefulness of this spectrum has not been fully established. Some ground measurements on rocket exhaust radiation in the 0.2 to 0.29 micron band exist at both short and relatively long range.[50,51] However, the data is somewhat unsatisfactory from an instrumentation standpoint. Targets can also be detected in the ultraviolet spectrum by *negative contrast* in daytime at low altitudes and fairly short ranges. *In negative contrast detection, the background is brightly lighted and the target appears as a dark spot on the background.* Ultraviolet detection has advantages over visible detection for this type of silhouette because of the suppression of background gradients by atmospheric scattering. Best detection occurs when background radiation is small. For ultraviolet, background radiation below 0.28 micron is much smaller than for visible or infrared systems at low altitudes,[52] but much worse above 30,000 feet. The scattering problem, while it reduces backgrounds, also attenuates signals so that only short ranges are possible. This same scattering problem has severely restricted the use of active systems. The principle source of background radiation in the ultraviolet spectrum is scattered sunlight, but between 0.21 and 0 30 micron, the Hartley bands of ozone strongly absorb this solar radiation. This ozone concentration is maximum at altitudes above 60,000 feet but little data exists at lower altitudes. Data which exists shows wide possible variations. Some attenuation coefficients for low level horizontal paths have been published[53] for the 0.22 to 0.46 micron region. These show smooth variations principally in accordance with Rayleigh scattering, inversely proportional to λ^{-4}.

Detectors for the ultraviolet region include Geiger-Muller counters and photo-multipliers. The prime need is for detectors which are *solar-blind*, that is, those which are sensitive only to ultraviolet in the ozone absorption band and are insensitive to the sunlight background outside this band. Thus one needs a very sharp cutoff at 0.29 micron.

7-6.3.4 Optical

The band of wavelengths between 0.7 and 0.4 micron is designated the visible spectrum in accordance with the spectral response of the eye. Detection equipment operating in the visible region generally uses negative contrast or sunlight illuminated targets and thus, are primarily useful during daylight hours. Automatic equipments using the visible spectrum are severely limited by background variations such as clouds and sky gradients. On the other hand, visible systems can be more effective than infrared equipments under certain conditions as, for example, poorly radiating targets such as aircraft viewed head on.[54,55] Night time operation is usually restricted to targets of the self-radiating type of sufficient temperature to give luminosity.

In spite of the background limitations imposed on visible light systems, they find many applications in missile launch tracking, star tracking and mapping due to their high resolution. Mapping techniques are probably most effective in the visible spectrum because maps so obtained bear high correlation with that which the eye sees and can, therefore, be easily interpreted.

Typical detectors of visible radiation, aside from the eye, are the photoconductors, the photo-multipliers, and various camera tubes such as the image orthicon, the vidicon and the more recent image intensifier orthicon.[56] The primary noise limitation on photo-multipliers

TABLE 7-9. COMPARISON OF VARIOUS SEEKER SYSTEMS

	Radar	Infrared	Visible	Ultraviolet
Mode of Operation	Conical Scan Doppler	Positive Contrast Reticle Modulated	Negative Contrast Reticle Modulated	Negative Contrast Reticle Modulated
All weather capabilities				
Water vapor	Excellent	Depends on λ	Excellent	Good
Haze-fog	Good	Poor	Poor	Operates at short range
Clouds	Good-long λ Fair-short λ	Poor	None	Low altitude and clear weather
Rain	Good-long λ Fair-short λ	Good	Fair to poor	
Acquisition capabilities (Jet aircraft)				
Nose	Fair	Poor	Poor-Fair	Poor-Fair
Beam	Good	Fair	Fair	Fair
Tail	Fair	Good	Poor-Fair	Poor-Fair
Acquisition Range	Depends on radiated power, target size	Depends on target radiation, aperture size	Depends on contrast, target size and aperture	Depends on contrast, target size and aperture
Acquisition Field of View	20-60°	3-5°	3-5°	3-5°
Track Accuracy	Increases, then decreases with range to go	Good (1-4 milliradians)	Good (1-4 milliradians)	Good (1-4 milliradians)
Best Time of Operation	Day-Night	Night	Day only	Day only
Tail Chase Capabilities	Poor	Excellent	Fair	Fair
Countermeasures	ECM Chaff etc.	Flares only	Balloons etc.	Balloons etc.
Complexity	Very	Simple	Simple	Simple

in the atmosphere is usually photon noise received from sky radiation. Sky radiation on a clear day falls off with zenith (angle being minimum at the zenith) and also decreases with altitude.

7-6.3.5 Hybrid

There are certain advantages and disadvantages which accrue to the use of each spectral region. For example, far better resolution can be obtained with optical systems in the infrared, visible and ultraviolet than with the longer wavelength radar systems with the same antenna or optical aperture. Water vapor which seriously degrades infrared performance in some spectral regions effects neither radar nor visible light systems. Ultraviolet systems which seem to offer a great deal of promise in short range low altitude applications, are virtually useless above 30,000 feet altitude due to absorption by ozone. In Table 7-9 the effects of the spectrum chosen on seeker performance are tabulated for radar, infrared, visible and ultraviolet systems. Such a table can indicate only the general trends. Nevertheless, the use of two or more different spectrums in the same seeker is suggested to take avantage of the best characteristics of the various spectra. For instance, radar which has long range and large acquisition angle capability, loses its accuracy at short range. Conversely, infrared with its narrower field of view retains and may even increase its accuracy with decrease in range. Furthermore, infrared can be added to a radar seeker without large size, weight, or complexity penalties. The combined infrared-radar seeker is often referred to as a dual-mode seeker.

While a dual-mode seeker possesses certain advantages, its overall kill probability may be limited by the limitations of each mode. For instance, the prime considerations of an infrared-radar seeker would be weather and range. As mentioned previously, a good weather-short range condition calls for infrared guidance; a bad weather-long range condition would necessitate radar guidance. Under adverse weather conditions at close range, the accuracy of an infrared-radar seeker would be limited to the degree of accuracy of the radar mode at close range.

7-7 TERMINAL GUIDANCE SEEKERS

7-7.1 GENERAL

While methods for designing the various radar seekers discussed previously are covered in Chapter 6, the same cannot be said for IR seekers. Rather than duplicate that effort in the following, pertinent references are given. It should be noted also that much of the basic IR information presented for seekers is applicable to ground based detection.

7-7.2 SEEKER FUNCTIONS

There are two classes of seeker problems associated with terminal guidance – acquisition and tracking.

Acquisition marks the beginning of the terminal guidance phase. In some systems, it occurs during pre-launch operations. In such a case, a ground radar and computer may be used to derive commands for training the launcher and starting the scanning operation of the seeker. When the seeker locks on to the target, the missile is launched. It is, then, in terminal guidance during its entire flight.

More generally, consider the missile to be in flight, and in a midcourse guidance phase. At some point (determined, for example, by a command transmitted from the ground, or an internal timer) the seeker begins to search for the target. When the seeker locks on to the target, acquisition is completed and the missile is in its terminal guidance phase.

After lock-on, the seeker becomes the source of guidance data for the missile. It must maintain its lock on the target. In doing so, it performs, essentially, a tracking function. The tracking data are the inputs to the missile guidance system. (See remarks in paragraph 7-6.3 concerning stabilization.)

7-7.2.1 Target Acquisition[42,57]

The factors which affect target acquisition are primarily

(a) scanning technique
(b) detection technique
(c) range capabilities of seeker

The fact that the detection process is probabilistic in nature adds to the complexity of the problem. A generally accepted criterion for acquisition is the range at which the probability of detection and lock-on reach some specified level (typically 70 percent to 90 percent).

SCANNING TECHNIQUE

Scanning may be viewed as the search mode of the seeker. When a platform-mounted antenna is used, the antenna is swept mechanically through a predetermined pattern. With this scheme, a narrow beamwidth (desirable for tracking after lock-on) may be used to search a relatively large volume of space. Two of the more common scanning patterns are depicted in Figure 7-52. The maximum angular displacement of the antenna *(maximum look angle)* with such patterns is typically of the order of 25° to 45°. The time to complete one scan may be of the order of 1 to 5 seconds. Area detectors such as vidicon or IR vidicon can be scanned electronically and, hence, much more rapidly.[58]

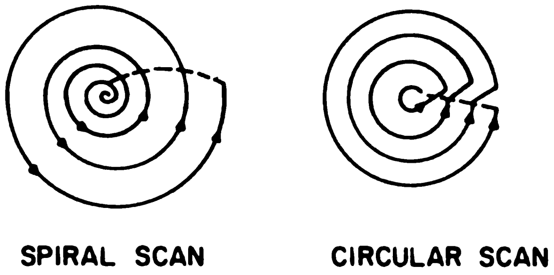

Figure 7-52. Possible Scan Patterns

When the target is detected, the seeker shifts to a conical scan (one form of *sequential lobing*) about the relative target bearing. These scanning actions are depicted in Figures 7-53 and 7-54.

In some systems, the search mode is not used. This would be the case when

(a) the seeker is locked on to the target prior to launch

(b) midcourse guidance errors are small enough to permit prepointing of the seeker.

In general, however, it is necessary to investigate the intercept problem in order to determine look-angle requirements consistent with acceptable system performance.

Information of considerable value can be obtained from idealized geometrical relations.[59] To illustrate this aproach, consider a system which is designed for a collision intercept. Assuming a two-dimensional representation, Figure 7-55 depicts the pertinent quantities involved.

It is assumed that the missile is on a perfect collision course to the target. Hence,

$$V_T \sin \phi = V_M \sin \Theta \qquad \text{(a)}$$

or, (7-89)

$$\sin \phi = r \sin \Theta \qquad \text{(b)}$$

Equation 7-89 may be used to plot a family of curves relating the three parameters Θ, ϕ, and r. From these, the maximum look angles (plotted in Figure 7-56) may be deduced.

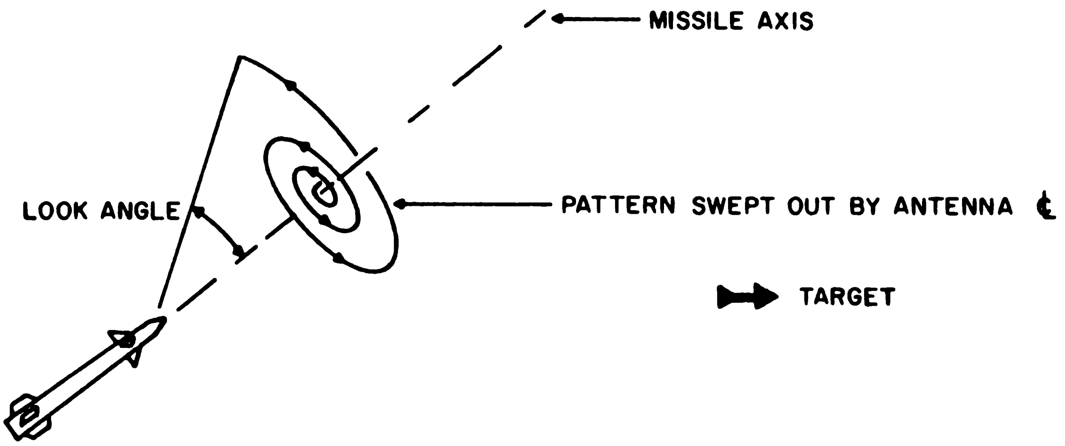

Figure 7-53. Scanning (Search Mode)

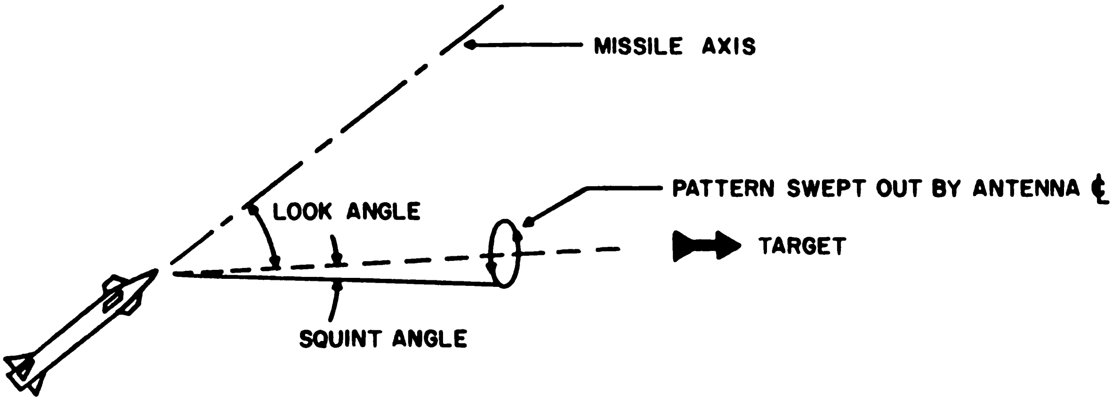

Figure 7-54. Conical Scan (Track Mode)

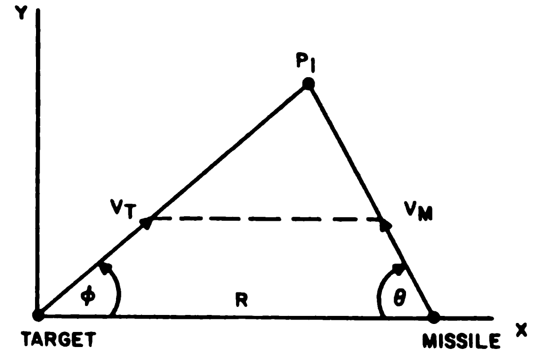

ϕ = TARGET ANGLE
θ = LOOK ANGLE
V_M = MISSILE VELOCITY
V_T = TARGET VELOCITY
R = RANGE, MISSILE TO TARGET
$r = \frac{V_M}{V_T}$ = SPEED RATIO
P_I = INTERCEPT POINT

Figure 7-55. Intercept Geometry

It is also necessary to find the conditions for which an intercept is possible. When r>1, an intercept is always possible provided the missile has sufficient range capability. For r<1, the angles Θ and ϕ have some influence. From equation 7-89, the region where an intercept is not possible is defined by

$$\frac{\text{Sin}\,\phi}{r} > \text{Sin}\,\Theta \;;\; r < 1 \qquad (7\text{-}90)$$

If the maximum look angle is allowed to be 90°, there results

$$\text{Intercept Impossible:} \frac{\text{Sin}\,\phi}{r} > 1 \;;\; r < 1 \qquad (7\text{-}91)$$

This region is shown in Figure 7-57.

This approach can be used further to develop relations involving the rate of closure, and the effects of simple target maneuvers. A detailed analysis of this problem is given in reference 58. This approach is useful for determining system requirements involving look angle, midcourse guidance accuracy, missile range, seeker detection range, and missile turning rates.

In systems which employ body-fixed antennas, a scanning technique in the sense depicted in Figures 7-52 and 7-53 (search mode) does not exist. Such systems depend on wide beamwidths to achieve the necessary coverage for reliable acquisition. A typical combination monopulse, for example, may have an effective beamwidth of the order of 45° to 60°. However, the problems of look angle, midcourse guidance accuracy, etc., are still present. Hence, the analysis outlined in this section is still applicable.

To complete the analysis, computer simulations will usually be required. In particular, simulations can incorporate the missile response characteristics, and probabilistic disturbances, into the analysis.

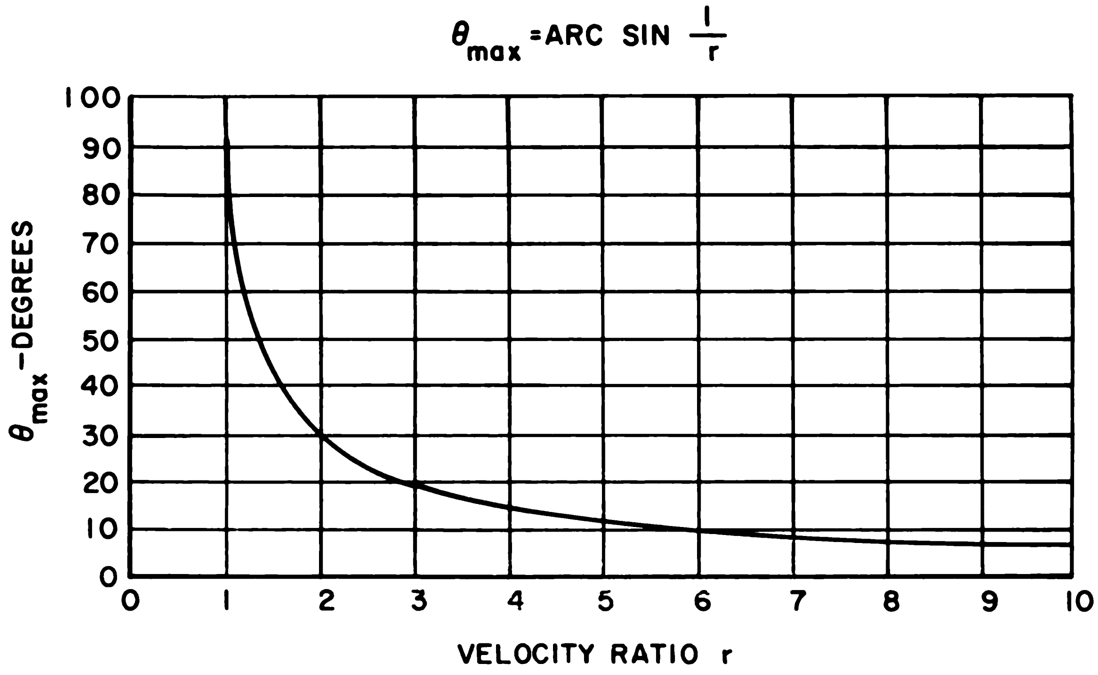

Figure 7-56. Maximum Look Angle Required for Successful Intercept

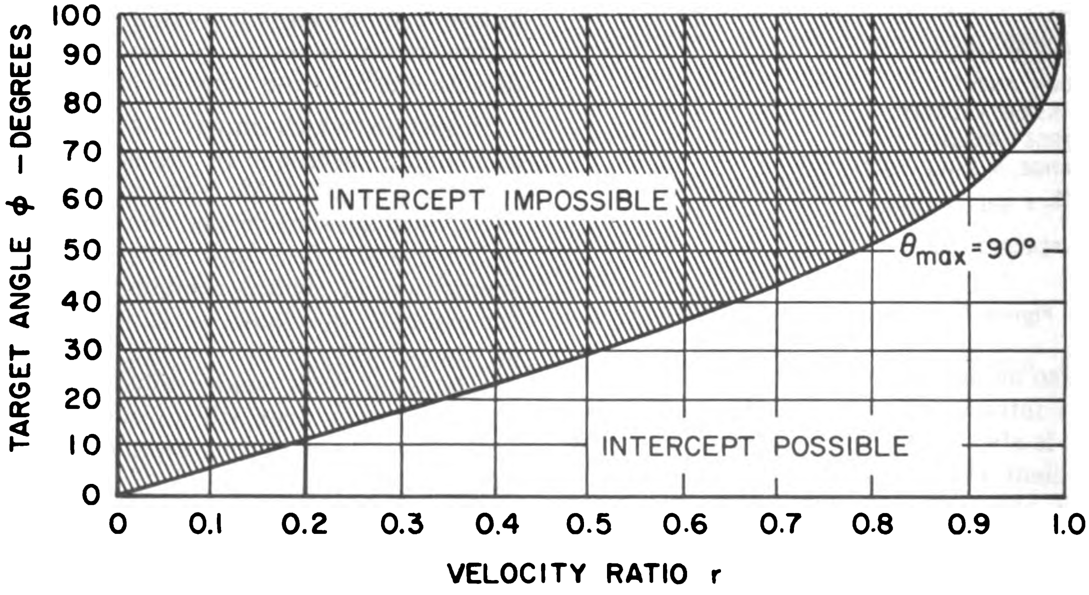

Figure 7-57. Region of Possible Intercept

DETECTION TECHNIQUE

The fundamental problem of detection is to achieve an acceptable probability of detection in the operating environment of the seeker. The usual problem is that the signal-to-noise ratio is very low at the required detection range. When this is the case, it may be possible to enhance the probability of detection through the use of special data-processing techniques. In addition, detection must be accomplished automatically. This is usually done by using a threshold device during the data processing.

Because the IR design data has not yet been presented, the detection problem will be discussed in terms of radar seekers. Similar considerations apply to IR.[57] (See paragraph 7-7.4.5, Infrared Range Equations.)

One of the primary considerations which affects the design of the entire radar seeker concerns the notion of coherence. A coherent system is one in which the target echo is referenced to the transmitted signal in phase and frequency. In a non-coherent system, such a relationship does not exist. The block diagrams in Figure 7-58 illustrate the principles involved. Coherence may be obtained by means other than that shown in Figure 7-58a. Several alternate schemes, applicable to active seekers, are described on pages 635-638 of reference 60.

For a semi-active seeker, the coherent reference signal must be derived via a transmission from the ground. Figure 7-59 illustrates this principle for a pulsed radar. Figure 7-49 is a complete block diagram for a coherent CW semi-active seeker.

The principal advantage in using coherent systems is that the Doppler principle may be used to derive velocity data on the target. By using velocity gates to lock on the target, some capability is obtained for resolving multiple targets. Coherent systems are particularly advantageous when the missile must operate in a strong clutter environment, such as for low-altitude intercepts. Velocity gating and pulse comparison techniques can be used to improve the discrimination between target echoes and clutter returns.

Doppler devices are discussed further in paragraph 7-6.2.2. The general aspects of MTI detection, cancellation ratio and subclutter visibility, calculation of clutter attenuation and a sample calculation for single pulse-to-pulse cancellation are discussed in paragraph 6-3.4.4 of Chapter 6. Rain and cloud cover are discussed in paragraph 6-5.3.4 of Chapter 6.

To provide for automatic detection, a threshold device must be used. Such a device would be set to a predetermined bias level. When the input signal exceeds this bias level (the *threshold*), detection is said to occur. In Figures 7-58 and 7-59 such a threshold device could be used to accept the output of the detector.

Because noise is always present in a radar receiver, false detection will occur from time to time when noise pulses exceed the threshold. A high threshold decreases the probability of such a *false alarm*. However, this also makes target detection more difficult. Extensive investigations in this problem area have been carried out by various researchers. References 61 and 62 are the outstanding works on this subject.

When detection is performed on the basis of a single pulse, high signal-to-noise ratios are required for reliable results. A signal-to-noise ratio in the order of 12 to 14 db will usually be necessary to achieve a probability of detection of about 70 percent.

A significant improvement over the single-pulse detection performance can be obtained through the use of integration. In such a scheme, successive pulses are added over a period of time called the integration time.

Two common types of integrators are the unweighted and exponential integrators. The unweighted integrator simply adds pulse amplitudes over the integration time. The exponential integrator usually takes the form of a simple RC filter, and performs averaging as well as integration. An exponential integrator causes a slight degradation in the range capability of a radar, as compared to a perfect (unweighted) integrator. As a rough figure of merit, range is decreased about 10 percent when the exponential integrator is used instead of an unweighted integrator.

Integration may be performed in the r-f, i-f, or video stages of a receiver. In all three cases, performance is essentially the same. R-f and i-f integration are usually used when the sys-

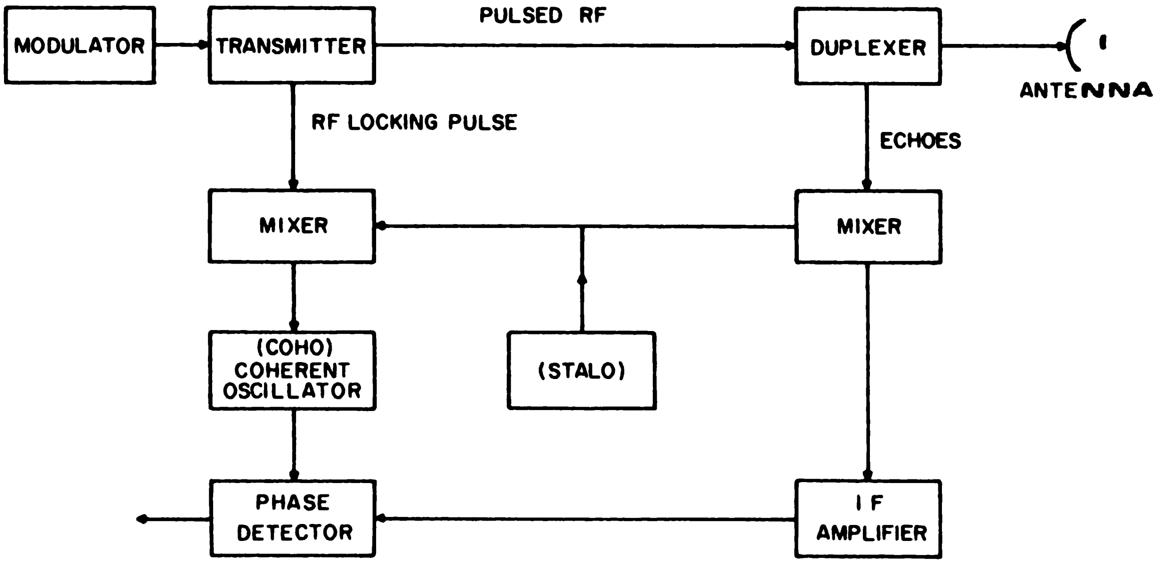

(a) COHERENT SYSTEM

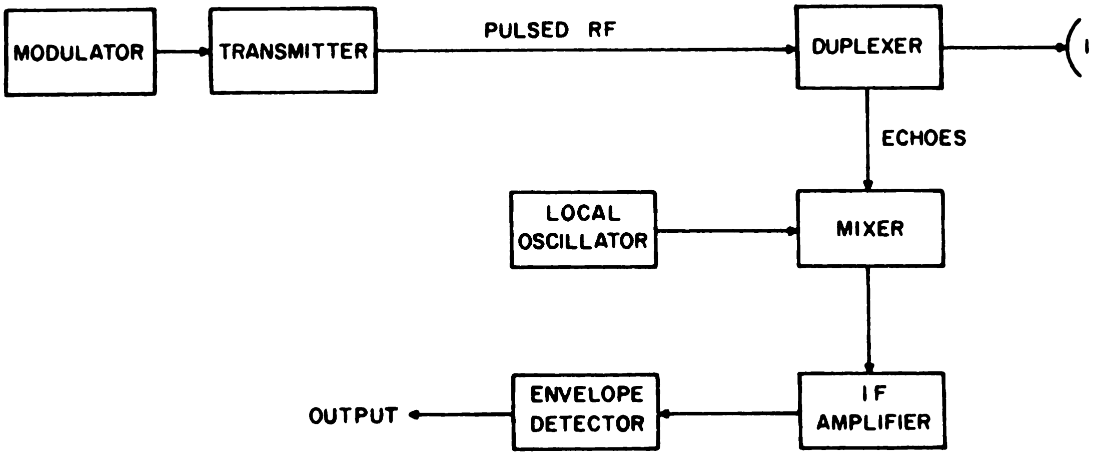

(b) NONCOHERENT SYSTEM

Figure 7-58. Radar Section of Typical Active Pulsed-Radar Seekers

tem is a coherent system. Figure 7-60 illustrates the integration and detection portion of a typical coherent pulsed-radar seeker.

When the threshold device has an output, the lock-on phase is initiated. The guidance servo-loop is closed, scanning (search mode) is stopped, and the antenna goes into a conical scan motion.

RANGE CAPABILITY OF SEEKER[43,44]

In evaluating or designing seekers, it ultimately becomes necessary to make computations of detection range. (See paragraph 7-7.4.5 for IR seeker range discussion.) Detection range must be computed for a specified probability of detection, and a specified false alarm rate. Integration time is a third significant parameter.

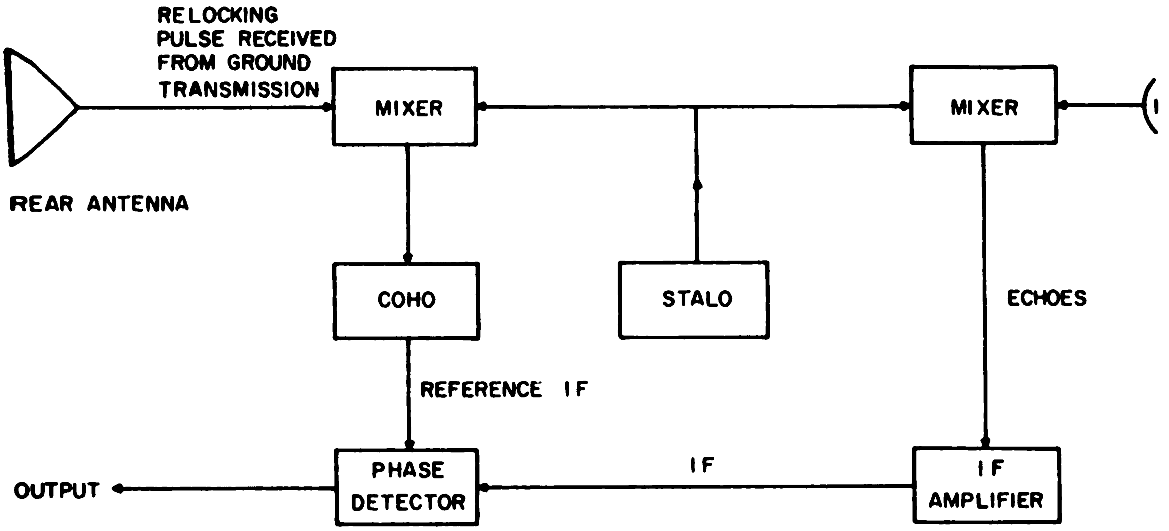

Figure 7-59. Radar Section of Typical Semi-Active Coherent Pulsed-Radar Seeker

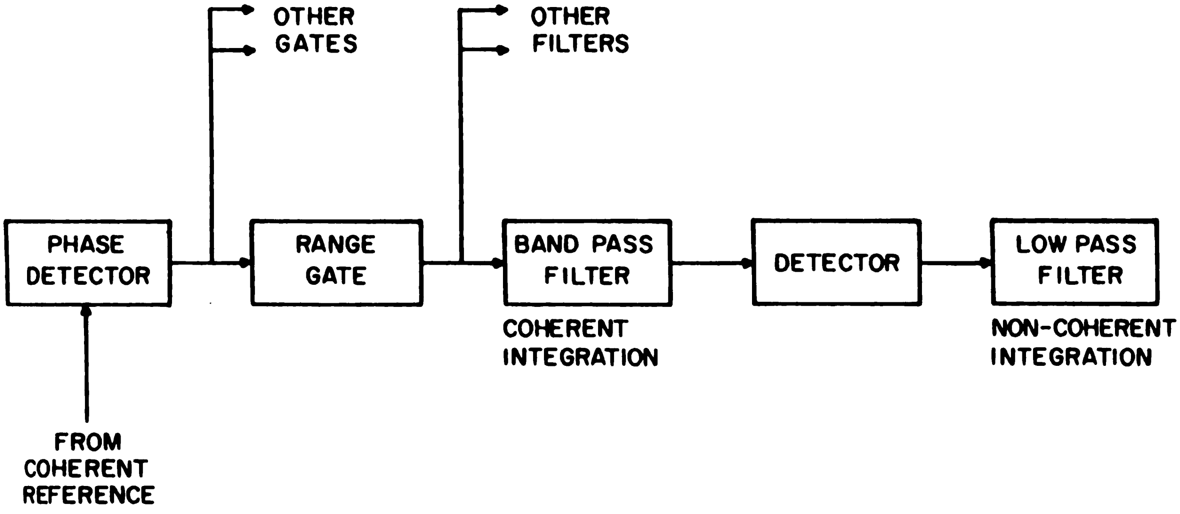

Figure 7-60. Integration and Detection Section of a Typical Coherent Pulsed-Radar Seeker

Seekers in which the transmitted energy must pass through a radome suffer an additional degradation in range performance due to absorption by the radome walls. Transmission coefficients are very difficult to estimate, and are known to change with temperature, and the angle of incidence of the radiation. Reference 63 contains some background information, and includes a tabulation of measured transmission coefficients. The highest one-way transmission coefficient listed is about 0.95 averaged over a 120°C temperature range. A conservative figure for a well-designed radome would be about 0.85. Additional transmission data is given in reference 20 (pp. 360, 361) while temperature data is given in reference 42 (p. 534) and reference 10 (p. 302).

7-7.2.2 Target Tracking[42]

When target echoes are detected, certain information becomes available to the guidance and control equipment. In all cases, angle information is necessary. This information is used to:

(a) position the antenna spin axis so that it is aligned with the target (if the seeker has a platform-mounted antenna, as opposed to a body-fixed antenna)

(b) provide steering information for the missile flight control equipment — For seekers which use platform-mounted antennas, such information is usually obtained from pickoffs, transducers, etc. mounted on the platform. Systems using body-fixed antennas must employ data-processing techniques to recover this information.

In some cases, range and/or range rate may also be available. This depends on the type of radar systems, and the data processing. This information is useful for resolution of multiple targets, gain-changing schemes for the guidance, and warhead detonation.

The tracking capabilities of a seeker are determined by its ability to provide accurate angle information to the guidance systems. To evaluate this capability, two figures of merit are usually used:

(a) sensitivity, K_s

(b) filter factor, K_f

Sensitivity is the figure which relates actual (physical) angular error to the magnitude of the error voltage. Its defining equation is

$$\frac{\Delta}{S} = K_s \frac{\varepsilon}{\Theta} \qquad (7\text{-}92)$$

where

Δ = rms error voltage

S = received signal strength (rms)

ε = rms angular error

Θ = beamwidth

The output of a radar is usually processed through some type of filter. In addition, the servos which position the antenna act like low-pass filters. The result is that angle noise (due to target scintillation, thermal noise, etc.) is reduced by this filtering action. The filter factor is a measure of this effect. Its defining equation is

$$K_f^2 = \frac{\text{Noise Power Input}}{\text{Noise Power out of Filter}} \qquad (7\text{-}93)$$

When the signal-to-noise ratio is high (e.g., near the intercept point), equations 7-92 and 7-93 may be combined by noting that

$$\frac{\Delta + N}{S + N} \cong \frac{\Delta}{S} + \frac{N}{S} = K_s \frac{\varepsilon}{\Theta} + \frac{N}{S} \qquad (7\text{-}94)$$

where N = input rms noise

When the antenna servo error is reduced to zero, there still remains an angular error ε. However, the rms noise level is reduced by the filter factor, so that equation 7-94 leads to

$$K_s \frac{\varepsilon}{\Theta} + \frac{N}{K_f S} = 0 \therefore \frac{\varepsilon}{\Theta} = \frac{1}{K_f K_s} \frac{N}{S} \qquad (7\text{-}95)$$

The tracking capabilities of various radars may be evaluated, and compared, by means of equation 7-95 K_f and K_s may be computed by referring to paragraph 6-5.2 of Chapter 6.

Error sources associated with the tracking problem are discussed in paragraph 6-5.3 of Chapter 6.

In addition to the various errors listed in Chapter 6, significant tracking errors can arise due to transmission through a radome. Two types of error exist:

(a) static or instantaneous errors cause a boresight shift, which results in a false angular indication.

(b) dynamic errors (error slope) can result in a false indicated angular velocity.

A typical boresight-shift curve is illustrated in Figure 7-61. Such curves are almost obtained experimentally, from a combined antenna-radome configuration. Its value at any point is the static error at that point. Its slope is the *error slope* (also called *radome rate*).

Radomes used in missiles are particularly liable to cause large errors due to their high fineness ratio (ratio of length-to-base diameter).

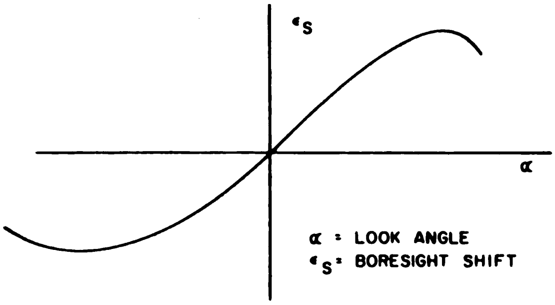

Figure 7-61. Typical Boresight Shift for a Combined Antenna-Radome

Well-designed antenna-radome combinations may have errors of

$$\max \epsilon_s = 5 \text{ to } 8 \text{ milliradians} \qquad \text{(a)}$$

$$\max k = 0.05 \text{ degree/degree} \qquad \text{(b)} \qquad (7\text{-}96)$$

where k = error slope

$$= \frac{d\epsilon_s}{d\alpha} \qquad \text{(c)}$$

The most pronounced boresight errors, and their rates, occur in the vicinity of the radome nose. Even slight disturbances (e.g., frequency shift from design value, radome-antenna misalignment) can increase the above values by a factor of 5 or 10. Reference 64 contains more quantitative information on various types of radomes.

Systems which use proportional navigation are particularly affected by radome errors. Unless special gain-changing techniques are used, the gain of such a system inherently increases as the range decreases. A serious radome rate error may cause an additional increase in the overall gain, and be the cause of attitude oscillations. [6, 10]

7-7.3 RADAR SEEKERS

Considerable information on radar seekers has been presented in preceding sections. Also much of paragraph 6-5 in Chapter 6 is applicable to radar seekers. Thus, the basic methods for implementing angle trackers and some aspects of the airborne problem that differ from ground trackers will be summarized here.

7-7.3.1 Conical Scan

As implied in Figure 7-53, the beam centerline repeatedly traces out a cone. The angle between the cone axis and the beam centerline is the squint angle. The squint angle is usually about one beamwidth, or a little less.

When a non-scintillating target is off-boresight, the returned signals are modulated at the scan frequency. Orthogonal error voltages may be derived from this modulation. These are used to drive the boresight axis on target, thus removing the modulation.

The most common source of errors arises from fading characteristics of the target. These cause amplitude modulation which appears as an angle error to the seeker, and ultimately cause guidance errors.

Further material is presented in Chapter 6, paragraph 6-5.2.1 and references 42 (pp 518, 519) and 1 (pp 362, 363).

7-7.3.2 Amplitude Monopulse

Amplitude monopulse customarily uses four antennas, spaced very close to one another. The antennas are mounted so that their beams diverge, causing a four-lobe free-space pattern.

When the target is on-boresight, all four antennas receive echoes of equal amplitudes. The four echoes are not all equal when the target is off-boresight. Hence, by comparing the four echo amplitudes, the target's position may be determined.

Amplitude monopulse does not require a physical scanning motion, hence fixed antennas may be used. Fading is not a problem, since angle information is derived from the processing of sets of simultaneous echoes.

Additional information is presented in Chapter 6, paragraph 6-5.2.2.

7-7.3.3 Phase Monopulse

Phase monopulse usually uses four antennas, spaced several wavelengths apart. The antennas are mounted so that their free-space radiation patterns coincide. By comparing the relative phases of the echoes received at the four antennas, the angular position of the target may be determined. Phase monopulse systems are also called *interferometers*.

Phase monopulse, like amplitude monopulse, is not affected by target fading. Also, body-fixed antennas may be used. However, ambiguities of the indicated target angle exist whenever the path lengths from the target to two feeds differs by an integral number of wavelengths.

Phase monopulse is discussed in Chapter 6, paragraph 6-5.2.3 and reference 11.

7-7.3.4 Combination Monopulse

Combination monopulse uses two antennas, spaced several wavelengths apart. The beams are made to coincide in azimuth, but are displaced *(squinted)* in elevation. Target echoes received at the antennas are compared in phase to derive azimuth information, and are compared in amplitude to derive elevation information.

The characteristics of combination monopulse are a composite of amplitude and phase monopulse systems. For additional information refer to Chapter 6, paragraph 6-5.2.4.

7-7.3.5 Additional Aspects of Radar Seekers[65,66]

EFFECT OF MISSILE ROLL[6]

Most missiles employ some form of roll control. With a platform-mounted antenna, the roll motion ordinarily causes no difficulty. With a body-fixed antenna, the roll must be controlled in order to make accurate scanning and tracking possible. It is also possible to secure scanning with a fixed antenna by causing the missile to roll at a constant rate. However, this makes the flight control problem more complex, by requiring commutation of the control surfaces, and because a gyroscopic effect takes place.

RADOME PROBLEMS

In addition to absorption and boresight errors, the presence of a radome in an active system creates problems due to internal reflections. Energy may be reflected to undesired directions, giving rise to a direct loss of radiated energy. Reflections can also create significant sidelobes which may collect clutter signals and contribute to system noise. In extreme cases, reflections may enter the antenna and waveguide, causing frequency pulling. This is a phenomenon in which the magnetron shifts frequency. The frequency shift can be so great as to cause the r.f. to fall outside the receiver bandwidth.

COMPARISON OF PULSE AND CW SYSTEMS

A significant difference between these two types of radars occurs when they operate in a clutter environment. CW radars have the inherent capability to reject clutter by using velocity gating, i.e., by detecting the Doppler-shifted r.f. However, this usually requires a forward hemisphere attack in order to effectively separate the target signal from the clutter. A straight pulse system does not have anti-clutter capability, unless special pulse comparison techniques are used.

In the matter of range performance, there is another significant difference in that a CW system can operate down to zero range. This is not possible with pulsed systems, which must have a finite recovery time following transmission of a pulse.

Range information can be obtained in CW systems, but with a little added difficulty. FM or AM *markers* are superimposed on the transmission, and the elapsed echoing time is then determined. Pulse systems may experience trouble with *second-time-around echoes.* There echoes are from very large and distant objects, which arrive at the receiver after a second pulse has been transmitted.

The most serious problem with CW seekers is spillover. This is a phenomenon where a portion of the transmitter signal, with the transmitter tube noise, enters the receiver. Radome reflections add to the problem. Poor isolation can cause a serious degradation of the maximum seeker range. The most effective way to overcome this problem is to use a double-dish seeker. With careful design, 50 db of isolation is possible.

7-7.4 INFRARED SEEKERS

A typical infrared seeker is shown in simplified schematic form in Figure 7-62. A hemispherical dome is generally used to protect the optical system while not distorting the optical image. Target radiation passing through the dome is collected by an optical system such as the Cassegrain telescope shown. This telescope consists of two front surface mirrors to reduce light transmission losses. The target is imaged on the reticle which is placed at or near the focal plane. The reticle modulates the target energy and provides an error signal. Spectral

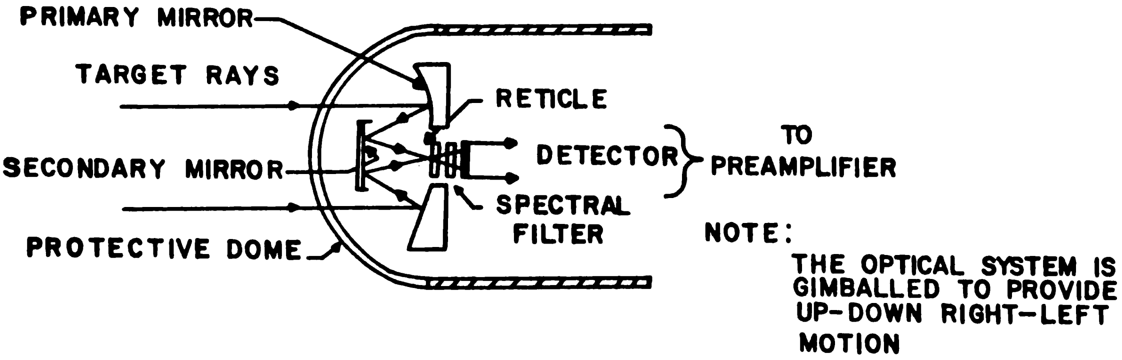

Figure 7-62. Typical Infrared Seeker

filters, which may be either coated on the reticle or independent elements, are used to help eliminate unwanted radiation such as sunlight reflected from clouds. The optical system is gimballed to provide up-down and right-left motion. Radiation signals are converted to electrical signals by the photodetector and then processed in a conventional way prior to being applied to the missile control actuators. Two reticles are shown in Figure 7-63. One provides an amplitude-modulated error signal, and the other a frequency-modulated error signal. In either case, the image of the target is focused on the reticle as a small blur circle of size comparable to a slit width. Either the reticle can be rotated about its center or the image can be optically rotated about the reticle center.[67]

An understanding of an infrared seeker can best be obtained from consideration of the amplitude-modulated reticle. The radiation passing through the reticle is converted into an electrical signal by the detector as shown in Figure 7-64. The target position is specified by a radius vector ρ, and an angle θ, relative to the reticle The blur circle is so adjusted that it just fills the slit near its edge. As the blur circle moves to the center of the reticle a portion of blur circle is cut off and the amplitude of the pulse train generated decreases, finally going to zero at the reticle center. The amplitude of the pulse train contains ρ information and the phase of the pulse train contains the θ position of the target relative to the θ_0 reference. The error signal frequency spectrum is centered at f_0 cps corresponding to N times the rotational rate of the reticle (f_s cps or rps) with sidebands at $\pm f_s$ cps.

Typically, a 12-bladed chopper might rotate at 60 rps so that the signal is at 720 cps ±60 cps. The 720 cps center frequency is removed by a second detector leaving the 60 cps component. A phase sensitive device is then used to determine the angle θ from 60 cps signal. Both angle and amplitude information are amplified and delivered to the seeker optics which corrects the heading of the optical boresight.

A typical infrared seeker system is shown in block form in Figure 7-65. The target is normally viewed against some background which may be illuminated by the sun. Target irradiance which is the radiant flux density at the seeker's optics, normally decreases inversely with range squared but is further attenuated by the atmosphere. The optical system and signal modulation has been discussed previously.

The seeker optic must be space stabilized. In some seekers, the optic is rotated and is itself a gyro. In others, separate stabilization is provided. A preamplifier and bandpass amplifier follow the detector. After band limiting, the signal is demodulated, further filtered and compared with a phase reference. The position of the seeker head is read from a position sensor, differentiated and used to control the missile aerodynamic surfaces or thrust deflectors. The infrared seeker system is extremely simple compared to most radar systems. Because of this simplicity, an infrared seeker is usually applicable to terminal guidance problems. Also,

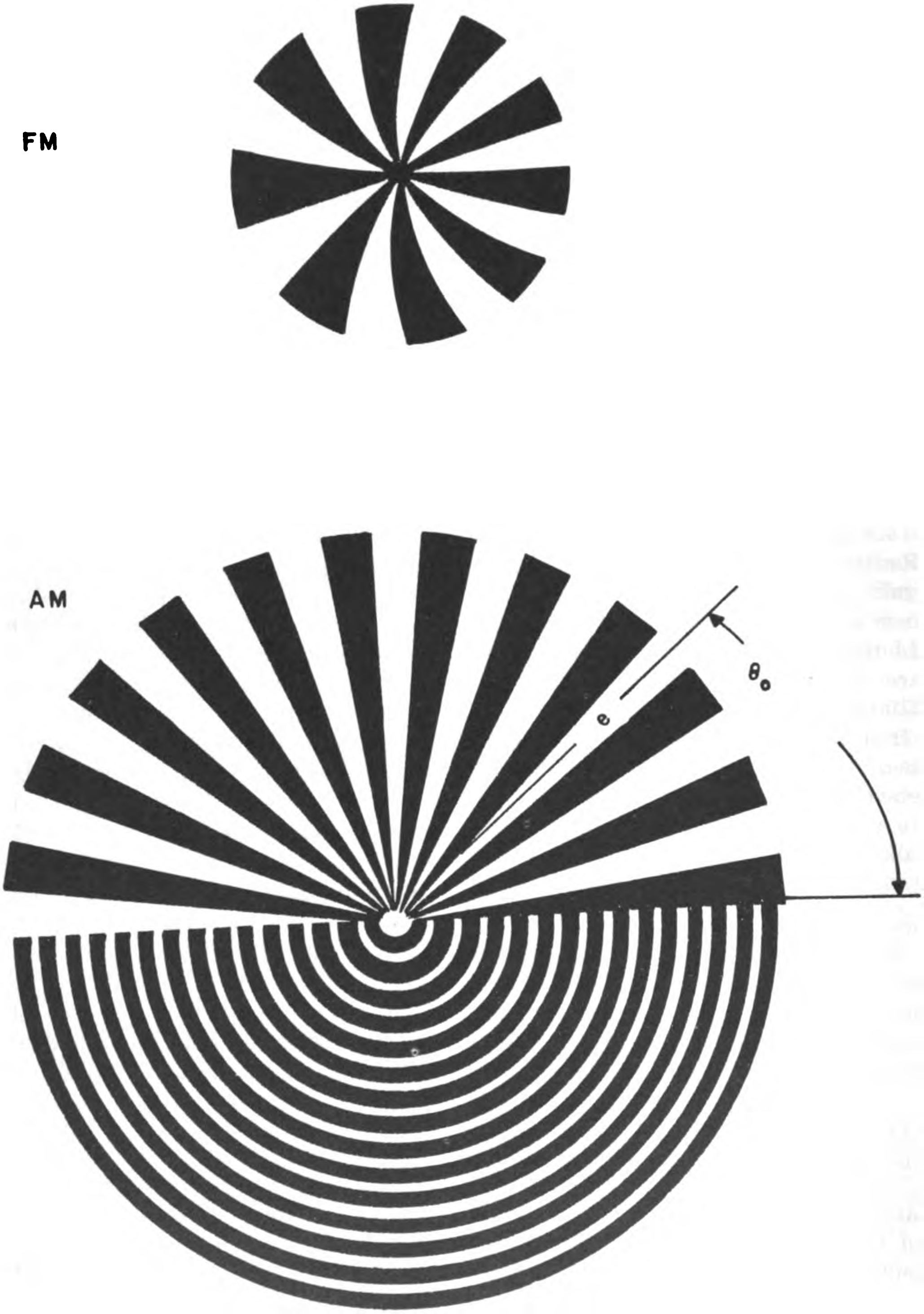

Figure 7-63. AM and FM Reticles

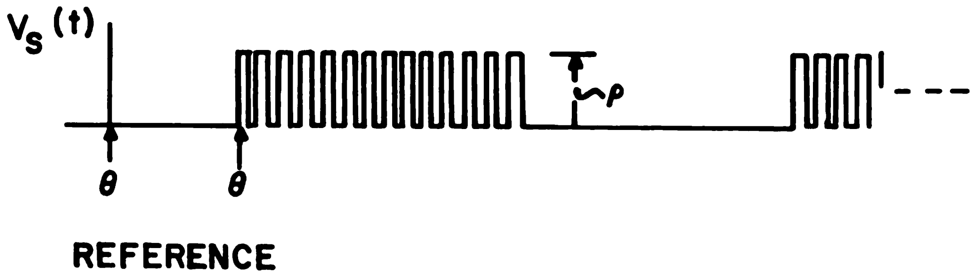

Figure 7-64. Amplitude Modulation Error Signal

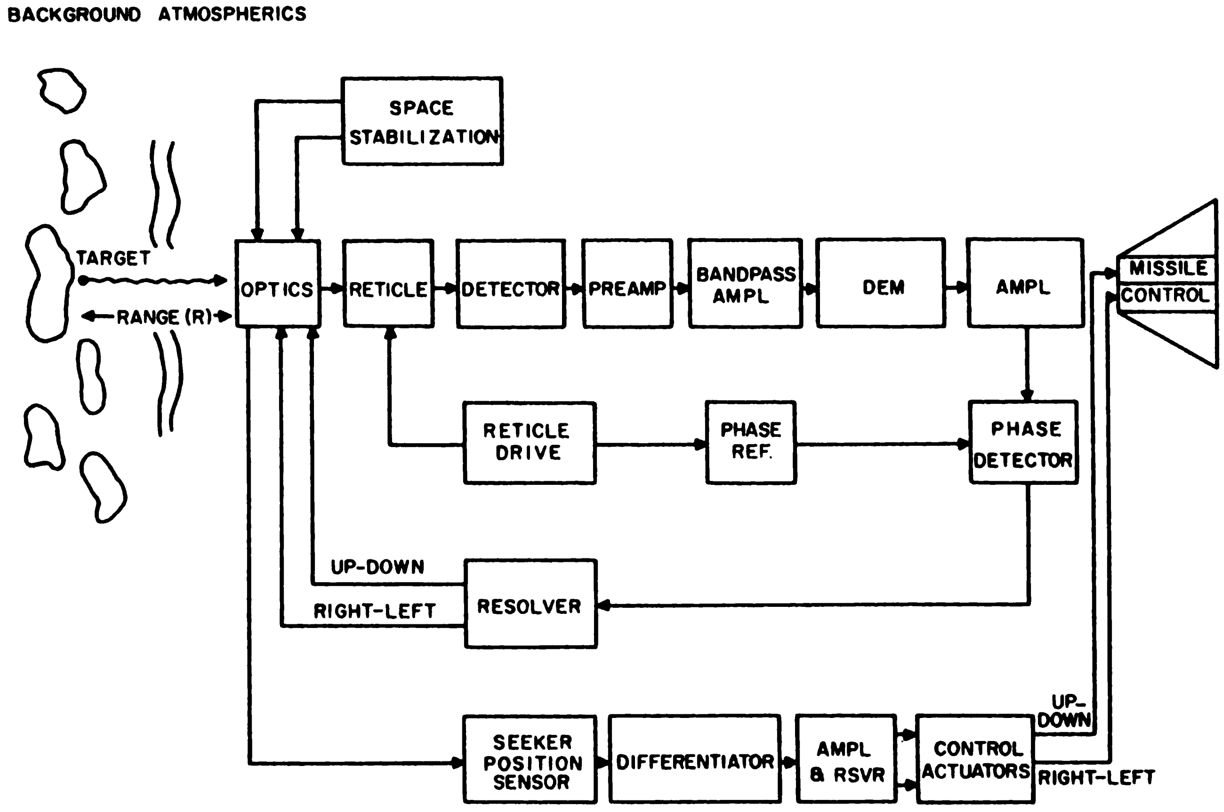

Figure 7-65. Typical IR Seeker System, Block Diagram

at higher altitudes the atmospheric and background problems are alleviated considerably. An infrared seeker's tail chase performance is usually much better than its nose aspect performance on jet or rocket driven targets. However, with very high speed targets in the atmosphere, skin temperatures are high enough so that serious degradation occurs only on the nose.

7-7.4.1 Radiation Laws

In order to effectively design IR seekers knowledge of the characteristics and limitations of IR radiation is necessary. Inherent to this knowledge is an understanding of the radiation laws. The spectral distribution of radiation emitted by a heated black-body can be calculated from *Planck's Law* where $W\ (\lambda, T)$ is the power

$$W\ (\lambda, T) = \frac{3.740 \times 10^4}{\lambda^5 \left[e^{\frac{1.4385}{\lambda T}} - 1 \right]} \ \frac{\text{watts}}{cm^2 - \text{micron}} \qquad (7\text{-}97)$$

radiated by a black-body per unit wavelength interval at wavelength λ and per unit area at temperature T (in degrees K). The total radiation emitted by the black-body is given by the *Stefan-Boltzmann Function.*

$$\int_0^\infty W\ (\lambda, T)\ d\lambda = 5.679 \times 10^{-12}\ T^4\ \frac{\text{watts}}{\text{cm}^2} \qquad (7\text{-}98)$$

The distribution $W(\lambda,\ T)$ goes through a maximum value at a wavelength λ_m. The value of λ_m is found by differentiating $W(\lambda,\ T)$ with respect to λ and equating to zero. The result, known as *Wien's Displacement Law,* is

$$\lambda_m = \frac{2897}{T}\ \text{micron} \qquad (7\text{-}99)$$

It should be noted that the above equations pertain to black-body radiation. The total radiation from a real body is given by the relation

$$\int_0^\infty W\ (\lambda, T)\ d\lambda = 5.679 \times 10^{-12}\ \varepsilon T^4\ \frac{\text{watts}}{\text{cm}^2} \qquad (7\text{-}100)$$

where ε is a quantity known as the *emissivity.* Emissivity depends on the nature of the radiation surface and lies between zero and one. Some bodies in nature, such as an opening in a cavity, approximate a black-body. A jet tailpipe is an example of such an opening. The net radiation surface and lies between zero and one. ated and that received by a body from its surroundings. If the body is completely surrounded by walls of temperature T_o the net rate of loss or rate of gain of energy by radiation is given by

$$W_{net} = 5.679 \times 10^{-12}\ \varepsilon\ (T^4 - T_o^4) \qquad (7\text{-}101)$$

Energy which is not absorbed by a body is reflected. At equilibrium, the rates of absorption and emission must be equal.

Planck's law, the Stefan-Boltzmann function and the Wien displacement law are presented in nomograph form in Figure 7-66. Radiation values obtained with them must be corrected by multiplying them by the emissivity values for the particular object involved. Four of the nomograph's seven scales for temperature conversion, degrees Rankine and Kelvin being °F +460 and °C +273, respectively. To convert from one temperature scale to another, lay a straight edge horizontally from the known temperature on one scale and read its equivalent temperature on the desired scale.

The scale at far left (watts per m^2) gives the total radiation emitted by a black-body of one m^2 area as a function of its temperature. To find total radiation, line up the straight edge horizontally with the object's temperature and read the watts scale where it intersects the straight edge. The two scales at right (wavelength and the integral of W with respect to λ) relate the spectral distribution of the radiation to source temperature. To use them, first express source temperature in degrees Kelvin. Then align a straight edge from the temperature (°K) with the wavelength of interest. The intersection of the straight edge with the scale at far right gives the percentage of energy falling below this wavelength. To find the percentage of energy in any spectral band, take the difference of the percentages obtained for the wavelengths at the ends of the spectral band.

SAMPLE PROBLEM

To find the energy in the 2 to 3 micron region radiated by the tailpipe of a jet engine of 0.5 meter² area at 600 degrees C.

First, place a straight edge horizontally at 600°C and read off total radiation on the scale at far left. Assuming an emissivity of one:

$$\text{Total } W_{600^\circ C} = (3 \times 10^4 \text{ watts/m}^2) \times 0.5\text{ m}^2$$
$$= 1.5 \times 10^4 \text{ watts.}$$

Converting the 600°C temperature yields 873°K. Now draw a line from the 873°K point first through the two-micron point and then through the three-micron point. On the percentage scale, this gives 3.1 and 18.5 respectively. The difference between these two values (18.5 and 3.1) is 15.4 percent. Thus, 15.4 percent of the energy

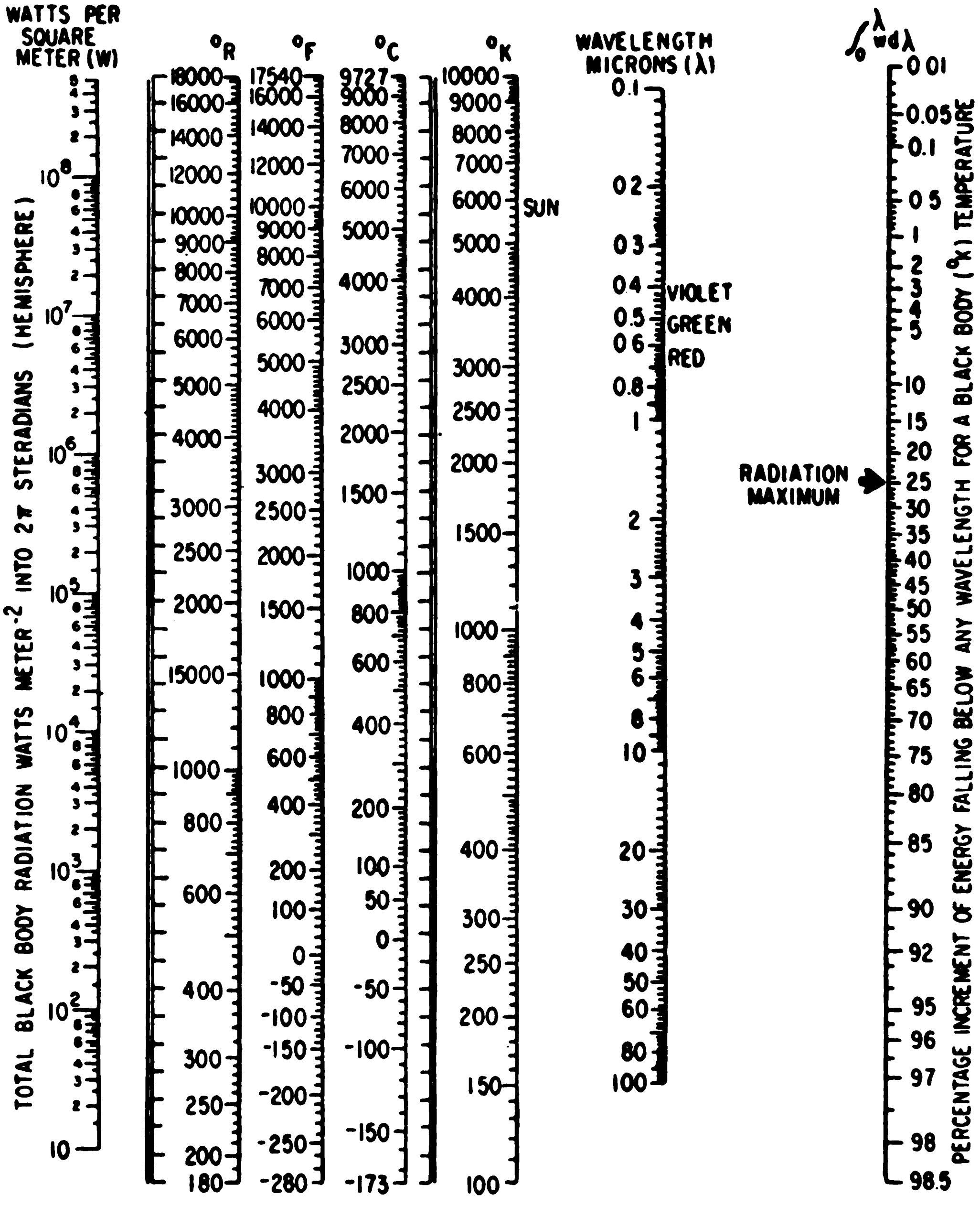

Figure 7-66. Nomograph for Calculation of IR Radiation

radiated by a 600°C body falls in the 2 to 3-micron region.

Applied to the total radiation, this percentage gives:

$$1.5 \times 10^4 \times 0.154 = 2.31 \times 10^3 \text{ watts.}$$

Thus, the energy radiated by the jet's tailpipe in the 2-to-3-micron region is 2.31×10^3 watts. The wavelength at which the radiation peaks can then be found by laying the straight edge from the K temperature scale to the radiation maximum error on the percentage scale. The intersection on the wavelength scale gives wavelength of peak radiation. For a 600°C source, the radiation is a maximum at 3.3 microns.

The above radiation laws and nomographs are given for calculation and reference purposes. More detailed descriptions are given in basic physics texts.[68,69,70]

7-7.4.2 Detectors[48]

Infrared detectors can be separated into two major categories, thermal and photon. Thermosensitive detectors depend on the measurement of temperature rise of the sensitive element caused by the conversion of infrared energy into heat. Photon detectors do not depend on a temperature change, but on the absorption of photons by a semiconductor. In this detector, a photon of the proper energy may drive an electron from a bound state to the conduction band whereupon the electron can be detected by an applied electric field. An example of a thermosensitive detector is the thermistor bolometer which depends on high negative thermal coefficient of resistance. The thermistor bolometer is blackened to extend its spectral sensitivity and is mounted on a good thermal conductor like quartz to improve its time constant which normally is longer than desirable. Since the thermal detector responds to heat change, its response is relatively independent of spectral distribution. Although photon detectors have limited spectral sensitivity, generally their sensitivity to certain spectral regions is quite high and their response time is relatively short. Although many other materials are used, the most popular photon detectors are the photoconductors lead sulfide, lead selenide, indium antimonide, and gold-doped germanium.

Electromagnetic radiation of wavelength (λ) incident upon a detector, results in an electrical signal at the detector output terminals. This signal is a function of the intensity and the spectral distribution of radiation illuminating the detector and the manner in which the radiation is modulated. The radiation incident on the detector is usually chopped to avoid d-c amplification and low frequency noise and to permit spatial discrimination. Thus, the electrical signal from the detector is time varying. For most photodetectors, the phase relation between the electrical signal and the radiation signal is independent of the radiation's wavelength but depends on the chopping frequency (f).

The maximum chopping rate which may be employed without signal attenuation is specified in terms of the detector's time constant. In most cases, detectors may be characterized by a single time constant. The responsivity of the detector to monochromatic radiation is defined as the response of the detector in volts/watt at frequency (f) and is given by

$$R_o(f) = \frac{R_o(o)}{\sqrt{1 + (2\pi f\tau)^2}} \qquad (7\text{-}102)$$

where $R_o(o)$ is the detector's response to steady illumination and τ is the detector's time constant. The rms voltage signal from the detector, $V_s(f)$, due to monochromatic radiation signal is

$$\left[\overline{V_S(f)^2}\right]^{1/2} = \sqrt{\int_{f_1}^{f_2} \left| R_o(f) \cdot P_S(f) \right|^2 df} \qquad (7\text{-}103)$$

where $(f_2 - f_1)$ is the frequency bandwidth of measurement. The detector is characterized by a noise energy density spectrum, $V_n(f)$, generated within the detector itself or by background noise. The rms noise voltage is

$$\left[\overline{V_n(f)^2}\right]^{1/2} = \sqrt{\int_{f_1}^{f_2} \left| V_n(f) \right|^2 df} \qquad (7\text{-}104)$$

and the rms signal-to-rms noise ratio is given by

$$\frac{S}{N} = \left[\frac{\overline{V_S(f)^2}}{\overline{V_n(f)^2}}\right]^{1/2} = \left[\frac{\int_{f_1}^{f_2} \left| R_o(f) \cdot P_S(f) \right|^2 df}{\int_{f_1}^{f_2} \left| V_n(f) \right|^2 df}\right] \qquad (7\text{-}105)$$

For a sinusoidal variation in incident radiation at frequency f_o, the above equation reduces to

$$\frac{S}{N} = \frac{R_o(f_o) \cdot P_S(f_o)}{\sqrt{\int_{f_1}^{f_2} \left| V_n(f) \right|^2 df}} \qquad (7\text{-}106)$$

A most important parameter in specifying detector performance is the noise equivalent power (NEP). The NEP, measured in watts, is defined as the rms radiant energy incident upon the detector which will give a signal-to-noise ratio of unity. NEP is also referred to as minimum detectable power. For a sinusoidal chopping of radiation at wavelength (λ)

$$NEP(\lambda, f_0) = \frac{\left[\int_{f_1}^{f_2} \left| V_n(f) \right|^2 df\right]^{1/2}}{R_o(f_o)} \qquad (7\text{-}107)$$

Thus, detectors are specified in terms of their responsivity to monochromatic radiation and by their noise power spectrum. In some cases, the detector's NEP due to black-body radiation is used instead of its monochromatic value. The inverse of NEP is also used and is referred to as *detectivity*.[71] The noise spectrums of detectors are, in general, quite complicated, but usually one or two types of noise are dominant. Most detectors exhibit a l/f low frequency noise spectrum and a *resistor* or Johnson noise spectrum which is uniform over all frequencies. The l/f noise spectrum usually drops below Johnson noise at between 1 and 10 kc. The responsivity of a long and a short time constant detector and a typical noise spectrum is plotted as a function of frequency in Figure 7-67. The detectivity for both cases is also plotted in Figure 7-68. In the case of a long time constant detector, it is seen that the detectivity reaches a maximum frequency of $\frac{1}{2\pi\tau}$ cps where τ is the detector time constant and, for a short time constant detector it reaches a maximum where l/f noise drops below Johnson noise and remains constant until it falls off beyond the frequency corresponding to the time constant.

In the case of photoconductors detector sensitivity and long wavelength limit may be increased by cooling. Time constant also increases with cooling such that the product of sensitivity and time constant remain about constant. This effect may be serious with long time constant detectors such as lead sulfide. Few photoconductors with response beyond 4 to 5 microns show appreciable sensitivity unless they are cooled to about liquid nitrogen temperatures. The reason is fundamental: long wavelength photons possess energy of the same order as thermal crystal lattice vibrations so that lattice vibrations themselves are sufficient to drive electrons from the bound to the conduction band. As one desires longer and longer wavelength response, the degree of cooling must be increased. Cooling beyond a certain point however, does not always increase sensitivity, because the detector, when ccoled, increases its sensitivity to background radiation.[72] Another

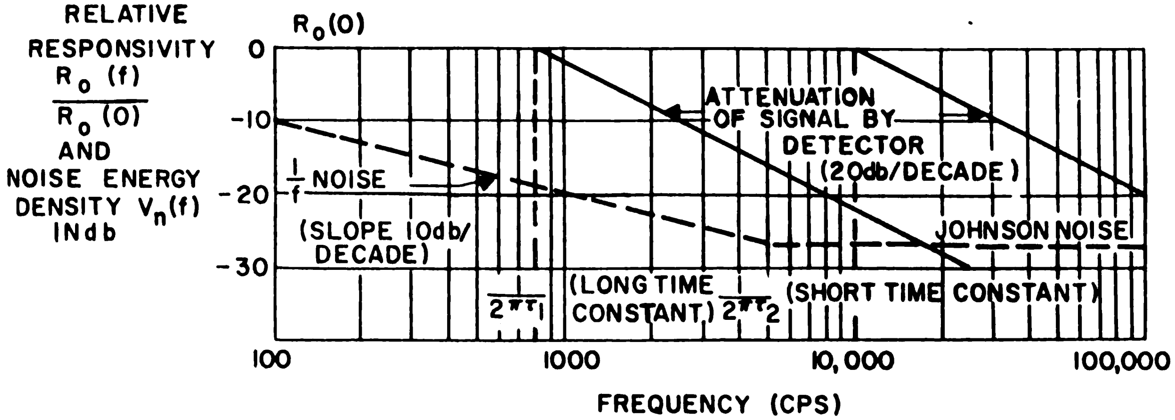

Figure 7-67. Responsivity and Noise Energy Density for a Long and a Short Time Constant Detector

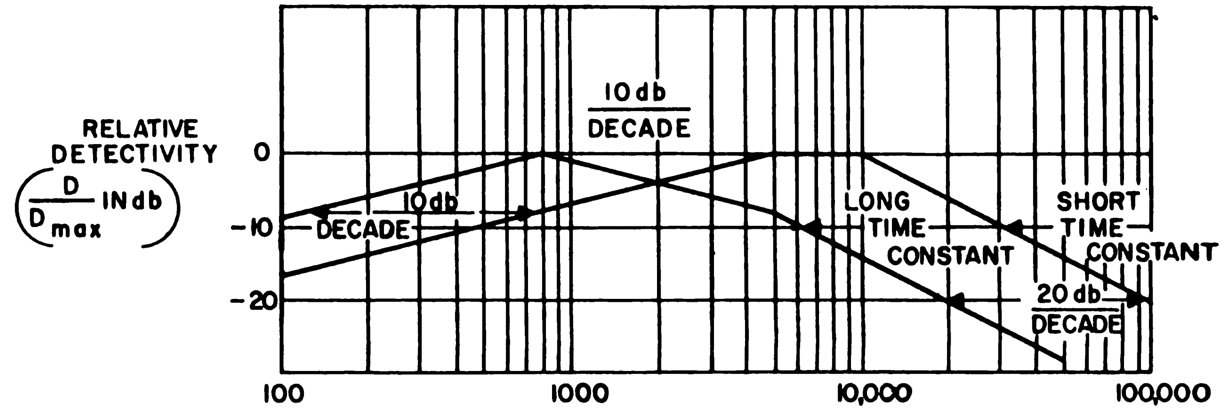

Figure 7-68. Detectivity for Two Detectors of Figure 7-67

phenomenon which occurs upon cooling, is that detector impedance increases. An increase in impedance of an order of magnitude upon cooling from room temperature to liquid nitrogen is not unusual. Since many detectors normally have a one-megohm impedance uncooled, the increase makes load impedance matching quite difficult. NEP, for a given detector, is a function of its area and the bandwidth of measurement. For most photoconductors, noise energy density varies with the square root of area and bandwidth. For purposes of comparing detectors, it would be desirable to normalize to unit area and bandwidth. It has been suggested that the following method[73,74] be used.

$$NEP\ (\lambda, f) = \frac{NEP\ (\lambda, f) \text{ measured}}{(A\ \Delta f)^{1/2}} \qquad (7\text{-}108)$$

where A is the cell area and Δf is the bandwidth of measurement. Formerly, when only the PbS detector was of military significance, it was standard practice to use *Jones "S"* which is particularly appropriate for this detector. *Jones "S"* is defined as

$$``S" = \frac{NEP\ (\lambda, f) \text{ measured}}{A^{1/2}\ [\ln f_2/f_1]^{1/2}} \qquad (7\text{-}109)$$

For small bandwidth of measurement

$$``S" = \frac{NEP\ (\lambda, f) \text{ measured}}{A^{1/2}} \left[\frac{f_e}{\Delta f}\right]^{1/2} \qquad (7\text{-}110)$$

This particular equation assumes that the detector is limited by 1/f noise. This is usually not the case beyond a few kilocycles for most detectors. Even so, data is often given in terms of *Jones "S"* even where it is not applicable. Such data can be used where noise is 1/f but not beyond the frequency at which the 1/f noise energy density drops below Johnson noise. The NEP for a group of lead sulfide detectors is shown in Figure 7-69. The variation in sensitivity and cutoff wavelength is plotted for different detector temperatures. Note that even with the same temperature, cell sensitivities and cutoff wavelengths can be varied in production. NEP for other detectors is shown in Figures 7-70 and 7-71. A more complete set of curves can be found in Reference 75. Time constants for typical detectors are tabulated in Table 7-10.

7-7.4.3 Atmospheric Transmission

In the design of infrared equipment, atmospheric transmission is one of the most variable parameters. It is predictable to a certain extent for given weather conditions, but the weather itself is the unpredictable element. Nevertheless, certain predictions must be made for systems design purposes; consequently, it is necessary to assume an average weather condition and work from this reference.

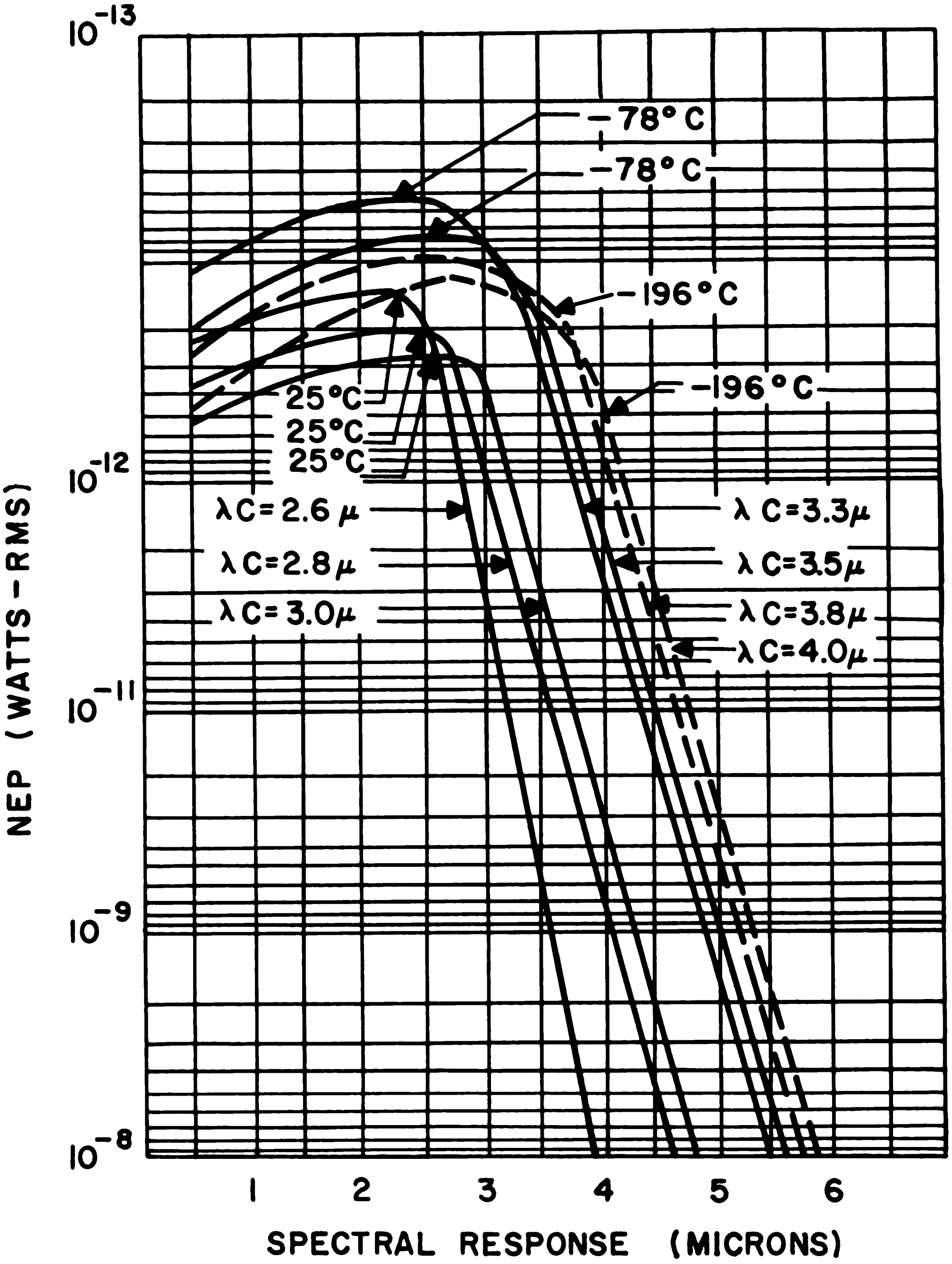

Figure 7-69. NEP Versus Spectral Response for PbS Detector

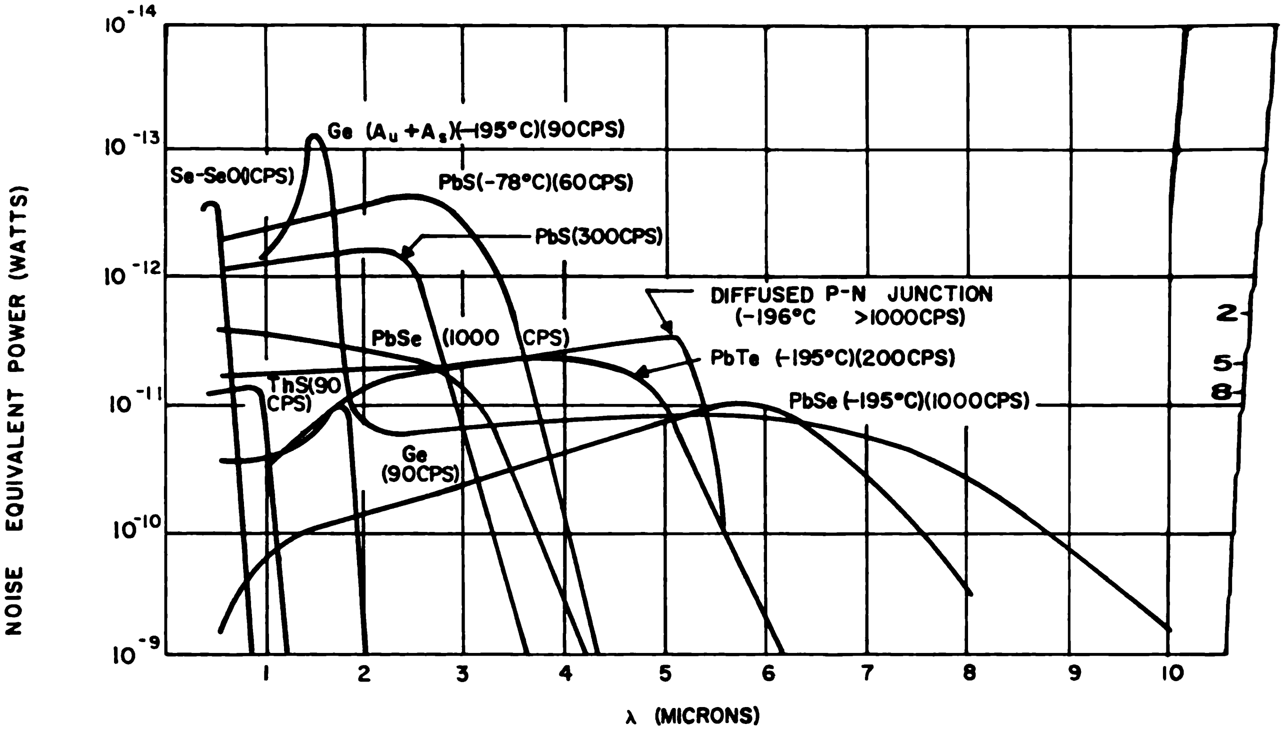

NOTE: ALL MEASUREMENTS AT 300°K UNLESS OTHERWISE NOTED.

Figure 7-70. NEP Versus Wavelength of Various Detectors

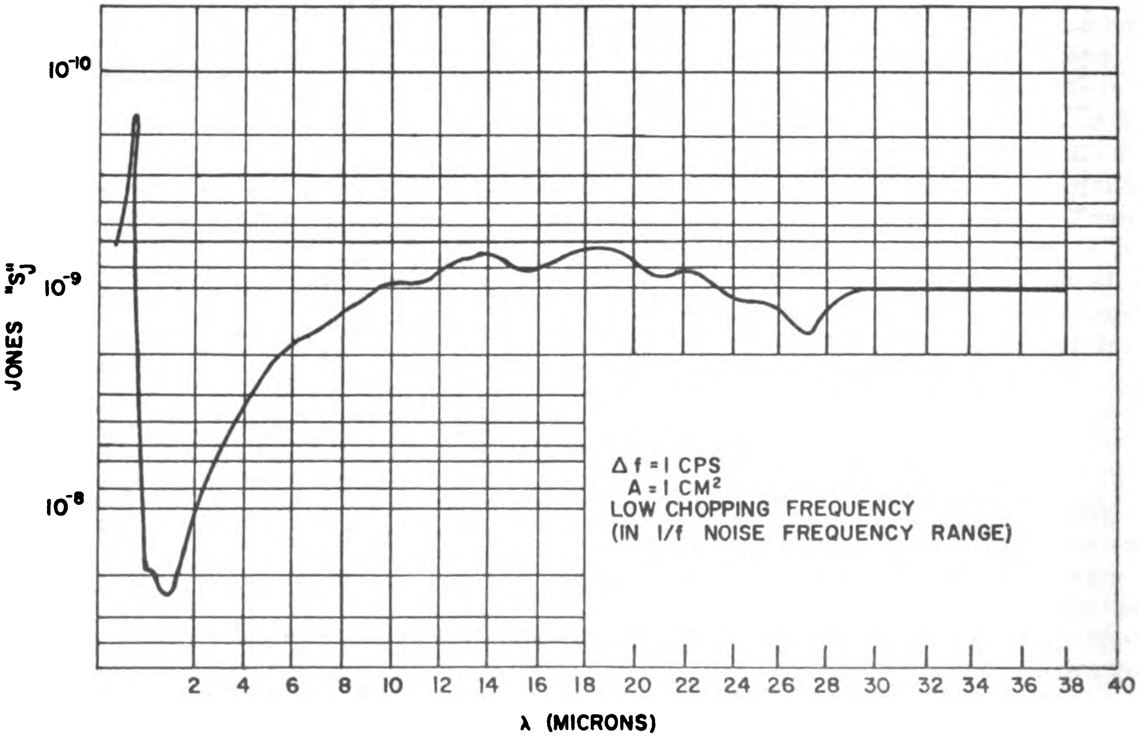

Figure 7-71. Jones "S" Versus Wavelength for PbS Detectors

TABLE 7-10. DETECTOR TIME CONSTANTS

Detector	Time Constant (Seconds)	Detector Temperature (°k)
Thermal Detectors		
Thermocouple	10^{-3}	300
Metal Bolometer	10^{-3}	300
Thermistor Bolometer	$0.25\text{x}10^{-3}$	300
Golay Cell	$3\text{x}10^{-3}$	300
Superconductive Bolometer	$0.3\text{x}10^{-3}$	3
Photoconductive Detector		
Lead Sulfide	$50\text{x}10^{-6}$ to 10^{-3}	300
Lead Selenide	$20\text{x}10^{-6}$ to $50\text{x}10^{-6}$	77
Lead Telluride	$20\text{x}10^{-6}$	77
Germanium		
Au-doped P Type	$4\text{x}10^{-6}$	77
Au-doped N Type	10^{-5}	77
Zn-doped	10^{-8}	4
Indium Antimonide (diffused Junction)	$4\text{x}10^{-6}$	77

Atmospheric absorption of infrared is due principally to molecular absorption, from water vapor and carbon and clouds, and absorption by solid particles such as dust and haze. For most applications in clear weather, only molecular absorption is important. In essence, the atmosphere acts like a window in certain spectral regions and is opaque to energy in other spectral regions. The atmosphere is relatively transparent between 2 and 2.6, 2.9 to 4.1, 4.4 to 4.9, and 8 to 13, and relatively opaque in the excluded regions. However, the degree of transmission is a strong function of CO_2 and H_2O concentration in the air. H_2O, in particular, varies by large amounts with ambient temperature and altitude.

With the aid of Figures 7-72 and 7-73, the molecular absorption of radiant energy can be calculated. Figure 7-72 assumes the ARDC model atmosphere with the top of the troposphere at 11 km altitude. The CO_2 content was assumed to be constant at all altitudes and equal of 0.032 percent by volume. The water vapor was assumed to have a constant relative humidity in the troposphere and a constant mixing ratio in the stratosphere. The optical thickness of the gasses was corrected for linear pressure, thicknesses, broadening, and square root

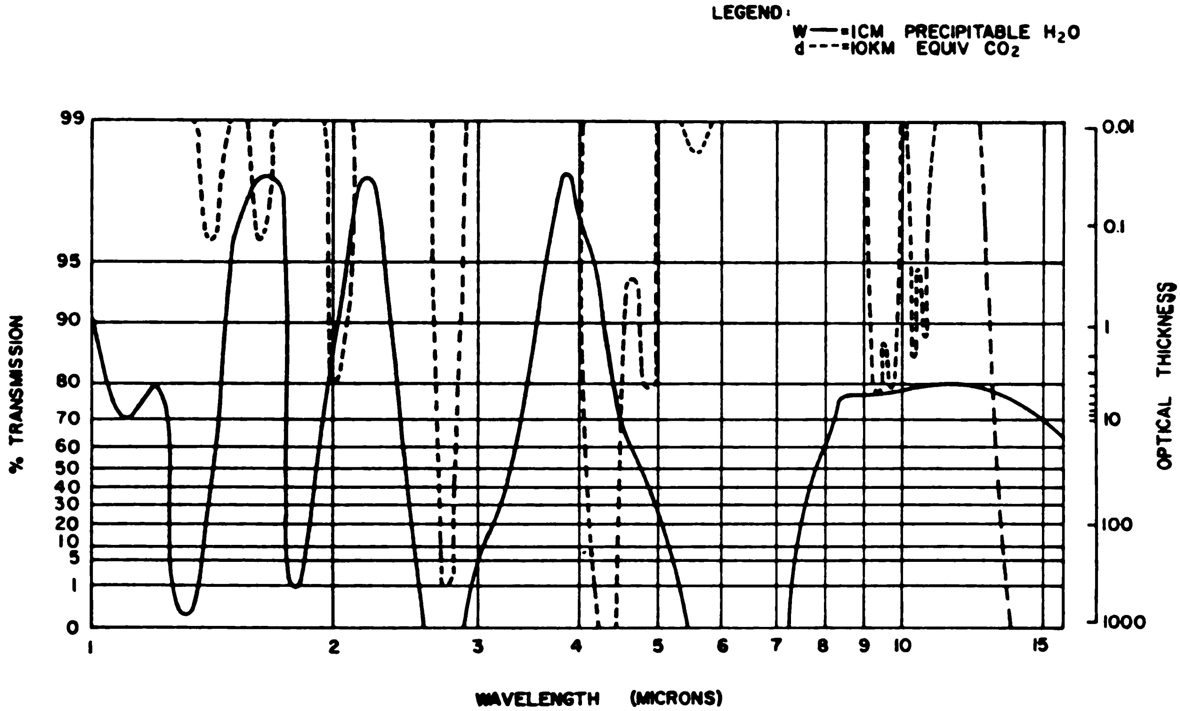

Figure 7-72. Transmission Versus Wavelength for H_2O and CO_2

temperature broadening. A flat earth was assumed. With these assumptions, the following procedure can be used to calculate atmospheric transmission.

Let:

d = equivalent sea level path length, *km* for CO_2 in infrared beam

d_h = horizontal equivalent sea level path length, *km* for CO_2 for one *km* actual path length

d_v = equivalent sea level path length, *km* for CO_2 in a vertical path from h to ∞

h_o = observer altitude, *km*

h_t = target altitude, *km*

h = altitude, *km*

R = range, *km*

R.H. = relative humidity (Take *R.H.* value of 0.80 if not given in a specific problem)

T_A = transmission of atmosphere

T_{H_2O} = transmission through water vapor in atmosphere

T_{CO_2} = transmission through CO_2 in atmosphere

W = precipitable centimeters water vapor in infrared path, corrected to *STP*

W_h = precipitable centimeters in a horizontal path 1 *km* in length, corrected to *STP*

W_v = precipitable centimeters in a vertical path from h to ∞, corrected to STP

λ = wavelength, microns

(a) To find d

(1) If $h_o = h_t$

Read d_h in Figure 7-71

$$d = d_h \times R$$

(2) If $h_o \neq h_t$

Read d_v in Figure 7-73 for both h_o and h_t

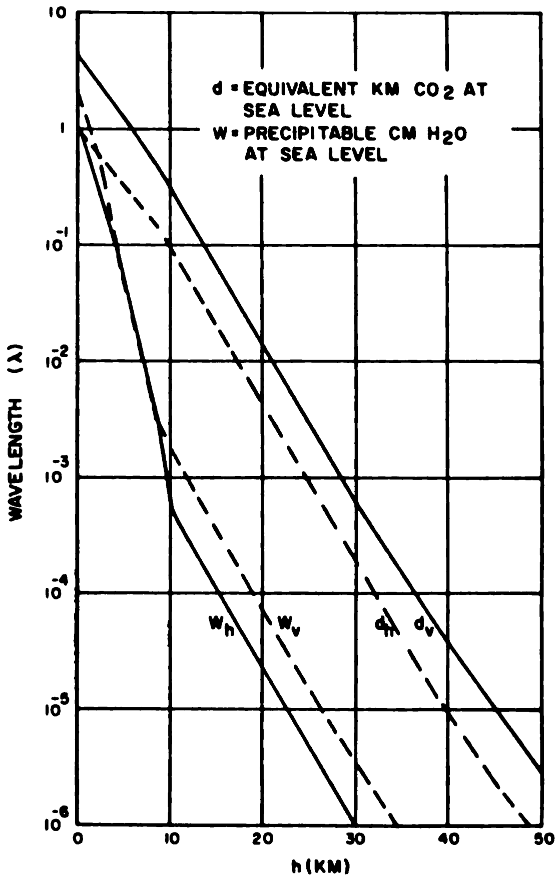

Figure 7-73. Wavelength Versus Altitude for H_2O and CO_2

$$d = \frac{(d_v \text{ for } h_o) - (d_v \text{ for } h_t)}{h_o - h_t} \times R$$

(b) To find W

(1) If $h_o = h_t$

Read W_h in Figure 7-73

$$W = R.H. \times W_h \times R$$

(2) If $h_o \neq h_t$

Read W_v in Figure 7-73

$$W = R.H. \frac{(W_v \text{ for } h_o) - (W_v \text{ for } h_t)}{h_o - h_t}$$

(c) To find T_{CO_2}

The dashed curve in Figure 7-72 gives the transmission of carbon dioxide versus wavelength for $d = 10$ *km*. For any other value of *d*, merely displace the curves vertically by the distance between the value of *d* on the "Optical Thickness" scale on the right hand side of Figure 7-72 and the value 10 on the same scale. Thus, for $d = 30$ *km*, $T_{CO_2} = 64$ percent for a wavelength of 4.9 microns.

(d) To find T_{H_2O}

The solid curve of Figure 7-72 gives the transmission of water vapor versus wavelength for $W = 1$ *cm* precipitable H_2O. For any other value of *W*, merely displace the curve vertically by the distance between the value of *W* on the "Optical Thickness" scale and the value one on the same scale. Thus, for $W = 0.2$ *cm.*, $T_{H_2O} = 61$ percent for a wavelength of 4.9 microns.

(e) To find T_A

$$T_A = T_{CO_2} \times T_{H_2O}, \text{ all the same wavelength}$$

Thus, in our previous example

$$T_A = 0.64 \times 0.61 = 0.391 = 39\%$$

7-7.4.4 Spectral and Spatial Discrimination

A target, to be observed in the presence of background must first be distinguished from the background. The primary difference between target and background is its spectral distribution of energy and its size. Background problems usually arise from sunlight reflected from clouds and other objects, and from radiation absorbed and reradiated from the atmosphere. Reflected sunlight approximates black-body radiation from the sun and is most serious in the 1- to 4-micron region. (See Figure 7-72.) Reradiated energy usually appears like 300°K radiation which peaks at 10 microns but has appreciable energy in the 5- to 25-micron region. Solar radiation is partially eliminated by a spectral filter which cuts off wavelengths shorter than two microns and the 300°K radiation is partially removed by proper choice of a detector with appropriate long wavelength cutoff. However, some radiation components in the spectral region of the target still remain.

A uniformly lighted background is not usually troublesome; its main effect is to raise the d-c level of the detector. Large extended background objects do not present excessive difficulties either. The major problems are experienced when viewing small objects like small fleecy clouds, fine grain sky variations, and sharp discontinuities, such as cloud edges.

From the preceding discussion, it can be inferred that sky gradients possess coarse and fine structure and could be described as having a frequency or wavelength in space attached to them.[76] Coarse objects such as large diffuse clouds would correspond to a low space frequency and fine grain objects, such as small fleecy clouds, have short wavelength and a high frequency structure. Targets which are essentially point sources are of high space frequency. This phenomenon can be utilized by using a reticle with small slit widths and a checkerboard appearance as shown in Figure 7-74. With this form of reticle, a large object covers many of the checkers and is not efficiently chopped while a small object is alternately passed and obscured by every checker and gives rise to a large a-c variation in the electrical output of the detector. This is known as spatial discrimination. In practice, it is usual to adjust the slit width so that it is about equal to the blur circle on the focal plane which represents a typical target.

As has been discussed, some sky radiation is generally observed in the target's spectral region primarily from reflection of solar radiation and from emitted radiation from objects at ambient temperatures. By measuring the intensity of the reflected solar radiation in one spectral region, between one and two microns, for example, one can predict the amount in the target's spectral region which might be concentrated in the 2- to 3.5-micron region. Thus, a cancellation scheme such as a two-color reticle can be devised. Note that atmospheric transmission variations can cause such a system to lose some effectiveness. Furthermore, the spectral properties of background in two different spectral regions are not necessarily related to their spatial properties. To be effective, spectral and spatial properties must be correlated if an efficient cancellation is to be obtained. Unless precautions are taken, a lack of correlation can be further aggravated by the reticle if a two-frequency, two-color reticle is used. The two-frequency reticle divides the reticle through a diameter and uses different slit widths in each half; thus, each half has different spatial filtering characteristics. One half of the slits pass radiation in one spectral region and the other half in another spectral region.

In some systems, chopping is accomplished by rotating the reticle and leaving the field stationary. In others, the reticle is held stationary and the view is rotated. Rotation of the field of view usually accentuates background problems since the background to the system is continually changing. Consequently, rotation of the field of view should be avoided if possible.

In the detection of jet tailpipes, the *PbS* detector is by far the most desirable from a target radiation-detector sensitivity viewpoint. Also, it can operate uncooled. However, the *PbS* detector also *sees* most solar reflections and if particularly difficult solar background problems are anticipated, it might pay to utilize the less sensitive 3- to 5-micron detectors which are

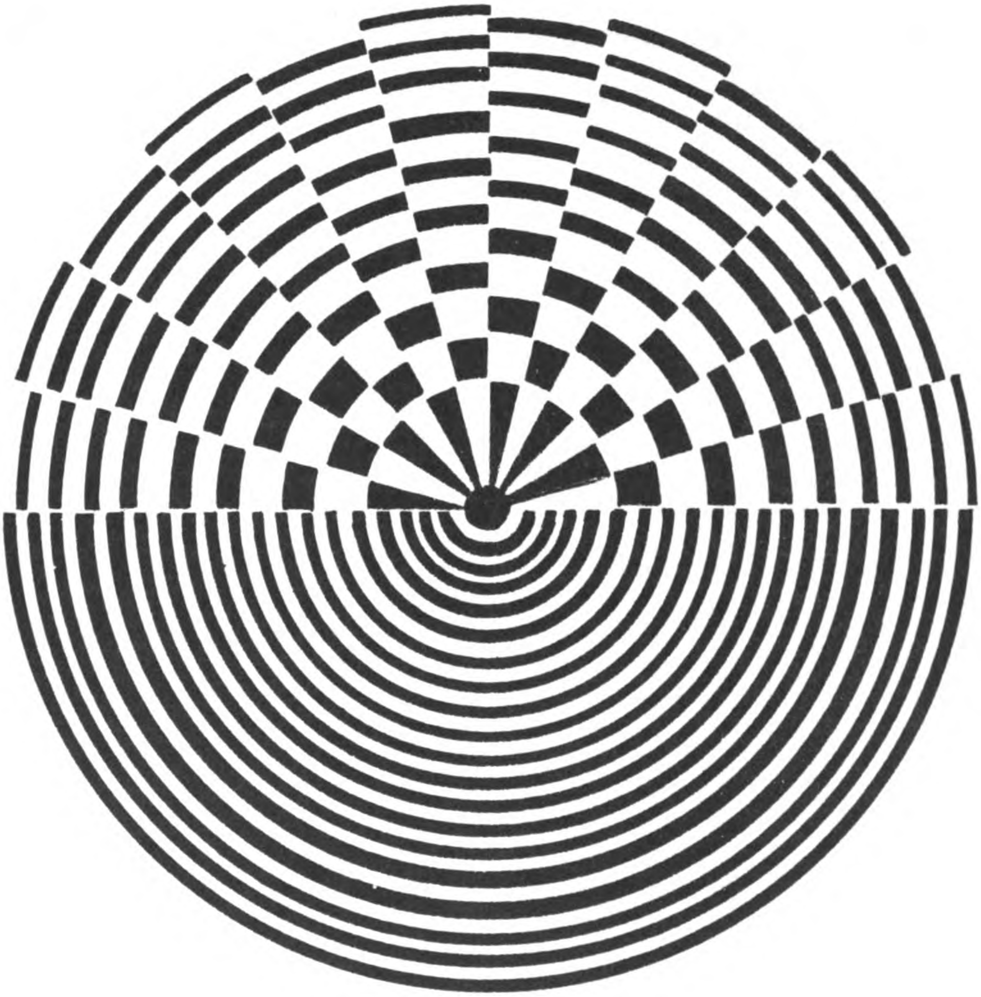

Figure 7-74. Amplitude Modulation Reticle, Checkerboarded for Spatial Discrimination

least affected by either solar reflection or by reradiation.

The background problem is the most difficult to solve. It is a noise which can be filtered out by appropriate reticle filters and some electronic techniques, but it cannot be solved by simply increasing optical aperture to increase the signal. In fact, background noise increases with aperture size.

7-7.4.5 Infrared Range Equations

As in radar systems, the range at which a target can be detected by an infrared system is statistical in nature and many of the statistical quantities involved cannot be stated except in a qualitative way. Nevertheless, it is often necessary to obtain a range capability estimate rather quickly for system design purposes. Range equations for these purposes generally neglect all but the most important first order effects and further, consider only system noise limitations. In reality, infrared systems are generally more vulnerable to sky noise than most radar systems and consequently, the infrared range equation is less indicative of expected range than might be expected. With these restrictions noted, the infrared range equation may be written as

$$R_{\max} = \left(A_o \int_{f_1}^{f_2} df \int_0^\infty \frac{J(\lambda)\ T_o(\lambda, R)\ T_o(\lambda)\ d\lambda}{NEP\ (\lambda, f)\ S/N} \right)^{1/2} \tag{7-111}$$

where

A_o = effective optical aperture (cm^2)

$T(\lambda)$ = target irradiance at the optical aperture $\frac{watts}{cm^2}$

$T_o(\lambda, R)$ = atmospheric transmittance at range R and wavelength λ

$T_o(\lambda)$ = optical and reticle transmittance at wavelength λ

$NEP(\lambda)$ = noise equivalent power of the detector at wavelength λ, (watts)

S/N = signal-to-noise ratio required to give reliable false alarm and detection performance

Most of the terms in the range equation are functions of spectral wavelength. The procedure is to plot or tabulate the various terms as a function of wavelength, do the required multiplications, and then integrate. Since atmospheric transmittance is a function of range, an estimate must be made of the value of range with which to begin. Using this range value, atmosphere attenuation can be obtained and R_{max} calculated. With the value of R_{max}, the estimate originally chosen can be revised and the integration reiterated until a satisfactory answer is obtained.

In some cases, it is desired to place specific system properties such as detector area and optical parameters into the range equation. For example, the optical system in Figure 7-75, which is often used in trackers, may be included in this range equation as follows:[77]

$$R_{max} = \left[A_d\left(\frac{1}{F_2\omega} - 1\right)^2 \int_{f_1}^{f_2} \int_0^{\infty} \frac{J(\lambda)\ T_a(\lambda, R)\ T_o(\lambda) d\lambda}{NEP(\lambda, f)\ (S/N}\right]^{1/2} \qquad (7\text{-}112)$$

where A_d is the detector area, F_2 is the focal length of the field lens and ω is the instantaneous field of view. For a search system, the detector area optical parameter relationships are usually different. For the case shown in Figure 7-76, the detector area, field of view, and the optical aperture and focal length are related as follows:

$$A_d = D^2 F^2 \omega \qquad (7\text{-}113)$$

where D is the diameter of the optics and F is the focal length. In this case, the range equation takes the form

$$R_{max} = \left[\frac{\pi}{4}\frac{A_d}{F^2\omega}\int_{f_1}^{f_2} df \int_0^{\infty} \frac{J(\lambda)\ T_a(\lambda, R)\ T_o(\lambda) d\lambda}{NEP(\lambda, f)\ (S/N)}\right]^{1/2} \qquad (7\text{-}114)$$

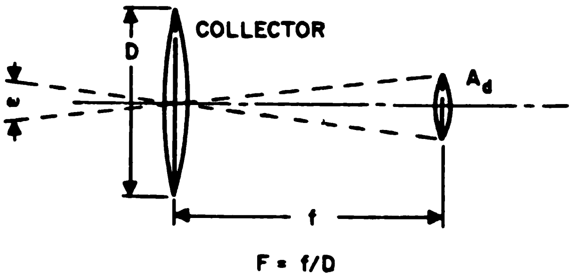

Figure 7-76. Optical System for Search

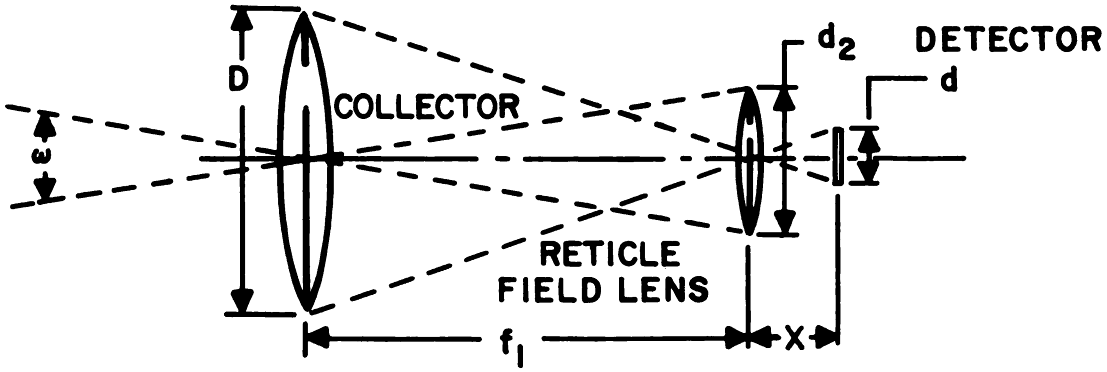

Figure 7-75. Optical System for Tracking

Other parameters can be entered into the range equation and additional factors included. However, it is inadvisable to over-complicate the range equation during the initial part of the design, but rather, to refine the equation as the final design evolves.

7-7.4.6 Optical Materials

In addition to transmitting infrared radiation, an optical material must be optically and mechanically suitable and low in cost. It should be hard but machinable, nonsoluble in water, and able to withstand thermal shock and rough handling. It should also be available in reasonably large pieces. The desirable properties vary with the application. For missile seeker domes, a hard material is required which withstands thermal shock and buffeting by particles. The material must have a low coefficient of expansion so that it will remain attached to the missile and must have a low index of refraction to keep optical distortion low. If used for missile application in volume production, its cost should be low even after fabrication into a dome. Some materials scatter incident radiation and others are bi-refringent, i.e., have different refraction indices in different directions. If material is protected, pertinent specifications may be less stringent. A soft material may be tolerated. However, in strong optical elements such as lenses, there is more concern with optical quality and machinability. A high index of refraction is desirable for refracting elements to keep required curvatures small.

Spectral transmissibility is not by itself a sufficient basis for material selection. Many of the common optical materials and some of their parameters are tabulated in Table 7-11.

7-8 GUIDANCE STUDIES

7-8.1 GENERAL

As indicated in the introduction, initial studies generally involve an examination of the basic relative merits of several guidance systems. This examination usually is accomplished with quite simple models obtained from gross approximations. These include the use of simple dynamics and control models as well as kinematics, and provide the basic requirements of primary sensors and controllers.

After reducing the number of approaches, considerable work of a preliminary nature remains, but it is characterized by more clearly defined objectives, requirements, and constraints. The translation of these into subsystem concepts generally amounts to properly choosing control parameters or designing compensation networks for the relatively fixed elements in the primary guidance loop.

7-8.2 SYNTHESIS

Those subsystems that may reasonably be described or approximated by linear, constant coefficient, ordinary differential equations may be subjected to several synthesis techniques that have been developed.[22,78] Generally all of the elements of the primary guidance loop, except the kinematics, may be treated in this way.

Usually, the kinematics relations are nonlinear and even when linearized they generally contain coefficients that depend explicitly on time. This fact severely limits the usefulness of standard synthesis techniques in connection with the primary guidance loop. However, progress in the theory of these areas has been made and fundamental results are available.[5,12-14,79-82]

7-8.3 BANDWIDTH

The kinematics relations developed in paragraph 7-2 make a precise discussion of the bandwidth of the primary loop difficult. With linearized kinematics, one might qualitatively state that the primary loop bandwidth depends on time. However, the material of paragraph 7-2 is useful for obtaining approximate spectral characteristics of the intercept intelligence which must be utilized by the primary sensors and flight control. In the material below it is the bandwidth of these elements that is referred to as *guidance loop bandwidth.*

The maneuverability necessary in a surface-to-air missile is determined by the speed of the target, the closure rate, and the angle between the flight paths of target and missile during closure. Also of great significance is the missile guidance philosophy (whether the missile flies toward the target or toward a predicted collision point) and the rate of change of either the magnitude or direction of the target flight path vector. The turning rate frequency spectrum was discussed for several

TABLE 7-11. INFRARED TRANSMITTING MATERIALS

MATERIAL		TRANSMISSION UNCOATED-ROOM TEMPERATURE		TEMPERATURE °C		HARDNESS		SOLUBILITY $\times 10^{-3}$ gm/100 gm H_2O	INDEX OF REFRACTION WAVELENGTH MICRONS			DENSITY gm/cc	COEFFICIENT OF LINEAR THERMAL EXPANSION TEMPERATURE $\times 10^{-6}$/°C		YOUNG'S MODULUS DYNES/cm²	REMARKS
		THICKNESS MM	WAVELENGTH MICRONS 2 4 6 8	MELTING	SOFTENING OR DEFORMATION	KNOOP	MOH	ROOM TEMPERATURE	2	6	10		RANGE °C			
As_2S_3	ARSENIC TRISULFIDE	4	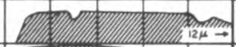	300	195	100·109	2	.05	2.423	2.398	2.380	3.20	24	26	1.6×10^9	COATED TO REDUCE REFLECTION LOSSES-LOW MELTING POINT AND SOFT.
Al_2O_3	SAPPHIRE	2	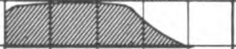	2030			9	.00	1.750	1.746		3.98	50	5.0-6.7	34.4×10^{11}	BIREFRINGENT-COSTLY. AVOID COMPLICATED SHAPES
Si	SILICON	6.4	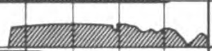	1420	1300		7	0	3.452	3.420	3.418	2.33	10-50	4.2	1.09×10^{11}	BECOMES OPAQUE AT ELEVATED TEMPERATURES-UNUSABLE BEYOND 350°c
SiO_2	QUARTZ	10	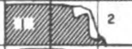	1750	1585		7	0	1.438			2.20	20-320	0.56	68.9×10^9	EXCELLENT IN ITS SPECTRAL REGION.
	CORNING #0160	2	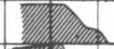		610	25·460	2-3	0	1.56			3.05				EXCELLENT IN ITS SPECTRAL REGION.
$SiO_2-B_2O_3-Na_2O-Al_2O_3$	PYREX	5	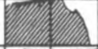		820		6	0	1.4			2.23	0-300	3.2	6.76×10^{11}	EXCELLENT IN ITS SPECTRAL REGION.
MgO	PERICLASE	5.4	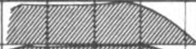	2800	2000	600·692	5	.012	1.709	1.597		3.58	0-1000	13.9	25.1×10^{11}	NOT AVAILABLE IN DIAMETERS OVER 2 INCHES
CaF_2	FLUORITE	33	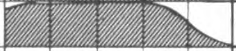	1360			4	1.7	1.424	1.386	1.300	3.18	0-100	19.5	7.6-14.5 X 1	SUSCEPTIBLE TO THERMAL SHOCK.
T/Br – I	KRS-5	2	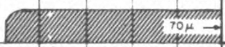	414.5		200·40	2	50	2.396	2.379	2.376	7.37	20-200	58	16-2.5 X 10	SUSCEPTABLE TO THERMAL SHOCK.
CF_2-CFCl	KEL-F	6.3	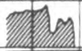		260	SHORE 65	~1	0	1.43			2.12	20-150	54.5	$11.5\text{-}12.2 \times 10^9$	SOFT-PLASTIC MATERIAL.
KCl	SYLVITE	12	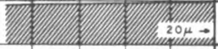	776		100·9.3	0.5	34700	1.475	1.468	1.457	1.98	(-50)-200	37	3.5×10^{11}	SOFT AND WATER SOLUABLE
TiO_2	TITANIA	6	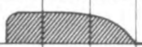	1825			7	0	2.4			4.25	40	7.1-9.2		NOT AVAILABLE IN DIAMETERS OVER 5/8"
AgCl	SILVER CHLORIDE	12.7	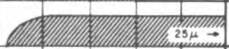	475	200		1.3	.15	2.006	1.994	1.980	5.56	(-50)-100	31	1.6-2.0 X 10	SOFT, LOW SOFTENING POINT AFFECTED BY ULTRAVIOLET.
Ge	GERMANIUM	6.4	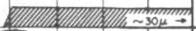	958	500		6	0	4.116	4.012	4.005	5.3	20-100	7		BECOMES OPAQUE AT ELEVATED TEMPERATURES-260°c
$CaAl_2O_4$	CALCIUM ALUMINATE	4	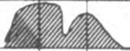	1600			2	40	1.635			3.67	20-400	8.4	10.5×10^{11}	SOFT AND WATER SOLUABLE UNLESS COATED-OTHERWISE SUITABLE FOR DOME APPLICATION.

guidance philosophies and is of particular interest here since it influences the guidance loop bandwidth. Specifically, the guidance loop must pass all significant frequency components of the turning rate spectrum or the desired missile flight path will not be effected.

In practice, competing functions and physical limitations impose restraints on guidance loop bandwidth in such a manner that an optimum implementation does not exist for all operating conditions.

Unavoidable noise inputs, for instance, indicate that a narrow band system is desirable. In addition to this, various guidance loop elements may act to limit bandwidth.

Rate gyros are made with a frequency response flat to 100-180 radians/second. This value is for a maximum dynamic range of 50°/second. If the dynamic range of the gyro is changed by changing the gradient of the restraining spring, the frequency response goes up or down with the range in proportion to the square root of the change.

Linear accelerometers are built with a frequency response of 40 to 60 radians/second for a unit with a ±½ g range. The frequency response varies with change of maximum range in the same manner as rate gyros.

The frequency response of actuators may vary widely depending on the requirements in the individual case. If little power is required, an actuator with a single time constant as small as 1/50 second is possible. With high hinge moments and low power available, the time constant may increase to 1/10 second or more. If dual actuators are used, the actuator will have two time constants or a transfer function as previously used consisting of a time constant and an under-damped quadratic. (The time responses given here are with a closed loop around the actuator and amplifier.)

It must be remembered that these time constants refer to the actuator when operating on small command signals that do not saturate the actuator system. The usual actuator has a maximum velocity such that the time necessary for full control deflection may be anywhere from 1/10 second to 1 second. If commands call for relatively small deflections, the frequency response is flat to 10 to 50 radians/second. For full deflection commands the frequency response drops to the 1 to 10 radians per second range.

The control system, in order to properly damp out the short period oscillatory mode must have a frequency response of at least the oscillatory range. The short period frequency may be as high as 20 radians/second.

With the correct feedback, the frequency response of the airframe as a rigid body can be made to approach the frequency response of the autopilot, or more specifically, the actuators. This response, (in some cases approaching 50 radians/second or more as actuators improve) is the source of other complications. It is above the frequency of bending modes of the airframe as a non-rigid body. The possibility of the actuator oscillating at an airframe bending frequency makes excitation of the bending mode possible.

If bending mode excitation occurs as a result of control deflection of tail surfaces, the airframe is, for practical purposes, a free-free beam having a sinusoidal force applied at one end. The result is shown in Figure 7-77. The cosine curves represent the center line deflection of the airframe for the fundamental and the second harmonic mode; *a* and *b* represent the mode or points of no deflection.

If these modes are excited by the control system, the excitation can be minimized by proper placement of the sensors. Linear accelerometers should be placed at the nodes where there is no linear deflection and rate gyros placed at the antinodes where linear motion is maximum but rotational motion is absent. Figure 7-77 shows the simplest form of bending mode deflection. Other frequencies and location of modes are possible if the surfaces are not at the end, as is true in the case of canard control surfaces. Also, the excitation of bending modes can result from aerodynamic forces, especially in the case of winged airframe. In this case, the bending mode can be damped by placing a sensor where the bending mode vibration causes a signal. This signal can be fed into the control system in the proper polarity to cause the control forces to oppose the oscillations. In many cases, however, it is considered best to cut the control system frequency response to a figure below bending mode frequencies.

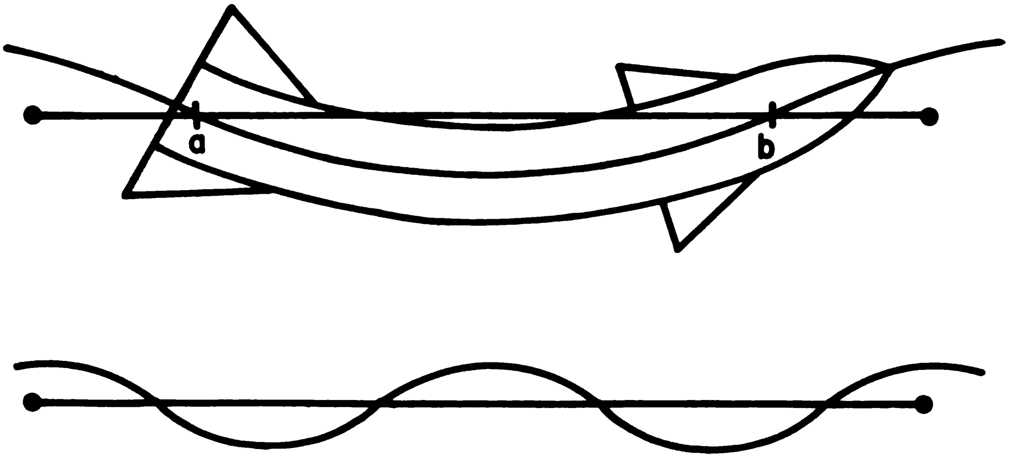

Figure 7-77. Airframe Bending Mode Excitation

If it is not possible to reduce the frequency response, the proper placement of sensors, and in severe cases, the inclusion of a notch filter in the feedback loop becomes necessary. The notch filter is a *band stop* filter at the resonant frequency. This solution is used when two or more frequencies are present.

It is significant that the control system frequency response necessary for short period stabilization generally covers a broader band than that needed for guidance purposes.

7-8.4 PRIMARY LOOP SYNTHESIS

The difficulties imposed by the nature of the kinematics generally leads to compensation *synthesis* for the primary loop by computer study or by the use of results from existing performance analyses.[2-18] Since the particulars of this approach are identical with those for evaluating the performance of a given system, paragraph 7-8.5 is applicable to this problem. While such a trial and error design procedure may seem primitive, it should not be forgotten that most of the linear models employed are approximations and the effects of nonlinearities such as deadband or saturation always raises a question regarding the extent of usefulness of results from strictly linear models.

7-8.5 PERFORMANCE EVALUATION

In order to state whether or not a specific guidance and control system provides adequate performance, some quantitative measure of the performance must be obtained and compared with a standard.

7-8.5.1 Criteria

Almost universally, miss distance is employed as the primary measure. Regardless of the complexity of the system or the detail of the model employed, suitable definitions of the miss distance can be made.

Additional criteria are also employed. The nature of these depend on the specific problem at hand. Warheads that do not have omnidirectional destructive capability, for instance, require that a more complete characterization of the miss than is provided by miss distance be investigated. Secondary performance criteria include maximum SAM maneuver and control energy needed to accomplish an intercept. Figures 7-14 and 7-15 indicated this for a simple model.

7-8.5.2 Simulation

The problem of determining the performance measures described above has received considerable attention. Although some analytical results are available[2-18] the most flexible approach appears to be offered by simulation. This conclusion results from the following observations about the environment of the preliminary design phase:

(a) Neither the standard for comparison nor control parameters have been firmly established. This requires that results be obtained for a range of values of (perhaps) several parameters.

(b) Initial errors and target motion can not be predicted exactly for use in evaluation. Additionally, various disturbances which can only be described statistically affect interceptor motion and result in performance measures that can only be described statistically. Thus, rather than using simply miss distance, the random nature of the miss distance is recognized by utilizing *rms miss distance.*

(c) Analytical results are available for predicting the rms miss distance for a wide range of linear models. This is not the case, however, for the secondary measures. Additionally, if effects of nonlinearities are to be studied, no general analytical approach is available.

LINEAR MODELS

In order to linearize the kinematics one usually studies perturbations about a nominal course as indicated in paragraph 7-2.7. Miss distance is then approximately given by the distance between the perturbed target and interceptor positions at $t = T_o$. Secondary measures can also be described in terms of the perturbed motions.

For these models the rms miss distance is conveniently obtained by the *adjoint method.*[83-86] Analytical results are also available but the simulation approach is more flexible and less demanding if one is designing by evaluating several systems.

Figure 7-78 illustrates the processing of adjoint system responses to obtain kill probability when it is adequately described as a function of only miss distance.

In case terminal guidance is initiated after a midcourse phase, additional contributions to miss distance will result. These are generally quite small if sufficient homing time is available.

If miss distance is not sufficient to describe kill probability, the last two operations in Figure 7-78 are not performed and only the mean and variance are extracted for use in the more complete functional relationship for kill probability.

In early design studies it is desirable to plot the individual contributions to the miss distance separately since subsequent calculations involving different relative magnitudes of the forcing functions can then be made independently.

NONLINEAR MODELS[85,87-90]

For nonlinear models it is generally necessary to generate the appropriate inputs and apply them to a simulator. The quantities needed to determine kill probability may then be measured as outputs of the simulation. If the inputs are stochastic, the measurements obtained will also be. Generally, kill probability studies require information at the instant of fuzing only so that complete time histories need not be generated but some of the secondary criteria may require a complete time history.

In such situations, provision is made for cycling the simulation. This provides a collection of measurements which are then subjected to statistical analysis to obtain estimates of the required distribution function parameters.

The question of accuracy of estimates and the number of samples that must be obtained is usually raised in the above procedure. These matters are treated in references 85, and 87-90.

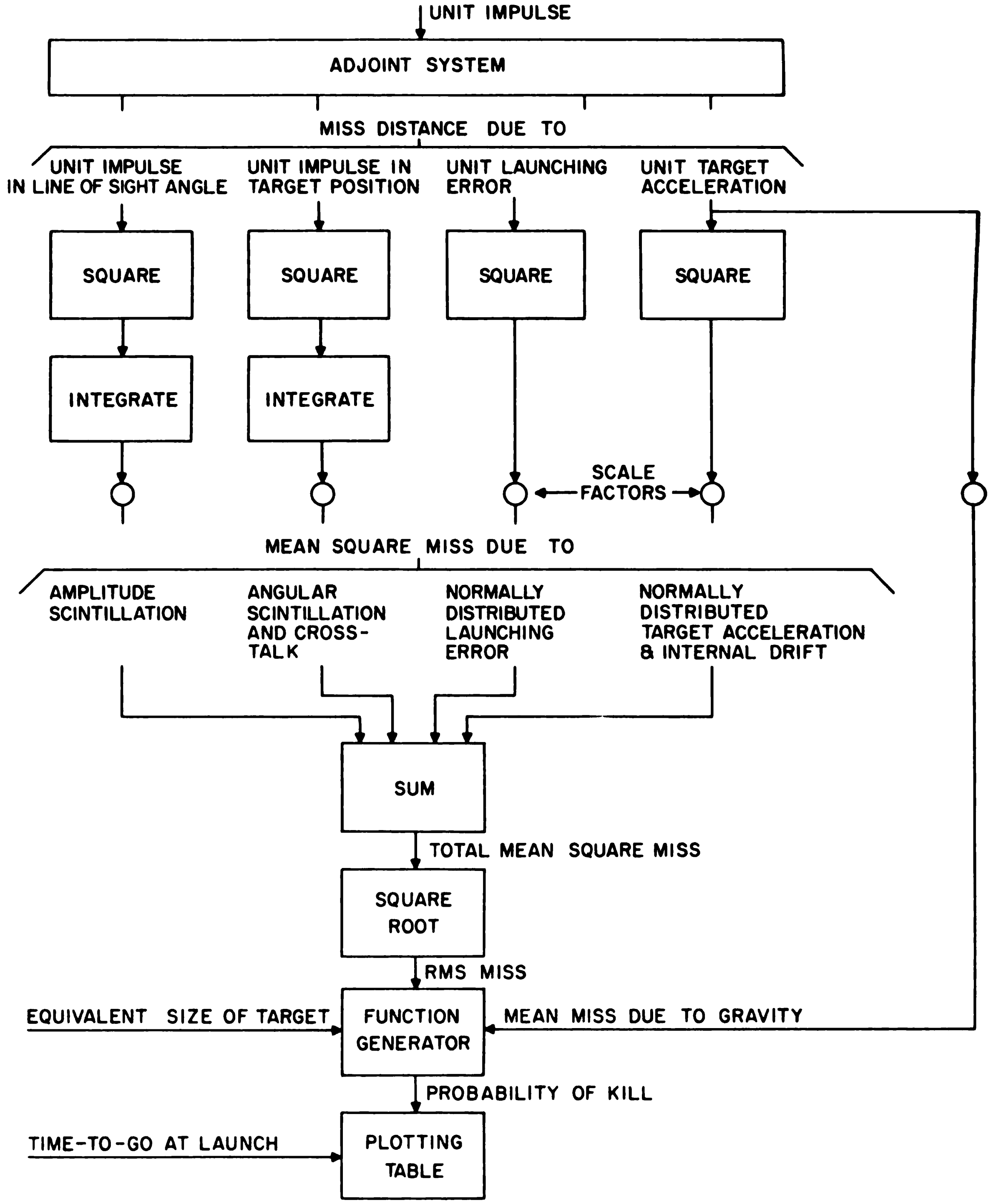

Figure 7-78. Kill Probability from Adjoint System

REFERENCES

1 Locke et al., *Principles of Guided Missile Design Series – Guidance*, D. Van Nostrand Co., Princeton, 1955.

2 D. Wooldridge, *Effects of Target Maneuvers, Tracking Errors, and Time Lags on a Proportional Navigation Missile Trajectory*, Hughes Aircraft Co., Tech Memo No. 194, March, 1949.

3 T. Jones et al., *The Effect of Time Lag on Proportional Navigation Trajectories*, MIT Meteor Rept. No. 38, Cambridge, 1949.

4 R. Booton Jr., *Effect of Circular Target Maneuvers on Homing Missile Trajectories*, MIT Meteor Rept. No. 47, Cambridge, 1949.

5 R. Booton Jr., *Optimum Design and Miss Distributions of Homing Missiles*, ASTIA #AT 178 076, 1950.

6 F. Adler, *Proportional Navigation in Three Dimensions*, Hughes Aircraft Co., Tech Memo No. 256, October, 1951.

7 R. Bennett and W. Mathews, *Analytical Determination of Miss Distances for Linear Homing Navigation Systems*, Hughes Aircraft Co., Tech Memo No. 260, March, 1952.

8 J.Gallagher and N. Trembath, *Basic Study of Proportional Navigation Systems with Linearized Kinematics*, MIT DACL Rept. No. 75, Cambridge, 1953.

9 *GEDA Report of the Dynamic Systems and Computations Laboratory on FS-11*, Goodyear Aircraft Co., Rept. No. GER-4957, 1953.

10 J. Jerger, *Principles of Guided Missile Design Series – Systems Preliminary Design*, D. Van Nostrand Co., Princeton, 1960.

11 R. Slaven, *Some Basic Characteristics of Interferometric Homing With Proportional Navigation*, Johns Hopkins Univ. APL Memo BBD-587, March 1959.

12 E. Stewart, *Application of Statistical Theory to Beam Rider Guidance in the Presence of Noise, I – Wiener Filter Theory*, NACA Research Memo A55E11, August, 1955.

13 E. Stewart, *Application of Statistical Theory to Beam Rider Guidance in the Presence of Noise, II – Modified Wiener Filter Theory*, NACA Tech Note 4278, June, 1958.

14 E. Stewart and G. Smith, *The Synthesis of Optimum Homing Missile Guidance Systems With Statistical Inputs*, NASA Memo 2-13-59A, April, 1959.

15 R. Bain, *The Analysis of Linear Homing Navigations Systems*, RAE Tech Note GW-427, August, 1953.

16 R. Slaven, *The Ideal Homing Law in Three Dimensions*, Johns Hopkins Univ. APL Memo BBD-734, December, 1959.

17 *Linear Theory for an Anti-Aircraft Missile*, Raytheon Mfg. Co., Rept. No. M/R-16/199, February, 1953.

18 R. Bain et al., *Intermittent Proportional Navigation*, Royal Aircraft Est. Tech Note GW452, March, 1957.

19 F. Adler, "Missile Guidance By Three-Dimensional Proportional Navigation", *Journal of Applied Physics*, Vol. 27, No. 5, May, 1956, pp. 500-7.

20 A. Puckett and S. Ramo, *Guided Missile Engineering*, McGraw-Hill Book Co., N.Y., 1959.

21 H. Chestnut and R. Mayer, *Servomechanisms and Regulating System Design*, John Wiley and Sons, N.Y., 1951.

22 J. Truxall, *Automatic Feedback Control System Synthesis,* McGraw-Hill Book Co., N.Y., 1955.

23 "Servomechanisms", *Ordnance Engineering Design Handbook,* Office of Ordnance Research, Duke University, 1957.

24 *Dynamics of the Airframe,* Northrup Aircraft Co., BuAer Rept. No. AE-61-4-II, September, 1952.

25 B. Etkin, *Dynamics of Flight-Stability and Control,* John Wiley and Sons, N.Y., 1959.

26 S. Chin, *Missile Configuration Design,* McGraw-Hill Book Co., N.Y., 1961.

27 M. Marx, "Design Aspects of Attitude Control Systems", *IRE Trans. on Automatic Control,* Vol. AC-4, July 22, 1958, pp. 65-8.

28 R. Bellman, *Adaptive Control Processes: A Guided Tour,* Princeton Univ. Press, Princeton, 1961.

29 P. Stromer, "Adaptive Or Self-Optimizing Systems – A Bibliography", *IRE Trans. on Automatic Control,* Vol. AC-4, July, 1958, pp. 65-8.

30 R. Buscher, "A Self Adaptive Control Without Test Signals", *Space/Aeronautics,* Part I, December, 1961, pp. 104-8.

31 P. Eykhoff, "Adaptive and Optimizing Control Systems", *IRE Trans. on Automatic Control,* Vol. AC-5, June, 1960, pp.148-51.

32 J. Pappas, *Mathematical Modeling for Missile Systems,* Special Rept. 13, White Sands Missile Range, March, 1959.

33 L. Davis et al., *Exterior Ballistics of Rockets,* D. Van Nostrand Co., Princeton, July, 1958.

34 G. Smith, "Synthesis of a Self-Adaptive Autopilot for a Large Elastic Booster", *IRE Trans. on Automatic Control,* Vol. AC-5, No. 3, August, 1960, pp. 229-36.

35 G. Knollman, *Aerodynamic Equations of Motion for Guided Missiles,* Engineering Experimental Status Rept. A 205/T2, Georgia Inst. of Tech., February, 1957.

36 G. Smith, "Synthesis of a Self-Adaptive Autopilot for a Large Elastic Booster", *IRE Trans. on Automatic Control,* Vol. AC-5, No. 3, August, 1960, pp. 229-36.

37 R. Hruby, "Design of Optimum Beam Flexural Damping in a Missile by Application of Root Locus Techniques", *IRE Trans. on Automatic Control,* Vol. AC-5, No. 3, August, 1960.

38 G. Tutt and W. Waymeyer, "Model Feedback Applied to Flexible Booster Controls", *IRE Trans. on Automatic Control,* Vol. AC-6, No. 2, May, 1961, pp. 135-42.

39 J. Truxal, *Control Engineers Handbook,* McGraw-Hill Book Co., N.Y., 1958.

40 J. Hanson, *Three Dimensional Coordinate Systems and Missile Dynamics,* Johns Hopkins Univ. APL Memo BBD-688.

41 A. Lange, "Automatic Control of Three Dimensional Vector Quantities", *IRE Trans. on Automatic Control,* Part I, May 1959, p. 21; Part II, January, 1960, p. 38; Part III, June 1960, p. 106; Correction, September 1961, p. 341.

42 D. Povejsil et al., *Airborne Radar,* D. Van Nostrand Co, Princeton, 1961.

43 J. Bussgang et al., "A Unified Analysis of Range Performance of CW, Pulse, and Pulse Doppler Radar", *Proc. of IRE,* Vol. 47, October, 1959, pp. 1753-62.

44 J. Bussgang et al., "Detection Range of CW and Pulse Doppler Radars", *Aeronautical Electronics National Conf. Proc.,* 1958.

45 "Symposium on Pulse Doppler Radar", *Proc. of 1956 Joint Services,* Bureau of Ordnance, Dept. of Navy.

46 A. Barrett, *Fundamentals of Beam Rider Receivers,* Capehart-Farnsworth, Fort Wayne, ASTIA #AD 66 453.

47 N. Jetta, *Gyroscopes for Army Missile Systems,* Redstone Arsenal Rept. 4R14F, March, 1958.

48 Smith, Jones, and Chasman, *The Detection and Measurement of Infrared Radiation,* Oxford Univ. Press, 1957.

49 Ballard, Larmore and Passman, *Fundamentals of Infrared for Military Applications,* Project Panel Report R297, Contract AF18(600)1600, March, 1956.

50 *Evaluation of Countermeasures Effectiveness,* Eastman Kodak Rept. No. EK-D-97-Q2, ASTIA #AD 118 864, 1956.

51 Perkin-Elmer Corp., Rept. No. 5034A, Norwalk, Conn., October 26, 1956.

52 W. Low, *Passive Detection of Intercontinental Ballistic Missiles,* Sylvania Electric Inc., July 31, 1956.

53 Baum and Dunkleman, "Horizontal Attenuation of Ultraviolet Light by Lower Atmosphere", *Journal of the Optical Soc. of America,* Vol. 45, 1955.

54 "Passive Detector by Solar Energy", *Project Hook,* Univ. of Calif., SIO Reference 55-9, February, 1955.

55 *Quarterly Engineering Reports: AN/DPN-18,* Ryan Aeronautical Co., 1955.

56 V. Zworykin and E. Ramberg, *Photoelectricity and its Applications,* John Wiley and Sons, N.Y., 1949.

57 R. Barbera, "Infrared Automatic Acquisition and Tracking System", *IRE Trans. on Military Electronics,* Vol. 4, October, 1961.

58 F. Rosell, "Imaging Tube Detectors", *Space/Aeronautics,* November, 1961.

59 F. Djorup Jr., *Missile-Target Intercept Geometry,* GE Rept. No. DF58ELC16, Ithaca, 1958.

60 *Radiation Laboratory Series,* Vol. 1, McGraw-Hill Book Co., N.Y., 1947.

61 J. Marcum, *A Statistical Theory of Target Detection by Pulsed Radar,* RAND Corp., RM-754 and RM-753, December, 1947.

62 P. Swerling, *Probability of Detection for Fluctuating Targets,* RAND Corp., RM-1217, March, 1954.

63 E. Schlieben, "Radomes and Aircraft Design", *Aeronautical Engineering Review,* May, 1952, p. 69.

64 M. Paiss et al., *Interim Report, Summary of Beam Deflection Investigations for the Period October 1950 to 1 February 1953,* NADC-EL-5399, Johnsville, Pa., October, 1953.

65 *Low Altitude Defense System Study, Final Report,* Vol. 4, Lockheed Aircraft Corp., Rept. MSD-1046, January, 1955.

66 R. DeLano, *A Comparison of Pulsed and CW Target Seekers,* Hughes Aircraft Co., Tech Memo No. 369, December 1954.

67 R. Carpenter, "Comparison of AM and FM Reticle System", *Proc. of IRIS,* Vol. 2, No. 2, December, 1957.

68 Jenkins and White, *Fundamentals of Optics,* McGraw-Hill Book Co., N.Y., 1950.

69 Sears, *Principles of Physics,* Addison-Wesley Press, Reading, Mass., 1947.

70 Zemansky, *Heat and Thermodynamics,* McGraw-Hill Book Co., N.Y., 1951.

71 R. Jones, "Methods of Rating the Performance of Photoconductive Cells", *Proc. of IRIS,* Vol. 2, No. 1, June, 1957.

72 Levinstein et al., "Cooled Infrared Detectors", *Proc. of IRIS* Vol. 3, No. 1, March, 1958.

73 R. Jones, *loc. cit.*

74 R. Jones, "Performance of Detectors for Visible and Infrared Radiation", *Advances in Electronics,* Vol. 5, 1953.

75 A. Cussen, "A Comparison of Photoconductive Cells", *Proc. of IRIS,* Vol. 2, No. 1, June, 1956.

76 D. Robinson, "Methods of Background Description and Their Utility", *Proc. of IRIS,* Vol. 3, No. 1, March, 1958.

77 M. Seymour, *Infrared Range Equations,* GE Rept. No. R58ELC1, Ithaca, 1958.

78 G. Newton Jr. et al., *Analytical Design of Linear Feedback Controls,* John Wiley and Sons, N.Y., 1957.

79 E. Peterson, *Optimization of Multi Output Linear-Time Varying Systems Subject to Multiple or Redundant Non Stationary Inputs*, GE Rept. No. SP-76, Santa Barbara.

80 E. Peterson, *Statistical Analysis and Optimization of Systems*, John Wiley and Sons, N.Y., 1961.

81 C. Merrian III, "An Optimization Theory for Feedback Control System Design", *Information and Control*, Vol. 3, No. 1, March, 1960, pp. 32-59.

82 E. Peterson and F. Remond, *Computation Methods for Optimization of Multi-Dimensional Nonlinear Processes*, GE Rept. No. RM61TMP52, Santa Barbara, 1961.

83 J. Laning, Jr. and R. Battin, "An Application of Analog Computers to the Statistical Analysis of Time Variable Networks", *IRE Trans. on Circuit Theory*, Vol. CT-2, No. 1, March, 1955, pp. 44-9.

84 J. Laning, Jr. and R. Battin, *Random Processes in Automatic Control*, McGraw-Hill Book Co., N.Y., 1956.

85 W. Mathews et al., *Analytical and Simulation Techniques Used in Predicting FALCON Probability of Hit*, Hughes Aircraft Co., Tech Memo No. 357, June, 1954.

86 M. Isaac, *Deterministic and Stochastic Response of Linear Time Variable Systems*, GE Rept. No. R62EML1, Utica, 1962.

87 R. Bennett, "Analog Computing Applied to Noise Studies", *Proc. of IRE*, Vol. 41, 1953, pp. 1509-13.

88 W. Dixon and F. Massey Jr., *Introduction to Statistical Analysis*, McGraw-Hill Book Co., N.Y., 1951, Chap. 13.

89 W. Vander Velde, "Make Statistical Studies on Analog Simulations", *Control Engineering*, Vol. 7, No. 6, June 1960, pp. 127-30.

90 T. Saaty, *Mathematical Methods of Operations Research*, McGraw-Hill Book Co., N.Y., 1959, pp. 292-5.

INDEX

ACCELERATION (Missile), 7-16, 7-26
ACCELEROMETER, 7-52
ACQUISITION, 6-5, 6-60
ACTUATORS (Missile Control), 7-43
ADJOINT SYSTEM, 7-95
AERODYNAMIC FORCES, 7-29
AIRFRAME CONTROL (Closed Loop), 7-33
  attitude control, 7-33
  attitude rate control, 7-35, 7-38
  lateral control, 7-39
  signal requirements, 7-41
  system root locus, 7-34
ALTIMETER, 7-1
AMPLIFIER
  ceramic tube, 7-41
  experimental, 7-42
  i-f, 6-34
  magnetic, 7-42
  packaging techniques, 7-42
  parametric, 6-37
  r-f, 6-35
  transistor, 7-41
  tube, 7-41
  video, 6-33
AMPLITUDE MONOPULSE, 6-89, 6-92
ANTENNA, 6-12
  beamwidth, 6-13, 6-15
  gain, 6-16
  patterns, 6-19, 6-85, 6-95
  phase errors, 6-16
  primary feeds, 6-19
  sidelobes, 6-13, 6-18
  waveguide, 6-19, 6-20
ANTENNAS, SEARCH, 6-20
  two-dimensional scanning arrays, 6-22
  inertialess scanning, 6-21
  line source scanners, 6-22
  point source scanners, 6-20
  rotating, 6-20
ANTENNAS, TRACK, 6-22, 6-82, 6-92, 6-95, 6-99
ASSIGNMENT, 6-3
ATMOSPHERE
  ARDC model, 7-85
  attenuation, 6-134
  exponential, 7-35
  IR transmission, 7-82
  "Standard", 6-138
ATTITUDE CONTROL, 7-28, 7-33
AUTOPILOT, 7-33
BEACONS, 7-45
BEAM ANGLE, 6-66
BEAM RIDER, 6-5, 7-3, 7-4
  geometry, 7-6, 7-10
  trajectories vs. launch angles, 7-9
  turning rates, 7-5, 7-10
BLACK-BODY, 7-63, 7-78, 7-81
BOLTZMANN'S CONSTANT, 6-7
BORESIGHT SHIFT, 7-73
CANCELLATION
  and sub-clutter, 6-55
  pulse-to-pulse 6-56, 6-59
CLUTTER
  attenuation, 6-56
  frequency, 6-57
  rain and ground clutter, 6-107
  sub-clutter, 6-55
COHERENT DETECTION SYSTEMS, 6-47
COMBINATION MONOPULSE, 6-99, 6-127, 6-129
COMMAND GUIDANCE, 6-5
CONICAL SCAN, 6-82, 6-102, 7-67
CONSTANT BEARING COURSE, 7-11
COORDINATE SYSTEMS (Missile)
  body axes, 7-22
  nomenclature, 7-24
  stability axes, 7-23
COUNTERMEASURES, 6-29
CRYSTAL BEACON, 6-158
DEAD-BAND, 6-111
DETECTION, 6-45
  discernibility, 6-40
  discrimination (IR), 7-88
  optical system, 7-90
  probability, 6-50, 6-77
  range (IR), 7-89
  range (radar), 6-2, 6-52
  search radar evaluation, 6-60
DETECTORS (IR), 7-80
  detectivity, 7-81
  Jones "S", 7-84
  NEP, 7-81
  responsivity, 7-81
  spectral response, 7-83
  time constants, 7-85
  wavelength, 7-86
DIFFERENTIAL DOPPLER REFLECTION, 6-118
DIFFRACTION, 6-123, 6-129, 6-133
  far-field, 6-13
  spherical, 6-131
  straight-edge, 6-131, 6-133
DISCERNIBILITY, 6-60
DITHER, 6-111
DOPPLER DEVICES, 7-46

DUTCH ROLL, 7-32
ECS, 6-117
EFFECTIVE NAVIGATION CONSTANT, 7-14
ELECTROMAGNETIC SPECTRUM, 7-61
EMISSIVITY, 7-78
ENGAGEMENT, 6-5
FADING, 6-118, 6-121
FALSE ALARM, 7-69
  number, 6-48
  time, 6-49
FLIGHT CONTROL, 7-21
  airframe as a loop element, 7-22
  attitude control, 7-28
  closed loop airframe control, 7-33
  component considerations, 7-40
  missile acceleration, 7-26
  missile axes, 7-22
  special features, 7-21
  system root locus, 7-34
FREE GYRO, 7-50
GEOMETRY FEEDBACK, 7-20
GUIDANCE MODES, 7-3
  constant bearing, 7-11
  flight path characteristics, 7-7
  line-of-sight, 7-4, 7-9
  measurement requirements, 7-17
  mechanization requirements, 7-18
  modified pursuit, 7-6
  nomenclature, 7-4
  perturbation analysis, 7-13
  proportional navigation, 7-11
  pursuit, 7-6, 7-10
  sensor requirements, 7-14
GUIDANCE PHASES, 7-1
GUIDANCE SERVO LOOPS, 7-17
  linear feedback controls, 7-19
  primary guidance loop, 7-20
GUIDANCE STUDIES, 7-91
GYROSCOPES, 7-49
HOMING, 6-6
HYDRAULIC FLUIDS, 7-43
I-F AMPLIFIERS, 6-34
IFF, 6-3
INDICATOR COLLAPSING FUNCTION, 6-75
INFRARED, 7-61
  atmospheric transmission, 7-82
  detectors, 7-80
  discrimination, 7-89
  nomograph, 7-79
  optical materials, 7-91
  radiated IR sample problem, 7-78
  radiation laws, 7-77
  range equations, 7-89
  seeker system, 7-77
  transmitting materials, 7-92
INITIAL AIMING ERROR, 7-15
INTEGRATION
  coherent, 6-52
  gain, 6-49
  loss, 6-53
  non-coherent, 6-45
  time, 6-68
INTERCEPT GEOMETRY, 6-2
INTERFEROMETERS, 7-73
JONES "S", 7-82
KINEMATICS, 7-20, 7-44
LATERAL DYNAMICS, 7-31
LINEAR FEEDBACK CONTROLS, 7-19
LOBE SWITCHING, 6-82
LONGITUDINAL MODE TRANSFER FUNCTIONS, 7-30
MASER, 6-40
MICROWAVE TRANSMITTING TUBES, 6-24
MISSILE ACCELERATION, 7-16
MISSILE MOTION EQUATIONS, 7-24
MODELS
  ARDC, 7-85
  high dynamic pressure, 7-30
  launch phase, 7-25
  linear, 7-95
  low dynamic pressure, 7-25
  non-linear, 7-95
MODIFIED PURSUIT COURSE
  definition, 7-6
  geometry, 7-10
MONOCHROMATIC RADIATION, 7-80
MTI, 6-54
NEGATIVE CONTRAST, 7-63
NEP (noise equivalent power), 7-81
NOISE
  additional noise sweeps, 6-70
  angular, 6-102, 6-160
  boxcarred, 6-102
  component instability, 6-55
  filtering, 7-72
  internal motion, 6-54
  Johnson, 6-43, 7-81
  local oscillator, 6-39
  man-made, 6-40, 6-102, 6-104
  natural, 6-40, 6-102, 6-104, 6-107
  partition, 6-39
  rain, 6-107
  receiver, 6-29, 6-38, 6-42, 6-107, 6-157
  r-f and i-f, 6-36, 6-103
  servo, 6-109
  shot, 6-39
  thermal, 6-103, 6-161
  transistor, 6-39
  tube, 6-35, 6-39
OPTICAL
  detection, 7-63, 7-90
  materials, 7-91
  tracking, 7-90

- PARAMETRIC AMPLIFIERS, 6-37
- PASS-COURSE GEOMETRY, 6-114
- PERFORMANCE EVALUATION (Guidance), 7-94
- PERTURBATION ANALYSIS, 7-13
- PHASE MONOPULSE, 6-96
  - elevation errors, 6-128
- PHASE SHIFT VERSUS AGC, 6-44
- PHUGOID OSCILLATION, 7-30
- PITCH RATE CONTROL, 7-35, 7-39
- PITCH RESPONSE, 7-28
- PRIMARY GUIDANCE LOOP, 7-20
- PROPAGATION ERRORS
  - diffraction, 6-123, 6-129
  - reflection, 6-123, 6-125
  - refraction, 6-133
  - regions of, 6-124
- PROPORTIONAL NAVIGATION
  - coordinate system, 7-13
  - definition, 7-11
  - geometry, 7-12
- PULSER
  - gas tube, 6-25
  - hard tube, 6-27
  - line type, 6-28
  - saturating reactor, 6-27
  - tube phase characteristics, 6-27
- PURSUIT COURSE
  - definition, 7-6
  - geometry, 7-10
- RADAR RANGE
  - calculation examples, 6-52, 6-76
  - coherent CW system, 6-52
  - coherent pulsed system, 6-53
  - CW system, 6-49
  - equation, 6-6
  - loss, 6-154
  - monopulse system, 6-89, 6-96
  - non-coherent CW system, 6-49
  - non-coherent pulsed system, 6-45
  - pulsed system, 6-45
  - scanned radar, 6-71
  - tracking errors, 6-147
  - wavelength factor, 6-9
- RADAR SYMBOLS, 6-60
- RADOME, 6-165
- RAIN, 6-107
- RATE GYRO, 7-51
- RECEIVER, 6-28
  - amplifiers, 6-33
  - bandwidth, 6-30
  - countermeasures, 6-29
  - gain, 6-12
  - maser, 6-40
  - measurement techniques, 6-41
  - noise, 6-38, 6-105
  - phase shift versus AGC, 6-44
  - representation factor, 6-77
  - selectivity, 6-32
  - stability, 6-32
  - typical receivers, 6-29, 6-31
- REFLECTION, 6-123
- REFRACTION
  - calculation of, 6-137
  - error calculation, 6-142
  - ionospheric, 6-135
  - tropospheric, 6-134
- RESPONSE STABILITY (Control), 7-21
- RESPONSIVITY, 7-81
- RETICLES, 7-76, 7-90
- R-F AMPLIFIERS, 6-35
- SEARCHLIGHT, 6-65
- SEARCH RADAR
  - additional noise sweeps, 6-70
  - discernibility, 6-60
  - evaluation, 6-60
  - i-f bandwidth and pulse length, 6-61
  - prf, 6-64, 6-68, 6-72
  - scanning, 6-65, 6-69, 6-79
  - video bandwidth and sweep speed, 6-63
- SEEKERS, 7-65
  - functions, 7-65
  - infrared, 7-74
  - radar, 7-73
  - range, 7-70
  - scanning, 7-66
  - tracking, 7-72
- SEEKERS (INFRARED), 7-74
- SEEKERS (RADAR), 7-73
- SENSITIVITY
  - crystal beacon, 6-158
  - interferometer, 6-98, 6-151
  - tracking radar, 6-102, 6-150
- SENSOR REQUIREMENTS, 7-14, 7-42, 7-44
- SENSORS (Midcourse)
  - basic measurements, 7-44
  - celestial, 7-58
  - inertial, 7-49
  - radar, 7-45
- SENSORS (Terminal), 7-59
  - hybrid, 7-65
  - infrared, 7-61
  - optical, 7-63
  - radar, 7-59
  - ultraviolet, 7-63
- SEQUENTIAL LOBING, 7-66
- SERVO
  - constant velocity errors, 6-113
  - ECS correction, 6-117
  - filter factor, 6-152
  - frictional drag, 6-112
  - guidance servo loop, 7-17
  - noise, 6-109
  - open loop response, 6-114
  - response curves, 6-111
- SERVOMECHANISM THEORY, 7-1, 7-19, 7-28

SIMULATION, 7-94
SLANT RANGE, 6-2, 6-12
SLIP ANGLE, 7-25, 7-31
SPIRAL DIVERGENCE, 7-32
STABILIZED PLATFORM, 7-57, 7-58
STAR TRACKERS, 7-58
STRUCTURAL RESONANCE, 7-21
SWEEP RECURRENCE FREQUENCY, 6-71
TARGET
  acceleration, 7-16
  area, 6-10, 6-108
  detection, 6-45
  displacement, 6-79
  scintillation, 6-118
TRACK
  definition, 6-5
  optical system for, 7-90
  radar, analysis and design, 6-82
TRACKING ERRORS, 6-102
  alignment, 6-165
  boresighting, 6-165
  boresight shift, 7-73
  combining of errors, 6-143
  external radio noise, 6-103, 6-105
  propagation errors, 6-123
  radome distortion, 6-165
  radome rate (error slope), 7-72
  r-f coupling, 6-165
  rain and ground clutter, 6-107
  servo noise and servo dynamic errors, 6-109, 6-115
  sun and windloading distortion, 6-165
  target scintillation, 6-118
  thermal noise, 6-103
TRACK RADAR, 6-82
  error sources, 6-102
  parameters, 6-88
  sample calculations, 6-145
  types, 6-82, 6-91
TRANSMITTERS, 6-24
ULTRAVIOLET, 7-63
UP-CONVERTER, 6-38
VELOCITY RESPONSE, 6-59
VIDEO AMPLIFIERS, 6-33
VIDEO BANDWIDTH AND SWEEP SPEED, 6-63
WANDER, 6-120

* U.S. GOVERNMENT PRINTING OFFICE : 1962 O—660916

ORDNANCE ENGINEERING DESIGN HANDBOOK SERIES

The Ordnance Engineering Design Handbook Series, when completed, is intended to provide a compilation of principles and fundamental data to supplement experience in assisting engineers in the evolution of new designs which will meet tactical and technical needs while also embodying satisfactory producibility and maintainability.

As of the date of this publication, the handbooks listed below have been published or publication is pending. Copies of these handbooks, and information on later publications which may be available, should be requested from the Ordnance Engineering Handbook Office, Ordnance Liaison Group, Durham, Box CM, Duke Station, Durham, N. C.

AMMUNITION SERIES

ORDP 20-210	Fuzes, General and Mechanical
ORDP 20-244	Section 1, Artillery Ammunition--General, with Table of Contents, Glossary and Index for Series
ORDP 20-245 (C)	Section 2, Design for Terminal Effects (U)
ORDP 20-246	Section 3, Design for Control of Flight Characteristics
ORDP 20-247 (C)	Section 4, Design for Projection (U)
ORDP 20-248	Section 5, Inspection Aspects of Artillery Ammunition Design
ORDP 20-249 (C)	Section 6, Manufacture of Metallic Components of Artillery Ammunition (U)

BALLISTIC MISSILE SERIES

ORDP 20-281 (S)	Weapon System Effectiveness (U)
ORDP 20-282	Propulsion and Propellants
ORDP 20-284 (C)	Trajectories (U)
ORDP 20-286	Structures

CARRIAGES AND MOUNTS SERIES

ORDP 20-341	Cradles
ORDP 20-342	Recoil Systems
ORDP 20-343	Top Carriages
ORDP 20-344	Bottom Carriages
ORDP 20-345	Equilibrators
ORDP 20-346	Elevating Mechanisms
ORDP 20-347	Traversing Mechanisms

EXPLOSIVES SERIES

ORDP 20-175	Solid Propellants, Part One
ORDP 20-176 (C)	Solid Propellants, Part Two (U)
ORDP 20-177	Properties of Explosives of Military Interest, Section 1
ORDP 20-178 (C)	Properties of Explosives of Military Interest, Section 2 (U)

EXTERIOR BALLISTICS SERIES

ORDP 20-140	Trajectories, Differential Effects, and Data for Projectiles

FIRE CONTROL SERIES

ORDP 20-331	Compensating Elements

GENERAL

ORDP 20-106	Elements of Armament Engineering, Part 1, Sources of Energy
ORDP 20-107	Elements of Armament Engineering, Part 2, Ballistics
ORDP 20-108	Elements of Armament Engineering, Part 3, Weapon Systems and Components

GENERAL (continued)

ORDP 20-110	Experimental Statistics, Section 1, Basic Concepts and Analysis of Measurement Data
ORDP 20-111	Experimental Statistics, Section 2, Analysis of Enumerative and Classificatory Data
ORDP 20-112	Experimental Statistics, Section 3, Planning and Analysis of Comparative Experiments
ORDP 20-113	Experimental Statistics, Section 4, Special Topics
ORDP 20-114	Experimental Statistics, Section 5, Tables
ORDP 20-134	Maintenance Engineering Guide for Ordnance Design
ORDP 20-135	Inventions, Patents, and Related Matters
ORDP 20-136	Servomechanisms, Section 1, Theory
ORDP 20-137	Servomechanisms, Section 2, Measurement and Signal Converters
ORDP 20-138	Servomechanisms, Section 3, Amplification
ORDP 20-139	Servomechanisms, Section 4, Power Elements and System Design
ORDP 20-170 (C)	Armor and Its Application to Vehicles (U)
ORDP 20-270	Propellant Actuated Devices
ORDP 20-290 (C)	Warheads--General (U)
ORDP 20-355	The Automotive Assembly

ORDNANCE MATERIALS HANDBOOKS

ORDP 20-301	Aluminum and Aluminum Alloys
ORDP 20-302	Copper and Copper Alloys
ORDP 20-303	Magnesium and Magnesium Alloys
ORDP 20-305	Titanium and Titanium Alloys
ORDP 20-306	Adhesives
ORDP 20-307	Gasket Materials (Nonmetallic)
ORDP 20-308	Glass
ORDP 20-309	Plastics
ORDP 20-310	Rubber and Rubber-Like Materials
ORDP 20-311	Corrosion and Corrosion Protection of Metals

SURFACE-TO-AIR MISSILE SERIES

ORDP 20-291	Part One, System Integration
ORDP 20-292	Part Two, Weapon Control
ORDP 20-293	Part Three, Computers
ORDP 20-294 (S)	Part Four, Missile Armament (U)
ORDP 20-295 (S)	Part Five, Countermeasures (U)
ORDP 20-296	Part Six, Structures and Power Sources
ORDP 20-297 (S)	Part Seven, Sample Problem (U)

Stanford University Libraries
3 6105 126 755 565